dmu.ac.uk
DE MONTFORT UNIVERSITY
LEICESTER

THE BIOMECHANCIAL PROPERTIES OF THE HUMAN VOCAL FOLD

ERIC N GOODYER

Submitted in partial fulfilment for the award of PhD by Published Works from

De MONTFORT UNIVERSITY

This research was financially supported by the EPSRC, The Royal Society and The Royal Academy of Engineering.

January 2008

EPSRC Engineering and Physical Sciences Research Council

The Royal Academy of Engineering

THE ROYAL SOCIETY
CELEBRATING 350 YEARS

Abstract

Phonation is a complex process requiring the controlled exhalation of air through the larynx. Within the larynx there is a specialist tissue structure known as the vocal folds, which under muscular control captures energy within the airflow and transfers it to a dynamic phenomena, analogous to a static fluid wave, known as the mucosal wave. This mucosal wave causes the vocal folds to open and close rhythmically, thus modulating the airflow, which can then be manipulated in the vocal tract to create the sounds that we know as speech.

The purpose of the research detailed in this thesis is the quantification of the biomechanical properties of the vocal folds. There is a major gap in knowledge relating to the elastic properties of the vocal fold as the only reliable apparatus available to determine these properties rely on dissecting the tissue out of anatomical context. The author's research is dedicated to developing methods to measure these properties from intact larynges, and from patients *in vivo*. This is to enable a better understanding of how this complex tissue structure works; to assist with the derivation of mathematical models of phonation; and to provide methods to assess objectively the effectiveness of tissue engineering therapies used to repair scarred vocal folds.

The author devised a new and novel apparatus to obtain data from excised tissue and *in vivo*. A key principle of these devices is that they directly measure the mechanical properties of intact larynges, which contrasts to methods reported by the majority of other researchers. The author also managed a number of research grant funded projects, in his capacity as PI, which deployed the devices. The author developed most of the software and the mathematical techniques used to analyse the data.

Details of the apparatus devised to obtain data from both excised larynges and *in vivo* are given, which required the derivation of devices capable of measuring micrograms of force and displacement resolutions at micron level. Also given are the mathematical models used to transform the raw data into the fundamental material property known as shear modulus.

The results include measurements of the shear modulus of a group of 20 excised vocal folds, of varying ages and both sexes. Also given are the results of similar data obtained from eight volunteer patients *in vivo*. The anisotropic nature of vocal

fold tissue is quantified and iso-contour maps presented showing the variation of elasticity with respect to anatomical position.

Early results are given that quantify the change in vocal fold tension with respect to electrical stimulation of the recurrent and superior laryngeal nerves in a canine model. Also given are the results of a study that demonstrated that hyaluronic acid tissue augmentation could restore vocal fold pliability in a rabbit model.

Acknowledgements

I would like to thank Assistant Professor Jim Kobler from Harvard Medical School for introducing me to this subject.

I would also like to thank Professor Markus Hess from UKE Hamburg for his continual support and advice.

Finally, my thanks go to Professors Bob John and Phil Moore from De Montfort University who encouraged me to write this thesis.

Contents

List of Figures

List of Tables

List of Abbreviations and Terms Used

DSR Dynamic Spring Rate: The DSR is the ratio of the peak force to peak displacement when a sinusoidally varying force is applied to any material, causing it to deform.

E Young's Modulus: E is the amount of longitudinal stress required to deform a solid material by a unit of longitudinal strain.

Epithelium: The epithelium is a general term for the outer covering of a tissue. In this thesis it refers to the outer layer of the vocal fold encapsulating the lamina propria.

ESR Elastic Spring Rate: The ESR is the in-phase ratio of peak force to peak displacement when a sinusoidally varying force is applied to a material, causing it to deform.

G Shear Modulus: G is defined as the amount of shear force required to deform a solid material bya unit of shear strain.

GBE Gas Bearing Electrodynanometer: The GBE is an electromechanical device design by Dr Hargens in the mid 20thC to measure the visco-elastic properties of the Stratum Corneum

LP Lamina Propria: The LP is soft tissue covering of the vocal fold.

LR Loss Rate: The LR is the out-of-phase ratio of peak force to peak displacement when a sinusoidally varying force is applied to a material, causing it to deform. It is also known as viscosity.

LSR Linear Skin Rheometer: The LSR is an electromechanical device originally devised to measure the visco-elastic properties of the Stratum Corneum

LVDT Linear Voltage Differential Transformer, a device that measures small linear displacements.

RLN Recurrent Laryngeal Nerve: The RLN is responsible for signalling the intrinsic muscles of the vocal tract, including the vocalis muscle to contract.

Shear Modulus: The relationship between shear stress applied to a material and the resultant shear strain, expressed as a ratio of shear stress/shear strain

SLN Superior Laryngeal nerve: The SLN is responsible for signalling cricothyroid muscle to contract

Vocal Fold: The Vocal Fold is a complex layered structure that includes the underlying vocalis muscle, the vocal ligament itself, and the outer covering of lamina propria and epithelium.

VP Vocal Process: The VP is the end of arytenoid cartilage to which the vocal ligament is attached. It is used in this research as a datum point for determining the anatomical position for point specific data measurements.

Young's Modulus: The relationship between linear stress applied to a material and the resultant linear strain, expressed as a ratio of linear stress/linear strain

1 The Research Context

This chapter sets out the background to the research detailed in this thesis. A brief explanation is given of how phonation is achieved, and the importance that biomechanical properties of the vocal fold play in enabling us to speak. An explanation is given as to how knowledge of these biomechanical properties is of value. Finally, the research objectives and boundaries are detailed.

Phonation, or our ability to speak, is a process that starts with the controlled and gentle exhalation of air from the lungs through the structure that is at the heart of this research study, the human vocal folds. Originally evolved as the means to prevent solid materials entering the lungs, that role is now undertaken by the epiglottis. The vocal folds have developed into the complex structure that is essential for modulation of the airflow as it passes from the trachea into the vocal tract, where the modulated flow is transformed into the sounds that we call speech. The vocal folds consist of a series of specialised layers; the lower being the vocalis muscle (part of the thyroarytenoid), which is overlaid by the vocal ligament which it controls. Above these structures are the lamina propria, and an outer covering of epithelium. This is shown in the images below taken and modified from the displayed sources [The Nurse 2006, Kim et. al. 2007]. Figure 7 shows a typical experimental setup with the key anatomical features displayed.

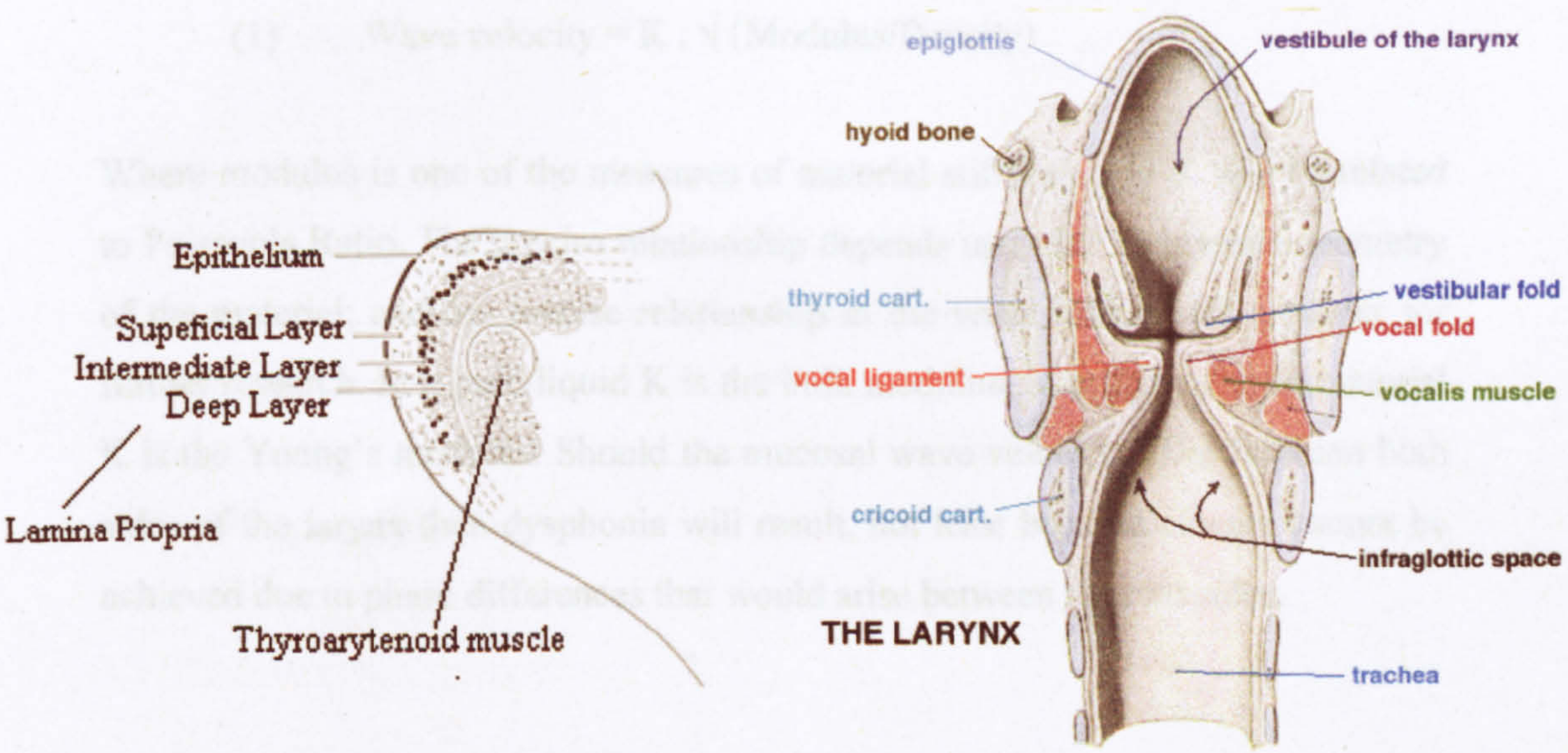

Figure 1 The structure of the vocal fold and its' anatomical context

Of most interest to this research are the mechanical properties of the vocal fold cover. The lamina propria (LP) consists mainly of rope like collagens, elastic like elastins, which are surrounded by an amorphous substance made up mostly of hyaluronic acid. This organ has complex visco-elastic properties. During phonation the airflow results in a drop of pressure above the vocal folds, causing them to rise up such that they meet and close the airway. Tension in the vocal ligament pulls the vocal fold cover back down again, thus creating a rhythmic cycle known as the myoelastic cycle [Hirano & Kakita 1985]; this causes a static wave to move through the LP structure known as the mucosal wave. It is this wave action, coupled with the rhythmic closures, that creates the modulation of the airflow.

A discourse on phonation is beyond the scope of this thesis. However, the key concept is that without the ability to generate a repetitive mucosal wave a person will suffer from either disordered voice (dysphonia) or in extreme cases total lack of voice (aphonia). A voice is termed "disordered" when the vocal quality of an individual is altered or changed in such a way that it is thought to be abnormal to the listener [Miller 2007].

Vocal fold scarring is a major challenge in the management of dysphonia. Scarring results in tissue stiffening, this impedes proper closure of the vocal folds, thus impacting on the quality of the mucosal wave. Fluid dynamics relates wave velocity to material stiffness by the simple relationship

$$(1) \qquad \text{Wave velocity} = K \cdot \sqrt{(\text{Modulus/Density})}$$

Where modulus is one of the measures of material stiffness, and K will be related to Poisson's Ratio. The precise relationship depends upon the nature and geometry of the material; and the precise relationship in the vocal fold is still a matter for further research. In a pure liquid K is the bulk modulus, in a strip of solid material K is the Young's modulus. Should the mucosal wave velocity differ between both sides of the larynx then dysphonia will result, not least because closure cannot be achieved due to phase differences that would arise between the two sides.

Scarring can arise from pathology, or because of the phono-surgery employed to address the pathology [Sulica 2004]. Research teams worldwide are engaged in a series of research programmes to devise tissue-engineering therapies to repair vocal fold scarring. These range from tissue augmentation using hyaluronic acid [Chan et.all 2002, Hertegard et. al. 2006-2, Hertegard et. al. 2004], Restylene, Cymetra and similar materials [Ford et. al. 1995, Dahlquist et.al. 2004], through to tissue engineering using growth factors [Duflo et. al. 2006], genetic transfection and stem-cell implants [Halun et. al. 2007, Hertegard et. al. 2006-1].

1.1 The Research Objectives

The overriding aim is to develop a constitutive equation that describes the biomechanical properties of the human vocal fold. This thesis represents a small step towards that goal.

The key objectives for this research were

- To measure the visco-elastic properties of the stratum corneum of the skin *in vivo*
- To measure the visco-elastic properties of the human lamina propria without dissecting the tissue out of anatomical context
- To device an apparatus to obtain visco-elastic data from the vocal folds of patients *in vivo*
- To formulate mathematical models to derive the fundamental rheological properties of the human tissue under test, to be presented in the results as the shear modulus

1.2 The Need for this research

This research has arisen because of the need of related research programmes into tissue engineering for methods to quantify the elastic properties of healthy tissue, the changes due to tissue damage, and a means to provide an objective assessment of tissue engineering therapies.

1.3 The Research Challenge

The research challenge was to devise an apparatus that is capable of measuring the visco-elastic properties of human tissue using excised intact organs and without dissecting samples out of anatomical context. Once the techniques had been

devised to obtain the raw stress/strain data the subsequent challenges were to devise a new device to obtain similar data *in vivo*, to derive mathematical methods to analyse the data, and to apply subsequently those methods to provide an objective assessment of the effectiveness of tissue engineering therapies.

1.4 The Boundaries of the Research

A key mathematical requirement is the derivation of a formal constitutive equation for the visco-elastic properties of the lamina propria. This is a major research programme that is beyond the scope of this thesis. Instead, the mathematical analysis is limited to presenting an experimentally derived method for estimating shear modulus.

In vivo measurements require the consent of the volunteer and must be minimally invasive. Our aim is to obtain experimental data in less than 1 minute. This constrained the apparatus formulation substantially, adding to the engineering challenge.

The *in vitro* studies rely on the availability of donor tissue. This cannot be guaranteed, nor is it possible to predict the range of tissue availability in terms of age and sex of the donors. This impacts on these studies as it is not possible to guarantee a representative range of age, and a balanced group of both sexes, within the study period.

2 The Instrumentation History

Here the history of the instrumentation devised to carry out this research is discussed. The earlier work that to quantify the effectiveness of various cosmetics and skin creams is briefly presented. The need to measure the elastic properties of dead or horny layers of the skin (stratum corneum) is explained, and how the Linear Skin Rheometer (LSR) was devised and evolved to take these measurements, together with some early-published results. The progression from skin measurement to the core of this research on the human vocal fold is presented.

Elasticity is a key parameter in determining the effectiveness of skin cream formulations. Some conditions, such as dry and cracked skin, require the skin to become more 'pliable'. Other conditions, and desires, require skin to become 'firmer'. Whatever the end requirement it is essential that the ability of a skin cream formulation to achieve that requirement is quantifiable through objective measurements. Amongst the methods formulated to support the skin cream research programmes is a device known as the Linear Skin Rheometer. The purpose of the device is to quantify changes in the visco-elastic response of the stratum corneum (upper layers of skin) when subjected to chemical changes, such as moisturisers (e.g. commercial products including Oil of Olay, Dove, Nivea etc.) and surfactants (e.g. soap).

This device was identified by a research team based at Harvard Medical School [Goodyer et. al. 2003] as a potential method to quantify the visco-elastic properties of the human vocal fold, and to quantify the effectiveness of tissue augmentation therapy. Since then a number of collaborative research programmes have been established with a range of different partners, including Harvard Medical School [Center for Laryngeal Research & Rehabilitation 2005], Universitat Klinic Eppendorf [Hess 2007], The Karolinska Institute Stockholm [Center for Hearing and Communication Research 2004], Wisconsin University Hospital [Otolaryngology Our Research 2007], UCLA, St. Thomas' Eye Hospital and Queen's Medical College.

The earlier publications [Matts & Goodyer 1998, Goodyer et. al. 2003, Hess et. al. 2006] deal with the research challenges that had to be overcome in order to formulate instrumentation capable of measuring the extremely small forces and displacements required to calculate the rheometric properties of human tissue. The

later publications [Goodyer et. al. 2007-1, Goodyer et. al. 2007-2, Goodyer et. al. 2006-1, Goodyer et. al. 2006-2] detail the research results. These include the first ever iso-contour maps produced showing the variation of elasticity over the surface of the vocal fold [Goodyer et. al. 2003, Hess et. al. 2006, Dailey et. al. 2007]. Also presented are interim results taken from a large-scale study of 20 excised human larynges [Goodyer et. al. 2007-3], and from eight volunteer patients who were measured *in vivo*. As well as demonstrating that the tissue is not homogeneous, as is widely accepted, the results also show that it is highly anisotropic in nature [Licht et. al. 2007]. The last finding has significant implications for other researchers investigating tissue-engineering therapies to repair scarred vocal folds. Finally, examples of work are presented that relate to the quantification of the effectiveness of hyaluronic acid tissue augmentation therapy [Hertegard et. al. 2004].

2.1 The Research Progression

- **Early Instrumentation**

The instrumentation is required to measure forces to milligram resolution, displacements to micron resolution, and do so without any frictional losses from the mechanical components. An earlier device, The Gas Bearing Electrodynanometer (GBE) [Bioengineering of the Skin 2002] invented by Dr Hargens, was used as a starting point by the author for the development of the LSR. The GBE applies a cyclical force of 3 grams to the skin by means of a solenoid that is floated within an air bearing. In effect, it is near frictionless. The force applied arises from the current that flows in the solenoid, and is induced by mutual inductance; therefore, it is not measured but inferred. Displacement is measured using a Linear Voltage Differential Transformer (LVDT). The data obtained is the peak force and peak displacement, from which the dynamic spring rate (DSR) of the material can be derived. DSR is the time-independent term given by the ratio of peak force/peak displacement. The author set up a development team to devise a new device, using modern components, that could replicate the performance of the GBE. The research challenge being the ability to deliver an extremely small force without frictional losses. The LVDT was retained in the new device, as it is a proven method for measuring displacement. Instead of inferring force, a force sensor was added to the system, and closed-loop control was used to create a known force cycle. The author acted as PI for the research programme, and developed the electronics and software for the new device. [Matts & Goodyer 1998]

- Studies on Animal Tissue

The earlier publications relate to a series of studies carried out using excised animal tissue. These took place at Harvard Medical School and UKE [Goodyer et. al. 2003, Hess et. al. 2006]. The key purpose of this early work was to refine the apparatus and methods. Some of this work was then duplicated by Wisconsin University Hospital. A key role undertaken by the author was to devise the methods for obtaining data from the animal tissue samples. The physiological data required by the clinicians was interpreted to obtain an engineering specification. The author specified new mechanical components, and designing new electronics and software techniques. The author undertook the analysis of the data obtained, and developed mathematical techniques to interpret the results. The major output of these early animal studies was the evolution of the devices, and proving of the methods. [Dailey et. al. 2007]

- Studies on Human Tissue

From 2003 onwards, the focus of the work moved to UKE Hamburg, where it was possible to obtain access to excised human cadaver tissue. From this point the bulk of the published material detailing the biomechanical properties of human vocal folds were produced. The author was PI for a series of studies using excised human tissue. This required devising new mechanical devices, and refinement of the real-time control strategies used to guide the measuring probe. New mathematical methods were developed and proved. Most important was the continual refinement of the attachment method, resulting in the use of a suctioned based cannula. [Goodyer et. al. 2007-1, Goodyer et. al. 2006-2, Licht et. al. 2007]

- *in vivo* Studies

Once the methods using excised tissue were proven the work began on formulating apparatus and methods for *in vivo* use. The joint DMU/UKE team are the second only to publish results for the biomechanical properties of the human vocal fold obtained *in vivo*. A major objective of this programme is the development of new devices to be used intra-operatively. The author managed the team that overcame the key challenges of producing a tool that can be deployed in an operating theatre, and is both safe and robust. [Goodyer et. al. 2006-1, Goodyer et. al. 2007-2]

- Tissue Engineering

The engineering methods formulated are now being applied in support of tissue engineering and other therapies. Most significant being the tissue augmentation work taking place at Karolinska, and tissue engineering at Wisconsin. In all these studies that author devised the measuring method to meet the Tissue

Engineering partners requirements, and analysed the results. [Hertegard et. al. 2004, Hertegard et. al. 2006, Dailey et. al. 2007]

2.2 Measurement of the Stratum Corneum

Cosmetic cream manufacturers have a strong interest in how their formulations change the elastic properties of the uppermost layer of the skin, known as the stratum corneum. This layer contains no living cells, but is of great importance in that it forms a barrier between a living body and the outer environment within which they are moving. It is not possible to measure the moisture content of the stratum corneum directly, without taking samples of skin for analysis; which is not practical. Therefore, it is necessary to infer the hydration level by secondary means.

There are two main techniques used to achieve this objective,

1) to measure the change in impedance of the stratum corneum
2) to measure the change in the visco-elastic response of the stratum corneum

Impedance methods are based on an electrical model of the stratum corneum, which represents cells as capacitive elements and surrounding fluids as resistive elements. Changes in impedance are determined by applying a sweep of AC signals to the skin via a pair of electrodes, and measuring the attenuation and phase shift that results from the effective reactive circuit created by the electrodes and the skin. Commercial products include the Nova Dermal Phase Meter and the Courage & Khazaka Corneometer. These, and similar instruments, are widely used for medical and cosmetic research. Visco-elastic measurement methods are based on the accepted theorem that the greater the hydration of the stratum corneum then the more pliable it becomes. Instruments that employ this technique include the Dia-Stron Dermal Torque Meter (DTM) and Ballistometer, the Courage & Khazaka Cutometer and the Hargens Gas Bearing Electrodynanometer (GBE). Neither group of techniques is truly satisfactory for determining hydration levels of the stratum corneum, but in the absence of an alternative to excising skin samples, they have become the 'industry norms'.

The driving factor that led Proctor & Gamble to prefer the use of electro-mechanical techniques to resistive techniques was commercial. The ability to make advertising claims for their moisturising cream product range using words such as

'supple' or 'smooth' has become commercially important in recent years. To support these advertising claims required the application of techniques that directly measured mechanical properties of the skin. Proctor & Gamble has long preferred the GBE device. This device was developed in the 1960's by Dr Hargens and is still in widespread use. The principle is based on applying a known force to the skin surface such that a shear stress is applied to the stratum corneum. The probe that is attached to the skin is held in a near-frictionless manner using an air bearing within the field of an electromagnetic component. By applying a known sinusoidally varying current of 0.3Hz to the primary coil, mutual inductance results in a known sinusoidal force being applied to the skin. The resultant strain is measured using a frictionless LVDT. P&G's preference for this device over other devices, such as the DTM and Cutometer is that the force is mainly applied to the stratum corneum and not the underlying dermis. The LSR design is the result of a requirement by P&G to reproduce the GBE concept using modern components [Matts & Goodyer 1998].

2.3 The Engineering Challenge

The engineering challenge was to devise an apparatus that operates in a similar manner to the GBE. That is, it has to apply a sinusoidally varying shear force to the surface of the skin whilst simultaneously logging the resultant displacement. The typical force is +-3g over 3 seconds, with displacements resolved to 1 micron and forces to 20 micrograms. The primary problem to be overcome in the mechanical design is to minimise the effect of friction as the skin attachment probe is moved. Figure 2 shows a schematic of the mechanical design solution adopted.

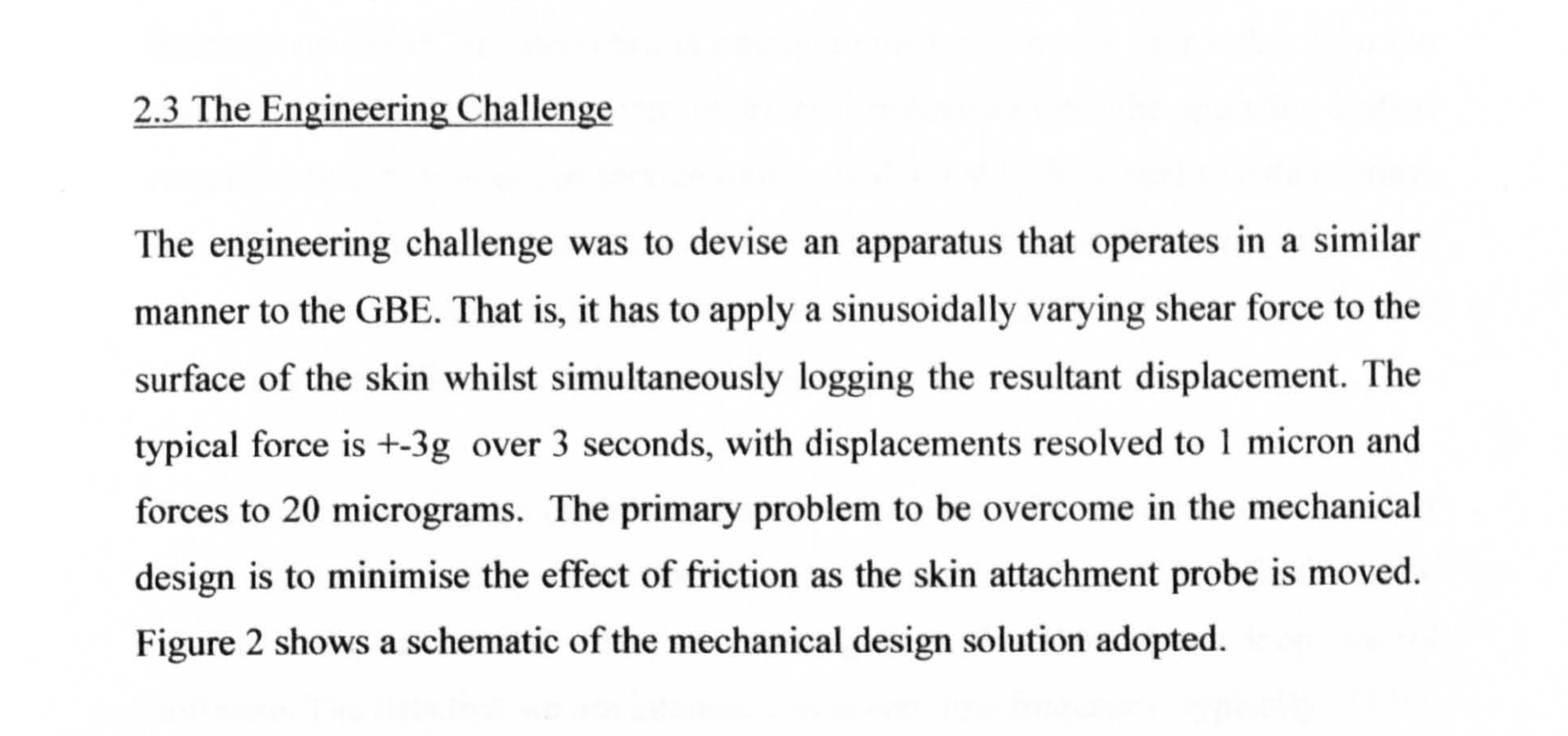

Figure 2 LSR schematic

The measuring probe is attached directly to the sensing head of a load cell, such that the shear forces acting along the axis of the probe are applied to both the load cell and to the skin surface. The probe is manufactured from stiff spring steel to minimise any internal mechanical losses. Thus, it is possible to measure directly the shear force applied to the skin surface. The displacement is directly measured using an LVDT that has had its' bearings removed. The frictional losses due to the mechanical movement are totally removed as the lead screw arrangement actuates the complete load cell, not the probe attachment. The load cell itself is inherently a very stiff device, and whilst there will be a momentary bending moment the resistance presented by the skin is extremely small. This arrangement is almost totally free of mechanical losses.

Data is captured from the sensors using a National Instruments ATMIO data multi-channel acquisition card. To achieve an acceptable sampling rate the real time interrupt on the PC motherboard is reprogrammed to run at 1 kHz rather than the usual 18.188 Hz. The BIOS interrupt driver is redirected from the operating system resources to a new interrupt service routine (ISR) that is dedicated to data capture. It is important to note that at the time of this research most PCs were still using DOS or WIN 3.1; this technique also works under WIN98 but is not guaranteed under any later Windows style operating systems.

The signal to noise ratio of the raw data is very poor, with a typical noise band of about 0.2 to 0.3g sitting on top of the +-3g sinusoidal signal. The primary noise source is the mechanical vibration resulting from the 1khz closed loop control software. The data that we are interested in is very low frequency, typically 1/3 Hz. The application of a simple mask filter removes most of this high frequency interference. Figure 3 below shows a typical trace after the application of the filter taken from a screen capture. Later mechanical refinements replaced the rod with a cannula, which is stiffer and less prone to producing mechanical noise.

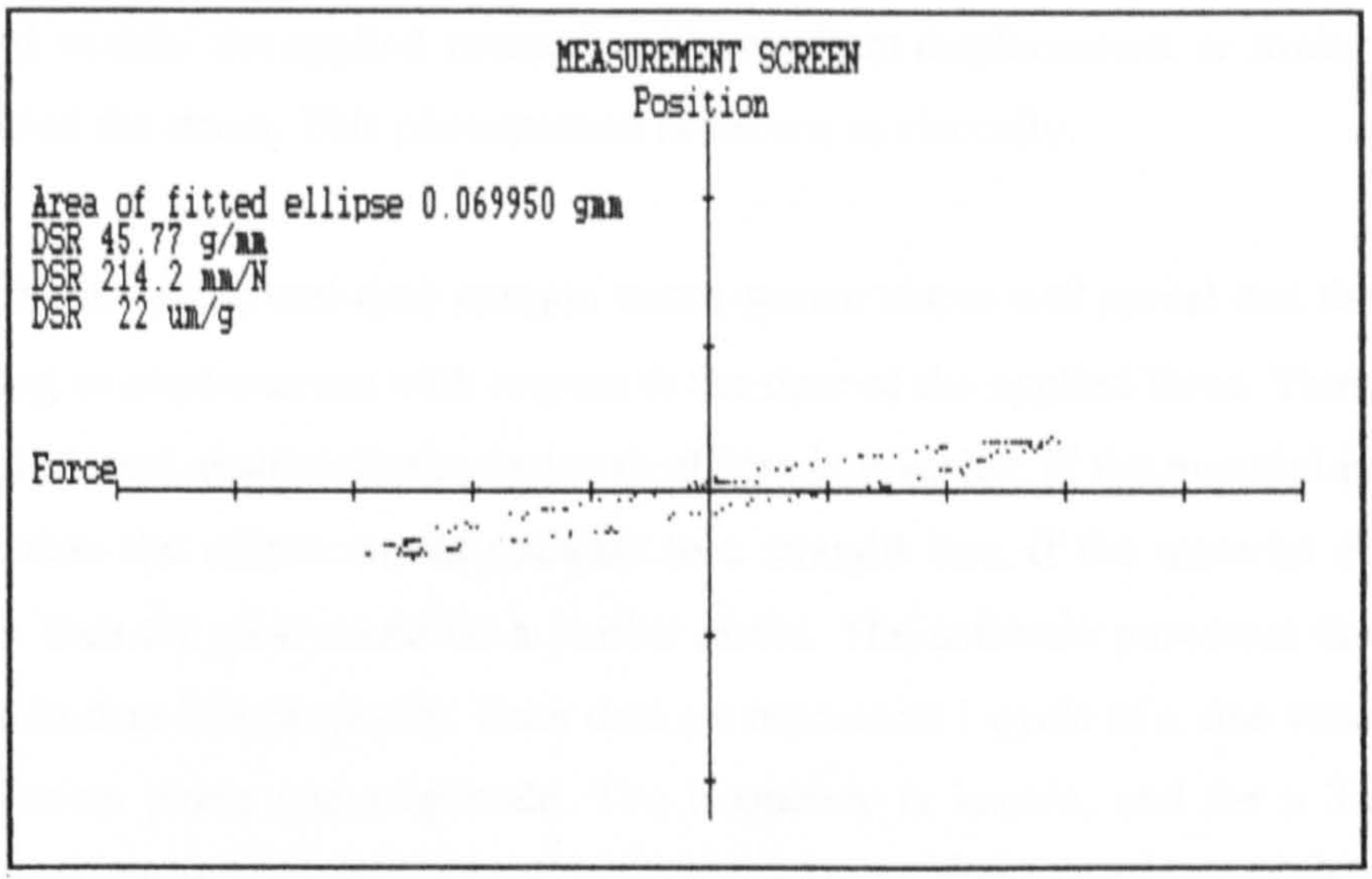

Figure 3 Typical measurement screen as presented by the LSR showing an elliptical plot relating force to resultant displacement

The elliptical trace shows the characteristic rheological response of a material under sinusoidal stress. It is derived from the force and displacement data, which when plotted against time are sinusoidal with a phase shift, as seen in the figure 4.

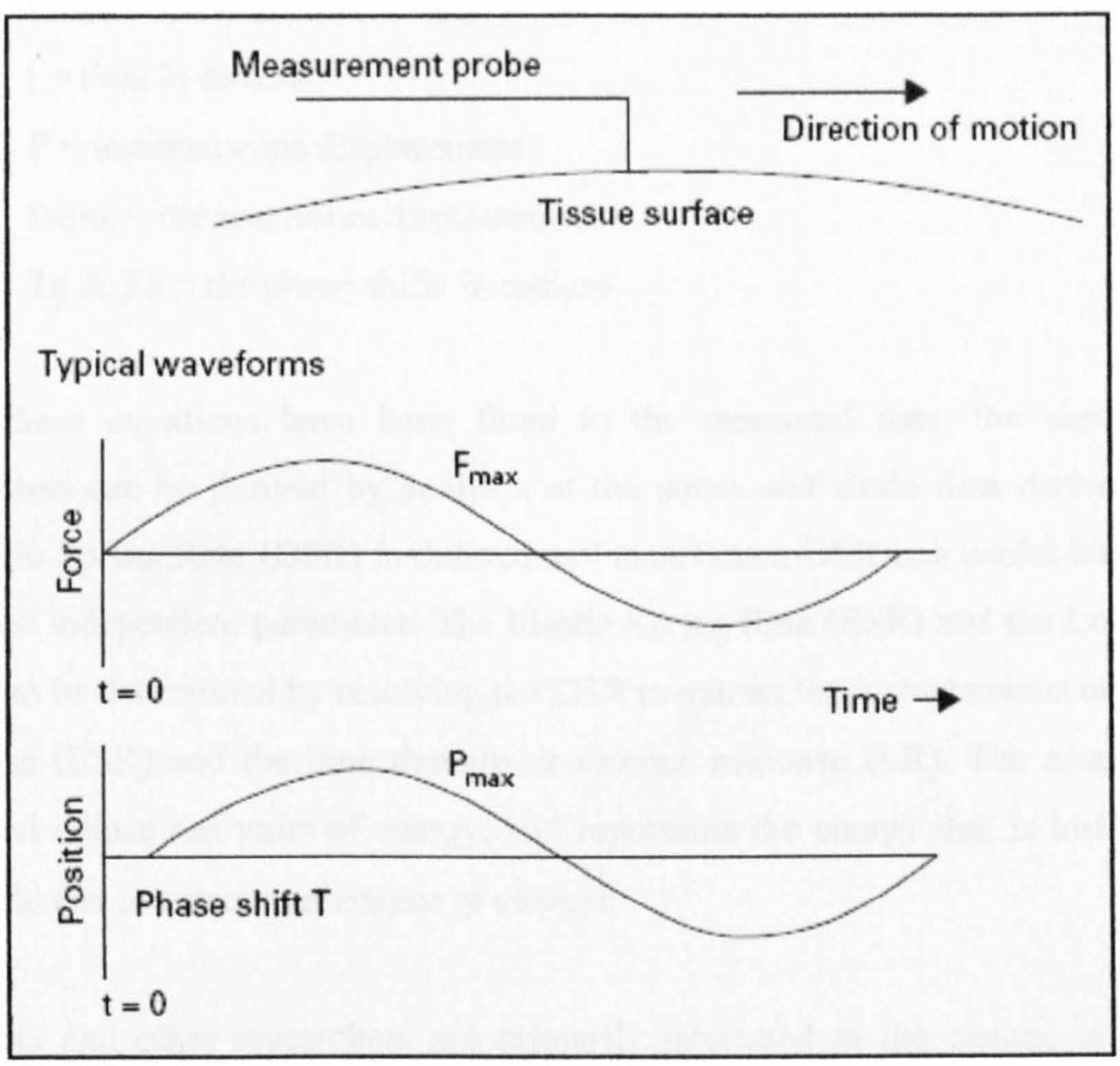

Figure 4 Typical waveforms of force & displacement with respect to time

If the material is totally elastic then the resultant displacement would be in phase with the applied force. If there is a time domain response, which means that the

material 'resists' the applied stress, then the resultant displacement, or strain, will lag behind the stress. This phenomenon is known as viscosity.

Examination of the real time domain traces shown above will reveal that there is a small lag in displacement with respect to the time of the applied force. Thus, when force is plotted against displacement an ellipse is revealed. If the material is 100% elastic then the ellipse would collapse to a straight line, if the material is 100% viscous then the plot would be a perfect circle. The software processes the stress and strain data independently. Each data set represents 1 cycle of a sine wave, with an unknown phase and amplitude. The frequency is known, and for a 3-second cycle time, there are 3000 data points. A regression algorithm is applied to each data set in order to converge on the best fit for the sine waves.

(2) $F = Fmax\ (Sin(t + Ta))$

(3) $P = Pmax\ (Sin(t + Tb))$

Where

F = instantaneous force

Fmax = the maximum force

t = time in radians

P = instantaneous displacement

Pmax = the maximum displacement

Ta & Tb = the phase shifts in radians

Once these equations have been fitted to the measured data, the rheological parameters can be derived by analysis of the stress and strain data derived. The Dynamic Spring Rate (DSR) is defined as Fmax/Pmax. DSR is a useful term as it is a time independent parameter. The Elastic Spring Rate (ESR) and the Loss Rate (LR) can be determined by resolving the DSR to extract the instantaneous or elastic response (ESR) and the time domain or viscous response (LR). The area of the enclosed ellipse has units of energy, and represents the energy that is lost during the cycle due to viscous resistance to change.

As P&G and other researchers are primarily interested in the change in elastic response, the results for this and similar studies are expressed in terms of DSR, ESR & LR. No attempt is made to derive any fundamental material properties such as Shear Modulus.

2.4 The Rheology Results

The primary purpose of the first paper reported here [Matts & Goodyer 1998] was to announce the existence of the LSR to the cosmetic science community. P&G had been using it for 6 years to provide claims support for a range of products, but had required that the LSR concept remained confidential to the company. This position could not be maintained as scientific data published to support a product claim can only be truly valid if the methodologies used to acquire that data are also open to examination.

To illustrate the application of the LSR two different skin creams were evaluated using sequential testing with the LSR and the Dermal Phase Meter. The study was carried out in a controlled environment chamber (temperature = 20±1°C; relative humidity 45±5%). Two different moisturising creams were applied to the back of the hand of 13 female volunteers, aged 18-35. The entire back of the hand was used, and the quantities applied were 2 micro-litres per square centimetre. Measurements of shear elasticity were taken at 1,3 and 6 hourly intervals. The results are expressed as change with respect to the pre-treated control. A parallel study was carried out with 12 female volunteers, aged 18-35. The volar forearm was used, with adjacent treated and untreated sections. Measurements were taken using a Dermal Phase Meter 9003 at 1, 2, 4 and 6 hourly intervals. The results are expressed as change with respect to the untreated control area. The results are shown in figures 5 & 6.

The DPM results clearly indicate an increase in hydration levels, as indicated by changes in skin impedance, with an early peak and excess hydration still measurable after 6 hours. This compares favourably with the LSR results, which show an early peak in the change in stratum corneum elasticity, which was still measurable after 6 hours. Both devices were able to separate out the different changes due to the same product.

Of interest is the way that the change in elasticity lags behind the increase in skin hydration. However, a more detailed discussion goes beyond the scope of this thesis.

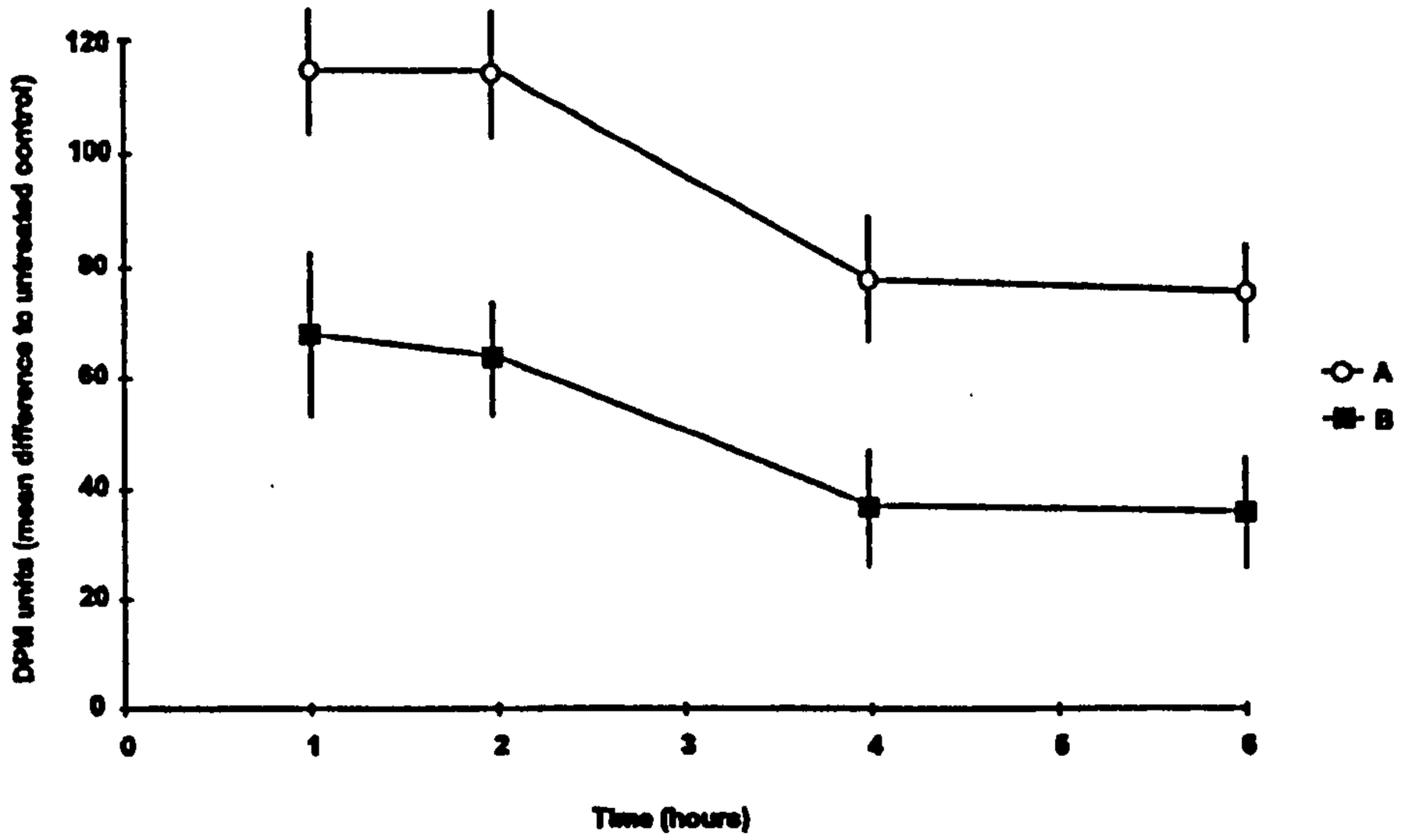

Figure 5 DPM impedance measurement of skin (copied from 1998 paper) showing change in dimensionless DPM units with respect to time

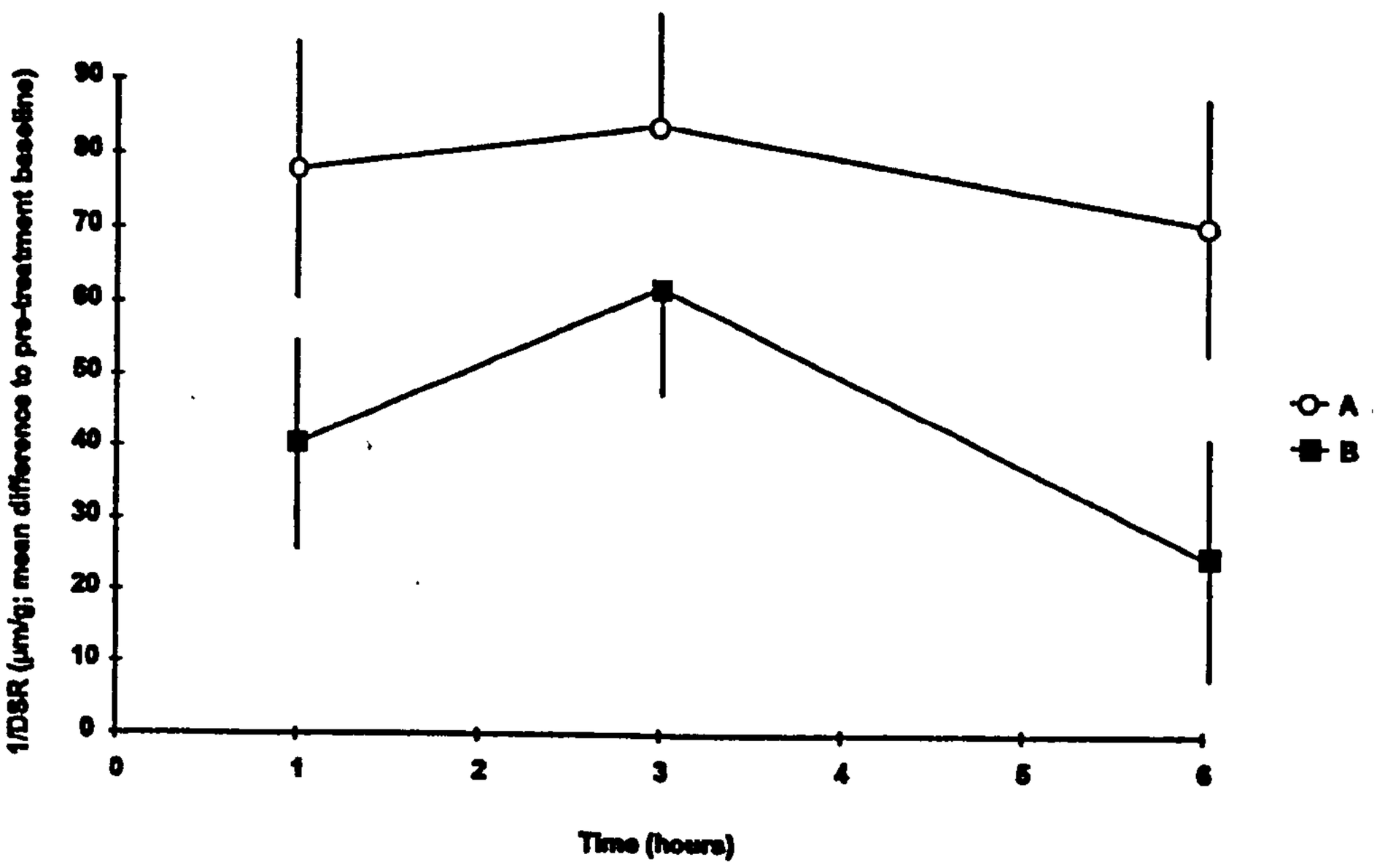

Figure 6 LSR shear measurement of skin (copied from 1998 paper) showing change in DSR with respect to time

2.5 The Position of the LSR Today

In total 10 LSR devices have been constructed. 4 have been supplied to P&G's Egham Laboratories, 1 to Ellen Betrix in Frankfurt, 1 to P&G's labs in Cincinnati USA, and three to Unilever laboratories in New Jersey, Connecticut and Bedfordshire. The device has been highlighted in a text book on skin measurement methods [Bioengineering of the Skin 2002], presented in an overview of *in vivo*

measurement techniques [Rodrigues 2001], cited in a range of studies and papers [Matts 2004, Ananthapadmanabhan et. al. 2004, Mok et. al. 2001, Rawlings et. al. 2005, Ducehemin et. al. 2005], and used to support 18 patents [US Patent 20040091446 and others]. A more recent application has been the evaluation of the friction coefficients for a range of lubricants used in condoms, which were tested on the forearm.

Much of the work carried out by P&G and Unilever is confidential, however there is a steady stream of conference papers that publish results that have employed the device. The latest device purchased by Unilever in 2007 is being used to examine the effect on skin by the application of textile based medications; representing the opening up a new field for the use of the device. A recent search (June 2008) of peer reviewed journals on Scopus for "Linear Skin Rheometer" found 14 papers, of which 7 were co-authored by myself. A definitive paper on the impact of skin cleansers [Ananthapadmanabhan et. al. 2004] was the result of extensive studies that included use of the LSR. I built, setup and delivered the apparatus to their New Jersey site; however I did not participate in the resultant study. This paper has 20 citations on Scopus.

3 The Vocal Fold

In this chapter, the existing knowledge of vocal fold biomechanics is presented. Most of this data was obtained from dissected tissue measured using standard industrial rheometric devices. The need to obtain data from intact larynxes and patients *in vivo* is considered a key advance required by researchers in the field. This was the most important outcome of the work that the author undertook, in that a series of devices were devised and deployed that are able to measure biomechanical data from intact larynxes, and from patients *in vivo*.

Phonation is achieved by the gentle and controlled exhalation of air from the lungs into the mouth and nasal passages via the larynx. The larynx is a complex structure, which can be simplified to three layers, the vocalis muscle, the vocalis ligament and the vocal fold cover (see figure 1 earlier). Muscular control by the vocalis muscle, and transmitted via the vocalis ligament results in physical changes to the position and tension of the vocal fold cover. This structure vibrates, which results in a fluid dynamic phenomena known as the mucosal wave flowing through the vocal fold cover. Thus the air stream is modulated and resultant sounds are shaped by a variety of anatomical features found in the vocal tract. This whole process is known as phonation.

A key anatomical feature that is essential to achieve phonation is the upper layers known collectively as the vocal fold cover. In humans this is stratified in to other layers, the epithelium, the superficial lamina propria and the lamina propria itself. The ability of the mucosal wave to propagate through the vocal fold is essential for phonation. Basic fluid dynamics tells us that the velocity of the wave is given by the square root of the ratio of the material modulus and density. To put that in to a more basic format the greater the modulus (i.e. stiffness) then the higher will be frequency of the mucosal wave. As energy is a function of frequency, then the stiffer the vocal fold the more energy that is required to make it vibrate. If the vocal fold is damaged or scarred then phonation will be impaired. Scarred tissue is normally stiffer than healthy tissue; and vocal fold scarring is a major cause of speech disorders as it can prevent proper closure of the vocal folds.

The following sections detail the application of the LSR and related techniques to gain a better understanding of the elastic properties of the human vocal fold. This knowledge is essential for other research teams deriving mathematical models of

phonation and those investigating tissue engineering therapies to repair vocal fold damage.

3.1 Current State of Knowledge

An examination of the existing literature relating to the measurement of the biomechancial properties of the human vocal fold places this work into context. Few researchers have reported data obtained by direct measurement of the mechanical properties of intact larynges. Results have either been inferred from observations of acoustic or optical effects, or the vocal fold cover has been excised and tested mechanically out of anatomical context.

Early work in this field is mainly attributed to Perlmann and Alipour, who obtained data from canine models. The references given are representative of their work and chosen because they both provide measurements of vocal fold elasticity against which the author's results can be compared. Adrienne Perlmann & Ingo Titze [Perlmann et. al. 1984, 1988] have obtained canine data using excised tissue with a range of 9,460 to 41,200 Pascals for a variety of conditions. Alipour's canine results [Alipour & Titze1990] give a shear modulus of 13,960 Pascals. In both cases, the vocal fold tissue was dissected out of the larynx prior to being mounted in the measurement apparatus.

Amongst the current leaders in this field are Roger Chan and Ingo Titze, with an impressive publications record. Out of their extensive work, I have selected a representative publication, which contains an extensive set of data obtained from excised human vocal fold tissue. Chan & Titze [1999] measured the shear modulus in excised tissue using a parallel plate rheometer. Their earlier work gives values of between 10 to 1000 Pascal for shear modulus. Their later papers report a range of values for different subjects, taken over a range of frequencies up to 10Hz. Values ranged from as low as 10 Pascal to 300 Pascal. Roger Chan's most useful recent contribution to this thesis is his work on the importance of hyaluronic acid in vocal fold biomechanics, which contains extensive data for elastic and viscous properties of the human vocal fold for a range of frequencies [Chan et. al. 2002].

Roger Chan has also published some excellent work that seeks to overcome the primary disadvantage of using a parallel plate rheometer, in that they cannot operate at frequencies anywhere near those that are exhibited during phonation [Chan 2001]

Kaneko [Kaneko et. al. 1981] and Tamura [Tamura et. al. 2002] amongst others have reported the derivation of visco-elastic properties using ultrasound techniques *in vivo* and using excised larynges. This technique infers elastic modulus from analysis of the reflected sound wave. However, they do not offer comparable data relating to the elastic modulus.

Hsiao [Hsiao et. al. 2002] has reported success in obtaining values for Young's modulus using colour Doppler imaging *in vivo*. If a Poissons ratio of 0.5 is assumed then these results translate to shear modulus ranges of 10,000 to 40,000 Pascals for men and 40,000 to 100,000 Pascals for women.

McGlashan [McGlashan et. al. 1998] reported a method to infer vocal fold properties using an *in vivo* optical technique that generated a series of dynamic surface maps, from which the authors derived the velocity of the mucosal wave. A more recent conference report gives a shear modulus of 2500 Pascals.

The *in vivo* data obtained by Tran et. al. [1993] offers a range of shear modulus from 2450 Pascals to 29,400 Pascals. Berke et. al. [1992] describes the apparatus used in more detail, and gives some results for Young's modulus using canine data, the medial result equates to a shear modulus of 1450 Pascals.

In summary most of the published work has measured the shear modulus of the vocal fold cover using excised tissue samples, with results ranging from 10 Pascal to over 100,000 Pascal. The consensus view today is that a figure of 300 Pascal is a reasonable estimate [Chan et. al. 2002]. However, what the author has been trying to achieve is to quantify a related but fundamentally different measurand. The elastic properties of the vocal fold cover, when measured *in vivo* or in an intact excised larynx is not the same as that obtained from a thin slice of tissue. This arises because the vocal fold is attached to surrounding tissue, thus it is tensioned and anchored. Like any membrane that is under tension, a measurement of its' elastic properties will not be the same as the measurement of its' fundamental elastic properties when taken in isolation. The best analogy is a kettle drum, as the skin that covers the drum is stretched it becomes stiffer, and a measure of its' elasticity will increase – however the fundamental material property of the skin remains unchanged.

The ability to measure the elastic properties of intact larynges is essential for two parallel strands of research. Mathematicians who are investigating numerical

models to explain how phonation works need to know the dynamic response characteristics of the whole structure. The other group of researchers who need to know the characteristics of complete larynges are teams who are investigating tissue-engineering therapies. In order to assess objectively the effectiveness of any tissue-engineering therapy it is necessary to be able to quantify the biomechanical properties of healthy tissue, and compare that baseline data to scarred tissue and treated tissue. Therefore, the key electro-mechanical design objective is to produce a surgical tool that can measure tissue elasticity *in vivo*.

The table below indicates how little data has been oblished in this field, and how wide-spread the results are

Researcher	Method	Results Pascal
Perlmann & Titze	Canine longitudinal data directly measured mechanically	9460 – 41200
Alipour	Canine longitudinal data directly measured mechanically	13960
Chan & Titze	Parallel plate rheometry under varying conditions – human excised tissue	10 - 1000
Kaneko & Tanura	Ultrasound - human	No results given
Hsiao	Colour doppler imaging - human	10000 - 40000
McGlashan	In-vivo optical imaging - human	2500
Tran & Berke	In-vivo transverse - human	1450

Table 1 – Summary of current knowledge based on published results for the shear modulus of the vocal fold

4 The Shear Modulus of the Vocal Fold – Methodology

The early research that the author undertook with the research team at Harvard Medical School is presented. The team deployed the original apparatus devised for use with the stratum corneum in a number of ingenious ways to enable measurements to be obtained from intact hemi-larynxes. Among the new results presented are the highly anisotropic nature of the vocal fold, the variation of elasticity with respect to anatomical position, and the derivation of the first iso-contour maps showing the variation of elasticity over the surface of a vocal fold. Also presented are the results of a similar study carried out at Wisconsin University Hospital that duplicated the Harvard findings.

In order to prove the apparatus was capable of measuring the human vocal fold a series of studies using animal larynges was carried out at Harvard Medical School [Goodyer et. al. 2003, Hess et. al. 2006]. Much of this work was repeated later at Wisconsin University [Dailey et. al. 2007]. Almost all of this early work was carried out using animal tissue for the purpose of developing the methods and apparatus, which were later deployed to quantify the far more complex properties of the human larynx. Sample tissue was typically used up to 1-week post-mortem.

The results presented here are from a variety of experiments intended to demonstrate that when measured in-situ the shear modulus of the vocal fold varies with both anatomical context and direction of applied stress. Data is presented in terms of DSR, which is the time-independent term given by the ratio of peak force/peak displacement. In effect, it is the amount of force in grams required to displace the epithelium by a distance of 1 mm.

Figure 7 shows a typical experimental setup, and shows the direction of the defined axes for transverse and longitudinal direction. The top of the cannula probe used for suction attachment is also visible.

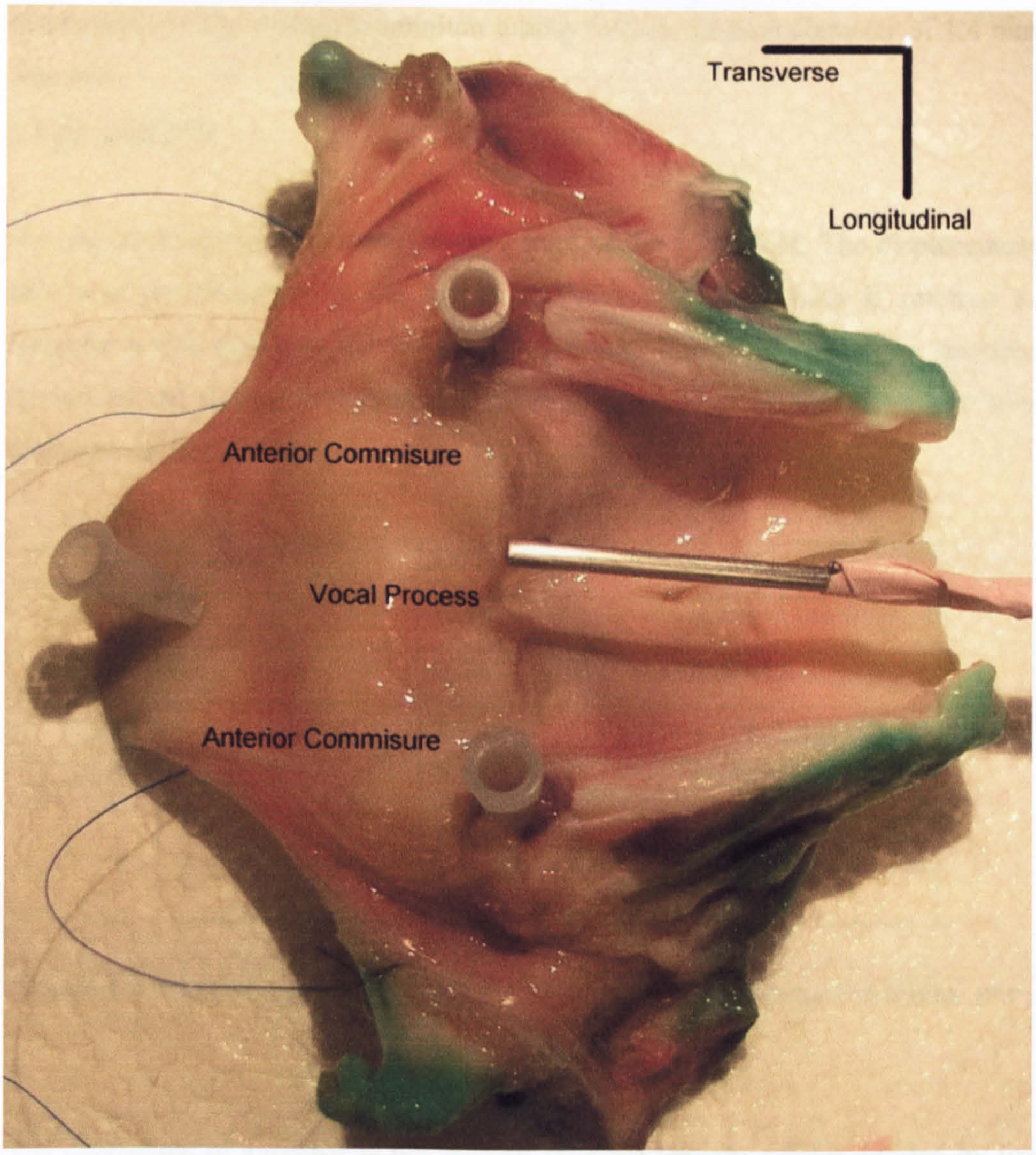

Figure 7 A typical experimental setup showing axes and key anatomical datums of a human larynx

4.1 Bench tests on Laryngeal Specimens

Laryngeal specimens were prepared by hemisection, taking care to leave the vocal fold attachment to the thyroid cartilage at the anterior commisure region intact. The specimens were pinned to a wooden base attached to small XY/rotary machinist's fixture that allowed for accurate positioning and rotation. The specimens were kept moist with physiological saline and measurements were made at room temperature (~ 20°C). Most measurements were made using needle tipped probes. The most effective of several designs tested was made from a spring steel rod 1mm in diameter and 10 cm in length, which was bent to a right angle 5 mm from one end. A fine (000) insect pin was soldered to the short bent section so that it protruded 1.5 mm beyond the end of the rod. This needle was inserted into the tissue up to the rod, which controlled insertion depth to 1.5 mm. In some instances a suction-based

probe made of lightweight aluminium tubing with an internal diameter of 1.4 mm was used.

4.2 Repeatability

Six pig larynges were measured at the centre of the vocal fold. The displacement axis was perpendicular to the length of the vocal fold, which is referred to throughout this thesis as the transverse direction. The table shows the standard deviations and means derived from 6 consecutive readings of the DSR taken from the same starting position.

Sample	DSR g/mm n = 6	CofV
1	0.69	4.1%
2	0.78	5.9%
3	0.7	2.1%
4	0.72	3.6%
5	0.49	1.2%
6	0.63	0.5%

Table 2 – Tests of repeatability of the LSR output data using 6 samples per measuring point

The coefficient of variance is the ratio of standard deviation (SD) divided by the mean of the 6 consecutive DSR readings, and is expressed as a %. They range from a 0.5% to 5.9%, The mean of the DSR results is 0.67g, which means that 1mm displacement of the vocal fold tissue, is achieved when a shear force of 0.67g is applied to the epithelium in a transverse direction.

4.3 Variations with respect to Anatomical Context

A series of studies were carried out using hemi-larynges. They were mounted without tension and the DSR measured in the transverse direction at different points along the axis created by the line between the vocal process and the anterior commisure. The variation along the axis is shown in the following graph.

The DSR peaks in the region of vocal process and the anterior commisure. This is a credible result as both these anatomical positions represent the cartilaginous attachment points that the vocal fold is effectively held by. The vocal process is stiffer than the anterior commisure, a fact that can be easily confirmed subjectively.

This is a key finding that forms the basis of two further studies, to map the variation of elasticity with respect to anatomical position.

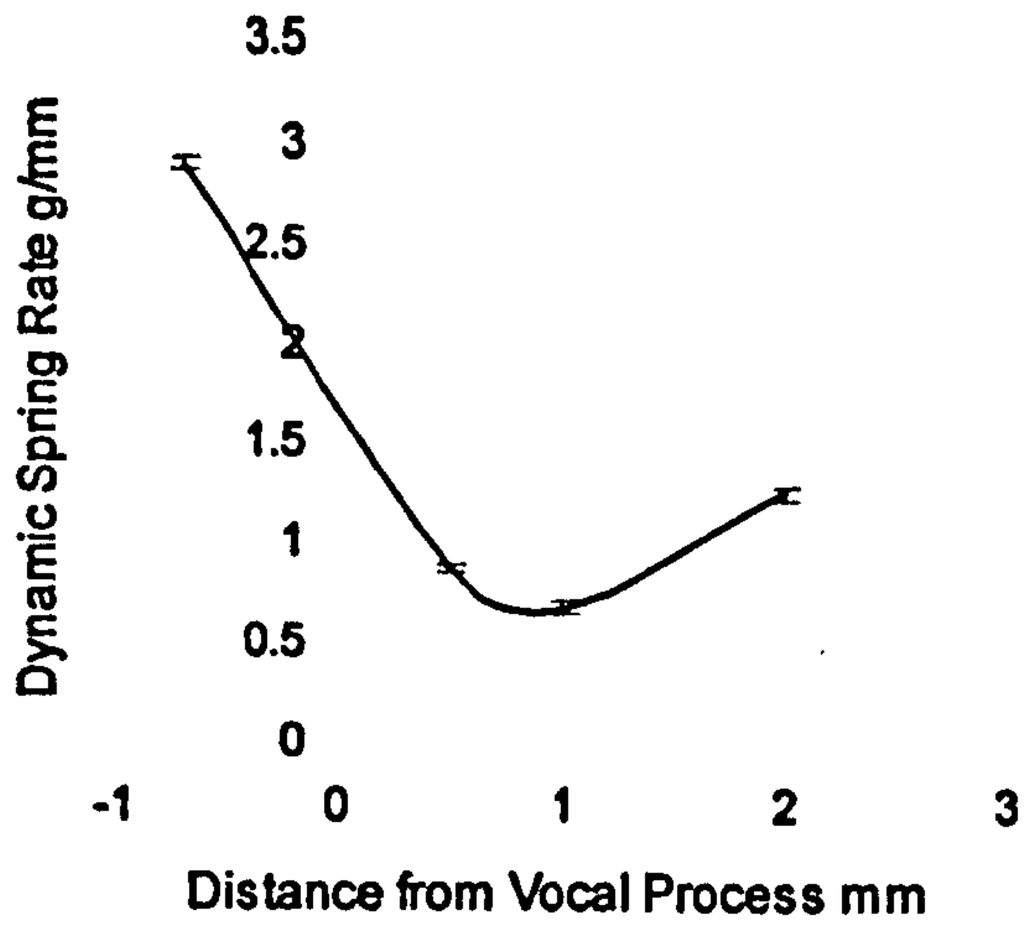

Figure 8 Variation of elasticity expressed as dynamic spring rate with respect to position along longitudinal axis

4.4 The Anisotropic Nature of the Vocal Fold

A key finding of this research is that the elastic properties of an intact vocal fold are highly anisotropic. If an axis is defined from the vocal process to the anterior commisure, known as the longitudinal axis, and measurements taken at different angles with respect to that axis this anisotropic nature becomes evident. The orthogonal axis, being the direction of airflow across the vocal fold, is known as the transverse axis. For this study the probe was attached to the mid-membranous point of the vocal fold, and the hemi-larynx was mounted on a rotary table.

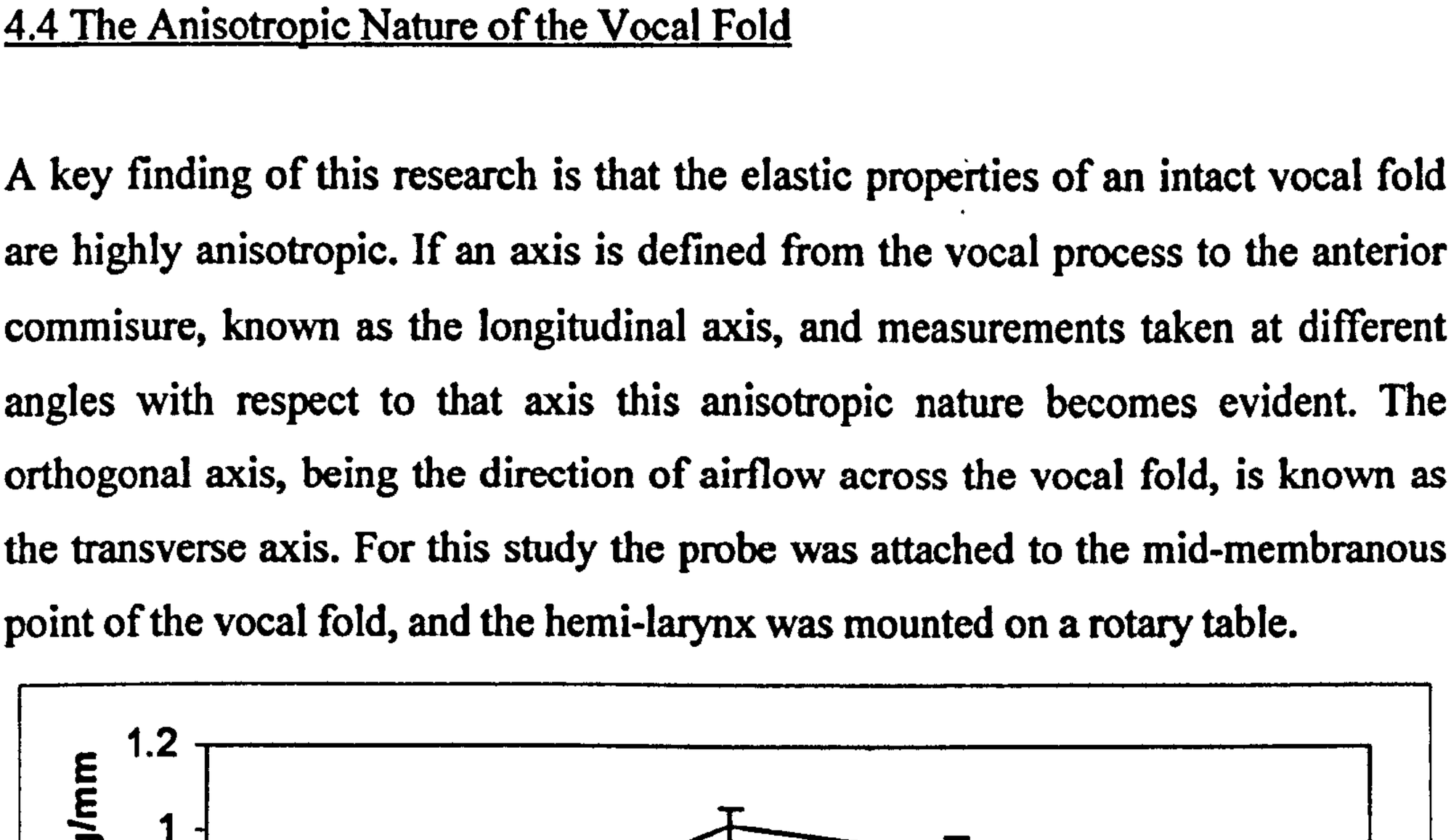

Figure 9 Anisotropic nature of the vocal fold showing variation of elasticity expressed as dynamic spring rate with respect to angle of applied stress

0 degrees is defined as the transverse direction, 90 degrees is defined as the longitudinal direction. 180 degrees returns to the transverse in the opposite direction. It can be seen that the tissue is far more pliable in the transverse direction than longitudinally. This phenomenon is well known from a subjective viewpoint, and this study is the first published results that quantifies this variation [Goodyer et. al. 2003]. It can be seen from this particular set of results that the spring rate in the transverse direction is about 50% of those obtained in the longitudinal direction. This phenomenon is now the basis of a major study currently under way at UKE Hamburg, and the interim results are set out in more detail later [Licht et. al. 2007]. The specific focus being to determine if the variation is solely due to the way the vocal fold is attached to the underlying ligament and muscles, or if the anisotropic nature is also inherent to the protein structures within the lamina propria itself.

4.5 Iso Contour Maps

The most important outcome is reproduced in figure 9, and is the first ever iso-contour map showing the variation of elasticity over the surface of an excised animal vocal fold; in this instance a calf. The right hand side photograph shows the sensing probe, with a small needle being used to take a point-specific data point from a hemi-larynx. Using an index table the iso-contour map on the left was constructed. This shows that the vocal fold cover is more pliable along the longitudinal axis of the line from the vocal process to the anterior commisure. As the probe moves away from this axis the tissue becomes stiffer; the tissue is also stiffer in the regions of the vocal process and anterior commisure. These facts are well known from a subjective point of view. What was achieved with this study is that the team showed these variations. [Goodyer et. al. 2003, Hess et. al. 2006]

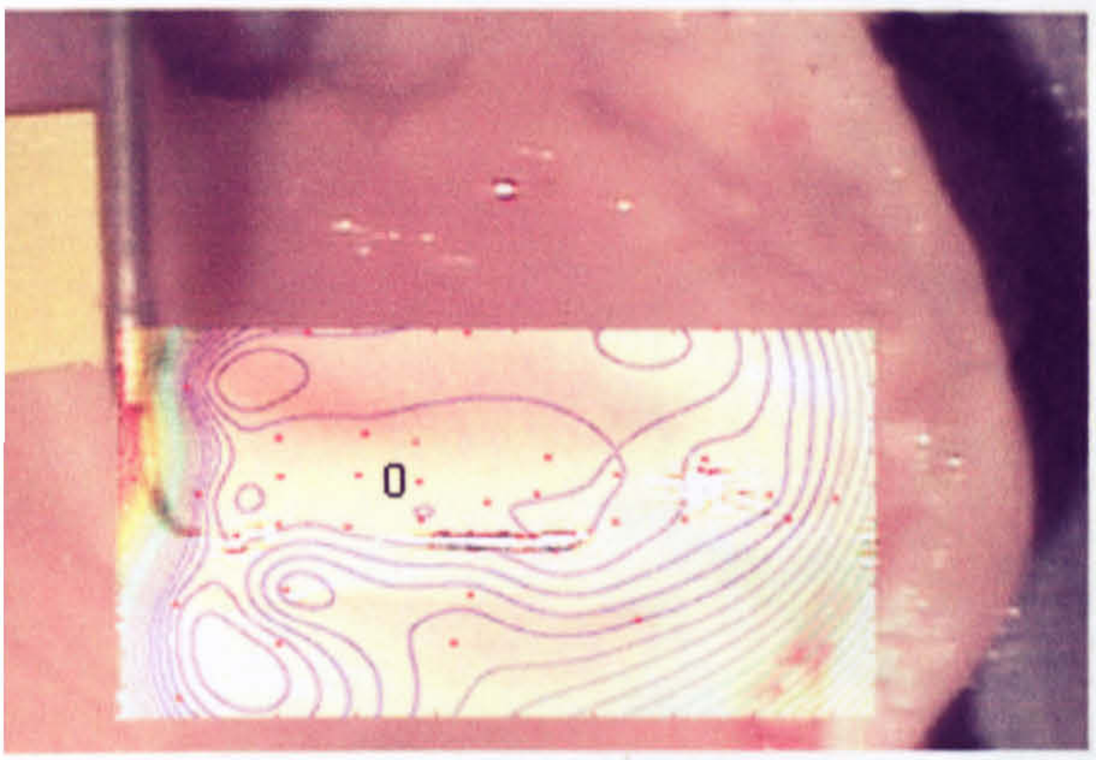

View of Vocal Fold with overlay of DSR contour map

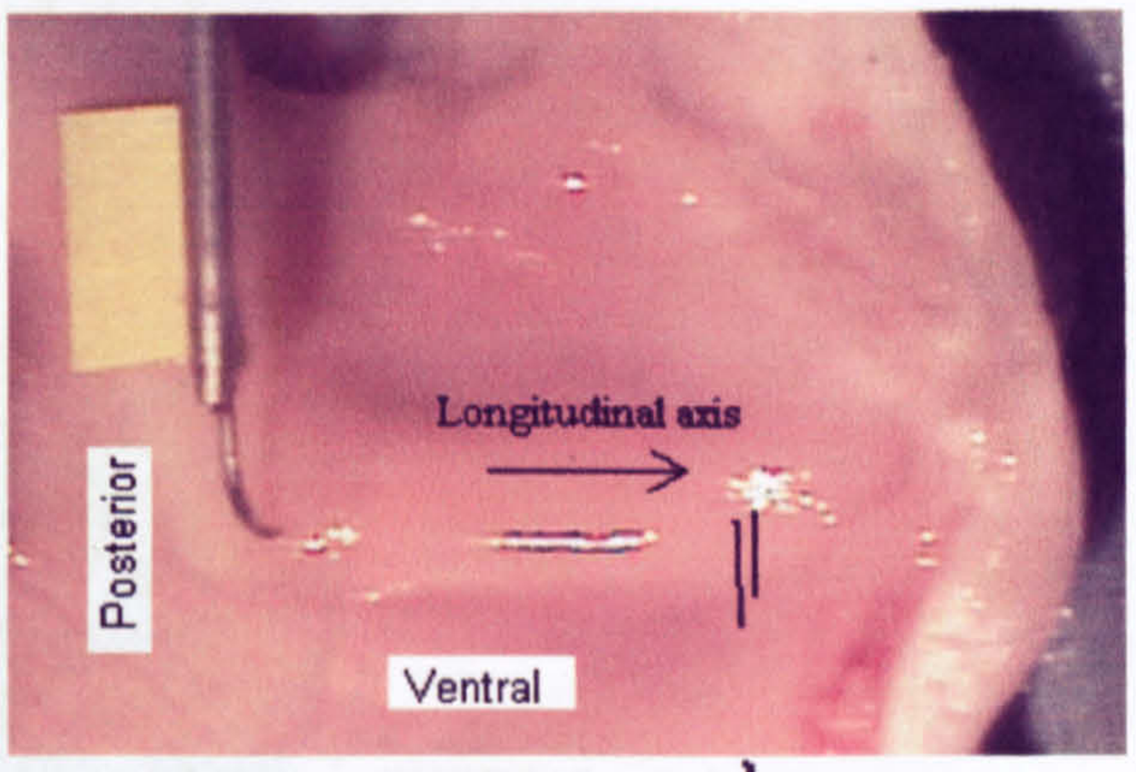

View of Vocal Fold with LSR probe attachment

mages taken at Harvard, showing experimental setup of LSR with ex-vivo focal-fold, together with results obtained from research data.

Figure 10 Elasticity iso-contour maps obtained by the Harvard team

The contour lines are DSR readings in units of g/mm where '0' is the region where DSR < 1g/mm

This experiment has since been independently verified by a team as Wisconsin University Hospital [Dailey et. al. 2007] using an excised canine larynx. The methodology was similar in that the larynx was mounted on an X-Y translation table. All readings were taken in the transverse direction using calibrated needles to ensure similar depth of penetration into the LP layer. The experimental setup can be seen in Figure 11. A mesh of readings was taken on a 2mm grid, resulting in the iso-contour map shown in Figure 12.

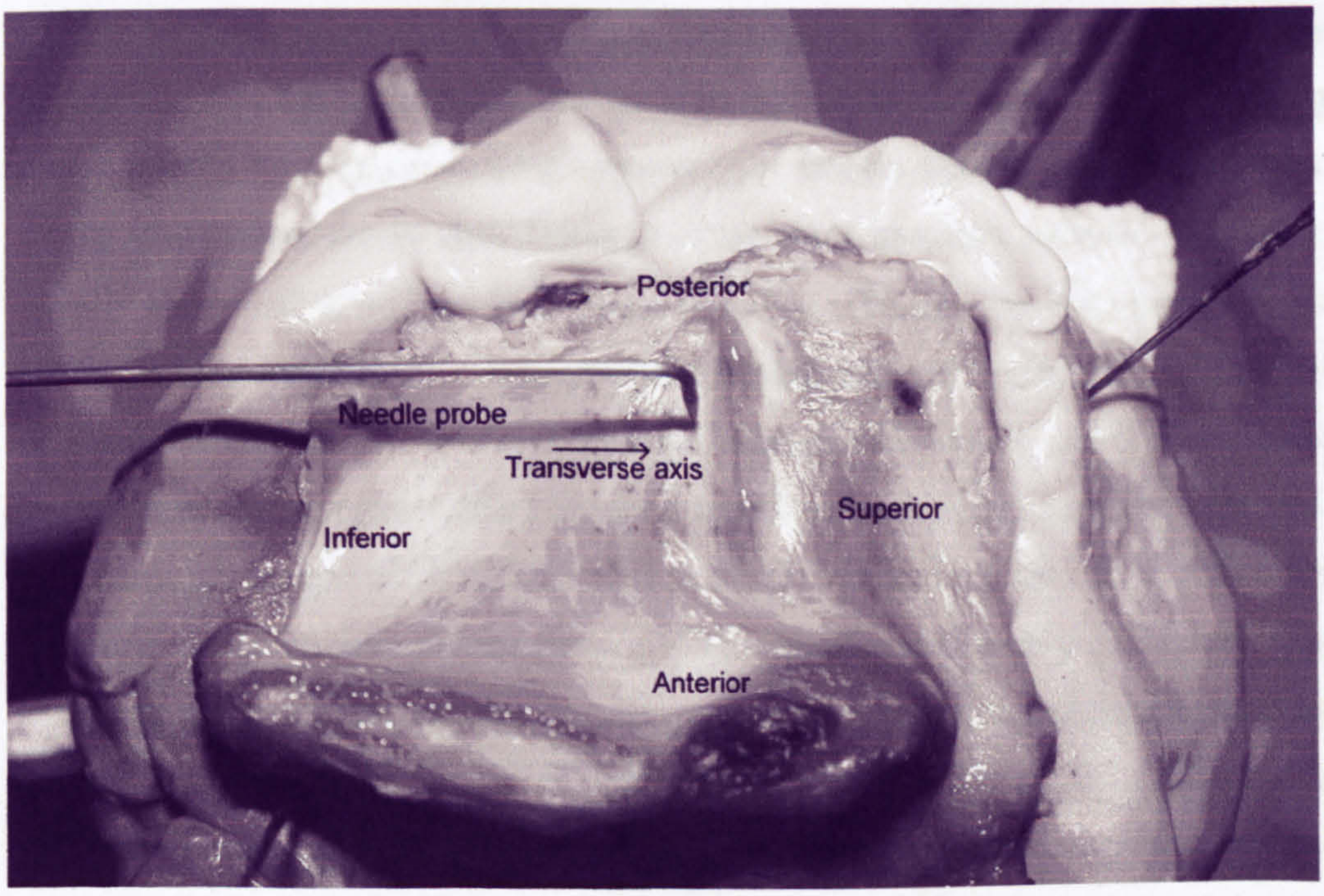

Figure 11 Iso-contour mapping of a canine larynx showing needle probe and key anatomical features

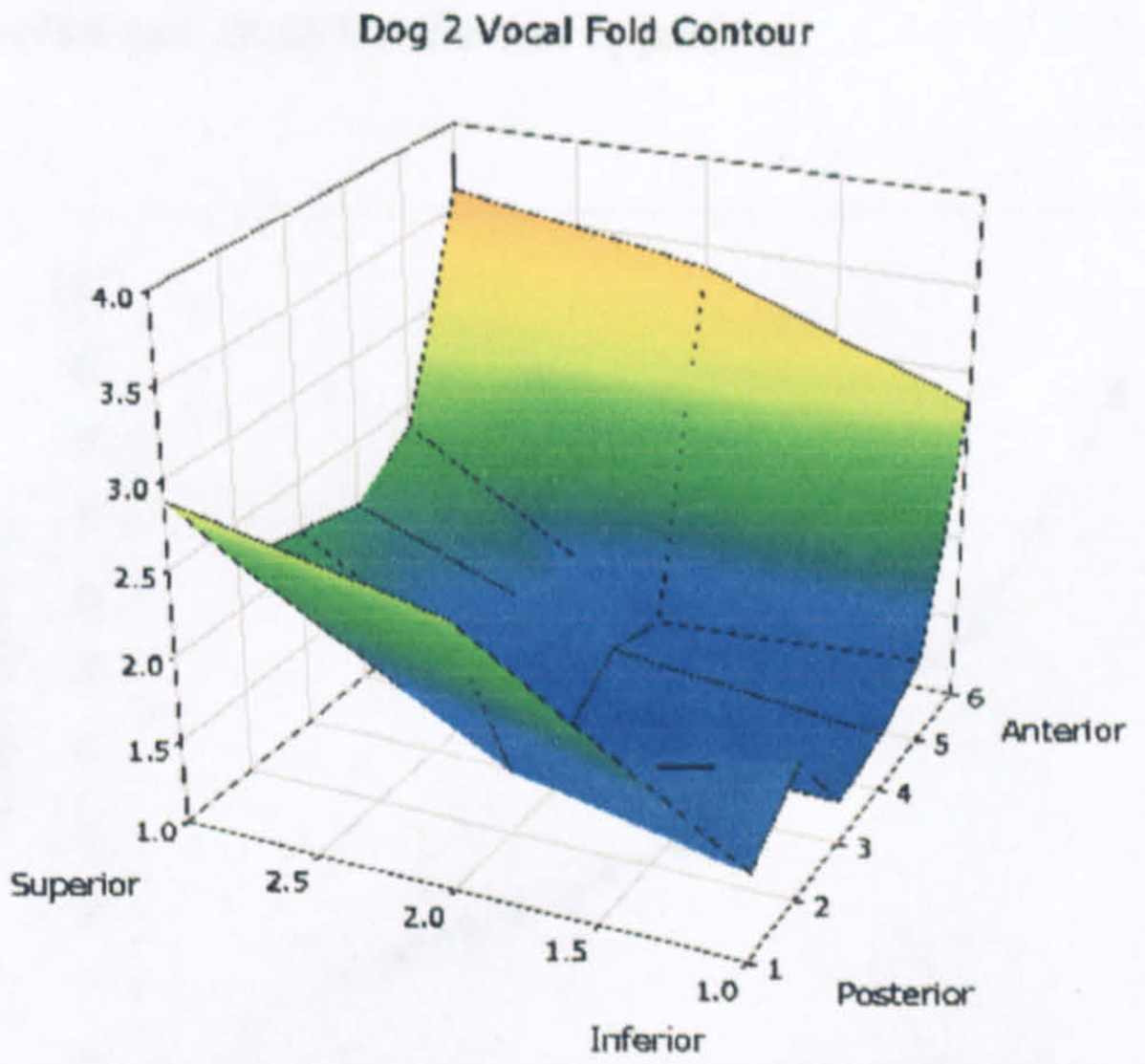

Figure 12 Iso-contour mapping of a canine larynx, showing change in DSR with respect to anatomical position

4.6 Comparison to Standard Test Apparatus

The key difference between the devices used for this research and other apparatus used to measure elastic properties of tissue, is that the new devices described here are able to obtain readings from a specific point with respect to anatomical position. The point specific shear measurement results determined for this research have to be peer reviewed and rigorously tested against other published results. The problem is that the majority of similar research results have been obtained using either Instron type tensile testing apparatus, or Bohlin parallel plate rheometers. These instruments report their findings in terms of absolute material properties, usually expressed as a shear or Young's modulus. The new devices used in these studies cannot intrinsically determine such fundamental properties, as is discussed in detail in Chapter 5. However, a study was carried out to see if the classic stress/strain characteristics obtained using tensile test equipment could be achieved. The purpose being to see if it is possible to obtain similar data sets, from which the modulus of the material can be obtained. The lamina propria of a calf larynx was dissected out and fixed at both ends. The tissue was mounted such that it could be pre-tensioned and then measured. The tissue was pre-tensioned to a measurable load and a sinusoidal force of +- 1.5 grams was applied. The initial 'draw length' was also measured. Figure 13 shows a plot of initial tension against measured DSR, and is directly analogous to extension section of a classic stress/strain curve found in literature that employed tensile test apparatus. The mathematics of

deriving modulus can be found in chapter 5. The resultant graph is typical of the extension data obtained from tensile test apparatus.

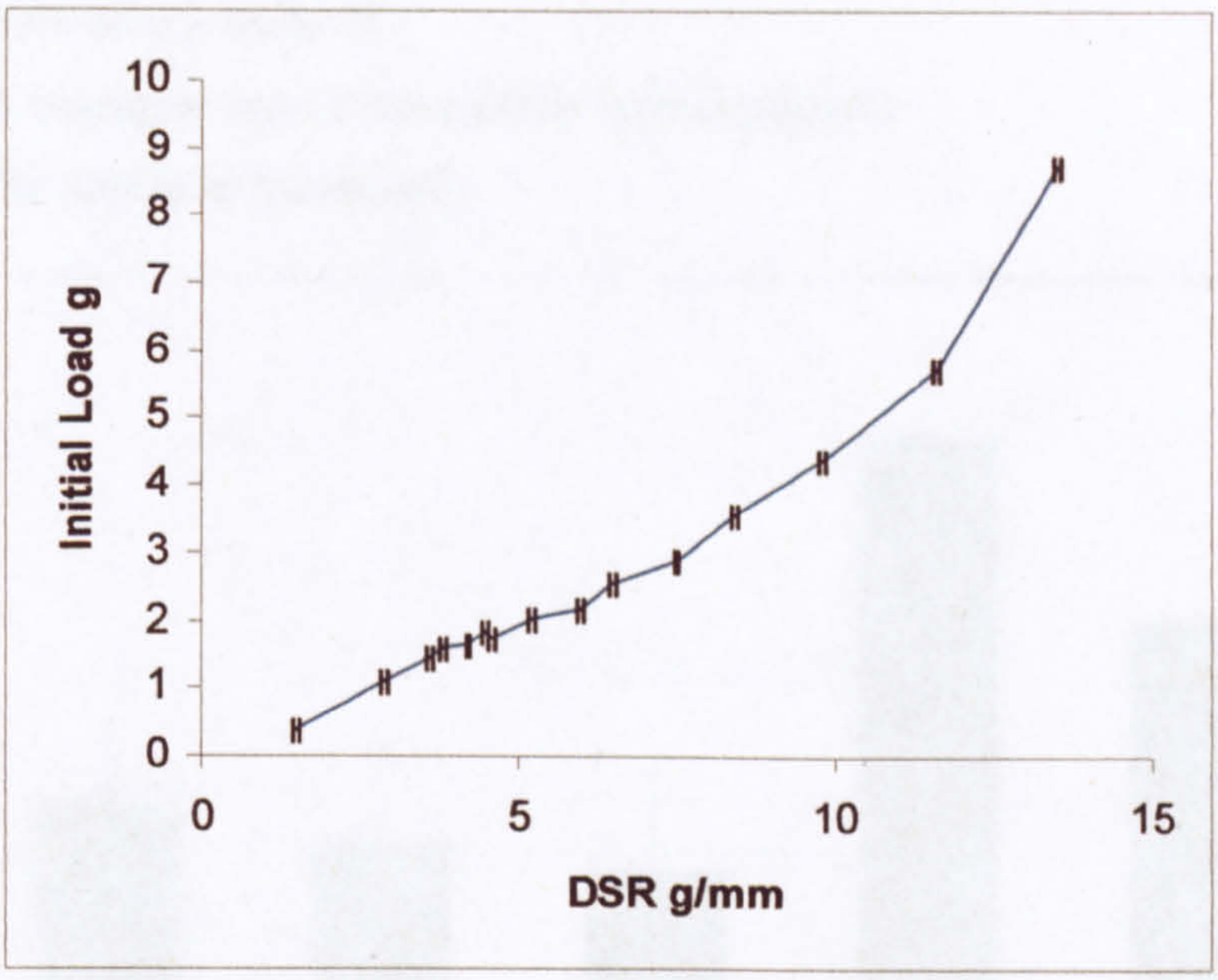

Figure 13 – Extension data from an excised calf lamina propria, showing DSR with respect to initial load

4.7 Resulting Changes in Methodology

All the above results arose from a series of studies primarily intended to prove the experimental methods. Peer review of the early results, some of which was highly critical of the methods [Goodyer et. al. 2003, Hess et. al. 2006], proved an essential aid to development of improvements to device designs, and the method of attachment to the tissue sample. Particular criticism was made of the use of needles to attach to the vocal fold [Dailey et. al. 2006] for two reasons –

1. The depth of penetration cannot be accurately controlled
2. Variation in depth results to ambiguity as to what layers within the vocal fold are being stressed

The second point is well illustrated by a small study undertaken by the Harvard team to evaluate the different effects of different layers. The DSR of different layers of a calf larynx were measured in a direction parallel to the vocal fold. This was achieved by sequentially removing layers, and retaking the measurement at the same position. These initial results demonstrate how the layers contribute to overall tension development as the vocal fold is stretched.

A. Typical epithelium measurements.

B. A small island of epithelium about 2 x 3 mm which indicates the relative contribution of the epithelium versus the underlying amorphous layer.

C. Epithelium removed.

D. Amorphous layer removed (the lamina propria)

E. Directly in to the muscle.

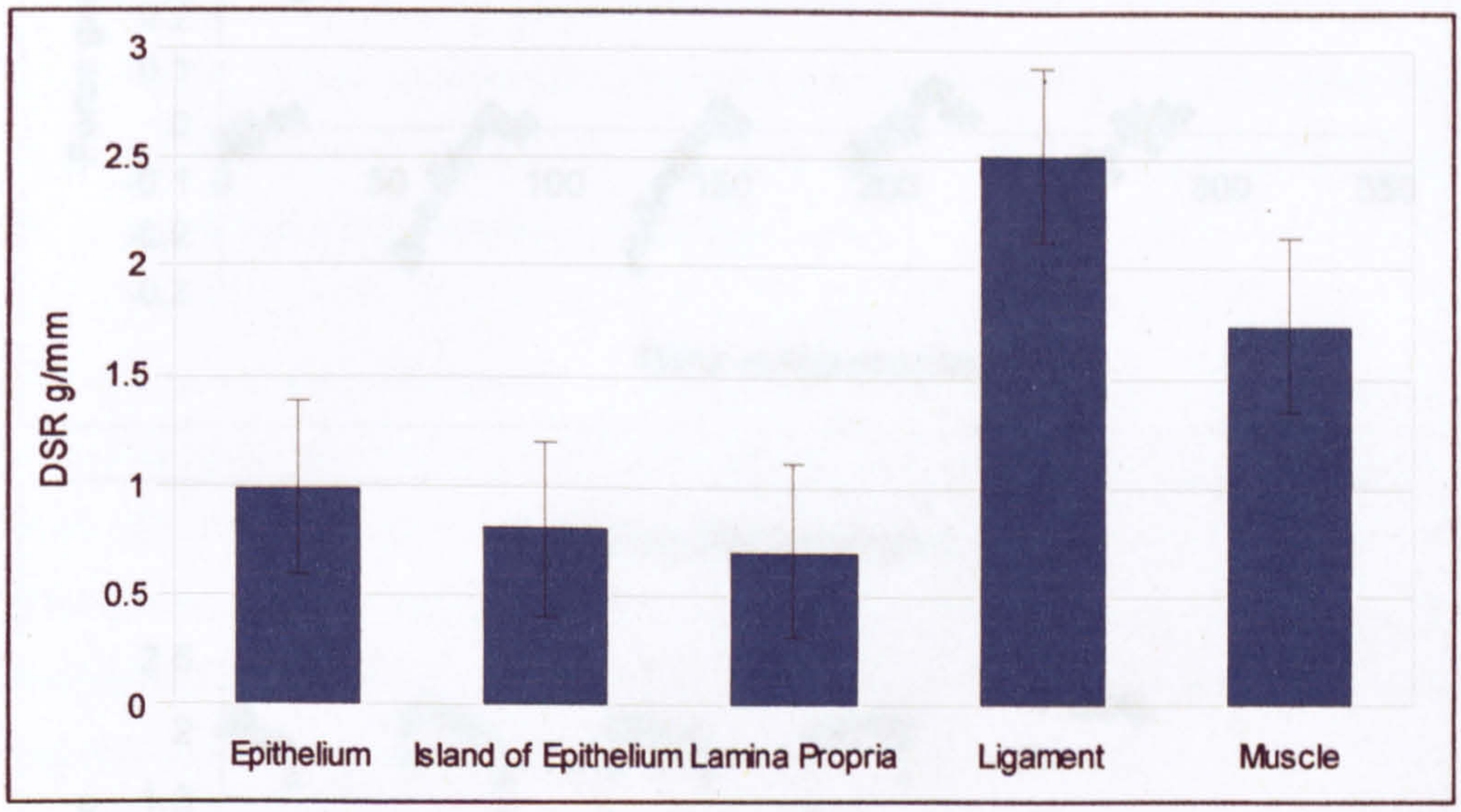

Figure 14 Variation of DSR with vocal fold layers

There are three clear differentiations, the lamina propria, the vocal ligament and the vocal muscle. This is to be expected and supports the critique that needle penetration depth is critical to securing good coefficients of variance in the results.

After much experimentation, using needles, adhesives and suction the preferred attachment method for all current studies is to use suction. Currently a cannular with a 2 mm internal diameter is used, which is attached to the epithelium using 50 mbar of suction. This has resulted in a dramatic improvement in repeatability of the measurements. The improvement in the quality of the data is illustrated well by Figure 15; the left hand trace is an *in vivo* measurement trace taken using a methylcellulose adhesive attachment to a volunteer patient under anaesthesia, the right hand side shows a similar trace obtained using suction. The other key advantage of suction is that the attachment is only to the epithelium, with a known diameter. The pin method penetrates to an unknown depth, as is not easy to repeat, and the glue tends to spread. Mechanically a cannular is stiffer than a metal probem as used for pins and glue, and this change will also greatly enhance the repeatability of the measuring devices.

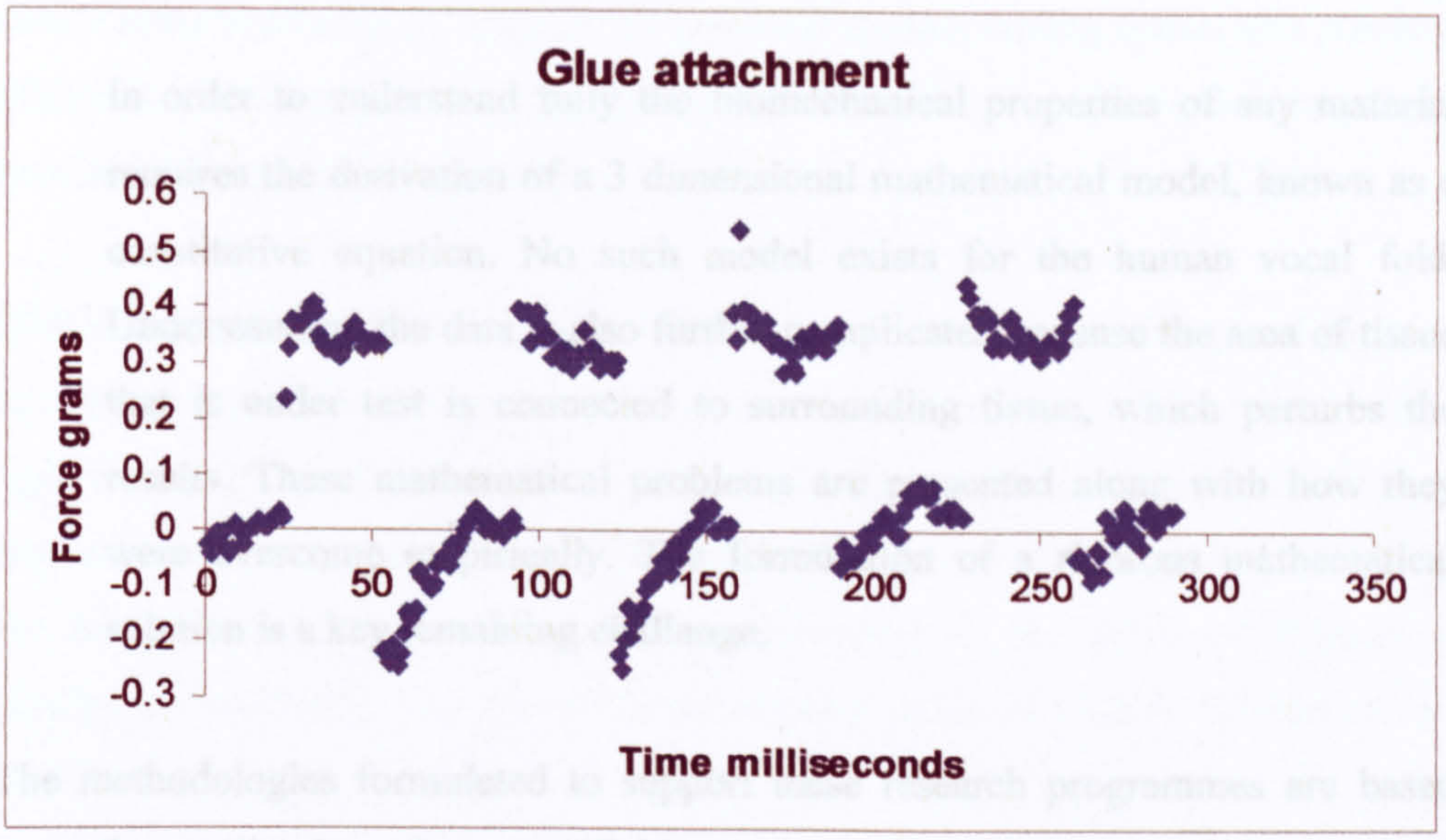

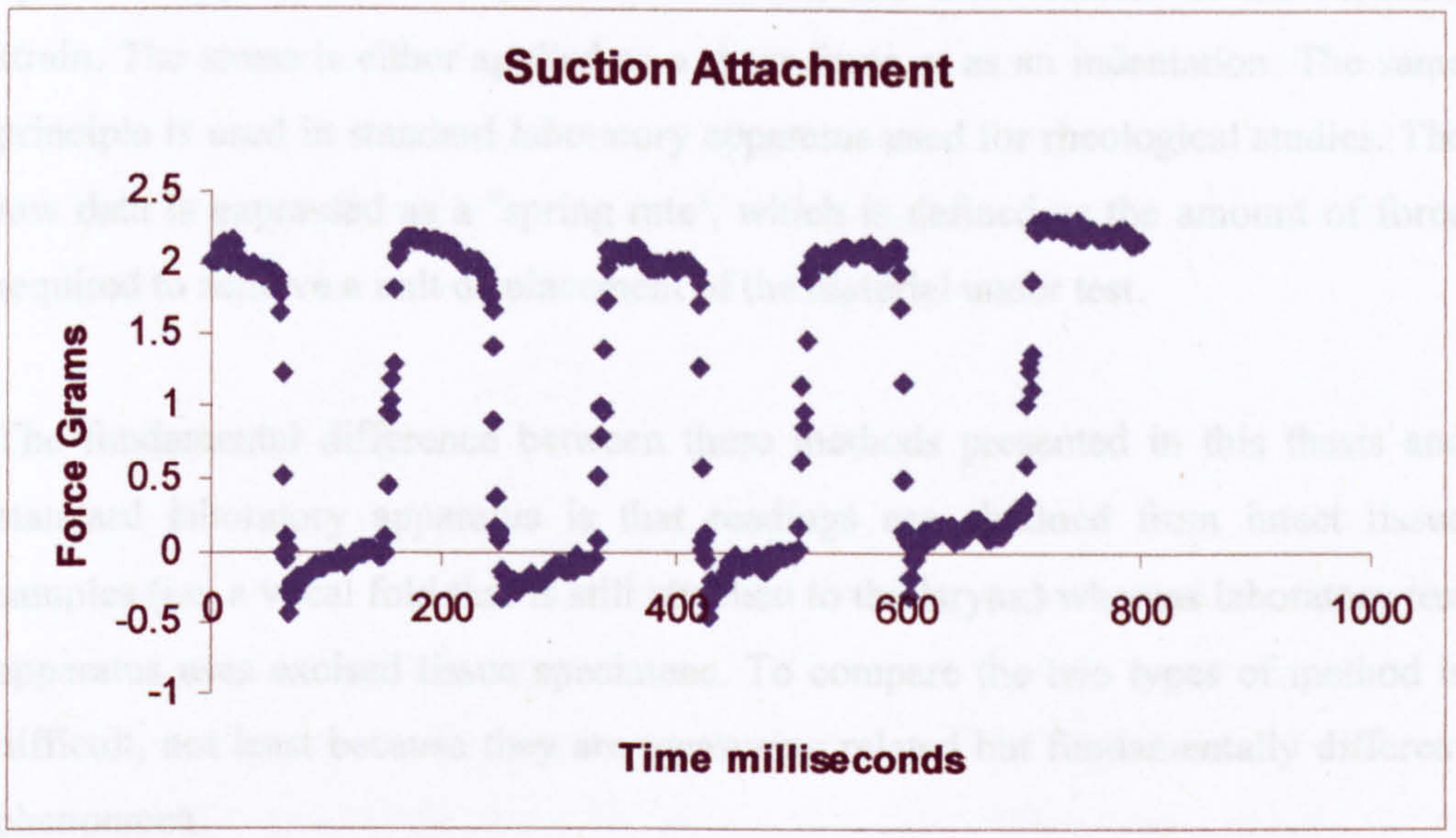

Figure 15 Enhancement of data resultant from use of suction instead of glue, expressed as force in g with respect to time in ms

It can be seen that the measured force changes when using glue, due to movement within the adhesive, whereas the measured force when using suction is far more stable. The time units are 10 ms.

5 Mathematical Presentation of the Results

In order to understand fully the biomechanical properties of any material requires the derivation of a 3 dimensional mathematical model, known as a constitutive equation. No such model exists for the human vocal fold. Understanding the data is also further complicated because the area of tissue that is under test is connected to surrounding tissue, which perturbs the results. These mathematical problems are presented along with how they were overcome empirically. The formulation of a rigorous mathematical solution is a key remaining challenge.

The methodologies formulated to support these research programmes are based upon the application of a quantifiable stress, and measurement of the resultant strain. The stress is either applied as a shear force or as an indentation. The same principle is used in standard laboratory apparatus used for rheological studies. The raw data is expressed as a 'spring rate', which is defined as the amount of force required to achieve a unit displacement of the material under test.

The fundamental difference between these methods presented in this thesis and standard laboratory apparatus is that readings are obtained from intact tissue samples (i.e. a vocal fold that is still attached to the larynx) whereas laboratory test apparatus uses excised tissue specimens. To compare the two types of method is difficult, not least because they are measuring related but fundamentally different phenomena.

Rheological test apparatus is used to determine the fundamental visco-elastic properties of the material under test, expressed in terms of its' modulus. The raw spring rate data is easily transformed into a measure of modulus as the specimens have a known geometric size and shape, thus the internal microelectronics can apply the well established formulae to derive absolute stress and strain from the force and displacement readings. Geometry of the tissue sample can then be used to derive Modulus.

De Montfort's tissue tensiometers and LSR devices take point specific measurements from intact tissue samples. The dimensions of the tissue being measured are not known; whilst it would be possible to dissect and measure the tissue samples taken from the mortuary this cannot be done with volunteers. Therefore the test site geometry is imprecise. The other reason why the methods

are not comparable is that when stress is applied to a point on a sample, the area that is subjected to direct stress is still attached to surrounding tissue, and this will affect the result. In effect a larger stress has to be applied to achieve the same strain than standard laboratory apparatus.

DMU's apparatus is therefore best suited to studies that are seeking to determine ratiometric data. Where such results have been published they are presented with a high degree of confidence; the best examples being the hyaluronic acid tissue augmentation study carried out at the Karolinska Institute [Hertegrad et. al. 2004], the iso-contour maps derived at Harvard [Goodyer et. al. 2003] and Wisconsin [Dailey et. al. 2007], and the nerve stimulation study at UCLA [Chettri et. al. 2008].

However because the bulk of published material is presented in terms of modulus [Chan & Titze 1999, Kaneko et. al. 1981, McGlashan et. al. 1998, Hsiao et. al. 2002, Alipour & Titze1990], these results have to be converted into estimates of modulus in order to enable credible peer-review.

5.1 The Indentor Model

The author is not the first researcher to have to overcome the problem of converting force/displacement data into a modulus to enable peer-review. For a homogeneous material, the resultant relationship will be logarithmic, forming a classic compression cycle curve. However many researchers have correctly stated that indentation of a soft tissue does not follow this simple rule because surrounding tissue remains in contact with the depressed section to which a shear stress is applied. Only one reliable source for a rigorous mathematical transformation that can be applied to soft human tissue was found. This was developed by W C Hayes [Hayes 1972] to describe the elastic properties of soft thin tissues overlaying a stiffer substrate. This method involved the use of a circular indentor to compress the upper layer of soft tissue into the underlying hard substrate.

One widely accepted model is that originally proposed by Y C Fung [Fung 1981], from which W C Hayes developed his rigorous mathematical solution that offers a 'correction factor' to Fung's equations which takes account of the shear strain surrounding the indentation

The correction factor (κ) is based on the ratio of the indentor radius (a), the tissue thickness and Poisson's ratio. Hayes gives the following expression in his paper as the definition of κ together with a table of solutions.

$$(4)\ \kappa = (F * (1 - P))/(4aGw)$$

which can be rearranged to give

$$(5)\ G = (F/w) * (1 - P) * 9.80665) / (4a\kappa)$$

where

κ = the Hayes correction factor obtained from the published table

F = applied force

P = Poisson's Ratio

a = indentor radius

G = Shear Modulus

w = depth of penetration

Hayes' original formulae presents results in terms of grams, whereas Pascals are unties of force expressed in Newtons. The conversion factor 9.80665 m/s^2 is gravitational acceleration which converts the units for Shear Modulus (G) into Pascals.

Using this method the force/displacement data can be transformed into a value for shear modulus.

The test apparatus is arranged to indent the tissue, in anatomical context, with a force normal to the surface, and log the compression characteristics.

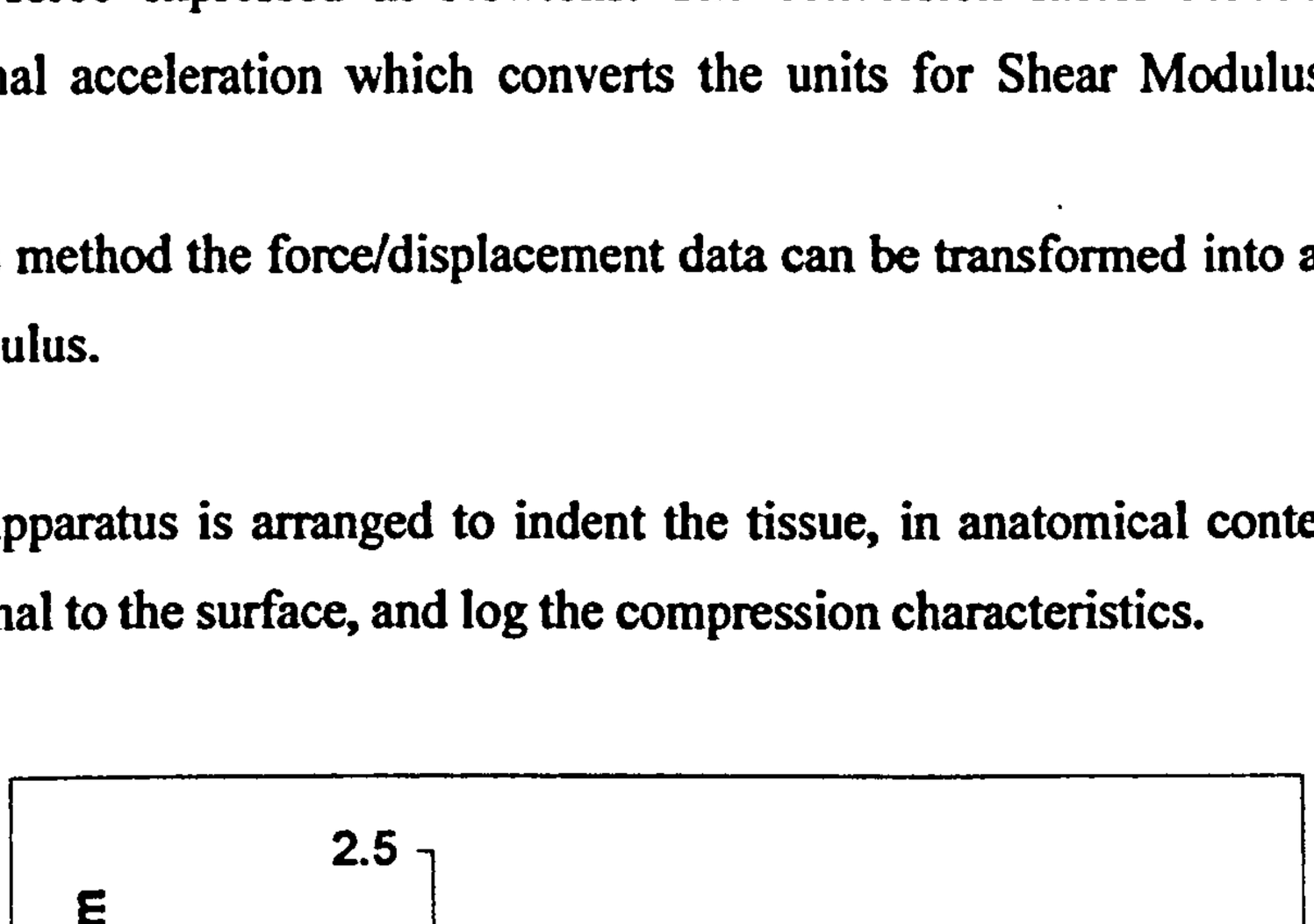

Figure 16 Indentation of an intact rabbit vocal fold

Figure 16 shows a typical trace, which was obtained by indenting a rabbit larynx using a 1 mm diameter flattened indentor [Hertegard et. al. 2004]. It can be seen that increasingly more force is required to compress the sample. Of interest is the first 0.5mm of compression, as that area approximates to a linear response, from which the ratio F/w can be derived. Testimony to the widespread acceptance of this formula is that there are currently 164 citations on Scopus for the paper [Hayes 1972], almost all of which have used the method to present rheological data of soft human tissues.

5.2 The Shear Model

Consider now a simple shear model. The LSR produces results in terms of DSR, which is the amount of force required to achieve a unit displacement of the tissue. However, the industry standard is to express elasticity in terms of a fundamental material property, such as shear modulus. Therefore, it is necessary to convert the value for DSR into shear modulus, which is achieved by an examination of the geometry of the test setup.

A sinusoidal force F is applied to the material under test and the resultant displacement P is logged.

$$F = F_{max} \sin(t) \quad (6)$$

$$P = P_{max} \sin(t+T) \quad (7)$$

Where

F = instantaneous force

Fmax = the maximum force

t = time over one cycle in radians

P = instantaneous displacement

Pmax = the maximum displacement

T = the phase shift in radians.

The Dynamic Spring Rate (DSR) of the tissue is F_{max} / P_{max}, and is expressed in units of grams force per millimetre. The DSR can then be used to determine the shear modulus using knowledge of the geometry of the test site as follows:

The stress τ is the applied force F per unit area A given by

$$\tau = F / A \quad (8)$$

The resultant strain ε is given by lateral displacement P per material thickness T, this is also expressed as the angle created by the distortion of the material, which is the arc tan of equation P/T.

$$(9)\ \varepsilon = P / T$$

Shear modulus G is defined as stress per unit strain

$$(10)\ G = \tau / \varepsilon$$

$$(11)\ G = (F / P) * (T / A)$$

As DSR = F / P then

$$(12)\ G = DSR * T / A$$

This simple shear model means that DSR can be easily converted into a value for shear modulus.

A flat probe is attached to the tissue surface using either cyanoacrylate glue for excised tissue, methylcellulose for *in vivo* studies, or suction. After the DSR data is obtained, the area of attachment can be measured and logged. Tissue thickness is assumed to be 1mm, as this is the value widely quoted in the published literature for the lamina propria [Hirano 1993]. Because the tissue under direct stress is attached to surrounding tissue, an allowance must be made to take account of the shear stress that is applied to the surrounding tissue. An extensive comparative study using both indentation and shear testing of 40 identical hemi-larynges determined that an optimum correction factor is to increase all attachment dimensions by 0.75mm. It must be stressed that this derivation is based on experimental observation. It remains an ongoing task of this research programme to derive a more rigorous mathematical correction for the derivation of shear modulus. [Goodyer et. al. 2007-3].

6 The Shear Modulus of the Human Vocal Fold

Here the results of the studies using excised human hemi-larynges are presented. There is a discussion of the early experiments that were used to derive the methods for later studies. Then the results obtained from an analysis of 20 human larynges are given. This represents the first known medium scale study to derive normative data for the biomechancial of the human vocal using intact hemi-larynges. A major area of controversy is whether the lamina propria is anisotropic. Prior to the successful deployment of the authors devices almost all published data was obtained using parallel plate rheometry, which applies a rotational shear to the tissue under test and are unable to differentiate the data with respect to a Cartesian direction. The authors devices apply a linear shear and are therefore able to resolve orthogonal data, revealing the anisotropic nature of the vocal fold.

As the methods for quantifying the shear modulus of the vocal fold, using a modified simple shear model and an indentometer had been demonstrated to produce credible results [Goodyer et. al. 2003, Hertegard et. al. 2004, Hess et. al. 2006] the focus of attention moved to carrying out a large-scale study using 20 excised human larynges, 10 from each sex. One outstanding issue was to determine if a delay between death and analysis of the donor larynx was a significant factor. A small study was completed which established that a brief delay of 1 or 2 days did not adversely affect the results. The opportunity was also taken to quantify the variance of transverse elasticity with respect to anatomical distance from the vocal process [Goodyer et. al. 2007-3]. The hemilarynx is typically mounted with a single pin through cartilage such that the vocal fold is not tensioned when being measured.

6.1 Initial, 2 Day Study

The key graphs are shown in figure 17. A single donor larynx was mounted, and a probe inserted into the structure and used to take a series of measurements at five different points on the left and right hand sides. 5 measurements were taken from each site. The measurements were repeated 24 hours later. Of significance are

1 The correlation between the left and right sides
2 The variation in elasticity with respect to anatomical positions
3 The fact that a 24 hour delay post-mortem yields similar results

Almost all currently published literature giving values for the elastic properties of the human vocal fold were obtained using tissue excised from the larynx, and measured using either a parallel plate rheometer or some form of tensiometer apparatus. The author's results are unique in that they were obtained from an intact excised human larynx. It proves that the method is able to obtain point specific biomechancial data without the need to dissect the tissue out of its' anatomical context.

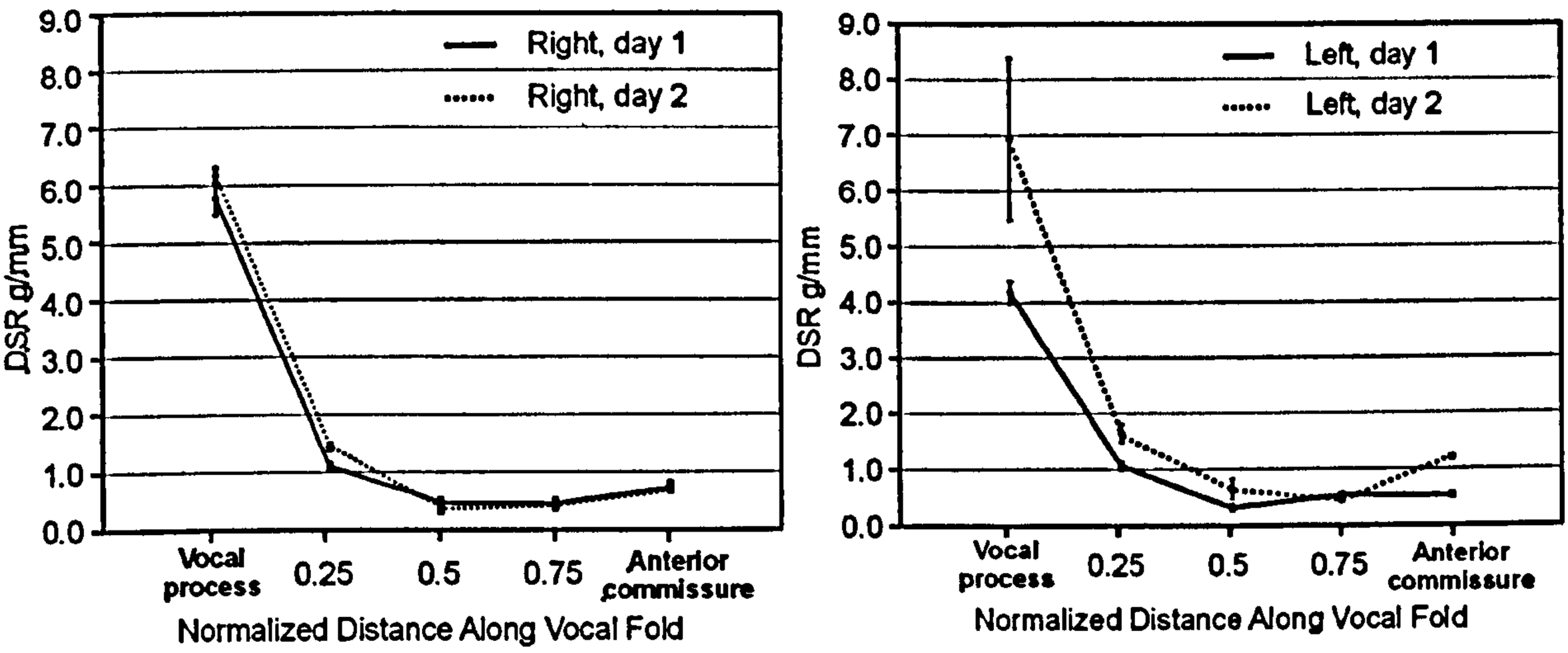

Figure 17 Comparisons between left & right sides of a hemisectioned human larynx

6.2 The Extended Study using 20 Excised Human Larynxes

Two methods were deployed for this study, one used the shear modulus measurement method that has already been outlined, and is referred to as the Shear Model in the article [Goodyer et. al. 2007-3]. The second method reconfigured the apparatus as an indentometer, and is referred to as the Indentometer Model in the article. The results for the study using both the indenter and the shear model are given here, and in a key publication [Goodyer et. al. 2006-2]. A similar but less extensive study carried out at Wisconsin reproduced the result for shear modulus in a transverse direction [Goodyer et. al. 2007-1].

	Male Shear Modulus Pascal	Female Shear Modulus Pascal
Shear Model	1008 CofV 38%	1237 CofV68%
Indentor Model	1008 CofV46%	1323 CofV 32%

Table 3 Comparison of shear moduli obtained using indentor and shear models

Whilst it is very pleasing that the two methods give similar mean results, the standard deviations are very poor. In addition, as is made clear in the article, the correlation coefficients between left and right hand side hemi-larynges are only just acceptable. Therefore, these results must be seen for what they are, which is an early announcement of preliminary results. The later use of a suction probe to replace the use of glue and pins has resulted in a substantial improvement in the coefficients of variance of the raw data.

A key area for further research is the derivation of mathematical formulae to express the 3D constitutive equations that will model tissue deformation of the vocal fold when shear stress is applied to a small section of the tissue. F C Fung [Fung 1981] in his widely respected book on tissue biomechanics is of the opinion that such equations can only be derived experimentally and not by the application of pure mathematics. However, it should be possible to develop mathematically based models that will allow the experimental results to have a better relationship to the tissue structure in a meaningful manner. This remains a key objective of future research. A more recent set of results were obtained at Wisconsin University Hospital using suction, are given in table 3.

Age	Sex	DSR g/mm	CofV %	G Pascal
78	F	1.202	2.96	1232
70	F	0.794	1.44	814
Unknown	F	0.848	8.31	869
89	M	0.996	1.14	1021
72	M	0.982	4.03	1006
33	M	1.752	5.00	1796

Table 4 Estimated shear modulus of the human vocal fold

The estimated shear modulus was derived using the modified shear model already presented in chapter 5; and the results are in the same order of magnitude as those derived using an adhesive for attachment. What is of interest mathematically is that the adhesive attachment used a rectangular surface, whilst the suction used a circular cannula; yet the same correction to the area of attachment of increasing the dimensions by 0.75mm enables the two sets of raw results to converge. This is indicative that this experimental result could enable us to begin the process of deriving a full set of constitutive equations for vocal fold shear, or at least to derive

a 2D model. The other significant result from this data is the substantially improved coefficients of variance in the data sets that are achieved by using suction.

6.3 Anisotropic Behaviour

There is clear evidence from the results in table 5, that the vocal fold is highly anisotropic. This runs counter to the published evidence, which in general assumes that the lamina propria is homogeneous and isotropic. There is no contradiction between these apparently different claims. The vast majority of published results has been derived from excised cadaver tissue; whereas DMU's methods measures the rheometric properties of the same tissue whilst it is still attached to its' underlying structures. In addition, the usual method of analysing excised tissue is with a rotating parallel plate rheometer, which by definition cannot resolve out directional differences.

A study is now under way at UKE to determine the extent of the anisotropic behaviour, and to determine which part of the vocal fold is primarily responsible for that behaviour. The early indicative results are compelling. So far, 14 larynxes have been examined. Each hemisection was mounted and measured in the transverse and longitudinal direction. The lamina propria and epithelium were removed and the test repeated on the ligament, then the ligament was removed and the muscle tested. The degree of the anisotropic nature may be derived by expressing the elasticity as a ratio of transverse and longitudinal results. These are shown in table 4 and have been published et. al. Licht 2007].

	Intact Larynx	Ligament & Muscle	Muscle Only
Mean	0.5376	0.6316	0.7336

Table 5 Anisotropic nature of the vocal fold expressed as a ratio the of transverse and longitudinal shear modulus

It can be seen that all three sections (complete, ligament/muscle and muscle only) exhibit anisotropic behaviour. The lower the ratio the more is the anisotropic behaviour. The muscle is highly anisotropic, as is to be expected, the ligament increase this effect; finally, the LP itself increases the variation further. It is not

known whether LP is inherently anisotropic in its' own right, and so the author is currently devising a new apparatus that is capable of measuring a sample of LP in isolation. As an excised LP has a typical dimension of 4mm x 2mm x 1mm this is a technical challenge still to be overcome.

The outcome of this study will be significant for our colleagues researching tissue-engineering therapies. The accepted wisdom is that the LP is homogeneous and isotropic, therefore it is possible to use a rectangular scaffold as the starting point to mount the growth factors; if however the LP is anisotropic, the scaffolds used would have to reflect this internal variation. However, the author has been informed by the Wisconsin that they have recently completed a series of as yet unpublished studies that found that the collagens in the lamina propria are aligned in the longitudinal direction, and this is a major reason for its' anisotropic nature.

7 *in vivo* results

A key research challenge was the invention of a device that is capable of obtaining *in vivo* measurements. Two devices [Goodyer et. al. 2007-2] have now been devised to achieve this, and the results obtained from eight volunteer patients are given.

A key objective of this extensive programme of work is to formulate methods to quantify the elasticity of the human vocal fold *in vivo*. Data are obtained in this way will complete the picture of how the structure is naturally tensioned. There is extensive data available on the fundamental elastic properties of the lamina propria in the published literature. Most of my published results to date are taken from excised tissue with the lamina propria remaining in its anatomical context. It is a reasonable assumption that data obtained *in vivo* will be similar, and a series of experiments have been carried to see if that is the case. As yet, the results are inconclusive, but indicative that similar values are obtained from excised tissue and *in vivo* [Goodyer et. al. 2007-2, Goodyer et. al. 2006-1].

7.1 The Laryngeal Tensiometer

Figure 18 is a schematic of the Laryngeal Tensiometer which clamps onto a standard laryngoscope once it has been inserted into the patient. The schematic diagram shows the mechanical assembly. A simple slide arrangement allows the investigator to apply a calibrated displacement of 1 mm along the main axis. The 50g load cell sensing axis is co-axial to the laryngoscope. A magnetised ball bearing is used to attach a steel rod, whose other end is then attached to the vocal fold tissue using a methyl-cellulose based adhesive. Figure 19 shows how the laryngeal tensiometer is deployed. For this paper the shear response of excised vocal folds were measured to prove the methods, and then the shear response from two female volunteer patients were obtained. One of the patients was suffering from a polyp on her left hand side, and we were able to contrast the tissue stiffness from the both sides of the larynx. Figure 20 shows the rod attached to the polyp on the first patient, and to a healthy vocal fold on the second patient.

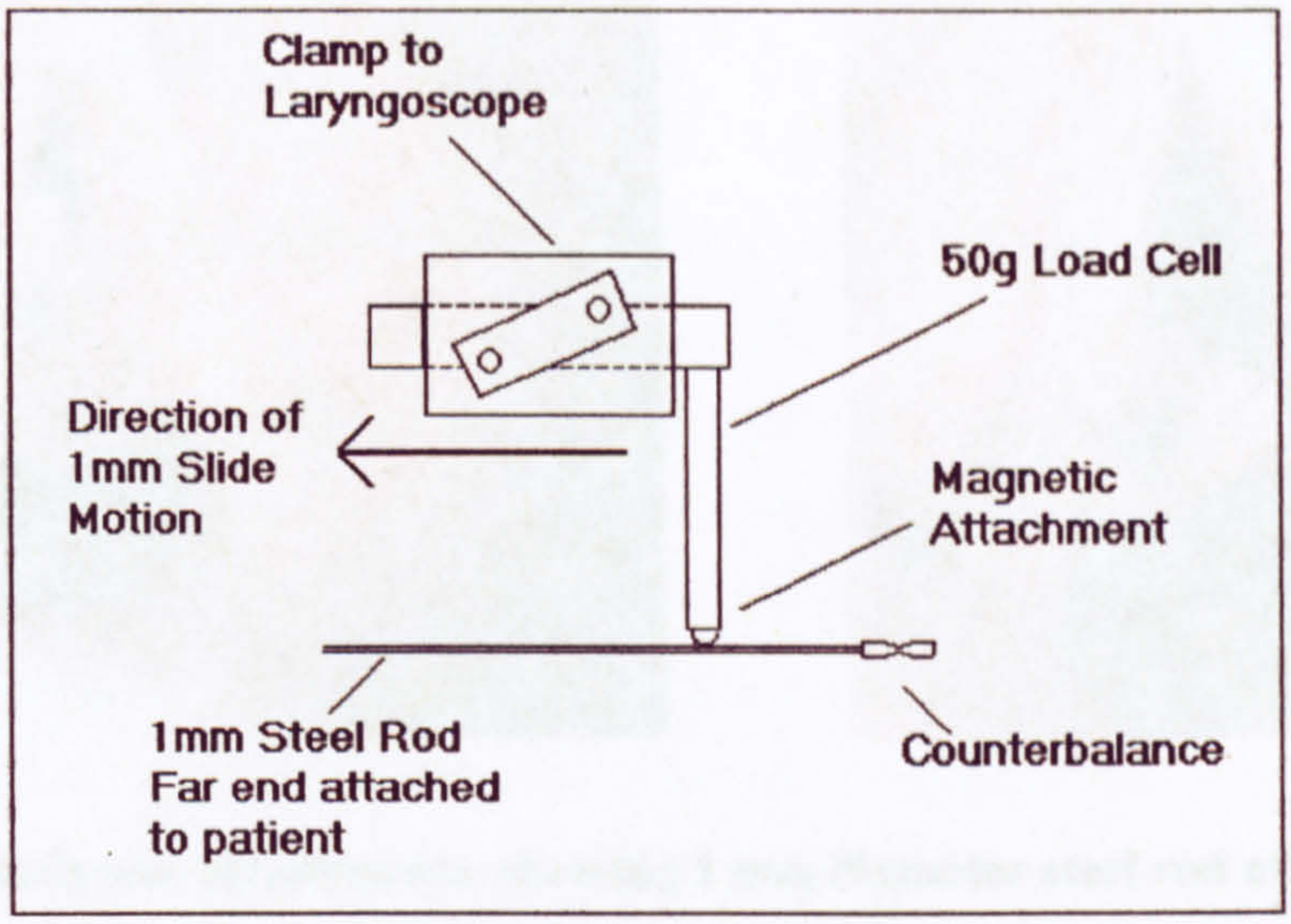

Figure 18 Laryngeal tensiometer schematic

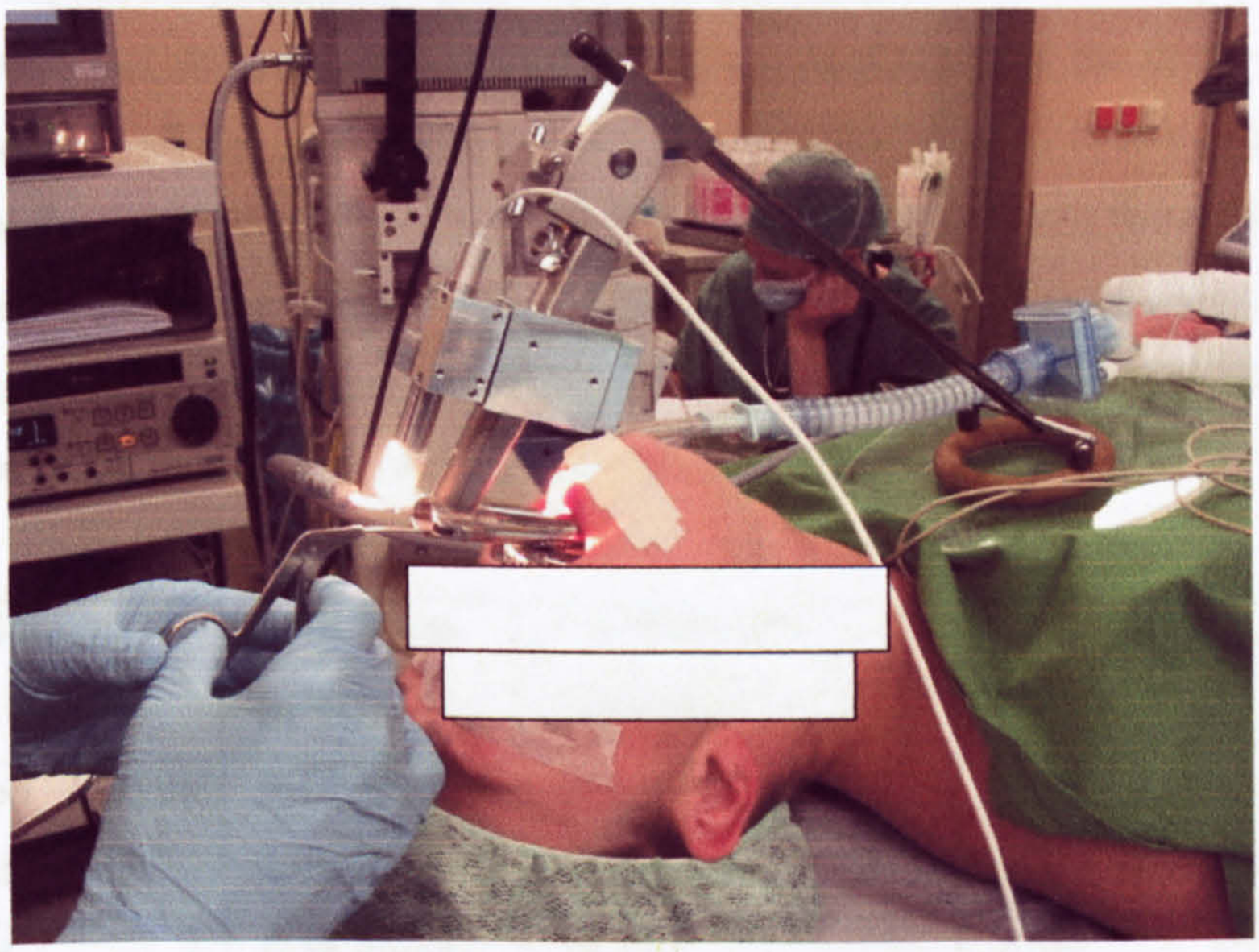

Figure 19 Deployment of laryngeal tensiometer

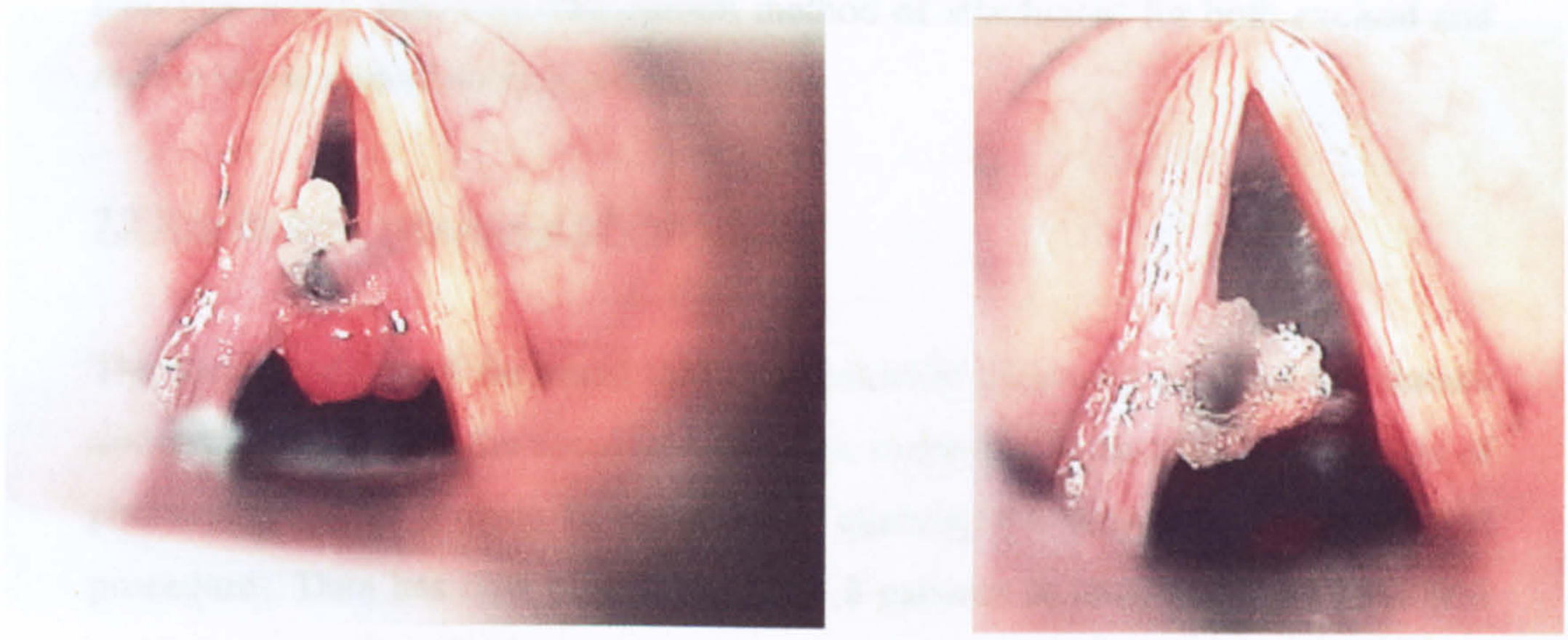

Figure 20 *in vivo* attachments, showing 1 mm diameter steel rod attached using methyl-cellulose glue

The raw data is expressed in terms of spring rate. Results were obtained from the excised larynx, the polyp on patient 1 and healthy vocal folds from both patients. It can be seen that the polyp has a far lower shear modulus than the healthy vocal fold, and that all the results are similar. It can also be seen that the standard deviation for the *in vivo* results is very poor, which is indicative of the difficulty of taking readings from a living person. There is also a high degree of uncertainty as to the area of attachment due to the use of adhesive; a problem that was overcome when the probe was changed to a cannula with suction.

Data Source	DSR Mean (n = 5)	Coefficient of Variance	Shear Modulus Pascal
Excised Larynx mid vocal-fold	0.40 g/mm	6.8%	1596
Patient 1 Healthy Tissue	0.58 g/mm	18.4%	2309
Patient 1 Diseased Tissue	0.26 g/mm	28.8%	1035
Patient 2 Healthy Tissue	0.53 g/mm	25.7%	2111

Table 6 Spring rate results from excised and *in vivo* sources

These initial results gave us the confidence to continue enhancing the methods, and to date data has been obtained from a total of 10 patients. The main case of the poor coefficients of variance was eventually determined to be the use of

methylcellulose adhesive. The current method of attachment for both excised and *in vivo* use is a small suction probe.

7.2 Results from subsequent *in vivo* studies

The shear modulus of the vocal fold is an essential parameter required to enhance understanding of how the vocal fold operates, to formulate mathematical models of phonation, and to provide benchmarks to quantify the effectiveness of surgical procedures. Data has now been taken from 8 patients *in vivo*, using the laryngeal tensiometer, and a further 3 patients have been measured using new device invented with financial support from the Royal Society. The new device includes an LVDT to measure the change in distance, replacing the calibrated gap used in the first device. The shear modulus was measured at the mid-membranous point, in a transverse direction with respect to the axis drawn between the anterior commisure and vocal process. The range of mean shear modulus results is 701 to 2225 Pascals, with a mean value of 1371 Pascals. [Goodyer et. al. 2006-1].

There are insufficient results to draw general conclusions; however, the mean result of 1371 Pascal is comparable with similar published results [Chan & Titze 1999, Goodyer et. al. 2007-3]. The instrument is currently being re-engineered to allow sinusoidally varying forces to be applied at frequencies up to 100 Hz. This will enable us to derive the viscous properties as well as elastic data.

The real significance of this work is the formulation of the methods to measure tissue parameters *in vivo*. This will be deployed in two ways; one will be as an aid to diagnosis and the other to enable real-time objective assessment of the effectiveness of tissue engineering therapies. A simple experiment using UV polymerised hyaluronic acid has already demonstrated that real-time measurements are achievable. An excised calf larynx was injected with a photosensitive HA based gel, and an LSR probe was attached. The change in tissue stiffness was successfully logged following brief periods of UV irradiation. The end objective will be to provide a phono-surgeon with a tool that will enable tissue stiffness to be tuned, by means of real-time monitoring of the current tissue stiffness.

7.3 Dynamic measurements

A new device is currently being devised that will enable data to be obtained *in vivo* at frequencies of up to 30 Hz. This is still well below the desired frequency of 100 Hz, which is closer to that achieved during phonation. No results are yet available.

8 Tissue Engineering Studies

In order to obtain an objective assessment of the effectiveness of a range of tissue engineering therapies it is necessary to measure the change in biomechancial properties of the augmented tissue. It is intended in time to deploy the new *in vivo* tools to support this work. Here are presented the results of a study where I obtained the data that enabled the team to conclude that Hyaluronic Acid augmentation could be used to restore the pliability of scarred vocal folds in a rabbit model.

A number of tissue engineering studies have been carried out in the last few years, the most significant being a study into the effectiveness of hyaluronic acid implants to restore vocal fold pliability in a rabbit model [Hertegard et. al. 2006]. Vocal fold scarring is accompanied by stiffness of the lamina propria and results in severe voice problems. Hyaluronic acid has been shown to improve the viscoelastic properties after injections in normal rabbit vocal folds and in patients with unilateral paresis and vocal fold atrophy. The main aim of the study was to analyse the short-term viscoelastic properties after injection of hyaluronic acid in scarred rabbit vocal folds. Another aim was to examine the degree of scarring achieved by the experimental model.

8.1 Hyaluronic Acid Augmentation in a Rabbit Model

Vocal folds of 15 New Zealand rabbits were scarred by a localised resection. After 8 weeks one group received injections with a cross-linked hyaluronic acid and another group was injected with saline. After 11 more weeks, both groups and a third group of control animals with normal vocal folds were sacrificed. The larynges were dissected out, 15 vocal folds were frozen for viscoelastic measurements, whereas 14 vocal folds were prepared and stained for histology. The histological analysis included measurements of the lamina propria thickness and of the relative content of connective tissue. Two methods were used for the viscoelastic measurements:

1. Analyses were made on intact vocal folds with a linear skin rheometer (LSR) adapted to laryngeal measurements.
2. The vocal folds were dissected and analysed in a parallel-plate rheometer.

Histological measurements on the digitized slides showed a thickened lamina propria and a higher content of connective tissue in the scarred samples as compared to the normal vocal folds ($p<0.05$). The viscoelastic LSR analysis on intact vocal folds showed stiffening of the scarred vocal folds as compared to the normal group ($p=0.05$). The parallel plate rheometry on the same samples after dissection showed a decreased dynamic viscosity and lower elastic modulus in the scarred samples injected with hyaluronic acid as compared to the normal and to the untreated scarred group ($p<0.01$)

The experimental model for vocal fold scarring resulted in deviation of the normal lamina propria structure with increased connective tissue content. Injection of scarred rabbit vocal folds with hyaluronic acid rendered improved viscoelastic parameters.

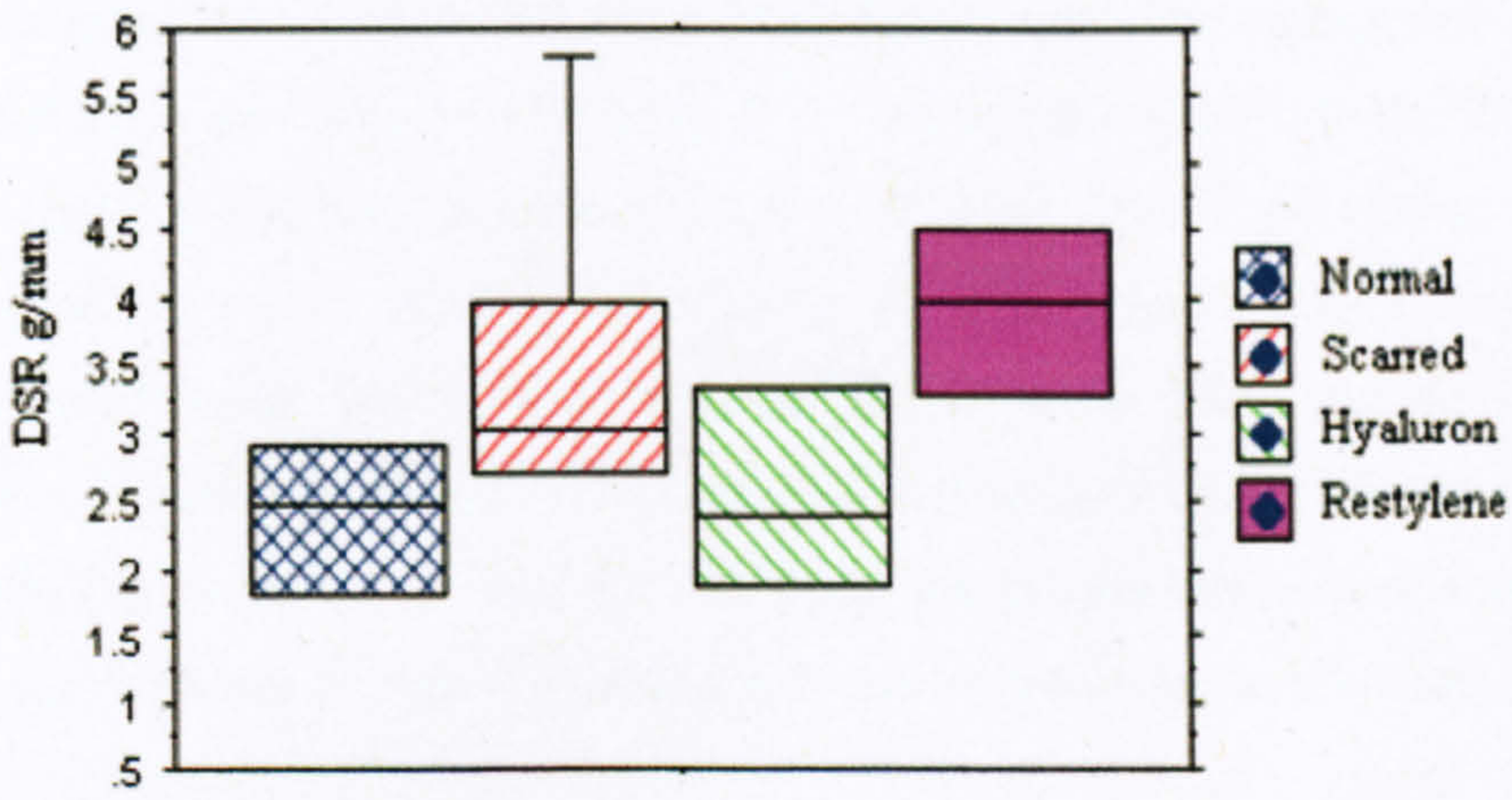

Figure 21 Results of the hyaluronic acid implant study

The rabbits were split into 4 groups. One group was a control. The other 3 groups had their vocal folds artificially scarred. One group of scarred rabbits was treated with hyaluronic acid, and the another group with restylene, which is another accepted tissue augmentation material. The results shown here were obtained from a blind measurement of the shear modulus of the excised larynges using an early indentometer method. The normal group is clearly differentiated from the scarred group. The group treated with hyaluronic acid have their elasticity restored back to normal conditions, whereas the control group treated with restylene are not restored.

Each larynx was split and mounted vertically. The LSR was setup such that it drove a 1 mm diameter polished rod into the tissue. The displacement was set to be

2 mm maximum. As the rod moved the force/and displacement data was captured. A typical compression graph is shown in figure 22.

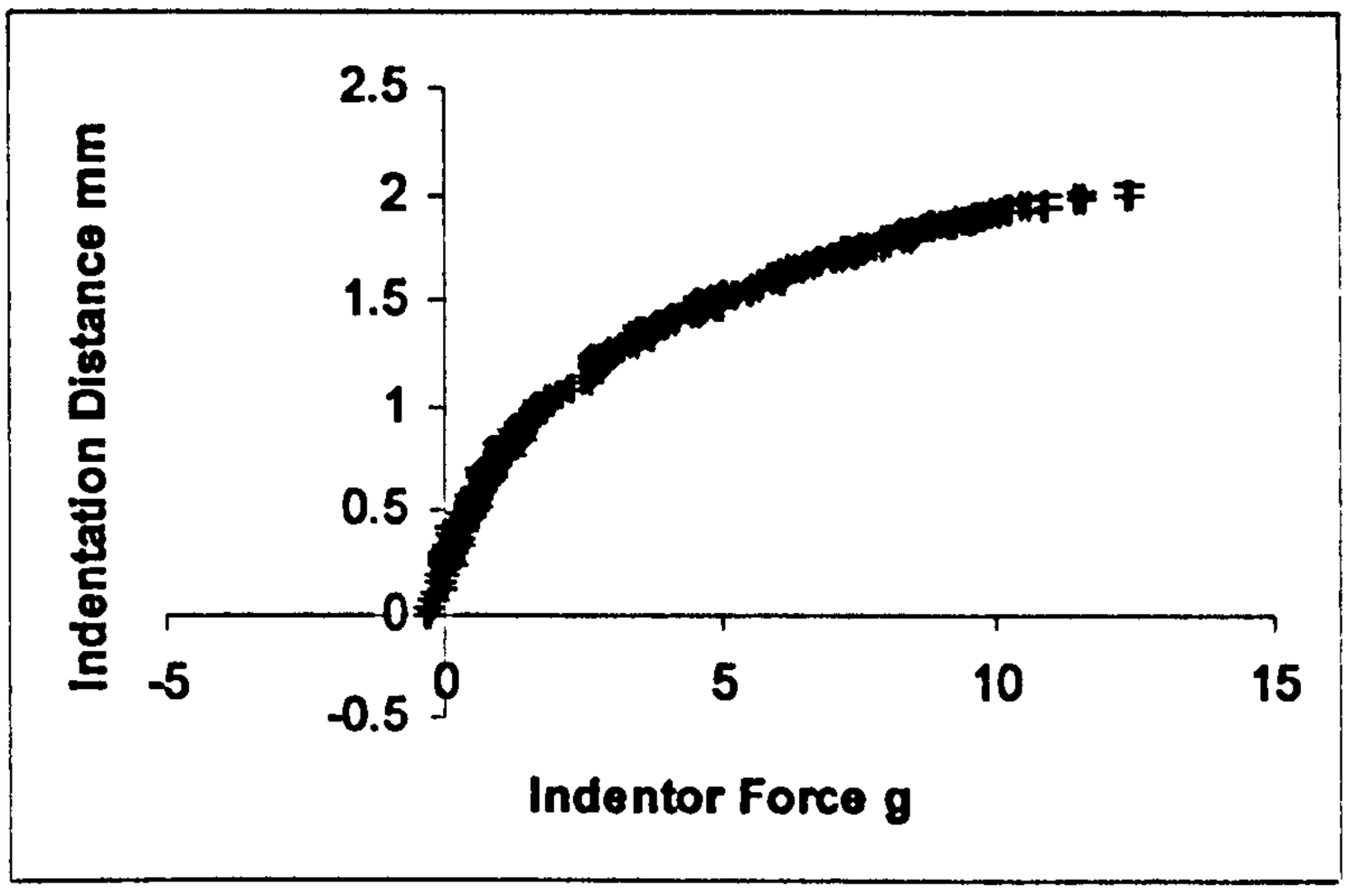

Figure 22 A typical compression graph obtained from a hemi-larynx

In this graph, the x-axis is applied force in grams, and the y-axis is the displacement. The curve shows the typical logarithmic relationship that is to be expected when materials are compressed; our interest is restricted to the initial part of the curve, which approximates to a liner response. The slope of this curve is directly related to the Young's modulus for the tissue, and the geometry of the experimental setup; which was the same for all vocal folds. As we are only interested in carrying a comparative study, not a derivation of an absolute value for modulus, the slope is sufficient for this study. Each hemi-larynx was measured 5 times and the average of the resultant slopes used to generate the box plot.

It can be seen form figure 21 that the scarred group had a higher modulus than the control group; this is as expected as scarred tissue is stiffer than healthy tissue. Treatment with an HA implant resulted in the near restoration of the elasticity of the scarred tissue. Restylene had no therapeutic affect at all, and seemed to increase stiffness. These results give a strong indication that HA implants can restore the elasticity of scarred vocal folds.

The Karolinska Institute has since moved on to demonstrate that stem-cell implants will also restore pliability into scarred vocal folds in a rabbit model [Hertegard et. al. 2006].

8.2 Preliminary Study in Support of Genetic Transfection Project

Wisconsin University Hospital has just started a 5-year programme that will investigate a range of tissue engineering therapies, including the use of genetic transfection to promote or suppress the production of growth factors. In order to

provide objective assessments of these techniques Wisconsin carried out an extensive evaluation of the apparatus devised by the author. The most important aspect is that they independently verified the methods used in the previous work over a period of 6 months. During this time, they carried out a range of experiments to map the variation of elasticity across the surface of vocal folds from different species. Tissue was collected from six larynges (four canine, one rat, one human), representing six vocal fold experimental conditions (normal canine, canine sulcus vocalis, normal rat, rat chronic scarred, normal human, human trichloroacetic acid exposure). Full details of the methods, preparation and ethical approvals can be found in the journal publication [Dailey et. al. 2007].

The overall findings confirmed previous studies obtained at other institutions. Significantly Wisconsin reproduced the iso-contour maps that derived by Harvard, demonstrating that the elasticity of the vocal fold is highly dependent upon anatomical position. Repeatability was found to be around 4.7% across canine and human samples. The team successfully measured the elasticity of the rat vocal fold, which will be of value in future research as it will enable the team to quantify changes in vocal fold elasticity in rat models without having to dissect the vocal fold out of context. One of the dog vocal folds was found to have scarring, which was visibly observed, and subsequently confirmed by staining. The area of observed stiffness was found to coincide with areas of measured stiffness found using the rheometric apparatus.

9 The Relationship Between Nerve Stimulation and Vocal Fold Tension

The LSR device was adapted to take readings from an *in vivo* canine model. The Recurrent and Superior Laryngeal Nerves were stimulated, and the apparatus used to determine the relationship between changes in vocal fold tension and applied stimulation current.

The author's most recent collaboration is with UCLA, who are investigating the feasibility of using reinnervation as a therapy for vocal fold paresis. Using a canine model an initial study investigated *in vivo* the relationship between Recurrent Laryngeal Nerve (RLN) and Superior Laryngeal Nerve (SLN) stimulation and the stiffness that results in the vocal fold. A mongrel dog (approximately 25 kg) was used. The dog was anaesthetised with intramuscular acepromazine (0.1 – 0.5 mg/kg), then intravenous sodium pentobarbital (Nembutal) (30 mg/kg) to maintain a level of general anaesthesia. Throughout the procedure, general anaesthesia was achieved using halothane. Maintenance intravenous fluid was be given at 2 ml/kg/hr. Core temperature was monitored with a rectal probe, and a heating pad will be used to maintain a homeostatic temperature. The vocal folds were visualised prior to operation to verify normal anatomy. Intravenous dexamethasone was given periodically to decrease nerve and vocal cord swelling.

The animal was placed supine, the neck prepped, and a midline incision from the hyoid bone to the sternal notch made. The sternocleidomastoid and strap muscles were exposed and retracted laterally to expose the larynx and trachea. Neck exploration was then performed to locate both recurrent RLN and SLN at their entrance into the larynx. Both RLN were isolated 5 cm inferior to the larynx. Custom designed rubber electrodes (monopolar, flexible, conductive neopreme with silicone, and silicone insulation KE45) were applied to the isolated nerves at the most proximal point dissected. Electrical isolation of the two nerves was confirmed by direct visualization of the vocal folds during phonation. The RLN was stimulated by a constant current nerve stimulator (WR Medical Electronics Co. Model 2SLH, St. Paul, Minnesota). These nerves were stimulated at 80 Hz with 0-3.0 mA for 1.5 msec pulse duration to achieve adduction. Subject to the outcome of these latter two studies, it is planned to extend the work to use freshly excised human larynges (typically less than 4 hours post-mortem). The results of these studies will lead directly to the development of the reinnervation therapy.

9.1 Summary of Nerve Stimulation Tests

Figure 23 shows the relationship between RLN stimulation and vocal fold tension. It can be seen that no change occurs for signals below 0.2 mA. Tension then changes with electrical stimulation up to just 0.3 mA, the muscle then appears to relax down to a maximum stiffness level. The values for shear modulus were derived using the Shear Model, but the real interest is the relative change in stiffness, which appear to increase by 75%, before falling back to an increase of 50%. However there is no clear relationship between tension and nerve stimulation.

Figure 24 shows the results when the SLN is stimulated. Little change occurs for stimulations below 0.22mA, then there is an apparent linear relationship between stiffness and stimulation up to about 0.3mA. The vocal fold then relaxes back to a constant stiffness. The degree of change appears to be far higher with SLN stimulation in that the peak change is almost 280%, falling back to 250% of the non-stimulated level.

These early studies have served two purposes. The results present an indication of the relationship between RLN & SLN stimulation and vocal fold tension from an *in vivo* canine model. The results also demonstrate that it should be possible to apply these methods in the future to develop and assess reinnervation therapy.

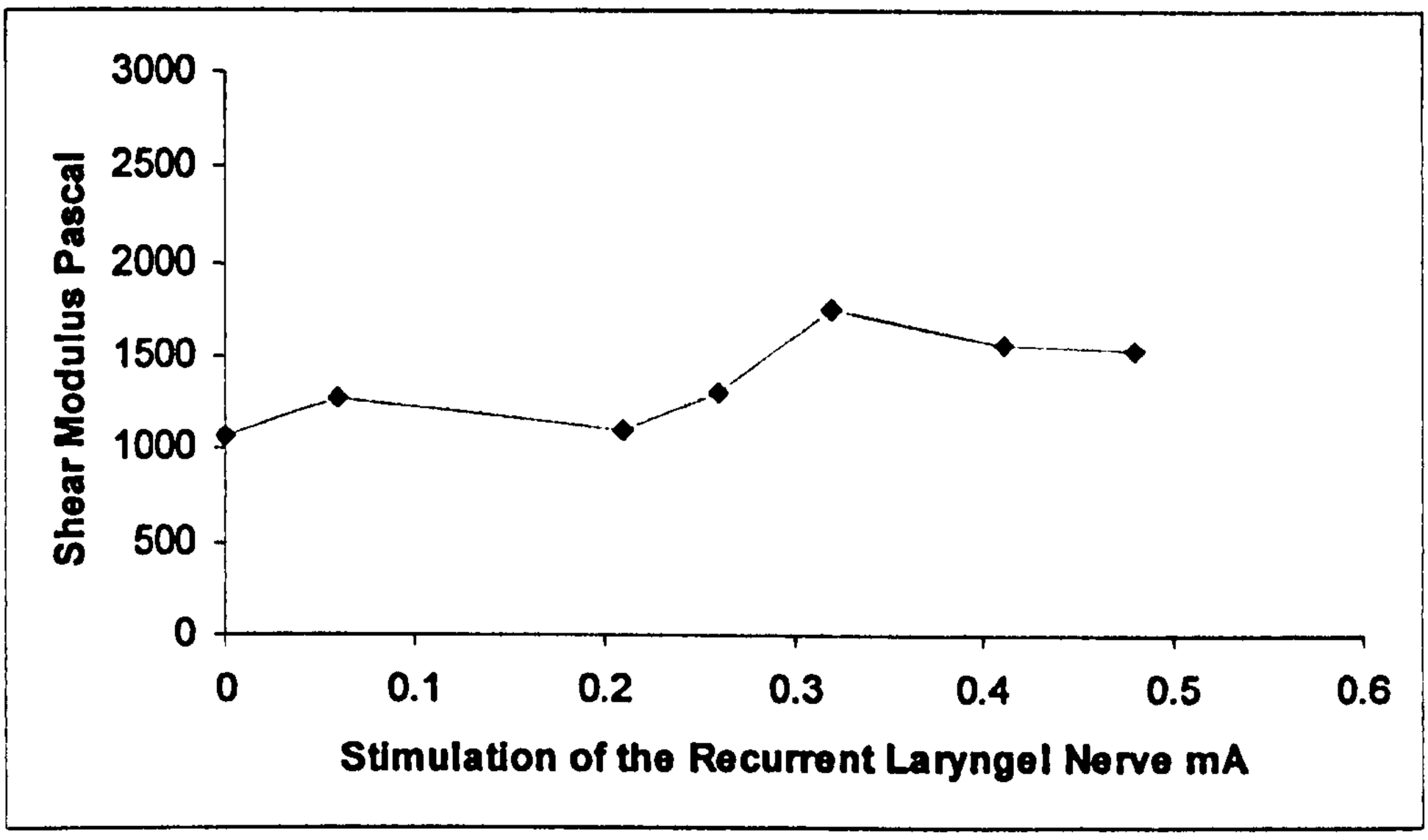

Figure 23 Vocal Fold Shear Modulus with respect to RLN stimulation

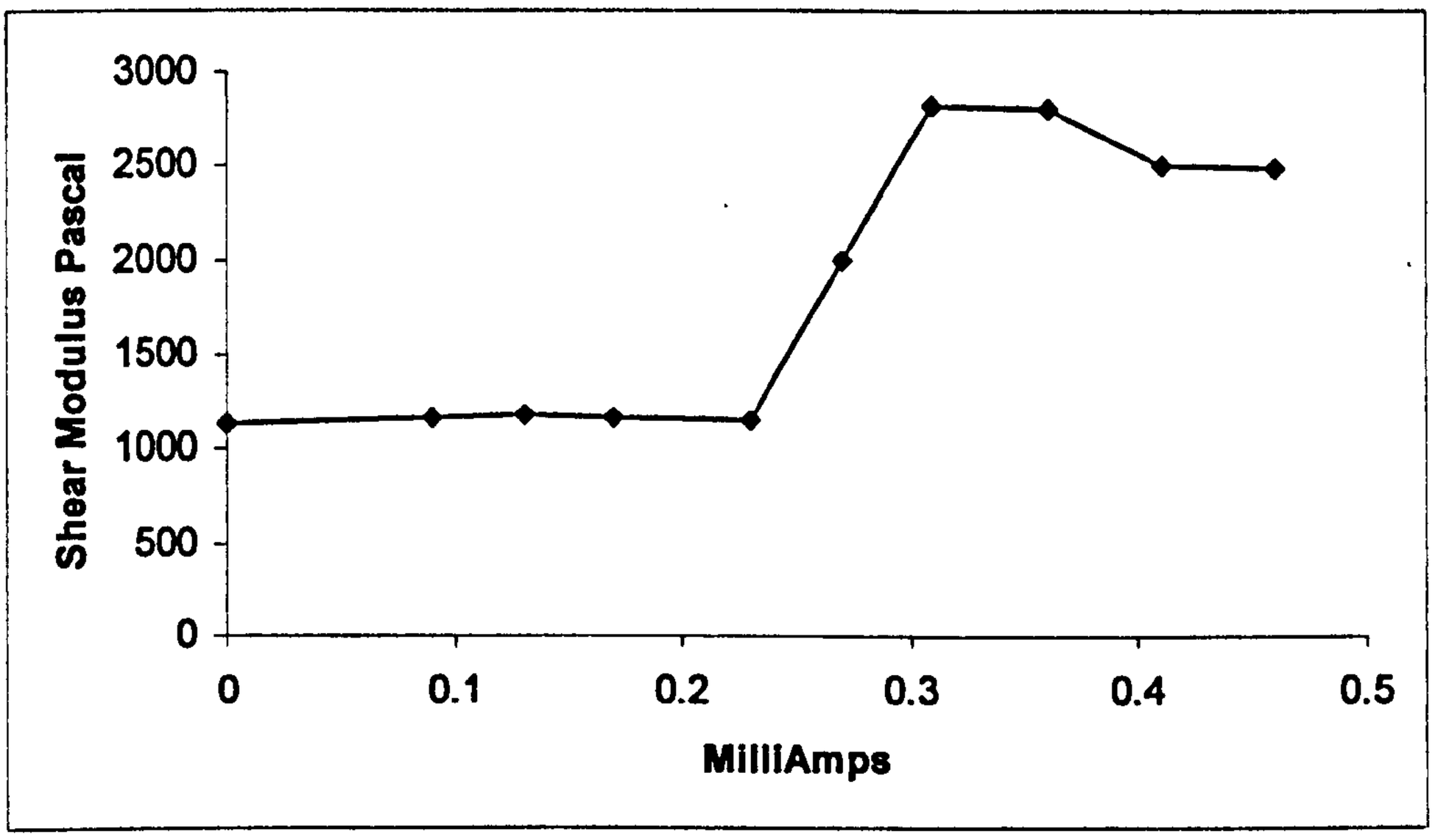

Figure 24 Vocal Fold Shear Modulus with respect to SLN stimulation

11 Summary of the Author's Contributions to the Field of Vocal Fold Biomechanics

The research work presented in this thesis has only been possible through the formation of a collaborative network bringing together the engineering skills to be found at DMU, with life scientists in the UK, Europe and the USA. Because of these collaborations, the author has led a team that has conceived, implemented and successfully deployed a range of new and novel devices have furthered fundamental medical research. The author specified the devices, developed the electronics and software, and devised mathematical techniques to analyse the resultant data.

The medical outputs arising from this research study can be summarised as follows:-

This research has made substantial progress with the characterisation of the human vocal fold, and the derivation of normative against which tissue engineering therapies can be assessed. The author is the first named author of a number of new papers in this field, presenting the new methods and devices that he devised for this research programme.

A large scale of excised human larynges has been completed, presenting data that demonstrated that vocal fold tension is highly dependant upon anatomical position and direction of applied stress. The author is the first named author of a published study that present results for the shear modulus of a large scale study of excised human larynges.

An easy to use device has been successfully deployed to obtain readings *in vivo*. Using this device, the shear moduli of the vocal fold in a transverse direction of 8 volunteers have now been obtained. The author is the first named author of two papers that present a set of results for the shear modulus of the human vocal fold obtained in-vivo.

The results show that there is a quantifiable relationship between nerve stimulation and vocal fold tension in a canine model. These results have been published, with the author named as a co-author.

The authors apparatus has been successfully deployed to quantify objectively the effectiveness of a range of tissue augmentation therapies.

The most successful being the use of Hyaluronic Acid augmentation to restore the elasticity of scarred vocal folds in a rabbit model. These results have been published, with the author named as a co-author.

11 Future Work

A number of new projects are currently started. These include the following

- Design of a new *in vivo* tool that will dynamically stimulate the vocal folds. This is a major challenge, in addition to the previous challenge of measuring very low forces the device is required to actuate the sensor, which will result in substantial noise overlaying the data. New mathematical techniques will be required to extract the data from the motor induced noise.
- Support for the tissue engineering studies at Wisconsin. This will require new methods to be devised as the Wisconsin team develop new tissue engineering techniques.
- The continuation of the normative data gathering and *in vivo* trials at UKE. The author has been asked to join a German/French team that will be examining the biomechanical properties of the false vocal fold. This will require a new class of devices and mathematical methods to be researched.
- Further work to determine the relationship between nerve stimulation and vocal fold tension at UCLA. Of particular interest is the intention to eventually use near post-mortem human donor tissue.

The major outstanding objective is to progress towards the development of a constitutive equation that describes the vocal fold's biomechanical behaviour.

References in Alphabetical Order

Alipour-Haghighi, F., Titze, I.R. (1990). Elastic Modulus of Vocal Fold Tissue. *Journal of the Acoustical Society of America.* **90** (3) p 1320-1331.

Ananthapadmanabhan, K.P., Moore, D.J., Subramanyan, K., Misra, M., Meyer, F. (2004). Cleansing without compromise: the impact of cleansers on the skin barrier and the technology of mild cleansing. *Dermatologic Therapy*, **17** (1) p 14.

Berke, G.S. (1992-1). Intraoperative measurement of the elastic modulus of the vocal fold. Part 1. Device development. *Laryngoscope* **102** (7) p 760-769.

Berke, G.S., Smith, M.E. (1992-2). Intraoperative measurement of the elastic modulus of the vocal fold. Part 2. Preliminary results. *Laryngoscope*, **102** (7) p 770-8.

Chan, R.W., Gray S.D., Titze, I.R. (2001). The importance of hyaluronic acid in vocal fold biomechanics. *Otolaryngology - Head and Neck Surgery*, **124**, (6), p 607-614.

Chan R.W. (2002). Estimation of viscoelastic shear properties of vocal-fold tissues based on time-temperature superposition. *Journal of the Acoustical Society of America*, **110** (3) p1548-1561.

Chan, R.W., Titze, I,R. (1999). Viscoelastic shear properties of human vocal fold mucosa: Measurement methodology and empirical results . *J. Acoustic Society of America*,. **106**, (4), p 2008-2021.

Elsner, P. (2002). Bioengineering of the Skin: Skin Biomechanics. 2002. The Gas Bearing Electrodynamometer and the Linear Skin Rheometer. Boca Raton, CRC Press, chapter 8 ISBN: 0849375215

Karolinska (2004) Center for Hearing and Communication Research, The Karolinska Institute [online], viewed 20th Dec 2007, available from World Wide Web <http://www.ki.se/cfh/research/principle_invest_en.html>

Massachusetts (2005) Center for Laryngeal Research & Rehabilitation, Massachusetts General Hospital [online] viewed 20th Dec 2007, available from World Wide Web http://www.massgeneral.org/voicecenter/research/

Dahlqvist, Å., Gärskog, O., Laurent, C., Hertegård, S., Ambrosio, L., Borzacchiello, A. (2004) Viscoelasticity of Rabbit Vocal Folds after Injection Augmentation. *Laryngoscope*, **114** (1) p 138-142

Duchemin, G., Maillet, P., Poignet, P., Dombre, E., Pierrot, F. (2005). A hybrid position/force control approach for identification of deformation models of skin and underlying tissues. *IEEE Transactions On Biomedical Engineering*, **52** (2) p160-170.

Duflo, S.A., Thibeault, S., Li, W., Xiao, Z., Prestwich, G. (2006). Effect of a synthetic extracellular matrix on vocal fold lamina propria gene expression in early wound healing. *Tissue Engineering*, **12** (11) p 3201-3207.

Ford, C.N., Staskowski, P.A., Bless, D.M. (1995). Autologous collagen vocal fold injection: A preliminary clinical study. *Laryngoscope*, **105** (9) p 944-948.

Fung, Y.C.(1981). Biomechanics: Mechanical Properties of Living Tissues. Springer-Verlag, New York

Halum, S.L., Naidu, M., Delo, D.M., Atala, A., Hingtgen, C.M., (2007). Injection of autologous muscle stem cells (myoblasts) for the treatment of vocal fold paralysis: A pilot study. *Laryngoscope*, **117** (5) p 917-922.

Hayes, W.C., Keer, L.M., Herrmann, G., Nockros, L.F. (1972). Mathematical Analysis For Indentation Tests Of Articular Cartilage. *Journal Of Biomechanics*, **5** (5) p 541-551.

Hertegård, S., Cedervall, J., Svensson, B., Forsberg, K., Maurer, F.H.J.., Vidovska, D., Olivius., Le Blanc, K. (2006). Viscoelastic and histologic properties in scarred rabbit vocal folds after mesenchymal stem cell injection. *Laryngoscope*, **116** (7) p 1248-1254.

Hess M (2006) , Department of Voice, Speech and Hearing Disorders [online]. viewed 20th Dec 2007, available from world wide web <http://www.uke.uni-hamburg.de/kliniken/phoniatrie/index_ENG_33113.php>

Hirano, M., Kakita, Y. (1985). Cover-body theory of vocal fold vibration. In Daniloff RG, editor. Speech Science. San Diego.

Hirano, M. (1983). Growth, development and aging of human vocal folds. In Vocal fold physiology: Contemporary research and clinical issues, edited by D.M. Bless and J.H. Abbs. College Hill Press: San Diego.

Hsiao, T., Wang, C., Chen, C., Hsieh, F., Shau, Y. (2002). Elasticity of Human Vocal Folds measured In Vivo Using Color Doppler Imaging. *Ultrasound in Medicine & Biology*, **28** (9) p 1145-1152

Kaneko, T., Uchida, K., Komatsu, K., Kanesaka, T., Kobayashi, N., Naito, J. (1981). Mechanical properties of the Vocal Fold:measurement in vivo" in Vocal Fold Physiology edited by Steven KN and Hirano M. p 365-376

Kim, K.H., Maguluri, G.N., Pierce, M.C., Burns, J.A., Klein, A., Shishkov, M., Park, B.H., Zeitels, S.M., de Boer, J.F. (2007). Layer Structure of the Vocal Cord, , Endoscopic imaging of the human vocal cords using polarization-sensitive optical coherence tomography, Harvard Medical School, [online] Viewed 20th Dec 2007. available from world wide web <www.massgeneral.org/wellman/people/jdeboer_project_5.asp>

Matts, P.J. (2004). Sensitive Measurement Of Stratum Corneum Mechanical Properties Using The Linear Skin Rheometer. Stratum Corneum IV, Paris

McGlashan, J.A., de Cunha, D.A., Hawkes, D.J., Harris, T.M. (1998). Surface Mapping of the Vibrating Vocal Folds. Proceedings of the 24th World Congress of the International Association of Logopedics and Phoniatrics (IALP), Amsterdam August 1998

Mok, W., Bautista, B., Hoybergm K., Kirnos, P., Subramanayam, K. (2001). Mechanical properties of ageing skin – Stratum Corneum vs. dermal changes. Stratum Corneum III, 12-14th September 2001, Basel Switzerland.

Miller, C.J. (2007). Voice Disorders [online]. viewed 20th Dec 2007, available from world wide web <http://mick.murraystate.edu/cdi624/fall97/disords.htm>

Otolaryngology Our Research, University of Wisconsin, (2007), [online], viewed 20th Dec 2007, available from world wide web <http://www.surgery.wisc.edu/Oto/research/index.shtml>

Perlmann, A.L., Titze, I.R., Donald, S.C. (1984). Elasticity of Canine Vocal Fold Tissue. *Journal of Speech & Hearing research*, **27** (2) p 212-219

Perlmann, A.L., Titze, I.R. (1988). Development of an in-vitro technique for measuring elastic properties of vocal fold tissue. *Journal of Speech & Hearing Research*, **31** (2) p 288-298.

Rawlings, A.V., Matts, P.J. (2005). Stratum Corneum Moisturization at the Molecular Level: An update in relation to the dry skin cycle. *Journal of Investigative Dermatology*, **124** (6) p 1099-1110.

Rodrigues, L. (2001). EEMCO Guidance to the *in vivo* Assessment of Tensile Functional Properties of the Skin. *Skin Pharmacology & Applied Skin Physiology*, **14** (1) p 52-67.

Sulica, L. (2004). Vocal Fold Scar, Voice Medicine. [online] Viewed 20th Dec 2007, available from word wide web <http://www.voicemedicine.com/vocal_fold_scar.htm>

Tamura, E., Kitahara, S., Kohno, N. (2002). Intralaryngeal Application of a Miniturized Ultrasonic Probe. 2002. *Acta Otolaryngology*, **122**, p 92-95

The Nurse (2006) In Depth Larynx Anatomy Overview, [online], viewed 20th Dec 2007, Available from World Wide Web <www.nurse-anesthesia.org/showthread.php?t=361>

Tran, Q.T., Berke, G.S., Gerratt, B.R., Kreiman, J. (1993). Measurement of Young's Modulus in the *In Vivo* Human Vocal Folds. *Annals of Otology, Rhinology and Laryngology*, **102**, (8 I), pp 584-591

United States Patent Application 20040091446.Liquid cleansing composition having simultaneous exfoliating and moisturizing properties

References to my peer-reviewed journal papers and conference presentations and a summary of my contribution to those papers.

[Chhetri 2008] I devised the apparatus, and analysed the data.

[Goodyer 2007-1] I devised the apparatus, the study and mathematics.

[Goodyer 2007-2] I devised the apparatus, assisted in the operating theatre to deploy the device, and analysed the data.

[Goodyer 2007-3] I devised the apparatus, most of the study methods, all of the mathematical analysis, and supervised the project [Goodyer 2006-1] I devised the apparatus and the mathematical analysis.

[Goodyer 2006-2] I devised the apparatus, some of the study methods, and all of the mathematical analysis.

[Goodyer 2003] I devised the apparatus, and a number of the study methods.

[Hess 2006] I devised the apparatus, some of the study methods, and developed the mathematical analysis.

[Dailey 2007] I devised the apparatus and assisted with the development of the methods.

[Hertegård 2006] I devised the apparatus and the development of the analytical methods.

[Hertegård 2004] I devised the apparatus and the development of the analytical methods.

[Licht 2007] I devised the apparatus and assisted with developing the methods.

[Matts 1998] I devised the apparatus, including the electronics and software, and managed the development of the mechanics.

Chhetri, D.K., Berke, G.S., Lotfizadeh, A., **Goodyer, E.N.** (2008). Control Of Vocal Fold Cover Stiffness By Laryngeal Muscles. In The American Laryngological Association, spring meeting, Orlando , May 2008.

Dailey, S.H., Tateya, I., Montequin, D., Welham, N., **Goodyer, E.N.** (2007) Viscoelastic Measurements of Vocal Folds Using the Linear Skin Rheometer (LSR). *Journal of Voice* (online) May 2007.

Goodyer, E.N., Welham, N.V., Choi, S., Yamashita, M., Dailey, S.H. (2007-1) The Shear Modulus of the Human Vocal Fold In A Transverse Direction. *Journal of Voice*. 2007. In Print.

Goodyer, E.N., Müller, F., Licht, A.K., Hess, M. (2007-2). *In Vivo* Measurement of the Shear Modulus of the Human Vocal Fold - Interim Results from 8 Patients. *European Archives of Oto-Rhino-Laryngology*, **264** (6) p 631-635.

Goodyer, E.N., Hemmerich, S., Müller, F., Kobler, J.B., Hess, M. (2007-3). The Shear Modulus of the Human Vocal Fold, Preliminary Results From 20 Larynxes. *European Archives of Oto-Rhino-Laryngology*, **264** (1) p 45-50

Goodyer, E.N., Muller, F., Bramer, B., Chauhan, D., Hess, M. (2006-1) *In Vivo* Measurement of the Elastic Properties of the Human Vocal Fold. *European Archives of Oto-Rhino-Laryngology*, **263** (5) p 445-462.

Goodyer, E.N., Hemmerich, S., Mueller, F., Licht, A.K., Hess, M. (2006-2). Characterisation of the Elasticity of the Human Vocal Fold using Electromechanical Measurement. Techniques. In 7th International Conference Advances in Quantitative Laryngology, Voice and Speech Research, Gronningen, October 2006.

Goodyer, E.N., Gunter, H.,Masaki, A., Kobler, J. (2003). Mapping the Visco-elastic Properties of the Vocal Fold, AQL 2003, Hamburg.

Hess, M., Muller, F., Kobler, J., Zeitels, S., **Goodyer, E.N.** (2006). Measurements of Vocal Fold Elasticity Using the Linear Skin Rheometer. *Folia Phoniatrica et Logopaedica*, **58** (3) p. 207-216

Hertegård, S., Dahlqvist, Å., **Goodyer, E.N.**, Maurer. (2006). Viscoelastic Measurements After Vocal Fold Scarring In Rabbits– Short Term Results After Hyaluronan Injection. *Acta Oto-Laryngologica* , **126** (7) p. 758-763

Hertegård, S., Dahlqvist, Å., **Goodyer, E.N.**, Maurer, E. (2004). Viscoelasticity In Scarred Rabbit Vocal Folds After Hyaluronan Injection - short term results. AAO-HNSF/ARO Research Forum during the 2004Annual Meeting of the American Academy of Otolaryngology-Head and Neck Surgery Foundation, New York, New York, September 19-22, 2004.

Licht, A.K., **Goodyer, E.N.**, Müller, F., Kobler, J.B., Hess, M. (2007). The Anisotropic Nature of the Vocal Fold. Pan European Voice Conference, Groningen August 2007.

Matts, P.J., **Goodyer, E.N.** (1998) A New Instrument to measure the mechanical properties of the human stratum corneum. *Journal of Cosmetic Science*, **49** (5) p 321-323.

CONTROL OF VOCAL FOLD COVER STIFFNESS BY LARYNGEAL MUSCLES

Dinesh K. Chhetri, MD, Gerald S. Berke, MD, Ali Lotfizadeh, MD, Eric Goodyer, MSc
Division of Head and Neck Surgery, Department of Surgery, UCLA School of Medicine Los Angeles, California 90095 USA (D.K.C., G.S.B., A.L.) and Department of Computer Science and Engineering, DeMontfort University, Leicester, United Kingdom

Corresponding author and reprint requests to:

Dinesh K. Chhetri, MD
62-132 CHS, Head & Neck Surgery
Mailcode 162418
UCLA School of Medicine
Los Angeles, CA 90095
Tel: (310) 794-4225
Fax: (310) 206-1393
E-mail: dchhetri@mednet.ucla.edu

This study was an oral presentation at the 2008 Annual Meeting of the American Laryngological Association, Orlando, Florida, May 2, 2008

ABSTRACT

Objectives: The objective of this study is to perform preliminary measurements of the shear modulus of the vocal fold cover layer during intrinsic laryngeal muscle contraction.

Study Design: Shear modulus was measured in an *ex vivo* human larynx and an *in vivo* canine larynx.

Methods: A modified linear skin rheometer adapted for laryngeal viscoelasticity measurement applied shear stress to the mid-membranous vocal fold medial surface via an attached suction probe. The measured probe displacement achieved at each level of laryngeal muscle contraction was used to derive the shear modulus using a simple shear model. In the *ex vivo* human larynx, lateral cricoarytenoid (LCA) muscle and cricothyroid (CT) muscle activity was simulated with gradual tension of arytenoid adduction sutures and manual cricothyroid approximation, respectively. In the *in vivo* canine, graded current applied to the recurrent laryngeal nerves (RLN) the superior laryngeal nerves (SLN), respectively.

Results: Baseline shear modulus was calculated between 1076 to 1307 pascals. In the *ex vivo* human larynx, the shear modulus increased gradually to maximum of 1.6 times baseline value with graded arytenoid adduction and maximum of 3.7 times baseline value with manual cricothyroid approximation. In the *in vivo* larynx, the shear modulus increased to a maximum of 1.6 times baseline value with RLN stimulation and 2.5 times baseline value with SLN stimulation.

Conclusions: While both RLN and SLN stimulation increase cover stiffness, cricothyroid muscle activity results in the most dramatic increase.

INTRODUCTION

The ability to control the fundamental frequency (F0) of voice is critical to human communication, expression, and singing. Hirano (1974) laid the groundwork for understanding of F0 control when he introduced the "body-cover" theory of phonation. He proposed that the histology of the vocal fold lends itself to division into two distinct layers: the "body" layer consisting of the thyroarytenoid (TA) muscle and the adjacent deep collagen fibers, and the "cover" layer consisting of the superficial lamina propria and the epithelium. The body layer is the "active" layer as it is able to shorten with neuromuscular stimulation while the cover layer is the "passive" layer whose tension is affected by the actions of the intrinsic laryngeal muscles. The cover layer has elastic properties necessary for the propagation of mucosal waves that is ultimately responsible for the quality of the generated sound.

The body-cover model of phonation facilitated an explanation of F0 control based on tension or stiffness of the vocal fold. In this model, cover layer stiffness is primarily responsible for F0 control and the TA and the cricothyroid (CT) muscles change the stiffness of the cover layer by altering its length. Contraction of the CT muscle elongates and stiffens the cover layer, thus increasing F0, while activation of the TA muscle shortens the body layer while concurrently creating a slack in the cover layer, thus decreasing F0. This model provides antagonistic roles for TA and CT muscles, and laid the groundwork for F0 control based on variable levels of TA and CT muscle contraction. Interestingly, this also allows for the theoretic possibility to obtain the same F0 at various combinations of TA and CT activation level. While other parameters such as subglottic pressure also affect F0, these

other factors are considered minor compared to the activity of the TA and CT muscle (Titze 1989).

The body-cover model has been further expanded upon using mathematical models where relative contributions of the TA and CT in F0 control have been assigned (Fujimura (1981), Titze (1988), and Lowell (2006)). Whereas computational models of F0 control have become more complex and sophisticated, *in vivo* data supporting these models is severely lacking. Current computational models are based on basic assumptions derived from measurements of the anatomic, histologic, acoustic, aerodynamic and biomechanical properties of the larynx, and consider the overall stiffness of the cover layer the most important factor in controlling F0. However, there is a paucity of *in vivo* measurements of vocal fold stiffness and there are no *in vivo* measurements of stiffness with concurrent laryngeal muscle activation. Such *in vivo* investigations have been hampered by lack of a reliable tensionometer to measure stiffness.

Study of vocal fold viscoelasticity has applications beyond the study of F0 control. A reliable quantitative method of measuring vocal fold pliability is necessary to understand vocal fold changes induced by diseases such as vocal fold edema, scar, and neoplasm. A reliable methodology is also necessary to objectively assess the results of vocal fold treatments such as laryngeal reinnervation, lamina propria replacement therapy, and tissue engineering. This study is a preliminary report on the measurement of vocal fold viscoelasticity with laryngeal muscle activation. While the ultimate goal is a systematic and detailed measurements of *in vivo* vocal fold stiffness with isolated as well as combinations of TA and CT muscle activation levels, this study is a preliminary step testing the feasibility of

and obtaining reliable measurements using the LSR with various levels of intrinsic laryngeal muscle activation.

MATERIALS AND METHODS

Ex vivo larynx: An adult human larynx was harvested from an autopsy case less than 48 hours post-mortem and kept quick-frozen at -80°C until the day before the experiment. The larynx was then removed from deep freeze and allowed to thaw overnight at -4°C in the refrigerator then kept soaked in isotonic saline in the morning of the experiment until it was thawed soft. The supraglottic structures, including the epiglottis and the false vocal cords, were excised. Arytenoid adduction sutures (3-0 nylon) were then placed through the left muscular processes and brought out through the anterior inferior thyroid lamina to adduct the vocal fold, thus simulating lateral cricoarytenoid (LCA) muscle contraction. A 3-0 nylon suture was placed circumferentially through the anterior cricoid and the anterior inferior border of the thyroid cartilages for manual cricothyroid approximation, thus simulating CT muscle contraction. The larynx was then mounted horizontally on a custom designed laryngeal holder for experimental measurements (Figure 1). Increasing weights in 10 gram increments were placed on the adduction sutures using a pulley mechanism to simulate increasing vocal fold adduction. The cricothyroid approximation suture was tightened to simulate CT muscle action and the shear modulus measured at baseline (no suture tension), medium (CT approximation midway between baseline and maximal), and maximum tension (maximum CT approximation possible with tightening of the CT approximation sutures). The larynx was periodically sprayed with saline to keep the surface moist.

In vivo canine model: A mongrel canine (25 kg) was used. The animal study was performed in accordance with the PHS Policy on Humane Care and Use of Laboratory Animals, the NIH Guide for the Care and Use of Laboratory Animals, and the Animal Welfare Act. Our institutional Animal Research Committee approved the research protocol. After anesthesia was induced with intravenous thiopental the animal was orally intubated and placed under halothane general anesthesia.

A vertical midline skin incision was then made on the anterior neck to widely expose the larynx and the trachea. Bilateral recurrent laryngeal nerves (RLNs) and superior laryngeal nerves (SLNs) were isolated. A low tracheotomy was performed for intra-operative ventilation and the oral endotracheal tube was removed. The larynx was exteriorized into the neck by first performing a suprahyoid pharyngotomy and division of the pharynx circumferentially at this level. The larynx was slightly lifted off the neck and fixed in placed using a custom designed laryngeal holder. This exposure allowed placement of the LSR probe on the vocal fold externally and unhindered by oral and pharyngeal structures. Custom designed monopolar electrodes with silicone insulation were applied to the isolated nerves bilaterally. The electrodes were attached to a constant current nerve stimulator (WR Medical Electronics Co., Model 2SLH, St. Paul, Minnesota). The nerves were stimulated at 80 Hz, 1.5 msec pulses, at approximately 0.06 mA increments.

The Linear Skin Rheometer: Measurements of the vocal fold shear modulus were obtained using a modified Linear Skin Rheometer (LSR) [Matts 1998]. This device was originally developed to measure the biomechanical properties of the stratum corneum of skin, and was identified [Goodyer 2003] as a potential method to quantify the viscoelastic properties of the human vocal fold, and to quantify the effectiveness of tissue augmentation

therapy. This device has been used to measure vocal fold viscoelasticity in a variety of reports (Goodyer 2007-3, 2006-2, Hess 2006, Licht 2007, Hertegaard 2006, 2004, Dailey 2007, Goodyer 2007-1) and the the device concept has also been successfully adapted to measure human vocal folds in-vivo (Goodyer 2007-2, 2006-1).

The LSR (Figure 2) is a programmable tensionometer capable of measuring displacement to a resolution of 4 μm using a linear variable displacement transducer (LVDT), and force to a resolution of 20 mg using a built-to-order force sensor with a full-scale reading of 50 g. The force sensor can be attached to the tissue under test using a variety of special probes. For this study, a suction cannula probe with a right angle tip and 2 mm diameter was used and the left vocal fold was selected for measurement. The LSR with the probe was aligned at right angles to the longitudinal axis of the vocal fold such that the there was no gap between the tip of the suction probe and the superior medial vocal fold epithelium, at which time 50mbar of suction was applied. The suction force was then released and the instrument zeroed prior to measurement. While some stress is applied to the vocal fold during this maneuver, this arrangement minimizes the effect and also maintains the probe in position. We found from experimentation with various probe designs that the suction probe was the most reliable at maintaining position after vocal fold stimulation. Also the LSR operates by applying a cyclical force and any DC offset due to initial loading is removed. The force sensor and suction attachment are gently cycled in a sinusoidal manner such that a cyclical shear force of one gram is applied to the vocal fold.

Calculation of the Shear Modulus: The LSR applies a known amount of force (one gram in this study) and measures the displacement achieved, and this force/displacement data is used to derive the "Dynamic Spring Rate" (DSR). In mechanical engineering the term

DSR defines the amount that a spring changes in length when a unit of force is applied to it. It is not a time dependant term. By applying knowledge of the probe geometry, it is possible to estimate the stiffness, or shear modulus, of the vocal fold. Using a simple shear model the geometry of this setup was defined as follows. The shear force (F) applied by the LSR is transmitted to the vocal fold cover over the area determined by the probe diameter (A). The displacement (P) is the resultant shear strain, which is tangential to the epithelial surface, and is measured by the LSR. The thickness of the lamina propria layer (H) is about 1 mm for the human larynx and 2 mm for the canine larynx. Thus an estimate for the shear modulus (G) is derived as further elaborated in the appendix.

RESULTS

In the *ex vivo* human larynx, with manual cricothyroid approximation, the shear modulus increased from a baseline value (1307 Pa) to 3.7 times baseline value (4786 Pa) at maximal CT approximation (Figure 3). With gradual increase in the force of arytenoid adduction with graded increase in weights, the vocal fold shear modulus gradually and linearly increased from a baseline value (1076 Pa) to a maximum of 1.6 times baseline value (1723 Pa) at an adduction force of 60 grams, and thereafter remained relatively unchanged with increasing weight (Figure 4).

In the *in vivo* canine larynx, with graded neuromuscular stimulation of bilateral SLNs, the vocal fold shear modulus remained stable around the baseline values (1134 Pa) until stimulation level reached 0.23 mA. At 0.27 mA a hint of cricothyroid activity was noted. Shear modulus increased from 0.23 mA to 0.31 mA to a maximum of 2.5 times baseline value (2818 Pa), and thereafter remained stable or slightly decreased with further stimulation.

(Figure 5). When graded neuromuscular stimulation was applied to the RLN, the vocal fold shear modulus remained stable around the baseline value (1077 Pa) until stimulation level 0.21 mA. At this point the onset of visible vocal fold motion was also appreciated. With further stimulation shear modulus increased to a maximum of 1.6 times baseline (1762 Pa) at 0.32 mA, and thereafter remained stable or slightly decreased with further increasing stimulation (Figure 6).

DISCUSSION

The results of this study indicate that while both RLN and SLN stimulation increase cover stiffness, cricothyroid muscle activity results in the most dramatic increase. In the human ex vivo larynx, CT approximation was applied manually and an almost four fold increase in shear modulus was achieved between baseline and maximal CT approximation. In the canine larynx, in vivo SLN stimulation could achieve only a 2.5 fold increase in the shear modulus despite maximal stimulation. The canine response is more physiologic because whereas with manual approximation it is physically possible to nearly completely appose the cricoid and the thyroid cartilages anteriorly this is not possible physiologically. The cricothyroid muscles insert at the edges of the thyroid and the cricoid cartilages and during muscular contraction the CT muscle will shorten but not to the degree that the cricoid and the thyroid cartilages would approximate completely.

Control of vocal fold stiffness via RLN stimulation appears more complex. Adductory muscles innervated by the RLN include the interarytenoid (IA), lateral cricoarytenoid (LCA), and the TA muscles. In the ex vivo human larynx, gradual increase in the force of arytenoid adduction lead to gradual increase in shear modulus to a maximum

increase of 1.6 times baseline value. This result is logical because during arytenoid adduction the vocal process rotates medially and posteriorly, thus adducting and lengthening the vocal fold, which would account for the increase in shear modulus. However, no furthere lengthening can take place once the limits of cricoarytenoid joint rotation is reached and further force of adduction does not lead to additional increase in the shear modulus. Interestingly, the increase in shear modulus with RLN stimulation also reached a maximal value 1.6 times baseline values. The *ex vivo* experiment would suggest that it would be possible to reach this increase in the shear modulus with arytenoid adduction (LCA action) alone. This could explain the excellent response to arytenoid adduction surgery for unilateral vocal fold paralysis (ref Chhetri). However, patients who undergo combined adduction and laryngeal reinnervation surgery for unilateral vocal fold paralysis do report an additional improvement three to six months after surgery, presumably when the laryngeal reinnervation kicks in. Therefore, what role does the TA play in modulating the cover stiffness? In a previous study from our laboratory, a gradual increase in F0 was seen with graded stimulation of the TA muscle in the present of constant LCA stimulation that maintained posterior glottic closure (Choi et al). While it seems reasonable to assume that both TA and LCA are contributing to cover stiffness their individual contributions are unknown. It is also entirely possible that the medial bulging of the vocal fold during TA activity affects phonation via mechanisms separate from viscoelastic changes of the cover layer, such as improving closure. Future studies measuring cover stiffness with isolated stimulation of adductor branches could delineate the role of each muscle.

The baseline shear modulus is similar in human and the canine larynx. The canine larynx is the closest match to the human larynx, both in its overall dimensions as well as

histopathologic characteristics (ref). The canine F0 (low 200 Hz range) is also similar to human larynx. Therefore, perhaps the similarity in the shear modulus between these larynges result from their overall common characteristics. It is possible that animals with higher F0 would have higher shear modulus.

CONCLUSION

Both RLN and SLN stimulation lead to increased viscoelasticity of the vocal fold. However, a more dramatic change in stiffness is seen with CT stimulation. Therefore, CT likely plays a more important role in F0 control.

REFERENCES

[Dailey 2007]
Dailey SH, Tateya I, Montequin D, Welham N, Goodyer EN. 2007. Viscoelastic Measurements of Vocal Folds Using the Linear Skin Rheometer (LSR). *Journal of Voice* (online) May 2007.

[Goodyer 2007-1]
Goodyer EN, Welham NV, Choi S, Yamashita M, Dailey SH. 2007-1. The Shear Modulus of the Human Vocal Fold In A Transverse Direction. *Journal of Voice*. 2007. In Print.

[Goodyer 2007-2]
Goodyer EN, Müller F, Licht AK and Hess M. 2007-2. In Vivo Measurement of the Shear Modulus of the Human Vocal Fold - Interim Results from 8 Patients. *European Archives of Oto-Rhino-Laryngology*, 264 (6) pp 631-635.

[Goodyer 2007-3]
Goodyer EN, Hemmerich S, Müller F, Kobler JB, Hess M. 2007-3. The shear modulus of the human vocal fold, preliminary results from 20 larynxes. *European Archives of Oto-Rhino-Laryngology*, 264 (1) pp 45-50

[Goodyer 2006-1]
Goodyer EN, Muller F, Bramer B, Chauhan D, Hess M. 2006-1. In Vivo Measurement of the Elastic Properties of the Human Vocal Fold. *European Archives of Oto-Rhino-Laryngology*, 263 (5) pp 445-462.

[Goodyer 2006-2]
Goodyer EN, Hemmerich S, Mueller F, Licht A-K, Hess M. 2006-2. Characterisation of the Elasticity of the Human Vocal Fold using Electromechanical Measurement. Techniques. In 7th International Conference Advances in Quantitative Laryngology, Voice and Speech Research, Gronningen, October 2006.

[Goodyer 2003]
Goodyer EN, Gunter H,Masaki A, Kobler J. 2003. Mapping the Visco-elastic Properties of the Vocal Fold, AQL 2003, Hamburg.

[Hayes 1972]
Hayes WC, Keer LM, Herrmann G., Nockros LF, Mathematical Analysis For Indentation Tests Of Articular Cartilage. J of Biomechanics. 1972;5,5,541-551

[Hertegard 2006]
Hertegård S, Dahlqvist Å, Goodyer EN, Maurer. 2006. Viscoelastic Measurements After Vocal Fold Scarring In Rabbits– Short Term Results After Hyaluronan Injection. *Acta Oto-Laryngologica* , 126 (7) pp. 758-763

[Hertegard 2004]
Hertegård S, Dahlqvist Å, Goodyer EN, Maurer E. 2004. Viscoelasticity In Scarred Rabbit Vocal Folds After Hyaluronan Injection - short term results. AAO-HNSF/ARO Research Forum during the 2004Annual Meeting of the American Academy of Otolaryngology-Head and Neck Surgery Foundation, New York, New York, September 19-22, 2004.

[Hess 2006]
Hess M, Muller F, Kobler J, Zeitels S, Goodyer EN. 2006. Measurements of Vocal Fold Elasticity Using the Linear Skin Rheometer. *Folia Phoniatrica et Logopaedica*, 58 (3) pp. 207-216

[Licht 2007]
Licht, A-K, Goodyer EN, Müller F,Kobler JB,Hess M. 2007. The anisotropic nature of the vocal fold. Pan European Voice Conference, Groningen August 2007.

[Matts 2998]
Matts PJ, Goodyer EN. 1998. A New Instrument to measure the mechanical properties of the human stratum corneum. *Journal of Cosmetic Science*, 49 (5) pp 321-323.

Appendix

Derivation of Shear Modulus

A sinusoidal force F is applied to the material under test and the resultant displacement X is logged.

(1) $F = F_{max}Sin(t)$

(2) (2) $X = X_{max}Sin(t+\tau)$

Where
F = instantaneous force
F_{max} = the maximum force
t = time
X = instantaneous displacement
X_{max} = the maximum displacement
τ = the phase shift in radians.

The DSR of the tissue is defined as F max / X max, and is expressed in g/mm. As we are not using the time dependant information associated with the sinusoidal nature of the applied force we can substitute F for F_{max} and X for X_{max}. DSR can then be used to estimate the shear modulus of the displaced vocal fold tissue using knowledge of the geometry of the test site, as follows:

The stress σ is the applied force F_{max} per unit area A given by

$$(2)\ \sigma = F_{max} / A$$

The resultant strain ε is given by tangential displacement X_{max} per material thickness H.

$$(3)\ \varepsilon = X_{max} / H$$

Shear modulus G is defined as stress per unit strain

$$(4)\ G = \sigma / \varepsilon$$

$$(5)\ G = (F_{max} / X_{max}) * (H / A)$$

As $DSR = F_{max} / X_{max}$ then

$$(6)\ G = DSR * H / A$$

It is important to note that this simple shear model does not make any allowance for the attached tissue, which is also subjected to shear stresses due to displacement of the tissue directly underneath and surrounding the suction attachment. This effect drops off rapidly as the force transmitted through a solid is inversely related to distance. However, a rigorous mathematical solution to describe the elastic processes involved has not been published. In the absence of a mathematical solution for the shear modulus of tissue attached to other tissue, we incorporated a simple correction derived experimentally based on a widely accepted mathematical model developed by W.C. Hayes. This model derives shear modulus from indentation data [Hayes 1972]. We first evaluated this correction methodology using data collected from 40 human hemilarynges at UKE [Goodyer 2006-2], which were tested using both the Hayes indentation method and the LSR. The data sets from the two methods correlated well when the surface area of attachment used to analyse the LSR data was increased by 0.75 mm in all dimensions. Based on these results, we employed a comparable correction to the data in this study by increasing the diameter of the area of attachment from 2 mm by 1.5 mm to 3.5 m

Figure 1

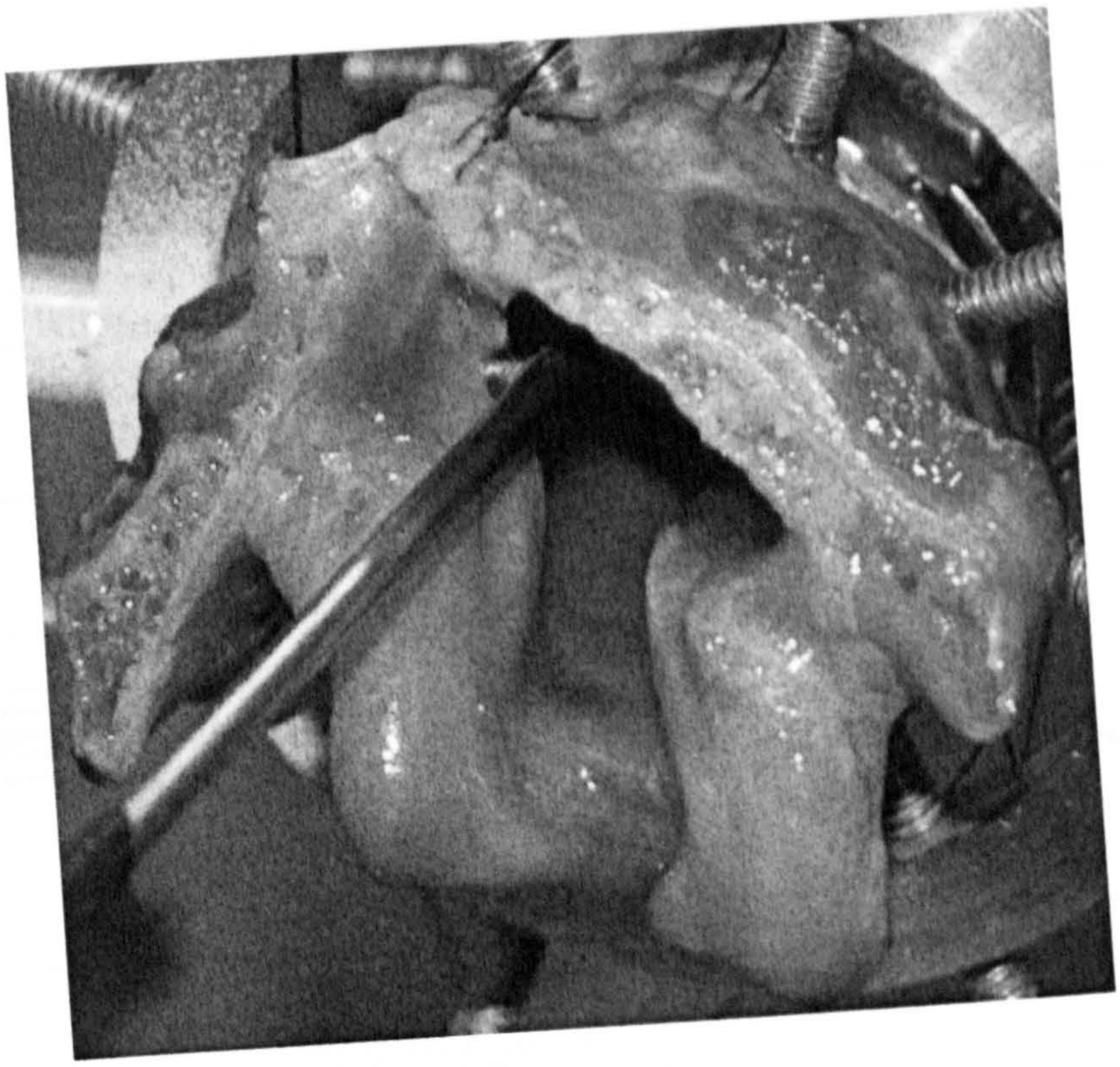

Figure 2

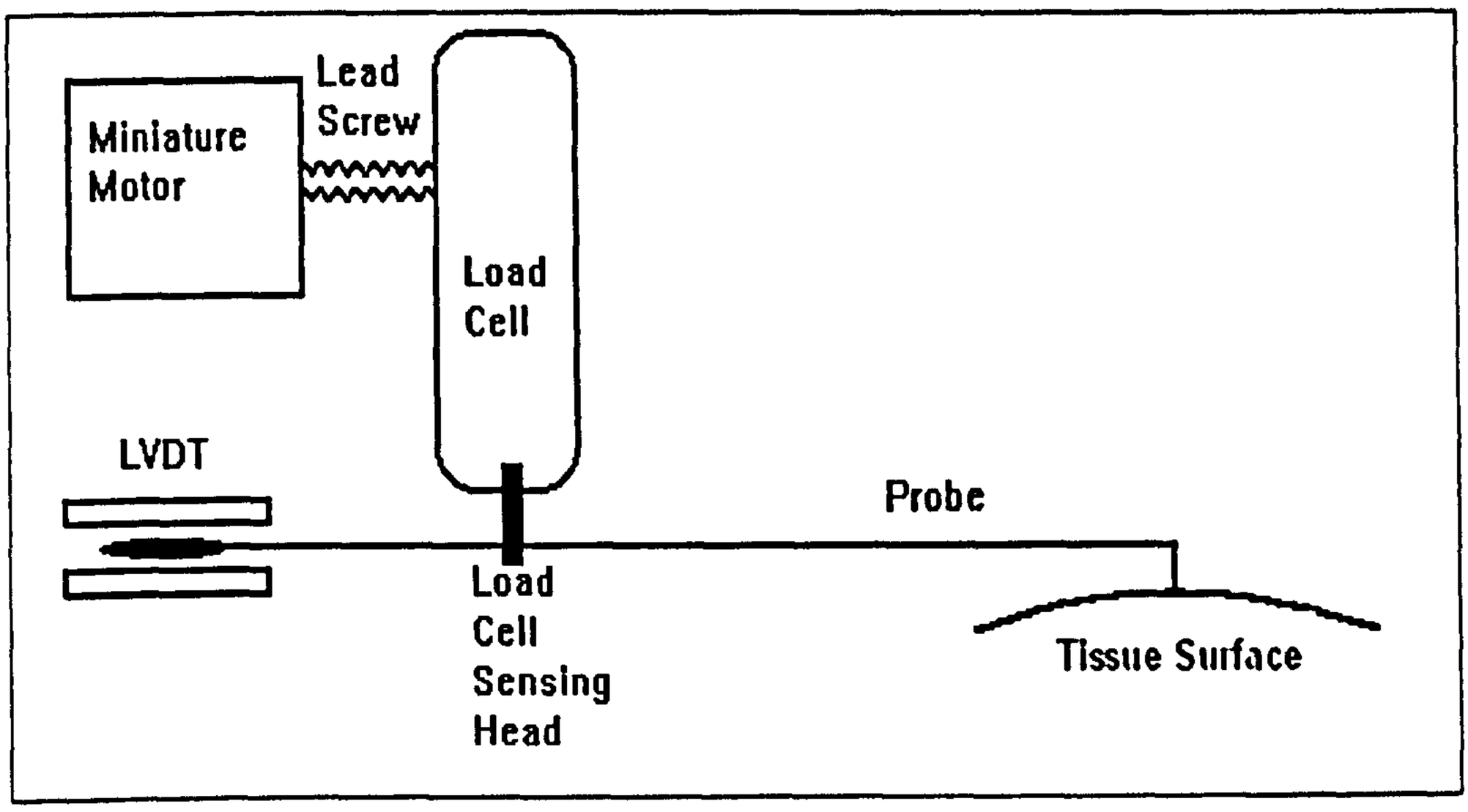
Miniature Motor
Lead Screw
Load Cell
LVDT
Probe
Load Cell Sensing Head
Tissue Surface

Figure 3

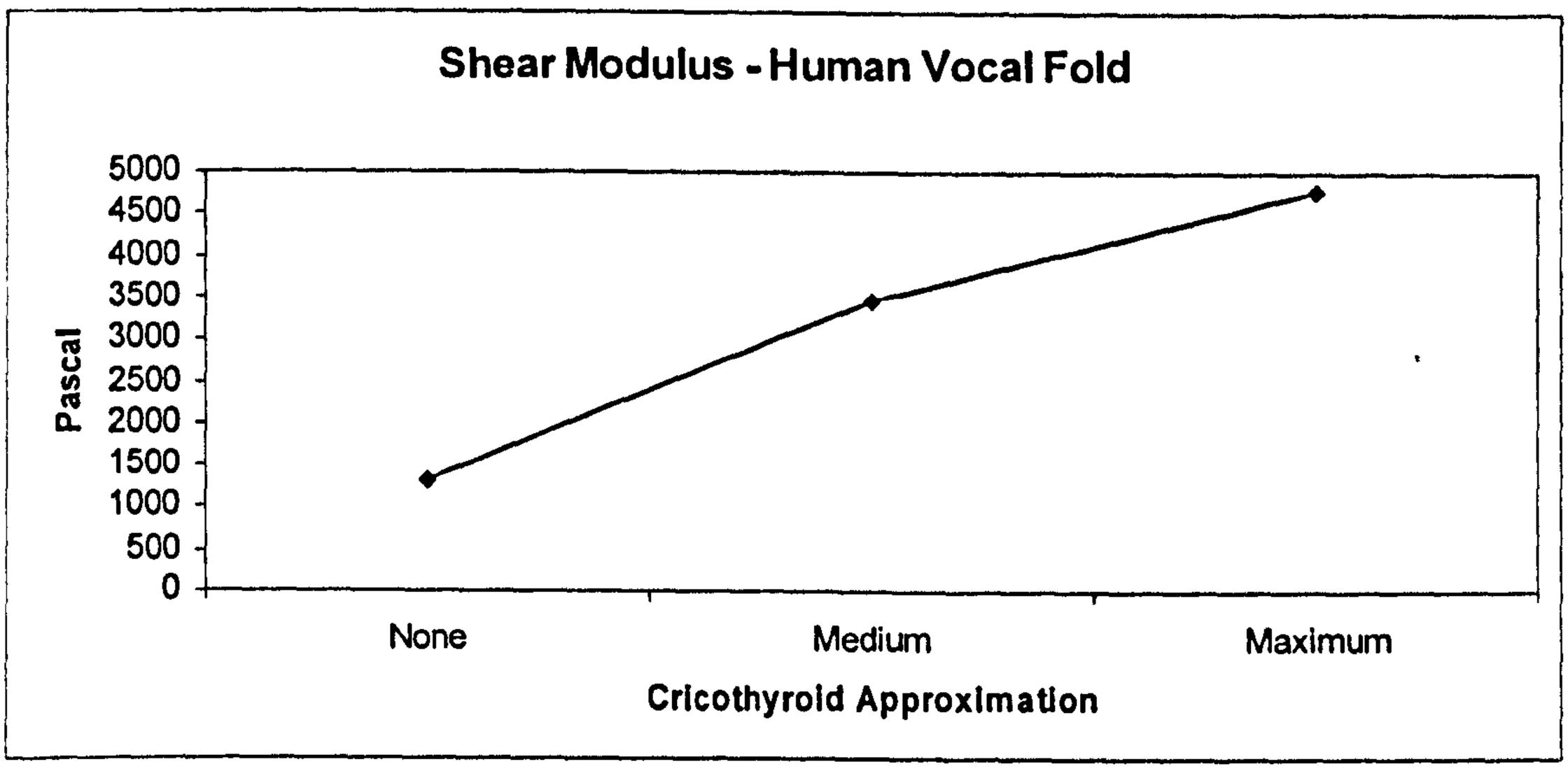

Figure 4

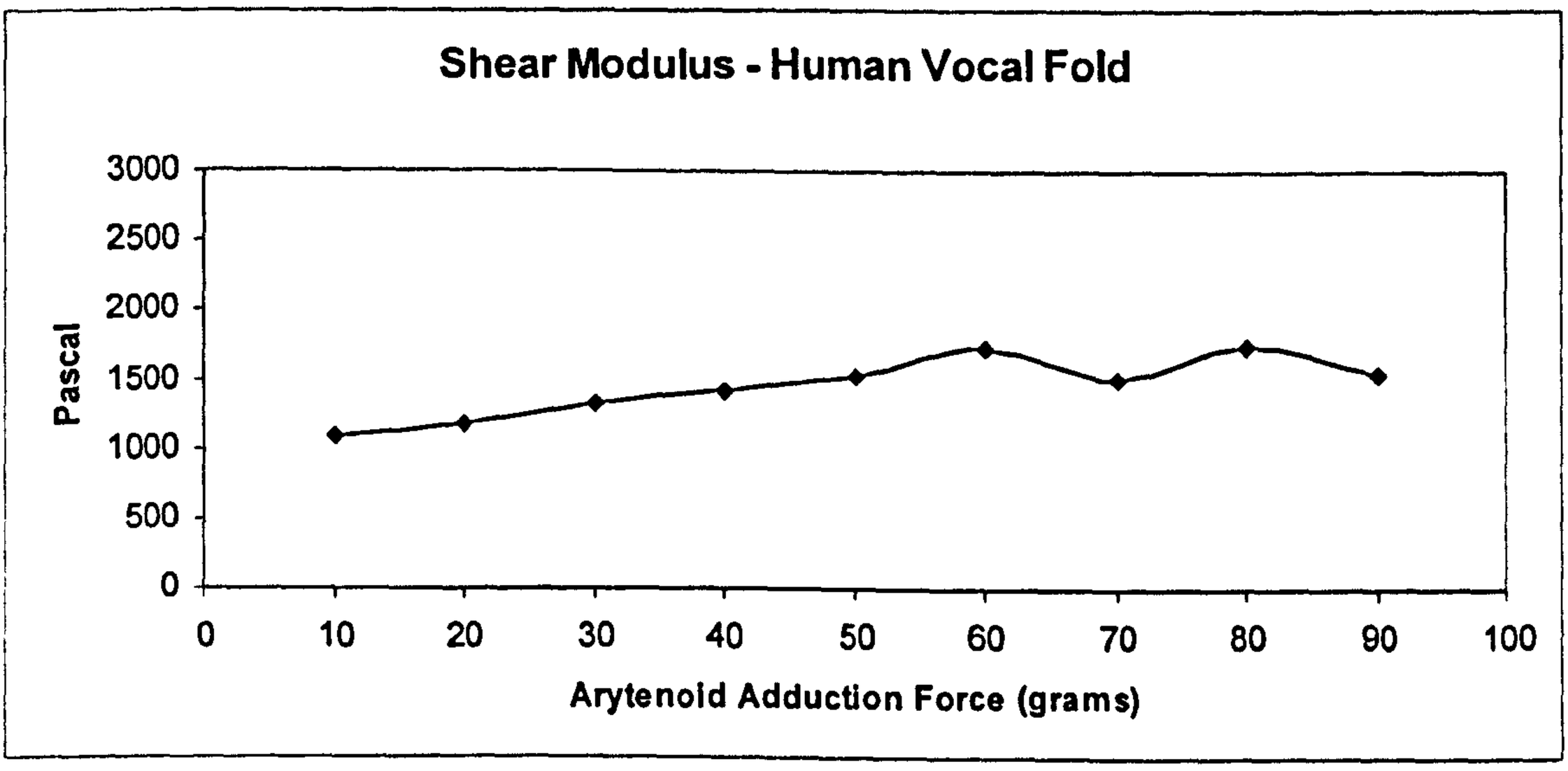

Figure 5

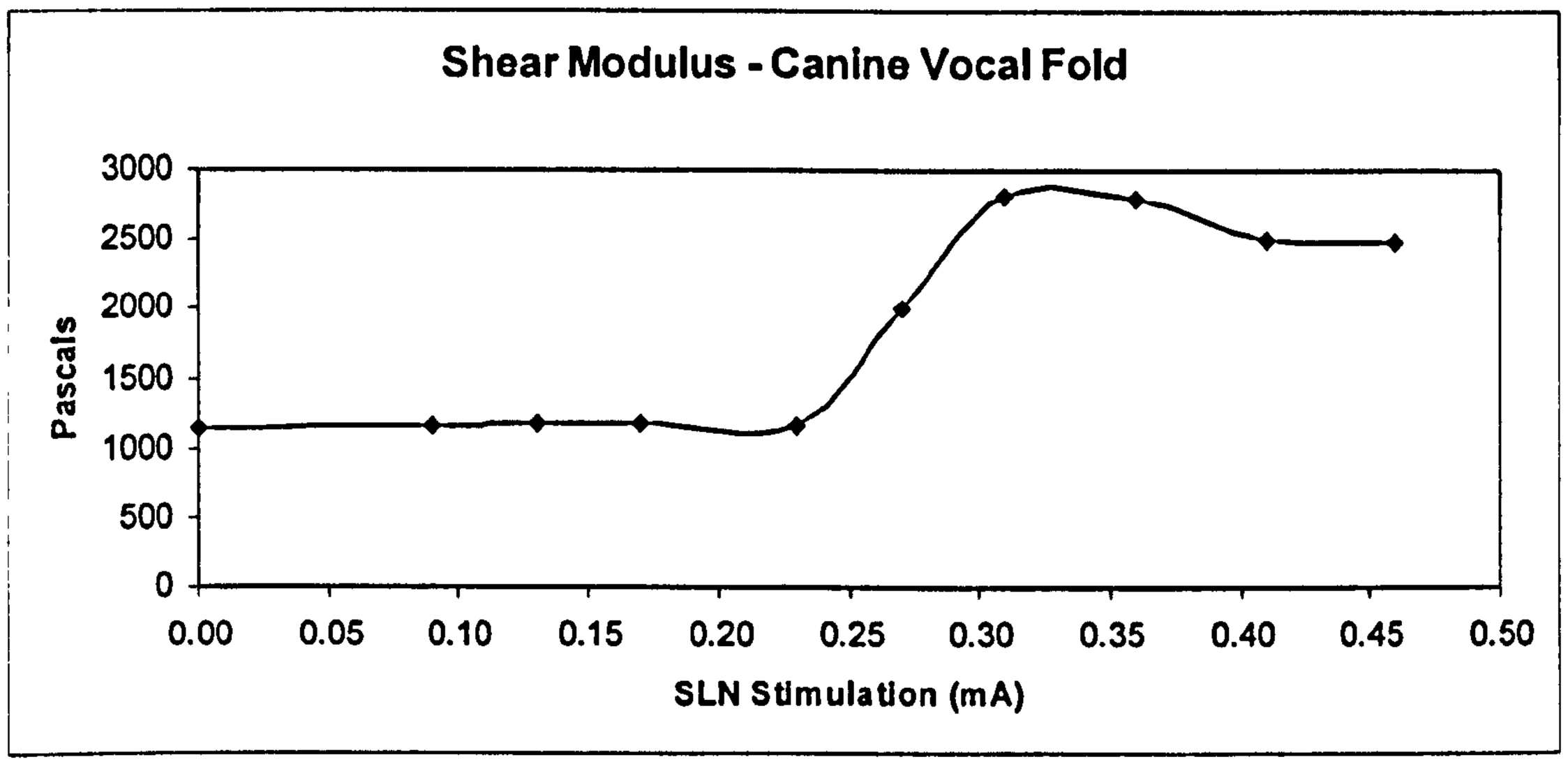

Figure 6

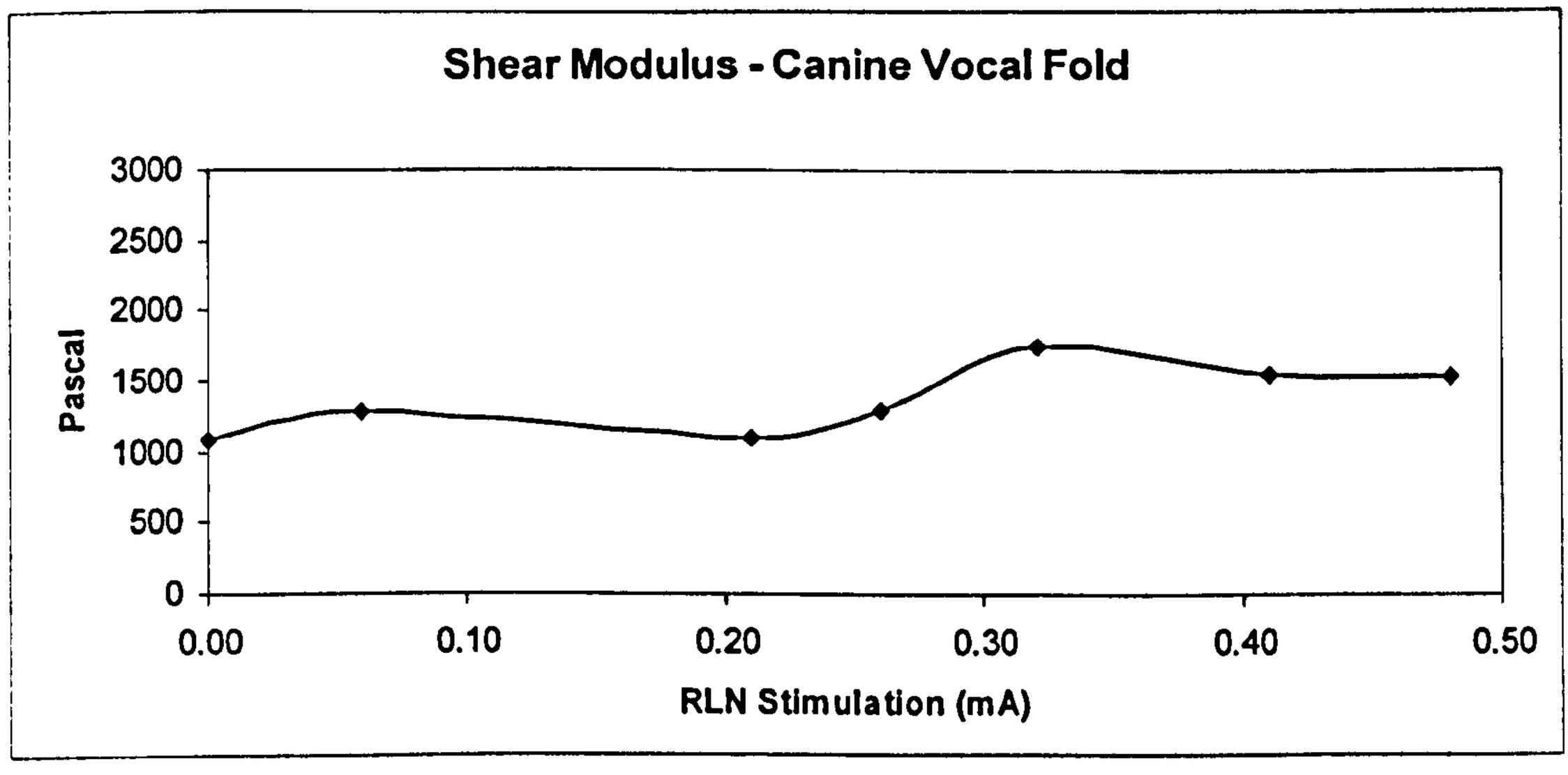

The Shear Modulus of the Human Vocal Fold in a Transverse Direction

*Eric Goodyer, †Nathan V. Welham, †Seonghee Choi, †Masaru Yamashita, and †Seth H. Dailey

Leicester, United Kingdom and †Madison, Wisconsin

Summary: The aim of this study was to measure the shear modulus of the vocal fold in a human hemilarynx, such that the data can be related to direction of applied stress and anatomical context. Dynamic spring rate data were collected using a modified linear skin rheometer using human hemilarynges, and converted to estimated shear modulus via application of a simple shear model. The measurement probe was attached to the epithelial layer of the vocal fold cover using suction. A sinusoidal force of 3 g was applied to the epithelium, and the resultant displacement logged at a rate of 1 kHz. Force measurement accuracy was 20 μg and position measurement accuracy was 4 μm. The force was applied in a transverse direction at the midmembranous point between the vocal process and the anterior commissure. The shear modulus of the three female vocal folds ranged from 814 to 1232 Pa. The shear modulus of the three male vocal folds ranged from 1021 to 1796 Pa. These data demonstrate that it is possible to obtain estimates for the shear modulus of the vocal fold while preserving anatomical context. The modulus values reported here are higher than those reported using parallel plate rheometry. This is to be expected as the tissue is attached to surrounding structures, and is under natural tension.

Key Words: Elasticity—Vocal fold—Rheometry—Shear modulus.

INTRODUCTION

Knowledge of the biomechanical properties of the vocal fold is an essential requirement for researchers seeking to develop mathematical models of phonation,[1] and to provide benchmarks against which novel medical and surgical procedures can be objectively assessed. Biomechanical properties can be expressed in many different ways, and one widely accepted property is the material's shear modulus (Figure 1). A material under stress has two flat surfaces, typically a rectangle or a column; one surface is fixed. A force F is applied to the upper surface such that the material deforms as shown. The stress (σ) is defined as the amount of

Accepted for publication September 19, 2007.

From the *Department of Computer Science and Engineering, DeMontfort University, Leicester, United Kingdom; and the †Division of Otolaryngology, Department of Surgery, University of Wisconsin School of Medicine and Public Health, Madison, Wisconsin.

Address correspondence and reprint requests to Eric Goodyer, Department of Computer Science and Engineering, DeMontfort University, Gateway 5.11, Leicester LE1 9BH, United Kingdom. E-mail: eg@dmu.ac.uk

Journal of Voice, Vol. ■, No. ■, pp. ■
0892-1997/$34.00

doi:10.1016/j.jvoice.2007.09.006

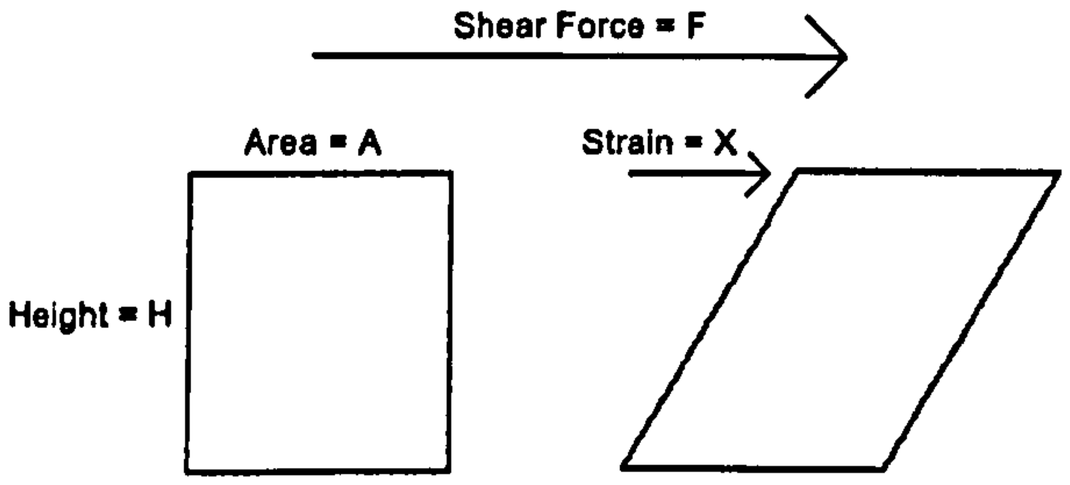

FIGURE 1. Simple shear model.

force applied divided by the surface area to which it is applied.

$$\sigma = \frac{F}{A}, \tag{1}$$

where A is the surface area.

The strain (ε) is defined as the maximum tissue displacement X divided by the thickness of the tissue H.

$$\varepsilon = \frac{X}{H}. \tag{2}$$

The shear modulus G is the ratio of stress to strain.

$$G = \frac{\sigma}{\varepsilon} \tag{3}$$

The value of G in effect defines how much a substance will deform when a force is applied to it. It is sometimes called "stiffness," as a "stiff" material will distort less than a "soft" material. Another common measurement is the Young's modulus (E), which defines how much a material is extended when a force is applied to it. There is a simple formula that relates E to G.

$$G = \frac{E}{2(1+\nu)} \tag{4}$$

where ν is Poisson's ratio, which is a measure of the compressibility of a material. Human tissue is almost incompressible; and ν is usually simplified to be 0.5 such that

$$G = \frac{E}{3} \tag{5}$$

Shear and Young's moduli are used to predict how the tissue moves when subjected to external forces. For example, the change in vocal fold length when muscular force is applied as a result of stimulation of the recurrent laryngeal nerve can be derived from knowledge of the Young's modulus. Another important physical property is the efficiency of the transfer of energy across boundaries, such as from aerodynamic into mechanical vibratory energy; which is directly related to the materials' shear modulus. Knowledge of a tissue's modulus therefore enables us to predict how it will work, and to develop rigorous mathematical models of phonation.

Research teams in Europe, the USA, and Japan are actively developing techniques to repair vocal fold tissue that has been damaged by scarring and other pathologies. Current approaches involve the use of hyaluronic acid implants,[2–6] growth factors,[7–10] and mesenchymal stem cells[11,12] to stimulate tissue regeneration and improve wound healing outcomes. The ability to measure the biomechanical properties of the vocal fold without dissecting it out of anatomical context is an essential pre-requisite to determining the viability of any new tissue repair technique. A valid and reliable solution to this measurement challenge could form the basis of an *in vivo* tool for the biomechanical assessment of vocal fold tissue injury and therapeutic outcomes.

Although many research teams have presented vocal fold viscoelasticity data obtained from excised vocal fold tissue, few have reported data obtained from human larynges. Further, most published approaches have inferred modulus from secondary phenomena. Kaneko et al[13] and Tamura et al[14] reported data collected with ultrasound technology, but did not derive elastic moduli. Hsiao et al[15] reported the use of color Doppler imaging. McGlashan et al[16] used stroboscopy to perform measurements of mucosal wave velocity. Only Tran et al[17–19] have deployed a method that directly measures vocal fold modulus *in vivo*. Their groundbreaking series of studies were completed in 1993, but were limited by a cumbersome apparatus.

Recently, a team based at Universitat Klinic Eppendorf (UKE) Hamburg successfully used novel instrumentation developed at DeMontfort University to obtain rheometric data from hemilarynges and human patients *in vivo*.[20–22] These devices are known as the linear skin rheometer (LSR) and

the laryngeal tensiometer. The LSR has also been deployed at Harvard Medical School[23] and the University of Wisconsin School of Medicine and Public Health[24] to develop isocontour maps showing the variation of modulus over the surface of the vocal fold of a hemilarynx. These mapping studies used a needle to attach a probe to the vocal fold, and were therefore only capable of producing reliable relative data, not absolute measurements of tissue elastic modulus. This limitation was due to the lack of a constitutive equation to transform stress/strain data into a value for modulus. This paper reports additional data from measurement of the transverse shear modulus of a group of six larynges using a modified suction attachment placed against the vocal fold epithelium. We demonstrate that this modified attachment technique enhances measurement reliability and provides a recognizable geometric framework (a simple shear model) that can form the basis of a credible deduction for shear modulus.

MATERIALS AND METHODS

Measurements were taken from the right vocal folds of six excised human larynges (three males and three females; age range 33–89 years). Data were obtained using a modified LSR instrument.

All larynges were harvested from autopsy cases within 12 hours after death, quick-frozen in liquid N_2 and stored at −80 °C until use. The larynges were thawed at 4 °C one day before experimentation. Once thawed, a midline incision was made to create two hemilarynges, and the right hemilarynx was mounted horizontally to expose the right vocal fold. All samples were secured using pins, with care taken not to place tension on the *in situ* vocal fold. Measurements were taken typically within 2 minutes of mounting, and the larynx was moistened using saline solution.

The LSR is a programmable tensiometer device capable of measuring displacement to a resolution of 4 μm, and force to a resolution of 20 μg.[25] The force sensor can be attached to the tissue under test using a variety of specialist attachments. For this study, a 2-mm bore cannula was used to attach the force sensor to the vocal fold epithelium, using a right-angled opening and 50 mbar of negative pressure was applied using a vacuum pump. The vacuum pump was disengaged during data collection.

The experimental setup is shown in Figure 2. The hemilarynx was mounted to expose the vocal fold. The LSR probe was attached to the epithelium such that resultant shear force was applied in the transverse direction, similar to the direction of airflow from the lungs. Using the simple shear model described in the introduction of this article, the geometry of this setup can be defined as follows. The shear force F applied by the LSR is transmitted into the vocal fold over the area determined by the probe diameter A. The displacement X is the resultant shear strain, which is tangential to the epithelial surface, and is measured by the LSR. The thickness of the tissue H is obtained from published data. This setup allowed derivation of an estimate for the shear modulus G.

The suction probe was attached to the LSR, which is mounted rigidly, and positioned such that the there was no gap between the suction probe and the epithelium, at which time 50 mbar of suction was applied. Although we cannot guarantee that this applies no stress to the vocal fold, this arrangement minimizes the effect. In addition, as the

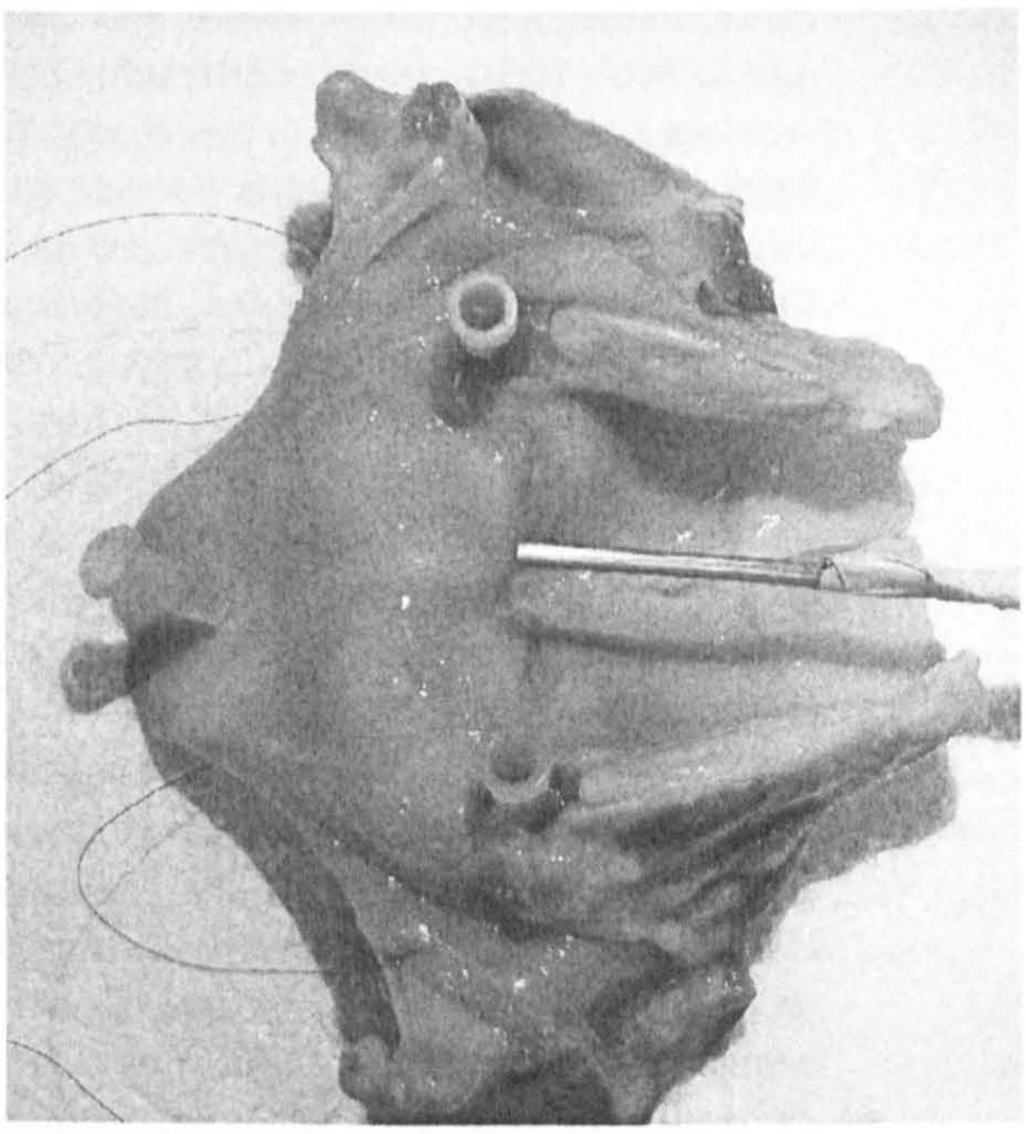

FIGURE 2. Experimental setup.

LSR operates by applying a cyclical force, any DC offset due to initial loading is removed. The force sensor and suction attachment were gently cycled in a sinusoidal manner such that a cyclical shear force of 1 g was applied to the vocal fold. Five measurements were taken from the same position without removing the suction probe. The LSR is mounted such that the probe rests in the tissue thus minimizing the applied vertical force. The built-to-order load cell used in the LSR was supplied by Maywood (Reading, UK), and has a full-scale reading of 50 g, with an overall accuracy of 0.02 g. The linear variable displacement transducer was supplied by Solartron (model DF 2.5, Farnborough, UK, type DF2.5), which has an accuracy of 4 μm. Force/displacement data were used to derive dynamic spring rate (DSR), defined below. DSR is a mechanical engineering term. It is defined as the change in length of a material when a unit of force is applied to it so that it is either stretched or compressed. It is not a time-dependent term. By applying knowledge of the geometry of the experimental setup, it is possible to estimate the shear modulus of the vocal fold.

Conversion of DSR data to an estimate of shear modulus is achieved by applying a simple shear model, with a correction to take account of effects due to adjacent attached tissue. The DSR is a measure of the amount of shear force required to achieve a unit of shear displacement.

A sinusoidal force F is applied to the material under test and the resultant displacement X is logged.

$$F=F_{max}\sin(t) \tag{6}$$

$$X=X_{max}\sin(t+\tau) \tag{7}$$

where F_{max} is the maximum force, t is the time, X_{max} is the maximum displacement, and τ is the phase shift in radians.

The DSR of the tissue is defined as F_{max}/X_{max}, and is expressed in grams per millimeter. As we are not using the time-dependent information associated with the sinusoidal nature of the applied force, we can substitute F for F_{max} and X for X_{max}. DSR can then be used to estimate the shear modulus of the displaced vocal fold tissue using knowledge of the geometry of the test site, as follows.

The stress σ is the applied force F_{max} per unit area A given by

$$\sigma=\frac{F_{max}}{A}. \tag{8}$$

The resultant strain ε is given by tangential displacement X_{max} per material thickness H.

$$\varepsilon=\frac{X_{max}}{H}. \tag{9}$$

Shear modulus G is defined as stress per unit strain.

$$G=\frac{\sigma}{\varepsilon} \tag{10}$$

$$G=\left(\frac{F_{max}}{X_{max}}\right)\left(\frac{H}{A}\right). \tag{11}$$

As $DSR=F_{max}/X_{max}$ then

$$G=DSR\frac{H}{A}. \tag{12}$$

The thickness of the adult human vocal fold lamina propria is typically 1 mm,[26] which is the figure used for H. The area of attachment is obtained by measuring the bore of the suction attachment, which in this study was 2 mm.

It is important to note that this simple shear model does not make any allowance for the attached tissue, which is also subjected to shear stresses due to displacement of the tissue directly underneath and surrounding the suction attachment. This effect drops off rapidly as the force transmitted through a solid is inversely related to distance. However, a rigorous mathematical solution to describe the elastic processes involved has not been published. In the absence of a mathematical solution for the shear modulus of tissue attached to other tissue, we incorporated a simple correction derived experimentally based on a widely accepted mathematical model developed by W.C. Hayes. This model derives shear modulus from indentation data.[27] We first evaluated this correction methodology using data collected from 40 human hemilarynges at UKE,[21] which were tested using both the Hayes indentation method and the LSR. The data sets from the two methods correlated well when the surface area of attachment used to analyze the LSR data was increased by 0.75 mm in all dimensions. Based on these results,

we used a comparable correction to the data in this study by increasing the diameter of the area of attachment from 2 mm by 1.5 mm to 3.5 m.

RESULTS

Table 1 contains demographic, DSR, and estimated shear modulus data. The shear modulus of the three female vocal folds ranged from 814 to 1232 Pa. The shear modulus of the three male vocal folds ranged from 1021 to 1796 Pa. The sample size in this study is too small to allow any generalized conclusions; however, these data are similar in magnitude to those obtained in the 40 larynges studied at UKE.

DISCUSSION

Finding similar published results to compare these findings with is challenging, as most of the published vocal fold viscoelasticity data are obtained from excised vocal fold covers. Chan and Titze, jointly and separately, have published extensive data using results obtained with a parallel plate rheometer taken at the same frequency as the LSR.[28] Their results ranged from 10 to 100 Pa. Our estimates of modulus are higher as we are measuring the same tissue, but in anatomical context; thus, the vocal fold is tensioned and anchored, resulting in higher values for modulus. The only other data set in the literature addressing vocal fold shear modulus in anatomical context was published by Tran et al,[17] who reported *in vivo* data from four subjects ranging from 2450 to 29 400 Pa. These values exceed those reported using excised mucosa with parallel plate rheometry, and hemilarynges with the LSR.

Of key interest are the results for the coefficient of variance (CofV) in the data set, which averaged 3.8%. This contrasts with previous work[21] that used adhesives, rather than suction, to attach the LSR probe to the vocal fold epithelium, and yielded a mean CofV of 8.4%. This demonstrates that suction, as opposed to a needle or adhesive, appears to be a superior means of attachment.

TABLE 1. *Estimated Shear Modulus of the Human Vocal Fold Using a Modified Simple Shear Model*

Age (y)	Sex	DSR	CofV	*G*
78	F	1.202	2.96	1232
70	F	0.794	1.44	814
Unknown	F	0.848	8.31	869
89	M	0.996	1.14	1021
72	M	0.982	4.03	1006
33	M	1.752	5.00	1796

CONCLUSIONS

The objective of this study was to measure the shear modulus of the vocal fold without dissecting the tissue out of a hemilarynx. This was successfully achieved using the LSR device, which appears to be a potentially useful tool for making point-specific measurements of vocal fold shear modulus in whole larynxes. The coefficients of variation obtained with the suction attachment in this study are superior to those obtained with alternative modes of attachment, such as pins or adhesives.[21–23]

A major obstacle that needs to be overcome is the lack of a mathematical model for deriving the shear modulus that takes account of the tissue that is attached to the area that is under direct stress. However, the results and methods under development are of great value. The LSR technique can be reliably used to measure relative changes in tissue modulus, and as such, holds value for comparative studies. Thus, it can be used to measure changes due to the application of tissue augmentation materials, or to quantify tissue stiffness resulting from vocal fold scarring. The ability to measure relative change will be used in a new study that will attempt to quantify change in vocal fold tension with respect to stimulation of the recurrent laryngeal nerve.

We are now pursuing development of an *in vivo* device to apply this methodology in the intraoperative setting, which can be used to measure relative change in modulus, but also requires a rigorous mathematical solution to enable derivation of absolute values. A mathematical derivation of shear modulus that takes account of attached tissue therefore remains an important area for theoretical progress. Although the analytical solution presented here appears to hold value in yielding a credible estimate of shear modulus, these data require further mathematical qualification. Regardless of this, however, the application of the LSR methodology to derive point-specific measurements with respect

to anatomical position and direction of stress means that this technique is presently most suited to obtaining relative, rather than absolute, measurements of modulus. To this end, we are presently collecting data using a ratiometric technique to quantify the anisotropic nature of the vocal fold, and initiating further work aiming to map variation in modulus with respect to anatomical position.

REFERENCES

1. Gunter HE. A mechanical model of vocal-fold collision with high spatial and temporal resolution. *J Acoust Soc Am.* 2003;113:994–1000.
2. Hertegård S, Dahlqvist Å, Goodyer E, Maurer F. Viscoelastic measurements after vocal fold scarring in rabbits. *Acta Otolaryngol.* 2006;126:758–763.
3. Hertegard S, Hallen L, Laurent C, Lindstrom E, Olofsson K, Testad P, Dahlqvist Å. Cross-linked hyaluronan used as augmentation substance for treatment of glottal insufficiency, safety aspects and vocal fold function. *Laryngoscope.* 2002;112:2211–2219.
4. Borzacchiello A, Mayol L, Garskog O, Dahlqvist A, Ambrosio L. Evaluation of injection augmentation treatment of hyaluronic acid based materials on rabbit vocal folds viscoelasticity. *J Mater Sci Mater Med.* 2005;16:553–557.
5. Chan RW, Titze IR. Hyaluronic acid (with fibronectin) as a bioimplant for the vocal fold mucosa. *Laryngoscope.* 1999;109:1142–1149.
6. Hahn MS, Teply BA, Stevens MM, Zeitels SM, Langer R. Collagen composite hydrogels for vocal fold lamina propria restoration. *Biomaterials.* 2006;27:1104–1109 [Epub Sep 9, 2005].
7. Hirano S, Nagai H, Tateya I, Tateya T, Ford CN, Bless DM. Regeneration of aged vocal folds with basic fibroblast growth factor in a rat model: a preliminary report. *Ann Otol Rhinol Laryngol.* 2005;114:304–308.
8. Hirano S, Bless DM, del Rio AM, Connor NP, Ford CN. Therapeutic potential of growth factors for aging voice. *Laryngoscope.* 2004;114:2161–2167.
9. Kriesel KJ, Thiebault SL, Chan RW, Suzuki T, VanGroll PJ, Bless DM, Ford CN. Treatment of vocal fold scarring, rheological and histological measures of homologous collagen matrix. *Ann Otol Rhinol Laryngol.* 2002;111:884–889.
10. Chhetri DK, Head C, Revazova E, Hart S, Bhuta S, Berke GS. Lamina propria replacement therapy with cultured autologous fibroblasts for vocal fold scars. *Otolaryngol Head Neck Surg.* 2004;131:864–870.
11. Kanemaru S, Nakamura T, Yamashita M, et al. Destiny of autologous bone marrow-derived stromal cells implanted in the vocal fold. *Ann Otol Rhinol Laryngol.* 2005;114:907–912.
12. Kanemaru S, Nakamura T, Omori K, et al. Regeneration of the vocal fold using autologous mesenchymal stem cells. *Ann Otol Rhinol Laryngol.* 2003;112:915–920.
13. Kaneko T, Uchida K, Komatsu K, Kanesaka T, Kobayashi N, Naito J. Mechanical properties of the vocal fold: measurement in-vivo. In: Steven KN, Hirano M, eds. *Vocal Fold Physiology.* Tokyo: University of Tokyo Press; 1981:365–376.
14. Tamura E, Kitahara S, Kohno N. Intralaryngeal application of a miniaturized ultrasonic probe. *Acta Otolaryngol.* 2002;122:92–95.
15. Hsiao T, Wang C, Chen C, Hsieh F, Shau Y. Elasticity of human vocal folds measured in vivo using color Doppler imaging. *Ultrasound Med Biol.* 2002;28:1145–1152.
16. McGlashan JA, de Cunha DA, Hawkes DJ, Harris TM. Surface mapping of the vibrating vocal folds. In: *Proceedings of the 24th World Congress of the International Association of Logopedics and Phoniatrics (IALP).* Amsterdam; August 1998.
17. Tran QT, Berke GS, Gerratt BR, Kreiman J. Measurement of Young's modulus in the in vivo human vocal folds. *Ann Otol Rhinol Laryngol.* 1993;102:584–591.
18. Berke GS. Intraoperative measurement of the elastic modulus of the vocal fold. Part 1. Device development. *Laryngoscope.* 1992;102:760–769.
19. Berke GS, Smith ME. Intraoperative measurement of the elastic modulus of the vocal fold. Part 2. Preliminary results. *Laryngoscope.* 1992;102:770–778.
20. Goodyer EN, Muller F, Bramer B, Chauhan D, Hess M. In vivo measurement of the elastic properties of the human vocal fold. *Eur Arch Otorhinolaryngol.* 2006;263:445–462.
21. Goodyer EN, Hemmerich S, Müller F, Kobler JB, Hess M. The shear modulus of the human vocal fold, preliminary results from 20 larynxes. *Eur Arch Otorhinolaryngol.* 2007;264:45–50.
22. Goodyer EN, Müller F, Licht AK, Hess M. In vivo measurement of the shear modulus of the human vocal fold—interim results from 8 patients. *Eur Arch Otorhinolaryngol.* 2007;264:631–635.
23. Hess M, Muller F, Kobler JB, Zeitels S, Goodyer EN. Measurements of vocal fold elasticity using the linear skin rheometer. *Folia Phoniatr.* 2006;58:207–216.
24. Dailey SH, Tateya I, Montequin D, Welham N, Goodyer EN. Viscoelastic measurements of vocal folds using the linear skin rheometer (LSR). *J Voice.* Online edition Jun, 2007.
25. Matts PG, Goodyer EN. A new instrument to measure the mechanical properties of the human stratum corneum. *J Cosmet Sci.* 1998;49:321–323.
26. Hirano S. Growth, development and aging of human vocal folds. In: Bless DM, Abbs JH, eds. *Vocal Fold Physiology: Contemporary Research and Clinical Issues.* San Diego, CA: College Hill Press; 1983.
27. Hayes WC, Keer LM, Herrmann G, Nockros LF. Mathematical analysis for indentation tests of articular cartilage. *J Biomech.* 1972;5:5541–5551.
28. Chan RW, Titze IR. Viscoelastic shear properties of human vocal fold mucosa. *J Acoust Soc Am.* 1999;106:2008–2021.

Viscoelastic Measurements of Vocal Folds Using the Linear Skin Rheometer☆

*Seth H. Dailey, *Ichiro Tateya, *Douglas Montequin,
*Nathan Welham, and †Eric Goodyer

Madison, Wisconsin and †Leicester, United Kingdom

Summary: As the number of interventions for vocal fold scar grows and with the advancement of mathematical modeling, greater accuracy and precision in the measurement of vocal fold pliability will become essential. Although indirect pliability measures have been used successfully, direct measurement of tissue pliability is essential. Indirect measurement with parallel plate technology has limitations; it requires the tissue to be removed from the surrounding framework, allows no site specificity, and offers no future for *in vivo* use in animals or humans. We tested the linear skin rheometer (LSR) in the evaluation of vocal fold pliability. We measured site-specific rheology of vocal folds thereby creating "pliability maps" in human, dog, and rat cadaveric larynges under conditions of altered stiffness; the canine vocal folds possessed sulci, the rat vocal fold was stiff secondary to controlled biopsy, and the human vocal fold was injected with trichloroacetic acid. Histology was performed to confirm the site and type of canine sulci. We found that the LSR reliably detected stiffness in the vocal folds of all species and created "pliability maps" consistent with previous data and clinical observations. The LSR should prove useful in the evaluation of vocal fold pliability for *ex vivo* and ultimately for *in vivo* applications.

Key Words: Microlaryngoscopy—Viscoelasticity—Rheology—Phonosurgery—Phonomicrosurgery—Vocal fold scar.

INTRODUCTION

Vocal fold scar continues to be a challenging clinical entity in the field of Laryngology.[1] Multiple surgical treatment options including medialization thyroplasty, scar/sulcus excision, and vocal fold augmentation with collagen, fascia, and fat have all been attempted with less than optimal results.[2] Failure to achieve an optimal approach is likely

Accepted for publication January 4, 2007.

☆This study was supported by grant ROl DC4428 from the National Institute on Deafness and Other Communication Disorders.

From the *Department of Surgery, University of Wisconsin School of Medicine, Division of Otolaryngology-Head and Neck Surgery – University of Wisconsin Hospital and Clinics, Madison, Wisconsin; and the †The Centre for Computational Intelligence - Bioinformatics Group, DeMontfort University, Leicester, UK.

Address correspondence and reprint requests to Seth H. Dailey, MD, Department of Surgery, University of Wisconsin Hospital and Clinics, Division of Otolaryngology-Head and Neck Surgery, K4/720, 600 Highland Avenue, Madison, WI 53792-7375. E-mail: dailey@surgery.wisc.edu

Journal of Voice, Vol. ■, No. ■, pp. ■
0892-1997/$32.00

doi:10.1016/j.jvoice.2007.01.002

based upon a lack of understanding of the fundamental nature of vocal fold scar and how to characterize it. Historically, vocal fold scar has been characterized by histologic, biochemical, aerodynamic, acoustic, stroboscopic, and rheologic parameters, including parallel plate technique.[1,3–5] Characterization of tissue rheology has been limited by technological barriers. Parallel plate technique requires excision of the entire vocal fold soft tissue away from its cartilaginous attachments and records measurements judging the multilayered vocal fold as one unit. The ability of this technique to record spatially important pliability changes is poor. Parallel plate technology cannot, for example, localize the site of the stiffness along the long and vertical axes of the vocal fold. Importantly, scarring is generally localized to the epithelium and superficial lamina propria and occupies particular sites along the long and vertical axes. This shortfall in parallel plate technology prevents precise characterization of vocal fold scar in both site and severity, limiting our ability to track focal interventions. Furthermore, mathematical modeling of vocal fold oscillation is based upon precise mapping of the vocal fold where even small tissue distortions in terms of volume or pliability will significantly alter calculations.[6–8] More precise rheometric spatial resolution will augment the power of these models. Lastly, clinical decision making is predicated upon an understanding of the tissue changes. Specifically, the site and severity of tissue volume loss and pliability loss will dictate the type of intervention to be attempted, for example, medialization for tissue volume loss versus softening of scar in an otherwise competent glottis. As the variety of interventions grows to accommodate the spectrum of problems that manifest in vocal fold scarring, a more refined characterization of the scar itself will be required to tailor the treatment to the problem. Use of the linear skin rheometer (LSR) in the characterization of vocal fold scarring addresses the shortfalls that parallel plate technology cannot.

The LSR is a precision electromechanical instrument that was designed to measure the viscoelastic properties of the stratum corneum of skin (Figure 1).[9] This measuring technique has been adapted to take viscoelastic measurements of vocal fold tissue.[10–13] The probe is attached to the tissue under test using

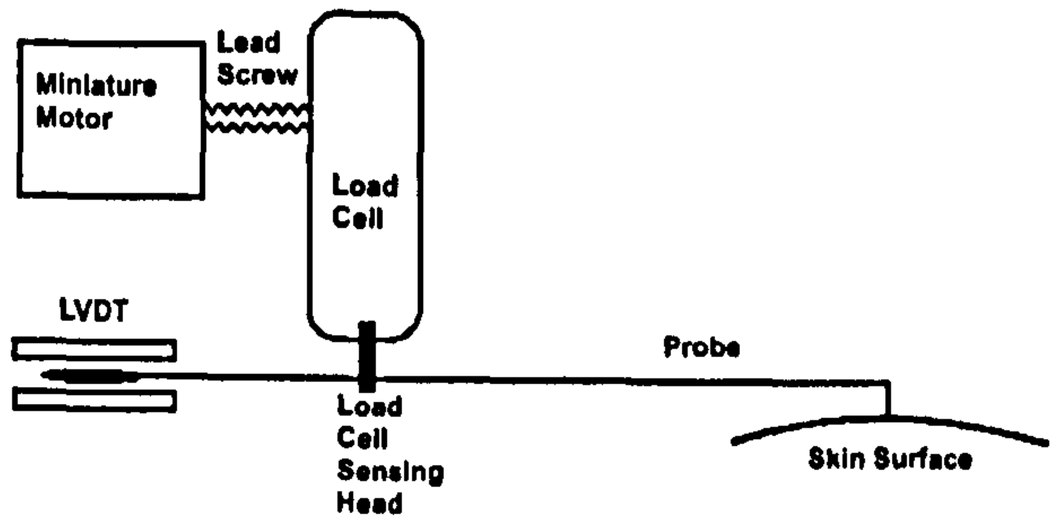

FIGURE 1. Schematic of the LSR device.

a needle mounted at right angles to the primary axis of the rod. The rod is capable of rotating through a full circle, allowing the needle to be inserted at any angle into the tissue. The needle probe is inserted onto the vocal fold epithelium, such that the direction of motion is perpendicular to the line that can be drawn between the vocal process and anterior commissure (Figures 2 and 3). Thus, the direction of the measurement is in the same axis as the motion generated by the mucosal wave generated during phonation. The force applied is sinusoidal, with peak amplitude of 1 g applied at a rate of 0.3 Hz. Three parameters may be obtained from these curves, F_{max}, the peak force that is applied to the skin surface, P_{max}, the peak displacement occurring as a result of that force, and T, the phase shift between the two signals. The dynamic spring rate (DSR) is given simply by the formula F_{max}/P_{max}. Derivatives are calculated and expressed as g/mm, mm/N, and

FIGURE 2. The LSR device as used for DSR measurements on hemilarynges.

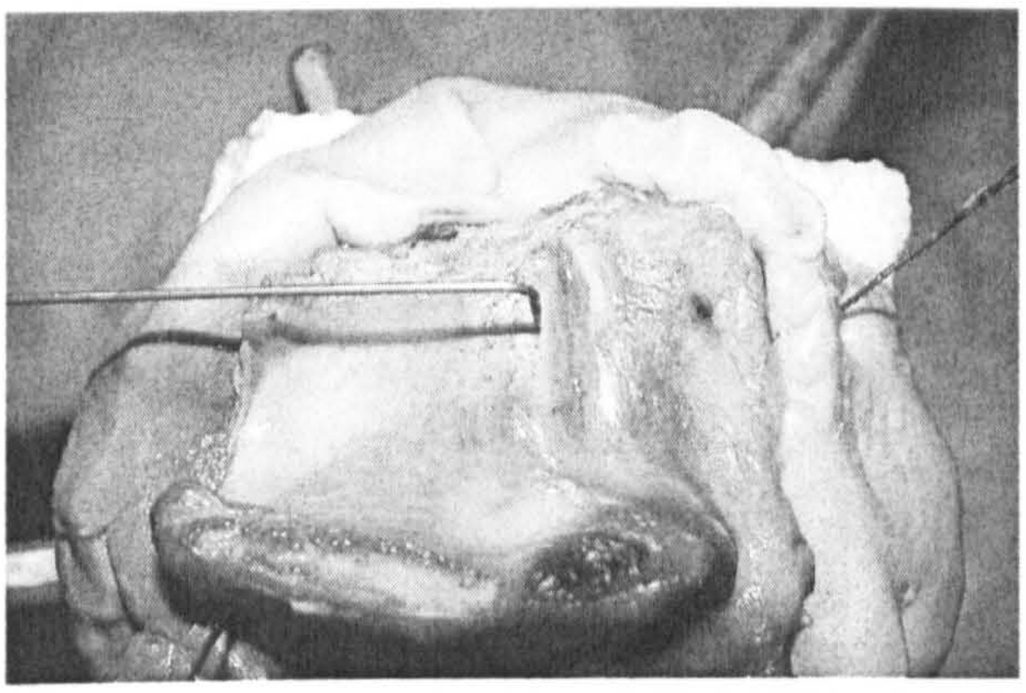

FIGURE 3. The DSR measurement setup. A custom needle probe (100 mm length, 1 mm diameter, 5 mm tapered tip) was inserted into each vocal fold region of interest, perpendicular to the plane of the vocal fold medial edge and at a depth of 1 mm. Data were collected across a matrix of 30 (6 × 5) measurement points to map variations in DSR as a function of vocal fold region. The dimension with six points was in the anterior-posterior plane: the most anterior point was placed 2 mm from the attachment of the vocal fold to the thyroid cartilage and the most posterior point was placed at the vocal process. The dimension with five points was in the inferior-superior plane: Hemilarynges were marked at the superior, mid, and inferior third positions of the vocal fold lumen surface in addition to the marking at the superior vocal fold surface and in the subglottal region.

μm/g. The DSR is a nonfrequency dependent measurement of the elasticity of the material under test where a higher value denoted increased stiffness. The *LSR* software (Eric Goodyer) yields information for both the elastic and viscous qualities of the tissue.

The *LSR* has been used in preliminary animal studies to measure vocal fold tissue pliability. These studies in pig, sheep, and rabbit models showed the ability of the LSR to measure superficial vocal fold pliability and to demonstrate geographic viscoelastic differences at different depths and sites along the vocal folds.[11,12] Also, viscoelastic changes were noted under experimental conditions, suggesting that the LSR will be a sensitive, reliable tool for site-specific identification of tissue stiffness. These studies, however, did not include histologic correlations and did not specifically examine sulcus deformities. We sought to examine the utility of the LSR in the reliable detection of tissue stiffness in a site-specific manner in three different species with three different conditions of tissue stiffness.

MATERIALS AND METHODS

The study was performed in accordance with the US Public Health Service Policy on Human Care and Use of Laboratory Animals, the National Institutes of Health Guide for the Care and Use of Laboratory Animals, and the Animal Welfare Act (7 U.S.C. et seq.); the animal use protocol was approved by the Institutional Animal Care and Use Committee of the University of Wisconsin-Madison (Madison, WI).

Tissue collection and preparation

Six larynges (four canine, one rat, one human), representing six vocal fold experimental conditions (normal canine, canine sulcus vocalis, normal rat, scarred rat, normal human, human with trichloroacetic acid [TCA] exposure), were used in this study.

Canine larynges were harvested from mongrel dogs sacrificed for purposes other than this study at the University of Wisconsin School of Veterinary Medicine. Visual inspection of the harvested larynges revealed three with normal appearing vocal folds and one with bilateral sulcus vocalis. Clinical records for the dog with bilateral sulcus vocalis revealed a history of kennel cough.

The rat larynx was harvested from a Sprague-Dawley rat, 2 months after unilateral vocal fold stripping as described by Tateya et al.[1] In brief, the rat was anesthetized using a mixture of ketamine HCL (90 mg/kg) and xylazine HCL (9 mg/kg) IP, the vocal folds were visualized using a telescope, and unilateral stripping was performed using a 25-G spinal needle and microforceps. Stripping continued until the thyroarytenoid muscle was exposed. The contralateral vocal fold remained intact. Laryngeal harvest was performed after humane euthanasia *via* intracardiac injection of beuthanasia (0.22 mL/kg).

The human larynx was obtained from an autopsy case. There was no evidence of previous laryngeal disease.

All harvested larynges were frozen immediately using liquid nitrogen and stored at −80°C until experimentation. Before each experiment, the larynges were thawed overnight at 4°C and then gradually warmed to 37°C. Hemilarynges were

created by sagittal section along the midline, taking care not to disturb the vocal fold attachment to the thyroid cartilage at the anterior commissure.

TCA application

The TCA was applied to one human vocal fold to examine the influence of chemical stiffening on DSR. After initial data collection under normal conditions, 1 mL of 20% TCA solution was applied topically for 2 seconds followed by saline wash. The DSR measurements were then repeated. Next, 0.3 mL of TCA solution was injected into the lamina propria through the deep to superficial layers. The injection of TCA was performed to chemically stiffen the lamina propria. Five minutes after the injection, the DSR measurements were again repeated.

DSR measurement

Hemilarynx specimens were affixed to a firm table top and kept moist with physiological saline. All measurements were made at 25°C. A custom needle probe (100 mm length, 1 mm diameter, 5 mm tapered tip) was inserted into each vocal fold region of interest, perpendicular to the plane of the vocal fold medial edge and at a depth of approximately 1 mm. Placement of the probe on the vocal folds was performed under careful visual inspection to allow for accuracy and consistency of probe depth placement. The probe tip had a sharpness that allowed it to maintain position on the vocal fold while not tearing the epithelium or lamina propria. Movement of the probe during DSR measurement followed the inferior-superior vocal fold axis, consistent with the direction of mucosal wave propagation during normal phonation. Sinusoidal force was applied at 0.3 Hz with a peak amplitude of 1 g. Resulting probe displacement was generally in the vicinity of 1 mm and therefore consistent with the range of normal tissue displacement observed during phonation. All measurements were repeated six times. No evidence of tissue damage was appreciated during or after the measurement process.

To map variations in DSR as a function of vocal fold region, data were collected across a matrix of 30 (6 × 5) measurement points in all canine and human hemilarynges except for two canine hemilarynges (one normal and one sulcus) from which data were collected across 18 (6 × 3) measurement points. The dimension with six points was in the anterior-posterior plane: the most anterior point was placed 2 mm from the attachment of the vocal fold to the thyroid cartilage and the most posterior point was placed at the vocal process. The dimension with three or five points was in the inferior-superior plane: hemilarynges with three points were marked at the superior, mid, and inferior third positions of the vocal fold lumen surface, beneath the free edge; hemilarynges with five points were additionally marked at the superior vocal fold surface and in the subglottal region.

In contrast with the human and canine specimens, the small size of the rat hemilarynx precluded more than a single measurement point on each vocal fold. Thus, a single measurement position was selected in the middle of the scarred and of the control vocal folds.

Histological analysis

The two canine vocal folds with sulcus vocalis were histologically analyzed by Elastin-van-Gieson (EVG) stain, as described by Rousseau et al.[5] In brief, the vocal fold tissues were fixed in a 10% buffered formalin solution immediately after the DSR measurement. The samples were then paraffin embedded. Ten micron-thick sections were prepared for histological examination, and EVG staining was used to identify collagen and elastin proteins.

Data analysis

Mapping of DSR variations by vocal fold region was performed as follows. The six repeated measurement values at each matrix point were averaged. Mean DSR values for each matrix point were then plotted using a contour mapping function within Sigmaplot 8.0 (*Systat Software*, Inc., Point-Richmond, CA).

The DSR measurement repeatability was calculated by dividing the standard deviation (SD) by the mean value of repeated measurements at each point. The resulting ratio, known as the coefficient of variation (CV), was averaged within subjects to

yield a mean per-subject CV. These per-subject means were then averaged to yield an overall CV.

Data conversion

Conversion of the LSR (g/mm) data into loss rate values was performed as follows. Five fluids of known viscosities (centipoise, cP) were obtained (Cannon Instrument Company, State College, PA) and placed into Petri dishes at 72°F; 4 × 4-inch gauze pads were placed into the fluids to act as a scaffold. Using the LSR machine, five consecutive measurements of each fluid were performed and the average for each set of values calculated. A plot of loss rate versus viscosity was then graphed.

RESULTS

DSR in canine and normal human vocal folds

In the canine (Figure 4), DSR values were consistently higher in the anterior and posterior vocal fold regions compared with the midmembranous region. In the midmembranous region, DSR values were highest near the free edge.

In the human (Figure 5), DSR values in the posterior vocal fold region were higher than all other vocal fold regions, including those measured in the canine. DSR was highest at the vocal process, with a value of 2.78 g/mm. DSR values in the infraglottic region, corresponding to the presence of the conus elasticus, tended to be greater than those observed in the vocal fold proper.

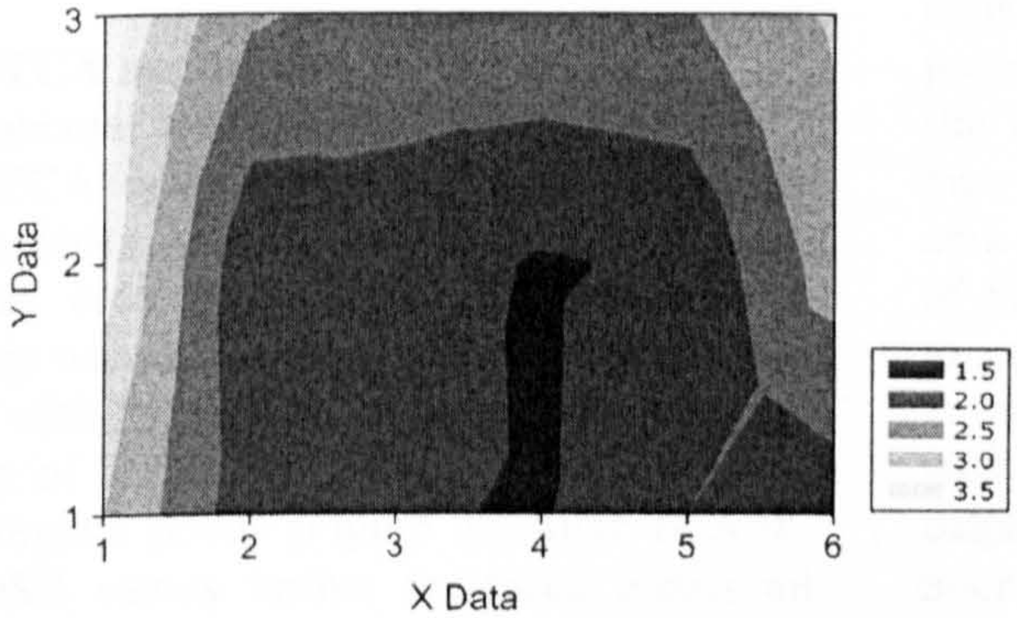

FIGURE 4. A representative 2-D map of variations in DSR by vocal fold region in a normal canine vocal fold. *Y*-axis values 1, 2, and 3 correspond to measurement points on the inferior, middle, and superior third of the medial surface of the vocal fold, respectively. *X*-axis values (1–6) correspond to measurement points progressing from the anterior to posterior end of the membranous vocal fold, respectively. DSR values are consistently higher in the anterior and posterior vocal fold regions compared with the midmembranous region. In the midmembranous region, DSR values are highest near the free edge. DSR units are g/mm.

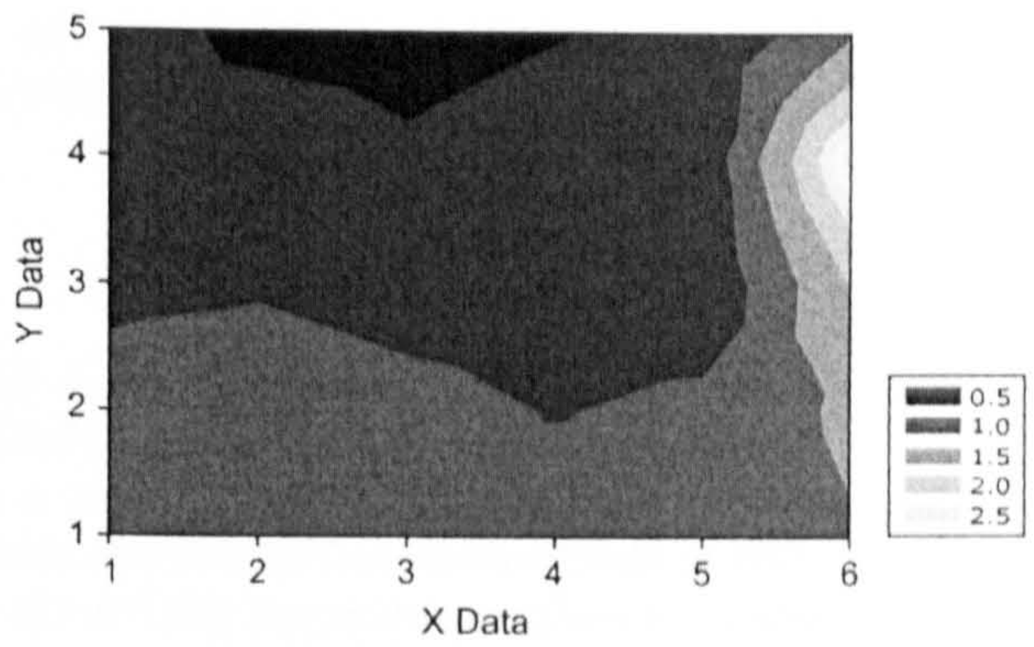

FIGURE 5. A representative 2-D map of variations in DSR by vocal fold region in a normal human vocal fold. *Y*-axis values 1, 2, 3, 4, and 5 correspond to measurement points on the subglottis, inferior, middle, and superior third of the medial surface, and superior surface of the vocal fold, respectively. *X*-axis values (1–6) correspond to measurement points progressing from the anterior to posterior end of the membranous vocal fold, respectively. DSR values in the posterior vocal fold region are higher than all other vocal fold regions. DSR is highest at the vocal process, with a value of 2.78 g/mm. DSR values in the subglottal region are greater than those observed in the vocal fold proper. DSR units are g/mm.

Repeatability measures across two canine and one human samples combined yielded a CV of 4.3%.

DSR in the scarred rat vocal folds

Mean DSR values (±SD) of the normal and scarred rat vocal folds were 1.35 (±0.20) and 2.37 (±0.23) g/mm, respectively (Figure 6). The

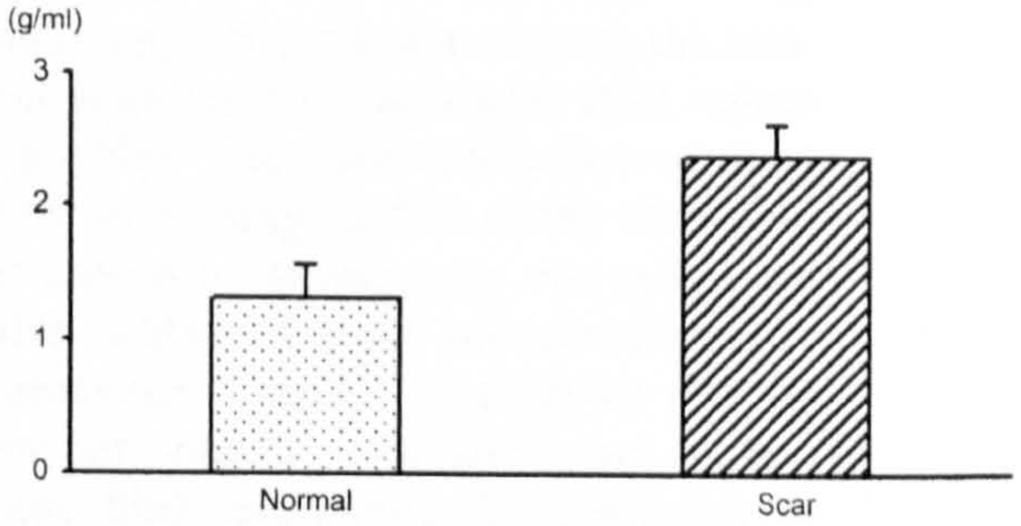

FIGURE 6. Mean DSR values of normal and scarred rat vocal folds (1.35 [±0.20] and 2.37 [±0.23] g/mm, respectively).

observations from the scarred vocal fold were higher than those from the normal fold.

Histology and DSR in canine vocal folds with sulcus vocalis

Although it is difficult to classify sulcus vocalis type in the canine due to absence of a vocal ligament, histological examination and gross appearance suggested the presence of a right side linear type 2 sulcus vocalis and left side pathologic type 3 sulcus vocalis[14] in the canine hemilarynges from the dog with a history of kennel cough (Figure 7). A focal lesion was observed in the superior third of both midmembranous vocal fold regions. EVG staining confirmed a deep sulcus extending to the deep layer of the lamina propria on the left, and a shallower sulcus extending to the superficial layer on the right. Both sulci were characterized by dense collagen deposition.

DSR values in the region of the left sulcus (white dashed line) were relatively higher than those in the surrounding area (Figure 5). In contrast, DSR values in the region of the right sulcus appeared consistent with those in the surrounding area. On both left and right sides, DSR values in the anterior and posterior vocal fold regions were higher than those in the midmembranous region.

Effect of TCA application on the DSR value in normal human vocal folds

Before TCA application, DSR values were higher in the anterior and posterior regions of the normal human vocal fold (Figure 8). Additionally, DSR values were elevated in the subglottal region compared with the vocal fold proper. After topical application of TCA, DSR values increased across all measurement points (Figure 9). After TCA injection, DSR values further increased across all measurement points (Figure 9). After both forms of TCA application, DSR values in the anterior, posterior, and subglottal regions remained higher than those in the midmembranous region, but they increased less than the midmembranous vocal fold did (Figure 8).

Data conversion

Conversion of LSR loss rate values into values of viscosity (cP) reflected a linear relationship with a slope of 15,089 cP/g/mm (Figure 10). R^2 value = 0.9491.

DISCUSSION

The LSR device was used in this study to evaluate its reliability and sensitivity in detecting pliability values at focally specific areas in three species of vocal folds and three different conditions of stiffness. The SD of DSR repeatability values in canine and human vocal folds of 4.3% is acceptable and is similar to the values of 5% or less found by Goodyer et al.[11] The "pliability maps" which we developed in human vocal folds using either 18 or 30 points of measurement yielded results similar to those of previous studies in sheep and pig vocal folds.[11] These maps demonstrate the sensitivity of the LSR device to the rheologic variability in normal vocal folds. Specifically, DSR values of areas with firm tissue, such as the vocal process and the infraglottis where the fibrous conus elasticus resides, were consistently higher than the midmembranous vocal fold where thin epithelium overlies the highly pliable superficial layer of lamina propria (SLP). Stiffness increased in either direction away from the midpoint of the musculomembranous vocal fold; thinning of the superficial lamina propria and the presence of the anterior and posterior maculae flavae may help to explain this trend. Sato and colleagues have demonstrated that the area of the macula flava has an increased number of fibroblasts and is thus hypercellular compared to the relatively hypocellular SLP, likely making it more stiff.[15,16] These stiffness values correlate well with clinical observations gleaned from the palpation of different vocal fold structures during microlaryngoscopy. Of particular interest, the midmembranous segment had the lowest DSR values (the most pliable). The midmembranous segment on the medial or striking surface of the vocal fold is the most critical in voicing such that evaluation of its pliability will be clinically and experimentally critical. Aerodynamic studies have shown that the midmembranous region undergoes the highest shear stresses, likely explaining the appearance of vocal fold nodules in those with elevated subglottic voicing pressures.[17] Mathematical modeling has

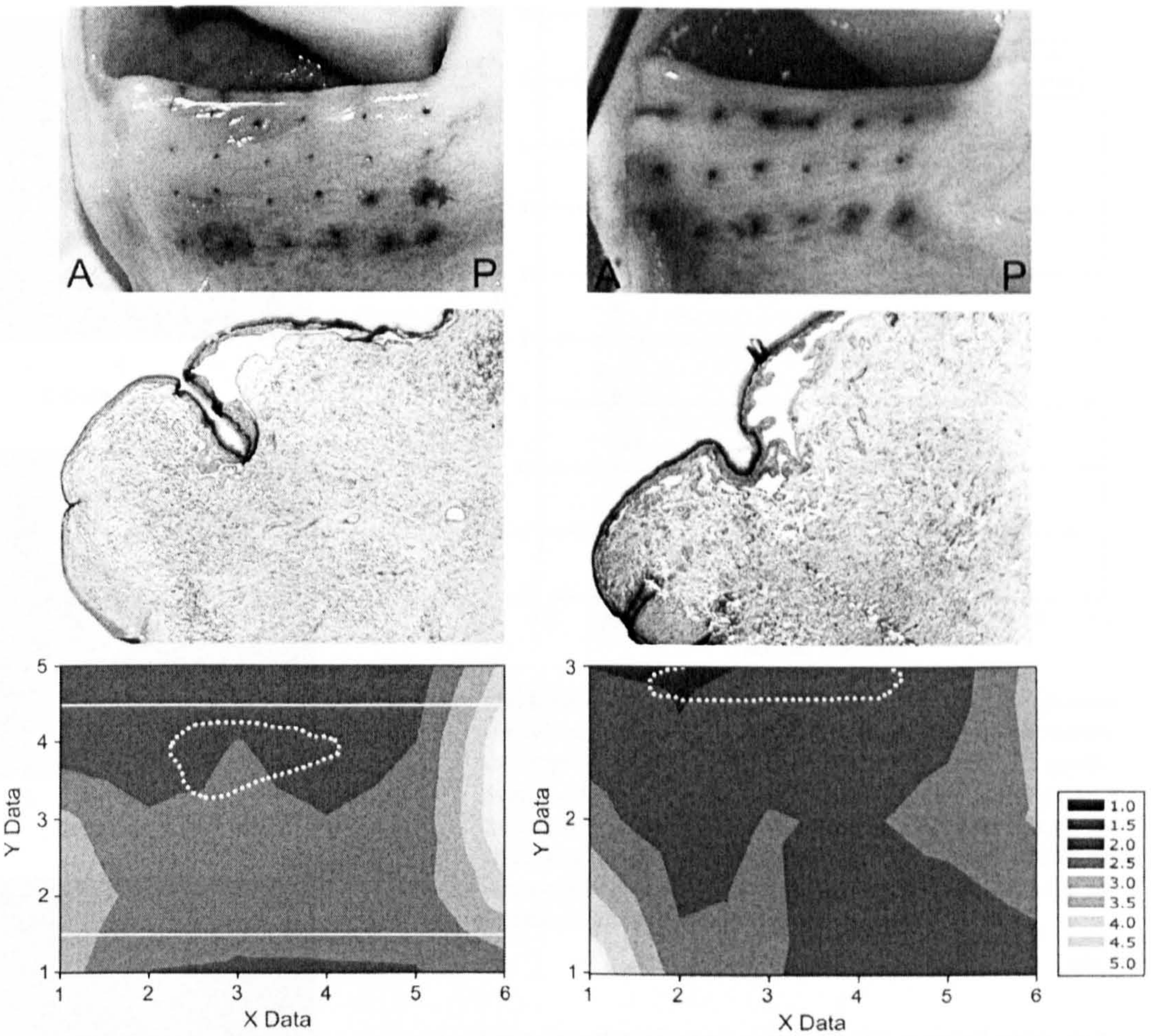

FIGURE 7. Gross appearance (upper row), EVG stain (middle row), and 2-D map of DSR value by vocal fold region (lower row), in canine vocal folds with bilateral sulcus vocalis. Gross appearance and 2-D DSR map of the left vocal fold are flipped horizontally. *Y*-axis values 1, 2, 3, 4, and 5 of the left vocal fold correspond to measurement points on the subglottis, inferior, middle, and superior third of the medial surface, and superior surface of the vocal fold, respectively. *Y*-axis values 1, 2, and 3 of the right vocal fold correspond to measurement points on the inferior, middle, and superior third of the medial surface, respectively. *X*-axis values (1–6) correspond to measurement points progressing from the anterior to posterior end of the membranous vocal fold, respectively. The upper and lower white lines indicate the free edge and lower margin of the vocal fold. DSR units are g/mm. (*Left*) Localized type 3 sulcus in the superior third of the left midmembranous vocal fold. DSR values in the sulcus region (white dashed line) are relatively higher than in the surrounding area. DSR values in the anterior and posterior vocal fold regions are higher than those in the midmembranous region. (*Right*) Localized shallow type 2 sulcus in the superior third of the right midmembranous vocal fold. DSR values in the sulcus region (white dashed line) appear consistent with those in the surrounding area. DSR values in the anterior and posterior vocal fold regions are higher than those in the midmembranous region.

shown that even tiny alteration of the configuration of this area will meaningfully affect vocal fold oscillation, confirming the importance of this region.[7,8,18,19] Furthermore, given that surgical interventions to eliminate midmembranous pathology will occasionally cause scarring and a subsequent loss of pliability, the ability of the LSR to detect pliability loss in this region will be of great utility.

As the characterization of vocal fold scarring in new experimental models must be credible, we examined whether chronic vocal fold scarring in the rat model could be reliably detected by the

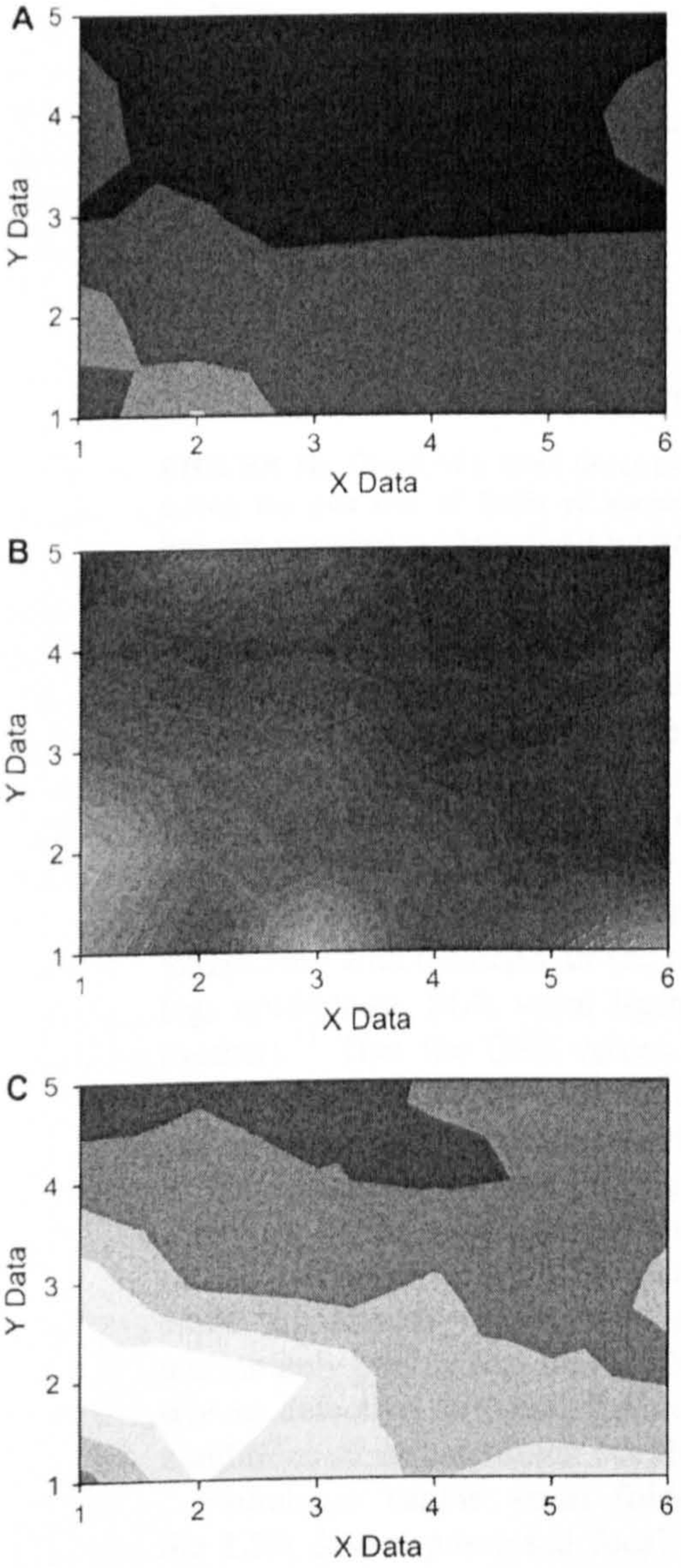

FIGURE 8. Effect of TCA application on DSR values in the human vocal fold. **A.** Pliability map before treatment with TCA. **B.** Pliability map after the treatment with topical TCA. **C.** Pliability map after the treatment with topical and injected TCA. *Y*-axis values 1, 2, 3, 4, and 5 correspond to measurement points on the subglottis, inferior, middle, and superior third of the medial surface, and superior surface of the vocal fold, respectively. *X*-axis values (1–6) correspond to measurement points progressing from the anterior to posterior end of the membranous vocal fold, respectively. DSR units are g/mm.

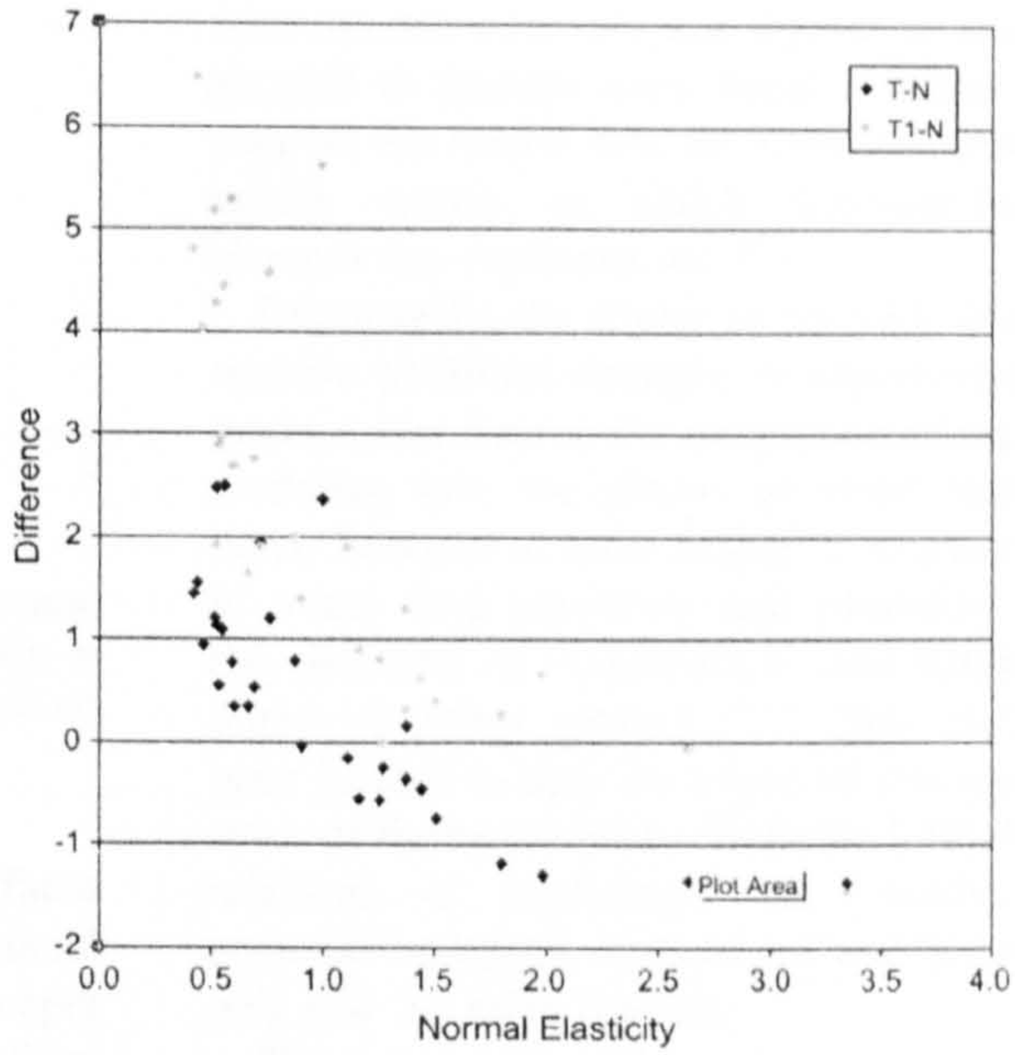

FIGURE 9. Plots of the differences in DSR values between normal and topical TCA injection (blue diamonds) and normal and topical + injected TCA vocal folds (yellow diamonds). Areas with higher pretest DSR rates (ie, stiff tissues such as cartilage) experience less alteration than areas with low pretest DSR rates (eg, midmembranous vocal fold). Values of DSR are measured in g/mm. *X*-axis is pretest elasticity. *Y*-axis is the difference in g/mm between pre- and posttest.

LSR.[20] Although the site specificity of the pliability changes was significantly reduced due to the tiny size of the rat vocal folds, differences were found between the scarred side and the normal side, confirming our hypothesis of validity. Statistical significance was not obtained because of the small number of test vocal folds.

The LSR was sensitive in detecting this midmembranous pliability loss in all three conditions of known stiffness (TCA application/injection, sulcus, and chronic scarring). This sensitivity helps to underscore the capacity of the device to detect stiffness in both depths and sites that are relevant to the characterization of vocal fold scarring. In the human TCA application and injection models, DSR values increased across all points measured. Gray et al found that distortion of the vocal folds at the junction of the epithelial basement membrane and SLP was a common finding in benign vocal fold pathology, such as nodules.[21] Furthermore, scarring from surgical biopsies occurs at this superficial site or deeper into the SLP or beyond depending on the nature of the biopsy/procedure. That the

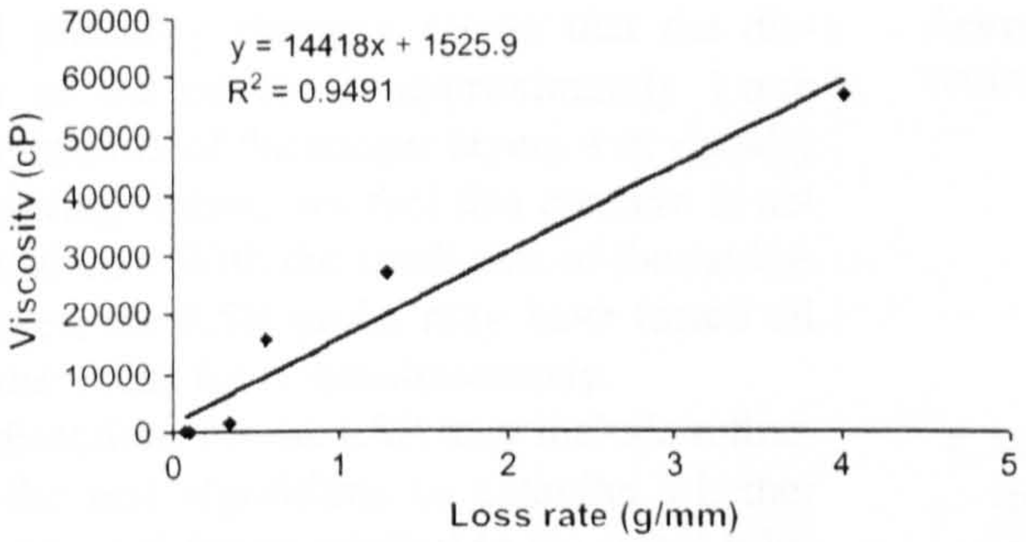

FIGURE 10. Graph of a fitted linear plot derived from measuring the loss rate of fluids of known viscosity. *X*-axis is loss rate measured in g/mm. *Y*-axis is viscosity measured in cP.

LSR was capable of reliably detecting stiffness changes under conditions of the most superficial type (TCA topical application) and slightly deeper (SLP proper) is encouraging and supports its utility as an experimental tool. This experience correlates well with studies in calf vocal folds, in which DSR values rose with the depth of vocal fold tissue tested (eg, epithelium, SLP, vocal ligament, and vocalis muscle).[11] That the DSR values rose more in the midmembranous region than at the vocal process and in the infraglottis offers additional face validity to the application of the LSR; areas already stiff (cartilage of the vocal process and conus elasticus of the infraglottis) would be not expected to become significantly more stiff versus tissues that are innately pliable (eg, SLP). The LSR was effective in detecting stiffness changes not only under conditions of varying depth but also of varying site.

Pathologic canine vocal folds measured with the LSR device possessed focal areas of stiffness (Figure 7). These vocal folds were taken from dogs known clinically to have "kennel croup," a disease involving excess coughing and therefore transiently elevated subglottic pressures from the coughing. When excised, the vocal folds were noted to have focal areas of contraction along the medial edge, one a longitudinal scar and the other a focal scar, corresponding to sulcus vocalis types 2 and 3, respectively.[14] These visually observed findings were confirmed by histologic sectioning and staining with EVG stain, helping to corroborate these findings (Figure 7). A direct comparison cannot be made to human vocal folds because canine vocal folds do not have a vocal ligament. However, the parallel to human vocal folds is close enough to support the notion that the LSR will detect human sulcus vocalis in which site-specific stiffness changes are characteristic.[14,22]

Importantly, the ability of the LSR to detect site-specific pliability changes in experimental models opens a new door to the integration of mathematical modeling into the effects of vocal fold interventions. Berry et al have helped to pioneer modeling of vocal fold geometry and pliability to predict the outcome of biochemical and surgical procedures on voice quality.[7,8,18] This modeling has been limited to date by a lack of site-specific measures of tissue pliability. With the LSR device, correlations of modeling with aerodynamic and acoustic measures, stroboscopy and tissue histology will now be more feasible.

The correlation of loss rate to viscosity revealed a linear relationship (Figure 10). Given the multiple different units used to measure tissue pliability, including dynamic elasticity and dynamic viscosity, a linear relationship of loss rate to viscosity helps to frame the discussion and will allow for a more clear understanding in studies to come.

Although the LSR device represents an advance in direct tissue evaluation, objections may be raised to certain technical points. The needle that contacts the tissue may damage the epithelium or SLP. Tissue destruction was not observed by our group in this set of larynges. Another concern may be directed at the ability of the device to discern differences in pliability of different layers of the vocal fold. Specifically, because the needle did not penetrate the epithelium, the LSR tested the epithelium and underlying SLP as one unit and did not differentiate between the two. This objection is well founded but perhaps irrelevant because the epithelium and SLP are bound by linking proteins and oscillate as one unit *in vivo*.[21,23] Furthermore, when conditions of scarring occur superficially, the epithelium and underlying SLP scar become even *more* adherent to one another, making differentiation of epithelium from SLP unimportant. Another objection may be that the displacement of the LSR needle on the vocal fold is really testing the pliability of all layers of the vocal fold, even down to vocalis muscle and that the device is not truly testing

superficial pliability changes. Given that the displacement of the needle is approximately 1 mm and that no motion of the deeper layers was visually observed during testing, we feel this concern is not a meaningful one. With the small size of the rat larynx, however, the LSR probe may have tested all layers of the vocal folds simultaneously.

Future directions for the LSR may include refinements in the test algorithms to examine whether displacements and forces applied to the vocal folds allow for more sensitive evaluations. Also, a smaller device may allow *in vivo* measurements of animal vocal folds while under anesthesia, making serial measures of pliability possible in multistage or longitudinal experiments. Furthermore, an LSR device that oscillates at physiologic frequencies may yield datasets that more accurately reflect physiologic function. Lastly, a device adapted for use in humans undergoing microlaryngoscopy has already been developed and will allow for real-time, direct measurements of tissue rheology. This capacity will improve our diagnostic abilities as well as our predictive models of surgical and biochemical interventions.

CONCLUSIONS

1. The LSR is a reliable tool for evaluation of vocal fold pliability in a research model in human, dogs, and rats.
2. Its sensitivity is satisfactory for the detection of focal stiffness in vocal folds of sufficient size.
3. Sites of focal stiffness correlate well with histologic findings of increased scar.
4. Pliability maps can now be plotted in normal, pathologic and test vocal folds with sufficient size.
5. Interventions to improve vocal fold stiffness in animal models can now be *directly* tested rather than relying upon indirect measures such as stroboscopic findings.
6. Second generation instruments are in evolution for the generation of human *in vivo* pliability maps derived during microlaryngoscopy.

Acknowledgments: We gratefully acknowledge the statistical assistance of Glen Leverson, PhD.

REFERENCES

1. Tateya T, Tateya I, Sohn JH, Bless DM. Histologic characterization of rat vocal fold scarring. *Ann Otol Rhinol Laryngol*. 2005;114:183–191.
2. Dailey SH, Ford CN. Surgical management of sulcus vocalis and vocal fold scarring. *Otolaryngol Clin North Am*. 2006;39:23–42.
3. Thibeault SL, Gray SD, Bless DM, Chan RW, Ford CN. Histologic and rheologic characterization of vocal fold scarring. *J Voice*. 2002;16:96–104.
4. Rousseau B, Hirano S, Chan RW, Welham NV, Thibeault SL, Ford CN, Bless DM. Characterization of chronic vocal fold scarring in a rabbit model. *J Voice*. 2004;18:116–124.
5. Rousseau B, Hirano S, Scheidt TD, Welham NV, Thibeault SL, Chan RW, Bless DM. Characterization of vocal fold scarring in a canine model. *Laryngoscope*. 2003;113:620–627.
6. Chan RW, Titze IR. Viscoelastic shear properties of human vocal fold mucosa: measurement methodology and empirical results. *J Acoust Soc Am*. 1999;106:2008–2021.
7. Berry DA, Clark MJ, Montequin DW, Titze IR. Characterization of the medial surface of the vocal folds. *Ann Otol Rhinol Laryngol*. 2001;110:470–477.
8. Berry DA, Herzel H, Titze IR, Krischer K. Interpretation of biomechanical simulations of normal and chaotic vocal fold oscillations with empirical eigenfunctions. *J Acoust Soc Am*. 1994;95:3595–3604.
9. Matts PM, Goodyer E. A new instrument to measure the mechanical properties of the human stratum corneum. *J Cosmet Sci*. 1988;49:321–323.
10. Hess MM, Mueller F, Kobler JB, Zeitels SM, Goodyer E. Measurements of vocal fold elasticity using the linear skin rheometer. *Folia Phoniatr Logop*. 2006;58:207–216.
11. Goodyer EN, Gunter H, Masaki A, Kobler JB. Mapping the visco-elastic properties of the vocal fold. *Advances in Quantitative Laryngology, Voice and Speech Research*, 2003.
12. Hertegård S, Dahlqvist Å, Goodyer EN, Maurer. Viscoelasticity in scarred rabbit vocal folds after hyaluronan injection short term results. *American Academy of Otolaryngology - Head and Neck Surgery Foundation*, 2004.
13. Goodyer E, Muller F, Bramer B, Chauhan D, Hess M. In vivo measurement of the elastic properties of the human vocal fold. *Eur Arch Otorhinolaryngol*. 2006;263:455–462.
14. Ford CN, Inagi K, Khidr A, Bless DM, Gilchrist KW. Sulcus vocalis: a rational analytical approach to diagnosis and

management. *Ann Otol Rhinol Laryngol*. 1996;105:189–200.
15. Sato K, Hirano M, Nakashima T. 3D structure of the macula flava in the human vocal fold. *Acta Otolaryngol*. 2003; 123:269–273.
16. Sato K, Hirano M. Histologic investigation of the macula flava of the human vocal fold. *Ann Otol Rhinol Laryngol*. 1995;104:138–143.
17. Zeitels SM, Hillman RE, Desloge R, Mauri M, Doyle PB. Phonomicrosurgery in singers and performing artists: treatment outcomes, management theories, and future directions. *Ann Otol Rhinol Laryngol Suppl*. 2002;190: 21–40.
18. Berry DA, Montequin DW, Tayama N. High-speed digital imaging of the medial surface of the vocal folds. *J Acoust Soc Am*. 2001;110:2539–2547.
19. Zhang Y, Jiang JJ. Chaotic vibrations of a vocal fold model with a unilateral polyp. *J Acoust Soc Am*. 2004;115: 1266–1269.
20. Hirano S, Nagai H, Tateya I, Tateya T, Ford CN, Bless DM. Regeneration of aged vocal folds with basic fibroblast growth factor in a rat model: a preliminary report. *Ann Otol Rhinol Laryngol*. 2005;114:304–308.
21. Gray SD, Hammond E, Hanson DF. Benign pathologic responses of the larynx. *Ann Otol Rhinol Laryngol*. 1995; 104:13–18.
22. Itoh T, Kawasaki H, Morikawa I, Hirano M. Vocal fold furrows. A 10-year review of 240 patients. *Auris Nasus Larynx*. 1983;10(suppl):S17–S26.
23. Hirano M. Morphological structure of the vocal cord as a vibrator and its variations. *Folia Phoniatr (Basel)*. 1974;26:89–94.

ur Arch Otorhinolaryngol (2007) 264:631–635
OI 10.1007/s00405-006-0239-z

LARYNGOLOGY

n vivo measurement of the shear modulus of the human vocal old: interim results from eight patients

ric Goodyer · Frank Müller · Katharina Licht · arkus Hess

Received: 5 September 2006 / Accepted: 13 December 2006 / Published online: 7 February 2007

Abstract The shear modulus of the vocal fold is an essential parameter required to enhance our understanding of how the vocal fold operates, to develop mathematical models of phonatation, and to provide benchmarks to quantify the effectiveness of surgical procedures. The authors announced the successful deployment of an instrument to measure vocal fold elasticity in vivo last year, and now present the data taken from eight patients in vivo. The shear modulus was measured at the mid-membranous point, in a transverse direction with respect to the axis drawn between the anterior commissure and vocal process. The range of mean shear modulus results is 701–2,225 Pa, with a mean value of 1,371 Pa.

Keywords Elasticity · Vocal fold biomechanics · Shear modulus

Introduction

Knowledge of the biomechanical properties of the vocal fold is an essential requirement for researchers seeking to mathematically model the operation of the vocal fold [1], and to provide benchmarks against which surgical procedures can be measured.

Research teams in Europe, USA and Japan are actively developing techniques to repair vocal fold tissue that has been damaged by scarring and other pathologies. Hyaluronic acid implants are a favoured technique [2–6]. However the use of growth factors [7–10] and groundbreaking research into the use of stem cells [11, 12] to stimulate self-healing is likely to prove more effective in the future. The ability to measure the biomechanical properties of the vocal fold in vivo is an essential prerequisite to determine the viability of any new tissue repair technique as this allows us to objectively assess the change that any tissue engineering procedure can achieve.

Whilst many research teams have presented vocal fold data obtained from excised tissue, few have reported data obtained in vivo. Most techniques employed infer elasticity from secondary phenomena. Kaneko [13] and Tamura [14] report the use of ultrasound, but do not publish any results for elastic modulus. Hsiao [15] reports the use of colour doppler imaging; if we assume a Poisson's ratio of 0.5, then these results translate to shear modulus ranges of 10,000–40,000 Pa for men and 40,000–1,00,000 Pa for women. McGlashan [16] reports the successful measurement of the velocity of the mucosal wave using stroboscopy, and has presented a value of 2,500 Pa for shear modulus at a conference. Only Tran and Berke [17–19] have deployed a method that directly measures the elasticity of the vocal fold in vivo.

The work by Tran, Berke, Gerratt and Kreiman in 1993 was groundbreaking, but relied on a cumbersome apparatus. Using modern components, the authors have duplicated their concept to develop a new, easy to

E. Goodyer (✉)
The Centre for Computational Intelligence,
Bioinformatics Group, DeMontfort University,
The Gateway, Leicester LE1 9BH, UK
e-mail: eg@dmu.ac.uk

F. Müller · K. Licht · M. Hess
Department of Phoniatrics and Pediatric Audiology,
University Medical Centre Hamburg-Eppendorf, Hamburg,
Martinistr. 52, 20246 Hamburg, Germany
e-mail: hess@uke.uni-hamburg.de

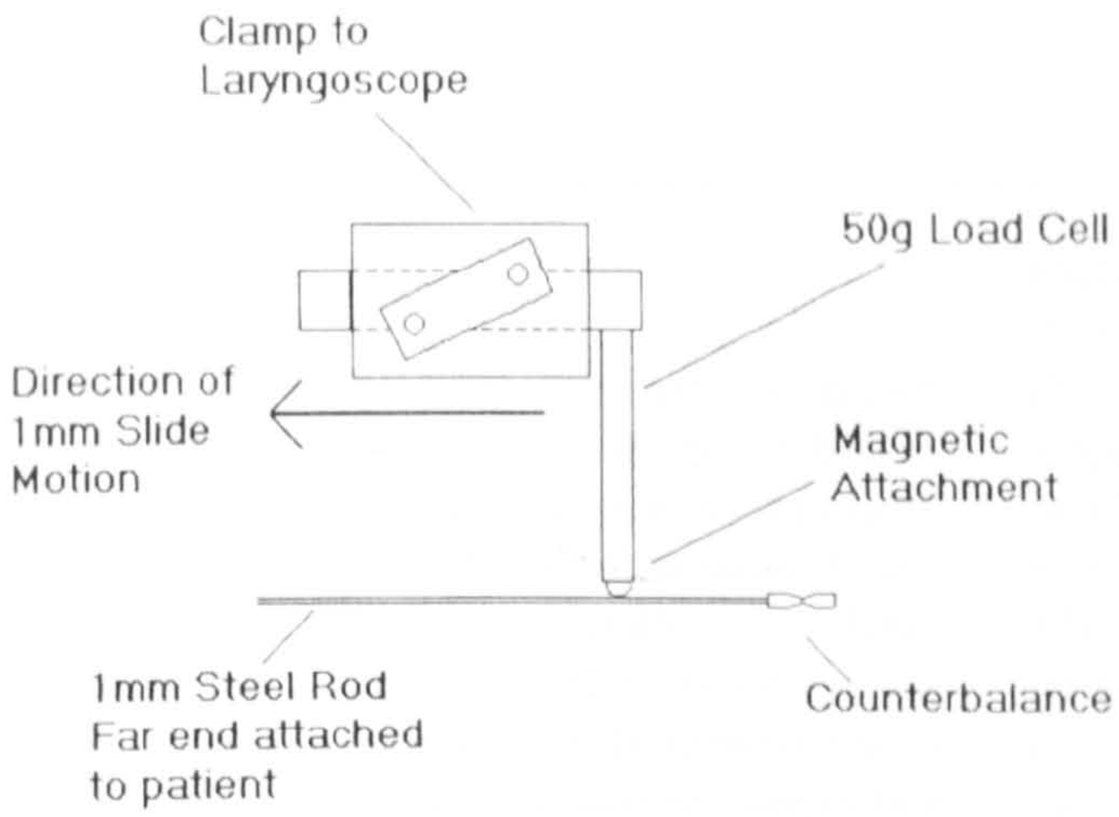

Fig. 1 Schematic of laryngeal tensiometer

use, instrument that is capable of repeatably obtaining in vivo elasticity data from anaesthetised patients [20].

This paper outlines this new instrument, the "laryngeal tensiometer" (LT), and presents our interim results obtained from eight volunteer patients. The range of shear modulus derived using this technique is comparable to that obtained by the same team from excised human larynxes [21, 22] using a linear skin rheometer (LSR). The range is also similar to those obtained by Chan [24] from excised human larynxes, and inferred by McGlashan.

The laryngeal tensiometer

The measuring apparatus consists of a load cell and slide arrangement that is securely clamped to the handle of a Storz laryngoscope. The clamp incorporates the horizontal slide arrangement that allows the user to displace a mounting block by a calibrated and repeatable distance. The distance has been set to be 1 mm.

Force data are obtained from a 25 g load cell supplied by RDP Electronics that is clamped to the moving block. The load cell is mounted such that the sensing element is located just above the viewing port of the laryngoscope. A hollow plastic chuck is fitted to the sensing element of the load cell; a bar magnet is located within the cavity, together with a steel ball bearing. Part of the surface of the ball bearing protrudes into the field of view of the laryngoscope. This bearing provides the user with a magnetic attachment to which the sensing probe can be attached.

The sensing probe is a steel rod, 1 mm diameter, which is inserted along the axis of the laryngoscope and attached to the vocal fold. The near end of the rod is magnetically coupled to the magnetised ball bearing. The holding force of the magnetic coupling has been measured to be 8 g. Previous research [20, 21] has demonstrated that the force exerted by vocal fold tissue in response to a 1 mm displacement is typically 0.3 g and is unlikely to be more than 2 g. This arrangement therefore is quite adequate to measure vocal fold tissue forces; it also provides the additional safety feature that the probe will slip rather than exert excessive force on the tissue.

Methodology

Figure 1 shows a schematic of the measurement apparatus. Figure 2 shows how the apparatus is clamped to the laryngoscope, with a close-up view of the magnetic attachment shown in Fig. 3.

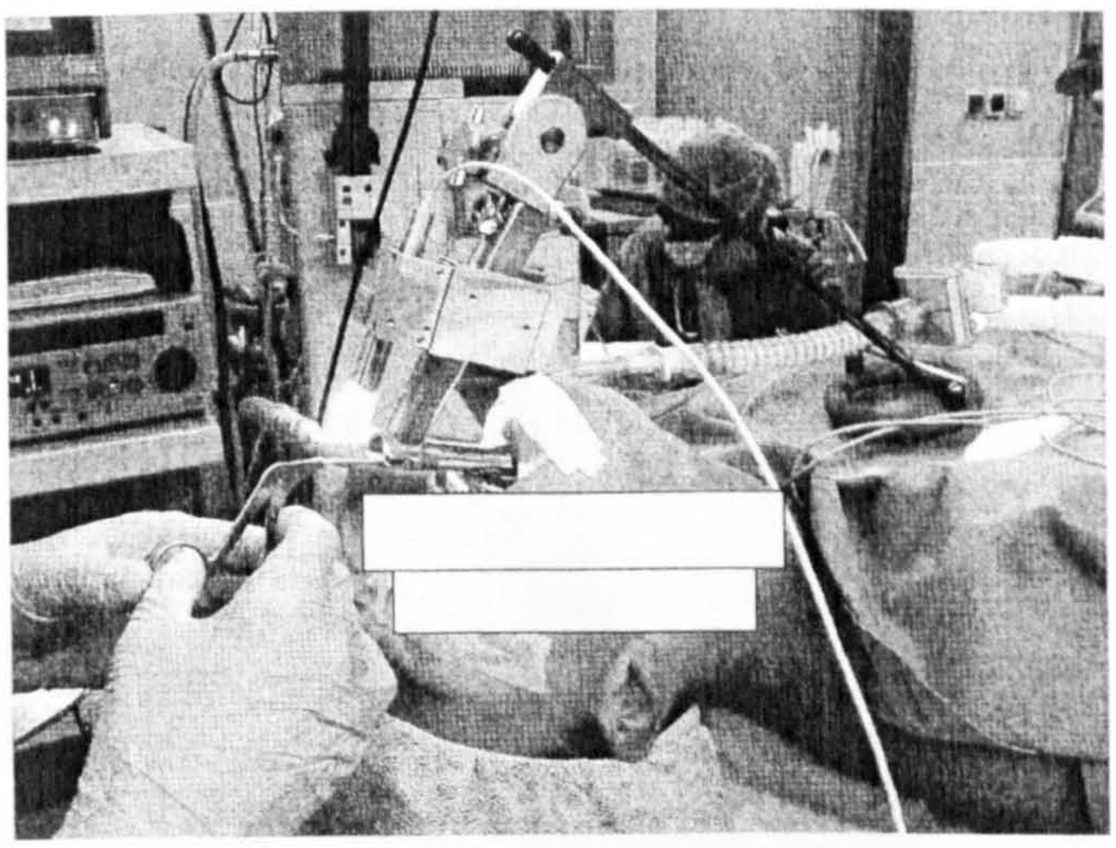

Fig. 2 In vivo laryngeal tensiometer set-up

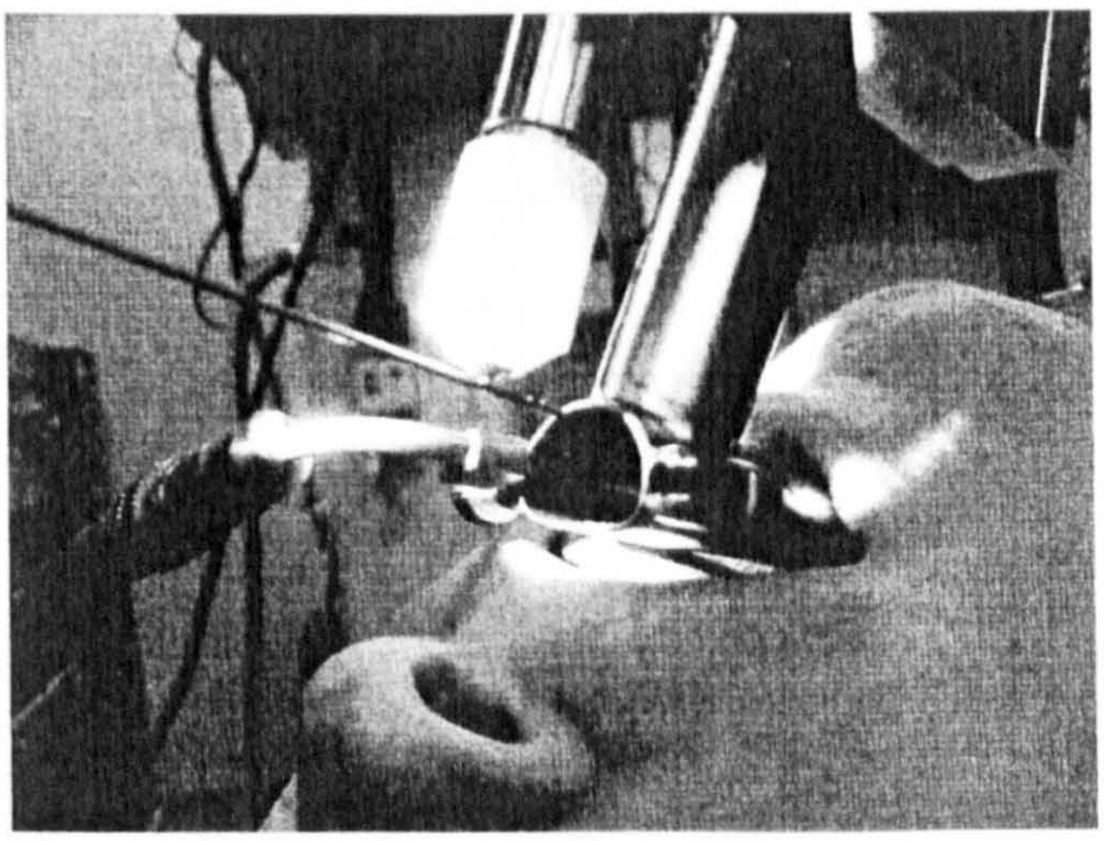

Fig. 3 Magnetic attachment of probe

Ssue attachment

he 1 mm rod is coated with a pharmaceutically anufactured mucosal adhesive, based on methylcellose, as used for dentures. This is a biocompatible, on-toxic and water soluble adhesive that sticks to the ucosa as long as it is not saturated with water. After nsing the adhesive with water, the stickiness de-eases rapidly and the adhesive is easily removed after e measurements. Meticulous mucosal inspection ter high magnification microlaryngoscopy revealed o mucosal changes at all.

As stated, the quality of this adhesive is critically ependent upon the moisture levels. The target site as dried with a cotton tip, and adhesive was applied nd held in place until it was fixed; this typically took p to a minute to occur. The lateral side of the steel rod as also coated with a small amount of adhesive, inerted down the laryngoscope and attached to the tisue at the mid-vocal fold (Fig. 4). The direction of otion is along the axis of the laryngoscope, such that he tissue is tangentially pulled towards the laryngoope, creating a shear stress on the tissue structure ike a billiards queue tangentially moving the skin rface of the resting hand's finger).

ata capture

he load cell signal-conditioning unit is an RDP S7DC. his gives an output that is proportional to the force applied to the load cell. Typical readings gave a signal change of less than 30 mV, therefore a Burr Brown IN114A instrument amplifier was used to provide an amplified signal prior to feeding the signal into a MAXIM 186 programmable analogue to digital converter (ADC). The ADC was controlled by an ATMEL T89C52RD2 microcontroller, which outputs the data on a serial line at a data rate of 115200BPS as three HEX-ASCII bytes terminated by a carriage return. This arrangement gave us the ability to transmit data at a maximum rate of approximately 2 kHz. The data acquisition rate was however set to be 1 kHz.

A portable laptop PC was used to capture the incoming data. The data capture programme was written using the DOS based Turbo C compiler from Borland.

The captured data were displayed graphically in real-time, providing essential visual feedback, and captured in a data file. The data files can then be subsequently analysed using off-line tools; in this instance we used Excel to extract the elastic data.

Data analysis

The raw data is the captured output from the load cell. The graph in Fig. 5 shows a typical trace obtained from a patient, the force difference being typically between 0.3 and 0.5 g. After each change in stress, there is a visible period of relaxation due to movement within the adhesive. The strain then tends to become linear. There are typically 15 readings within this linear section, which are averaged to obtain a value for the applied stress in units of grams force. The standard deviation within the linear section is typically less than 0.02 g, which is less than 10% of the force difference. It is our opinion that the cause of these perturbations is due to the fact that we are measuring extremely small forces in vivo, as these errors are not present when similar readings are taken from excised and rigidly mounted larynxes.

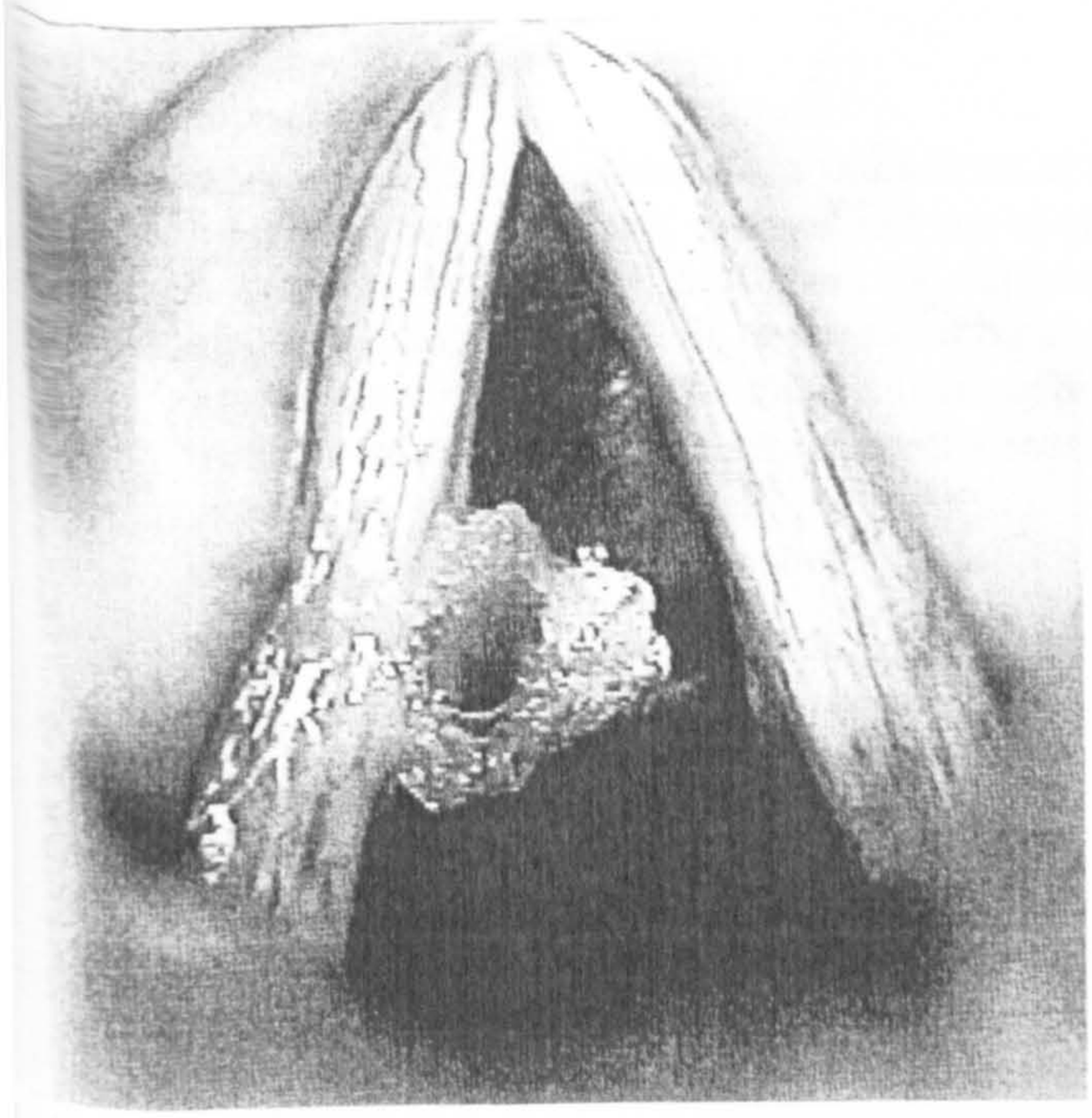

Fig. 4 Typical in vivo attachment

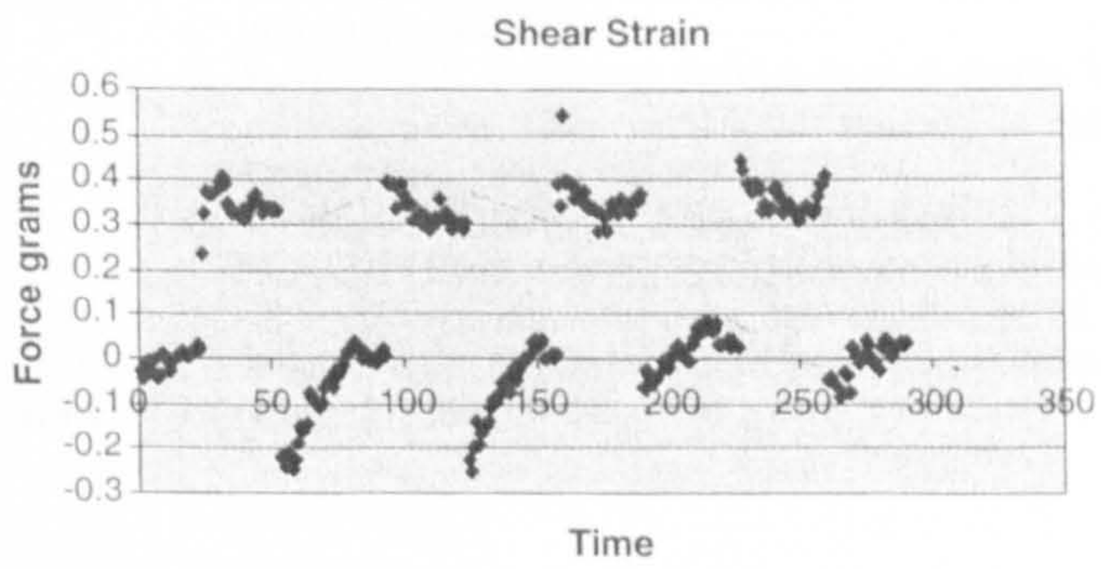

Fig. 5 A typical set of in vivo data

The tissue is stressed at least 5 times, and the force difference between each step change is determined. The average change in force is determined, and the standard deviation determined. This value is the force exerted as a result of a vocal fold tissue displacement of 1 mm.

The geometry of the test area was determined by measurement of the probe diameter, and inspection of images taken during the test. The area was typically 1 × 2 mm; however this assessment is the main cause of error in our final readings, which is why they are expressed as a range in the results table.

The shear stress σ is the applied force F per unit area A given by

$$\sigma = F/A \quad (1)$$

The resultant shear strain ε is given by lateral displacement P per tissue thickness T.

$$\varepsilon = P/T \quad (2)$$

Shear modulus G is defined as stress per unit strain

$$G = \sigma / \varepsilon \quad (3)$$

$$G = (F/P) * (T/A) \quad (4)$$

The force (F) is derived from the captured data, the displacement (P) is set to be 1 mm, the tissue thickness is assumed to be 1 mm and the area of attachment is estimated to be 1 × 2 mm. Using this geometry it is possible to derive the shear modulus of the vocal fold, which is expressed as a range to take account of the geometric uncertainties.

Results

Please see Table 1, which gives the full set of results in terms of shear modulus, the age and sex of the volunteer patients, and the coefficient of variance of the original data. The range is determined by applying an uncertainty of 10% to the dimensional estimates and the full effect of the standard deviation to the mean results.

The mean reading for the shear modulus is 1,371 Pa, with a range 701–2,225 Pa.

Discussion

Successful deployment of the LT device has yielded a range of results for the shear modulus of the vocal fold that is comparable with the few published results obtained by other researchers working in vivo, and with whole excised larynxes. The in vivo data obtained by Tran [17] offers a range of shear modulus from 2,450 to 29,400 Pa; which is the only comparable experimental setup to that used by us. McGlashan has reported a value of 2,500 Pa obtained by analysis of in vivo measurement of the mucosal wave.

Table 1 Range of shear modulus obtained from eight volunteer patients

Age	Sex	Coefficient of variance (%)	Shear modulus mean (Pa)	Shear modulus range (Pa)
36	F	15	933	681–1,184
37	F	19	777	553–1,000
28	F	11	701	526–877
70	F	Only 1 reading	1,972	1,582–2,363
28	F	10	1,819	1,364–2,274
52	F	27	901	609–1,194
63	M	22	1,637	1,220–2,055
55	M	17	2,225	1,605–2,843

Chan and Titze [23] have measured shear modulus in excised tissue using a parallel plate rheometer. Their earlier work gives value of between 100 and 1,000 Pa for shear modulus. Their later papers report a range of values for different subjects, taken under differing conditions. Values ranged from as low as 10 to 300 Pa.

Our results are also in line with data that we have obtained from a study of 20 excised larynxes, using a different direct measurement technique, which indicate an initial range of 1,000–1,500 Pa for shear modulus.

We are therefore confident that the results are valid. The poor coefficient of variance is a reflection of the difficulty of obtaining data in vivo; the other main cause of uncertainty is the determination of the surface area of contact of the measuring probe. It is our intention to continue to obtain more data in vivo in order to improve the statistical validity of the results. We also intend to modify the instrumentation to reduce the geometrical uncertainties of our methods.

References

1. Gunter HE (2003) A mechanical model of vocal-fold collision with high spatial and temporal resolution. J Acoust Soc Am 113(2):994–1000
2. Hertegård S, Dahlqvist Å, Goodyer E (2006) Viscoelastic measurements after vocal fold scarring in rabbits. Acta Otolaryngol 126(7):758–763
3. Hertegard S, Hallen L, Laurent C, Lindstrom E, Olofsson K, Testad P, Dahlqvist A (2002) Cross-linked hyaluronan used as augmentation substance for treatment of glottal insufficiency, safety aspects and vocal fold function. Laryngoscope 112:2211-9

Borzacchiello A, Mayol L, Garskog O, Dahlqvist A, Ambrosio L (2005) Evaluation of injection augmentation treatment of hyaluronic acid based materials on rabbit vocal folds viscoelasticity. J Mater Sci Mater Med 16(6):553–557
Chan RW, Titze IR (1999) Hyaluronic acid (with fibronectin) as a bioimplant for the vocal fold mucosa. Laryngoscope 109:1142–1149
Hahn MS, Teply BA, Stevens MM, Zeitels SM, Langer R (2006) Collagen composite hydrogels for vocal fold lamina propria restoration. Biomaterials 27(7):1104–1119, Epub 2005 Sep 9
Hirano S, Nagai H, Tateya I, Tateya T, Ford CN, Bless DM (2005) Regeneration of aged vocal folds with basic fibroblast growth factor in a rat model: a preliminary report. Ann Otol Rhinol Laryngol 114(4):304–308
Hirano S, Bless DM, del Rio AM, Connor NP, Ford CN (2004) Therapeutic potential of growth factors for aging voice. Laryngoscope 114(12):2161–2167
Kriesel KJ, Thiebault SL, Chan RW, Suzuki T, VanGroll PJ, Bless DM, Ford CN (2002) Treatment of vocal fold scarring, rheological and histological measures of homologous collagen matrix. Ann Otol Rhinol Laryngol 111:884–889
Chhetri DK, Head C, Revazova E, Hart S, Bhuta S, Berke GS (2004) Lamina propria replacement therapy with cultured autologous fibroblasts for vocal fold scars. Otolaryngol Head Neck Surg 131(6):864–870
Kanemaru S, Nakamura T, Yamashita M, Magrufov A, Kita T, Tamaki H, Tamura Y, Iguchi F, Kim TS, Kishimoto M, Omori K, Ito J (2005) Destiny of autologous bone marrow-derived stromal cells implanted in the vocal fold. Ann Otol Rhinol Laryngol 114(12):907–912
Kanemaru S, Nakamura T, Omori K, Kojima H, Magrufov A, Hiratsuka Y, Hirano S, Ito J, Shimizu Y (2003) Regeneration of the vocal fold using autologous mesenchymal stem cells. Ann Otol Rhinol Laryngol 112(11):915–920
Kaneko T, Uchida K, Komatsu K, Kanesaka T, Kobayashi N, Naito J (1981) Mechancial properties of the vocal fold: measurement in vivo. In: Steven KN, Hirano M (eds) Vocal fold physiology. Tokyo University of Tokyo Press, Tokyo, pp 365–376
14. Tamura E, Kitahara S, Kohno N (2002) Intralaryngeal application of a miniturized ultrasonic probe. Acta Otolaryngol 122:92–95
15. Hsiao T, Wang C, Chen C, Hsieh F, Shau Y (2002) Elasticity of human vocal folds measured in vivo using color doppler imaging. Ultrasound Med Biol 28(9):1145–1152
16. McGlashan JA, de Cunha DA, Hawkes DJ, Harris TM (1998) Surface mapping of the vibrating vocal folds.In: Proceedings of the 24th world congress of the international association of logopedics and phoniatrics (IALP), Amsterdam. August 1998
17. Tran QT, Berke GS, Gerratt BR, Kreiman J (1993) Measurement of Young's modulus in the in vivo human vocal folds. Ann Otol Rhinol Laryngol 102:584–591
18. Berke GS (1992) Intraoperative measurement of the elastic modulus of the vocal fold. Part 1. Device development. Laryngoscope 102:760–769
19. Berke GS, Smith ME (1992) Intraoperative measurement of the elastic modulus of the vocal fold. Part 2. Preliminary results. Laryngoscope 102:770–778
20. Goodyer EN, Muller F, Bramer B, Chauhan D, Hess M (2006) In vivo measurement of the elastic properties of the human vocal fold. Eur Arch Otorhinolaryngol 263(5):445–462
21. Goodyer EN, Gunter H, Masaki A, Kobler J (2003) Mapping the viscoelastic properties of the vocal fold. AQL 2003, Hamburg
22. Hess M, Muller F, Kobler JB, Zeitels S, Goodyer EN (2006) Measurements of vocal fold elasticity using the linear skin rheometer. Folia Phoniatrica Logop 58(3):207–216
23. Goodyer EN, Hemmerich S, Müller F, Kobler JB, Hess M (2007) The shear modulus of the human vocal fold, preliminary results from 20 larynxes. Eur Arch Otorhinolaryngol 264(1):45–50
24. Chan RW, Titze IR (1999) Viscoelastic shear properties of human vocal fold mucosa. J Acoust Soc Am 106:2008–2021

Eur Arch Otorhinolaryngol (2007) 264:45–50
DOI 10.1007/s00405-006-0133-8

LARYNGOLOGY

The shear modulus of the human vocal fold, preliminary results from 20 larynxes

Eric Goodyer · Sandra Hemmerich · Frank Müller · James B. Kobler · Markus Hess

Received: 23 April 2006 / Accepted: 11 July 2006 / Published online: 19 August 2006

Abstract Quantification of the elastic properties of the human vocal fold provides invaluable data for researchers deriving mathematical models of phonation, developing tissue engineering therapies, and as normative data for comparison between healthy and scarred tissue. This study measured the shear modulus of excised cadaver vocal folds from 20 subjects. Twenty freshly excised human larynxes were evaluated less than four days post-mortem. They were split along the saggital plane and mounted without tension. Shear modulus was obtained by two different methods. For method 1 cyclical shear stress was applied transversely to the mid-membranous portion of the vocal fold, and shear modulus derived by applying a simple shear model. For method 2 the apparatus was configured as an indentometer, and shear modulus obtained from the stress/strain data by applying an established analytical technique. Method 1 shear model for male larynxes yielded a range from 246 to 3,356 Pa, with a mean value of 1,008 and SD of 380. The range for female larynxes was 286–3,332 Pa, with a mean value of 1,237 and SD of 768. Method 2 indentometer model for male larynxes yielded a range from 552 to 2,741 Pa, with a mean value of 1,000 and SD of 460. The range for female larynxes was 509–1,989 Pa, with a mean value of 1,332 and SD of 428. We have successfully demonstrated two methodologies that are capable of directly measuring the shear modulus of the human vocal fold, without dissecting out the vocal fold cover tissue. The sample size of nine female and 11 male larynxes is too small to validate a general conclusion. The high degree of variability in this small cohort of subjects indicates that factors such as age, health status, and post-mortem delay may be significant; and that there is range of 'normality' for vocal fold tissue.

Keywords Elasticity · Shear modulus · Vocal fold biomechanics · Shear modulus of the vocal fold

This project received financial support from the Engineering Physics and Science Research Council of Great Britain (EPSRC) and the Eugene B Casey Foundation (JBK).

E. Goodyer (✉)
The Centre for Computational Intelligence—Bioinformatics Group, DeMontfort University,
The Gateway, Leicester LE1 9BH, UK
e-mail: eg@dmu.ac.uk

S. Hemmerich · F. Muller · M. Hess
Department of Phoniatrics and Pediatric Audiology,
University Medical Centre Hamburg-Eppendorf,
Martinistr. 52, 20246 Hamburg, Germany
e-mail: hess@uke.uni-hamburg.de

J. B. Kobler
Center for Laryngeal Surgery and Voice Rehabilitation,
Massachusetts General Hospital,
One Bowdoin Sq., Boston, MA 02114, USA

Introduction

Intraoperative measurements of vocal fold pliability would be very useful in the practice of phonosurgery. As a preliminary step in designing a system to make such measurements we conducted a study on fresh cadaver vocal folds. The purpose of this study was to obtain some preliminary data regarding the range of normal shear modulus values for male and female vocal folds, and to compare two methods for obtaining these data. Two different techniques were developed to measure the shear modulus of the tissue at the

mid-membranous position without the need to dissect out the vocal fold out of the larynx. One method was the application of cyclical shear stress transversely to the axis between the vocal process and the anterior commisure; the resultant stress/strain characteristics are used to derive the tissue modulus using a simple shear model. The second method was the use of an indentometer to compress the tissue normal to the surface; the mathematical model developed by Hayes et al. [5] can then be applied to the resultant stress/strain data to obtain another measure of the tissue modulus.

There are very few published reports that give the shear modulus for a group of human vocal folds. Those that do exist employed a range of different techniques, such as ultrasonics, optics, and mechanics. The ultrasonic and optical methods infer shear modulus from secondary phenomena, whereas the mechanical methods directly measured the biomechanical response of the tissue. Our results compare most favourably with those obtained from human tissue using mechanical methodologies.

Materials and methods

All measurements were made with a Linear Skin Rheometer (LSR) [10, 14]. The LSR is a precision instrument originally designed to measure the viscoelastic properties of the stratum corneum. Based upon the concept of the Gas Bearing Electrodynanometer (GBE) [14] developed by Hargens in the 1960s, the LSR uses modern micro-mechanical components to achieve force feedback control in real time and precision position measurement. It is now being successfully used to measure the more delicate tissue of the vocal fold [4, 6, 7].

Method 1: simple shear model

A flat probe is attached to the vocal fold epithelium, mid-membranous between the anterior commisure and vocal process. A sinusoidal force F is applied to the material under test in a transverse direction so as to apply a shear stress to the vocal fold, and the resultant displacement P is logged. The driving force was set to be 0.5 g, which typically results in a displacement of 1 mm. The frequency of operation was set to be 0.3 Hz. The value of 1 mm was chosen as this represented a realistic displacement with respect to the geometry of the tissue structure, the measurement frequency is the one used by researchers when applying the LSR to analysis of the stratum corneum; the results can therefore only be used to measure the elasticity of the tissue and not the viscosity. When comparing our results with other published results we have whenever possible selected data obtained using comparable frequencies; and the closest methodology to ours is the study carried out by Tran et al. [15], which was effectively at DC.

$$F = F_{max} \sin(t). \tag{1}$$

$$P = P_{max} \sin(t + R). \tag{2}$$

where F is the instantaneous force, F_{max} the maximum force, t the time over one cycle in radians, P the instantaneous displacement, P_{max} the maximum displacement, and R the phase shift in radians.

The Dynamic Spring Rate (DSR) of the tissue is F_{max}/P_{max}, and is expressed in units of grams force per millimetre. The DSR can then be used to determine the shear modulus using knowledge of the geometry of the test site as follows:

The shear stress σ is the applied force F per unit area A given by

$$\sigma = F/A. \tag{3}$$

The resultant shear strain ϵ is given by lateral displacement P per material thickness T.

$$\varepsilon = P/T. \tag{4}$$

Shear modulus G is defined as stress per unit strain

$$G = \sigma/\varepsilon. \tag{5}$$

$$G = (F/P) \cdot (T/A). \tag{6}$$

As DSR = F/P then

$$G = \mathrm{DSR} \cdot T/A. \tag{7}$$

Data are obtained by gluing the flat tip of a probe arm to the tissue with cyanoacrylate. This is a very fast acting adhesive that internally polymerises in the presence of a small amount of water, achieving the bond by in-filling crevices on the surface of the epithelium. The adhesive works by first forming a surface skin, with polymerisation continuing at a high rate internally. In view of the speed of action, and the manner of the bonding, we consider that it is highly improbable that the adhesive solvents would have time, or be able to penetrate into the tissue to the extent that it would perturb the results.

The area of attachment (A) is determined by direct measurement. The simple shear model does not take account of tissue that is attached to the column that is directly stressed. The Hayes formula provides a mathematically rigorous correction for indentometer data, which in addition to compressing tissue with the indentor also exerts shear stresses to surrounding tissue. No such similar rigorous solution has been found for pure shear stresses; the derivation of such a solution will form part of a new study.

The additional surface area that was subjected to the applied stress was observed to be typically 0.75 mm around the area of direct attachment; therefore, the dimensions were increased by this amount on all four sides. The thickness of the vocal fold tissue (T) is typically 1 mm.

Using these geometric values a range of shear moduli can be derived for each sample. Ten readings were taken from each test site, and middle of each range was averaged. These results are referred to as the 'shear model' in the text.

Method 2 indentometer

In the second approach the LSR was used as an indentometer. In this arrangement a 1 mm diameter flattened probe tip is pushed into the tissue, and the force-displacement data is then captured in real time. The measurement point was chosen to be the centre of the area used for the shear model method already described in order to enable a meaningful comparison. The indentor was located clear of the tissue with an air gap of 1 mm. it was then driven into the vocal fold for a distance of 2 mm at a speed of 1 mm/s.

For a homogeneous material the resultant relationship will be logarithmic, forming a classic compression cycle curve. However, many researchers have correctly stated that indentation of a soft tissue does not follow this simple rule because surrounding tissue remains in contact with the depressed section to which a shear stress is applied.

One widely accepted model is the one originally proposed by Fung, from which Hayes et al. [5] developed a rigorous mathematical solution. This mathematical device is based upon a solution for Yung's 3D partial differential equations that explain the deformation of soft tissue [16]. This solution offers a 'correction factor' to Yung's equations that takes account of the shear strain surrounding the indentation. which requires knowledge of the tissue's Poisson's ratio (v). v is the relationship between a materials' elongation and sheer strains. For an incompressible material it is 0.5.

The correction factor (κ) is a function of the indentor radius (a), the tissue thickness and Poisson's ratio (v), assumed to be 0.5. Our indentor radius (a) is 0.5 mm, and we assume the thickness of the tissue to be 1 mm. Hayes gives the following expression in his paper as the definition of κ together with a table of solutions.

$$k = (F \cdot (1 - v))/(4aGw), \tag{8}$$

which can be rearranged to give

$$G = \frac{(F/w) \cdot (1 - v) \cdot 9.80665}{(4a\kappa)}. \tag{9}$$

where κ is the Hayes correction factor obtained from the published table, F the applied force, v the Poisson's ratio, a the indentor radius, G the shear modulus, and w the depth of penetration.

The 9.80665 converts the units for shear modulus (G) into Pa.

Each sample was indented ten times. From the resultant stress/strain curves we select the initial linear section, apply a least squared fit, and obtain the best value for F/w in units of g/mm. All the other values are known. These results are referred to as the 'indentometer model' in the text.

Results

Overall results

Please refer to tables and graphs for the full set of results (Figs. 1, 2; Tables 1, 2). The graphs show the distribution of shear modulus with respect to the donor's age.

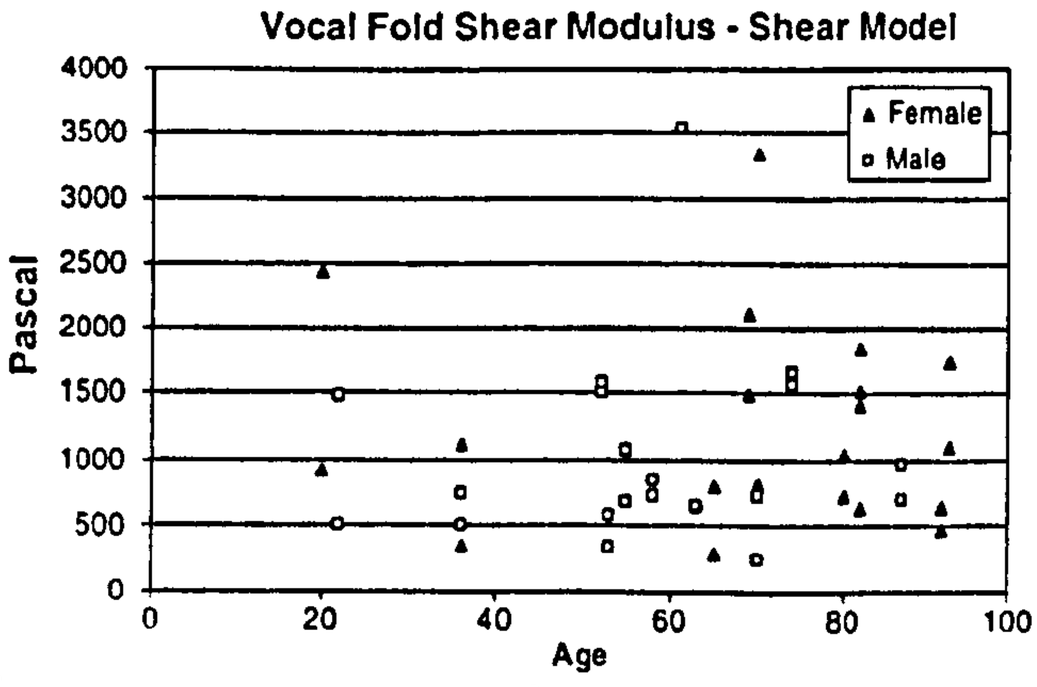

Fig. 1 Distribution of shear model modulus with age

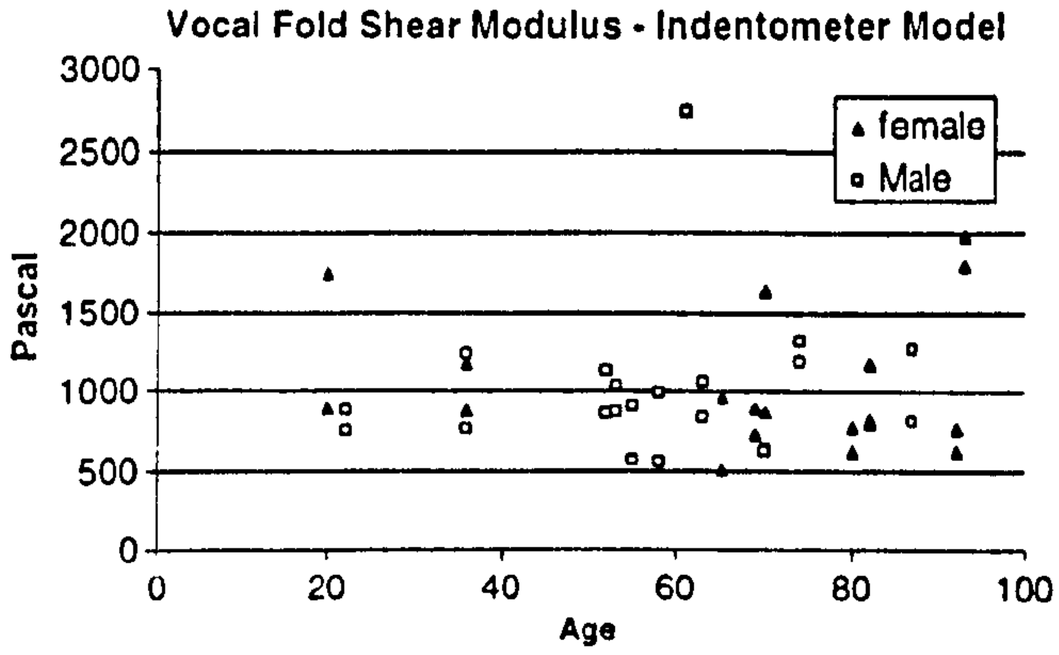

Fig. 2 Distribution of indentometer model shear modulus with age

Table 1 Shear modulus of female larynxes

Age (left then right)	Shear model (Pa)	CofV %	Indentation model (Pa)	CofV %
20	912	2 9	893	18
20	2,439	8.1	1,746	8.2
36	351	9	1,179	3.3
36	1,110	3	879	15
65	286	14	963	40
65	802	17.5	509	16
69	1,491	3.3	892	18
69	2,101	5.9	735	33
80	1,749	5.8	1,796	14
80	1,100	4.9	1,989	11.5
82	1,844	15.4	827	24
82	1,520	8.2	1,181	18.6
82	628	8.8	809	22
82	1,408	4	802	25
92	723	21.1	782	19.7
92	1,042	3.5	627	12.3
93	472	10.5	765	16
93	633	2	621	29

The results can be summarised as follows:
Male shear modulus

1. Range = 246–3,536 Pa (shear model).
2. Mean = 1,008 Pa (shear model).
3. SD = 380 (shear model).
4. Range = 552–2,741 Pa (indentometer model).
5. Mean = 1,000 Pa (indentometer model).
6. SD = 460 (indentometer model).

Female shear modulus

1. Range = 286–3,332 Pa (shear model).
2. Mean = 1,237 Pa (shear model).
3. SD = 768 (shear model).
4. Range = 509–1,989 Pa (indentometer model).
5. Mean = 1,332 Pa (indentometer model).
6. SD = 428 (indentometer model).

Table 2 Shear modulus of male larynxes

Age	Shear model (Pa)	CofV %	Indentation model (Pa)	CofV %
22	1,474	3.5	877	7.3
22	501	5.2	753	33.7
36	491	6.1	1,241	12.7
36	742	4.2	761	9.2
52	1,507	3.4	1,134	9.4
52	1,582	13	856	16
53	336	7.2	868	22
53	565	32	1,031	16
55	1,069	9.4	904	23.5
55	684	14	567	23
58	840	11.3	984	19.6
58	729	8.3	552	17.2
61	3,536	2.3	2,741	7.7
63	637	6.1	1,056	26
63	644	6	832	18.9
70	718	4.5	631	25
70	246	19	618	16.9
74	1,658	3.5	1,188	14.9
74	1,652	11.3	1,321	19.9
87	958	5.4	1,272	22
87	696	3.9	808	22

Comparison between methods 1 and 2

We can compare the data obtained by both methods from the same tissue sample as a validation procedure. The total data set consists of 39 pairs of data from the left- and the right-hand sides of the 20 larynxes (one hemi-larynx was damaged during hemisection).

A standard statistical tool that is used to compare two sets of results with each other is the correlation coefficient (CC), on a scale of 0–1; where 1 is a perfect match.

Using all 39 pairs of data we obtain a CC of 0.66. This is a fair result, but not perfect. By selectively rejecting ~20% of the data set the CC rises to a far more acceptable value of 0.8; indicating that we require a larger sample group to improve our confidence in both methods.

Comparison between left- and right-hand sides

A further validation of the methodology can be obtained by comparing the results obtained from the left- and the right-hand sides of the same larynx. In total there are 19 left/right pairs of data available for each method. The CC for all data pairs is poor, being 0.22 for the shear model and 0.47 for the indentometer model. By rejecting a few obvious outliers it is possible to obtain a CC of 0.7 or better. This result again demonstrates the need for expanding the size of the data set.

Discussion

Few researchers have reported data obtained by direct measurement of the mechanical properties of intact larynxes. Results have either been inferred from observations of acoustic or optical effects, or the vocal fold cover has been excised and tested mechanically out of anatomical context.

Kaneko et al. [9] and Tamura et al. [13] amongst other have reported the derivation of visco-elastic properties using ultrasound in vivo and with excised larynxes. However, they do not offer comparable data relating to the elastic modulus.

Hsiao et al. [8] have reported success in obtaining values for Young's Modulus using colour Doppler imaging in vivo. If we assume a Poisson's ratio of 0.5 then these results translate to shear modulus ranges of 10,000–40,000 Pa for men and 40,000–100,000 Pa for women.

McGlashan et al. [11] have reported a method to infer vocal fold properties using an in vivo optical technique that generated a series of dynamic surface maps, from which they derived the velocity of the mucosal wave. A more recent conference report gives a shear modulus of 2,500 Pa.

Chan and Titze [3] have measured shear modulus in excised tissue using a parallel plate rheometer. Their earlier work gives a value of between 10 and 1,000 Pa for shear modulus. Their later papers report a range of values for different subjects, taken under differing conditions. Values ranged from as low as 10 to 300 Pa, for low frequency cycling.

The in vivo data obtained by Tran et al. [15] offers a range of shear modulus from 2,450 to 29,400 Pa. Berke and Smith [2] describe the apparatus used in more detail, and give some results for Young's Modulus using canine data. The medial result equates to a shear modulus of 1,450 Pa. Perlmann et al. [12] have obtained canine data using excised tissue with a range of 9,460–41,200 Pa for a variety of conditions. Alipour's excised canine results [1] for Young's Modulus equate to a shear modulus of 13,960 Pa for a Poisson's ratio of 0.5.

Our results are indicative of a transverse shear modulus for the vocal fold of between 300 and 4,500 Pa. As yet there is insufficient data to enable us to draw generalised conclusions; and the difficulty of obtaining repeatable measurements from soft tissue is demonstrated by the poor coefficients of variance relating to the original raw data. Our results compare most favourably with those obtained from intact larynxes, by direct mechanical measurements (Tran and Berke), or by inference using the optical technique (McGlashan). We believe that this is because these techniques measured or derived shear modulus from intact larynxes, with the vocal fold cover still attached to the underlying structures.

Our intention is to continue this study in order to improve the repeatability of the results, to reduce the CofV of the raw data, and to expand the data sets to achieve a statistically acceptable sample size. Our measure for success will be an improved convergence of data obtained by both methods and an improved correlation between data obtained from the left- and right-hand sides.

The resultant strains that both our methods are applying are small, typically between 0.5 and 1 mm; we believe that we are mainly acting on the vocal fold cover, but this hypothesis needs to be demonstrated. In future studies we will complete the analysis by dissecting out the vocal fold tissue and measuring it in isolation enabling a more in-depth analysis of our results.

Conclusion

We have shown that it is possible to directly measure the shear modulus of the vocal fold without dissecting the tissue from its surroundings, using two mechanical methodologies. Thus, the data obtained is more representative of the elastic response during phonation than data obtained from dissected tissue measured in isolation.

The two techniques outlined offered similar results and therefore support each other. They are also similar to data obtained by other researchers using direct mechanical methodologies, and obtained from intact larynxes. Insufficient data have yet been obtained to make generalised conclusions, or to provide a statistically acceptable data set. Both methods are promising, and will be improved in future studies. For the shear modulus method the primary cause of error is the uncertainty relating to the area of attachment. This will be addressed by the use of a more repeatable probe design and the development of a mathematical model that adequately takes account of the attached tissue that is not under direct stress. The indentometer has consistently shown more consistent results, and this apparatus will be redesigned to remove observed mechanical problems.

References

1. Alipour-Haghighi F, Titze IR (1990) Elastic modulus of vocal fold tissue. J Acoust Soc Am 90(3):1320–1331

2. Berke GS, Smith ME (1992) Intraoperative measurement of the elastic modulus of the vocal fold. Part 2. Preliminary results. Laryngoscope 102:770–778
3. Chan RW, Titze IR (1999) Viscoelastic shear properties of human vocal fold mucosa. J Acoust Soc Am 106:2008–2021
4. Goodyer EN, Gunter H, Masaki A, Kobler J (2003) Mapping the visco-elastic properties of the vocal fold. AQL, Hamburg
5. Hayes WC, Keer LM, Herrmann G, Nockros LF (1972) Mathematical analysis for indentation tests of articular cartilage. J Biomech 5(5):541–551
6. Hertegård S, Dahlqvist Å, Goodyer E, Maurer (2005) Viscoelastic measurements after vocal fold scarring. In: Rabbits—short-term results after hyaluronan injection acta oto-laryngologica (in press)
7. Hess M, Muller F, Kobler J, Zeitels A, Goodyer EN (2005) Measurements of vocal fold elasticity using the linear skin rheometer folia phoniatrica (in press)
8. Hsiao T, Wang C, Chen C, Hsieh F, Shau Y (2002) Elasticity of human vocal folds measured in vivo using color doppler imaging. Ultrasound Med Biol 28(9):1145–1152
9. Kaneko T, Uchida K, Komatsu K, Kanesaka T, Kobayashi N, Naito J (1981) Mechancial properties of the vocal fold: measurement in-vivo. In: Steven KN, Hirano M (eds) Vocal fold physiology, Tokyo University of Tokyo Press, Tokyo pp 365–376
10. Matts P, Goodyer EN (1998) A new instrument to measure the mechanical properties of the human stratum corneum. J Cosmet Sci 49:321–323
11. McGlashan JA, de Cunha DA, Hawkes DJ, Harris TM (1998) Surface mapping of the vibrating vocal folds. In: Proceedings of the 24th world congress of the international association of logopedics and phoniatrics (IALP), Amsterdam, August 1998
12. Perlmann AL, Titze IR, Donald SC (1984) Elasticity of canine vocal fold tissue. J Speech Hear Res 27:212–219
13. Tamura E, Kitahara S, Kohno N (2002) Intralaryngeal application of a miniturized ultrasonic probe. Acta Otolaryngol 122:92–95
14. The gas bearing electrodynamometer and the linear skin rheometer in bioengineering of the skin, skin biomechanics. CRC Press, Boca Raton, Chap. 8; ISBN 0-8493-7521-5
15. Tran QT, Berke GS, Gerratt BR, Kreiman J (1993) Measurement of young's modulus in the in vivo human vocal folds. Ann Otol Rhinol Laryngol 102:584–591
16. Fung YC (1981) Biomechanics: mechanical properties of living tissues. Springer-Verlag, New York

THE ANISOTROPIC NATURE OF THE VOCAL FOLD

A.-K. Licht*, E. Goodyer#, F. Müller*, JB Kobler♦, K Püschel°, M Hess*

*Department of Phoniatrics and Pediatric Audiology, °Institute for Forensic Medicine, University Medical Centre Hamburg-Eppendorf, Germany, # The Centre for Computational Intelligence-Bioinformatics Group, DeMontfort University, Leicester, UK, ♦ Center for Laryngeal Surgery and Voice Rehabilitation, Massachusetts General Hospital, Boston, MA, USA

1. INTRODUCTION

The human vocal fold is a complex, multilayered structure. The different layers present themselves with different visco-elastic properties. This makes them ideally suited for phonation. The elastic properties of vocal fold are important for understanding the mechanical properties of this tissue in general, and for understanding alterations in the mechanical response of vocal fold tissue due to polyps, aging, scars and phonosurgical procedures.

Research teams worldwide are actively developing new techniques to repair vocal fold tissue damaged by scars or other pathologies. Matching the properties of the repair techniques and augmentation materials to the properties of the vocal fold are essential to ensure the recreation of the correct biomechanical properties of a healthy vocal fold. As a consequence, fundamental biomechanical property data of the vocal fold is required. This knowledge is also important to help clinicians understand how these new procedures react under clinical conditions as well as to help to predict behavior of the vocal fold/ restoration material interface.

The biomechanical properties have been reported in many studies. These research projects observe the biomechanical properties solely of excised laryngeal tissue, which is tested as a whole. A better understanding of the oscillatory nature is only possible if we quantify the biomechanical properties of the tissue within its anatomical context and orientation, i.e. if we don't dissect the vocal fold tissue out of its underlying structures and use intact larynges for our measurements.

The authors have announced the successful development of a new, easy to use instrument to measure vocal fold elasticity in-vivo, the Laryngeal Tensiometer [1]. Preliminary results from 8 patients were presented in 2006 [2]. Parallel to the in-vivo studies we have used a Linear Skin Rheometer to obtain in-vitro biomechanical data from 34 excised human larynxes. The methods employed were direct application of a shear strain and the use of an indentometer. The preliminary results of the first 20 freshly excised cadaver larynges were published in 2007 [3]. For male larynxes the mean shear modulus was found to be 1008 Pascal (shear

method) and 1327 Pascal (indentation method). For female larynxes the mean shear modulus was found to be 1327 Pascal (shear method) and 1332 Pascal (indentation method). The LSR is being successfully used to measure the more delicate tissue of the vocal fold in a range of other published studies ([4], [5], [6]).
The purpose of this work was to determine layer dependent and directional variations of the elastic properties of the vocal fold, in short the anisotropic behavior. Our hypothesis is that vocal fold tissue shows broad variations of elastic modulus with respect to age, layer and direction of applied shear force.

Our specific prospective objective is to obtain visco-elastic measurement data from a large cohort of human larynxes. So we can keep sight of our goal to provide quantitative data to go ahead with the development of new procedures, for example augmentation, tissue engineering and stem cell therapy. Patients which have lost the ability to phonate because of an affected vocal fold will profit by a better knowledge of the biomechanical structures.

2 MATERIALS AND METHODS

Tissue collection

Human cadaver larynges were obtained within 3 days (mean) of death. There were no cases with a prior history of endotracheal intubation, laryngeal disease, or laryngeal trauma before death. The past medical history was known for age, sex, diseases and cause of death. 14 larynges were evaluated in the following groups: 7 adult males (age range, 47–76 y) and 7 adult females (age range, 47–92 y).

Tissue preparation

The larynges were extracted and split along the sagittal plane and mounted without tension. The LSR probe was attached primarily to the vocal fold epithelium mid-membranous between the anterior commisure and vocal process using suction catheter of 2 mm inner diameter, and the results analysed using the mathematical transformations shown in our earlier publications [3].
In order to quantify the anisotropic behavior, the elastic response was measured at 5 different angles of applied stress. The longitudinal direction axis from the vocal process to the anterior commisure is defined as 0°. Measurements were taken at 0°, 45°, 90°, 135° and 180°.
In addition, the multilayered vocal fold was measured at all 5 different angles in 4 consecutive steps. First we measured the complete vocal fold. Subsequently, we removed the epithelial layer, composed of nonkeratinized stratified squalous cells, with the aid of opthalmological

dissecting instruments, and repeated the measurement on the lamina propria. The lamina propria was then removed and we measured the ligament and the muscle. Finally, we removed the vocal ligament and repeated the measurement on the thyroarytenoid muscle alone.

Histochemical method

Both hemilarynxes were obtained either with the entire vocal fold or following division into the different layers from each larynx en bloc and fixed in 10% paraformaldehyde for 24 hours. After fixation, two 5 mm thick transverse sections were cut in the midregion of the vocal fold, dehydrated in 70% alcohol. Afterwards the specimens were embedded in paraffin, stained with haematoxylin and eosin and 4 µm thick sections were cut in the coronal direction. The samples were observed under a standard light microscope using optical polarization.
The layer preparation process was successful, subsequent macroscopic inspection of the histological images established that the result was the desired single vocal fold layer (Figures 1–4). Consequently, the successive exposure of different layers was correlated with histology.

Figure 1. Frontal histologic section of the vocal fold, stained with Haematoxylin-eosin and observed under conventional light microscope. Note the epithelium, superficial, intermediate and deep layers and vocal muscle.

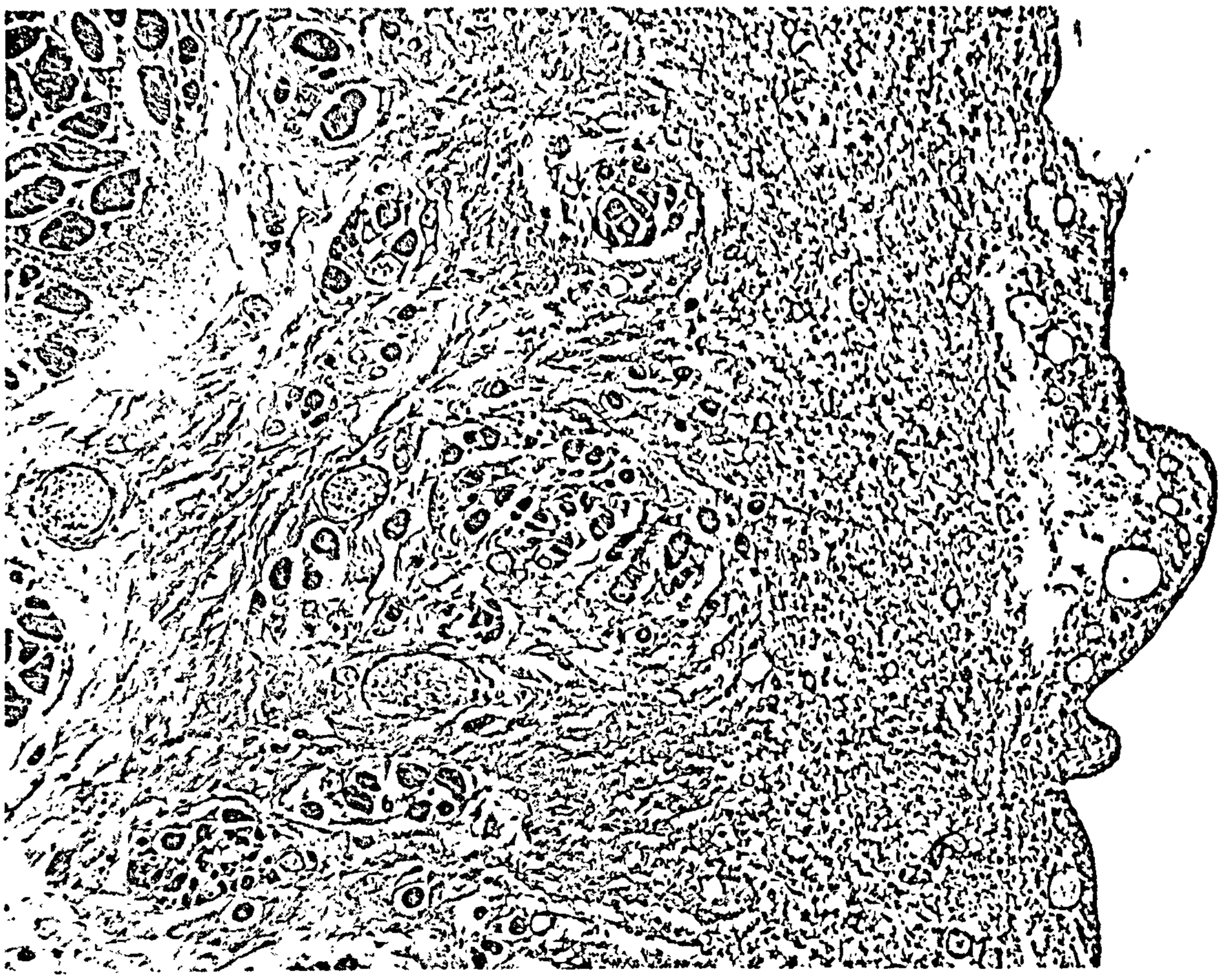

Figure 2. Frontal histologic section of the vocal fold, stained with Haematoxylin-eosin and observed under conventional electronic light microscope (magnification??). Following elaborate microsurgical removal of the epithelium you can note the superficial, intermediate and deep layers and vocal muscle.

Figure 3. Frontal histologic section of the vocal fold, stained with Haematoxylin-eosin and observed under conventional electronic light microscope (magnification??). Following elaborate microsurgical removal of the epithelium and superficial and intermediate layer of the vocal fold you can note the deep layer, i.e. the ligament and the vocal muscle.

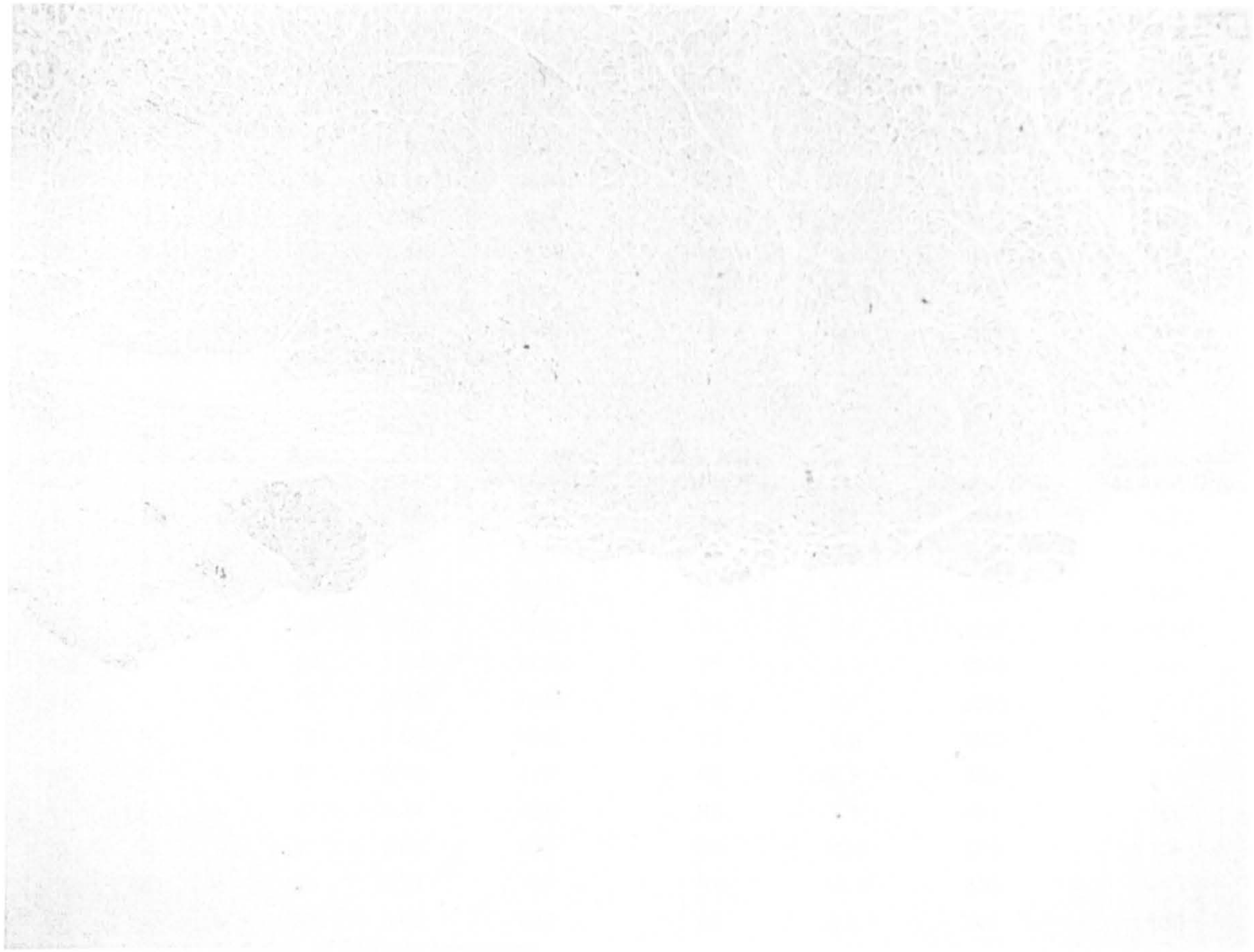

Figure 4. Frontal histologic section of the vocal fold, stained with Haematoxylin-eosin and observed under conventional electronic light microscope (magnification??). Following elaborate microsurgical removal of the epithelium and the all lamina propria you can note the the vocal muscle.

3. RESULTS

3.1 DSR value and Shear Modulus

The mean reading for the DSR is 0.88 g/mm, with a range from 0.30 to 3.43 g/mm, and for the shear modulus 1078 Pascals, with a range from 436 to 3398 Pascals.

3.1.1 Shear Modulus and Gender

The tables 1 and 2 show the full set of results for male (table 1) and female larynxes (table 2).

Larynx Number	Side	Sex	Age (years)	Mean DSR (g/mm)	Mean shear modulus (Pa)	SD of shear modulus (Pa)	CofV (%)	Minimum shear modulus (Pa)	Maximum shear modulus (Pa)
1	L	m	49	0.41	678	52	7.7	545	744
1	R	m	49	0.30	492	161	32.8	297	711
2	L	m	76	0.43	703	57	8.2	628	810
2	R	m	76	0.86	1414	31	2.2	1388	1471
3	L	m	47	0.30	501	51	10.2	463	578

3	R	m	47	0.51	849	68	8.1	744	958
4	L	m	68	0.72	1192	90	7.6	1124	1405
4	R	m	68	1.62	2680	52	1.9	2627	2760
5	L	m	73	1.83	3029	56	1 9	2958	3107
5	R	m	73	1.00	1650	432	26.2	942	2231
6	L	m	55	0.45	446	40	8.9	407	526
6	R	m	55	0 48	479	40	8.3	436	535
7	L	m	56	0.83	824	92	11.1	714	962
7	R	m	56	0.63	623	35	5.6	555	674

Table 1. Shear modulus of male larynxes.

Larynx Number	Side	Sex	Age (years)	Mean DSR (g/mm)	Mean shear modulus (Pa)	SD of shear modulus (Pa)	CofV (%)	Minimum shear modulus (Pa)	Maximum shear modulus (Pa)
8	L	w	80	0.96	950	54	5.7	892	1071
9	L	w	92	0.51	501	38	7.6	446	555
9	R	w	92	0.50	499	28	5.7	466	555
10	L	w	68	1.59	1576	41	2.6	1527	1646
10	R	w	68	1.44	1430	29	2.0	1398	1487
11	L	w	76	3.43	3398	241	7.1	3005	3947
11	R	w	76	1.06	1053	29	2.8	1002	1081
12	R	w	57	0.78	770	68	8.9	684	912
13	L	w	47	0.44	436	25	5.7	407	486
13	R	w	47	0.68	670	67	10.0	555	764
14	L	w	80	0.71	707	109	15 4	575	883
14	R	w	80	0.49	483	42	8.6	446	585

Table 2. Shear modulus of female larynges.

Table 1 gives the full results for 7 male larynxes. Please notice, we could take measurements for the larynx 8 only on the left side, and for larynx 12 only on the right side. Table 2 gives the full results for 7 female larynxes. Column 5 is the shear modulus (average of up to 10 readings), column 7 is the coefficient of variance of the column 5 data. Using the mean values from tables 1 and 2, the results can be summarized as follows:

Male Shear Modulus =

i) Mean: 1111 Pa
ii) Standard Deviation = 31–432 Pa

Female Shear Modulus =

i) Mean: 1039 Pa
ii) Standard Deviation: 25–241 Pa

3.1.2 Shear Modulus and age

The graphs use the values shown in the full results tables to demonstrate the distribution of the transversal shear modulus with respect to the gender of the donors and the side of the larynx. An LSR probe was attached using suction to the mid-membranous point of the vocal fold

and the elastic response was displayed only for 90 degrees (transverse direction to the axis from the vocal process to the anterior commissure) of applied stress.

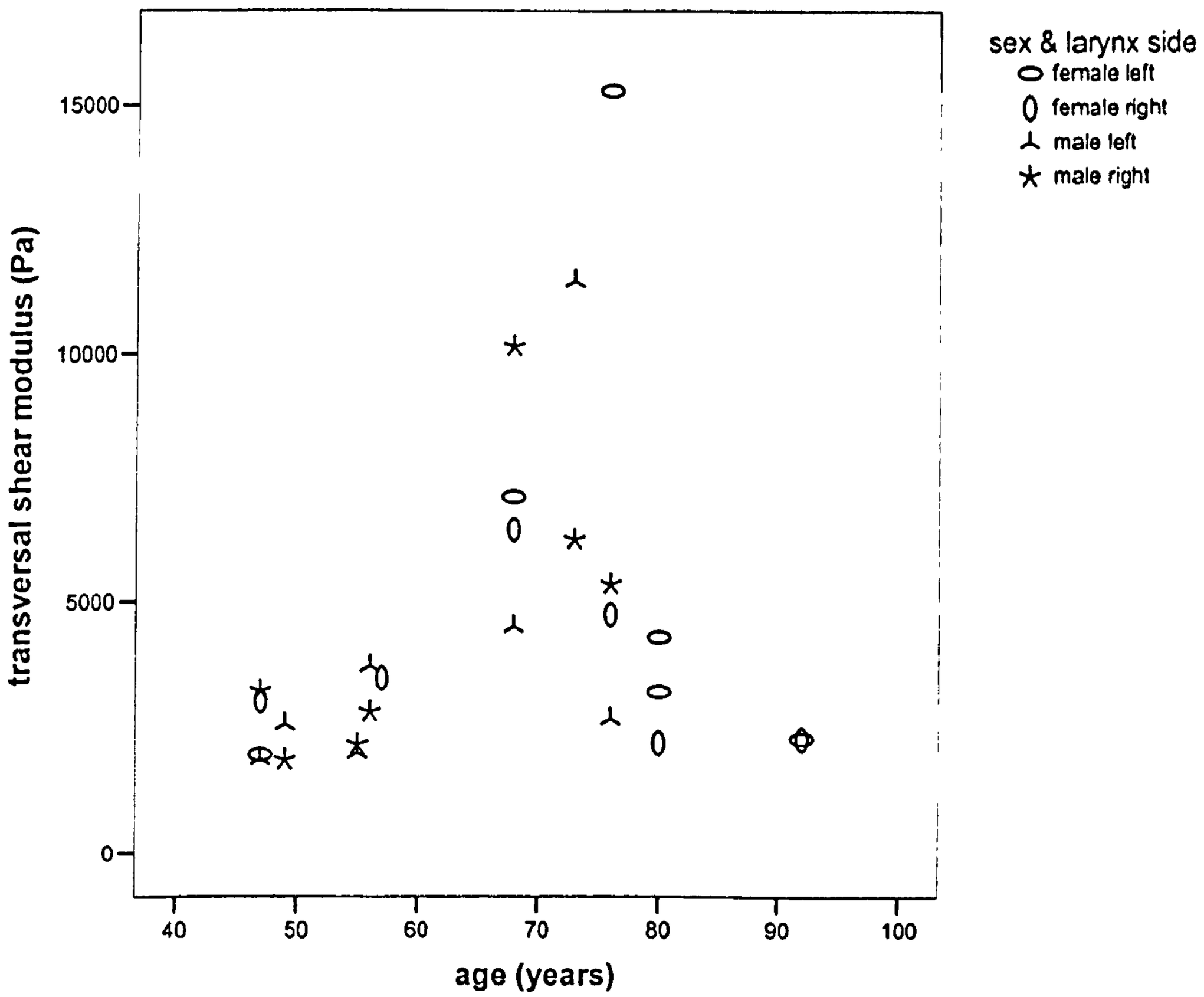

Graph 1. Distribution of vocal fold shear modulus with respect to age (only mid-position of vocal folds, transversal (90°), non-dissected)

Comparing the values of the vocal fold shear modulus from only mid-position of vocal folds in the transversal direction with respect to age cohorts, the younger age cohort (47 to 57 years old) showed smaller data range irrespectively of side and sex in comparison to the older cohort. As from the age of 68 years you can observe a wider range of transversal shear modulus. The values of the older cohort aren't dependent on side and sex, too.

3.2 Anisotropic Nature of the Vocal Fold

The key advantage to measuring the biomechanical properties of the vocal fold using intact larynges is that it is possible to differentiate the

elastic response with respect to the direction of the applied stress. We want to present the preliminary results of the anisotropic nature of the vocal fold.

3.2.1 Relative shear modulus and angle of applied stress

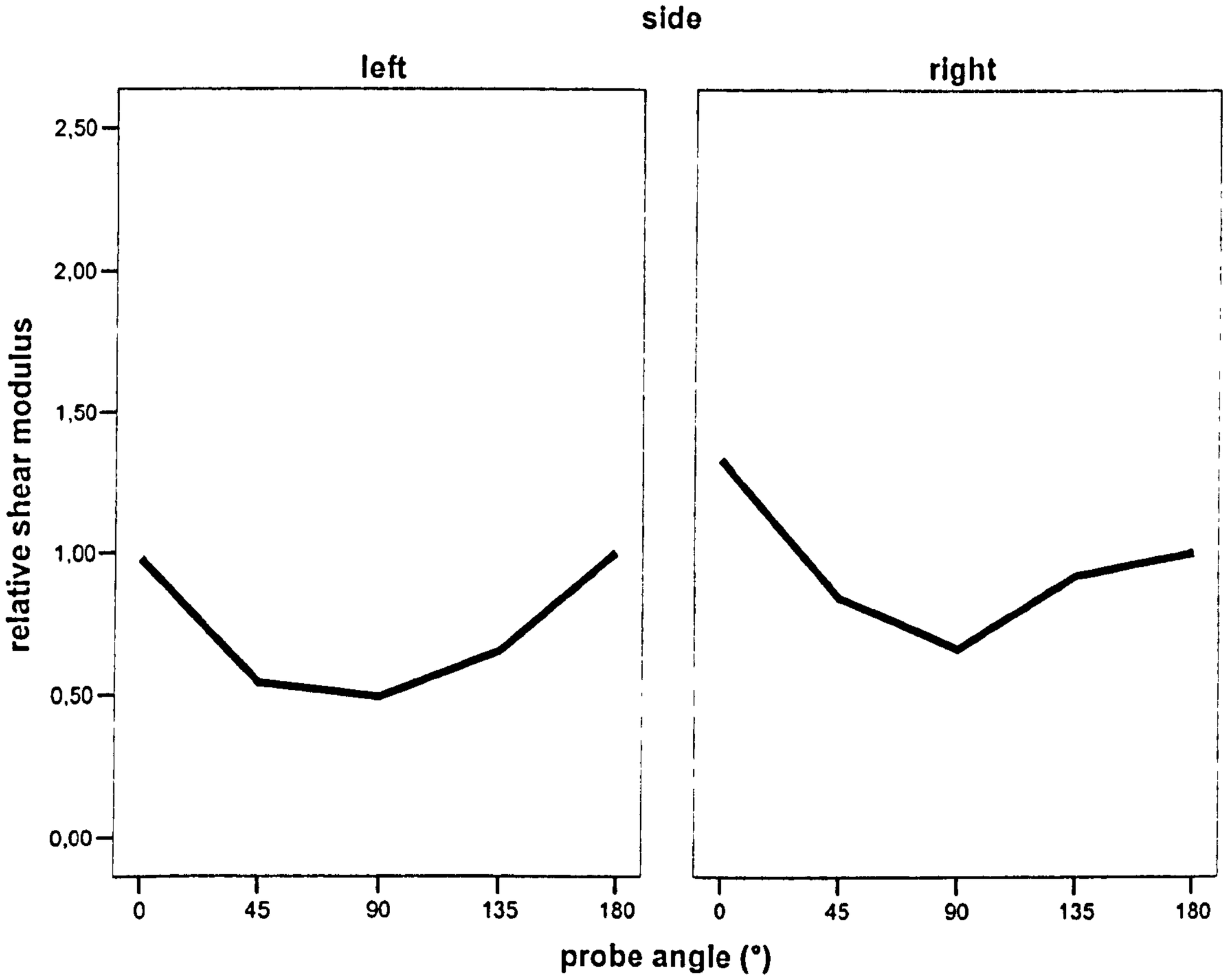

Graph 2. The relative shear modulus of every single larynx (altogether 14 larynges) with respect to different angles (only mid-position of vocal folds, non-dissected). All values are given in relation to the value at 180° of each vocal fold. The thick line represents the mean relative shear modulus of all measurements.

From 5 different angles (0, 45, 90, 135 and 180 degrees) and from 2 different sides (left, right), values for the shear modulus were obtained. Graph 2 shows the overall results obtained only at the mid-position of the non-dissected vocal folds. All larynxes exhibited higher shear moduli if values were obtained at 180 degrees and 0 degrees. The mean value is declining at 135 and 45 degrees to a minimum at 90 degrees. The 45 and 0 degrees stood for the possibility of a backup and obviously comply with our requirements.

3.2.2 Relative shear modulus and layer

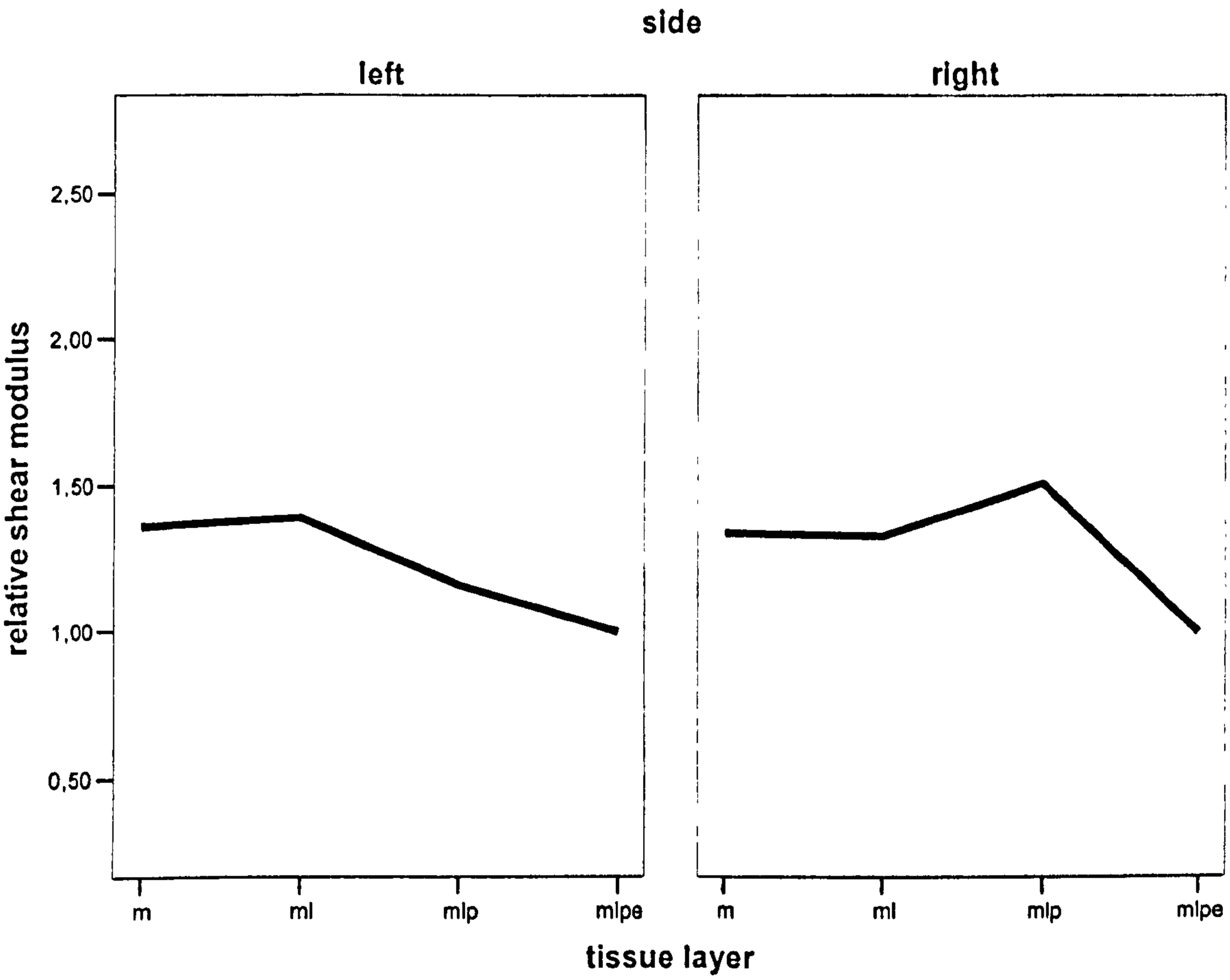

Graph 3. The relative shear modulus of every single larynx (altogether 14 larynges) with respect to different layers (only mid-position of vocal folds, transversal): complete vocal fold (mlpe), lamina propria, ligament and muscle (mlp), ligament and muscle (ml) and muscle alone (m). All values are given in relation to the value of the complete vocal fold. The thick line represents the mean relative shear modulus of all measurements.

The relative shear modulus with respect to different layers of altogether 14 larynxes shows an upwards tendency towards deeper layers.

3.2.3 Ratio of transversal to longitudinal direction

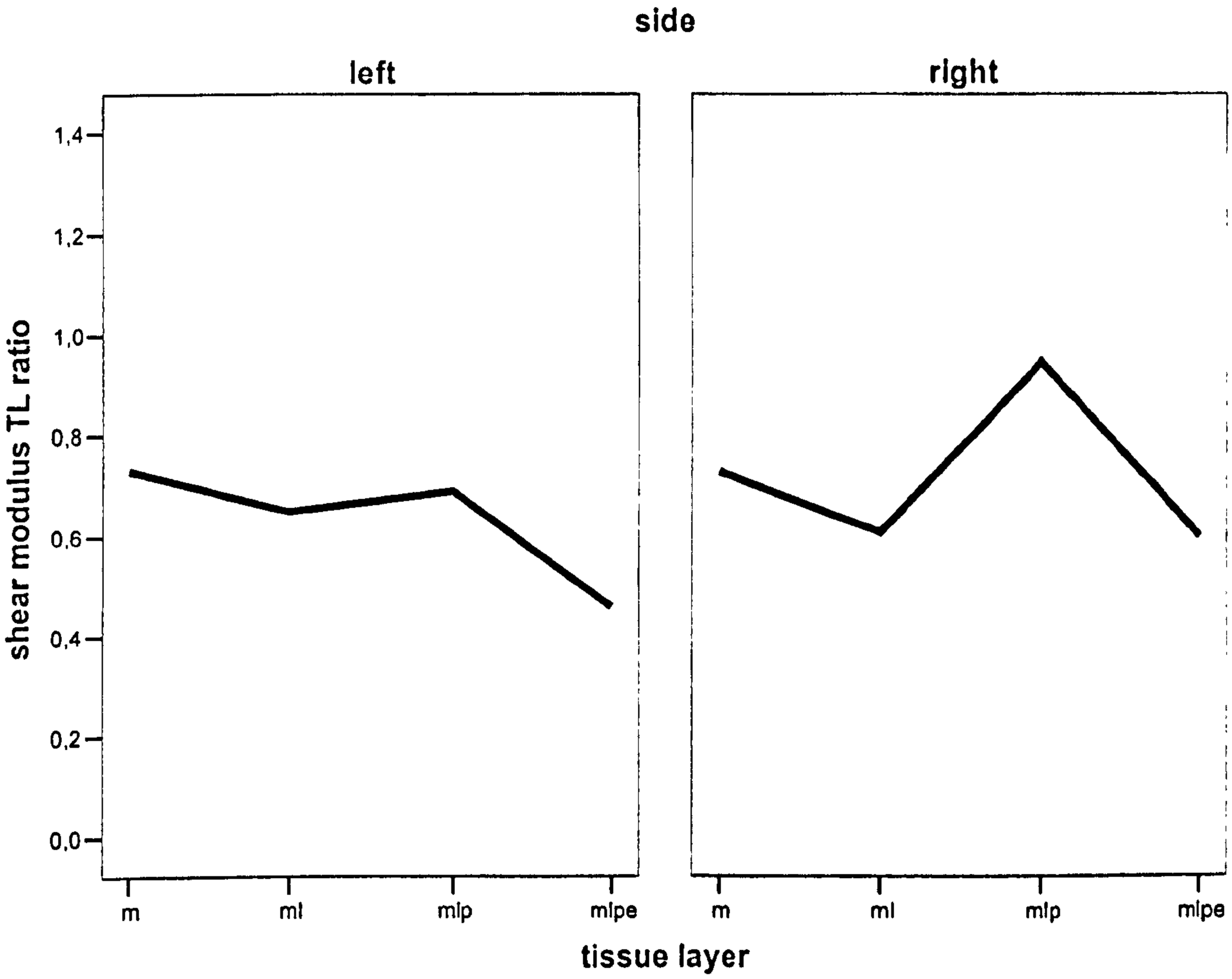

Graph 4. Ratio of elasticity in the transverse direction with respect to the longitudinal direction for the complete vocal fold (mlpe), for the lamina propria, ligament and muscle (mlp), the ligament and muscle (ml) and the muscle alone (m). The thick line represents the mean shear modulus TL ratio of all measurements.

From 14 larynxes from which data were obtainable, the average ratio of the elasticity in the transverse direction with respect to the longitudinal direction is 0.53. If we remove the vocal fold epithelium and repeat the measurement successively on the lamina propria, the vocal ligament and the vocalis muscle, the anisotropic behavior is still present but is less prominent. The ratio for the measurements taken from the lamina propria is 0.82, from the vocal ligament is 0.63 and from the exposed muscle is 0.73. The value is always less than 1 for all layers. By comparing both sides, right and left, a similar upward trend is cognoscible towards deeper layers. In consideration of only a few measuring points the maverick of the mlp value is explainable.
The greatest imbalance of transversal/ longitudinal axis applies for the wholesome vocal fold. Recapitulating we can say the vocal fold requires all layers for a strong anisotropic behavior. Removing the epithelium leads to a decreased, but still present anisotropic behavior of the underlying structures.

4. DISCUSSION

This study demonstrates the distribution of anisotropy between the single layers and the different angles in the vocal fold.

The human vocal fold is known to dispose of viscoelastic properties and therefore is an important source of biomechanical behavior in soft tissue. There are many key features of soft tissue including anisotropy.
Traditionally, complex mechanical behavior of planar soft biological tissue is characterized by multiaxial tensile testing. While uniaxial tests do not provide sufficient information for a full characterization of the material anisotropy, in this study a biaxial test was applied. The major result of this study is that the complete vocal fold is softer than without the epithelium (transverse direction). The inhomogeneity of the vocal fold is characterized by the anisotropy of transversal/longitudinal direction and a dependency from the different layers.

Method improvements

In this study, a suction experiment is applied. After several attempts, this method proved to be the adequate means for the mechanical contact of delicate tissue. The steel needle used in previous experiments [5] could have damaged the tissue and offered no possibility to control the indentation depth. Though Dailey et al. [4] couldn't point a tissue damage out, they allowed for epithelium damage by the needle. Gluing a probe on the tissue [3] avoids these problems but leaves surface damages on the vocal fold when changing the probe angle at the same position.

Biomechanical properties of layered vocal fold

DSR

The mean DSR value in vocal folds of 0.88 g/mm (complete vocal fold, measurement taken at 90°) is similar to the values of 0.5 to 1.5 g/mm found by Dailey et al. [4].

Shear modulus

The findings of the shear modulus of the vocal fold presented here are in order of magnitude comparable with our previous published results obtained by indentometer and shear stress model [3] and the published results by other research groups obtained in-vivo or with whole excised larynges ([7], [8], [9], [10], [11, 12]). We are therefore confident that our results obtained by the suction method are valid.
We can observe a wider range of shear modulus in the aged vocal folds. Anatomical and histopathological studies observe advanced ossification of the laryngeal skeleton, morphologic and metabolic changes of elastic

fibers in the most important vibrating portion (superficial layer of the lamina propria) of the aged vocal folds, a larger intermediate layer with a larger fiber diameter and an increasing loss of glycosaminoglycans in the vocal ligament tendon. These changes could contribute to generation of negative functional consequences during voice production.

Anisotropic nature

To the author´s knowledge, a systematic study of the directionality-specific mechanical response of human vocal fold is not available. By contrast, evaluation of mechanical properties of other soft tissues, for example blood vessel walls, revealed the presence of directionality [13]. But anisotropic mechanical properties for tubular specimens like blood vessels are not comparable with planar specimens like vocal fold, not to mention the diverse function. What is behind all this? With respect to the different functions of the vocal fold (mucosal wave and pitch adjustment) a directionality could make sense: Different functions require different biomechanical properties.

The vocal fold tissue shows higher pliability in the transverse direction. In addition, the whole structure is anisotropic, decreasing as you go down the layers. The results rule the composition of isotropic material for vocal fold tissue out and provide the development of a direction specialisation due to the varying biomechanical needs. Similarily, the anisotropy in cobra leather has adjusted to the functional locomotion of the skin [14].

In contrast to these findings the commonly used phonosurgical materials inserted to restore appropriate shape and pliability show a clear isotropic material behavior. Most conventional indentation techniques assume material homogeneity and isotropy due to an axisymmetry [15], although most biological tissues such as skin, bone and myocardium are known to be anisotropic.

Moreover, the relative shear modulus conditioned by age reveals a mainstream trend (results not represented in this publication): The anisotropy seems to decrease by age. If voicing is enhanced by anisotropy, we can hypothesise that the younger vocal folds are in better form. This assumption applies to a great extent to the midmembranous segment in the transverse direction (90°) on the surface of the vocal fold that is the most critical segment in voicing.

The disadvantage of the presented method lies in the indirect assessment of the layer properties: instead of measuring each kind of tissue separately, we consider the difference of being present or absent. The existence of inter-layer pliability can not be separated from the tissue pliability itself. This is left for the next step in the project: a cooperation with a biomaterial modeling group. Computer models will then close the gap between the measured differential values and the real material properties. A second benefit of this cooperation could be a

more accurate correction method for the real measured tissue volume, which may be of an greater influence than assumed by Dailey et al. [4]. The long term objective is to develop novel methods and accordingly pliable substrates with properties comparable to the native tissue for engineering vocal fold replacement tissue. An anisotropic material would more accurately reflect the true physical nature of vocal fold.

5. LITERATUR

[1] Goodyer, E., Muller, F., Bramer, B., Chauhan, D., and Hess, M., 2006, "In vivo measurement of the elastic properties of the human vocal fold," European Archives of Oto-Rhino-Laryngology, 263(5), pp. 455-462.

[2] Goodyer, E., Muller, F., Licht, K., and Hess, M., 2007, "In vivo measurement of the shear modulus of the human vocal fold: interim results from eight patients," European archives of oto rhino laryngology official journal of the European Federation of Oto Rhino Laryngological Societies EUFOS affiliated with the German Society for Oto Rhino Laryngology Head and Neck Surgery, 264(6), pp. 631-635.

[3] Goodyer, E., Hemmerich, S., Muller, F., Kobler, J. B., and Hess, M., 2007, "The shear modulus of the human vocal fold, preliminary results from 20 larynxes," European archives of oto rhino laryngology official journal of the European Federation of Oto Rhino Laryngological Societies EUFOS affiliated with the German Society for Oto Rhino Laryngology Head and Neck Surgery, 264(1), pp. 45-50.

[4] Dailey, S. H., Tateya, I., Montequin, D., Welham, N., and Goodyer, E., 2007, "Viscoelastic measurements of vocal folds using the linear skin rheometer," J Voice, in press.

[5] Hess, M. M., Mueller, F., Kobler, J. B., Zeitels, S. M., and Goodyer, E., 2006, "Measurements of vocal fold elasticity using the linear skin rheometer," Folia phoniatrica et logopaedica official organ of the International Association of Logopedics and Phoniatrics IALP, 58(3), pp. 207-216.

[6] Hertegard, S., Dahlqvist, A., and Goodyer, E., 2006, "Viscoelastic measurements after vocal fold scarring in rabbits--short-term results after hyaluronan injection," Acta oto laryngologica, 126(7), pp. 758-763.

[7] Chan, R. W., and Titze, I. R., 1999, "Viscoelastic shear properties of human vocal fold mucosa: measurement methodology and empirical results," Journal of the Acoustical Society of America, The, 106(4 Pt 1), pp. 2008-2021.

[8] Berke, G. S., and Smith, M. E., 1992, "Intraoperative measurement of the elastic modulus of the vocal fold. Part 2. Preliminary results," Laryngoscope, The, 102(7), pp. 770-778.

[9] Tran, Q. T., Berke, G. S., Gerratt, B. R., and Kreiman, J., 1993, "Measurement of Young's modulus in the in vivo human vocal folds," Annals of otology, rhinology, and laryngology, The, 102(8 Pt 1), pp. 584-591.

[10] McGlashan, J., de Cunha, D., Hawkes, D., and Harris, T., 1998, "Surface mapping of the vibrating vocal folds," Proceedings of the 24th world congress of the international association of logopedics and phoniatrics (IALP)Amsterdam.

[11] Hsiao, T. Y., Wang, C. L., Chen, C. N., Hsieh, F. J., and Shau, Y. W., 2002, "Elasticity of human vocal folds measured in vivo using color Doppler imaging," Ultrasound in medicine and biology, 28(9), pp. 1145-1152.

[12] Hsiao, T. Y., Wang, C. L., Chen, C. N., Hsieh, F. J., and Shau, Y. W., 2001, "Noninvasive assessment of laryngeal phonation function using color Doppler ultrasound imaging," Ultrasound in medicine and biology, 27(8), pp. 1035-1040.

[13] Ohashi, T., Abe, H., Matsumoto, T., and Sato, M., 2005, "Pipette aspiration technique for the measurement of nonlinear and anisotropic mechanical properties of blood vessel walls under biaxial stretch," Journal of biomechanics, 38(11), pp. 2248-2256.
[14] Niitsuma, K., Miyagawa, S., and Osaki, S., 2005, "Mechanical anisotropy in cobra skin is related to body movement," European journal of morphology, 42(4-5), pp. 193-200.
[15] Jurvelin, J., Kiviranta, I., Arokoski, J., Tammi, M., and Helminen, H. J., 1987, "Indentation study of the biochemical properties of articular cartilage in the canine knee," Engineering in medicine, 16(1), pp. 15-22.

Eur Arch Otorhinolaryngol (2006) 263: 455–462
DOI 10.1007/s00405-005-1034-y

LARYNGOLOGY

Eric Goodyer · Frank Muller · Brian Bramer
Dilip Chauhan · Markus Hess

In vivo measurement of the elastic properties of the human vocal fold

Received: 12 May 2005 / Accepted: 18 August 2005 / Published online: 22 February 2006

Abstract The ability to measure the biomechanical properties of the vocal fold in vivo is both an aid to diagnosis and enhances our knowledge of how the vocal folds operate. This paper details a new instrument that is capable of taking readings of the spring rate of the vocal fold in a repeatable manner. We also present three sets of readings taken from two volunteer patients. Patient 1 was suffering from polyp growth, and the data presented are taken from both the damaged vocal fold and the healthy vocal fold. The third set of readings was obtained from a similar volunteer and taken from a healthy vocal fold. It can be seen that the data obtained from the healthy vocal folds are similar and that the data obtained from the diseased vocal fold is at variance.

Keywords Elasticity · Vocal fold · Biomechanics

Introduction

Research teams in Europe and the USA are actively developing techniques to repair vocal fold tissue that has been damaged by scarring and other pathologies [5, 10, 12]. Currently, the most favoured technique is the use of hyaluronic acid implants. However, ground-breaking research into the use of stem cells to stimulate self-healing is likely to prove more effective in the future. The ability to measure the biomechanical properties of the vocal fold in vivo is therefore an essential pre-requisite to determining the viability of any new tissue repair technique. It is essential that we are able to quantify the biomechanical properties of healthy vocal fold tissue and to objectively assess the change that any tissue-engineering procedure can achieve.

Many researchers have obtained and published data from excised larynxes, most of which were of animal origin [1, 3, 4, 6, 8, 15, 17, 18, 19]. Only one paper [20] details a technique that was used to measure the elasticity of the human vocal fold in vivo. This work by Tran, Berke, Gerratt and Kreiman in 1993 was groundbreaking, but relied on a cumbersome apparatus. No similar studies have since been presented.

The authors have been collaborating for a number of years to develop techniques to map the elastic properties of excised vocal folds repeatedly and reliably. A direct result of this work has been the development of a new, easy-to-use instrument that is capable of obtaining in-vivo elasticity data from anaesthetised patients. This paper outlines this new instrument, the Laryngeal Tensiometer, and presents our initial data. Measurements were taken from two volunteer patients. The elasticity results taken from healthy tissue from both patients were similar and in line with data obtained from excised larynxes using the same instrument and a different technique. Typical readings obtained from the mid-vocal fold are in the region of 0.5 g per mm displacement. We first present the background to the development of the instrument, which was developed from an earlier instrument designed to measure the visco-elastic properties of the stratum corneum. We present data obtained from an excised human larynx, which enabled us to refine the measurement techniques. Finally, we present the first data obtained from volunteer patients under anaesthesia.

E. Goodyer (✉) · B. Bramer · D. Chauhan
Centre for Computational Intelligence and Bioinformatics Group, DeMontfort University, The Gateway, Leicester LE1 9BH, UK
E-mail: Eric Goodyer eg@dmu.ac.uk

F. Muller · M. Hess
Department of Phoniatrics and Pediatric Audiology, University Medical Centre Hamburg-Eppendorf, Martinistr. 52, 20246 Hamburg, Germany

Materials and methods

The apparatus

Linear skin rheometer

The Laryngeal Tensiometer is a simplification of the Linear Skin Rheometer (LSR) [2, 13, 14, 16], which is

used to measure the visco-elastic properties of skin and has been successfully modified to take similar measurements from excised vocal folds [7, 9, 11]. The major simplification arises from the need to have a compact apparatus that can be easily and speedily clamped to a laryngoscope in the operating room environment. The motorised cyclical motion arrangement has been discarded and replaced with the simple slide arrangement. The integral displacement sensor has been replaced with a calibrated slide arrangement. The proven force sensing mechanism employing a load cell that is coupled to the tissue under test remains unchanged. The advantage of using the LSR as a starting point is that it is a proven design. The primary disadvantage of the simplification is that it is only possible to measure the elastic properties of the tissue and not the time-dependant viscous properties.

Laryngeal tensiometer

The measuring apparatus consists of a load cell and slide arrangement that is securely clamped to the handle of a Storz laryngoscope. The clamp incorporates the horizontal slide arrangement that allows the user to displace a mounting block by a calibrated and repeatable distance. The distance has been set to be 1 mm. Force data are obtained from a 25-g load cell supplied by RDP Electronics, which is clamped to the moving block. The load cell is mounted so that the sensing element is located just above the viewing port of the laryngoscope. A hollow plastic chuck is fitted to the sensing element of the load cell; a bar magnet is located within the cavity, together with a steel ball bearing. Part of the surface of the ball bearing protrudes into the field of view of the laryngoscope. This bearing provides the user with a magnetic attachment to which the sensing probe can be attached.

The sensing probe is a steel rod of 1-mm diameter, which is inserted along the axis of the laryngoscope and attached to the vocal fold. The near end of the rod is magnetically coupled to the magnetised ball bearing. The holding force of the magnetic coupling has been measured to be 8 g. Previous research [7, 9] has demonstrated that the force exerted by vocal fold tissue in response to a 1-mm displacement is typically 0.3 g and is unlikely to be more than 2 g. This arrangement therefore is quite adequate to measure vocal fold tissue forces; it also provides the additional safety feature that the probe will slip rather than exert excessive force on the tissue.

Methodology

Tissue attachment

Three techniques have been used in our previous research [7, 9, 11]: a pin, suction and adhesion. The adhesive used for the in-vivo studies was a pharmaceutically manufactured mucosal adhesive, based on methylcellulose, as is used for dentures. This is a biocompatible, non-toxic and water-soluble adhesive that sticks to the mucosa as long as it is not saturated with water. After rinsing the adhesive with water, the stickiness decreases rapidly and the adhesive is easily removed after the measurements. Meticulous mucosal inspection after high magnification microlaryngoscopy revealed no mucosal changes at all.

As stated, the quality of this adhesive is critically dependent upon moisture levels. The target site was dried with a cotton tip, and adhesive was applied and held in place until it was fixed; this typically took up to a minute to occur. The lateral side of the steel rod was also coated with a small amount of adhesive, inserted down the laryngoscope and attached to the tissue at the mid-vocal fold (Figs. 1 and 2). The direction of motion is along the axis of the laryngoscope, such that the tissue is tangentially pulled towards the laryngoscope, creating a shear stress on the tissue structure (like a billiards queue tangentially moving the skin surface of the resting hand's finger).

Data capture

The load cell signal-conditioning unit is an RDP S7DC. This gives an output that is proportional to the force applied to the load cell. Typical readings gave a signal change of less than 30 mV; therefore, a Burr Brown IN114A instrument amplifier was used to provide an amplified signal prior to feeding the signal into a MAXIM 186 programmable Analogue to Digital Converter (ADC). The ADC was controlled by an ATMEL T89C52RD2 microcontroller, which outputs the data on a serial line at a data rate of 115200BPS as three HEX-ASCII bytes terminated by a carriage return and line feed. This arrangement gave us the ability to transmit data at a maximum rate of approximately 2 kHz. The data acquisition rate was however set to be 1 kHz. A portable laptop PC was used to capture the incoming data. The data capture programme was written using the DOS-based Turbo C compiler form Borland. The captured data were displayed graphically in real-time, providing essential visual feedback, and captured in a data file. The data files can then be subsequently analysed using off-line tools; in this instance, we used Excel to extract the elastic data.

Calibration

Calibration was achieved using the LSR calibration jig [5]. This apparatus consists of two secondary standards for force and displacement, which can be coupled to the transducers under test. A secondary standard is a portable sensor that is calibrated by a recognised test house and is issued with a calibration certificate that is traceable to a National or International standard. The load cell is coupled to a second load cell using a spring cou-

Fig. 1 Attachment to patient 1

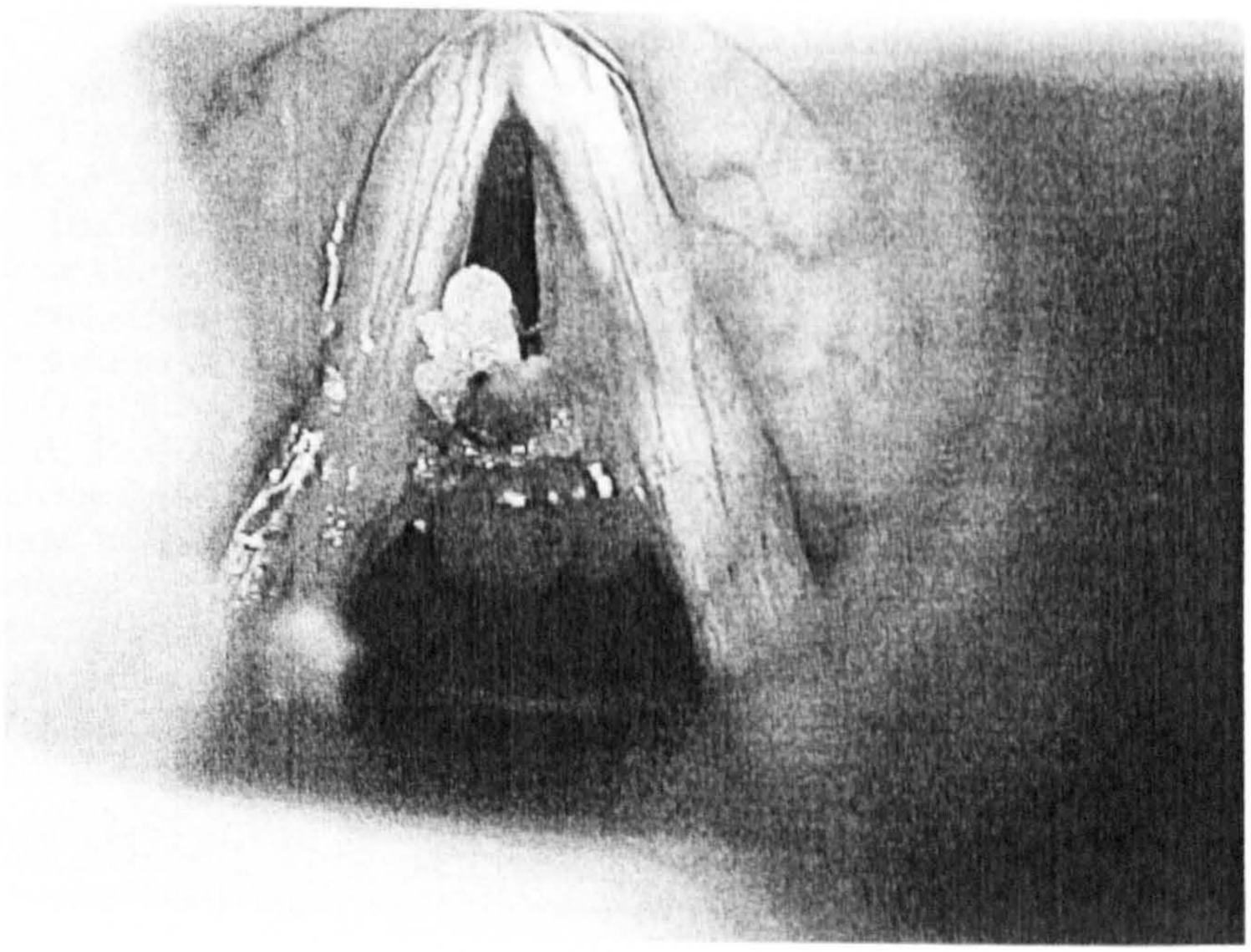

Fig. 2 Attachment to patient 2

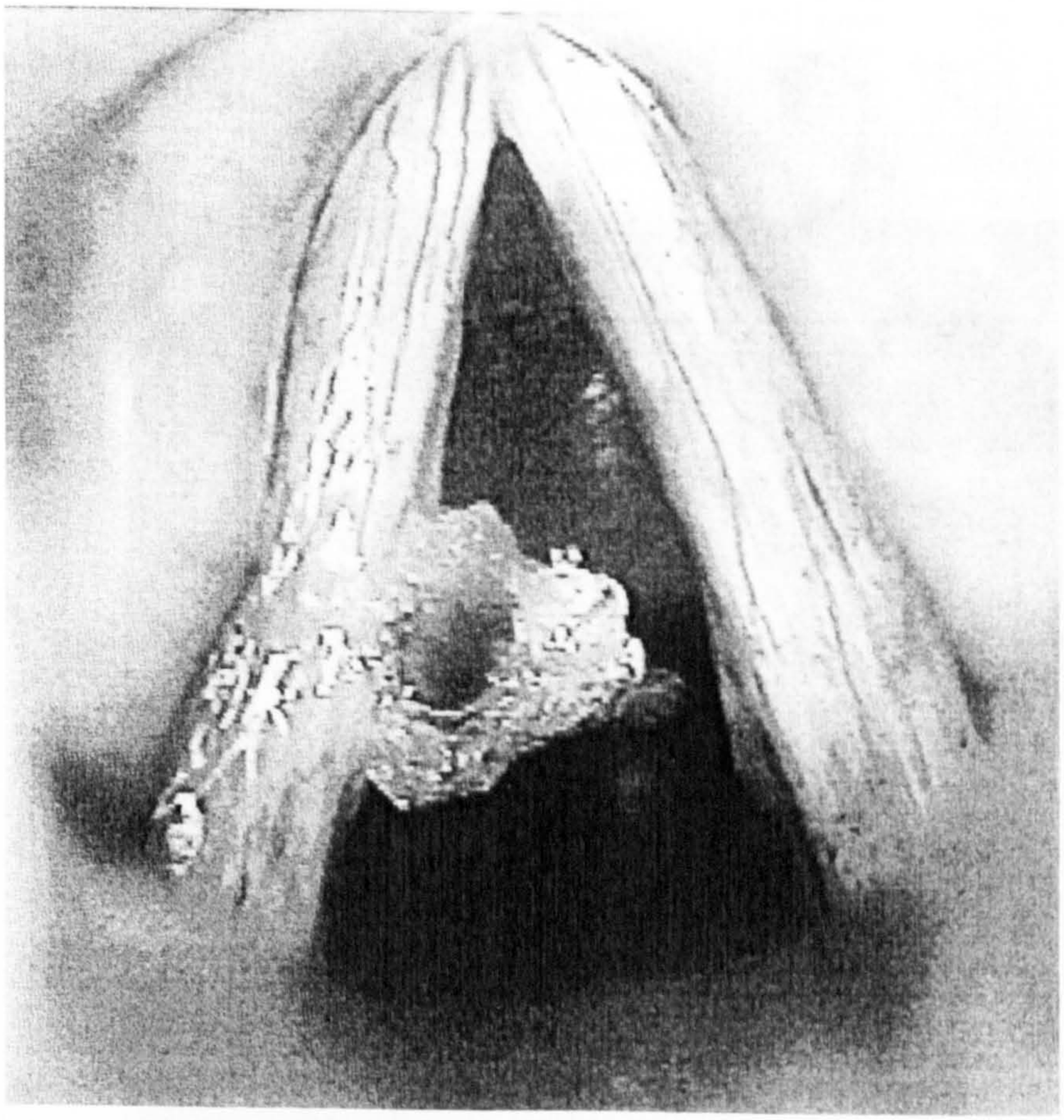

pling, such that any force acting on one load cell is also applied to the second load cell. A digital readout unit displays the load applied to the second load cell and gives a traceable measurement of the load acting on the load cell under test. These readings are then related back to the digital output of the ADC. The displacement is calibrated using a Mitutoyo linear displacement sensor. The slide arrangement is coupled to the sensing element

of the readout unit, and the total displacement distance is measured.

Results

Please see Table 1, which contains all the results obtained from the excised larynx and the in-vivo studies. All data given are the spring rate (SR) of the tissue under test expressed in terms of g/mm. The table gives the mean of multiple readings taken from each site and the standard deviation of each set of data. Using a simple shear model, it is possible to derive a value of the shear modulus of the tissue under test: (1) G = stress/strain; G = shear modulus; (2) stress = F/A; F = the applied force; A = the surface area to which the force is applied; (3) strain = X/L; X = the change in length of the material; L = the depth of the material; (4) G = (F * L)/(X * A); (5) DSR = F/X in units of gf/mm per metre, which is converted to N/m by multiplying through by 9.80665; (6) G = (SR * 9.80665 * L)/A. If all units of length are expressed in metres, and force in units of Kgf, then the units of G are Pascal. The SR is obtained from the tensiometer. A is the cross-sectional area of the attached probe. L is the depth of the tissue. Both L and A were estimated visually using the images taken in surgery. A range of values for shear modulus is given that takes account of these estimates.

Ex-vivo trials

Two sets of readings were obtained from an excised split human larynx. The experimental set-up is shown in Figs. 3 and 4, together with a schematic drawing in Fig. 5. The first set was taken from a position 2 mm superior to the mid-vocal fold and the second set from the mid-vocal fold itself. Table 1 shows the results, in terms of g/mm. The purpose of these trials was to assess the viability of the adhesive and the feasibility of moving towards in-vivo measurements. The results obtained (0.94 g/mm superior to the vocal fold, and 0.4 g/mm mid vocal fold) are comparable with those achieved

Table 1 Spring rate results from excised and in-vivo sources

Data source	DSR-mean	SD	Estimated shear modulus
Excised larynx 2 mm superior to the mid-vocal fold	0.94 g/mm	0.073 g/mm	2304–5184 Pascal
Excised larynx mid vocal fold	0.40 g/mm	0.027 g/mm	980–2205 Pascal
Patient 1: healthy tissue mid vocal fold	0.58 g/mm	0.107 g/mm	1421–3197 Pascal
Patient 1: diseased tissue tangentially attached to medial surface of polyp	0.26 g/mm	0.075 g/mm	637–1433 Pascal
Patient 2: healthy tissue mid vocal fold	0.53 g/mm	0.136 g/mm	1299–2922 Pascal

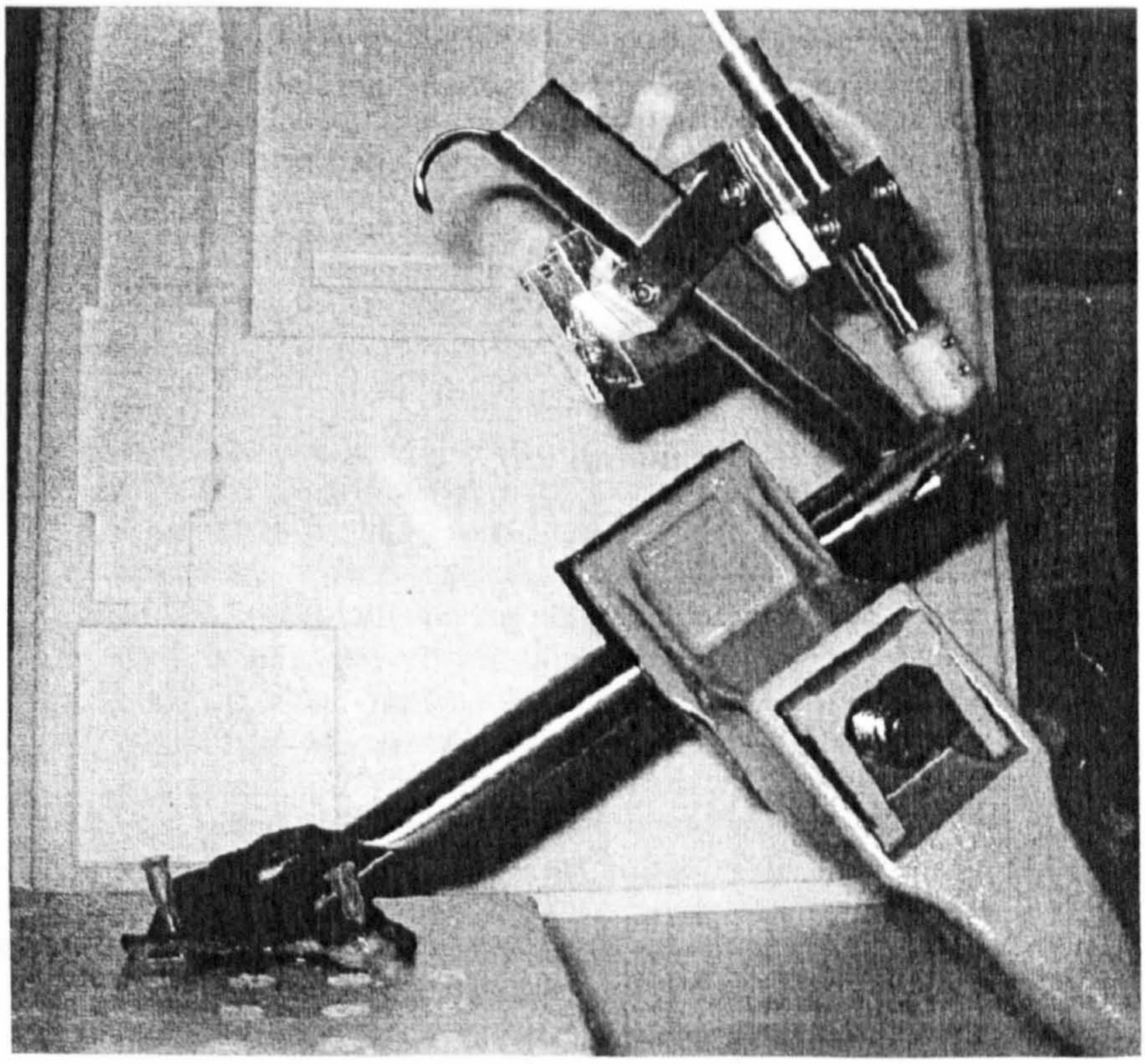

Fig. 3 Experimental set-up for excised laryngeal measurements

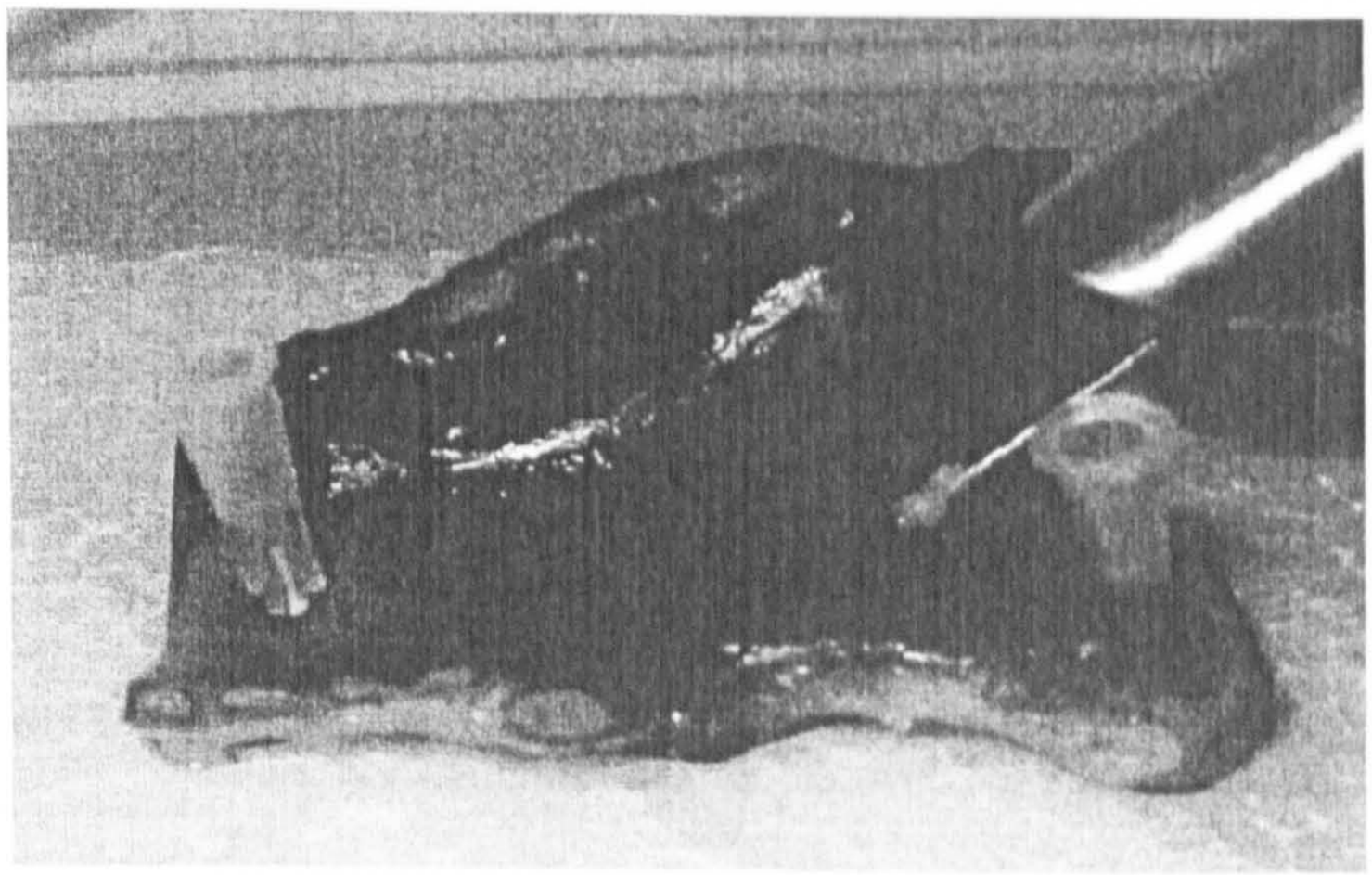

Fig. 4 Excised tissue study 2

using the LSR [7] and a needle. These results gave us sufficient confidence to attempt similar measurements with volunteer patients.

In-vivo trials

Figure 6 shows the experimental set-up that was used to take the in-vivo readings. The laryngeal tensiometer is clamped to the laryngoscope, as shown in Fig. 6. Figure 7 shows a close up of the magnetic attachment arrangement, whereby the probe that is inserted along the laryngoscope is coupled to the load cell. The far end of the probe is adhered to the vocal fold, where the measurements are taken by gently compressing and releasing the linear slide.

Patient 1

A female volunteer was suffering from a polyp of the right vocal fold. The opportunity was used to take readings from the area just above the polyp and from the healthy tissue on the opposite side. An image of the probe attachment is shown in Fig. 1. The result from the healthy tissue was 0.58 g/mm, and from the diseased tissue 0.26 g/mm.

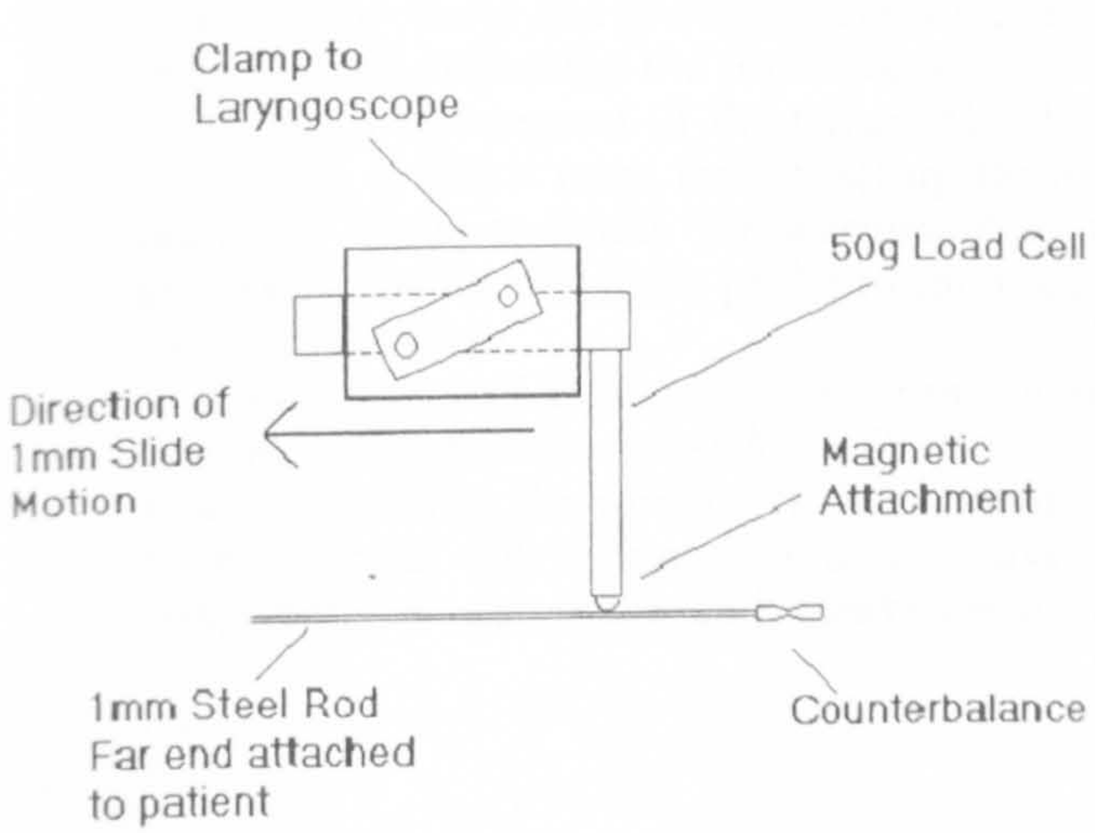

Fig. 5 Schematic of laryngeal tensiometer

Patient 2

A second female volunteer received a tissue augmentation procedure of the left vocal fold. Readings were taken from the healthy tissue of the right vocal fold prior to treatment. An image of the probe attachment is shown in Fig. 2. The result from the healthy tissue was 0.56 g/mm, which is very similar to that obtained from patient 1, and comparable with the data obtained from the excised larynx.

Discussion

The data obtained from both the excised tissue and in-vivo trials were noisy, with a SD/mean ratio ranging from 6.8% for the excised tissue up to 28% for the in-vivo trials. This can be seen from the typical result trace shown in Fig. 8. The results must therefore be considered as indicative only until we have obtained more data and can then improve the uncertainty. However, the general results are in accordance with previous measurements using different techniques and demonstrate that the in-vivo laryngeal tensiometer will be capable of being used as part of a larger study.

Data were obtained only from two female volunteers. Our parallel work with excised tissue uses donor tissue from both male and female donors. This data will enable us to determine if there is a correlation between the variance of the measured elasticity of the vocal tissue with respect to the length of the vocal fold.

These obtained results demonstrate that the laryngeal tensiometer is capable of taking in-vivo measurements of the elastic properties of the vocal fold, in a repeatable

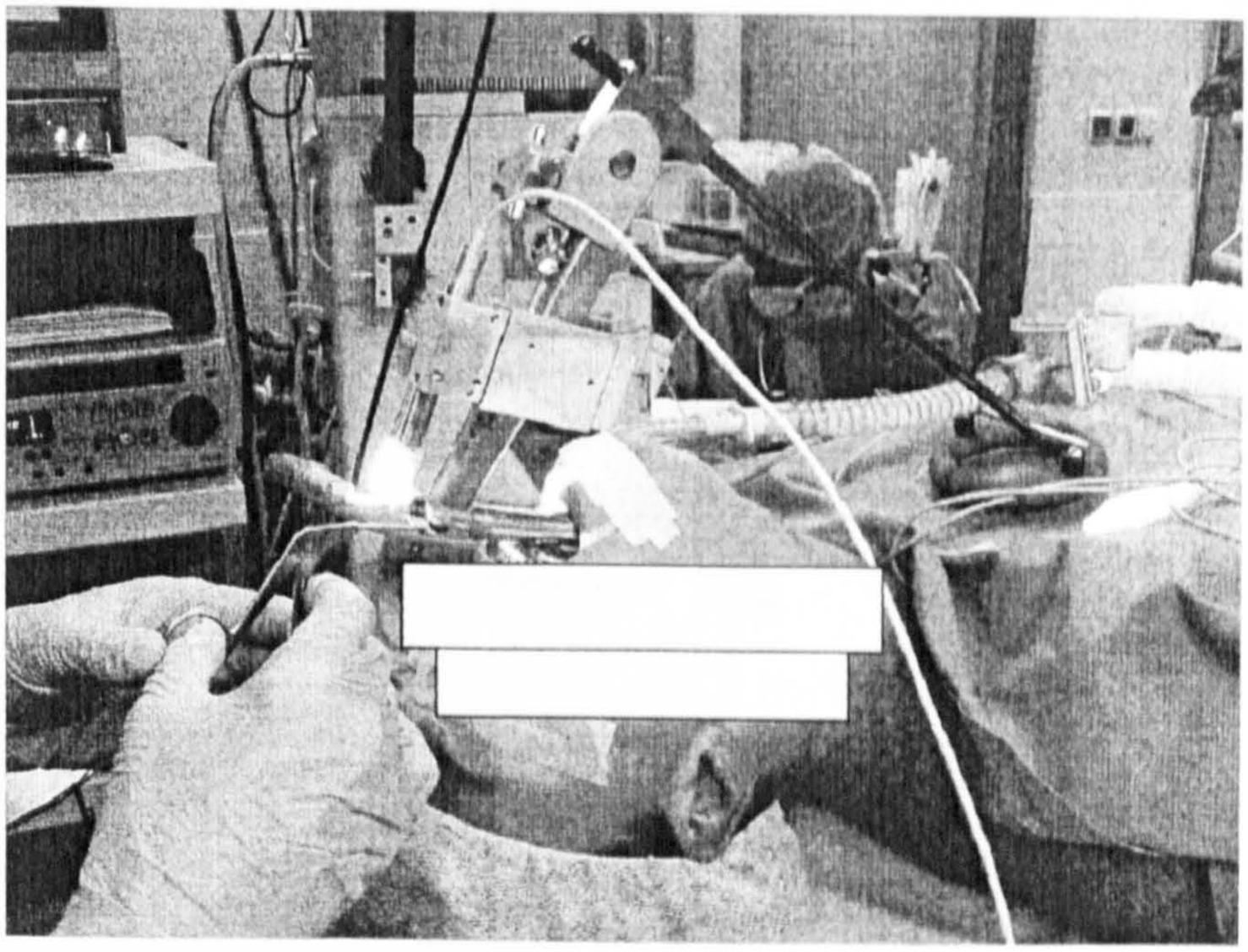

Fig. 6 In-vivo laryngeal tensiometer set-up

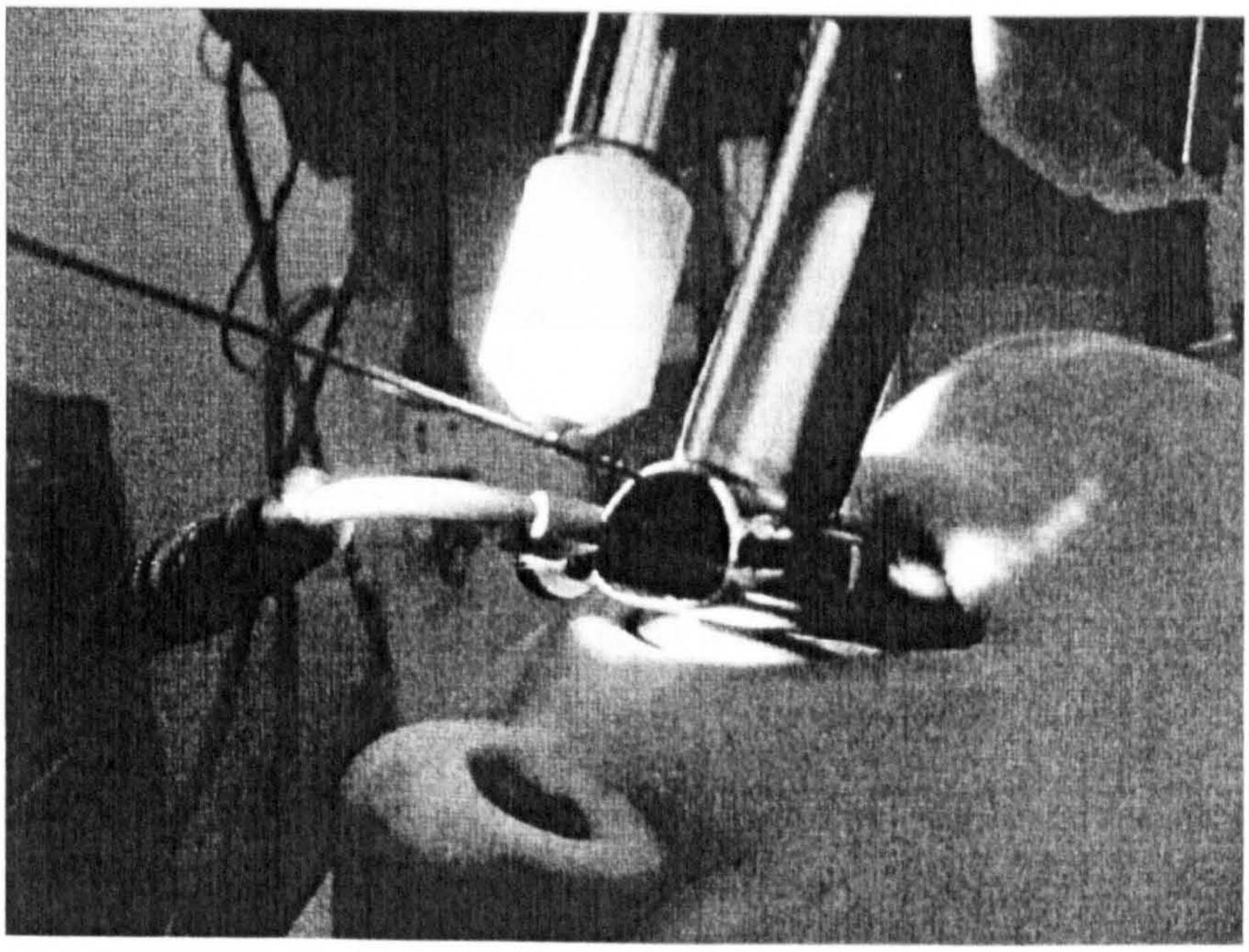

Fig. 7 Magnetic attachment of probe

manner. This represents a substantial improvement on the only previously published work, in that the instrument is easy to use and provides data using the empirical technique of measuring the force required to cause a 1-mm shear displacement of the tissue. The drawback of the design is that it takes time to set up the experiment: typically, 5 min to clamp the instrument to the laryngoscope, then to attach the probe to the vocal fold and capture the data.

Presentation of elastic data in terms of the fundamental values for shear and Young's modulii is preferable to providing the spring rate. Shear modulus can be derived from the spring rate if we have a precise knowledge of the tissue and measurement geometry. Young's modulus can be derived by applying an exponential fit to indentometer data. The mechanical design will be reviewed to improve the confidence with which geometric measurements can be made and to reconfigure the mechanics such that indentometer data can be obtained. Table 1 includes our estimates for shear modulus, which are comparable with previously published results. The values derived for shear modulus are lower than those derived by parallel plate rheometry. This variance is explained because our readings were taken at DC as opposed to a typical value of 100 Hz for parallel plate rheometry.

To progress this work, the authors are planning two new large-scale studies. One will be the detailed exami-

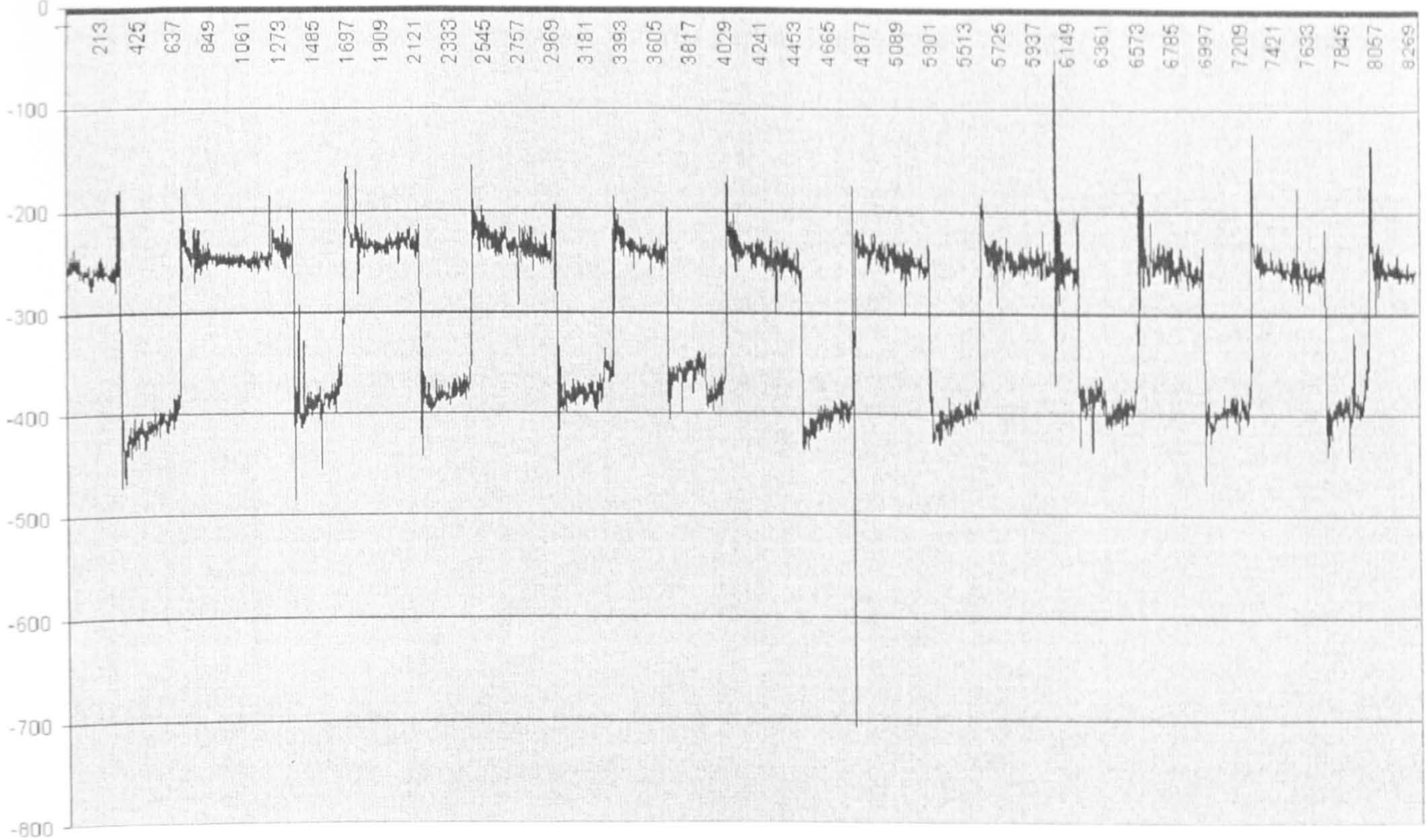

Fig. 8 A typical set of stress/strain readings

nation of a large sample of excised larynxes using the LSR device. The other will be a long-term programme to collect in-vivo data from a large sample of volunteer patients over the next 2 years, during which time the design of the tensiometer will be enhanced to address our concerns relating to its use. The data obtained from these and other related studies will be analysed in order to develop a generalised mathematical model of human vocal fold biomechanical properties.

References

1. Alipour-Haghighi F, Titze IR (1985) Viscoelastic modelling of canine vocalis muscle in relaxation. J Acoust Soc Am 78:1939–1943
2. Ananthapadmanabhan KP, Moore DJ, Subramanyan K, Misra M, Meyer F (2004) Cleansing without compromise: the impact of cleansers on the skin barrier and the technology of mild cleansing. Dermatol Ther 17:16
3. Berke GS (1992) Intraoperative measurement of the elastic modulus of the vocal fold. Part 1. Device development. Laryngoscope 102:760–769
4. Berke GS, Smith ME (1992) Intraoperative measurement of the elastic modulus of the vocal fold. Part 2. Preliminary results. Laryngoscope 102:770–778
5. Chan RW, Titze IR (1999) Hyaluronic acid (with fibronectin) as a bioimplant for the vocal fold mucosa. Laryngoscope 109:1142–1149
6. Chan RW, Titze IR (1999) Viscoelastic shear properties of human vocal fold mucosa, measurement methodology and empirical results. J Acoust Soc Am 106:2008–2021
7. Goodyer EN, Gunter H, Masaki A, Kobler J (2003) Mapping the visco-elastic properties of the vocal fold. AQL, Hamburg
8. Haji T, Mori K, Omori K, Isshiki N (1992) Mechanical properties of the vocal fold. Stress-strain studies. Acta Otolaryngol 112:559–565
9. Hertegård S, Dahlqvist Å, Goodyer EN, Maurer E (2004) Viscoelasticity in scarred rabbit vocal folds after hyaluronan injection—short term results. AAO-HNSF/ARO Research Forum of the American Academy of Otolaryngology-Head and Neck Surgery Foundation, New York
10. Hertegard S, Hallen L, Laurent C, Lindstrom E, Olofsson K, Testad P, Dahlqvist A (2002) Cross-linked hyaluronan used as augmentation substance for treatment of glottal insufficiency, safety aspects and vocal fold function. Laryngoscope 112:2211–2219
11. Hess M, Muller F, Kobler J,Zeitels A, Goodyer EN (2005) Measurements of vocal fold elasticity using the linear skin rheometer. Folia Phoniatr (in print)
12. Kriesel KJ, Thiebault SL, Chan RW, Suzuki T, VanGroll PJ, Bless DM, Ford CN (2002) Treatment of vocal fold scarring, rheological and histological measures of homologous collagen matrix. Ann Otol Rhinol Laryngol 111:884–889
13. Matts P, Goodyer EN (1988) A new instrument to measure the mechanical properties of the human stratum corneum. J Cosmetic Sci 49:321–323
14. Matts PJ (2004) Sensitive Measurement of Stratum Corneum Mechanical Properties Using the Linear Skin Rheometer. Stratum Corneum IV, June 2004, Paris
15. Min YB, Titze IR, Alipour-Haghighi F (2005) Stress-strain response of the human vocal ligament. Ann Otol Rhinol Laryngol.104, 563–9.
16. Mok W, Bautista B, Hoyberg K, Kirnos P, Subramanayam K (2001) Mechanical Properties of Ageing Skin – Stratum Corneum vs. Dermal Changes. Stratum Corneum III, 12–14th September 2001, Basel Switzerland.
17. Perlman AL, Titze IR (1988) Development of an in vitro technique for measuring elastic properties of vocal fold tissue. J Speech Hear Res. 31, 288–98.
18. Perlman AL, Titze IR (1984) Cooper DS. Elasticity of canine vocal fold tissue. J Speech Hear Res. 27, 212–9.

19. Tanaka S, Hirano M (1990) Fiberscopic estimation of vocal fold stiffness in vivo using the sucking method. Arch Otolaryngol Head Neck Surg. 116, 721–4.

20. Tran QT, Berke GS, Gerratt BR, Kreiman J. (1993) Measurement of Young's modulus in the in vivo human vocal folds. Ann Otol Rhinol Laryngol. 102, 584–91

Characterisation of the Elasticity of the Human Vocal Fold using Electromechanical Measurement Techniques

Eric Goodyer (1), Sandra Hemmerich, Frank Mueller, Anna-Katharina Licht, Markus Hess (2)

(1) The Centre for Computational Intelligence - Bioinformatics Group, DeMontfort University, The Gateway, Leicester LE1 9BH UK.

(2) University Medical Centre Hamburg-Eppendorf, Department of Phoniatrics and Pediatric Audiology, Hamburg, Martinistr. 52, D-20246 Hamburg/Germany

Eric Goodyer eg@dmu.ac.uk

Markus Hess hess@uke.uni-hamburg.de

Abstract: Characterisation of the bio-mechanical properties of the human vocal fold is an essential aid to understanding vocal fold oscillation, as an aid to diagnosis,
and to support surgical as well as tissue engineering therapies. The authors will present preliminary results of an extensive study that has examined 20 excised human larynxes, and obtained data from 8 volunteer patients in-vivo during surgery under general anaesthesia. Three electro-mechanical measuring techniques were employed, which either applied shear stress to the tissue, or indented the tissue. The excised larynxes were split along the sagittal plane, mounted without tension, and measured
using a linear skin rheometer (LSR). Two techniques were used; one applied a sinusoidal shear stress in a transverse direction; the other indented the same point using a circular 1mm indentor. In both cases the applied stresses and resultant strains were logged. A new instrument was deployed for the in-vivo study, the laryngeal tensiometer (LT). The LT is clamped to a standard laryngoscope; a probe is inserted down the laryngoscope and adhered to the vocal fold, a slide arrangement is used to apply a known displacement of 1mm and the resultant force is logged. Analysis of the stress/strain characteristics of all three methods indicates a typical shear modulus with the order of magnitude at approx. 1000 Pascals for the mid-membranous section of the vocal fold.

1 Introduction

There are very few published reports that give the shear modulus for a group of human vocal folds. Those that do exist employed a range of different techniques, such as ultrasonics, optics and mechanics. The ultrasonic and optical methods infer shear modulus from secondary phenomena, whereas the mechanical methods directly measured the biomechnical response of the tissue; invariably by excising the lamina propria and measuring it outside of its' anatomical context. This presentation outlines a number of different techniques that were specially designed to enable the quantification of the biomechanical properties of the vocal from intact excised larynxes, and in-vivo.

2 The Laryngeal Tensiometer for In-Vivo use

The measuring apparatus consists of a load cell and slide arrangement that is securely clamped to the handle of a Storz laryngoscope. The clamp incorporates the horizontal slide arrangement that allows the user to displace a mounting block by a calibrated and repeatable distance. The distance has been set to be 1mm.

Force data are obtained from a 25g load cell supplied by RDP Electronics, that is clamped to the moving block. The load cell is mounted such that the sensing element is located just above the viewing port of the laryngoscope. A hollow plastic chuck is fitted to the sensing element of the load cell; a bar magnet is located within the cavity, together with a steel ball bearing. Part of the surface of the ball bearing protrudes into the field of view of the laryngoscope. This bearing provides the user with a magnetic attachment to which the sensing probe can be attached.

The sensing probe is a steel rod, 1mm diameter, which is inserted along the axis of the laryngoscope and attached to the vocal fold. The near end of the rod is magnetically coupled to the magnetised

ball bearing. The holding force of the magnetic coupling has been measured to be 8g. Previous research [3,5] has demonstrated that the force exerted by vocal fold tissue in response to a 1mm displacement is typically 0.3g and is unlikely to be more than 2g. This arrangement therefore is quite adequate to measure vocal fold tissue forces; it also provides the additional safety feature that the probe will slip rather than exert excessive force on the tissue.

3 The Linear Skin Rheometer for Excised Tissue

The LSR [1] is a precision instrument originally designed to measure the visco-elastic properties of the stratum corneum. Based upon the concept developed by Hargens in the 1960's (The Gas Bearing Electrodynanometer or GBE), the LSR uses modern micro-mechanical components to achieve force feedback control in real time, and precision position measurement. It is now being successfully used to measure the more delicate tissue of the vocal fold [2,3,4,5,6]. Force is measured to a precision of 10 micrograms, and displacement to a precision of 1 micron.

Method 1: Simple Shear Model

A flat probe is attached to the vocal fold epithelium, mid-membranous between the anterior commisure and vocal process. A sinusoidal force F is applied to the material under test in a transverse direction so as to apply a shear stress to the vocal fold, and the resultant displacement P is logged. The driving force is set to be 0.5g, which typically results in a displacement of 1mm. The frequency of operation is set to be 0.3Hz. As the measurement frequency is low; the results can only be used to quantify the elasticity of the tissue and not the viscosity. The value of 1mm was chosen as this represented a realistic displacement with respect to the geometry of the tissue structure.

(1) $F = FmaxSin(t)$

(2) $P = PmaxSin(t+T)$

Where

F = instantaneous force

$Fmax$ = the maximum force

t = time over one cycle in radians

P = instantaneous displacement

$Pmax$ = the maximum displacement

T = the phase shift in radians.

The Dynamic Spring Rate (DSR) of the tissue is $F\ max\ /\ P\ max$, and is expressed in units of grams force per millimetre. The DSR can then be used to determine the shear modulus using knowledge of the geometry of the test site as follows:

The shear stress σ is the applied force F per unit area A given by

(3) $\sigma = F / A$

The resultant shear strain ε is given by lateral displacement P perthickness T.

(4) $\varepsilon = P / T$

Shear modulus G is defined as stress per unit strain

(5) $G = \sigma / \varepsilon$

(6) $G = (F / P) * (T / A)$

As DSR = F / P then

(7) $G = DSR * T / A$

Data was first obtained by gluing the flat tip of a probe arm to the tissue with cyanoacrylate. This is a very fast acting adhesive that internally polymerises in the presence of a small amount of water, achieving the bond by in-filling crevices on the surface of the epithelium. The adhesive works by first forming a surface skin, with polymerisation continuing at a high rate internally. In view of the speed of action, and the manner of the bonding, we consider that it is highly improbable that the adhesive solvents would have time, or be able to penetrate into the tissue to the extent that it would perturb the results. Our more recent studies uses suction to attach the measuring probe, which is producing far more repeatable results.

The area of attachment (A) is determined by direct measurement. The simple shear model does not take account of tissue that is attached to the column that is directly stressed. The additional surface area that was subjected to the applied stress was observed to be typically 0.75 mm around the area of direct attachment; therefore the dimensions were increased by this amount on all 4 sides. The thickness of the vocal fold tissue (T) is typically 1mm.

Using these geometric values a range of shear moduli can be derived for each sample. Ten readings were taken from each test site and middle of each range was averaged. These results are referred to as the 'Shear Model'.

Method 2 Indentometer

In the second approach the LSR was used as an indentometer. In this arrangement a 1mm diameter flattened probe tip is pushed into the tissue and the force~displacement data is then captured in real time. The measurement point was chosen to be the centre of the area used for the shear model method already described in order to enable a meaningful comparison. The indentor was located clear of the tissue with an air gap of 1mm, it was then driven into the vocal fold for a distance of 2mm at a speed of 1mm per second.

For a homogeneous material the resultant relationship will be logarithmic, forming a classic compression cycle curve. However many researchers have correctly stated that indentation of a soft tissue does not follow this simple rule because surrounding tissue remains in contact with the depressed section to which a shear stress is applied.

One widely accepted model is that originally proposed by Y C Fung, from which W C Hayes et. al [11] developed a rigorous mathematical solution. This mathematical device is based upon a solution for Yung's 3D partial differential equations that explain the deformation of soft tissue. This solution offers a 'correction factor' to Yung's equations that takes account of the shear strain surrounding the indentation, which requires knowledge of the tissue's Poisson's ratio (ν). ν is the relationship between a materials' elongation and sheer strains. For an incompressible material it is 0.5. The correction factor (κ) is based on the ratio of the indentor radius (a), the tissue thickness and Poisson's ratio, assumed to be 0.5. Our indentor radius (a) is 0.5 mm and we assume the thickness of the tissue to be 1mm. Hayes gives the following expression in his paper as the definition of κ, together with a table of solutions.

$$(8)\ \kappa = (F * (1 - \nu))/(4aGw)$$

Which can be rearranged to give

$$(9)\ G = (F/w) * (1 - \nu) * 9.80665) / (4a\kappa)$$

Where

κ = the Hayes correction factor obtained from the published table

F = applied force

ν = Poisson's Ratio

a = indentor radius

G = Shear Modulus

w = depth of penetration

The 9.80665 converts the units for Shear Modulus (G) into Pascal

Each sample was indented 10 times. From the resultant stress/strain curves we select the initial linear section, apply a least square fit and obtain the best value for F/w in units of g/mm. All the other values are known. These results are referred to as the 'Indentometer Model' in the text.

4 LT Methodology

Figure 1 shows a schematic of the measurement apparatus. Figure 2 shows how the apparatus is clamped to the laryngoscope, with a close-up view of the magnetic attachment shown in figure 3.

4.1 Tissue Attachment

The 1mm rod is coated with a pharmaceutically manufactured mucosal adhesive, based on methylcellulose, as is used for dentures. This is a biocompatible, non-toxic and water soluble adhesive that sticks to the mucosa as long as it is not saturated with water. After rinsing the adhesive with water, the stickiness decreases rapidly and the adhesive is easily removed after the measurements. Meticulous mucosal inspection after high magnification microlaryngoscopy revealed no mucosal changes at all.

As stated, the quality of this adhesive is critically dependent upon moisture levels. The target site was dried with a cotton tip, and adhesive was applied and held in place until it was fixed; this typically took up to a minute to occur. The lateral side of the steel rod was also coated with a small amount of adhesive, inserted down the laryngoscope and attached to the tissue at the mid-vocal fold (figure 4). The direction of motion is along the axis of the laryngoscope, such that the tissue is tangentially pulled towards the laryngoscope, creating a shear stress on the tissue structure (like a billiards queue tangentially moving the skin surface of the resting hand's finger).

4.2 Data Capture

The load cell signal-conditioning unit is an RDP S7DC. This gives an output that is proportional to the force applied to the load cell. A portable laptop PC was used to capture the incoming data.The captured data were displayed graphically in real-time, providing essential visual feedback, and captured in a data file. The data files can then be subsequently analysed using off-line tools; in this instance we used Excel to extract the elastic data.

4.3 Data Analysis

The raw data is the captured output from the load cell. The graph in figure 5 shows a typical trace obtained from a patient, the force difference being typically between 0.3 to 0.5g. After each change in stress there is a visible period of relaxation due to movement within the adhesive. The strain then tends to become linear. There are typically 15 readings within this linear section, which are averaged to obtain a value for the applied stress in units of grams force. The standard deviation within the linear section is typically less than 0.02 grams, which is less than 10% of the force difference. It is our opinion that the cause of these perturbations is due to the fact that we are measuring extremely small forces in-vivo; as these errors are not present when similar readings are taken from excised and rigidly mounted larynxes.
The tissue is stressed at least 5 times, and the force difference between each step change is determined. The average change in force is determined, and the standard deviation determined. This value is the force exerted as a result of a vocal fold tissue displacement of 1mm.

The geometry of the test area was determined by measurement of the probe diameter, and inspection of images taken during the test. The area was typically 1mm x 2mm; however this assessment is the main cause of error in our final readings, which is why they are expressed as a range in the results table. The force is derived from the captured data, the displacement is set to be 1mm, the tissue thickness is assumed to be 1mm. Using this geometry it is possible to derive the shear modulus of the vocal fold, which is expressed as a range to take account of the geometric uncertainties.

5 Results

5.1 In Vivo Data

Please see table 1, which gives the full set of in-vivo results in.terms of shear modulus, the age and sex of the volunteer patients, and the coefficient of variance of the original data. The range is determined by applying an uncertainty of 10% to the dimensional estimates and the full effect of the standard deviation to the mean results. The mean reading for the shear modulus is 1371 Pascals, with a range 701 to 2225 Pascals.

Age	Sex	CofV	Shear Modulus Mean Pascals	Shear Modulus Range Pascals
36	F	15%	933	681-1184
37	F	19%	777	553-1000
28	F	11%	701	526-877
70	F	Only 1 reading	1972	1582-2363
28	F	10%	1819	1364-2274
52	F	27%	901	609-1194
63	M	22%	1637	1220-2055
55	M	17%	2225	1605-2843

Table 1 – Range of Shear Modulus Obtained from 8 Volunteer Patients

5.2 Excised Tissue Data

The graphs show the distribution of shear modulus with respect to the age of the donors to age. The results can be summarised as follows:

Male Shear Modulus =

i) Range = 246 – 3536 Pascal (shear model)
ii) Mean = 1008 Pascal (shear model)
iii) Standard Deviation = 380 (shear model)
iv) Range = 552 - 2741 Pascal (indentometer model)
v) Mean = 1000 Pascal (indentometer model)
vi) Standard Deviation = 460 (indentometer model)

Female Shear Modulus =

i) Range = 286 - 3332 Pascal (shear model)
ii) Mean = 1237 Pascal (shear model)
iii) Standard Deviation = 768 (shear model)
iv) Range = 509 - 1989 Pascal (indentometer model)
v) Average = 1332 Pascal (indentometer model)
vi) Standard Deviation = 428 (indentometer model)

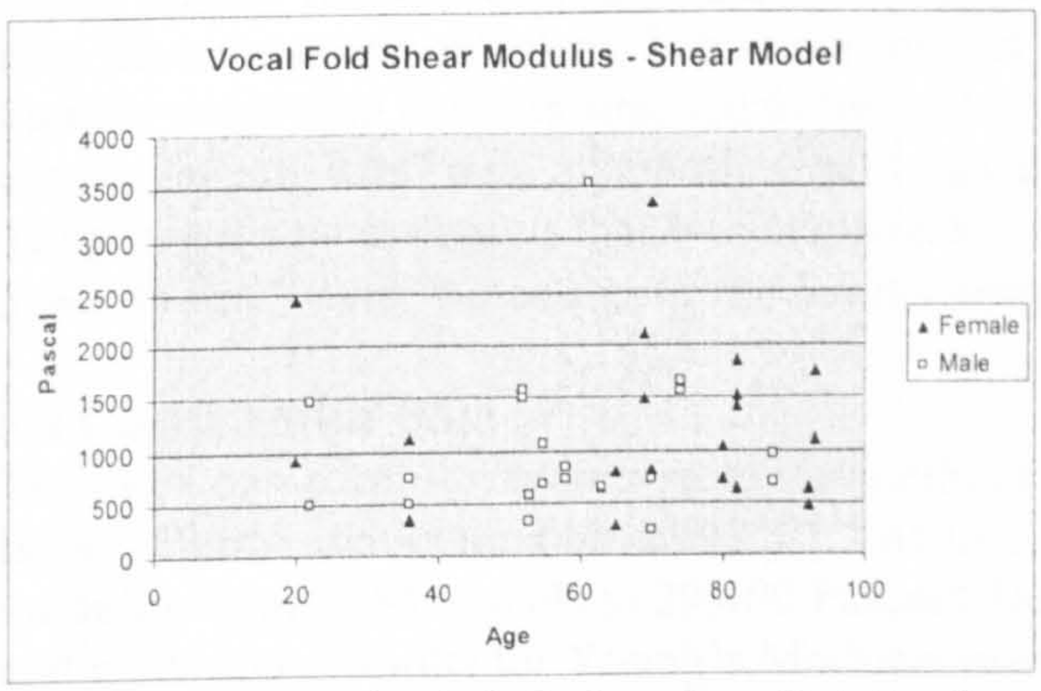

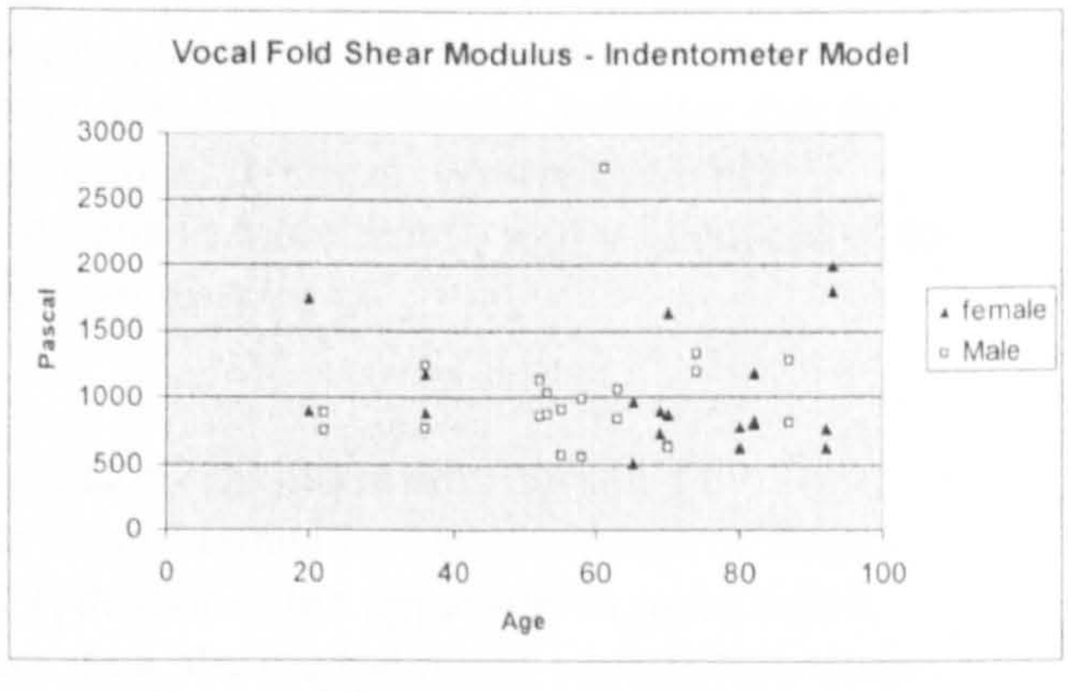

Graphs 1 & 2 showing distribution of shear modulus with respect to age

5.3 Anisotropic Nature of the Vocal Fold

The key advantage to measuring the biomechancial properties of the vocal fold using intact larynxes is that it is possible to differentiate the elastic response with respect to the direction of the applied stress. Currently we are part way through a study to examine the anisotropic nature of the vocal fold, and our early findings are presented here.

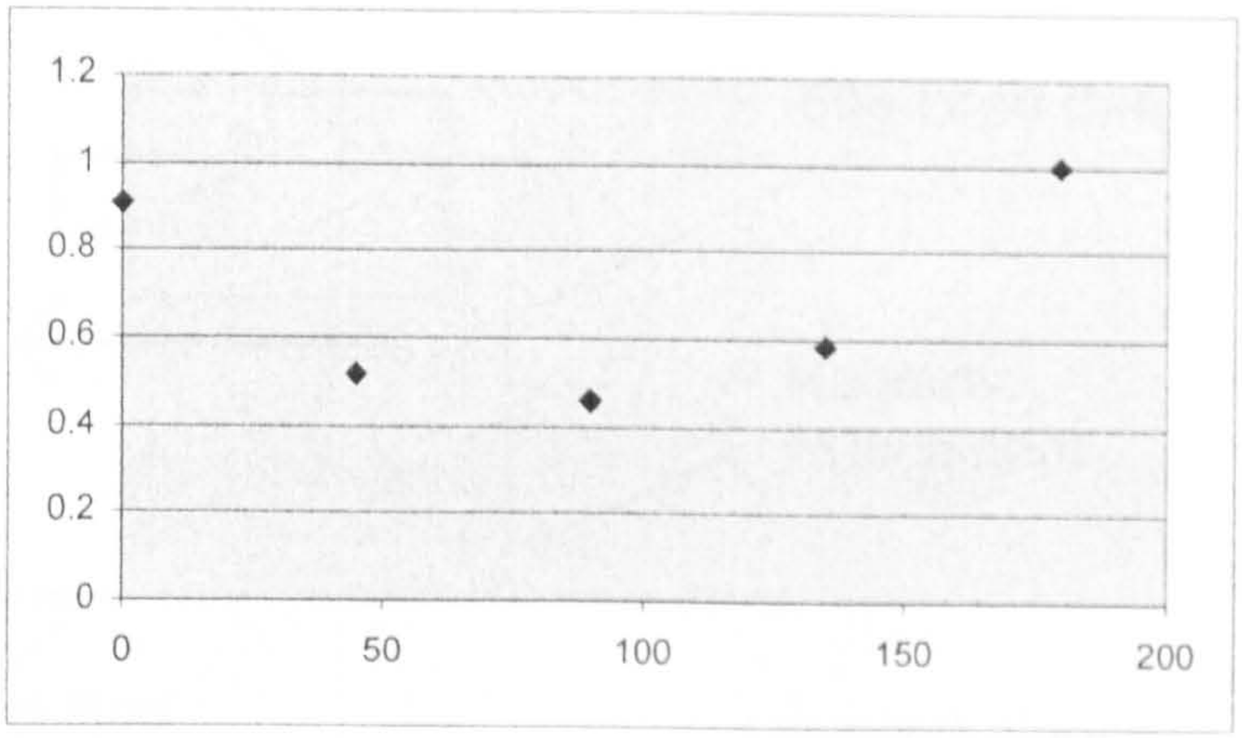

Graph 3 The variation in elasticity of a complete hemi-larynx with respect to angle

An LSR probe was attached using suction to the mid-membranous point of the vocal fold, and the elastic response measured at different angles of applied stress. 0 degrees is the longitudinal direction along the axis from the vocal process to the anterior commisure; 90 degrees is transverse to this axis, and 180 degrees returns to the longitudinal axis in the opposite direction. So far only 5 larynxes have been examined, and all of them exhibit the anisotropic behaviour as shown in graph 3. From 8 hemi-larynxes from which data was obtainable, the average ratio of the elasticity in the transverse direction with respect to the longitudinal direction is 0.4. If we remove the vocal fold cover and repeat the measurement on the vocal ligament and then the vocalis muscle the anisotropic behaviour is still present but is less prevalent. The ratio for the measurements taken from the ligament is 0.56 and from the exposed muscle is 0.63.

It is far too early to make any firm conclusions from this study. The indications are that the vocal fold tissue is more pliable in the transverse direction than in the longitudinal direction. The fact that removing the vocal fold cover and measuring the pliability of the underlying ligament and muscle also shows a strong anisotrpic behaviour implies that the phenomena is primarily due to the way that the vocal fold cover is attached to the underlying structures. However it also indicates that the lamina propria itself may inherently react in an anisotrpic manner to stress. We are currently designing a new apparatus that will investigate this phenomena in more detail, as it will enable us to quantify the Young's modulus of the lamina propria in known directions.

5.4 Comparative Data

The most comparable experiment to our methods is the groundbreaking results obtained by Tran, Berke, Gerrat and Kreiman in 1993 [7]. The in-vivo data they obtained by offers a range of shear modulus from 2450 Pascals to 29,400 Pascals. Berke [8,9] describes the apparatus in more detail, and gives some results for Young's Modulus using canine data, the medial result equates to a shear modulus of 1450 Pascals. McGlashan [10] recently reported a shear modulus of 2500 Pascals, using an optical in-vivo technique that infers modulus by determining the velocity of the mucosal wave.

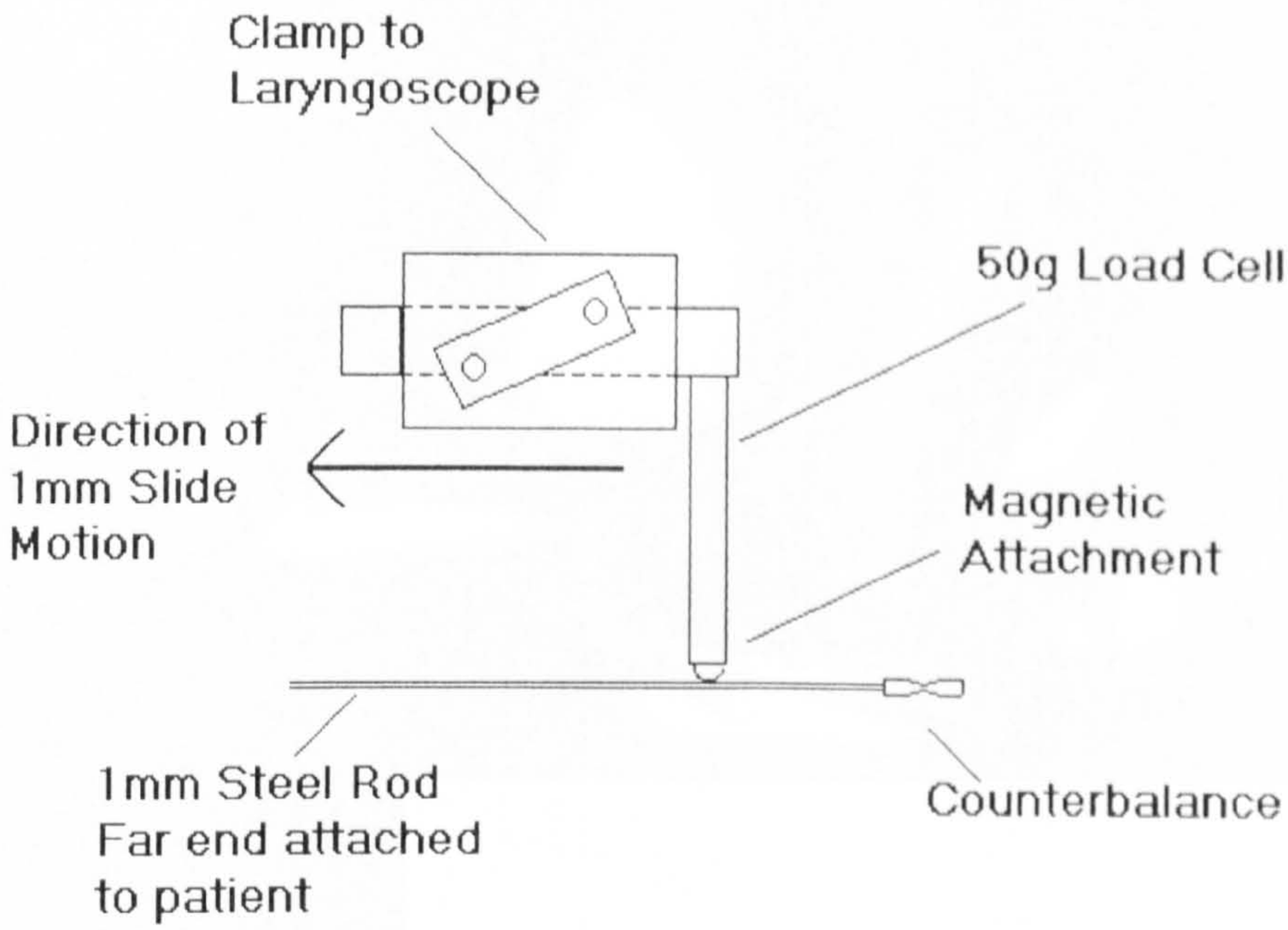

Figure 1 Schematic of Laryngeal Tensiometer

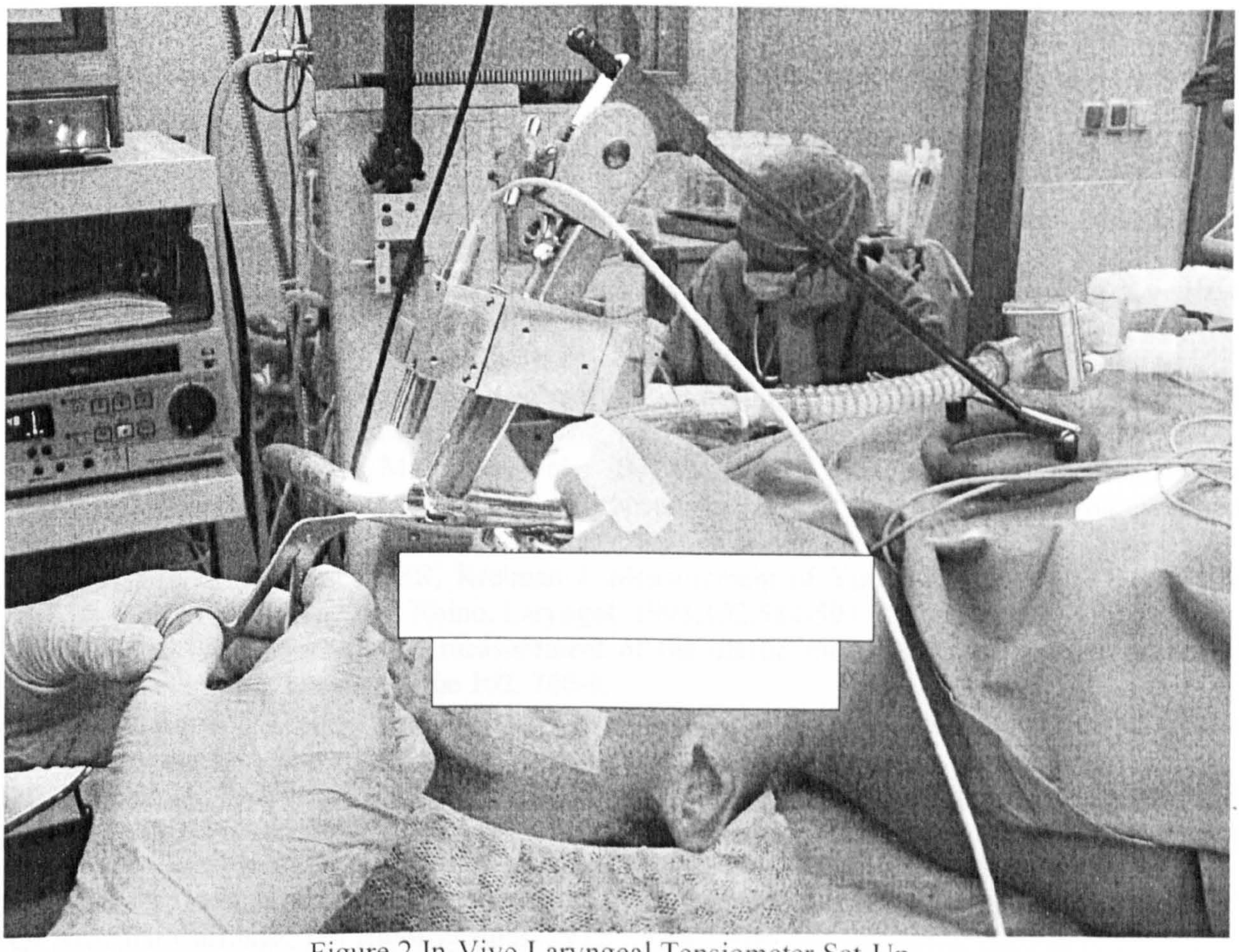

Figure 2 In-Vivo Laryngeal Tensiometer Set-Up

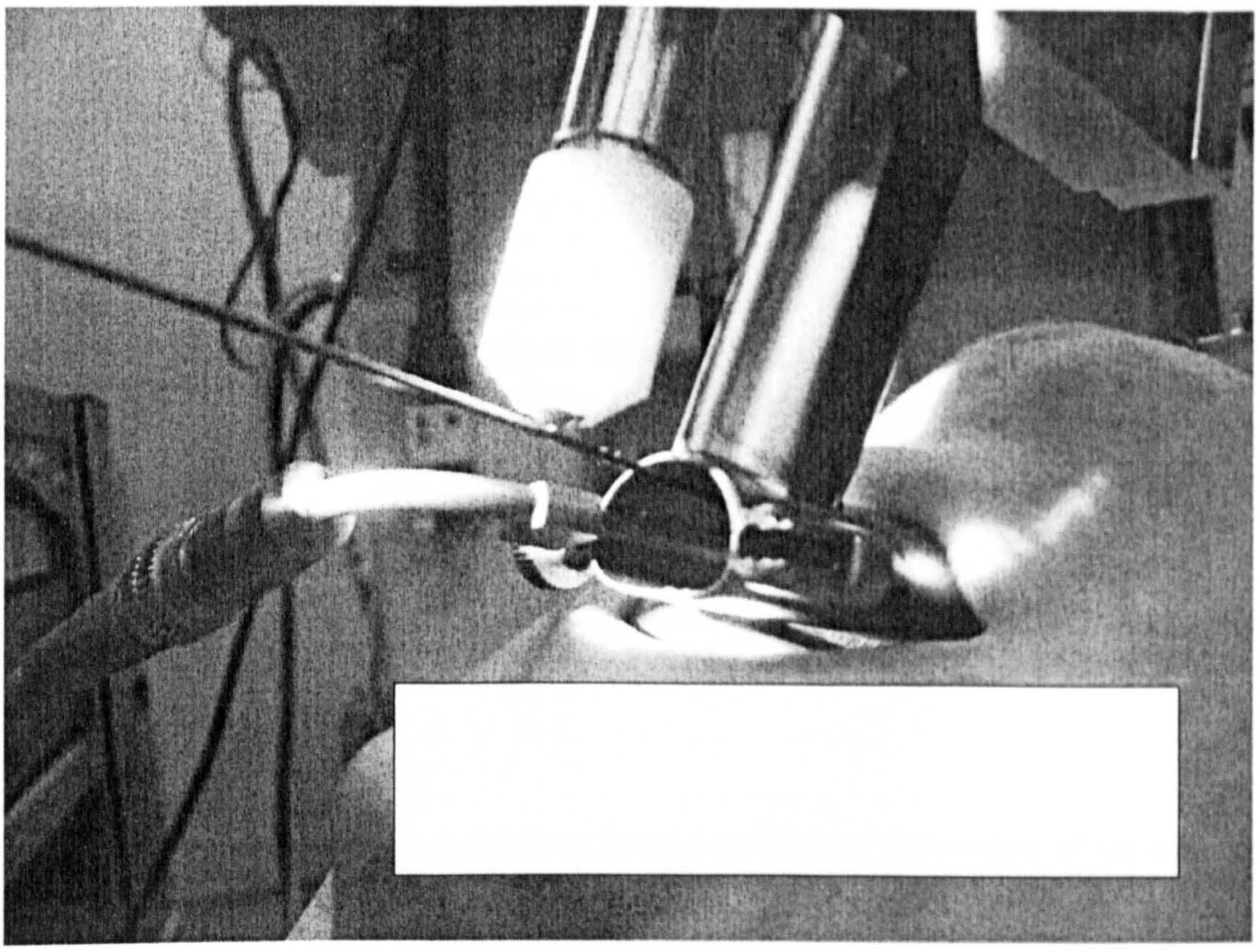

Figure 3 Magnetic Attachment of Probe

References

1. Matts P, Goodyer EN. A New Instrument To Measure The Mechanical Properties Of The Human Stratum Corneum. J of Cosmetic Science. 1998;49,321-323
2. Hertegård S, Dahlqvist Å, Goodyer E, Maurer. Viscoelastic Measurements After Vocal Fold Scarring In Rabbits. Acta Oto-Laryngologica, 2006 July; 126(7):758-763.
3. Hess M, Muller F, Kobler J,Zeitels A, Goodyer EN. Measurements Of Vocal Fold Elasticity Using The Linear Skin Rheometer Folia Phoniatrica. 2006,58(3):207-216
4. Goodyer EN, Muller F, Bramer B, Chauhan D, Hess M. In Vivo Measurement of the Elastic Properties of the Human Vocal Fold. European Archives of Oto-Rhino-Laryngology. 263(5):445-462, May 2006.
5. Goodyer EN, Gunter H, Masaki A, Kobler J (2003) Mapping the visco-elastic Properties of the Vocal Fold, AQL 2003, Hamburg.
6. Goodyer EN, Hemmerich S, Müller F, Kobler JB, Hess M. The shear modulus of the human vocal fold, preliminary results from 20 larynxes. European Archives of Oto-Rhino-Laryngology. Online August 2006.
7. Tran QT, Berke GS, Gerratt BR, Kreiman J. Measurement of Young's Modulus in the In Vivo Human Vocal Folds. Ann Otol. Rhino. Laryngol. 1993;102,584-591
8. Berke GS (1992) Intraoperative measurement of the elastic modulus of the vocal fold. Part 1. Device development. Laryngoscope 102, 760-9.
9. Berke GS, Smith ME (1992) Intraoperative measurement of the elastic modulus of the vocal fold. Part 2. Preliminary results. Laryngoscope 102, 770-8.
10. McGlashan JA, de Cunha DA, Hawkes DJ, Harris TM. (1998) Surface Mapping of the Vibrating Vocal Folds. Proceedings of the 24th World Congress of the International Association of Logopedics and Phoniatrics (IALP), Amsterdam August 1998
11. Hayes WC, Keer LM, Herrmann G., Nockros LF, Mathematical Analysis For Indentation Tests Of Articular Cartilage. J of Biomechanics. 1972;5,5,541-551

Acta Oto-Laryngologica, 2006; 126: 758–763

Taylor & Francis

ORIGINAL ARTICLE

Viscoelastic measurements after vocal fold scarring in rabbits – short-term results after hyaluronan injection

S. HERTEGÅRD[1], Å. DAHLQVIST[2]* & E. GOODYER[3]

[1]*Department of Logopedics and Phoniatrics, Karolinska Institute, Huddinge University Hospital, Sweden,* [2]*Department of Otorhinolaryngology, University of Umeå, Sweden and* [3]*Department of Computer Science & Engineering, De Montfort University, Leicester, UK*

Abstract

Conclusions. The scarring model resulted in significant damage and elevated viscoelasticity of the lamina propria. Hyaluronan preparations may alter viscoelasticity in scarred rabbit vocal folds. *Objectives.* Vocal fold scarring results in stiffness of the lamina propria and severe voice problems. The aims of this study were to examine the degree of scarring achieved in the experiment and to measure the viscoelastic properties after injection of hyaluronan in rabbit vocal folds. *Materials and methods.* Twenty-two vocal folds from 15 New Zealand rabbits were scarred, 8 vocal folds were controls. After 8 weeks 12 of the scarred vocal folds received injections with 2 types of cross-linked hyaluronan products and 10 scarred folds were injected with saline. After 11 more weeks the animals were sacrificed. After dissection, 15 vocal folds were frozen for viscoelastic measurements, whereas 14 vocal folds were prepared and stained. Measurements were made of the lamina propria thickness. Viscoelasticity was measured on intact vocal folds with a linear skin rheometer (LSR) adapted to laryngeal measurements. *Results.* Measurements on the digitized slides showed a thickened lamina propria in the scarred samples as compared with the normal vocal folds ($p < 0.05$). The viscoelastic analysis showed a tendency to stiffening of the scarred vocal folds as compared with the normal controls ($p = 0.05$). There was large variation in stiffness between the two injected hyaluronan products.

Keywords: *Vocal fold scarring, viscoelasticity, hyaluronan*

Introduction

Vocal fold scarring may have different etiologies, such as trauma, defect healing after vocal fold surgery, post radiotherapy, or inflammation [1]. This results in tissue defects and/or disturbance of the vocal fold lamina propria viscoelasticity. The voice is often breathy or aphonic and the phonation threshold pressure which corresponds to 'easiness of phonation' [2] is elevated. Effective treatment is lacking; many injection substances have been tried. Bovine or autologous human collagen has been used for superficial injections into the vocal fold ligament [3,4]. Autologous fat implantation into the lamina propria has also been tried in selected cases [5]. Drawbacks with collagen and fat are the need for allergy testing (for bovine collagen) and the unpredictable degree of resorption over time (for both) [6].

Because of the different drawbacks with all existing materials for augmentation, there is an ongoing search for new materials [7]. The ideal substance has to fulfil various criteria, for example, to be non-toxic and non-allergenic, and to allow precise injection and superficial implantation into the vocal fold lamina propria. It should persist for a long time.

Hyaluronan (HYA) is a glycosaminoglycan that is identical for all vertebrate species. It is present in high concentrations in the extracellular matrix of many tissues in the body [8] and has also been found in the vocal fold lamina propria [9,10]. HYA is a major constituent of extracellular soft connective tissue matrix where it provides lubrication, shock

---

This paper was presented at the American Academy of Otolaryngology – Head and Neck Surgery, New York, 21 September 2004.

*Dr Dahlqvist was a tsunami victim in Thailand on 26 December 2004

Correspondence: Stellan Hertegård, MD, PhD, Department of Logopedics and Phoniatrics, Karolinska Institute, Karolinska University Hospital Huddinge, S-141 86 Stockholm, Sweden. Fax: +46 8 5858 1505 E-mail: stellan.hertegard@klinvet.ki.se

(Received 30 July 2005; accepted 10 November 2005)

ISSN 0001-6489 print/ISSN 1651-2551 online
DOI: 10.1080/00016480500470147

absorption, filtering, exclusion of particles and many biological functions in, for example, wound healing [8,11]. The viscoelastic properties of native exogenous HYA showed a similar dynamic viscosity to that of normal vocal fold mucosa [12]. Its rheological properties, however, vary substantially with concentration, molecular weight and degree of molecular cross-linking [13,14].

Pure cross-linked hyaluronan in a gel-like form (hylan b gel, Hylaform®) was found to be persistent in rabbit vocal folds for up to at least 1 year after injection, with no inflammatory reaction or granuloma formation [15]. Our previous results using hyaluronan in patients with glottal insufficiency due to unilateral vocal fold paresis and atrophy showed no side effects, and improved voice and glottal closure for up to at least 2 years [16,17]. Parameters related to improved viscoelasticity, such as amplitude of vocal fold vibrations and phonation threshold sound pressure, were also improved. No vocal fold stiffening or signs of scarring were found after injection in the superficial lamina propria with hylan b gel. The drawbacks are related to some resorption with need for re-injections. The effects of hylan b gel in treatment of vocal fold scarring have so far only been studied in a few patients but the substance seemed to have the potential for improving vocal fold function [16].

The first aim of the experiment was to study the degree of scarring in the lamina propria achieved in an experimental model for vocal fold scarring. The second aim of this experiment was to investigate the short-term viscoelastic properties of scarred rabbit vocal folds after injections of cross-linked HYA as compared to scarred vocal folds injected with saline. Vocal fold mucosa from non-injected rabbit larynges served as controls.

Materials and methods

Fifteen New Zealand white rabbits (body weight 2.9–3.5 kg) were used in the experiment. The American principles of laboratory animal care and the Swedish National law on animal care ethics were followed. The experiment was approved by the local ethic committee of Karolinska Institute (S-149-01, 2001-10-15).

Vocal fold scarring

Before surgery premedication was administered consisting of glycopyrron (Robinul®, 0.1 mg/kg s.c.) and Hypnorm (a mixture of fluanizonum 10 mg/ml and fentanyl 0.3 mg/ml), 0.3 ml/kg i.m. The animals were then anaesthetized with diazepam 1–2 mg/kg i.v. The laryngeal structures were found to be normal on examination by means of a modified 4.0 mm paediatric laryngoscope (model 8576E, Karl Storz Endoscope, Tuttlingen, Germany) and a Storz-Hopkins 0 2.7 mm rigid endoscope (model 7218A). The scarring procedure was performed with a 2 mm microcup forceps and microscissor (Micro-France) [18,19]. A 2–3 mm biopsy was taken from the mid-membranous mucosa and superficial thyroarytenoid muscle under direct vision through an otomicroscope (Figure 1). Seven animals were operated on both vocal folds and eight animals were operated on one side only. Thus a total of 22 vocal folds was operated (scarred) and 8 normal vocal folds were kept as the control group. All animals survived the procedure.

Vocal fold injections

After 8 weeks the animals were again examined with direct laryngoscopy under general anaesthesia. Injections were made under vision through a microscope into the lamina propria and/or to the superficial part of the thyroarytenoid muscle of the vocal fold using a Medtronic Xomed laryngeal injector with a 27 gauge needle (Figure 1). Systematic injections into either of the structures mentioned above were not possible due to the narrow space and the equipment available at the time of the experiment. Ten of the 22 operated (scarred) vocal folds were injected with 0.1 ml saline each. Six of the 22 vocal folds were injected with 0.1 ml Hylaform®, hylan b gel, a cross-linked pure HYA at 5.5 mg/ml concentration (Genzyme Biosurgery, Ridgefield, MA, USA), and 6 of the 22 vocal folds were injected with Restylane®, a non-animal stabilized HYA from bacterial fermentation at 20 mg/ml concentration (Q-Med Inc., Uppsala, Sweden). The eight non-scarred vocal folds were not injected. No animal

Figure 1. Left: image of a rabbit larynx after a resection (arrow) in the left vocal fold. Right: image of a larynx of another animal during the second procedure after injection of hyaluronan into the left vocal fold.

suffered from breathing problems or bleeding after the injections.

Dissection

Eleven weeks after the injections the animals were killed by an i.v. overdose of sodium pentobarbital. The larynges were dissected out and each larynx was divided in the posterior midline. Sixteen of the hemilarynges were immediately fresh frozen at −20 C until viscoelastic analysis. This included five non-injected (normal), five operated (scarred) vocal folds injected with saline, three operated (scarred) vocal folds injected with Hylaform® and three operated (scarred) samples injected with Restylane®.

Fourteen of the hemilarynges were placed in 10% formaldehyde for later preparation and histological analysis: three non-injected (normal), five operated (scarred) folds injected with saline, three operated (scarred) folds injected with Hylaform® and three operated folds injected with Restylane®.

Histological measurements

Fourteen vocal folds removed from the hemilarynges were further processed in 2% formaline and 0.5% glutaraldehyde in 0.1 M PBS, fixed in a microwave owen at 630 W, paraffin-embedded, dried and cut into 5 µm thick sections [20]. These were stained with haematoxylin and eosin (H&E) and van Giesson for histological analysis. Image analysis of the stains at ×20 magnification was carried out after digitization of the microscopic images (using a Nikon Digital Camera, DXM 1200 attached to a Nikon Ecclipse, E600 microscope). The thickness of the lamina propria was measured with the software Image Pro Plus® (version 3.0 Media Cybernetics). The thickness measurements of lamina propria were enhanced by a colour filtering and normalization process with Photoshop (version 8.0) and custom-made software (written by Hans Larsson at Karolinska Institute, Stockholm, Department of Logopedics and Phoniatrics) (Figure 2).

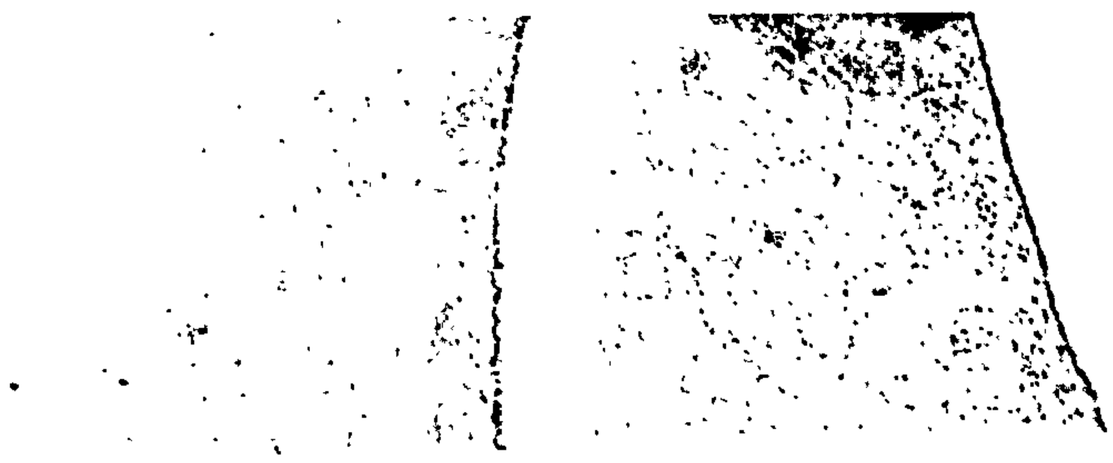

Figure 2. Haematoxylin and eosin-stained sections (×20) after digital colour filtering of the lamina propria (red colour). Left, a normal vocal fold; right, a scarred vocal fold.

Viscoelastic measurements

For linear skin rheometry, analyses were made on intact vocal folds with a linear skin rheometer (LSR) adapted to laryngeal measurements. This device was originally developed for measurements of skin viscoelasticity [21,22]. A lightweight tipped probe with a cross-section surface of 1 mm^2 is driven to produce a sinusoidal compression over a distance of 1–2 mm at 0.3 Hz. The resulting relative Young's modulus (ΔY) [23] parameter is derived from analysis of stress/strain curves. These parameters are related to tissue stiffness. An advantage with the method is that the measurements can be made without dissecting the tissue samples. The hemilarynges were thawed at room temperature, kept moist with saline and fixed with needles at a plate during the measurements. Measurements were made at the vocal fold edge on mid-membranous position during compression of the vocal folds (four untreated samples, five scarred folds injected with saline, three scarred folds injected with Hylaform® and three with Restylane®). One normal vocal fold was used to test the experimental set-up and the results for this were not further analysed in the experiment. The measurements of each vocal fold lasted 15–20 min.

Statistics

Non-parametric comparisons between the groups were made (Statview program, SAS Institute Inc., version 5.0). The two types of HYA treatments were analysed as one group because of the small number of samples. Due to the exploratory nature of the study, significance levels with $p < 0.05$ are reported.

Results

Histological analysis

In four of the six scarred vocal folds treated with HYA (Hylaform® or Restylane®) there was remaining HYA substance, either in smaller well localized islands in the lamina propria or deep in the thyroarytenoid muscle. No inflammatory changes or granuloma were observed. These aggregates were surrounded by a thin capsule of connective tissue. The measurements of the vocal fold lamina propria showed that both the scarring groups (scarring+saline and scarring+HYA) had significantly thicker lamina propria than the non-scarred folds ($p < 0.05$). There was no difference in lamina propria thickness between the scarred folds that were treated with HYA or injected with saline.

Viscoelastic analyses (LSR analysis)

As shown in Figure 3 the relative Young's modulus (ΔY) was lowest for the normal vocal folds and higher for both the scarred groups. This indicates a stiffening for the scarred groups. The variation was large within the scar group treated with different HYA substances, the Hylaform® samples had the lowest stiffness. The difference between the normal vocal folds and the scarred folds injected with saline was close to significant ($p = 0.05$) (normal versus scar + HYA, ns; scar + saline versus scar + HYA, ns).

Discussion

Many attempts have been made to find a treatment for vocal fold scarring. The main aim of the study was to examine the degree of scarring achieved in a rabbit animal model. The rabbit vocal folds are similar in structure to human vocal folds, although the lamina propria is less well developed [20]. We operated rabbit vocal folds in a surgical scarring procedure that was similar to procedures used by other researchers [18,19]. The total observation time was close to 5 months after the scarring procedure.

The main histological finding was a significant thickening of the lamina propria. Previous research with scarring models in rabbits showed ultrastructural changes of the lamina propria with increased pro-collagen and fibronectin and a decrease in elastin at 2 months after surgery [24]. Studies on scarred canine vocal folds showed similar findings to those for the rabbits 2 months after surgery and a co-deposition of collagen in the lamina propria developing 6 months after scarification [19,25]. Levels of fibronectin were also elevated both 2 and 6 months after surgery. Although we did not analyse the mechanisms of the lamina propria thickening this finding indicates that significant damage was achieved by our scarring procedure.

Viscoelastic testing by the LSR method showed an elevated relative Young's modulus for the scarred vocal folds injected with saline as compared with the normal folds. This corresponds to tissue stiffening. Rheological analyses in other studies in scarred larynges in both rabbits and dogs have shown increased stiffness and viscosity [25,26]. Thus both the histological and rheological findings indicate that a significant degree of scarring was achieved by the vocal fold surgery in this experiment. The injection in itself might also have contributed to some scarring (no animals in the experiment were operated but not injected). However, no scarring was found in a previous study in which rabbits' vocal folds were injected with HYA substances without any surgical scarring procedure [27]. Furthermore, no signs of scarring were noted in our previous injection studies on patients with glottal insufficiency caused by vocal fold paresis or atrophy [16].

To restore the vibratory capacity of scarred vocal folds the characteristics of a bio-implant used for injection or implantation should match the viscoelastic properties of normal vocal fold mucosa. Previous studies in normal rabbit vocal folds after injection of hylan b gel showed similar dynamic viscosity after injection as for native rabbit vocal folds [27,28]. Furthermore, it was demonstrated that the level of hyaluronan was lowered in vocal folds of pigs and rabbits within 15 days after a scarification procedure with a simultaneous increase in tissue stiffness [29,30]. The results after treating a few patients with vocal fold scarring were also promising [16]. Both HYA substances used in this study (Restylane® and Hylaform®) are easy to handle and inject. The difficulties of injecting or

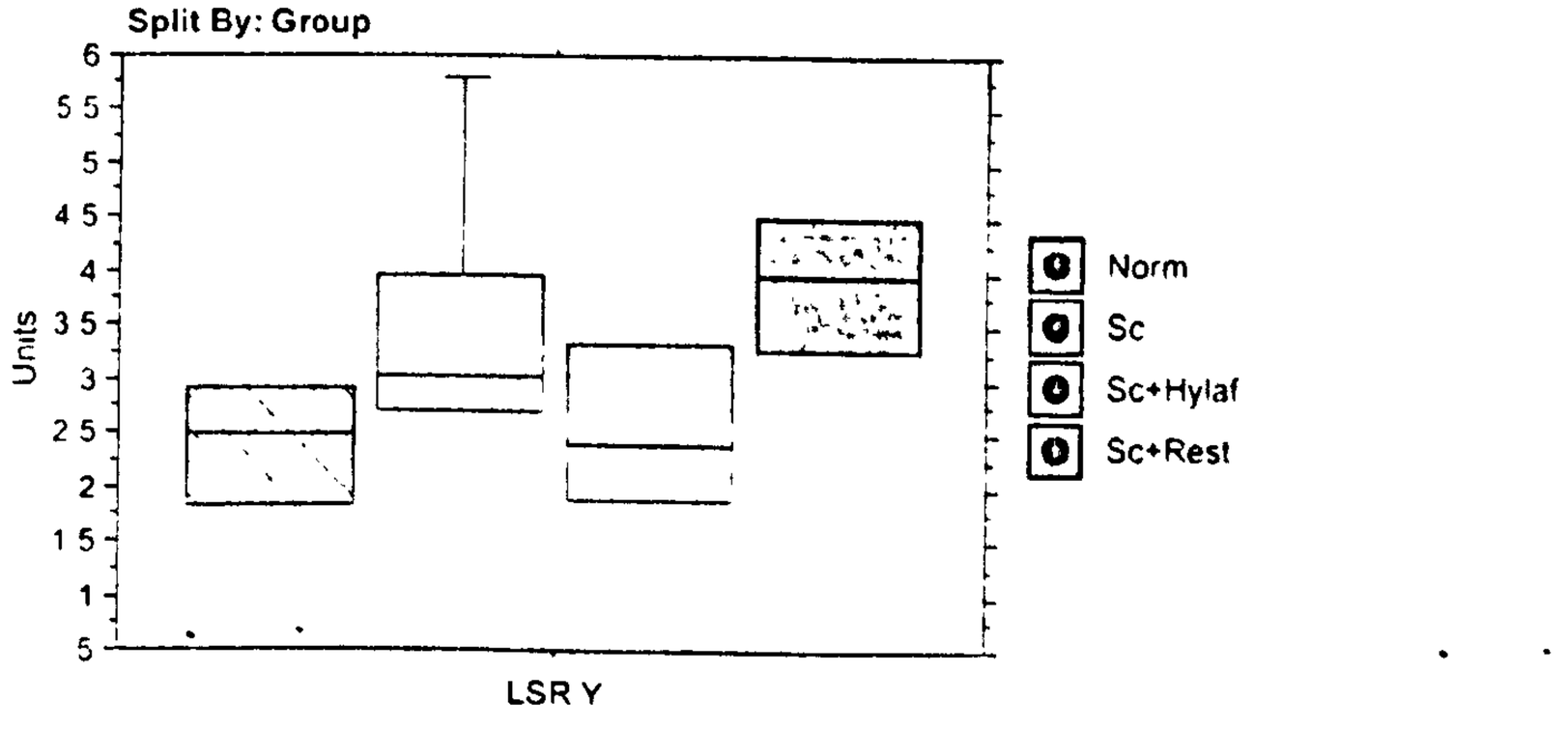

Figure 3. Box plots showing the relative Young's elastic modulus (LSR Y) from the linear skin rheometer (LSR) analysis for the normal vocal folds (Norm, $n = 4$), scarred vocal folds (Sc, $n = 5$) and scarred folds treated with HYA (Hylaform® Sc + Hylaf, $n = 3$, and Restylane® Sc + Rest, $n = 3$)

augmenting with precision in scarred vocal folds are well known. This may explain the results of the histological analysis showing that the HYA injected was found at various locations in the vocal folds and the HYA was surrounded by a thin capsule. This is similar to the findings by Hallén et al. [15]. Remaining HYA was found at histological analysis in four of the six injected samples. The observation time after injection was 11 weeks. Thus for two animals either we did not succeed in injecting into the scarred tissue or there was resorption of the material.

Reological testing by the LSR method showed no significant difference between the scarred folds injected with saline or with HYA (Hylaform® or Restylane®). The variation was large for the HYA-treated samples, but Hylaform® had a lower relative Young's modulus close to the normal controls. This indicates less stiffening, which corroborates the results noted for some patients treated for vocal fold scarring [16]. Chan et al. performed parallel plate rheometry analysis on normal human vocal folds before and after removal of the natural hyaluronan [12]. Their results showed a higher viscoelasticity without hyaluronan. Hansen and Thiebeault injected a HYA scaffold hydrogel in newly scarred rabbit vocal folds. Viscoelasticity was improved after 3 weeks with well organized collagen fibrils [31]. It was hypothesized that HYA accelerated wound repair and altered the viscoelasticity directly in a favourable way in vocal fold scarring

Conclusions

The results showed that the experimental model used resulted in thickening of vocal fold lamina propria. The LSR viscoelastic analysis showed elevated elasticity for the scarred vocal folds injected with saline as compared with the normal controls. These findings indicate that significant damage to the lamina propria was achieved by the surgical procedure. The reometry also showed improved biomechanical properties in some of the scarred vocal folds treated with HYA. However, these results must be confirmed to permit definite conclusions.

Acknowledgements

We are grateful to Professor Claude Laurent, Department of Otorhinolaryngology, Rikshospitalet, Oslo, for valuable comments and discussions on the manuscript; to Kristina Forsgren at Umeå University Hospital for performing the histological preparations and to Anna Tolf at the Institution of Pathology, Karolinska University Hospital Huddinge for assistance with histological analysis. The study was supported by the Swedish Research Council (grant no. 2002-3897) and by the Karolinska Institute.

References

[1] Benninger MS, Alessi D, Archer S, Bastian R, Ford C, Koufman J, et al. Vocal fold scarring: current concepts and management. Otolaryngol Head Neck Surg 1996;115:474–82.

[2] Titze IR. Phonation threshold pressure: a missing link in glottal aerodynamics. J Acoust Soc Am 1992;91:2926–35

[3] Ford C, Bless DM, Loftus J. Role of injectable collagen in the treatment of glottic insufficiency: a study of 119 patients. Ann Otol Rhinol Laryngol 1992;101:237–47.

[4] Remacle M, Lawson G, Delos M, Jamart J. Correcting vocal fold immobility by autologous collagen injection for voice rehabilitation. Ann Otol Rhinol Laryngol 1999;108:788–93.

[5] Neuenschwander MC, Sataloff RT, Abaza MM, Hawshaw MJ, Reiter D, Spiegel JR. Management of vocal fold scar with autologous fat implantation: perceptual results. J Voice 2001;15:295–304.

[6] Shindo ML, Zaretshy LS, Rice DH. Autologous fat injection for unilateral vocal fold paralysis. Ann Otol Rhinol Laryngol 1996;105:602–6.

[7] Chan RW, Titze IR. Viscosities of implantable biomaterials in vocal fold augmentation surgery. Laryngoscope 1998;108:725–31.

[8] Laurent T. Biochemistry of hyaluronan. Acta Otolaryngol Suppl 1987;442:7–24.

[9] Butler JE, Hammond TH, Gray SD. Gender related differences of hyaluronic acid distribution in the human vocal fold. Laryngoscope 2001;111:907–11.

[10] Hammond TH, Zhou R, Hammond EH, Pawlak A, Gray SD. The intermediate layer: a morphologic study of the elastin and hyaluronic acid constituents of normal human vocal folds. J Voice 1997;11:59–66.

[11] Toole BP. Hyaluronan from extracellular glue to pericellular cue. Nat Rev Cancer 2004;4:528–39.

[12] Chan RW, Gray SD, Titze IR. The importance of hyaluronic acid in vocal fold biomechanics. Otolaryngol Head Neck Surg 2001;124:607–14.

[13] Ambrosio L, Borzacciello A, Netti PA, Nicolais L. Rheological study on hyaluronic acid and its derivatives solutions. J Macromol Sci-Pure Appl Chem 1999;A36[7&8]:991–1000.

[14] Ferry JD. Viscoelastic properties of polymers. New York: John Wiley; 1980.

[15] Hallén L, Johansson C, Laurent C. Cross-linked hyaluronan (Hylan B gel): a new injectable remedy for treatment of vocal fold insufficiency – an animal study. Acta Otolaryngol (Stockh) 1999;119:107–11.

[16] Hertegård S, Laurent C, Olofsson K, Lindström E, Hallén L, Testad P, et al. Cross-linked hyaluronan used as augmentation substance for treatment of glottal insufficiency: safety aspects and vocal fold function. Laryngoscope 2002;112:2211–9.

[17] Hertegård S, Dahlqvist A, Laurent C, Olofsson K, Sederholm E, Hallén L, et al. Cross-linked hyaluronan for injection treatment of glottal insufficiency – a two-year follow-up. Acta Otolaryngol (Stockh) 2004;124:1208–14.

[18] Kriesel KJ, Thibeault SL, Chan RW, Suzuki T, Vangroll PJ, Bless DM, et al. Treatment of vocal fold scarring: rheological and histological measures of homologous collagen matrix. Ann Otol Rhinol Laryngol 2002;111:884–9.

[19] Rousseau B, Hirano S, Scheidt TD, Welham NV, Thiebeault SL, Chan RW, et al. Characterization of vocal fold scarring in a canine model. Laryngoscope 2003;113:620–7.

[20] Hallén L, Johansson C, Laurent C, Dahlqvist Å. Hyaluronan localization in the rabbit larynx. Anat Rec 1996;246:441–5.

[21] Matts P, Goodyer E. A new instrument to measure the mechanical properties of the human stratum corneum. Journal of Cosmetic Science 1988;49:321–3.

[22] Goodyer E, Gunter H, Masaki A, Kobler J. Mapping the visco-elastic properties of the vocal fold. In: Proceedings of Advances in Quantitative Laryngology, Voice and Speech Research (AQL), April 2003, Hamburg. www.uke.uni-hamburg.de/kliniken/hno/phoniatrie/aql2003/

[23] Tran QT, Berke GS, Gerrat BR, Kreiman J. Measurement of Young's modulus in the in vivo human vocal folds. Ann Otol Rhinol Laryngol 1993;102:584–91.

[24] Hirano S, Bless DM, Rousseau B, Welham N, Scheidt T, Ford CN. Fibronectin and adhesion molecules on canine scarred vocal folds. Laryngoscope 2003;113:966–72.

[25] Rousseau B, Hirano S, Scheidt TD, Welham NV, Thiebeault SL, Chan RW, et al. Characterization of vocal fold scarring in a canine model. Laryngoscope 2003;113:620–7.

[26] Thiebeault SL, Gray SD, Bless DM, Chan RW, Ford CN Histologic and rheologic characterization of vocal fold scarring. J Voice 2002;1.96–104.

[27] Dahlqvist Å, Gärskog O, Laurent C, Hertegård S, Ambrosio L, Borzacchiello A. Viscoelasticity of rabbit vocal folds after injection augmentation. Laryngoscope 2004;114 138–42.

[28] Hertegård S, Dahlqvist Å, Laurent C, Borzacchiello A, Ambrosio L. Viscoelastic properties of rabbit vocal folds after augmentation. Otolaryngol Head Neck Surg 2003;128 401 6.

[29] Rousseau B, Sohn J, Montequin DW, Tateya I, Bless DM. Functional outcomes of reduced hyaluronan in acute vocal fold scar. Ann Otol Rhinol Laryngol 2004;113:767 76.

[30] Thibeault SL, Rousseau B, Welham NV, Hirano S, Bless DM. Hyaluronan levels in acute vocal fold scar Laryngoscope 2004;114:760–4.

[31] Hansen J, Thibeault SL. Current understanding and review of the literature: vocal fold scarring J Voice 2005 (Epub ahead of print).

Original Paper

Folia Phoniatr Logop 2006;58:207–216
DOI: 10.1159/000091734

Folia Phoniatrica et Logopaedica

Measurements of Vocal Fold Elasticity Using the Linear Skin Rheometer

Markus M. Hess[a] Frank Mueller[a] James B. Kobler[b]
Steven M. Zeitels[b] Eric Goodyer[c]

[a]Department of Phoniatrics and Pediatric Audiology, University Medical Center Hamburg-Eppendorf, Hamburg, Germany; [b]Department of Surgery, Massachusetts General Hospital and Harvard Medical School, Boston, Mass., USA; [c]Department of Computer Science and Engineering, DeMontfort University, Leicester, UK

Key Words
Vocal fold elasticity · Linear skin rheometer · Dynamic spring rate

Abstract

Objective: The linear skin rheometer (LSR), which measures skin visco-elasticity, was adapted for measurements of vocal fold properties. A series of studies was performed on animal and human excised larynges to determine if the LSR technique can be applied to the vocal fold. ***Methods:*** In excised larynges, small patches of mucosa were driven sinusoidally at 0.3 Hz over distances of 1–2 mm using a small probe. Forces in the order of 1 g equivalent gave optimal measurements. Stiffness and viscosity values were derived from stress/strain data. ***Results:*** The instrument was able to measure the visco-elasticity of the tissue in a repeatable manner and it could detect areas where the tissue was artificially stiffened. Two-dimensional maps of the mechanical properties of the laryngeal mucosa were obtained showing local variations in elasticity both parallel and perpendicular to the vocal fold edge. Initial studies were undertaken using animal tissue; more recently, the LSR has been successfully used to obtain similar data from human tissue. ***Conclusion:*** The LSR was been demonstrated to be capable of measuring the elastic properties of the vocal fold in a repeatable and reliable manner. Further studies will now be undertaken to obtain data from a larger sample of human tissue.

Introduction

In phonosurgery there is a need for an instrument that can measure the pliability of vocal fold mucosa (epithelium and superficial lamina propria). The superficial lamina propria, which is the primary oscillator, is critical for normal phonation and

KARGER
Fax +41 61 306 12 34

1021–7762/06/0583–0207$23.50/0

Univ.-Prof. Dr. Markus M. Hess, Poliklinik für Hör-, Stimm- und Sprachheilkunde, Universitätsklinikum Hamburg-Eppendorf, Martinistrasse 52

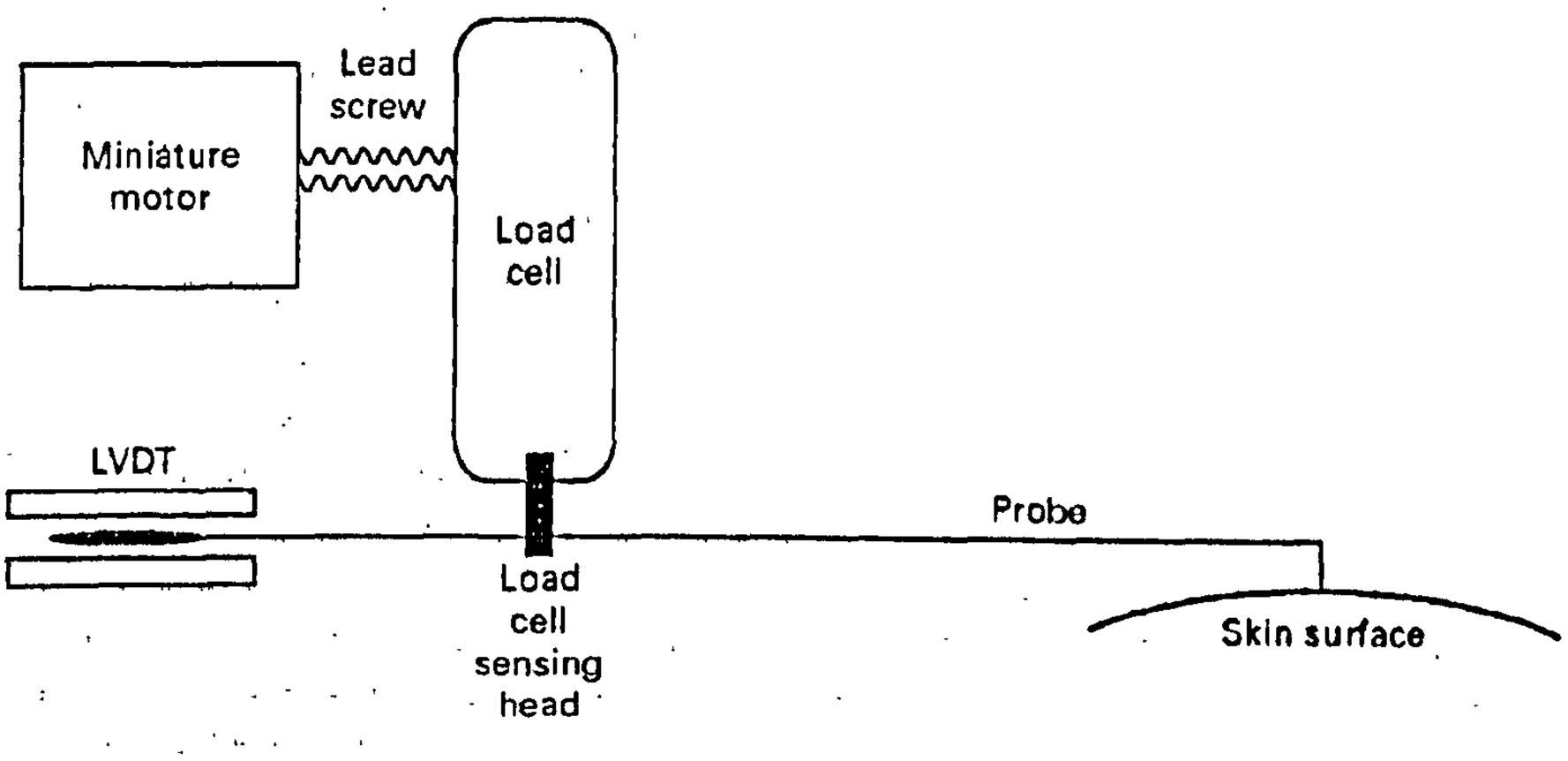

Fig. 1. The LSR sensor head. LVDT = Linear variable displacement transducer.

There was no histological evaluation of tissue damage but neither was there any obvious damage or tearing of the tissue. The small displacements of typically 1 mm, and maximum force of 1 g equivalent, are within the range of the normal motion of the tissue during phonation.

All components fit into one casing measuring 20.0 × 14.8 × 6.9 cm, and the whole unit weighs 1.7 kg. The probe housing itself is a light-weight machined perspex chuck mounted on a low-friction swivel assembly allowing 360-degree movement. This is protected from damage during routine usage by a metal collar. The chuck contains wire grips to allow the wire probes to be inserted or withdrawn by a simple, firm push or pull. A single lead connects the unit to a PC via a 25-pin D-type connector. Power for the LSR unit is taken from the PC via the connector.

Instrument Control

An IBM (or compatible) PC is used to control the movement of the probe and to log force and displacement data. Both force and displacement are monitored continuously at a rate of 1 kHz using a 12-bit ADC plug-in card (National Instruments ATMIO16). The motor is controlled with an analogue output signal also generated by the PC. The desired force/time cycle, which is normally a single sinusoid, is calculated initially and then stored in memory as a table of values. The actual force applied to the probe is compared with the desired value in the table 1,000 times a second. A feedback loop is used to control the motor, which moves the load cell in such a way as to minimize any discrepancy. The force applied thus follows the desired force/time cycle extremely closely. The control loop uses an algorithm with proportional and integral terms, whose weightings can be varied.

The PC logs all the force and displacement values over a complete measurement cycle, which is usually set at 0.33 Hz, thus generating 3,000 pairs of points over a 3-second cycle. Two waveform plots are then obtained, as seen in figures 2 and 3.

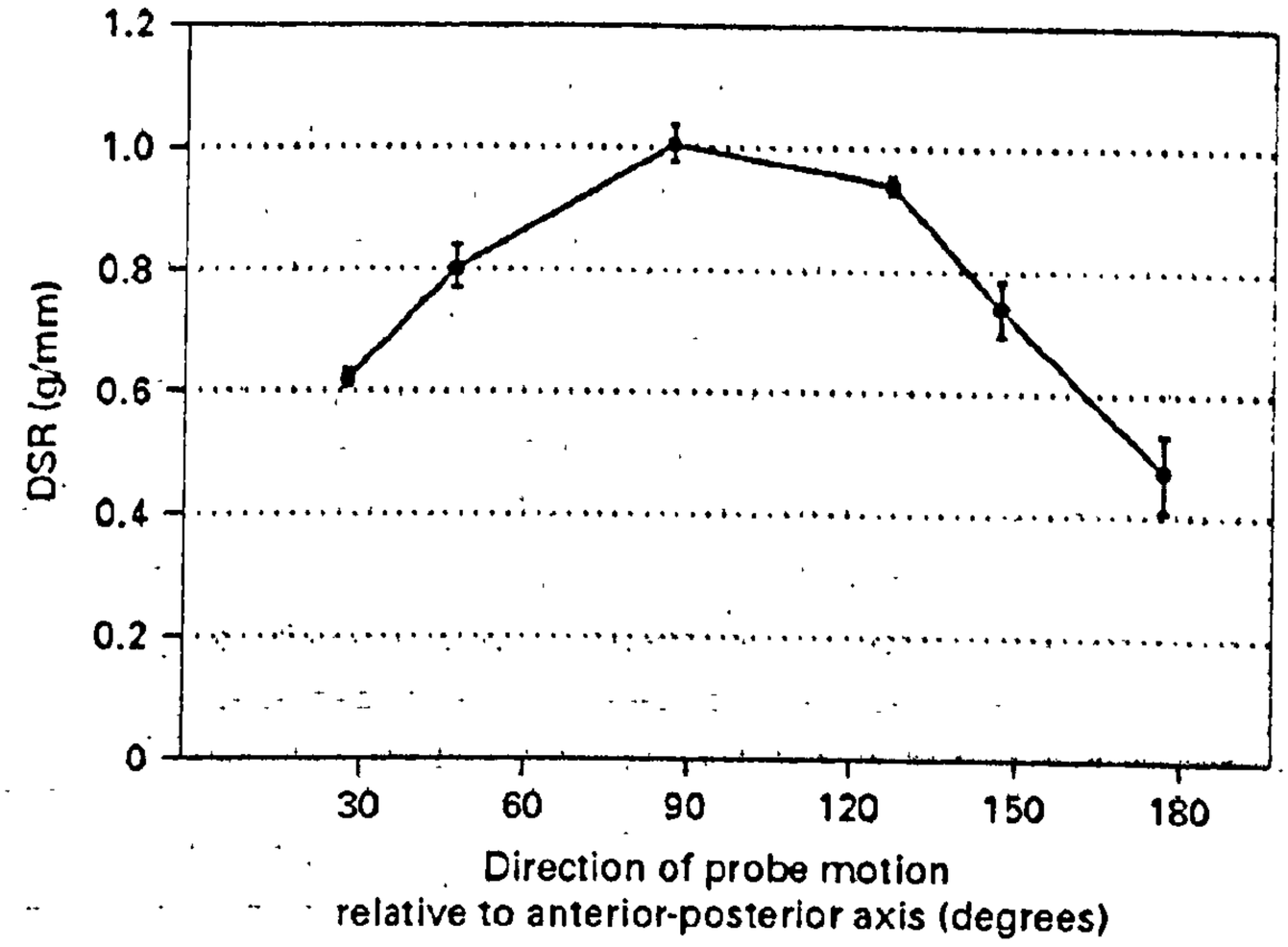

Fig. 4. Relationship between DSR and direction.

The DSR is given simply by the formula F_{max}/P_{max}. Derivatives are calculated and expressed as grams per millimetre, millimetres per newton and micrometres per gram. The DSR is a non-frequency-dependent measurement of the elasticity of the material under test.

The viscous component is often inferred by calculating the area of the ellipse shown in figure 4. A more rigorous approach is to perform a regression on the original sinusoidal data in order to solve the equations:

$$F = F_{max} \sin(t) \qquad (1)$$

$$P = P_{max} \sin(t + T) \qquad (2)$$

where F = instantaneous force, F_{max} = peak force, t = time for one complete cycle in seconds, P = instantaneous displacement, P_{max} = peak displacement, T = phase shift in radians.

Having solved these equations, it is then a straightforward problem to solve the integral over one cycle that represents the area of the ellipse:

$$\int_0^{2\pi} F_{max} \sin(t) P_{max} \cos(t + T)$$

The LSR software solves the above equations for both elastic and viscous components of the data. These are subsequently displayed, directly after measurement. For this study only the non-frequency-dependent DSR readings were recorded.

Bench Tests on Laryngeal Specimens

Laryngeal specimens from animal sources were prepared by hemisection, taking care to leave the vocal fold attachment to the thyroid cartilage at the anterior commissure region intact. The specimens were pinned to a wooden base attached to a

help identify abnormal regions, provide feedback during augmentation surgery and aid in the objective assessment of surgical procedures designed to manipulate vocal fold material properties. Methods that have been applied to intact vocal folds include indentation with a probe attached to a servo motor-controlled force sensor [20, 21], lateral displacement of the vocal fold with a transoral calibrated lever [14, 22, 23] and medial aspiration of the mucosa with a calibrated suction catheter [24]. The latter two methods have been tested on human subjects under general anaesthesia.

In contrast to standard in vitro rheological methods, the LSR is not capable of determining absolute values for visco-elasticity parameters on a unit area or volume basis because the exact volume of tissue that is deformed cannot be determined. Data obtained so far are comparable to previous intact larynx methods. Like the indentation approach and in contrast to the transoral lever, there is good spatial resolution. Relative measurements are potentially very useful in many clinical scenarios if abnormal tissue can be identified or changes resulting from a treatment can be documented. The results demonstrated that this method has the ability to make sensitive and repeatable punctate measurements that may allow for mapping areas of pathology and for side-by-side comparison of a normal with an abnormal vocal fold. It is also well suited for testing the properties of the clinically important superficial lamina propria because it can be attached non-invasively to the epithelium with a suction cannula and gently oscillate the vocal fold cover. This is similar to the way surgeons intuitively test vocal fold properties by palpating the tissue with small surgical instruments.

Future Directions

The most recent studies have demonstrated that the technique can be used to extract measurement data from an intact human larynx. We now have sufficient confidence in this measuring technique to justify a more extensive study using a quantity of freshly excised human larynges.

We further intend to examine the feasibility of developing a compact LSR device that will be capable of being inserted through a direct laryngoscope speculum, thereby allowing in vivo measurements to be taken from patients during general anaesthesia.

Acknowledgements

This work was funded in part by the Eugene B. Casey Foundation.

VISCOELASTICITY IN SCARRED RABBIT VOCAL FOLDS AFTER HYALURONAN INJECTION – SHORT TERM RESULTS

The paper was presented at the American Academy of Otolaryngology –Head and Neck Surgery, New York September 21 2004.

Hertegård S, M.D., Ph.D. [1], Dahlqvist Å, M.D., Ph.D.[2], Goodyer E, M.Sc.[3],

Maurer F. Ph.D. [4]

[1]Dept of Logopedics and Phoniatrics, Karolinska Institute, Huddinge University Hospital, Sweden [2]Dept of Otorhinolaryngology, University of Umeå, Sweden, [3]Dept of Computer Science& Engineering, De Montfort University. Leicester UK, and [4]Dept of Polymer Science& Engineering, Lund University, Sweden

Short title: Viscoelasticity in scarred rabbit vocal folds after hyaluronan

Keywords: vocal fold scarring, viscoelasticity, hyaluronan.

Corresponding author:

Stellan Hertegård MD PhD, Department of Logopedics and Phoniatrics, Karolinska Institute

Karolinska University Hospital Huddinge.S-141 86 Stockholm Sweden

Email: stellan.hertegard@klinvet.ki.se fax:+468 5858 1505

Abstract

Vocal fold scarring is accompanied by stiffness of the lamina propria and results in severe voice problems. Hyaluronan has been shown to improve the viscoelastic properties after injections in normal rabbit vocal folds and in patients with unilateral paresis and vocal fold atrophy.

Objectives: The main aim of the study was to analyze the short term viscoelastic properties after injection of hyaluronan in scarred rabbit vocal folds. Another aim was to examine the degree of scarring achieved by the experimental model.

Material and Methods

Vocal folds of 15 New Zealand rabbits were scarred by a localized resection. After 8 weeks one group received injections with a cross-linked hyaluronan and another group was injected with saline. After 11 more weeks both groups and a third group of control animals with normal vocal folds were sacrificed. The larynges were dissected out, 15 vocal folds were frozen for viscoelastic measurements, whereas 14 vocal folds were prepared and stained for histology. The histological analysis included measurements of the lamina propria thickness and of the relative content of connective tissue. Two methods were used for the viscoelastic measurements: 1. analyses were made on intact vocal folds with a linear skin rheometer (LSR) adapted to laryngeal measurements. 2. the vocal folds were dissected and analyzed in a parallel-plate rheometer.

Results

Measurements on the digitized slides showed a thickened lamina propria and a higher content of connective tissue in the scarred samples as compared to the normal vocal folds ($p<0.05$). The viscoelastic LSR analysis on intact vocal folds showed a tendency to stiffening of the scarred vocal folds as compared to the normal group ($p=0.05$). The parallel plate rheometry on the same samples after dissection showed a decreased dynamic viscocity and lower elastic

modulus in the scarred samples injected with hyaluronan as compared to the normals and to the untreated scarred group ($p<0.01$)

Conclusions

The experimental model for vocal fold scarring resulted in deviation of the normal lamina propria structure with increased connective tissue content. Injection of scarred rabbit vocal folds with hyaluronan rendered improved viscoelastic parameters in short term.

Background

Vocal fold scarring may have different etiology, such as trauma, surgical defects of the vocal folds, post radiotherapy, or inflammation (1). This results in tissue defects and/or disturbance of the vocal fold lamina propria viscoelasticity. Voice is often breathy or aphonic and the phonation threshold pressure which corresponds to "easiness of phonation" (2) is elevated. The treatment is usually difficult, and may include voice therapy by a speech and language therapist and injection augmentation. Many substances have been tried. Bovine or autologous human collagen has been used for superficial injections into the vocal fold ligament (3, 4). Autologous fat implantation into the lamina propria has also been tried in selected cases (5). Drawbacks with collagen and fat is the need for allergy testing (for bovine collagen) and the unpredictable degree of resorption over time (for both) (6).

Due to different drawbacks with all existing materials for augmentation, there is an ongoing search for new materials (7). The ideal substance has to fulfil various criteria, e.g. to be non-toxic, non-allergic, can be precisely injected or implanted superficially into the vocal fold lamina propria, and persists for a long time.

Hyaluronan (HYA) is a glycosaminoglycan identical for all vertebrae species. It is present at high concentrations in the extracellular matrix of many tissues in the body (8) and has also been found in the vocal fold lamina propria (9, 10). HYA functions as a space filler, lubricates, is a shock-absorbing substance and has important biological functions in, e.g., wound healing (8). The viscoelastic properties of native HYA showed a similar dynamic viscosity as that of normal vocal fold mucosa (11). Its rheological properties, however, vary substantially with concentration, molecular weight and degree of molecular cross-linking (12, 13).

Pure cross-linked hyaluronan in the gel form (hylan b gel) was found to be persistent in rabbit vocal folds for up to at least one year after injection, with no inflammatory reaction

or granuloma formation (14). Our previous results using hyaluronan in patients with glottal insufficiency due to unilateral vocal fold paresis and atrophy showed no side effects, improved voice and glottal closure up to at least 2 years. Parameters related to improved viscoelasticity, such as amplitude of vocal fold vibrations and phonation threshold sound pressure were also improved. No vocal fold stiffening was found after injection in the superficial lamina propria with hylan b gel (15, 16). The drawbacks are related to some resorbtion with need for reinjections. The effects of hylan b gel in treatment of vocal fold scarring has so far only been studied in a few patients but in the substance seemed to have the potential for improving vocal fold function (15) .

The *aim* of this experiment was to investigate the short-term viscoelastic properties of scarred rabbit vocal folds after injections of cross-linked HYA as compared to scarred vocal folds injected with saline. Vocal fold mucosa from non-injected rabbit larynges served as controls. A second aim of the experiment was to study the degree of scarring in the lamina propria achieved in the experimental procedure.

Material and Experimental procedures

Fifteen New Zealand white rabbits (bw 2.9-3.5 kg) were used in the experiment. The American principles of laboratory animal care and the Swedish National law on animal care ethics were followed. The experiment was approved by the local ethic committee of Karolinska Institute (S-149-01, 2001-10-15).

Vocal fold scarring. After premedication with glycopyrrolate (0.1mg/kg s.c.) and fluanizonum (10mg/ml fentanyl 0.3/mg/ml, 0.3ml/kg diazepam, 0.3ml/kg i.m.) the animals were anaesthetized with diazepam 1-2mg/kg i.v. The laryngeal structures and mobility were found normal at examination by means of a modified 4.0 mm pediatric laryngoscope (model 8576E, Karl Storz Endoscope, Tuttlingen, Germany) and a Storz-Hopkins 0° 2.7 mm rigid endoscope,

(model 7218A). The scarring procedure was performed with a 2 mm microcup forceps and microscissor (MicroFrance). A localized excision of the mucosa and superficial thyroarytenoid muscle was made under direct vision through an otomicroscope (Figure 1). The procedure yielded 22 excised (scarred) vocal folds and 8 normal vocal folds without scarring. All animals survived the procedure.

Vocal fold injections. After 8 weeks the animals were again examined with direct laryngoscopy under general anaesthesia. Injections were made under vision through a microscope into the lamina propria and/or to the superficial part of the thyroarytenoid muscle of the vocal fold using a Medtronic Xomed laryngeal injector with a 27 gauge needle. Systematic injections in either of the structures mentioned above was not possible due to the narrow space and the equipment available at the time of the experiment. Eleven out of the 22 scarred vocal folds were injected with 0.1ml saline each. Six vocal folds were injected with 0.1 ml Hylaform®, hylan b gel, a cross-linked pure HYA at 5.5 mg/ml concentration (Genzyme Biosurgery, Ridgefield, MA, USA), and 6 vocal folds were injected with Restylane®, a non-animal stabilized HYA from bacterial fermentation at 20mg/ml concentration (Q-Med Inc. Uppsala, Sweden). The 8 non-scarred vocal folds were not injected. No animal suffered from breathing problems or bleeding after the injections.

Dissection

Eleven weeks after the injections the animals were killed by an i.v. overdose of sodium pentobarbital. The larynges were dissected out and each larynx was divided in the posterior midline. Sixteen of the hemilarynges were immediately fresh frozen at –20°C until viscoelastic analysis (5 non-injected, 5 scarred vocal folds injected with saline, 3 scarred vocal folds injected with Hylaform® and 3 scarred samples injected with Restylane®).

Fourteen of the hemilarynges were placed in 10% formaldehyde for later preparation and histological analysis (4 non-injected, 5 scarred folds injected with saline, 2 scarred folds injected with Hylaform® and 3 folds injected with Restylane®).

Histological measurements

Fourteen vocal folds removed from the hemilarynges were further processed, dryed in microwave owen at 630W, paraffin-embedded and. cut into 5µm thick sections (17). These were stained with hematoxyline eosine and van Gieson for histological analysis. Image analysis on the stains at 20x magnification were made after digitization of the microscopic images (..... ....). The thickness of the lamina propria (LP) was measured with the software Image Pro Plus® (version 3.0 Media Cybernetics). The relative content of connective tissue in LP was measured from the digitized stains after a colour filtering and normalization process with Photoshop (version 8.0) and a custom made software (written by Hans Larsson at Karolinska Institute, Stockholm, Dept of Logopedics and Phoniatrics), Figure 2.

Viscoelastic measurements

1. Linear skin rheometry (LSR)

Analyses were made on intact vocal folds with a linear skin rheometer (LSR) adapted to laryngeal measurements. This device was originally developed for measurements of skin viscoelasticity (18, 19). A lightweight tipped probe with a cross section surface of 1mm^2 is driven to produce a sinusoidal compression over a distance of 1-2mm at 0.3Hz. The resulting relative Youngs's modulus (ΔY) (20) parameter is derived from analysis of stress/strain curves. These parameters are related to tissue stiffnes. An advantage with the method is that the measurements can be made without dissecting the tissue samples. The hemilarynges were thawed at room temperature, kept moist with saline and fixed with needles at a plate during the measurements. Measurements were made at the vocal fold edge on midmembranous position during compression of the vocal folds (4 untreated samples, 5 scarred folds injected

with saline, 3 scarred folds injected with Hylaform® and 3 with Restylane®). One vocal fold was used to test the experimental set-up and the results for this were not further analyzed in the experiment. The measurements of each vocal fold lasted 15-20 minutes. After the measurements the hemilarynges were again frozen at –20°C until the parallel plate rheometry.

2. Parallel-plate rheometry

The linear viscoelastic shear properties of vocal fold tissue has been studied by several researchers (11, 21-23). A parallel-plate rheometer produces sinusoidal shear small amplitude oscillations at increasing frequency (from 0.01-15Hz). We used an AR 2000 Rheometer (TA Instrument) with a stationary lower plate (15mm diameter) separated by about 0.5mm from a rotating upper plate. Tissue samples from the same fifteen vocal folds as in the LSR experiments were dissected and analyzed at 37°C in the parallel plate rheometer (4 untreated, 5 scarred fold injected with saline, 3 scarred folds injected with Hylaform® and 3 with Restylane®). The samples included vocal fold lamina propria and the superficial part of the thyroarytenoid musce. The tissue were kept most with saline during the measurements. All rheometric measurements were performed in the linear region with constant stress level transferred from the sample to the upper plate where it is measured with a linear variable displacement transducer. The dynamic viscocity (η', Pas) and elastic modulus (G', Pa) were derived as a function of frequency. Dynamic viscocity is a measure of a material´s resistance to shear flow. The elastic modulus (G') represents a measure of a materials stiffness in shear. In this experiment the gap between the plates was not completely filled with tissue. Thus the absolute level of η' and G' may not be accurate. However, the same dissection procedure and amount of tissue was used for all samples which allows for comparison between the different treatment groups.

Statistics

Non-parametric comparisons between the groups were made (Statview program, SAS Institute Inc., version 5.0). The two types of HYA treatments were analyzed as one group due to the small number of samples. Due to the exploratory nature of the study a significance levels with $p<0.05$ are reported.

Results

Histological analysis

In 4 out of the 5 scarred vocal folds treated with HYA (Hylaform® or Restylane®) showed remaining substance. HYA was identified either in smaller well localized islands in the lamina propria or deep in the thyroarytenoid muscle. These aggregates were surrounded by a thin capsule of connective tissue. The measurements of the vocal fold lamina propria (LP) showed that both the scarring groups (scarring+saline and scarring+HYA) had significantly thicker LP than the non-scarred folds ($p<0.05$). There was no difference in LP thickness between the scarred folds who were treated with HYA or injected with saline. Analysis of the relative content of connective tissue in LP also showed that both scarring groups had higher relative connective tissue content in LP as compared to the untreated vocal folds, $p<0.05$ (scar+saline versus scar+HYA ns).

Viscoelastic analyses

1. LSR analysis

As shown in Figure 3 the relative Young's modulus (ΔY) was lowest for the normal vocal folds and higher for both the scarred groups. This indicates a stiffening for the scarred groups. The difference between the normal vocal folds and the scarred folds injected with saline was close to significant ($p=0.05$). (normal versus scar+HYA: ns, scar+saline versus scar+HYA: ns).

2. Parallel plate rheometry

Figure 4 shows that the dynamic viscocity was lower for the scarred vocal folds treated with HYA as compared to both the untreated samples and to the scarred samples injected with saline ($p<0.05$). There was no significant difference between the untreated samples and the scarred samples injected with saline). Figure 4 also shows that the elastic modulus was significantly lower for the scarred vocal folds treated with HYA as compared to both the untreated and to the scarred samples who were injected with saline, $p<0.01$ (untreated versus scar+saline: ns).

Discussion

Many attemps have been made to find a treatment for vocal fold scarring. In order to restore the vibratory capacity of scarred vocal folds the characteristics of a bio-implant used for injection or implantation should match the viscoelastic properties of normal vocal fold mucosa. Previous studies in normal rabbit vocal folds after injection of hylan b gel (Hylaform®) showed similar dynamic visocity after injection as for native rabbit vocal folds (22, 23). The results after treating a few patients with vocal fold scarring were also promising (15). The in vitro characteristics of Restylane® are similar as Hylaform® and both substances are easy to handle and inject. The rabbit vocal folds are similar to human in structure although the lamina propria is less well developed. We used rabbits vocal folds in a similar experimental model for vocal fold scarring as other researchers (21, 24). The total observation time was about five months after the scarring procedure. Hirano et al. recommended an observation time in the "chronic" scar model close to six months in order to obtain a realistic deposition of collagen in the vocal fold which probably correlates to a stiffening of scarred folds. The results of the colour analysis and measurements of the lamina propria thickening in the present study also indicates that significant scarring was achieved.

The difficulties to inject or augment with precision in scarred vocal folds are well known. This may explain the results of the histologic analysis showing that the HYA injected was

found at various locations in the vocal folds. No inflammatory changes or granuloma were observed and the HYA was surrounded by a thin capsule. This is similar to the findings by Hallén et al. (14). Remaining HYA was found at histological analysis in 4 out of the 5 injected samples. The observation time after injection was 11 weeks. Thus for one animal either we did not succeed to inject into the the scarred tissue or there was resorbtion of the material.

We performed two types of viscoelastic analyses. The LSR analysis has the advantage that it can be made on intact vocal folds, but on the other hand the vocal fold tissue is compressed at only a single slow rate (not corresponding to phonation). The LSR analysis showed an elevated relative Young's modulus for the scarred vocal folds as compared to the normal folds. This corresponds to stiffening probably due to scarring. There was no significant difference between the scarred folds injected with saline or with HYA (Hylaform® or Restylane®). The parallel plate reometry is performed after dissecting the vocal folds, but the method permits measurements at different frequencies (0-10 Hz in this experiment). The results of this analysis showed a lowered dynamic viscocity and elastic modulus for the HYA treated samples as compared to the scarred folds treated with saline. This indicates less stiffening which corroborates the results noted for some patients treated for vocal fold scarring (15). Titze, Gray and Chan performed parallel plate reometry analysis on normal human vocal folds before and after removal of the natural hyaluronan (11). Their results showed a higher viscoelasticity without hyaluronan. It may be that HYA alters the viscoelasticity directly in a favourable way in vocal fold scarring Our results must, however, be interpreted with caution. The HYA samples had lower viscocity than the normal controls. We have no clear explanation for this, but possibly there may be some degenerative changes due to the repetitive analysis which affected the normal samples more than the sacrred folds.

Conclusions

The results showed that the experimental model used resulted in vocal fold scarring both at histological analysis and indicated from the LSR viscoelastic analysis. The parallel plate reometry showed improved biomechanical properties for the scarred vocal folds treated with HYA. This results must however be confirmed in order to permit definite conclusions.

Acknowledgements

To Professor Claude Laurent Department of Otorhinolaryngology Rikshospitalet Oslo for valuble comments and discussions on the manuscript. To Kristina Forsgren at Umeå University Hospital for performing the histolological preparations. To Anna Tolf at the Institution of Pathology, Karolinska University Hospital Huddinge for assistance with histological analysis. To Daniella Vidovska at the Department of Polymer Science& Engineering, Lund University for the reological analysis.

The study was supported by the Swedish Research Council (grant no. 2002-3897), by the Karolinska Institute.

References

1.Benninger MS, Alessi D, Archer S, Bastian R, Ford C, Koufman J et al. Vocal fold scarring: current concepts and management. *Otolaryngol Head Neck Surg.* 1996;115(5):474-482.

2. Titze IR. Phonation threshold pressure: a missing link in glottal aerodynamics. *J Acoust Soc Am.* 1992;91(5):2926-2935.

3. Ford C, Bless DM, Loftus J. Role of injectable collagen in the treatment of glottic insufficiency: a study of 119 patients. *Ann Otol Rhinol Laryngol.* 1992;101:237-247.

4. Remacle M, Lawson G, Delos M, Jamart J. Correcting vocal fold immobility by autologous collagen injection for voice rehabilitation. *Ann Otol Rhinol Laryngol* 1999;108:788-793.

5.Neuenschwander MC, Sataloff RT, Abaza MM, Hawshaw MJ, Reiter D, Spiegel JR. Management of vocal fold scar with autologous fat implantation: perceptual results. *J Voice* 2001;15(2):295-304

6. Shindo ML, Zaretshy LS, Rice DH. Autologous fat injection for unilateral vocal fold paralysis. *Ann Otol Rhinol Laryngol* 1996;105:602-606

7. Chan RW, Titze IR. Viscocities of implantable biomaterials in vocal fold augmentation surgery. *Laryngoscope* 1998;108:725-731.

8. Laurent T. Biochemistry of hyaluronan. *Acta Otolaryngol. (Stockh)* 1987;Suppl. 442: 7-24.

9. Butler JE, Hammond TH, Gray SD. Gender related differences of hyaluronic acid distribution in the human vocal fold. *Laryngoscope* 2001;111:907-911.

10. Hammond TH, Zhou R, Hammond EH, Pawlak A, Gray SD. The intermediate layer: a morphologic study of the elastin and hyaluronic acid constituents of normal human vocal folds. *J Voice.* 1997 Mar;11(1):59-66.

11. Chan RW, Gray SD, Titze IR. The importance of hyaluronic acid in vocal fold biomechanics. *Otolaryngol Head Neck Surg.* 2001 Jun;124(6):607-14.

12. Ambrosio L, Borzacciello A, Netti PA, et al. Rheological study on hyaluronic acid and its derivatives solutions. J Macromol Sci-Pure Appl Chem 1999;A36[7&8]:991-1000.

13.Ferry JD. Viscoelastic properties of polymers. New York: John Wiley, 1980.

14. Hallén L, Johansson C, Laurent C. Cross-linked hyaluronan (Hylan B gel): a new injectable remedy for treatment of vocal fold insufficiency--an animal study. *Acta Otolaryngol (Stockh)* 1999;119(1):107-111.

15. Hertegård S, Laurent C, Olofsson K, Lindström E, Hallén L, Testad P, Dahlqvist Å. Cross-linked hyaluronan used as augmentation substance for treatment of glottal insufficiency: safety aspects and vocal fold function. *Laryngoscope* 2002;112:2211-2219.

16. Hertegård S., Dahlqvist Å., Laurent C., Olofsson K., Sederholm E., Hallén L., and Testad P. Cross-linked hyaluronan for injection treatment of glottal insufficiency – a two-year follow-up. *Acta Otolaryngologica (Stockholm).* In Press.

17. Hallén L, Johansson C, Laurent C, Dahlqvist Å. Hyaluronan localization in the rabbit larynx. *Anat. Rec.*1996;246:441-445.

18. Matts P, Goodyer E. A new instrument to measure the mechanical properties of the human stratum corneum. *J of Cosmetic Science.* 1988;49:321-323.

19.Goodyer E, Gunter H, Masaki A, Kobler J. Mapping the visco-elastic properties of the vocal fold. In Proceedings of Advances in Quantitative Laryngology, Voice and Speech Research (AQL) www.uke.uni-hamburg.de/kliniken/hno/phoniatrie/aql2003/ . April 2003.Hamburg.

20.Tran QT, Berke GS, Gerrat BR, Kreiman J. Measurement of Young's modulus in the in vivo human vocal folds. *Ann Otol Rhinol Laryngol* 1993;102:584-591.

21. Kriesel KJ, Thibeault SL, Chan RW, Suzuki T, Vangroll PJ, Bless DM, Ford CN. Treatment of vocal fold scarring: rheological and histological measures of homologous collagen matrix. *Ann Otol Rhinol Laryngol* 2002;111(10):884-889.

22. Hertegård S., Dahlqvist Å., Laurent C., Borzacchiello A., Ambrosio L. Viscoelastic properties of rabbit vocal folds after augmentation. *Otolaryngology –Head and Neck Surgery.* 2003;128(3):401-406.

23. Dahlqvist Å., Gärskog O., Laurent C., Hertegård S., Ambrosio L., Borzacchiello A. Viscoelasticity of Rabbit Vocal Folds after Injection Augmentation. *Laryngoscope* 2004;114 (1):138-142.

24.Hirano S, Bless DM, Rousseau B, Welham N, Scheidt T, Ford CN. Fibronectin and adhesion molecules on canine scarred vocal folds. *Laryngoscope* 2003;113:966-972.

Figures Hertegård et al Viscoelasticity in scarred rabbit vocal folds

Figure 1

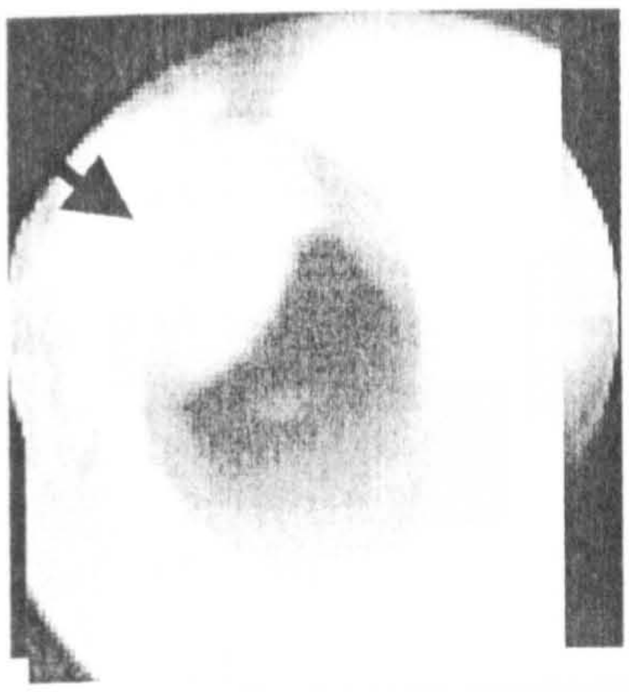

Figure 1. To the left: image of a rabbit larynx efter a resection (arrow) in the left vocal fold. To the right: image of a larynx of another animal after injection of hyaluronan into the left vocal fold.

Figure 2

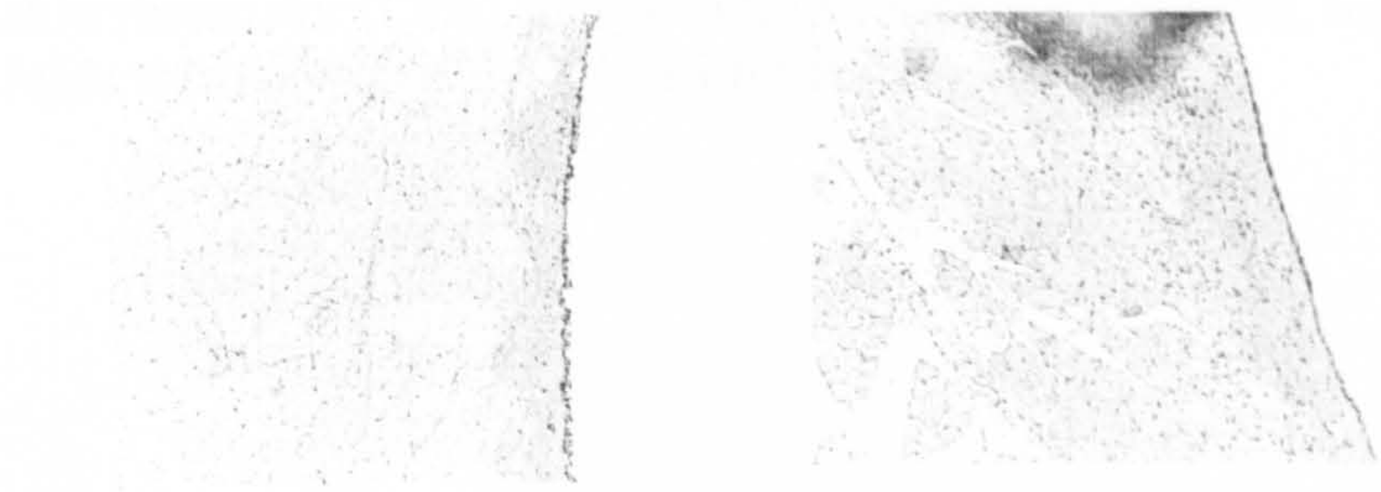

Figure 2. Hematoxyline-eosine stained sections (at 20x) after digital color filtering of connective tissue of the lamina propria (red color). left: a normal vocal fold. right: a scarred vocal fold

Figure 3.

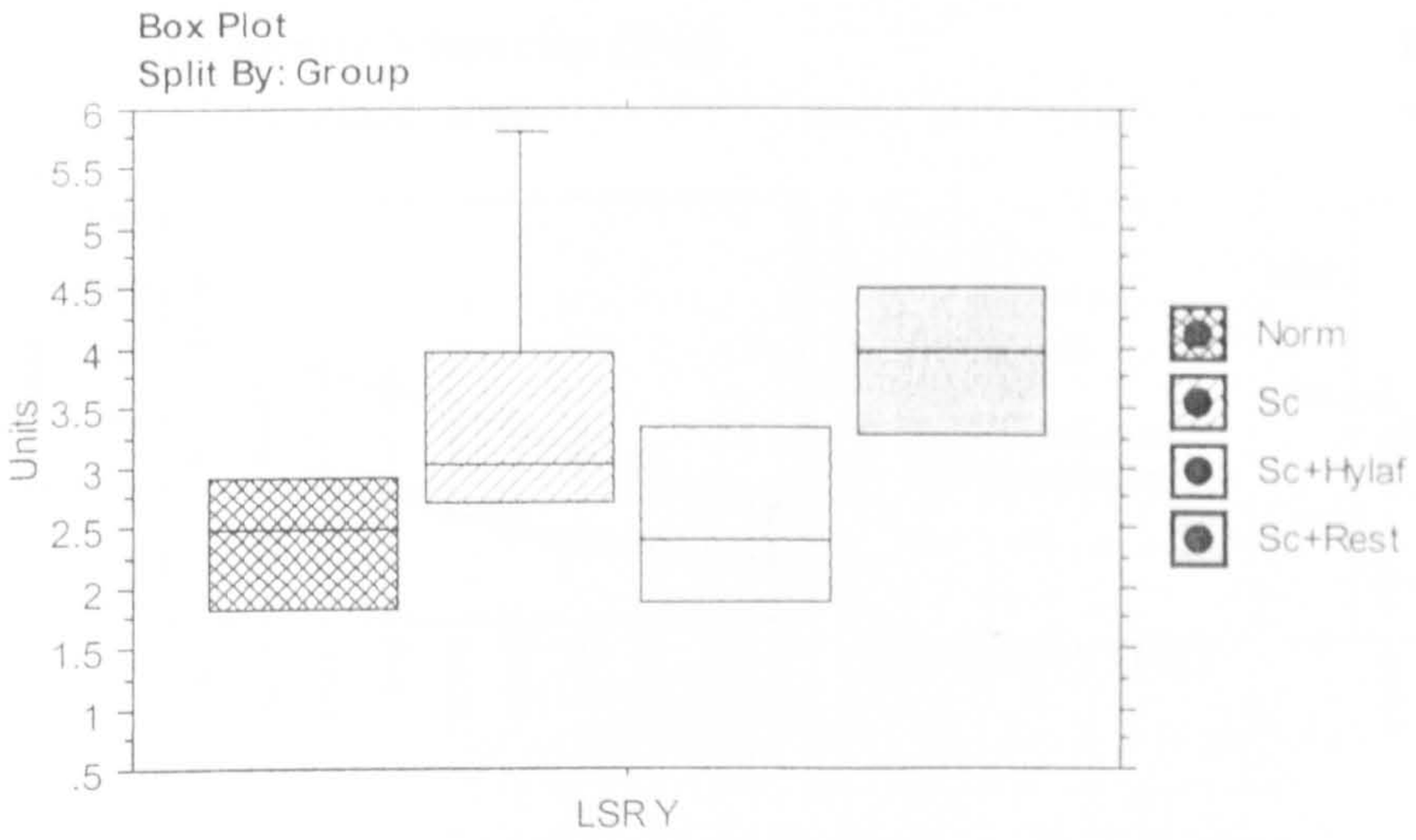

Figure 3. Box plots showing the relative Young's elastic modulus (LSR Y) from the Linear skin rheometer (LSR) analysis for the normal vocal folds, scarred vocal folds and scarred folds treated with HYA (Hylaform and Restylane).

Mapping The Visco-Elastic Properties of the Vocal Fold

Eric Goodyer (1), Heather Gunter (2,3), Asa Masaki (3), and James B. Kobler (3,4)

(1) DeMontfort University, Leicester, UK, eg@dmu.ac.uk.; (2) Division of Engineering and Applied Science, Harvard University, Cambridge, MA.; (3) Division of Health Sciences and Technology, Massachusetts Institute of Technology, Cambridge, MA.; (4) Harris Peyton Mosher Laryngological Research Laboratory, Massachusetts Eye and Ear Infirmary, Boston, MA, 02114, USA, James_Kobler@meei.harvard.edu

Abstract: The Linear Skin Rheometer (LSR), which measures skin visco-elasticity, was adapted for measurements of vocal fold properties. In excised larynges small patches of mucosa were driven sinusoidally at .3 Hz over 1-2 mm distances using a small probe. Forces on the order of one gram gave optimal measurements. Stiffness and viscosity values were derived from stress/strain data and using a simple shear model. The instrument was able to measure the visco-elasticity of the tissue in a repeatable manner and it could detect areas where the tissue was artificially stiffened. 2D maps of the viscous and elastic properties of the laryngeal mucosa were obtained showing local variations in elasticity and viscosity both parallel and perpendicular to the vocal fold edge.

Introduction: In phonosurgery there is a need for an instrument that can measure the material properties of the superficial lamina propria of the vocal fold, a layer that is critical for normal phonation, that is frequently damaged and that is a key target for novel vocal fold augmentation techniques. Such an instrument would ideally help the surgeon sense the extent and degree of tissue abnormality and provide objective measures before, during and after treatment.

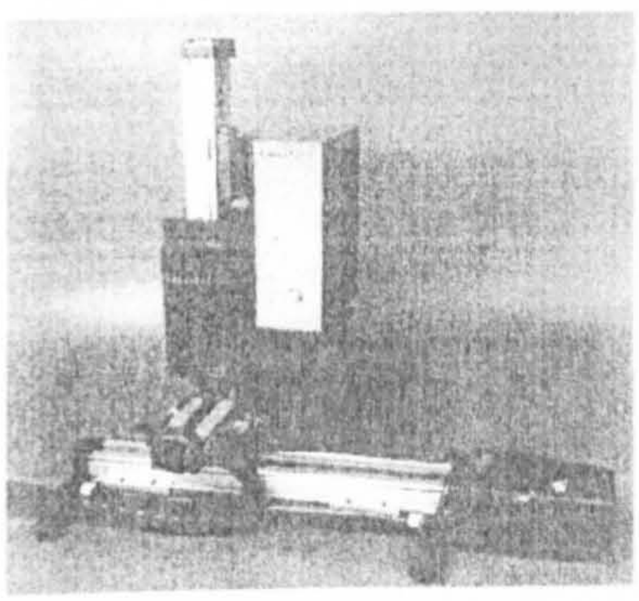

The Linear Skin Rheometer

We undertook a pilot study to see if a commercially available rheological device, the Linear Skin Rheometer, or LSR, could be used to make measurements of vocal fold viscoelastic properties. An important feature of this instrument is the long lightweight tissue probe, which makes it suitable for potential use via a surgical laryngoscope. A series of bench tests of the LSR was conducted to address the following questions: (1) Is the LSR adequately sensitive to measure vocal fold mucosal material properties? (2) Can reproducible measurements be obtained? (3) Can differences in tissue properties be detected and correlated with different anatomical locations or tissue modifications?

The experiments to be described have been directed towards establishing the feasibility of using the LSR as a measurement tool rather than the gathering of normative data. The results suggest that the LSR has potential for providing clinically useful intraoperative assessment of vocal fold material properties.

Methods: The LSR is a precision mechatronic instrument that was designed to measure the visco-elastic properties of the stratum corneum of the skin [1]. Based upon an original concept developed by Hargens in the 1960's (The Gas Bearing Electrodynanometer or GBE) [2,3], the LSR uses modern micro-mechanical components to achieve force feedback control in real time, and precision position measurement.

LSR Measurement principles: When measuring the elastic and viscous properties of a material we are seeking to determine how far the material moves when a lateral force is applied to it. If we apply a sinusoidal force, then we expect to see a resultant displacement that also changes sinusoidally. The phase shift between the force and displacement curves is also of great interest. This technique has been used to measure skin elasticity, infer hydration levels [4] and assess skin ageing [5].

To make a measurement a probe is attached to the surface of the skin or larynx, and a sinusoidal force is then applied along its axis and thereby onto the tissue. Typically the peak force applied will be in the region of 3g for skin and 1g for the larynx. By simultaneously measuring the displacement caused by the force then a pair of readings is obtained as shown schematically in figure 1.

Three parameters can be obtained from the curves - *F Max* which is the peak force that is applied to the skin surface, *P Max* which is the peak displacement that occurs as a result of that force, and *T* which is the phase shift between the two signals. The elastic component of the skin is given simply by *F max / P max*, and is usually expressed in units of grams force per millimetre. The usual way of presenting this data is to plot force directly against displacement, in which case an ellipse will be formed, as the component parts are two sine waves with an identical period, but shifted in time. Such a picture, as taken from the LSR, is shown in figure 2. The phase shift is due to the viscous properties of the tissue. The LSR captures the force and displacement waveforms, and performs a linear regression on that data in order to determine the coefficients of the biodynamic equations for variation of force and displacement with time. (1) $F = FmaxSin(t)$ and (2) $P = PmaxSin(t+T)$, where F = instantaneous force, $Fmax$ = the maximum force, t = time over one cycle in radians, P = instantaneous displacement, $Pmax$ = the maximum displacement, and T = the phase shift in radians. To summarise, the slope of the ellipse along its major axis is the elastic parameter, and the area of the ellipse is the viscous parameter [6].

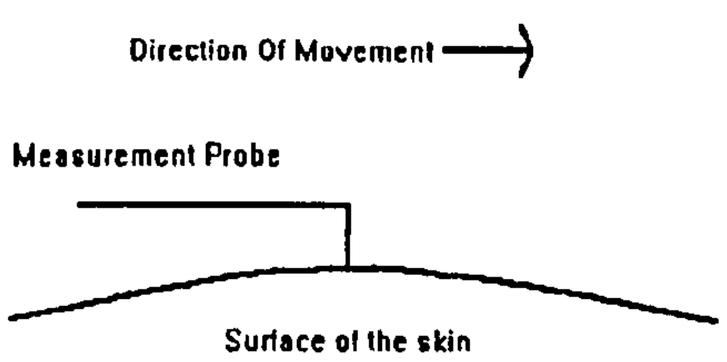

Figure 1 Typical Waveforms of Force and Displacement

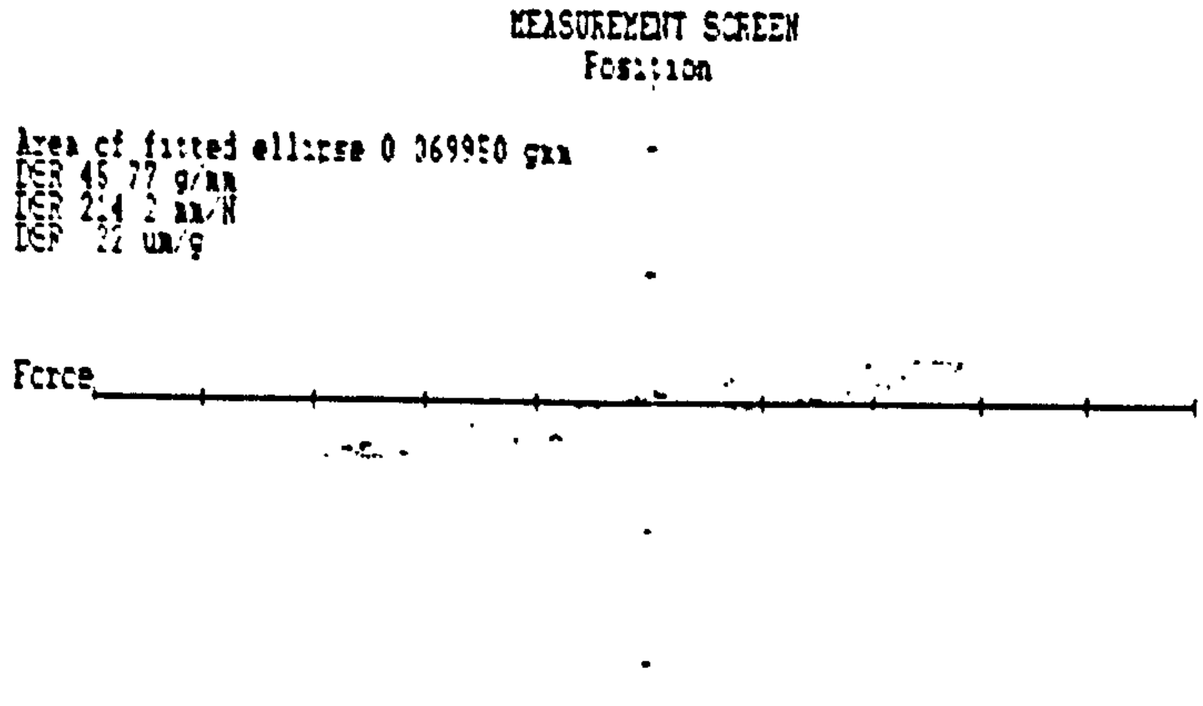

Figure 2 Typical measurement screen

LSR device: The key to the design of the LSR is the means to apply a continuously varying, but controlled, force to the surface of the tissue. From the measuring head a light stiff probe protrudes, the far end of which is bent through a right angle and its tip is modified to attach to tissue. For laryngeal measurements we have used a variety of fine needle-tipped probes and also suction probes connected by flexible silicone tubing to a source of negative pressure. Inside the measuring head, the

probe is attached to a load cell, which is moved along the probe axis by a motor-driven lead screw. An LVDT is used to monitor the position of the load cell and probe.

A PC is used to control the movement of the sensing head. Both force and position are continuously monitored at a rate of 1 kHz using a 12-bit ADC plug-in card. The motor is controlled with an analogue output signal also generated by the PC. The desired force/time cycle, which is normally a single sinusoid, is initially calculated from an equation, and then stored in memory as a table of values. The actual force applied to the probe is compared with the desired value in the table 1000 times per second. A feedback loop is used to control the motor, which moves the load cell in such a way as to minimise the discrepancy. The force applied thus follows closely the desired force/time cycle. The control loop uses an algorithm with proportional and integral terms, whose relative weighting can be varied.

The PC logs all the force and displacement readings over the complete measurement cycle, which is usually set to be 3 seconds thus generating 3000 pairs of points. This data is then used to generate the graphs that are shown above, and are analysed to determine the elastic and viscous parameters. Measurements of elasticity are expressed in terms of the Dynamic Spring Rate, in units of g/mm. The load cell used in the LSR is supplied by Maywood and has a full scale reading of 10g, with an overall accuracy of better then 0.02g. The LVDT is supplied by Solartron, type DF2.5, which has an accuracy of better than 4 microns. The motor is supplied by Maxon. Minor modifications were made to the LSR design to make it more suitable for measuring the visco-elastic properties of the larynx, but the underlying principles remain unchanged.

Bench tests on Laryngeal Specimens: Laryngeal specimens were prepared by hemisection, taking care to leave the vocal fold attachment to the thyroid cartilage at the anterior commisure region intact. The specimens were pinned to a wooden base attached to small XY/rotary machinist's fixture that allowed for accurate positioning and rotation. The specimens were kept moist with physiological saline and measurements were made at room temperature (roughly 20°C). Most measurements were made using needle tipped probes. The most effective of several designs tested was made from a spring steel rod 1mm in diameter and 10 cm in length, which was bent to a right angle 5 mm from one end. A fine (000) insect pin was soldered to the short bent section so that it protruded 1.5 mm beyond the end of the rod. This needle was inserted into the tissue up to the rod, which controlled insertion depth to 1.5 mm. In some instances we used a suction-based probe made of lightweight aluminum tubing with an internal diameter of 1.4 mm.

Results:

Tests of repeatibility: Six pig larynxes were measured at the centre of the vocal fold. Displacement axis was perpendicular to the length of the vocal fold. The table shows the standard deviations and means derived from 6 consecutive readings of the DSR taken from the same starting position.

Repeatability Tests	SD	Mean	SD/Mean
' middle' of sample 1	0.040591	0.691429	0.058706
' middle' of sample 2	0.058878	0.776667	0.075809
' middle' of sample 3	0.020659	0.69625	0.029672
' middle' of sample 4	0.036425	0.72125	0.050503
' middle' of sample 5	0.01169	0.488333	0.023939
' middle' of sample 6	0.005164	0.633333	0.008154

TABLE 1 – *Tests of repeatibility*

Variation in properties along length of vocal fold: The LSR was used to measure the DSR using a needle probe along the length of the vocal fold in a fresh pig vocal fold. The probe was placed perpendicular to the long axis of the vocal fold. Five readings were taken at each point, and the average plotted with respect to position of the measurement from the vocal process. The complete set of measurements is given in table 1. Stiffness was greatest near the vocal process and anterior

commisure. The DSR over the vocal process was about 3-fold higher than over the membranous vocal fold

Position from Vocal Process (inches)	DSR 1	DSR 2	DSR 3	DSR 4	DSR 5
-0.07	2.81	2.89	2.98	2.84	2.97
0.05	0.88	0.9	0.9	0.86	0.88
0.1	0.69	0.68	0.69	0.69	0.71
0.2	1.28	1.29	1.26	1.25	1.25

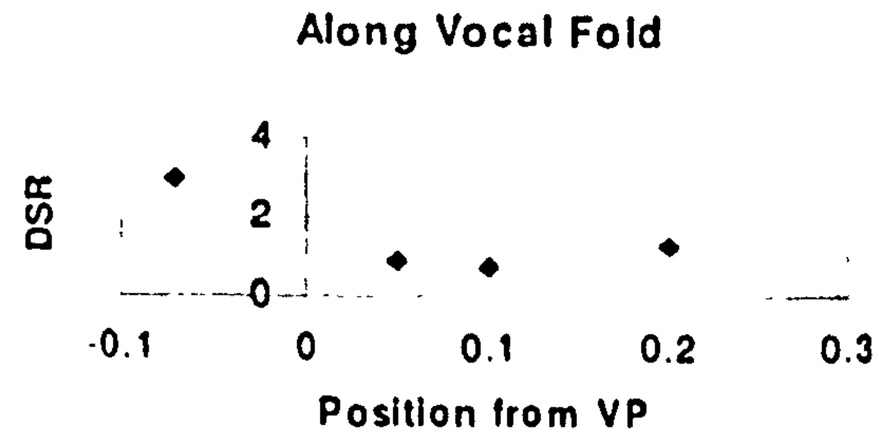

TABLE 2 – *Variation in DSR along length of vocal fold*

Effect of displacement direction relative to vocal fold axis: Readings were taken from the mid-membranous region of a pig vocal fold with the probe producing displacements at different angles relative to the long axis of the vocal fold. Five readings were taken at each angle, and the average DSR was plotted against that angle. The stiffness was least for displacements perpendicular to the long axis, and maximal for displacements along the long axis.

Angle	DSR 1	DSR 2	DSR 3	DSR 4	DSR 5
30	0.6	0.64	0.62	0.62	0.62
50	0.83	0.85	0.8	0.79	0.76
90	0.98	0.98	1.05	1.02	1.01
130	0.95	0.95	0.92	0.95	0.93
150	0.73	0.78	0.74	0.78	0.67
180	0.58	0.44	0.46	0.45	0.42

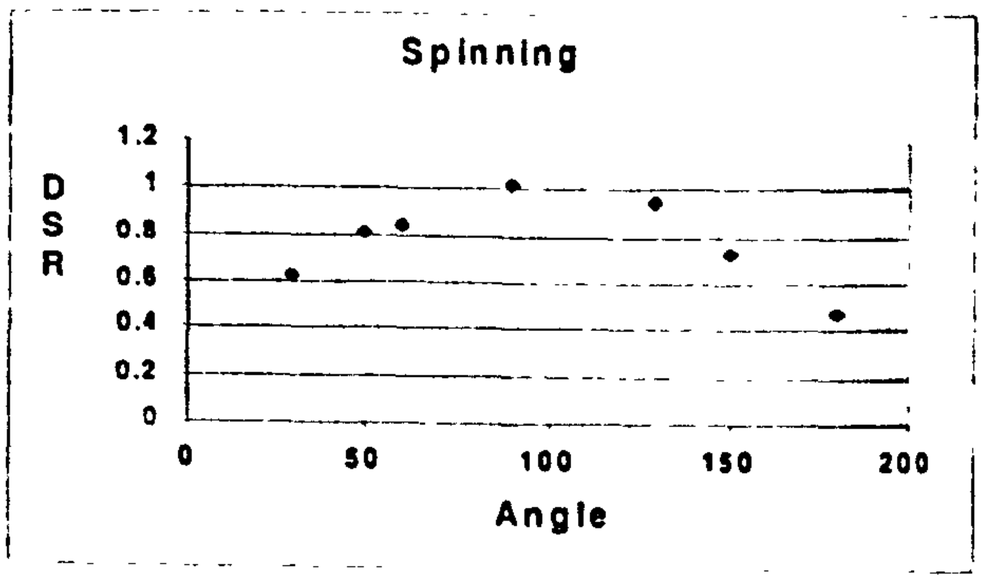

TABLE 3 – *Effect of displacement direction relative to vocal fold axis on DSR*

Measurements of excised lamina propria: In one calf larynx the lamina propria of the vocal fold was dissected out with attached vocal process and small attached piece of thyroid cartilage. The tissue was mounted such that it could be pre-tensioned and then measured. The tissue was pre-tensioned to a 'starting force', and a sinusoidal force of +- 1.5g was applied. The initial 'draw length' was also measured. The purpose of this trial was to determine if it would be possible to construct a classic stress/strain curve. The graph shown simply plots initial tension against measured DSR.

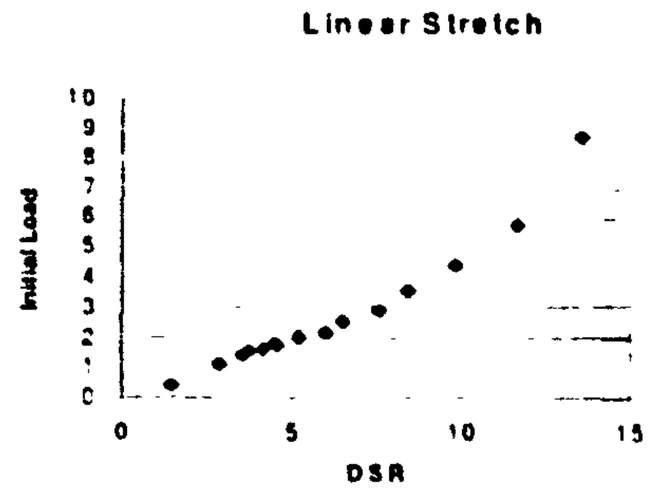

Draw length	0	0.05	0 065	0.075	0.085	0 095	0.095	0.11	0.125	0.155	0.17	0.185	0.2	0.215
Starting force	1.5	2.9	3.6	3.8	4.2	4.5	4.6	5.2	6	7.5	8.4	9.8	11.6	13.5
DSR	0.4	1.13	1.46	1.58	1.62	1.82	1.73	2.03	2.16	2.9	3.56	4 38	5.77	8.73

TABLE 4 – *Linear stress 'strain data excised lamina propria*

Two-dimensional mapping of DSR: Using the XY table to position a sheep larynx, a systematic map of DSR at different locations on, above, and below the vocal fold was made. A reference digital photograph was taken at each point of measurement. Using this data, a 2D plot showing the variance of elasticity across the surface of the specimen was created by registering an isocontour 2D plot of elasticity (generated using Matlab software) to a lateral photographic view of the vocal fold. Contours reflect increments of .06 g/mm and range from .6 g/mm along vocal fold to 12 g/mm over arytenoids.

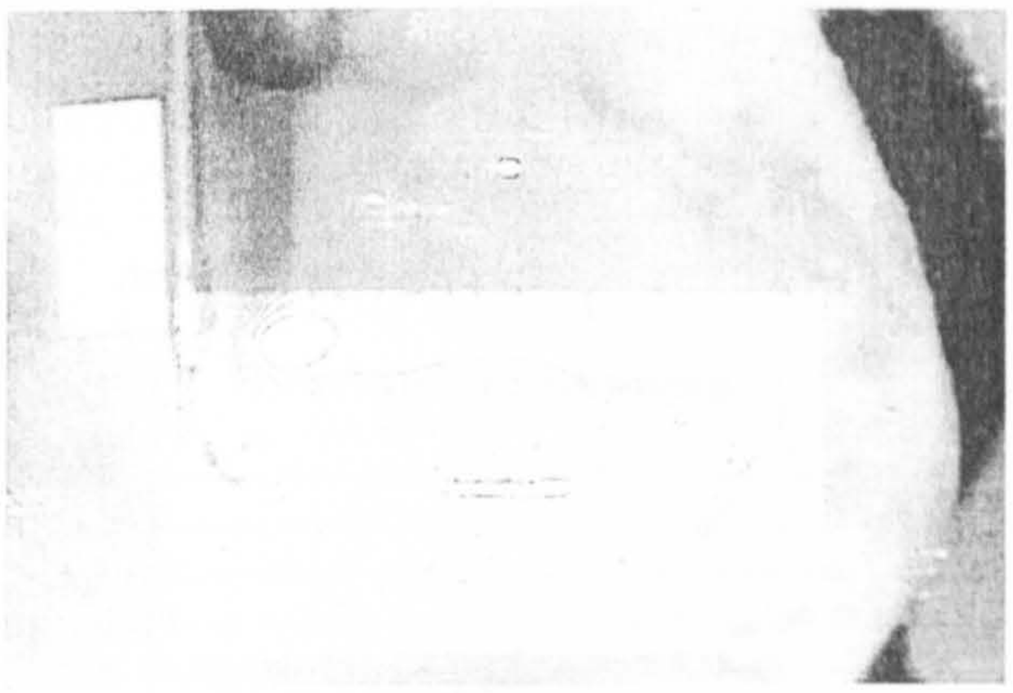

View of Vocal Fold with overlay of DSR contour map

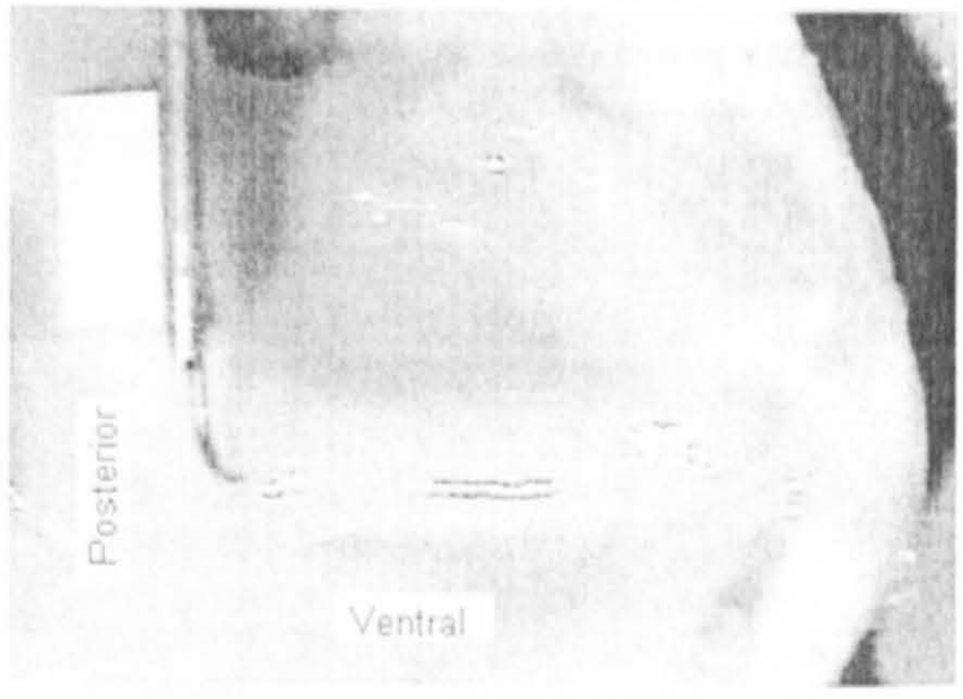

View of Vocal Fold with LSR probe attachment

Images taken at Harvard, showing experimental setup of LSR with ex-vivo focal-fold, together with results obtained from research data

FIGURE 3 *Visco-Elastic Isocontour Map*

Application of a simple model of shear viscoelasticity to derive viscosity estimates: The LSR derives viscous properties of a tissue by measuring the phase shift between the applied force and the resultant displacement. As we know the cycle time of the applied force, this measurement can be converted into the viscosity parameter for shear damping.

Assuming that the tissue can be characterised by shear stiffness *(k)* and shear damping *(B)* parameters that are in parallel, and that a sinusoidal shear force *(A*sin(wt))* is applied on the tissue surface, then the displacement of the surface *(x)* is *C*sin(wt + z)*:

amplitude of force/amplitude of movement	*A/C = sqrt(B^2w^2 + k^2)*	1.
Phase difference between force and movement	*z = tan^-1 Bw/k*	2.
Simplify (2) to obtain equation for B	*B = tan(z)k/w*	3.
Simplify (1) to obtain equation for k	*(A/C)^2 = tan(z)^2k^2 + k^2*	4.
Take out k^2	*(A/C)^2 = k^2(tan(z)^2 +1)*	5.
Apply trig. Rule sin^2 = 1/(tan^2+1)	*(A/C)^2 = k^2/sin(z)^2*	6.
Solution for Shear Stiffness	*k = (A/C)sin(z)*	7.
Replace k in (3)	*B = tan(z) (A/C) sin(z)/w*	8.
Apply trig. Rule tan(z)sin(z)=cos(z)	*B =(A/C) cos(z)/w*	9.

w is known since it is the applied frequency in Hz divided by 2*Pi. *A* is known since it is the applied amplitude of the force. *C* is known since it is the measured amplitude of the movement. *z* is the phase difference and is derived by a linear regression of the data obtained by the LSR with respect to time.

This basic relationship can be used to separate out the viscous and elastic components of the vocal fold biodynamics. The plot below shows the variation of these properties along the axis of the vocal fold. Shear damping units are given as gs/mm and the elastic units are given as g/mm.

Position	Elastic g/mm	Viscous gs/mm
2.54	0.686	0.460631
5.08	1.252	0.796346
-1.778	2.874	1.751961
1.27	0.8775	0.538705
0.71882	0.635	0.468439

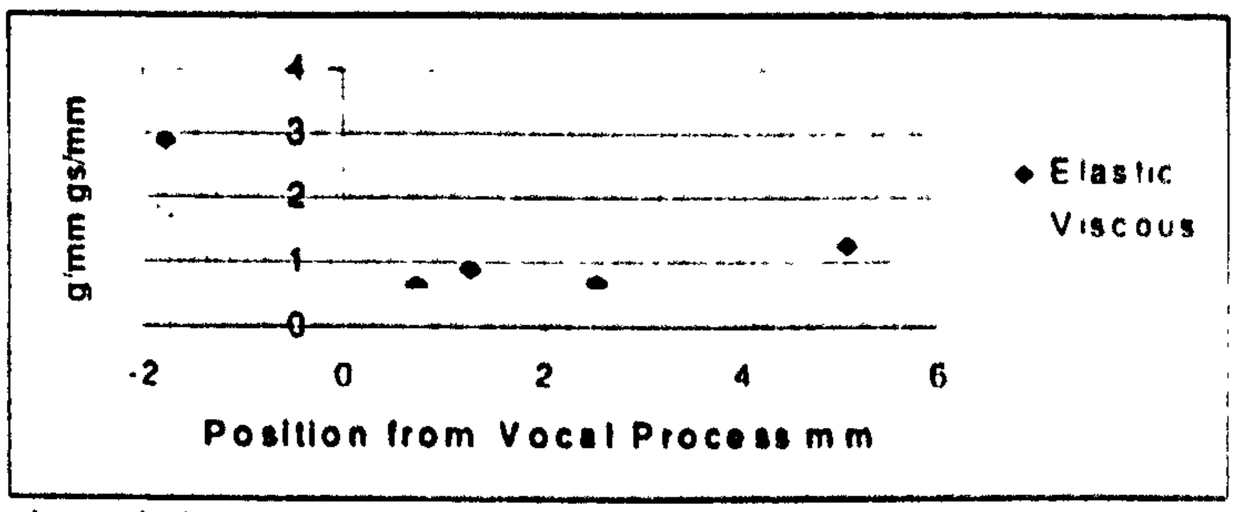

TABLE 5 – *Resolving out pure elastic and viscous components*

Artificial Stiffening:

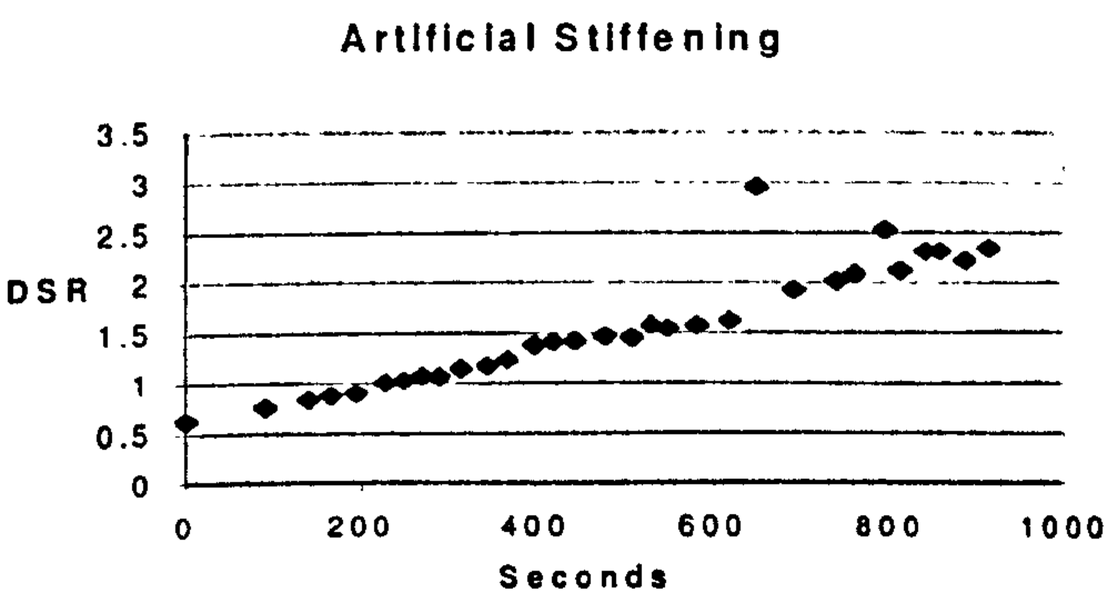

A pig vocal fold was injected subepithelially with .1cc of 10% formaldehyde solution, and the DSR was measured over a period of 15 minutes. The graph shows change in DSR of the specimen as the tissue was artificially stiffened.

FIGURE 4 *Change in Stiffness over Time*

Effect of Differing Layers: The DSR of different layers of a calf larynx were measured in a direction parallel to the vocal fold. This was achieved by sequentially removing layers, and retaking the measurement at the same position. These initial results demonstrate how the layers contribute to overall tension development as the vocal fold is stretched.

A. Typical epithelium measurements.
B. A small island of epithelium about 2 x 3 mm which indicates the relative contribution of the epithelium versus the underlying amorphous layer.
C. Epithelium removed.
D. Amorphous layer removed
E. Directly in the muscle.

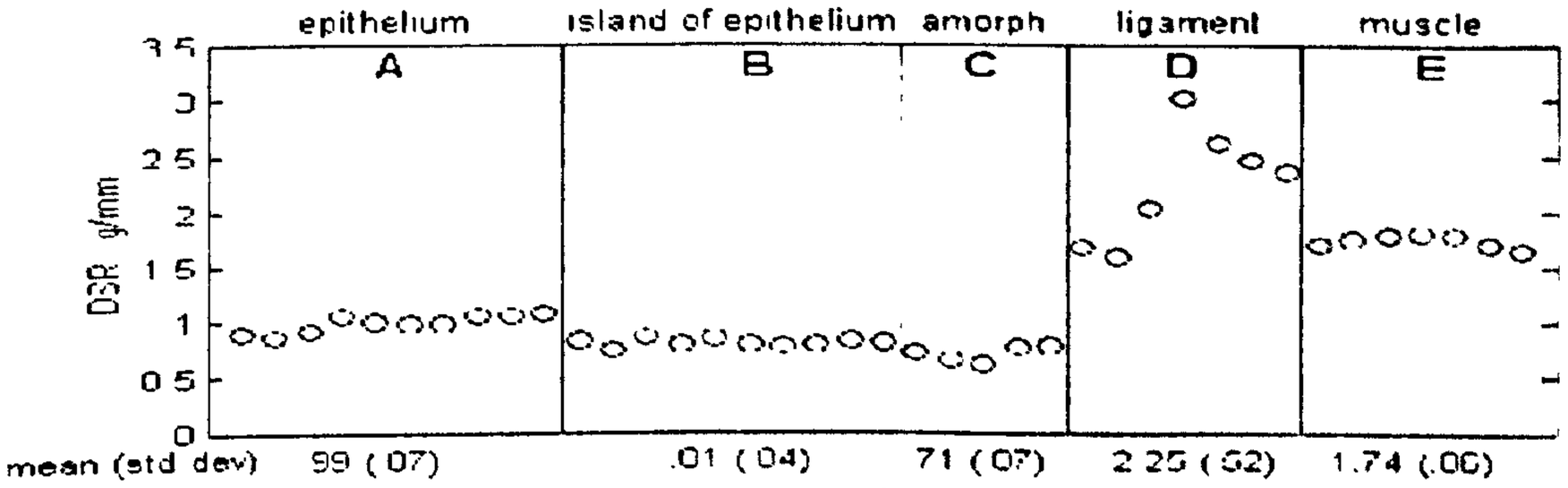

FIGURE 5 *Variation of DSR with Vocal Fold Layers*

Discussion: Over the last decade there has been a surge of interest in vocal fold material properties and a widening appreciation of the relevance of such data to better understanding the anatomy, pathology, aging, modeling and repair of the vocal folds.

For excised specimens, parallel plate rheometry has been become a standard for determining the shear viscoelasticity parameters of tissue from animals, cadavers or surgical specimens, of candidate augmentation materials and of animal vocal folds previously implanted with augmentation materials [10-17, 21, 29]. Complimentary stress/strain studies on excised vocal fold layers have provided data on longitudinal viscoelastic properties essential for understanding vibratory behaviour and contributions of the different layers to vibration as a whole [7,22,23,24].

Measurements on intact vocal folds has been technically difficult, but is clearly essential for many clinical applications. In vivo measurement could potentially help identify abnormal regions, provide feedback during augmentation surgery and aid in the objective assessment of surgical procedures designed to manipulate vocal fold material properties. Methods that have been applied to intact vocal folds include indentation with a probe attached to a servo motor-controlled force sensor [18,19], lateral displacement of the vocal fold with a trans-oral calibrated lever [8,9,27], and medial aspiration of the mucosa with a calibrated suction catheter [25]. The latter two methods have been tested on human subjects under general anesthesia.

In contrast to the *in vitro* rheological methods, the LSR is not capable of determining absolute values for viscoelasticity parameters on a unit area or volume basis because the exact volume of tissue that is deformed cannot be determined. Data obtained so far is comparable to previous intact larynx methods. Like the indentation approach and in contrast to the transoral lever, there is good spatial resolution. Relative measurements are potentially very useful in many clinical scenarios if abnormal tissue can be identified or changes resulting from a treatment can be documented. The results demonstrated that this method has the ability to make sensitive and repeatable punctate measurements that may allow for mapping areas of pathology, and for side-by-side comparison of a normal with an abnormal vocal fold. It is also well suited for testing the properties of the clinically important superficial lamina propria because it can be attached non-invasively to the epithelium with a suction cannula and gently wiggle the vocal fold cover. This is similar to the way surgeons intuitively test vocal fold properties by palpating the tissue with small surgical instruments.

Future Directions: While the LSR was able to reliably measure the most pliable tissues of the larynx, it was originally designed for measurements of skin on the dorsum of the hand, which is about 5 times more stiff than the vocal fold. Some adaptations to the hardware and software would improve performance of the feedback control system for vocal fold tissue. Following these improvements further in vitro testing of human and animal vocal folds will be pursued to obtain normative data under well-controlled conditions.

We have found that the probe of the LSR can be adapted to work through a surgical laryngoscope, but the arrangement is somewhat cumbersome. Our current technical review has indicated that the application of Surface Acoustic Wave (SAW) technology offers the potential to further miniaturize the LSR to the point where it is convenient for routine clinical use in the operating room.

[1] Matts, P, Stratum Corneum Podium Presentation Abstracts, item 23, – 10-12 Sep 1998, Cardiff (P&G)
[2] Hargens, CW, Handbook of Non-invasive Methods and the Skin, pages 353-357 "The Gas Bearing Electrodynanometer": CRC Press 1995.
[3] Maes D, Short J, Tureck BA, and Reinstein JA. In vivo measuring of skin softness using the gas bearing electrodynamometer. J. Cosmetic Sci. 1983: 5, 189-200, 1983
[4] Matts P, Goodyer E, A new instrument to measure the mechanical properties of the human stratum corneum. J.I of Cosmetic Sci.. 1988: 49, 321-323.

[5] Mok W, Bautista B, Hoyberg K, Kirnos P, Subramanayam K. Mechanical properties of ageing skin – Stratum Corneum vs. dermal changes. Stratum Corneum III, presented 12-14th September 2001, Basel Switzerland.
[6] Peter Elsner (editor) Bioengineering of the Skin, Skin Biomechanics Chapter 8 the Gas Bearing Electrodynamometer and the Linear Skin Rheometer. Published by CRC Press ISBN 0-8493-7521-5
[7] Alipour-Haghighi F, Titze IR. Viscoelastic modeling of canine vocalis muscle in relaxation J Acoust Soc Am. 1985: 78, 1939-43.
[8] Berke GS. Intraoperative measurement of the elastic modulus of the vocal fold Part 1.Device development. Laryngoscope. 1992: 102, 760-9.
[9] Berke GS, Smith ME. Intraoperative measurement of the elastic modulus of the vocal fold Part 2.Preliminary results.Laryngoscope. 1992: 102, 770-8.
[10] Chan RW, Titze IR. Viscosities of implantable biomaterials in vocal fold augmentation surgery. Laryngoscope. 1998: 108, 725-31.
[11] Chan RW, Titze IR. Viscoelastic shear properties of human vocal fold mucosa. measurement methodology and empirical results. J Acoust Soc Am. 1999: 106, 2008-21.
[12] Chan RW, Titze IR. Hyaluronic acid (with fibronectin) as a bioimplant for the vocal fold mucosa. Laryngoscope. 1999: 109, 1142-9.
[13] Chan RW, Titze IR. Viscoelastic shear properties of human vocal fold mucosa. theoretical characterization based on constitutive modeling. J Acoust Soc Am. 2000: 107, 565-80.
[14] Chan RW. Estimation of viscoelastic shear properties of vocal-fold tissues based on time-temperature superposition. J Acoust Soc Am. 2001 110, 1548-61.
[15] Chan RW, Gray SD, Titze IR. The importance of hyaluronic acid in vocal fold biomechanics. Otolaryngol Head Neck Surg. 2001 124, 607-14.
[16] Chan RW, Tayama N. Biomechanical effects of hydration in vocal fold tissues. Otolaryngol Head Neck Surg. 2002: 126, 528-37.
[17] Gray SD, Titze IR, Chan R, Hammond TH. Vocal fold proteoglycans and their influence on biomechanics. Laryngoscope. 1999: 109, 845-54.
[18] Haji T, Mori K, Omori K, Isshiki N. Mechanical properties of the vocal fold. Stress-strain studies. Acta Otolaryngol. 1992: 112, 559-65.
[19] Hemler RJ, Wieneke GH, van Riel AM, Lebacq J. Dejonckere PH. A new method for measuring mechanical properties of laryngeal mucosa. Eur Arch Otorhinolaryngol. 2001: 258, 130-6.
[20] Hertegard S, Hallen L, Laurent C, Lindstrom E, Olofsson K, Testad P, Dahlqvist A. Cross-linked hyaluronan used as augmentation substance for treatment of glottal insufficiency. safety aspects and vocal fold function. Laryngoscope. 2002: 112, 2211-9.
[21] Kriesel KJ, Thiebault SL, Chan RW, Suzuki T, VanGroll PJ, Bless DM, Ford CN. Treatment of vocal fold scarring, rheological and histological measures of homologous collagen matrix. Ann Otol Rhinol Laryngol. 2002: 111, 884-9.
[22] Min YB, Titze IR, Alipour-Haghighi F. Stress-strain response of the human vocal ligament. Ann Otol Rhinol Laryngol. 1995: 104, 563-9.
[23] Perlman AL, Titze IR, Cooper DS. Elasticity of canine vocal fold tissue.
J Speech Hear Res. 1984: 27, 212-9.
[24]Perlman AL, Titze IR. Development of an in vitro technique for measuring elastic properties of vocal fold tissue. J Speech Hear Res. 1988: 31, 288-98.
[25] Tanaka S, Hirano M. Fiberscopic estimation of vocal fold stiffness in vivo using the sucking method. Arch Otolaryngol Head Neck Surg 1990: 116, 721-4
[26] Thibeault SL, Gray SD, Bless DM, Chan RW, Ford CN. Histologic and rheologic characterization of vocal fold scarring. J Voice. 2002: 16, 96-104.
[27] Tran QT, Berke GS, Gerratt BR, Kreiman J. Measurement of Young' s modulus in the in vivo human vocal folds. Ann Otol Rhinol Laryngol 1993 : 102, 584-91.

Return to Index

A new instrument to measure the mechanical properties of human stratum corneum *in vivo*

PAUL J. MATTS† and ERIC GOODYER*, *Procter & Gamble Health & Beauty Care, Rusham Park Technical Centre, Whitehall Lane, Egham, Surrey TW20 9NW*

Received

Synopsis

The Gas Bearing Electrodynamometer (GBE)(1) has been used for the last 20 years to obtain sensitive measurements of the stratum corneum. A new instrument for measuring the mechanical properties of the stratum corneum incorporates all of the measurement principles of the GBE but none of its components. A force-controlled miniature d.c. servo, gearing and leadscrew replace the magnet / solenoid arrangement of the GBE. Error resulting from conversion of an electrical signal to a mechanical force is automatically compensated. Consequently, this control renders the need for a friction-free bearing redundant. The original Linear Variable Differential Transformer (LVDT) has been replaced with a unit with a sensitivity of 0.01% and force is now measured by a calibrated 50g load beam. The function generator, signal conditioner and storage oscilloscope have been replaced by user-friendly software run by a small portable computer. The new design offers greater inherent accuracy than the GBE and requires minimal servicing. The new instrument (Linear Skin Rheometer, "LSR") has been shown to provide sensitive measurements of stratum corneum mechanics and was used to measure the mechanical responses of the stratum corneum to two topical moisturising treatments of differing relative hydration performance (as determined by impedance measurements using the Nova™ DPM9003). The relative performance of the two products as measured by the LSR compared favourably with corresponding impedance data, indicating the ability of the LSR to differentiate varying degrees of stratum corneum plasticisation in response to hydration.

* Present Address: E & C Consultancy, 20 Gladstone Street, Hathern, Leicestershire, U.K.

† To whom requests for reprints should be addressed

INTRODUCTION

There are a wide variety of methods available to the dermatological researcher to determine

changes in the mechanical properties of human skin, *in vivo*. However, to measure sensitive changes in the mechanical properties of the stratum corneum, there is only a small number of instruments and methods that may be used with confidence. This is principally because the majority of available

instruments and methods involve relatively large displacements of the stratum corneum, either parallel or perpendicular to the skin surface (1). Consequently, the tissue underneath the stratum corneum will have an unacceptably large effect on the measurement.

The instrument that appears to have been most widely used over the last 20 years to obtain sensitive measurements of the stratum corneum, is the Gas Bearing Electrodynamometer (GBE; 1,2,3,4,5). It is able to apply a sinusoidal loading stress of less than 5g parallel to the skin surface, with a resulting displacement of less than 1mm in each direction. This is achieved by suspending an armature in a gas bearing to create near friction-free movement. Changes in the magnetic field generated by a surrounding coil cause the armature to oscillate at a known frequency and amplitude. The coil is activated by a sinusoidal signal from a low frequency function generator or from a suitable software trigger. The armature of the instrument is typically attached to the skin surface by a stiff wire probe bent to 90ºat its free end. A small plastic stub is usually cemented to the free end of the probe and used to attach the probe to the skin surface using a circular piece of double-sided sticky tape. Displacement of the armature is measured by a sensitive LVDT, mounted coaxially with the coil. Coil and LVDT outputs (force and displacement) are amplified and then supplied for analysis to either a storage oscilloscope or a computer equipped with suitable software. Equipment used in a "classic" GBE workstation is shown in Figure 1.

Results of force and displacement measurements of skin are typically displayed as a hysteresis loop (Figure 2). Analysis of the gradient of the loop (force/displacement or displacement/force) yields derivatives of the dynamic spring rate (DSR) usually expressed as g/mm (a measure of the force required to stretch or compress the skin per unit extension), mm/N or µm/g (measures of stretching or compression of the skin in response to a given applied force). Such analysis yields information about the elastic properties of the skin. Analysis of the phase lag between force and displacement responses yields information about the viscous properties of the skin.

After 20 years of experience with the GBE within our laboratories we believe that the principle of the GBE measurement is still the best available for measuring sensitive changes in the mechanical properties of the human stratum corneum *in vivo*. Subtle though important changes in skin elasticity (dubbed "softness" by Maes *et al.*, (3)) in response to the application of moisturising formulae have been measured, as have changes in skin "tightness" due to surfactant damage. Our experience has, however, also highlighted the draw-backs of employing the original Hargens GBE

instrument in a modern laboratory. These are as follows:

1. Importantly, the instrument employs an "open-loop" method of control, i.e. during calibration of the instrument, and subsequently in routine operation, one assumes that an applied current equals a given force. As the GBE is calibrated on one point only (3g), linearity is not guaranteed over the whole measurement range of the GBE. In addition, calibration drift over time is certain.

2. The components needed to run the GBE are bulky and dated (function generator, signal conditioner, storage oscilloscope, compressed gas / air).

3. The probe components are fragile and, in our experience, break easily and require excessive servicing when used routinely (for example, the fine copper wires connecting the armature to the body of the probe).

4. The air-bearing employed in the probe design is inherently susceptible to misalignment, soiling and malfunction.

In recent years, the cost of precision has improved greatly. We can now achieve using conventional technology what was achieved previously through Hargens' (1) considerable ingenuity. We have designed and built a new instrument that retains and builds on all the principles of the original GBE, but contains *none* of the components. This instrument, designated the Linear Skin Rheometer (LSR) is described in the following sections.

MATERIALS AND METHODS

INSTRUMENT HARDWARE AND DESIGN

A schematic diagram of the new instrument is shown in Figure 3. A force-controlled miniature d.c. servo (Maxon 23-12, 0.5W rating, supplied in U.K. by Trident Engineering), gearing and leadscrew now replace the GBE solenoid arrangement, and drive the LSR probe. The original Schaevitz 050 HR LVDT in the GBE has been replaced with a unit of linearity 0.3% (15μm) and sensitivity 0.01% (0.5μm) (Solartron type DF2.5, Schlumberger Industries). The force exerted on the probe is now measured directly by a calibrated load beam (Minigram Beam Load Cell, type MBH50, rated 50g, supplied in UK by RDP Electronics) with an overall accuracy of <20mg. The load beam is mounted vertically within the instrument casing.

All components fit into one casing measuring 20.0 x 14.8 x 6.9cm and the whole unit weighs 1.7kg. The probe housing itself is a light-weight machined perspex chuck mounted on a low-friction swivel assembly allowing 360o movement (analogous to the GBE). This is protected from damage during routine usage by a metal collar. The chuck contains wire grips to allow the wire probes to be inserted or withdrawn by a simple, firm push or pull. A single lead connects the unit to a PC via a 25-pin D-type connector. Power for the LSR unit is taken from the PC via the connector. The unit can be seen in Figure 4.

INSTRUMENT CONTROL

An IBM (or compatible) PC is used to control the movement of the probe and to log force and displacement data. Both force and displacement are monitored continuously at a rate of 1KHz using a 12 bit ADC plug-in card (National Instruments MIO16). The motor is controlled with an analogue output signal also generated by the PC. The desired force/time cycle, which is normally a single sinusoid, is calculated initially and then stored in memory as a table of values. The actual force applied to the probe is compared with the desired value in the table 1000 times a second. A feedback loop is used to control the motor which moves the load cell in such a way as to minimise any discrepancy. The force applied thus follows the desired force/time cycle extremely closely. The control loop uses an algorithm with proportional and integral terms, whose relative weighting can be varied.

The PC logs all the force and displacement values over a complete measurement cycle, which is usually set at 0.33Hz, thus generating 3000 pairs of points over a 3 second cycle. Two waveform plots are then obtained (Figure 5). Three parameters may be obtained from these curves:

F_{max} the peak force that is applied to the skin surface

P_{max} the peak displacement occurring as a result of that force

T the phase shift between the two signals

The Dynamic Spring Rate (DSR) of the stratum corneum is given simply by the formula F_{max}/P_{max}. Derivatives are calculated and expressed as g/mm, mm/N and µm/g.

The viscous component of the stratum corneum is often inferred by calculating the area of the ellipse shown in Figure 2. A more rigorous

approach is to perform a regression on the original sinusoidal data in order to solve the equations:

$F = F_{max}Sin(t)$ (1)

$P = P_{max}Sin(t+T)$ (2)

where

F = instantaneous force, F_{max} = peak force, t = time for one complete cycle in seconds,

P = instantaneous displacement, P_{max} = peak displacement, T = phase shift in radians

Having solved for these equations, it is then a straightforward problem to solve the integral over one cycle that represents the area of the ellipse:

$$\int_0^{2\pi} F_{max}SIN(t)P_{max}COS(t+T) \quad (3)$$

The LSR software solves the above equations for both elastic and viscous components of the data. These are subsequently displayed, directly after measurement. Note: units of µm/g (1/DSR, a measure of stretching or compression of the stratum corneum in response to a given applied force) will be used as a convenient expression of skin softness in the rest of this paper.

INSTRUMENT SOFTWARE

The LSR software runs on a standard IBM (or compatible) PC of at least 386 33MHz speed, and is sourced in C programming language. The closed loop control employed by the LSR is achieved as follows. As the LSR control loop is a sampled data system, it is essential that a fast real time clock is generated which triggers the measurement of data samples and updates the control signal output. All IBM PCs have as standard a user interrupt (on interrupt vector 0x1c) called the TIMER TICK, which is available for programmers to use as a regular timing source. This timing signal is generated from the 4.192MHz system clock via an Intel 8253 programmable interval timer. The BIOS presets this timer to its full scale of 65536 and,

therefore, the TIMER TICK interrupt is normally 18.188Hz. This is far too slow for a sampled data system.

This problem is overcome by reprogramming the 8253 divider to give the desired frequency during the measurement cycle, in this case 1KHz. In order, however, not to disrupt important internal functions such as monitoring disk drive heads, the timing of interrupt 0x8 (the interrupt number actually triggered by the 8253 output) needs to be restored. This may be achieved by not using interrupt 0x1c, but replacing the BIOS interrupt function at 0x8 with the control programme itself. The original timing is derived within the new interrupt 0x8 by installing a simple counter and calling the BIOS interrupt at the correct interval. In this way, a fast timer is generated that allows data sampling at 1KHz but which does not harm other internal PC operations.

CALIBRATION OF THE LSR

A simple calibration jig has been designed and built that allows rapid, absolute calibration of *actual* force and displacement (Figure 6). Displacement is measured by a 10μm resolution Digimatic Indicator (Mitutoyo (UK) Ltd, Warwick, UK) traceable to NAMAS calibration standards. Force is measured by a 10g load beam (Maywood Load Beam type 49034, Maywood Instruments Ltd, Basingstoke, UK) with <10mg accuracy, also traceable to NAMAS calibration standards.

The load cell calibration factor is expressed in terms of mV signal per volt per gram measured. The output signal is then amplified through a proprietary amplifier (Maywood Amplifier type D2000, Maywood Instruments Ltd) set to a nominal gain of 325. The amplified signal is then converted via the MIO16 interface card (ADC) such that a full-scale reading of 2048 is equal to an input of 10V. The calibration factor is expressed in terms of ADC input reading that equals 1g. The following values are required:

The load cell calibration value taken from its certificate L

The bridge supply voltage measured with a NAMAS calibrated digital volt meter B

The gain of the amplifier measured with a calibrated digital volt meter G

The correction for the digital volt mefer taken from its certificate C

Thus, L = mV per V per g at a nominal voltage of 10V,

Output from the sensor for a 1g load = (L * B * C) / 10,

Output from the amplifier for a 1g load = (L * B * C * G) / 10,

ADC input reading for a 1g load = (L * B * C * G * 2048) / (10 * 10).

The LVDT calibration factor is expressed in terms of mV output per volt per mm displacement. The final slope is expressed in terms of ADC input per mm displacement. The following values are required:

The LVDT calibration value from its certificate L

The excitation voltage measured with a NAMAS calibrated digital volt meter V

The correction factor for the digital volt meter taken from its certificate C

The slope value is derived as follows:

Output voltage for 1mm displacement = (L * V * C)

ADC input reading for 1mm displacement = (L * V * C * 2048) / 10

In practice, these calculations are performed automatically by a simple software programme, allowing rapid and simple calibration of absolute force and displacement.

SKIN MEASUREMENT USING THE LSR

For direct comparison with the GBE reproducibility data obtained by Maes*et al.* (3), the reproducibility of the LSR was estimated by the same method. 40 consecutive identical measurements were performed on the back of the hand of a female volunteer. Results were analysed to determine the coefficient of variation of the measurement.

To determine the ability of the LSR to measure sensitive changes in stratum corneum mechanics in response to simple hydration, the following study was performed. Two moisturising formulae of differing hydration performance (products A and B; hydration performance was determined by impedance measurements using a Nova™ Dermal Phase Meter 9003, see below) were applied to the back of the hands of 13 female subjects (aged 18 - 35)..The dorsal surface of the hand was chosen for mechanical measurements (i) to conform to previous measurement sites using the GBE (3) and (ii) because it

is relatively simple to immobilise the hand effectively. The study was performed in a controlled-environment chamber (temperature 20±1oC; relative humidity 45±5%). The plastic stub on the end of the LSR wire probe was attached to skin on the back of the hand via a circular piece of double-sided tape (5mm diameter). LSR measurements were then performed in triplicate. Baseline measurements were performed before product application. Test products were then applied at a rate of 2µl/cm2 to the entire back of the hand according to a pre-determined randomisation schedule. LSR measurements were performed at 1, 3 and 6 hours after product application. As the whole dorsal surface of each hand was used for product treatment, inclusion of an untreated control was not possible. Results were, therefore, expressed as mean difference to initial pre-treatment baseline.

Hydration performance of products A and B was assessed by randomised application at the same rate as above (2µl/cm2) to 5x5cm sites on the volar forearms of 12 female subjects (aged 18 - 35; the volar forearm was chosen as the site for hydration measurements because of its smooth, hairless morphology and utility as a standard in this type of testing (6). Each forearm also contained an untreated 5x5cm control site. The study was performed within a controlled-environment chamber (temperature 20±1oC; relative humidity 45±5%). Impedance measurements were performed using a Nova™ Dermal Phase Meter 9003 with the standard measuring probe DPM 9103 (Nova Instruments, USA) at 1, 2, 4 and 6 hours after application, and results expressed as mean difference to untreated control.

RESULTS

40 consecutive measurements on the same subject and same site indicated that the coefficient of variation of the measurement was only 2.9% (Figure 7). This demonstrates very good reproducibility of the measurement technique and compares very favourably with the value of 3% obtained by Maes*et al.* (3) for the GBE. The variation measured is almost certainly due to movement of the subject during the probe cycle. This has always been the main source of error in these types of sensitive measurements and various means have been employed to minimise subject movement during readings (e.g. use of a pre-cast plaster mould by Maes *et al.* (3)). However, like Cooper *et al.* (4), we have found that the use of no restraint is preferable and employ a simple sloping table on which subjects rest their hands.

The results of the study using the Nova DPM 9003 to measure the hydration efficacy of products A and B can be seen in Figure 8. Both products induced significant increases ($p<0.05$; paired t-test vs untreated control) in apparent stratum corneum hydration (as measured by impedance changes) up to, and including, 6 hours after application. Moreover, product A increased stratum corneum hydration significantly more ($p<0.05$; paired t-test) than product B at all time-points up to and including 6 hours after application. Water exerts considerable influence on the mechanical properties of the human stratum corneum due to its complex interactions with keratin (7,8). This plasticisation of the stratum corneum, an essentially viscoelastic material, has been described as skin "softening" (2,3). In the case of topical application of a moisturising formula, the extent of this softening effect is directly related to the ability of the product to deliver and maintain increased water concentrations within the stratum corneum. This is usually achieved by the delivery of humectant compounds such as glycerol and / or use of occlusive lipidic films. Indeed, in the case of products A and B, product A might be expected to leverage greater increase in stratum corneum hydration due to its higher glycerol content (4% (w/w) glycerol in A, in contrast to 3% (w/w) in B) and formulation (gel network, in contrast to a simple oil-in-water emulsion in B). For products A and B, therefore, one would expect to be able to measure (i) absolute significant increases in softness for both treatments and (ii) differing relative changes in skin softness for both treatments in accordance with their apparent hydration performance.

Results of the study using the LSR to measure the effects of products A and B on stratum corneum mechanics are presented in Figure 9. Both products induced significant increases ($p<0.05$; paired t-test vs pre-treatment baseline) in skin softness at all time-points up to and including 6 hours after application. Moreover, product A induced greater increases in skin softness than product B throughout the time-course, significantly so ($p<0.05$; paired t-test) at 6 hours after application. These results compare favourably with the relative hydration profiles of the two products (Figure 8). The LSR is, thus, able to measure subtle changes in stratum corneum mechanics in response to hydration and to distinguish between the effect of topical application of moisturising products with differing relative hydration performance.

CONCLUSIONS

The control system used for the LSR provides the instrument with an inherently more accurate and reliable measurement capability because it

employs closed loop (feedback) control. The GBE, in contrast, uses an open loop method of control whereby a predetermined current is applied to the solenoid and assumed to be transformed into the desired force. As no determination of the actual force generated is made at the time of measurement, it is difficult to know with certainty the true force applied to the skin. Whilst open loop techniques can be used successfully in perfectly stable environments, no account can be taken of instantaneous fluctuations in such a system (notably, in this case, subject movement). With the LSR closed loop system, the true force applied to the skin is measured at a rate of 1KHz and corrective action taken within 1ms to restore that measured force to the required value. This system helps ensure that the test sequence is reliable, repeatable and can dynamically adjust for the inevitable variations that occur during *in vivo* testing. Put another way, because this system allows instantaneous compensation of error resulting from the conversion of an electrical signal to a mechanical force, the need for the friction-free gas-bearing arrangement of the GBE is eliminated. This allows the deployment of a compact, efficient and flexible new instrument.

ACKN OWLEDGEMENTS

The authors wish to thank Dr Paul Stevens (Paul Stevens Mechanical Design, Tunbridge Wells, Kent, UK) for his significant skill and expertise in the design of the LSR and also Dr Chris Gummer of Procter & Gamble HABC Ltd for his guidance throughout the development project.

REFERENCES

(1) M.S. Christensen, C.W. Hargens III, S.B., S. Nacht, and E.H. Gans, Viscoelastic properties of intact human skin: instrumentation, hydration effects and the contribution of the stratum corneum,*J. Invest. Derm.*, **69**, 282-286 (1977).

(2) C.W. Hargens, III, "The Gas Bearing Electrodynamometer (GBE) applied to measuring mechanical changes in skin and other tissues", in *Bioengineering and the Skin*, R. Marks and P.A. Payne, Eds. (MTP Press, Hingham, MA, 1981), pp. 113-122.

(3) D. Maes, J. Short, B.A. Turek, and J.A. Reinstein,*In vivo* measuring of skin softness using the Gas Bearing Electrodynamometer,*Int. J. Cosmet. Sci.*,·**5**, 189-200 (1983).

(4) E.R. Cooper, P.J. Missel, D.P. Hannon, and G.B. Albright, Mechanical properties of dry, normal, and glycerol-treated skin as measured by the Gas

Bearing Electrodynamometer, *J. Soc. Cosmet. Chem.*, **36**, 335-348 (1985).

(5) C.W. Hargens III, "The Gas Bearing Electrodynamometer", in *Handbook of non- invasive methods and the skin*, J. Serup and G.B.E. Jemec, Eds. (CRC Press, 1995), pp. 353-357.

(6) V. Rogiers, M.P. Derde, V. Verleye and D. Roseeuw, Standardised conditions needed for skin surface hydration measurements, *Cosmet. Toil.*, **105**, 73-82 (1990).

(7) J.L. Leveque, M. Escoubez, and L. Rassneur, Water-keratin interaction in human stratum corneum, *Bioeng. Skin*, **3**, 227-230 (1987).

(8) J.L. Leveque, "Water-keratin interactions", in *Bioengineering of the skin: water and the stratum corneum*, P. Elsner, E. Berardesca, and H.I. Maibach, Eds. (CRC Press, 1994), pp. 13-22.

An Intelligent Colour Graphics Display for use in Vehicle Dashboard Instrument Clusters

E. Goodyer

An intelligent display system for use in vehicles is described, that uses miniature single board PC's (90mm x 95mm), interfaced to '4 inch' full colour TV displays. Both these components are embedded within the instument cluster. Graphics are generated using a resident intepreter, that allows the design of new screens in less than a day, and can support animation of better than 10 frames per second. There are no user interfaces to the embedded PC, as all data is obtained from transduced inputs, which are attached to software variables in the intepreter, and thereby dynamically drive the graphics. Systems are now in use by Ford and Jaguar.

1 INTRODUCTION

In recent years developments of new intelligent systems for automotive applications, such as engine management and active suspension, has led to a growing need to provide system developers with more meaningful graphics displays.

One solution has been to interface the system elements to a central computer, usually an IBM or compatible PC, via a range of transducers and transmitters. Even though PC's have come down in size, embedding them into vehicle dashboards is not always a practical proposition. Even if the computing mother board can be lost somewhere behind the dashboard, the problem of locating a suitable miniature graphics display into the viewing area still remains.

The smallest commercially available colour graphics display is still 5.6 inches, which is too large for many vehicle dashboards. There are however a range of smaller 4 inch colour displays available that have been developed for the growing 'camcorder' and small TV market. These are perfectly suitable for installing into vehicle dashboards. There are two technical problems however; they comform to television scan rates (PAL or NTSC) and not computer scanrates, and the video signals conform to different electrical standards.

This paper outline the technical solutions, both software and hardware, to overcome the differences between TV and computer video signals, with reference to actual systems now installed into test vehicles belonging to the Ford Motor Company and Jaguar Cars Ltd.

Two electrical solutions will be outlined; one being how to interface CGA signal to NTSC or PAL monitors, and the other being how to interface VGA signals to NTSC or PAL monitors. These solutions were developed specifically for use with SHARP and TOSHIBA 4 inch full colour LCD TV screens, but are applicable in general to all such monitors.

Building a suitable electrical interface is not sufficient. In addition it was also neccesary to develop software that reprogrammes the PC display driver devices to provide video signals with the correct timings. These solutions will also be outlined.

The packaging problem was resolved by utilising the new range of 'credit card' PC's now coming onto the market. It is now possible to purchase a complete PC, which can slip into a pocket; and the new PC104 connector standard allows the user of such devices access to a wide range of peripheral and interface cards from different manufacturers. All of the systems outlined below make use of DSP Design's GCAT series of miniature PC cards, but the solutions are applicable to all such devices that use standard VGA & CGA driver devices.

Finally, in order to provide the fastest achievable graphics update rate and to make the design of new graphics screens simple, a 'graphics intepreter' was developed specifically for use with 4 inch colour displays. This intepreter is permanently resident on the embedded PC that drives the colour display, it defines a range of primitive graphics functions, such as sliding bars and moving dials, which are 'attached' to transduced inputs. A new screen is defined solely by an ASCII based definitions file, giving system developers the ability to design new dynamic graphics screens in hours.

2 THE DISPLAY TIMINGS

In order to understand the software it is neccesary to first have an understanding of the differences between PAL, NTSC, CGA and VGA display timings; and the relationship between those timings and the number of horizontal and vertical pixels that can be defined by each of these standards.

2.1 CGA

CGA screens are refreshed at a rate of 60Hz, which is the rate required by NTSC (US National Television System Committee) television monitors. In theory therefore CGA driver cards should be the easiest to interface to TV monitors that support NTSC signals.

The total number of visible lines varies depending upon the selected mode. Alphanumeric modes have 25 text lines, each character being 8x8 pixels. This gives a total of 200 lines containing pixel data. In order to allow for flyback and picture sync, additional lines with no picture information are added. It is these additional lines that bring the refresh rate back towards 60Hz. The IBM XT technical reference manual states that the low resolution alphanumeric mode (40 x 25) can be used by an NTSC "home colour television".

The graphics modes have either 100 or 200 lines. The 100 line mode is archaic, and even though the standard CGA 6845 CRT controller device can support it, the code to do so is not present in any PC's BIOS. Timing and operation is therefore similar to the 200 line alphanumeric modes described above, and again the 'medium' resolution mode is stated to be suitable for direct connection to NTSC television monitors.

Of interest is the horizontal scan time. The default BIOS programmes the horizontal line scan to be 56 characters long. As there are 8 bits per character width, this gives a total of 56 x 8 = 448 pixel clocks per line. As the character clock in 40 column text and medium resolution graphics is 7MHz, that gives us a scan rate of 0.064 ms per line.

The horizontal pixel count varies with the selected mode, 40 column text and medium resolution graphics mode have 320 pixels, 80 column text mode and high resolution graphics offer 640 pixels.

2.2 VGA

VGA driver cards support a wide range of different VGA display modes, most of which are listed in the table below -

Table 1 List c

TYPE
40 x 25 Text
40 x 25 Text
40 x 25 Text
80 x 25 Text
80 x 25 Text
80 x 25 Text
80 x 25 Text
80 x 25 Text
Graphics
Graphics
Graphics
Graphics
Graphics
Graphics
Graphics
Graphics
Graphics
Graphics

The mode nu
mode. It is int
horizontal an
a limited set c

All of these m
which effectiv

Of particular
closest match

2.3 PAL

PAL screens
As only half t
2/(refresh rat

2.4 NTSC

NTSC screen
therefore in n

2.5 Matching

In order to giv
endeavour to
possible. This
monitor, and
that monitor.

As already di
information.
blanking and
200 line mod

If we are usin
visible scan li
ourselves to
13, which off

Table 1 List of VGA Display Modes

TYPE	PIXELS	COLOUR	MODE NUMBER
40 x 25 Text	360 x 400	16 colours	0,1
40 x 25 Text	320 x 350	16 colours	0,1
40 x 25 Text	320 x 200	16 colours	0,1
80 x 25 Text	720 x 400	16 colours	2,3
80 x 25 Text	640 x 350	16 colours	2,3
80 x 25 Text	640 x 200	16 colours	2,3
80 x 25 Text	720 x 400	Mono	7
80 x 25 Text	720 x 350	Mono	7
Graphics	320 x 200	4 colours	4,5
Graphics	640 x 200	2 colours	6
Graphics	320 x 200	16 colours	13
Graphics	640 x 200	16 colours	14
Graphics	640 x 350	Mono	15
Graphics	640 x 350	16 Colours	16
Graphics	640 x 480	2 Colours	17
Graphics	640 x 480	16 Colours	18
Graphics	320 x 240	256 Colours	19

The mode number is the parameter passed to the mode set BIOS routine when selecting a new video mode. It is interesting to note that even though a wide range of different modes, in terms of horizontal and vertical lines and number of colours, are available, many popular compilers only offer a limited set of these alternatives.

All of these modes , with the exception of numbers 17 & 18, have a screen refresh rate of 70Hz, which effectively means that none of them have any relationship to any TV scan rates.

Of particular interest to the technical solution given below is mode number 13, as this gives the closest match to an NTSC screen, whilst also offering a 16 colour solution.

2.3 PAL

PAL screens have a 50Hz refresh rate, with 625 transmitted lines including top and bottom blanking. As only half the lines are used in a non interlaced mode the horizontal scan time is given by 2/(refresh rate x number of lines) = 0.064ms .

2.4 NTSC

NTSC screens have a 59.94 Hz refesh rate, with 525 transmitted lines. The horizontal scan rate therefore in non interlaced modes is 0.63556 ms.

2.5 Matching The Different Scans

In order to give a TV screen a chance of synchronising onto a CGA or VGA signal we must endeavour to modify the video driver output such that it provides signals that are as compatible as possible. This requires us to select a total number of lines that matches that expected by the TV monitor, and to adjust the timings such that the horizontal and vertical scan rates are acceptable to that monitor.

As already discussed both NTSC & PAL in non interlaced modes expect less than 320 of visible information. To send more than that is pointless as the picture information will just be lost in vertical blanking and flyback periods. Therefore the best that we can hope to achieve in the conversion is a 200 line mode.

If we are using a CGA driver then we have an almost perfect match with NTSC, as the number of visible scan lines will be 200. with a screen refresh rate of 60Hz. With VGA we must restrict ourselves to one of the 200 line scan modes, else information will be lost. Our chosen option is mode 13, which offers 320 x 200 pixel pictures. Adjusting the actual scan rates is discussed later.

3 THE ELECTRICAL SOLUTION

Electrical compatibility is the easiest part of our problem. The colour information for all the standards outlined above is supplied on three analogue signals, designated Red, Green and Blue; or simply just RGB. PAL, NTSC and VGA colour information are analogue signals with a peak to peak voltage of 0.7V, they are therefore directly compatible. CGA colour information signals are however TTL signals, and need to be attenuated in order to drive a TV monitor.

The difficulty comes with the sync signals. Both VGA and CGA supply independant horizontal and vertical signals, at TTL levels, on a standard video connector. Whereas both the Sharp & Toshiba displays require a composite sync signal.

The solution to the design of a suitable interface is given in the circuit below. The RGB signals can be either attenuated by the potential divider for CGA, or directly connected for VGA by simply not fitting the resistors. A composite sync signal, at TTL levels, is generated from the separate horizontal and vertical sync signals, by means of a simple FET switch.

More complex solutions have been proposed elsewhere, but this simple circuit is more than adequate for connecting standard computer outputs to a Sharp or Toshiba LCD display.

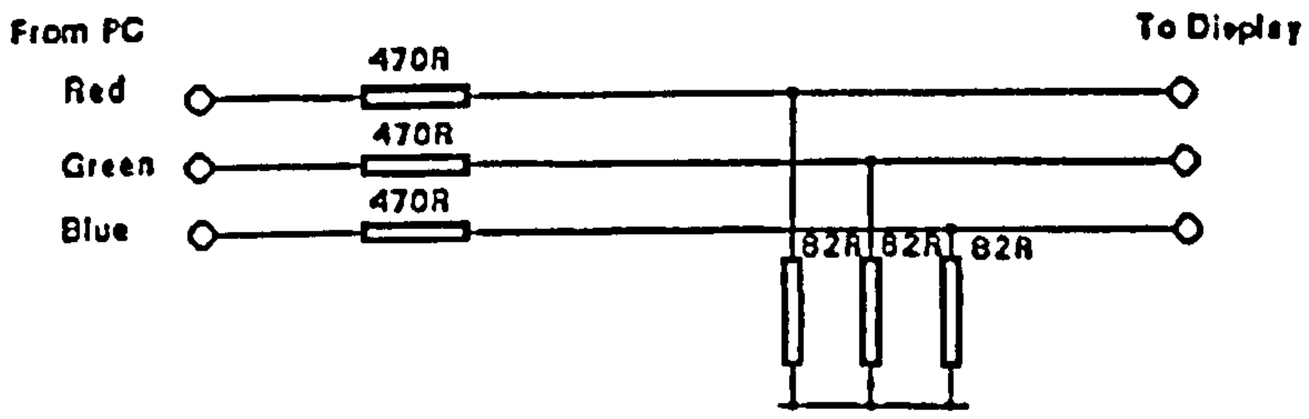

Figure 1 RGB & Sync Conversion Circuit

4 THE SOFTWARE SOLUTION

The fine detail of any software solution depends solely upon the video mode selected, Therefore what is detailed below is the method that needs to be adopted in order to achieve that solution.

Intelligent

4.1 CGA M
As has alre
be suitable
used in the

The major
equivilent.
vertical syn
respect to t

Given belo

TABLE 2

Register N
0
1
2
3
4
5
6
7

All the regi
write the d

The dot cl
bits in both
set to 40 w
the length
value of 5
us a time

Registers
generated

Registers
of the who
(31 x 8), r
As each li
60Hz (1 /

Register 6
set to 25,
vertical sy

In theory i
medium r
practice th

Fortunatel
to the Vid
the BIOS
vertical sy

4.1 CGA Modes

As has already been discussed 40 column text and medium resolution graphics modes are claimed to be suitable for direct connection to an NTSC screen. Therefore these are the modes that have been used in the in-vehicle displays when a CGA display driver was installed.

The major component that needs to be considered is the Motorola 6845 CRT controller device, or it's equivilent. This device contains a set of registers that determine the timings of the horizontal and vertical synchronisation signals, and how the picture data is output on the RGB signal lines with respect to those sweeps. For a detailed description you should obtain a copy of the full data sheet.

Given below are a list of the principle registers that need to be considered.

TABLE 2 CGA CRT CONTROL REGISTERS

Register Number	Function
0	Total number of horizontal characters
1	Number of horizontal characters to be displayed (<=register 0)
2	Horizontal sync position
3	Horizontal sync width
4	Total number of vertical rows
5	Vertical total adjust
6	Number of vertical rows to be displayed (<=register 4)
7	Vertical sync mode

All the registers are located at address 0x3d5. To select a specific address it is neccesary to first write the desired register number to address 0x3d4, and then to output the desired data.

The dot clock for 40 column and medium resolution modes is 7MHz. The total number of horizontal bits in both these modes is 320 (the characters are laid out on an 8x8 matrix). Register 1 therefore is set to 40 which means that the visible part of the line is 0.045 ms long. Register 0 is used to extend the length of the horizontal line to our desired width, in terms of character widths. So by entering a value of 56, we define that line to be 448 dot clocks wide (56 characters x 8 dots each); which gives us a time of 0.064 ms.

Registers 2 and 3 determine at what point in the horizontal line the horizontal sync signal is generated, and how long that pulse is.

Registers 4 & 5 determine how many lines are transmitted in total, thus determining the refresh rate of the whole screen. In 40 column mode register 4 is set to 31 rows, which gives a total of 248 lines (31 x 8), register 5 is set to 6, which adds a further 12 lines to the total display, giving a total of 260. As each line is 0.064 ms long the total screen refresh rate is slightly over the desired NTSC rate of 60Hz (1 / (260 x 0.064) = 60.096Hz);

Register 6 determines how many of the transmitted lines contain visible data, in our case this will be set to 25, for 25 rows of 8 pixels each, or 200 lines in total. Register 7 determines at what point the vertical sync signal is started.

In theory if a Sharp or Toshiba display is set to NTSC mode then CGA signals in 40 column text and medium resolution modes will drive them without any further interference by the programmer. In practice this is not so, and some minor adjustments need to be made.

Fortunately we do not need to worry about most of the registers, as they can be set up for us by a call to the Video BIOS, either through a high level language function as given below, or by a direct call to the BIOS via an interrupt. What we do need to do is to adjust the timings of the horizontal and vertical sync pulses in order to centre the picture onto the screen. This is best achieved by trial and

error, using a simple programme that calls the new video mode, sets the sync registers to different values, and then displays a test pattern such as a grid or bars.

After experimentation with both a Sharp and a Toshiba display the optimum set up was found to be as detailed in the programme below.

```
_setvideomode(_MRES4COLOR) ; // CGA medium resolution graphics 4 colour mode
outp(0x3d4,2);               // Select register 2
outp(0x3d5,0x2c);            // Start horizontal sync at position HEX 2C
outp(0x3d4,3);               // Select register 3
outp(0x3d5,4);               // Set horizontal sync width to 4
outp(0x3d4,7);               // Select register 7
outp(0x3d5,0x75);            // Start vertical sync at position HEX 75
```

Programme 1 CGA Medium Resolution Graphics to NTSC Conversion

A similar solution exists for PAL screens. Registers 4 & 5 need to be increased to add more blank lines, thus reducing the screen refresh rate to 50Hz. The picture however will be slightly smaller as PAL screens expect to receive more lines than NTSC, and the PC can only ever put out a maximum of 200 visible lines.

So to summarise, select your display mode in the normal manner, then adjust the horizontal and vertcal pulse widths to centre the picture. Medium resolution graphics and 40 column text modes are the most suitable for use on a TV. NTSC is preferable to PAL but solutions exist for both types of screen.

4.2 VGA Modes

VGA is far more entertaining, not just because we have such a wide range of different modes, but because we have substantially more control registers to worry about. The objective is however the same as CGA, to match the computer generated video output to the TV screen.

VGA display drivers have substantially more programmable registers than CGA drivers. Fortunately only a small group of them are of interest to us. These are the CRT controller registers as listed in the table below. To access them it is neccesary first to output the register number to address HEX 3D4, and then to write the data to address HEX 3D5, but see the section on 'Group Protection' below.

TABLE 2 KEY VGA CRT CONTROLLER REGISTERS

REGISTER NUMBER	FUNCTION	UNITS
00	Horizontal Total	Pixel Clocks
01	Horizontal Display End	Characters
02	Horizontal Blank Start	Characters
03	Horizontal Blank End	Characters
04	Horisonal Sync Start	Characters
05	Horizontal Sync End	Characters
06	Vertical Total	Lines
07	Vertical Overflow Register	Various

It is beyond the scope of this paper to give a full solution to all the VGA to TV conversion modes. What is detailed below is the method that needs to be adopted to determine each solution in the lab.

Two specific solutions were developed for Ford & Jaguar, based on 640 x 480 graphics, and 320 x 200 graphics. The chosen display for both systems was the Sharp LQ4RA 4 inch panel, which has 234 lines of 479 dots each. There is no point in using a VGA mode with greater dot resolution than can be displayed, otherwise fine detail that can be seen on a VGA screen will not be visible on the LCD. So even though a solution for 640 x 480 dots can be found, care must be taken when developing graphics as the images will not look the same when downgraded to a TV scan rate.

In both cases the displays were set to NTSC mode, so the first task is to adjust the horizontal scan time to be 0.064ms, and the screen refresh rate to be 60Hz.

VGA control register 0 determines the total horizontal line scan time, in units of character clocks. So first determine how long each character clock is, by simply dividing the pixel clock by 8, and then choose a number that will set the total line length to be approximately 0.064 ms. A good starting point would be around 45. The VGA controller adds 5 to this number to determine how long the line is, so 45 gives a line length of 50 characters.

Next set the frame refresh rate to be 60Hz. This is achieved by adjusting the total number of horizontal lines transmitted, with VGA control registers 06 and 07. Register 06 holds the lower 8 bits of the number of lines that are transmitted, register 07 holds the upper two bits of a 10 bit word; bit 0 of register 07 is bit 8, and bit 5 of register 07 is bit 9. A good number to choose here is 262 lines, so as the VGA controller adds 2 to the programmed number of lines, we need to programme in a number of 260, which is achieved by writing 04 to register 06 and 01 to register 07.

Once this is done the picture should now at least be visible. The rest of registers are best set up experimentally, as they adjust the actual position of the screen with respect to the borders of the display.

Given below are some typical sections of code. The first achieves the conversion of the VGA output from 320 x 200 lines to NTSC scan rate for a Toshiba display; the second is for use with a Sharp display in PAL mode.

```
void toshiba(void)
        {
        OUTPORTB(0x3d4,0x00) ;      // select CR0
        OUTPORTB(0x3d5,0x2d) ;      // set to approximately 0.064 milliseconds
        OUTPORTB(0x3d4,0x01) ;      // select CR1
        OUTPORTB(0x3d5,0x27) ;
        OUTPORTB(0x3d4,0x02) ;      // select CR2
        OUTPORTB(0x3d5,0x28) ;
        OUTPORTB(0x3d4,0x03) ;      // select CR3
        OUTPORTB(0x3d5,0x80) ;
        OUTPORTB(0x3d4,0x04) ;      // select CR4
        OUTPORTB(0x3d5,0x2a) ;
        OUTPORTB(0x3d4,0x05) ;      // select CR5
        OUTPORTB(0x3d5,0x0e) ;
        OUTPORTB(0x3d4,0x06) ;      // select CR6
        OUTPORTB(0x3d5,0x04) ;      // set to 262 lines
        OUTPORTB(0x3d4,0x07) ;      // select CR7
        OUTPORTB(0x3d5,0x11) ;      // vertical overflow register
        }
```

Programme 2 VGA to NTSC conversion for Toshiba Display

```
void pal(void)
        {
        OUTPORTB(0x3d4,0x00) ;      // select CR0
        OUTPORTB(0x3d5,0x30) ;
        OUTPORTB(0x3d4,0x01) ;      // select CR1
        OUTPORTB(0x3d5,0x27) ;
        OUTPORTB(0x3d4,0x02) ;      // select CR2
        OUTPORTB(0x3d5,0x28) ;
        OUTPORTB(0x3d4,0x03) ;      // select CR3
        OUTPORTB(0x3d5,0x80) ;
        OUTPORTB(0x3d4,0x04) ;      // select CR4
        OUTPORTB(0x3d5,0x2d) ;
        OUTPORTB(0x3d4,0x05) ;      // select CR5
        OUTPORTB(0x3d5,0x0e) ;
        OUTPORTB(0x3d4,0x06) ;      // select CR6
        OUTPORTB(0x3d5,0x36) ;      // set to 312 lines
        OUTPORTB(0x3d4,0x07) ;      // select CR7
        OUTPORTB(0x3d5,0x15) ;      // vertical overflow register
        }
```

Programme 3 VGA to PAL conversion for Sharp Display

2.4.1 Protection Bits

When reprogramming VGA registers it is important to be aware that they are usually write protected by a mechanism known as 'protection' or 'lock' bits. This means that other registers in the VGA I/O map area contain protection (or lock) bits, which when set will prevent all write accesses to various groups of registers. A full description of these operations can be found in the VGA controller device manual. In the examples given above control registers 0 through to 7 are 'Group 0 Protected'. This means that unless the Group 0 Protect Bit is clear you will not be allowed to write to any of these registers.

In the case of the Chips & Technology 65535 VGA controller, the Group Protection Bits are held in the VGA extension register number 15 HEX. The Group 0 Protection Bit is bit number 6, so the code that allow writes to Group 0 registers is as follows -

```
OUTPORTB(0x3d6,0x15) ;      // select XR 15
OUTPORTB(0x3d7,0xBF) ;      // unprotect group 0
```

Programme 4 Code to Unprotect Group 0 VGA Control Registers

It is essential that you closely examine the data sheets of the VGA controller that you are using in order to determine where the Protection Bits are.

2.4.2 The Preferred Video Mode

The chosen mode for both the Sharp and Toshiba displays was VGA mode 13, which has a layout of 320 by 200 pixels, and offers 16 colours. The reason for this selection is that it is the VGA mode that most closely matches the pixel layout of the LCD displays themselves. For example the Sharp display claims to offer 234 vertical lines with 479 horizontal dots. As there is no point in generating more dots than the display can support, the 320 x 200 line mode is the best choice. This mode also has the advantage over the more usual 640 x 480 mode, in that far more full page images can be stored in the same amount of video RAM, thus offering more scope for animation to be achieved by the relatively fast process of switching the currently active video page.

The standard VGA pixel clock is set to 25.175MHz for all modes up to 640 pixels in the horizontal direction, and 28.322 for the higher resolution 720 pixel modes. This clock needs to be adjusted when the CRT control registers are set for VGA mode 13, because the standard set up only fills half a

```
OUTPORTB(0x3d7,0x00);       // select VCLK
OUTPORTB(0x3d6,0x30) ;      // select XR 30
OUTPORTB(0x3d7,0x02);       // halve the clock rate
OUTPORTB(0x3d6,0x31) ;      // select XR 31
OUTPORTB(0x3d7,0x58);       // halve the clock rate
OUTPORTB(0x3d6,0x32) ;      // select XR 32
OUTPORTB(0x3d7,0x57);       // halve the clock rate
OUTPORTB(0x3d6,0x15) ;      // select XR 15
```

Programme 4 Halving the Pixel Clock for the C&T 65535 CRT Controller

5 THE FINAL SYSTEM

5.1 Hardware

Due to the restricted space available in the vehicle all the displays were driven by single card PC's housed in purpose designed boxes. Of particular interest were the cards supplied by DSP Design Ltd, who can offer a 'credit card PC' with integral PCMCIA slot, and a range of PC104 type cards as well.

The 'credit card' device was one of their GCAT range, which has a dimension of only 84mm x 65mm with a height of 24mm. This device is an XT device, with a full range of user interfaces (keyboard CGA output serial and parallel ports) and a PCMCIA memory card slot. The memory card is configured as a disk drive, which means that we have a complete PC with no moving parts.

A more recent development has been a similar range of devices, up to 486 capability with VGA outputs, laid out using the new PC104 miniature PC connector standard. These devices are also very small, 95mm x 90mm, and have the advantage of being compatible with a wide range of other manufacturers' PC104 peripheral devices. Again memory card 'hard disks' can be fitted to improve reliability.

5.2 Software

The final development was to provide a software environment that allowed the user to design and create new graphics screens with minimum fuss, and supported animation of better than 10 frames per second.

This was achieved through the design of a Graphics Intepreter that is made resident on the embedded PC & Display system. The language supports a range of primitive graphics images, such as circles, lines, horizontal and vertical sliders, predefined Icons and text blocks. New screens are defined simply by a list of ASCII commands, each line of which defines the type of graphic primitive that needs to be display, its' position, colour and orientation. An example is given below.

91/030

n overview of a range of novel automotive nsors

OODYER, MSc, CEng, MIEE
imited, Chislehurst, Kent

SIS This paper is a relatively non-technical summary of sensors developed at Sira Ltd which may t to automotive use. The following sensors as developed for various companies will be presented:

ge of low cost steering wheel position sensors which offer resolutions better than 0.5 degrees.

tical fuel flow sensor that detects light scattered by particles moving along with the fuel.

hly accurate electromechanical road tanker liquid level sensor and its' derivatives including a ost sensor for use in car petrol tanks.

m Dip" which optically detects an oncoming car or the tail lights of a preceding car and atically dips the car's main beam.

tical linear displacement sensor, which uses a handful of widely available optical components. ble applications include suspension arm extension, and wheel to road measurements.

STEERING WHEEL POSITION SENSORS

Ltd has developed a range of steering wheel ion sensors for First Inertia Switch Ltd. e sensors have been specifically designed a number of European car manufacturers to their differing specifications and rements.

and low angular resolutions from 2 degrees to 0.3 degrees can be achieved. Absolute position signals can be included for one or turns of the steering column. A variety of al outputs can be provided depending upon nput specification for the unit that ts data from the sensor. The basic unit des a pair of digital pulsed outputs that sent left and right turns of the steering n, but existing systems may prefer to ve quadrature signals and to derive tion, which can also be supplied. Analogue ts can also be added if required, and basic al processing (eg rate of change of angle) be incorporated with the addition of a computer.

Confined Space Option

arly requirement was to design a steering tion sensor that would fit into the confined e between a 23mm diameter steering column an outer sleeve of 35mm diameter, with a lution of better than two degrees. This ws only 4mm total space between the column the outer sleeve for the sensor optics. The nique employed in currently available ors is to obtain quadrature signals from two cent detectors viewing an LED through a ted wheel (see fig 1.a). The wheel would ire 45 slots 1.2mm wide at the edge, down to 0.8mm wide next to the steering column inner shaft. The detectors would also need to have a similar geometry and be carefully positioned. Such an approach is unlikely to provide a low cost solution.

Sira overcame the confined space problem by using a wedge of light guides as shown in figure 1.b and a chopper wheel with only 24 2mm wide slots. The light guides overcome the problem of mounting the detectors accurately in the confined space, as the wedge can be assembled separately and 'slotted' into place. The light is then taken externally and can be detected by any reasonable detector regardless of it's geometry. Using 4 light guides effectively quadruples the resolution available from the chopper wheel, which can be more easily manufactured because of the wider slot width.

Simple thresholding electronics provide a set of pulse trains that is decoded by a PLD to provide a pair of pulsed outputs that represent left and right rotations of the steering column, so that the car does not have to decode quadrature signals. An error signal is also available should a fault be detected.

The sensor resolution is 1.875 degrees, with an accuracy of better than 0.2% of full scale, and can operate up to 1500 degrees per second.

1.2 Use of Photodetector Array

Later models of the sensor use a photodetector array (figure 1.c). instead of the light wedge. Use of the array reduces the mechanical complexity of the sensor, and improves the electronic performance. The active elements are laid down to match the the geometry of the light guides, thus retaining the advantage of

CHAPTER 1

Introduction to automotive sensory systems

1.1 INTRODUCTION

Within the automotive industry, it is known that a quiet technological revolution is progressively taking place in the area of vehicle system performance and control. This revolution is undoubtedly fuelled by the fact that at the present, automotive component and vehicle manufacturers are confirmed with ever-increasing demands from their customers and government legislation for high-quality, reliable, safe and environmentally less damaging products. Compounded with these demands, there is continuing competition within the industry for the available market share, which is normally influenced by the national and international economic cycle.

The increase in road vehicle automation is through the application of sensory systems for control of vehicle components and subsystems. As part of the sensory systems, the application of information technology and electronics in road vehicles has meant that control, monitoring and information display functions normally carried out mechanically or manually are now performed with the enabling sensors and computer processing systems. Some of these functions include: engine control, chassis control, vehicle safety, vehicle–infrastructure interactions, systems diagnostics, emission control information systems and communications. In all these functions integrated sensory systems play a very important role.

Currently, there is a continued drive towards the development of the so-called 'smart' or intelligent vehicles. If the vehicle of the future is to be made more intelligent with some elements of autonomous control, integrated sensory systems will form the most important and central aspects of the vehicle.

This chapter will define automotive sensory systems in terms of an integrated part of a vehicle. Current applications of sensors and systems are discussed. Future development in vehicle sensory systems is discussed.

1.2 WHAT ARE AUTOMOTIVE SENSORY SYSTEMS?

To define automotive sensory systems, a general definition of some of the devices which make up a basic sensory system will be useful. These devices can be classified into one distinct category, namely measurement or sensory system. The measurement system consists of devices which can obtain a quantitative comparison between a predefined standard and a measured. The word measured is used in this instance to designate the particular physical parameter being sensed and quantified within an automotive system. Transducers, sensors and detectors are some of the names used to describe a measurement system.

Transducers are devices capable of converting one form of energy or physical quantity to another. Often this energy or stimulus determines the quantity of the signal obtainable.

Sensors are devices used for the purpose of detecting, measuring or recording physical phenomena and subsequently responding by transmitting information, initiating changes or effecting systems control.

Detectors are devices capable of sensing the presence of something such as physical phenomena, heat, radiation, etc. within the automative system's environment.

It is apparent from this definition that any difference between these devices will be difficult to distinguish. Therefore for the purpose of defining automotive sensory systems, these devices can generally be classified as sensory systems. Typically, sensory systems will comprise a number of elements integrated into component blocks. Most basic sensory systems will contain the sensor, a signal conditioning element, an analysis element and a recorder or display system. Within the sensory system's structure, a feedback sensory signal can be provided in order to optimize the behaviour of the system.

As part of the evolving application of computers, electronics devices and communication systems in vehicles, automotive sensory systems can be difficult to define completely, since many views are possible within this developing technology. To capture the most important aspects of automotive sensors and systems, an automotive sensory system is defined as the integrated part of the vehicle sensors and systems with the functions of detecting, transmitting, analysing and displaying vehicle performance information from a given stimulus within the internal and external environment of the vehicle. This definition will in future include the capacity of the sensory system to memorize and logically store vehicle performance information for the purpose of performance diagnostics and prognostics with inbuilt intelligence and self-calibration. It is possible that a full definition of automotive sensory systems will also include the ability of the sensory systems to form part of a specialized distributed and multi-tasking capability within a networked multiprocessing system. As shown in Figure 1.1, at a low and normal driving task levels, the driver forms part of the sensory system. An integrated sensory system takes account of the ability of the

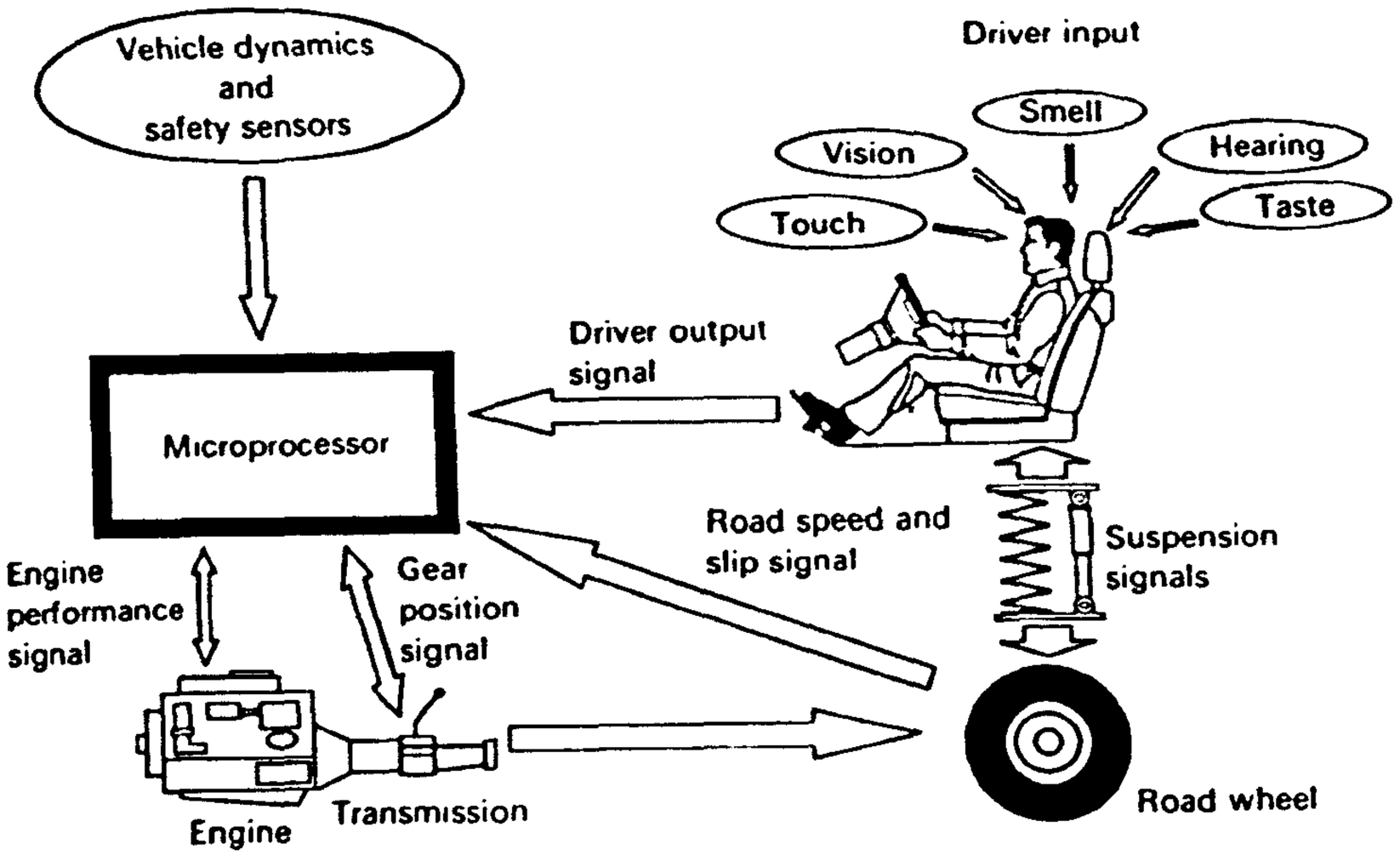

Figure 1.1 Driver as part of the sensory system

decisions on the progress and state of the road vehicle during driving and parking conditions. The responsibility of the driver in this respect will obviously be reduced as the sensory systems and the vehicle are made more intelligent.

1.3 THE BACKGROUND

The use of sensors and systems in road vehicles was, a decade ago, restricted to the acquisition and display of fairly inaccurate information on vehicle and engine speed. This was extended to simple sensing and display of water temperature, fuel level in the tank and lubrication system failure. With this basic level of sensor technology the demand put on the driver to make up for the deficiency was too high. As can be testified by most drivers under normal driving conditions, this can result in pressures and stress on the driver in busy traffic conditions and during long-distance travel. The stresses and pressures can be even higher on people who drive as part of their job (taxi drivers, bus and heavy goods vehicle drivers).

Today, however, an increasingly competitive market coupled with

- stringent environmental and safety legislation;
- expected high-level driveability and performance;
- moves towards a vehicle with self-management and diagnostics;
- improvements in luxury and comfort;
- the availability of low-cost electronic devices

has encouraged manufacturers to integrate into their vehicles sophisticated sensory systems capable of enhancing the performance and safety of the vehicle. Basic mechanical and some manual operations are now controlled and monitored by these sensory devices. The use of these devices has increased rapidly since early 1970 [1, 2]. This growth has been accentuated by various technical papers [3–6]. The high-level materials discussed in this book indicate that this growth will continue at a rapid rate in the future.

1.4 SOME CURRENT SYSTEMS

Various sensory systems are currently used in road vehicles. The majority of the sensors are used for monitoring and control of powerplants and transmissions. There is also a rapid growth in the use of sensory systems for vehicle ride and chassis control. Sensory systems for passive and active driver and passenger safety continue to be applied as an integrated part of recent road vehicles. Some of the current systems used on road vehicles will now be discussed.

1.4.1 Powerplant and transmission

The types of sensors and systems used for powerplant and transmission control depend on the parameters which will be monitored. Some of these parameters and the sensor systems used are as follows.

Inlet manifold absolute pressure

This is an engine parameter which can be sensed for speed/density and control of fuel mixture. Inlet manifold vacuum pressure allows for ignition control incorporating the appropriate timing sensor. It allows for engine load sensing because as the engine load is increased, the engine slows down and the inlet manifold vacuum pressure tends towards atmospheric pressure; this is accentuated by depressing the accelerator pedal, and thus increasing the opening of the throttle.

The mechanical method of manifold vacuum measurement has generally been in existence since the early days of automotive powerplant (engine) design. The current method uses a piezoresistive silicon diaphragm or other type of electronic pressure sensor connected to the manifold with a system which allows for a frequency or voltage input that represent engine rotational speed.

Crankshaft angle position

As the crankshaft rotates the ignition timing or the injection timing indexes, this yields angular velocity or frequency which is used for ignition and fuel control. Several sensors and systems are available for monitoring the rotational position of the crankshaft. For example, Hall-effect sensors, Wiegand-effect sensors, optical sensors and variable-inductance sensors are used for crankshaft angle position. The sensor signal forms part of the ignition, fuel and powertrain control.

Other powerplant parameters

Apart from the manifold pressure and crankshaft positions, there are other parameters which can be sensed and used to control the performance of a powerplant. The mass airflow into the engine manifold can be sensed using a hot-wire anemometer, a vortex-shedding flowmeter, an ion-drift flowmeter, etc. The output signal is used to control the air/fuel demand of the engine. Throttle position can be monitored with a sensor which helps to control the amount of fuel in the carburettor. The exhaust gas emitted from the engine can be monitored to detect the oxygen content in the gas. This is used as a means of controlling the emission characteristic of the engine. This type of sensory system incorporates an exhaust-gas-oxygen sensor, known as the λ sensor (Figure 1.2(a,b,c)). The sensor voltage is monitored, and, as shown in Figure 1.3, the voltage output can be related to the air/fuel ratio.

The temperature of the engine can be sensed and used as a variable for an engine control system. There are some well-established sensors, such as wirewound resistor temperature sensors and thermistors. These are used in various control systems.

To optimize engine performance and fuel economy, ignition timing and control must be adjusted so that combustion will occur during a specific number of crankshaft degrees, beginning at top dead centre of the power stroke. If it occurs any sooner, knock or detonation will occur. If it occurs any later, less pressure will be produced in the cylinder, and hence there will be a loss of engine efficiency. Even when an ignition system is fitted with electronic advance control, and is used to optimize the engine for best performance and economy, it can, under some conditions, be set sufficiently advanced to cause 'knocking' or 'detonation'. Knock can result in physical damage to the combustion chamber. In order to be able to provide an optimized engine performance without the effect of knock, knock sensors and systems are used. Most of the knock sensor (Figure 1.4) contains a piezoelectric crystal, which acts as an accelerometer for sensing the vibrational response of a knock. Another method of sensing the knock conditions is by measuring the ionization current across the spark plug after a normal firing in the engine [7].

The most recent development is in the in-process combustion monitoring. This is by use of optical fibres and a high-speed camera [8]. There are also other methods, such as the use of combustion chamber pressure sensors [9] and ionization flame front sensor [10].

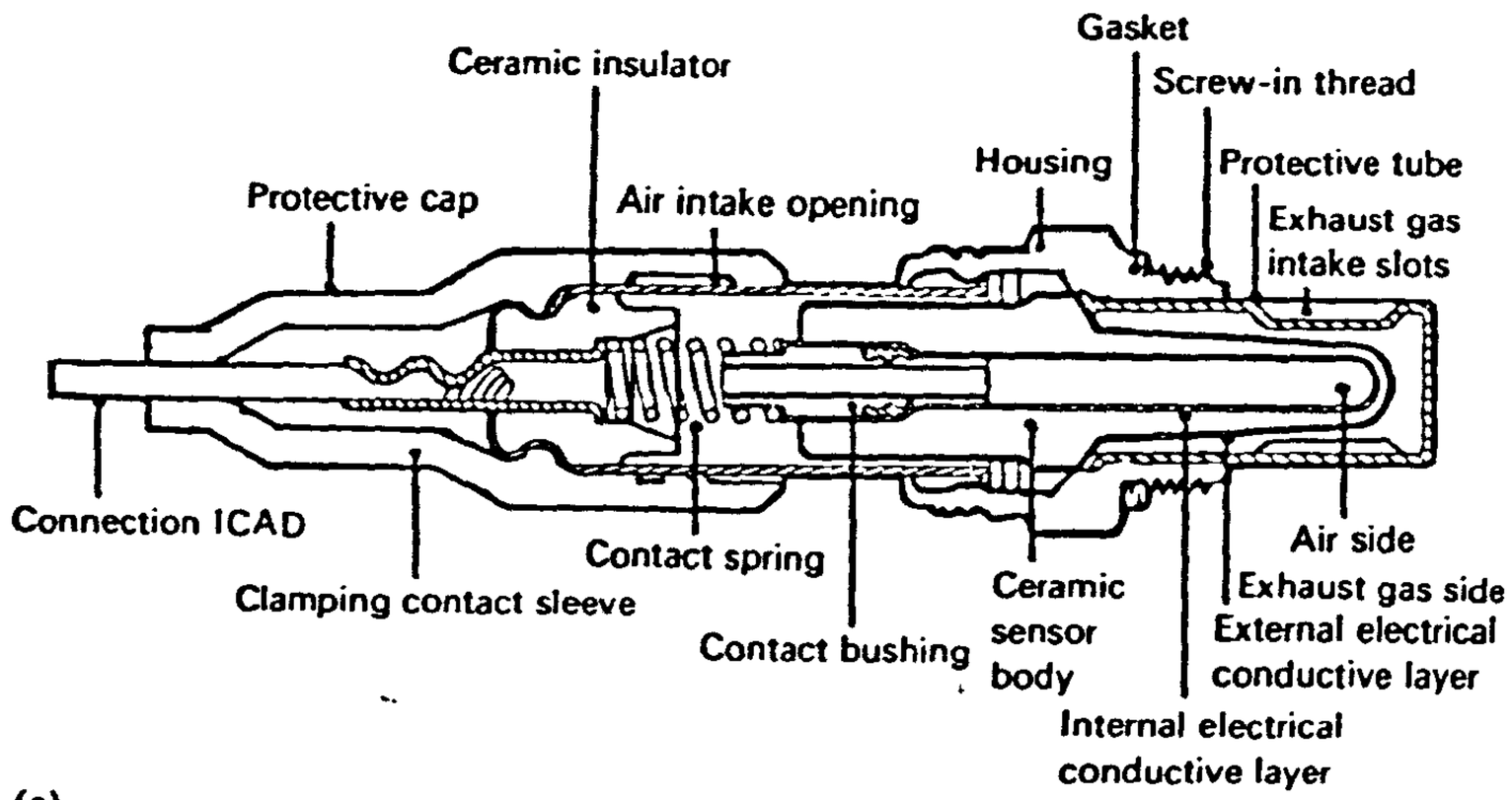

(a)

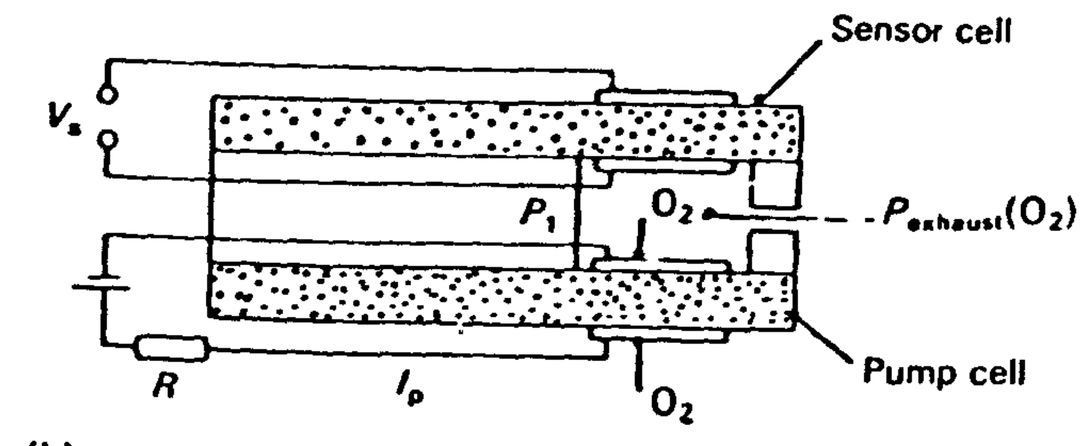

(b)

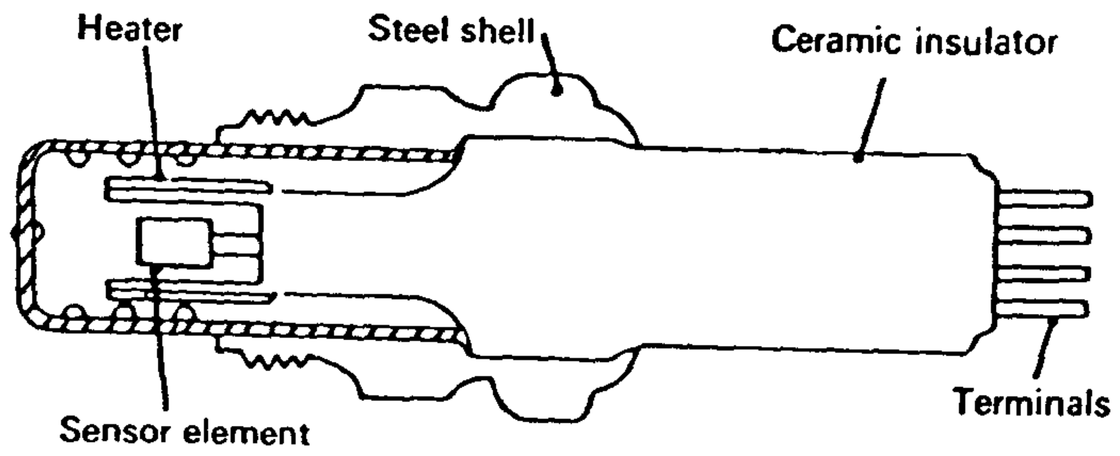

(c)

Figure 1.2 Exhaust-gas-oxygen sensor.

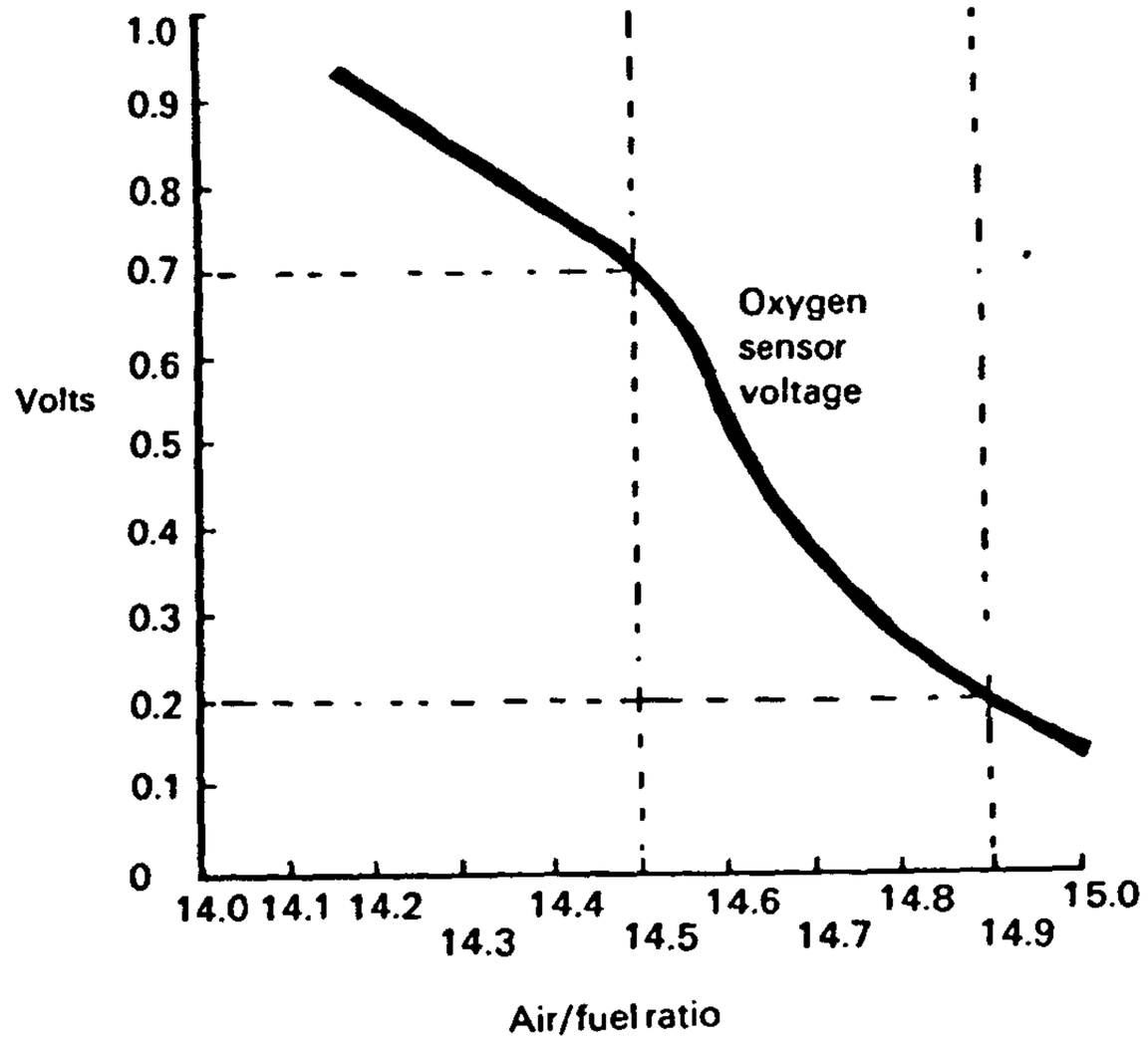

Figure 1.3 Approximate relationship of oxygen sensor voltage to air/fuel ratio.

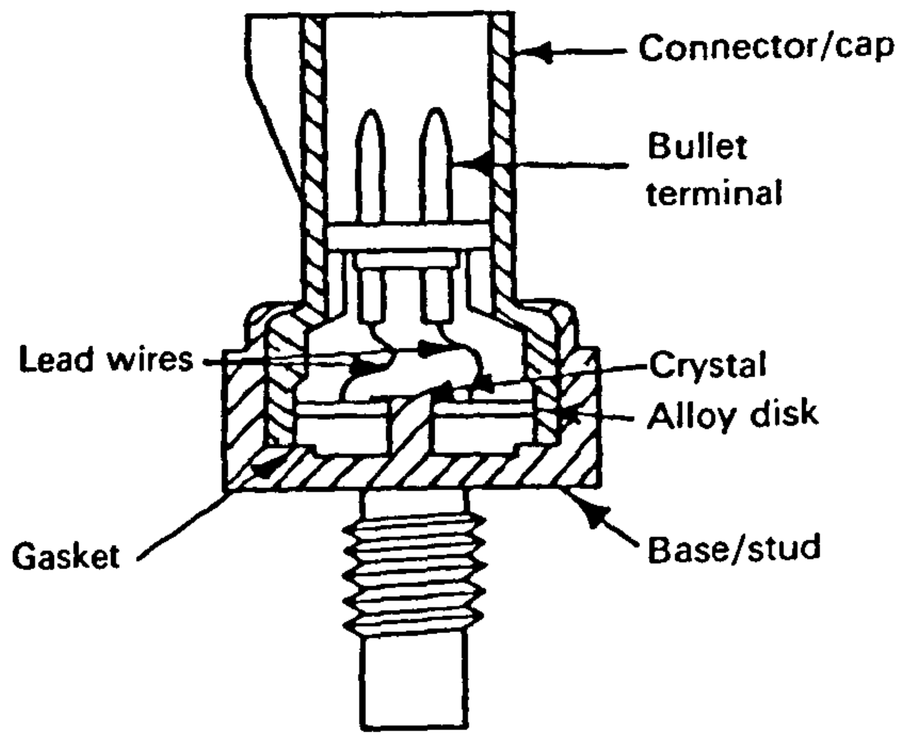

Figure 1.4 Sensor for ignition knock monitoring.

Transmission control

The transmission system provides the interface between the powerplant and the road wheels. As shown in Figure 1.5, it acts as a power match system device which is at the disposal of the driver who has the function of engaging

control. For a manual transmission system, the driver acts as part of the feedback loop of an otherwise open loop system, by sensing the engine speed and road wheel speed, and thus changing the gear ratio to match the required road torque (load). This process can be represented as shown in Figure 1.6,

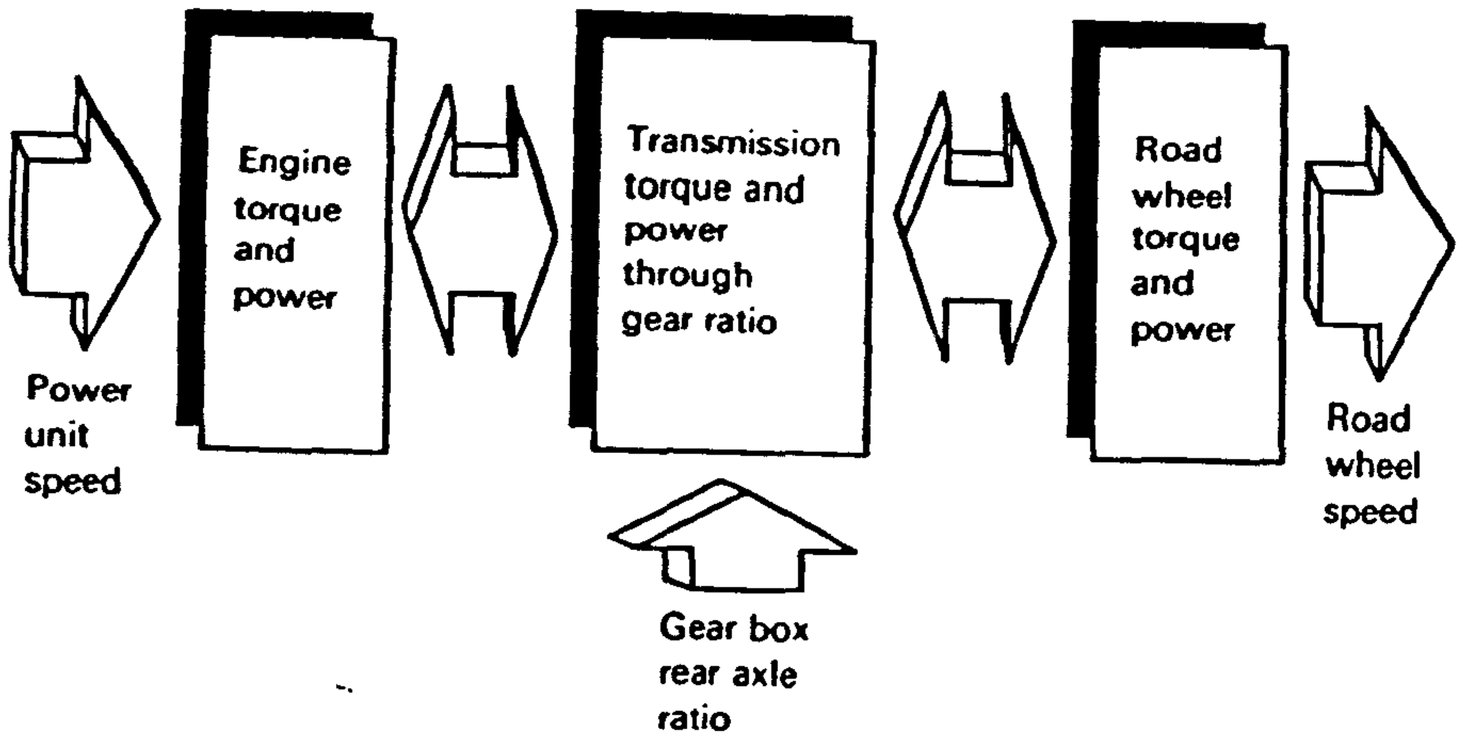

Figure 1.5 Powerplant–transmission interface.

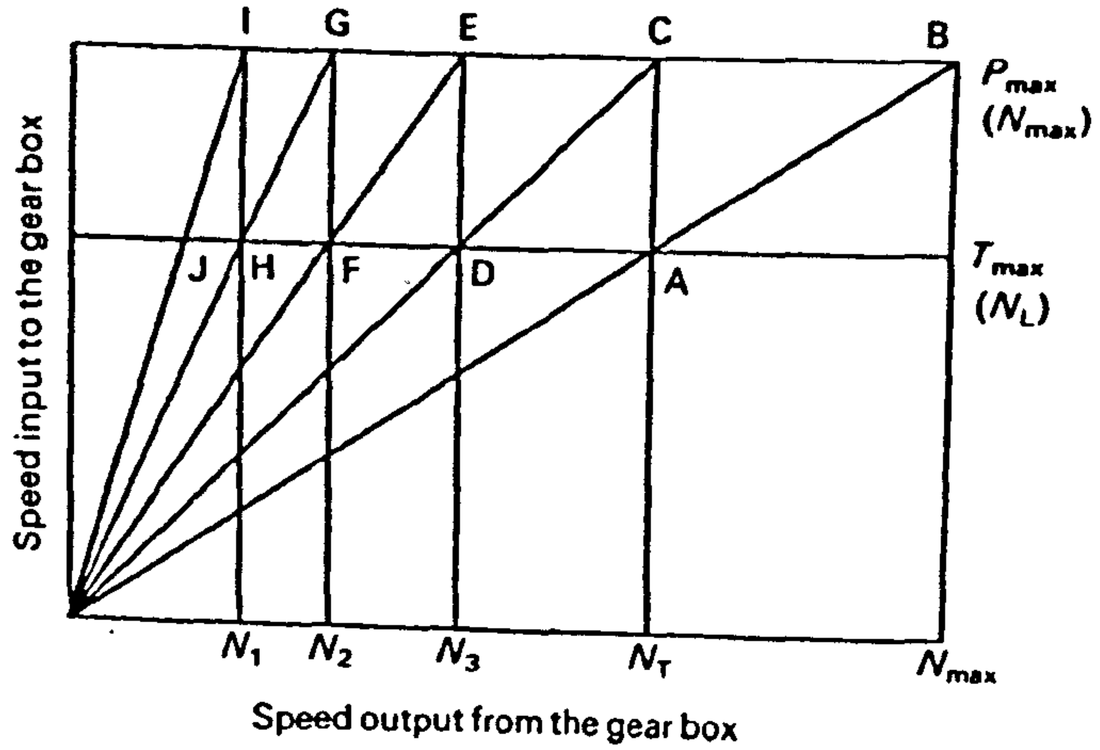

Figure 1.6 Intermediate gear ratio chart.

the load speed when the driver changes from one ratio to the other. Engine speed in the form of the pitch and noise level is one of the parameters intuitively sensed by the driver in order to provide the necessary acceleration and driveability. This is not satisfactory as a means of providing the optimum performance of the vehicle. In changing the gear ratio, the driver has the extra task of ensuring that the right gear ratio is selected.

Against this background, it is now possible to look at various sensing requirements for the transmission control. Powerplant speed information, which can be obtained from the crankshaft, gear box output shaft sensor

gear ratio required can be used [11]. There will be a need to have a sensory system (e.g. with optical sensor) which will monitor the wear conditions of the clutch plate. Some of these sensors can also be used even when operating electronically controlled automatic transmission systems designed to give a better overall performance.

1.4.2 Vehicle ride and control

The sensory systems required for vehicle ride, comfort and handling are defined as those sensors and systems aimed at vehicle chassis management and control systems [12,13]. These include vehicle suspension systems, advanced braking systems and traction control systems. The majority of the sensors used in chassis management and control systems assist the vehicle ride, which is subsequently affected by the vehicle suspension system. The suspension system will provide the focus for the different types of sensors which will be discussed.

The primary function of the suspension system is to control the attitude of the vehicle body with respect to the road surface. This includes the monitoring and control of parameters such as pitch, roll, bounce and yaw motions (Figure 1.7) of the vehicle. There are several types of suspension systems used (e.g. passive, semi-active, active) and they are well defined in

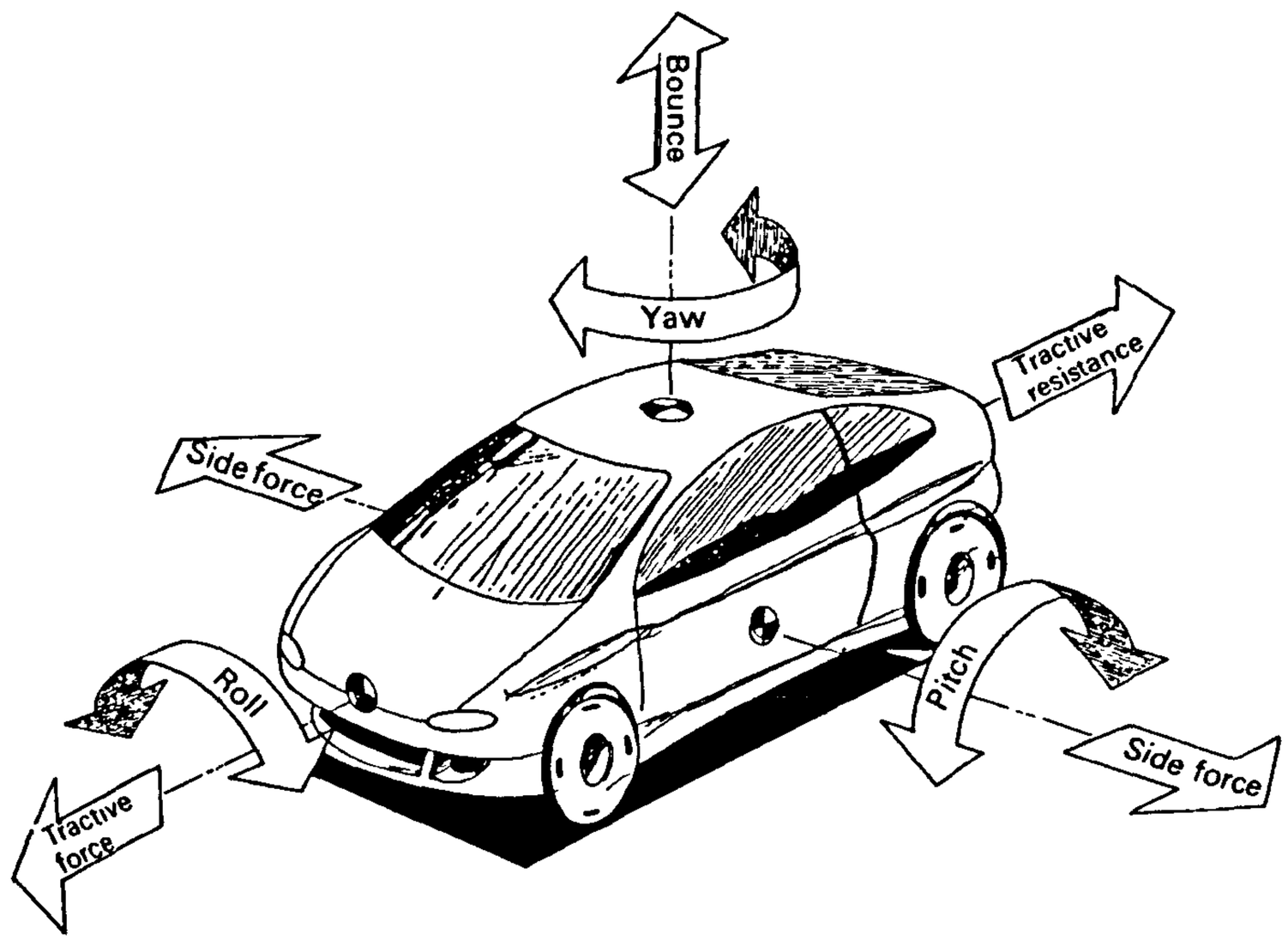

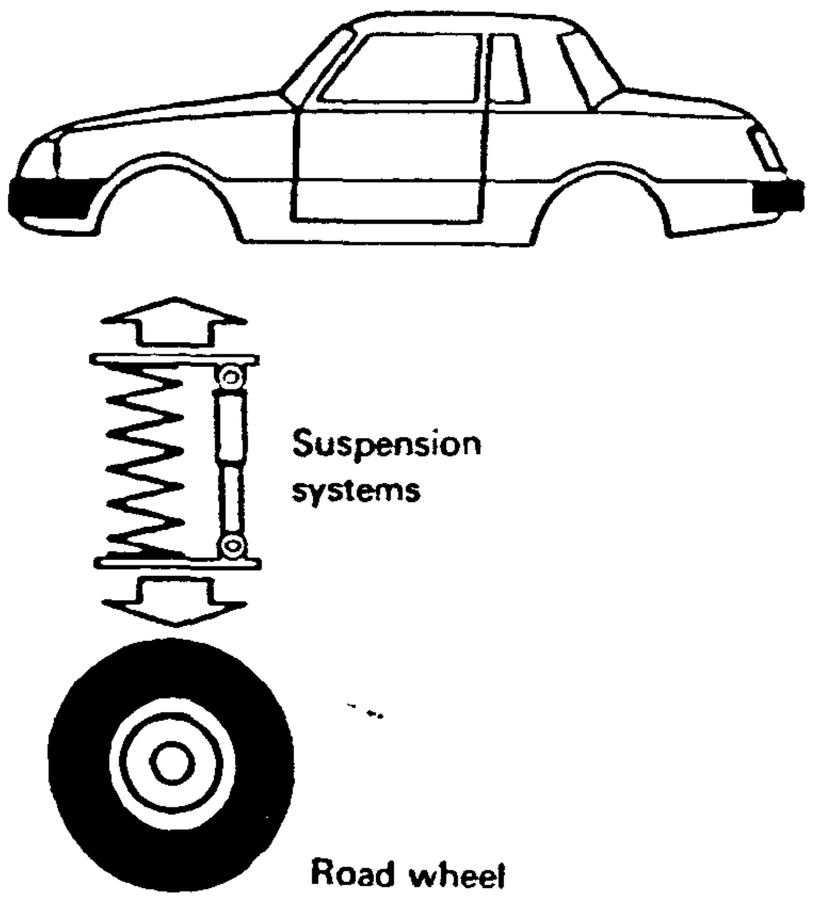

Figure 1.8 Passive suspension.

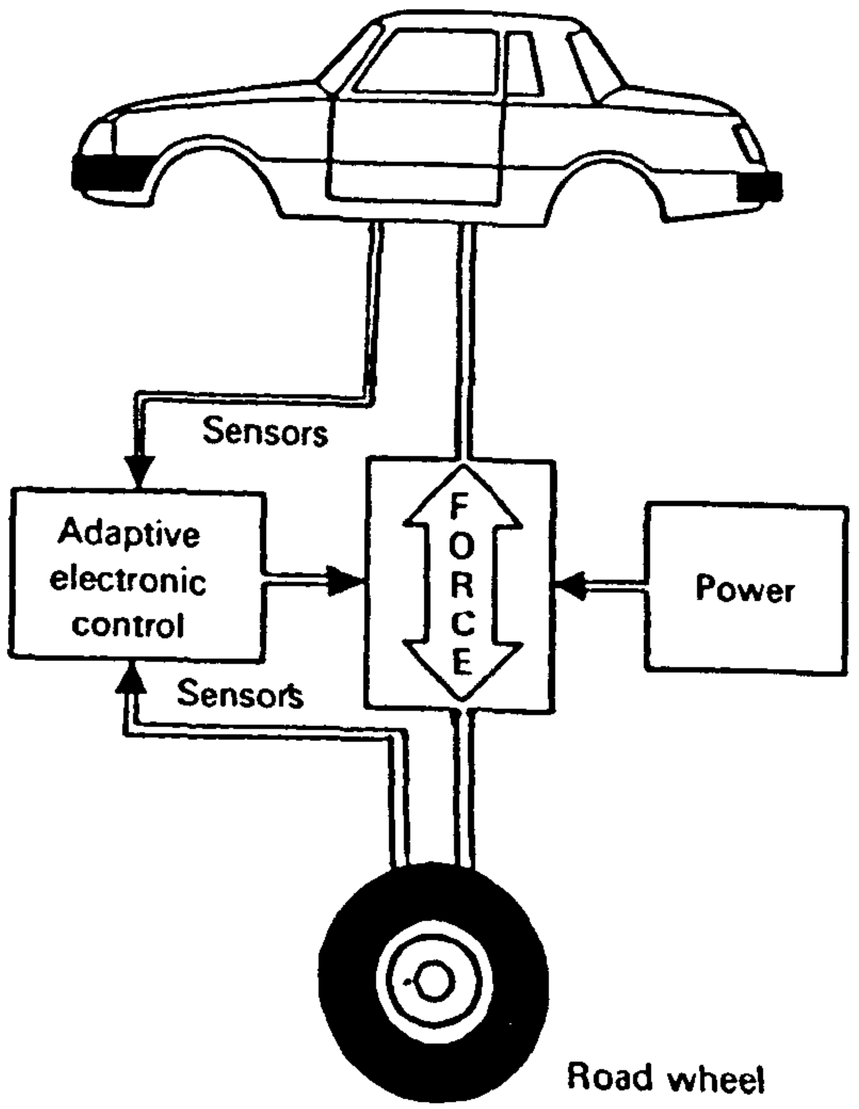

ref. 14. Although contemporary vehicle suspension systems predominantly contain passive systems which include springs and dampers (Figure 1.8), there are several advances in adaptive and active systems (Figure 1.9).

In suspension control, the main objective is to provide a suspension system which will give a suitable and comfortable ride and handling for all conditions. This requires the use of appropriate sensors and systems to monitor the necessary suspension parameters (Figure 1.7) with the necessary electronic control strategy. A control strategy is required in order to minimize the disturbance to the sprung mass and the passengers. It is also required to control the motion of the unsprung mass in order to maximize adhesion of the tyre to the ground surface during handling and ride control (e.g. traction control).

There are several controlled suspension systems available [13, 15–22], but the majority of the sensors and systems used are similar; some examples are described in ref. 22. For a typical controlled suspension system, there are sensors for monitoring the vertical displacement (bounce) of the road wheels relative to the vehicle body. This type of sensor can range from a simple potentiometer to more complex sensors such as linear variable-inductance position sensors and optical sensors which employ the principles of optical

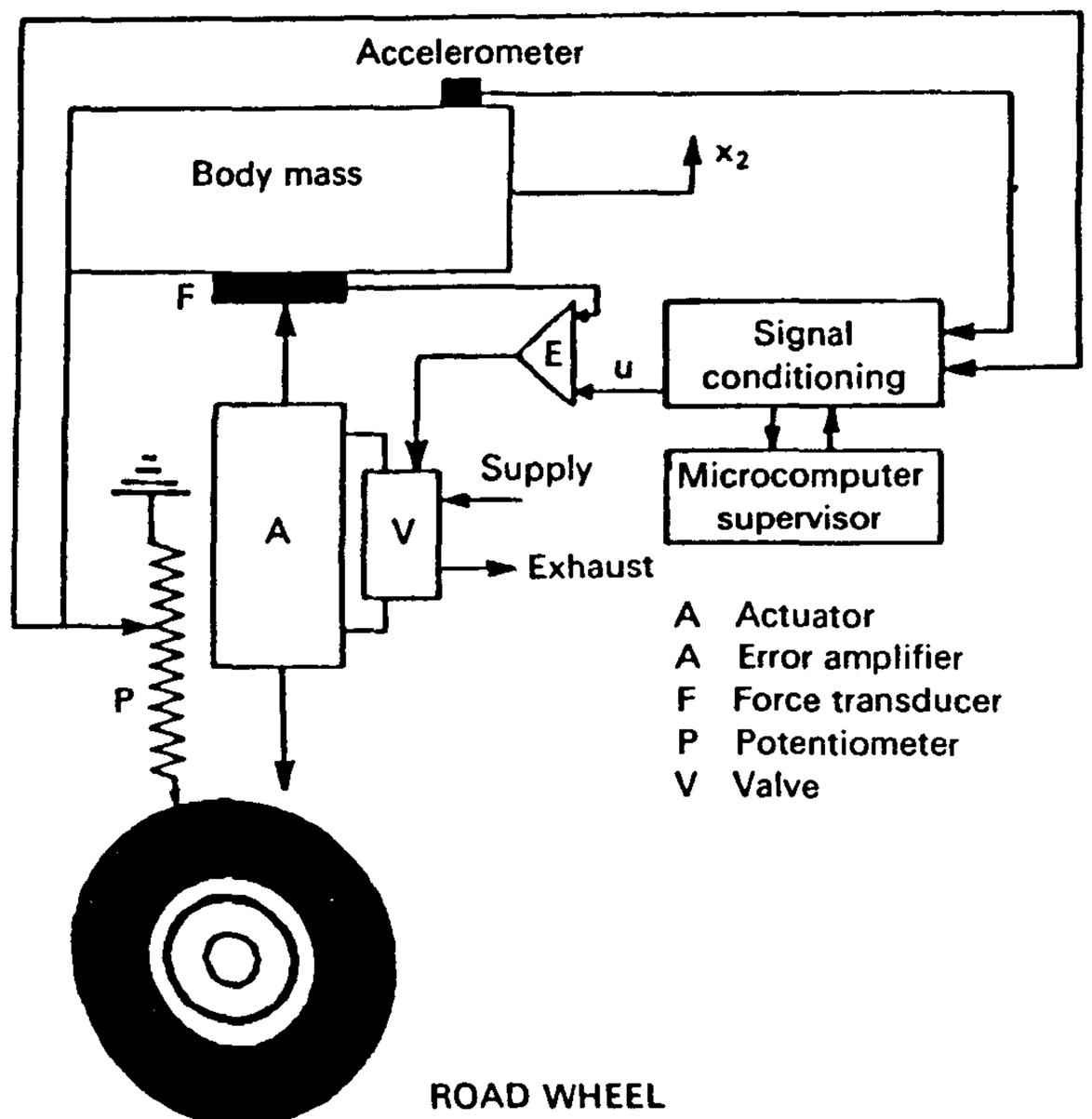

grating/Moire fringe technique for linear displacement monitoring. In some cases, sonar sensors can be used to monitor the relative vehicle body to ground vertical displacements. An accelerometer sensor and system is used to monitor vehicle body motion during cornering. As shown in Figure 1.10, the signal from the accelerometer and displacement sensors can be used to empower and control the suspension actuator with an error signal. Accelerometer sensors can also be used for advanced braking systems incorporating antilock braking (ABS)/traction control, steering systems and safety systems (e.g. airbag systems).

For the suspension control, the combination of these sensors is used to monitor and control the bounce, roll and pitch motions of the vehicle, but yaw motion can be monitored by the use of a yaw rate sensor (e.g. optical fibre gyroscope, solid-state piezoelectric devices). An integrated control strategy will include steering wheel rotation sensor (e.g. angular optical sensors–encoders), vehicle velocity sensor (e.g. road speed sensors – Hall-effect sensor) and throttle position sensors (e.g. optical sensory systems or potentiometric sensors – Figure 1.11).

1.4.3 Vehicle safety sensors

It was in 1769 that Nicholas Joseph Cugnot in France made history by constructing the world's first road vehicle. This vehicle, which was a steam-powered tricycle, sped along for 20 min at approximately 3.2 km/h. He also made history by having the world's first road vehicle accident. Since then, safety has increasingly become a very important factor to be considered during vehicle design and development. In recent times, safety requirements have necessitated the development of various sensory techniques for enchancement of vehicle safety.

Sensory systems can be used for passive and active safety systems. An example of the passive system is the supplemental inflatable restraint, which is the airbag system. This is well covered in Chapter 8. Examples of active systems are antilock brakes, traction control systems and, in some measure, tyre performance control.

Antilock braking system

Antilock brakes are an accident avoidance system which, by incorporating relevant sensory systems such as accelerometers, pressure sensors etc., can prevent wheel locking during hard braking in an emergency, especially when the road is slippery. Vehicles lose steering when the front wheels lock. An antilock braking system uses sensors at each wheel to monitor deceleration

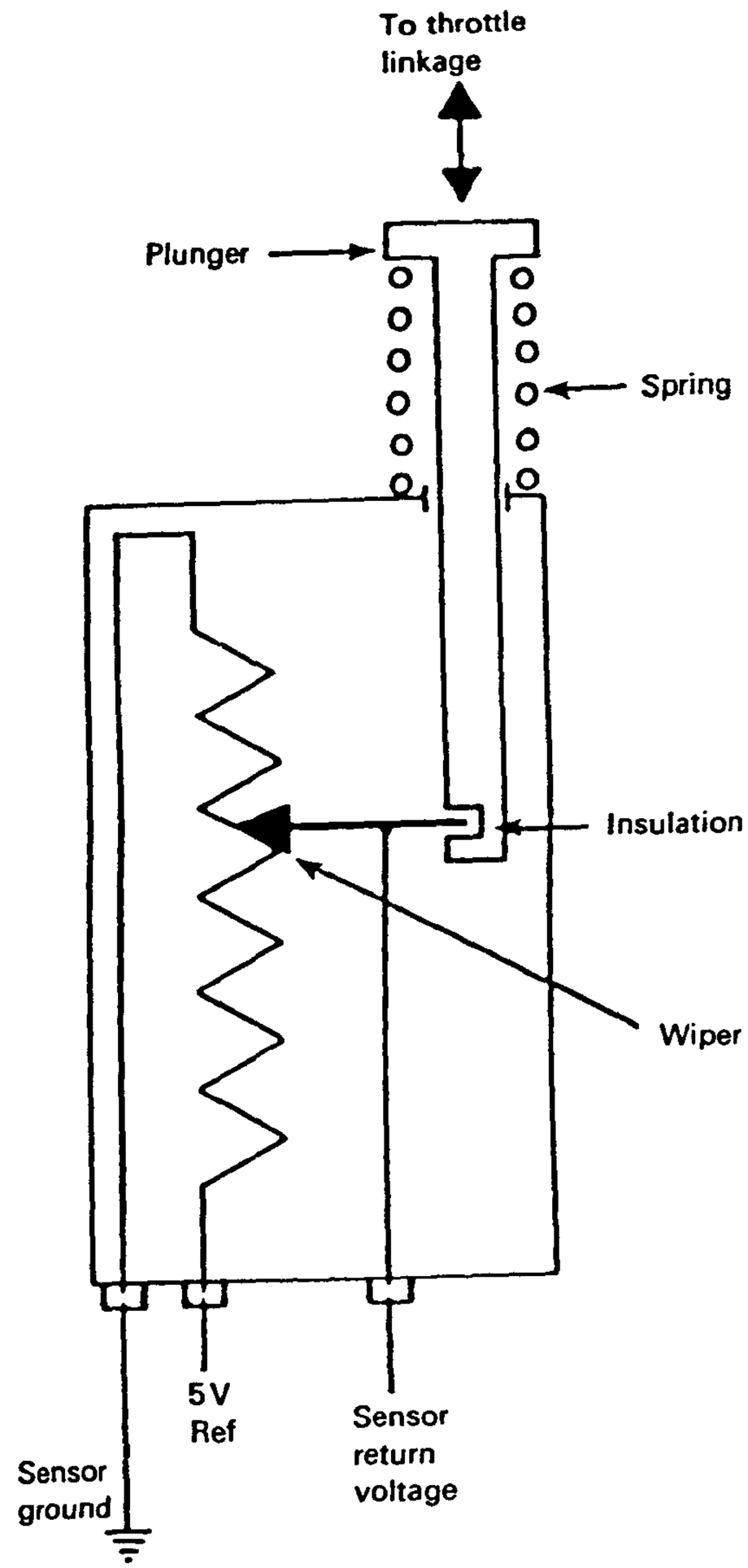

Figure 1.11 Potentiometric throttle position sensor.

wheel. So, by using the appropriate sensory system, an antilock braking system allows a driver to steer a vehicle during emergency braking.

surfaces. In most vehicles with traction control, the system works only during low-speed acceleration and is then disconnected. In more expensive vehicles, the system operates at all speeds.

The same sensors that can detect wheel lock during braking with an ABS can be used to detect uncontrolled wheel spin. In operation, the traction control system senses when one driving wheel spins faster than the other and applies pulses of brake pressure to limit its slippage. This will then allow other wheels to receive and transmit engine power, thus improving steerability and traction. The operation of the system can be linked to engine control where, if the system is in operation for more than a given time (e.g. 2 s), the engine controller cuts fuel delivery to the engine cylinder on a selective basis to limit engine rev/min. This helps to minimize stresses on the brakes, transmission and engine prolonged traction control operation. A dashboard display can be provided to show when the system is in operation.

Tyre performance monitoring

A number of parameters affect the performance of road vehicle tyres. The operational adjustable parameters which can be monitored to ensure safe and economical driving are the tyre pressure and temperature. Other parameters, such as the tyre width, tyre deflection/oscillation and wheel speed in relation to other wheels on the vehicle, can also be measured in order to ascertain tyre performance status. The parameters to monitor depend on the types of sensor, system and measurement strategy used.

The most common sensory systems used for monitoring tyre performance are the pressure and temperature sensory systems. There are various systems available which can be used for the monitoring tasks during dynamic and static conditions [23, 24]. One of the methods of monitoring tyre performance is by the use of piezoresistive pressure sensors mounted on the wheel. The pressure sensor monitors the air pressure in the tyre. A sensor for monitoring the heat generated by the tyre can also be mounted on the wheel. As the wheel rotates relative to the axle, a means must be provided to power up the sensor and transmit the sensor signal for processing and display. This can be done by a signal pick-up device such as a circular antenna mounted on the wheel. As shown in Figure 1.12, to interface with the antenna mounted on the wheel, a fixed antenna is mounted on the brake caliper with a corresponding signal decoder. This type of system operates in two phases. In the first phase, the power supply is sent to the sensor through the two antennas. This is stored in a capacitor and used in the second phase to power the sensors as they measure temperature and pressure of the tyre; there is a decoder for analysis and display. This system can be used for continuous and reliable verification of the actual tyre pressure and temperature to an accuracy of a few per cent. With efficient software, the information

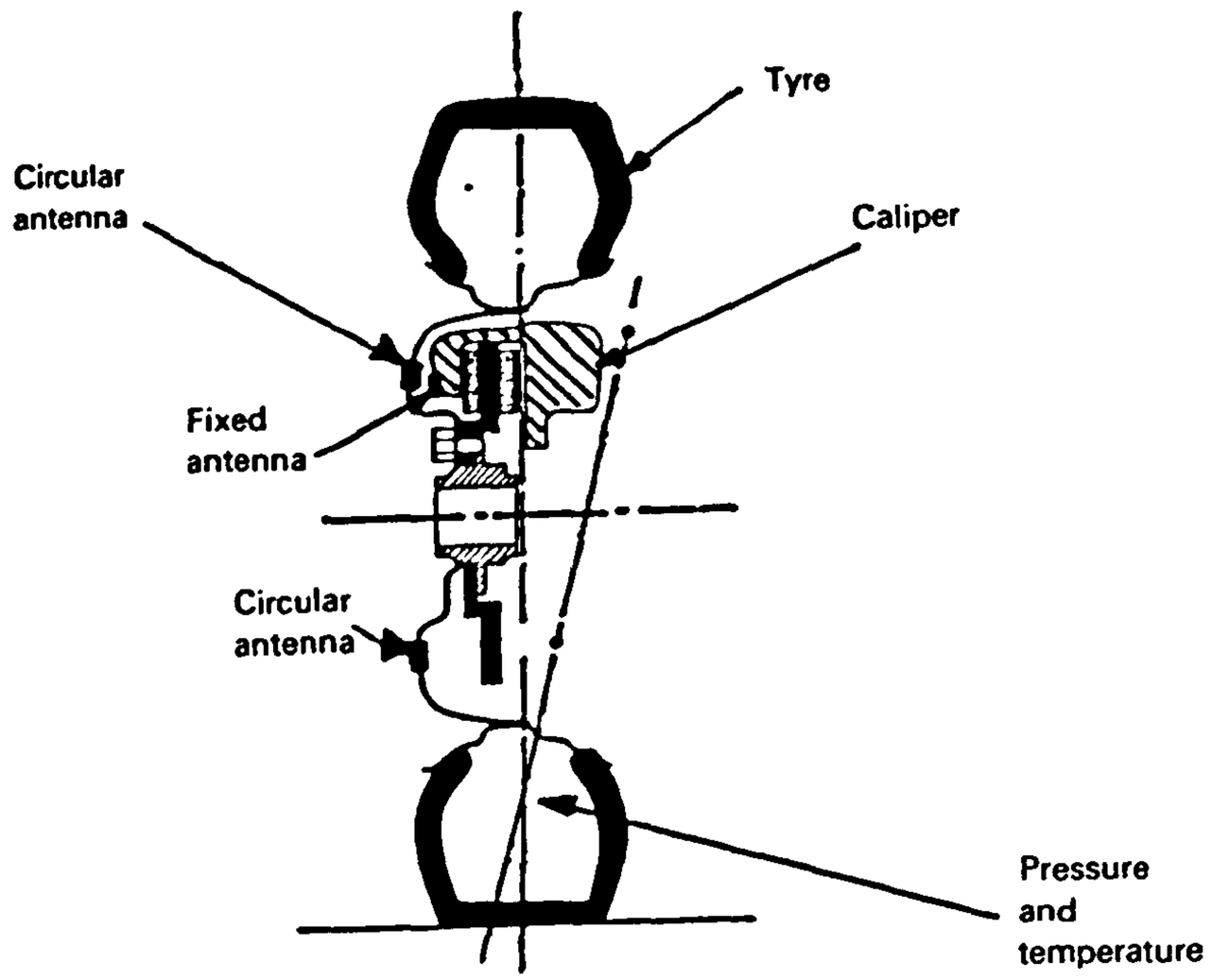

Figure 1.12 Tyre performance monitoring system.

1.5 BASIC AUTOMOTIVE OPTICAL SENSORS

As the advances in other types of sensory system for automotive applicatio continue, so also does the growth in the use of optical sensors and system for road vehicles. To complete the discussion on the current systems, som applications of optical sensors and systems for sensing linear and angula displacements will now be described.

Three major optical sensors and systems will be described; these will includ the technique which provides the signal that may be processed by oth integrated systems such as a computer processing system.

1.5.1 Linear position sensor

Linear displacement sensing has a wide range of applications in the automoti field, such as suspension systems, automated seat adjustments, and gear leve position monitoring. There have been several developments of optical senso which can sense linear positions, one of which is shown in Figure 1.13.

The sensor consists of a pair of detectors, one located at the focal poin of a lens and the other in the same plane but shifted vertically. A light source

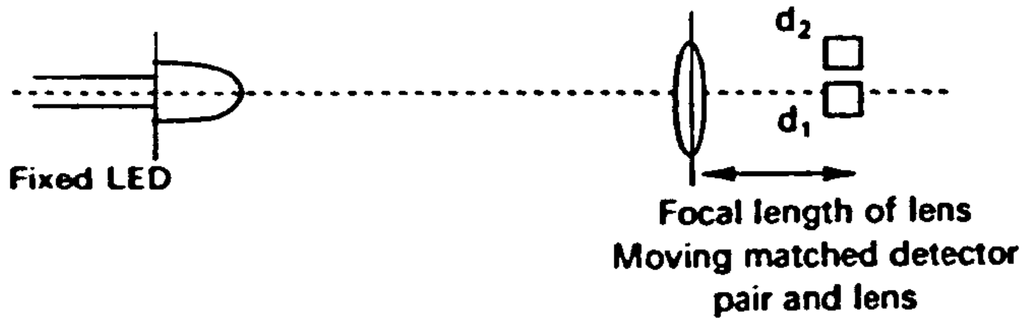

Figure 1.13 Optical linear position sensor (courtesy SIRA Ltd): d_1 = on-axis overfilled detector; d_2 = off-axis underfilled detector.

such that it is overfilled by the light that is focused onto it by the lens. The other detector is placed such that no light falls on it when the source is furthest away; as the light source moves closer, the amount of out-of-focus light falling on this detector increases.

The signal from the detector placed at the focal point is independent of the light source distance from the lens. This signal can be used as a normalizing reference. The output from the other detector is related to the inverse square of the separation between the light source and the lens, and hence it is used as the basis of the output signal.

The working principle described has the disadvantage that a light source and the detectors have to be fitted to different ends of the moving part. This can be overcome by using a retroflective device, but such a device must be kept clean and free of dirt.

1.5.2 Steering wheel rotation sensor

The type of optical sensor used for monitoring the rotation of the steering wheel is normally determined by the resolution of the steering wheel turn (e.g. 2° down to 0.3°), the space in which the sensory system will be fitted, the type of signal output to be provided, etc.

The optical sensor to be described was developed by SIRA [25] and is integrated with the steering column as shown in Figure 1.14. It consists of two types of optical sensor to take account of different styles of steering columns. The optical sensing method is the same in both types, the difference being the method of delivering light onto the sensor. One type uses a transmissive method and the other uses a reflective method. As shown in Figure 1.15, the transmissive method uses a perspex wheel fitted around the steering column. A series of darkened notches are etched on the wheel such that the wheel acts as a chopper. This provides output signals that represent right and left turns of the steering wheel. This is similar to the optical encoder

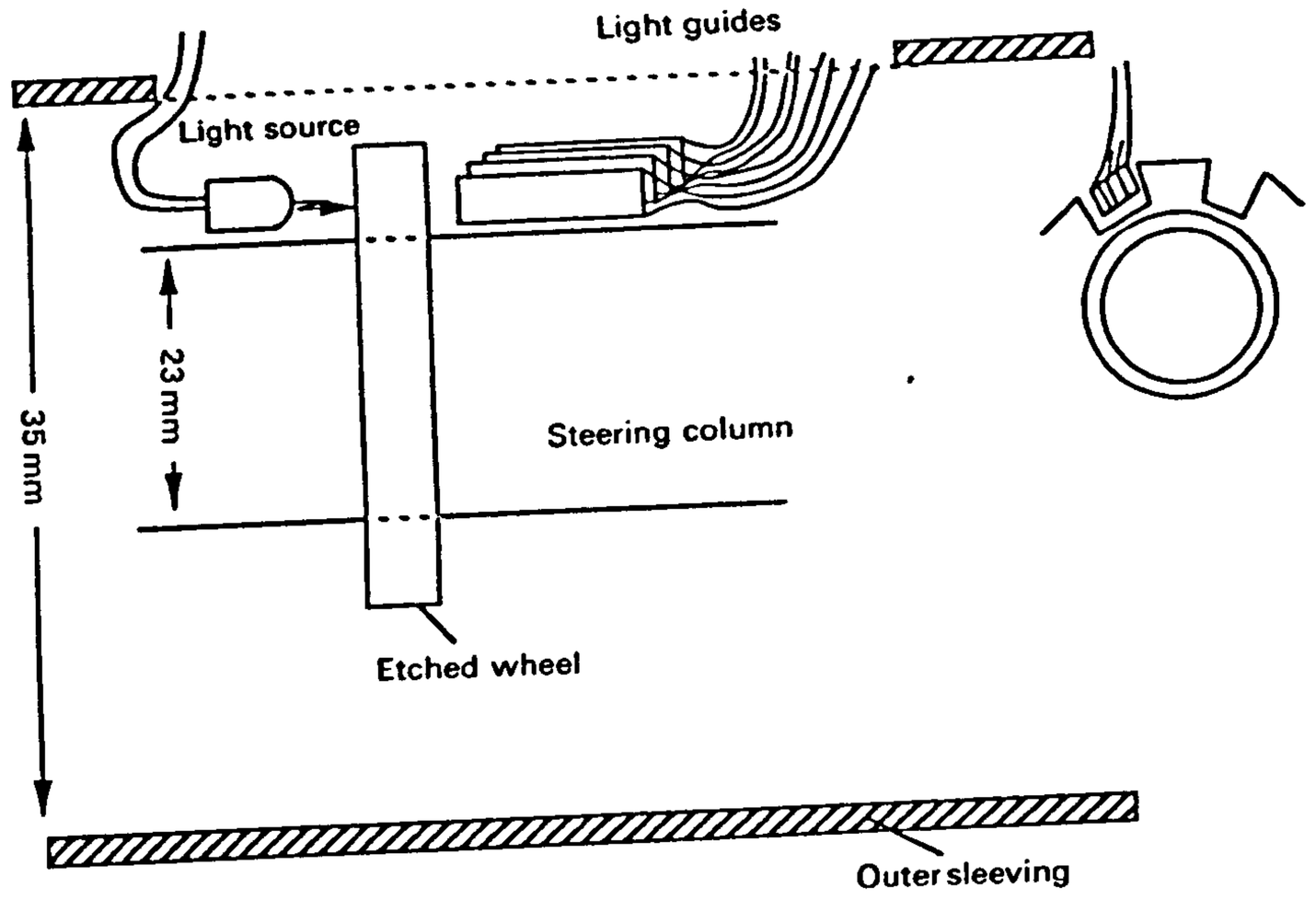

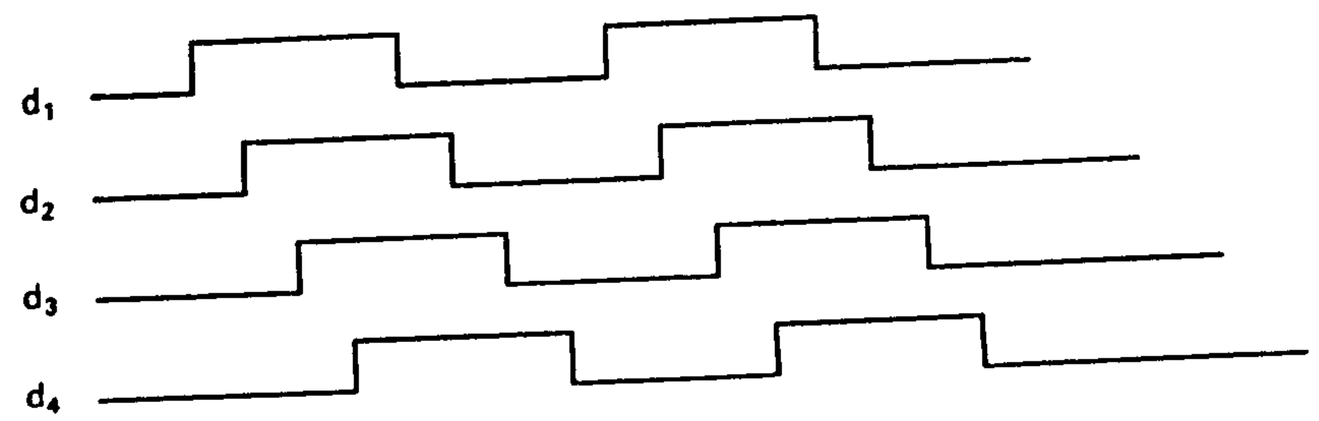

Figure 1.14 Steering wheel position sensor (courtesy SIRA Ltd).

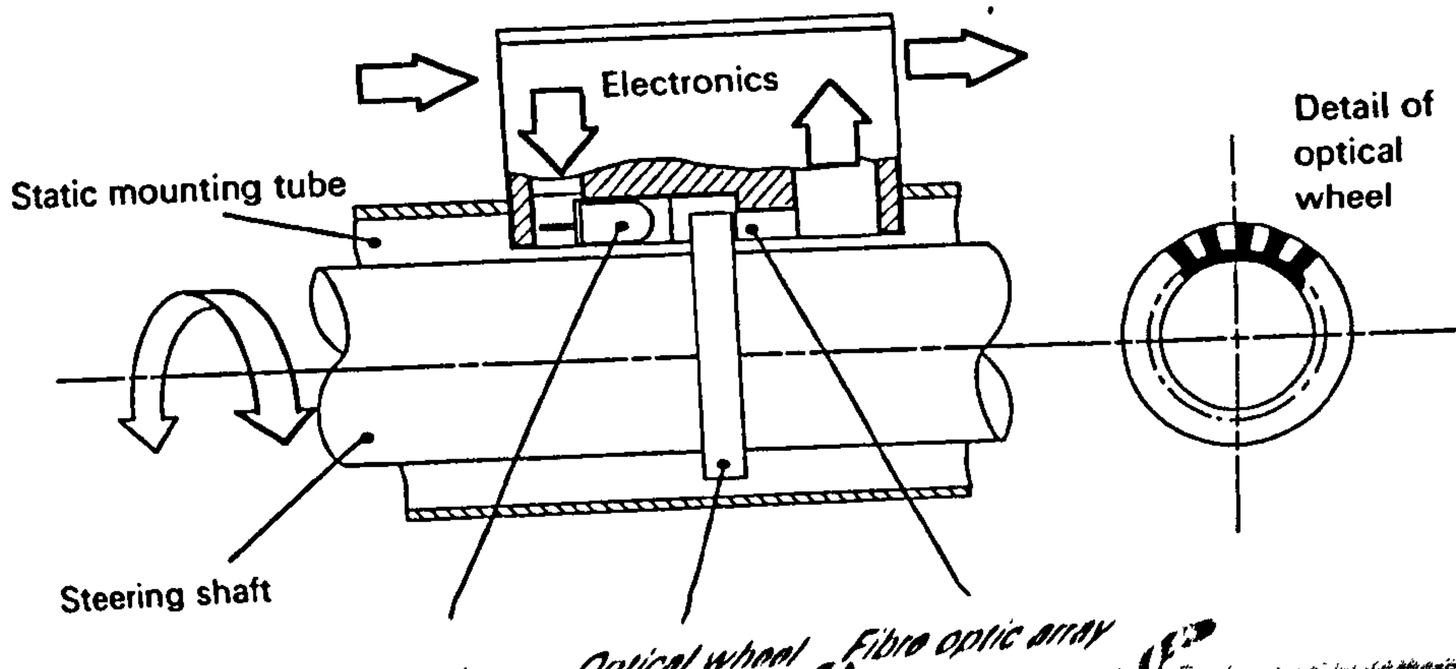

notches *N where N is the number of the light guides in the sandwich that fit into a single notch gap. The effective resolution is limited by the width of the light guides used.

A reflective method can be used, where the perspex wheel is replaced by a reflective tape, with black lines stuck coaxially onto the steering column. The light guide sandwich consists of alternate illuminating and detecting elements which are directed normally to the surface of the steering column.

The sensory signal can be in a pulse train or analogue format. With the digital pulse output, the pulse train is decoded to provide a pair of output signals that represent left and right rotations of the steering column.

1.5.3 Optical shaft encoders

To sense the angular displacement and velocity of shafts such as steering columns, propeller shafts and drive shafts (road speed sensing), adapted optical shaft encoders may be used. An optical shaft encoder is an arrangement where a circular glass disk is encoded by etching rows of broken concentric arcs of transparent and opaque regions in the form of a binary pattern. As shown in Figure 1.16, a light source is assigned to each row with a corresponding detector on the opposite side of the disk. The arcs and sensors are arranged so that, as the light is projected through the disk, the pattern of the activated light sensors is a unique encoding of the position of the shaft to within a given angular resolution. The accuracy of the encoder disk is a function of how many light sensors (binary digits) are used to make up the binary code; the number of such sensors can range up to 12.

The pattern of the activated sensors is in computer-readable binary code. The binary code generated at each of the radial positions on the disk (Figure 1.16b) is generated by a unique combination of light sensors that are 'on' or 'off'. However, problems of accuracy can occur if the angular shaft position is represented in the standard set of sequential binary numbers, as given by the encoder disk (Figure 1.16b). Such problems can occur during the change of state between the sensors when the system becomes skewed from the radial line. Another problem can occur during the change of state between the sensors when the systems become unstable. To overcome this problem the natural binary code is modified so that, at any transition point, a change in only one binary digit is required. The resulting code is known as the Gray code (Figure 1.16c); absolute encoders usually employ this type of Gray code. Gray code disk increase reliability but require the use of additional decodes circuitry to complete the sensory systems.

1.6 FUTURE DEVELOPMENTS

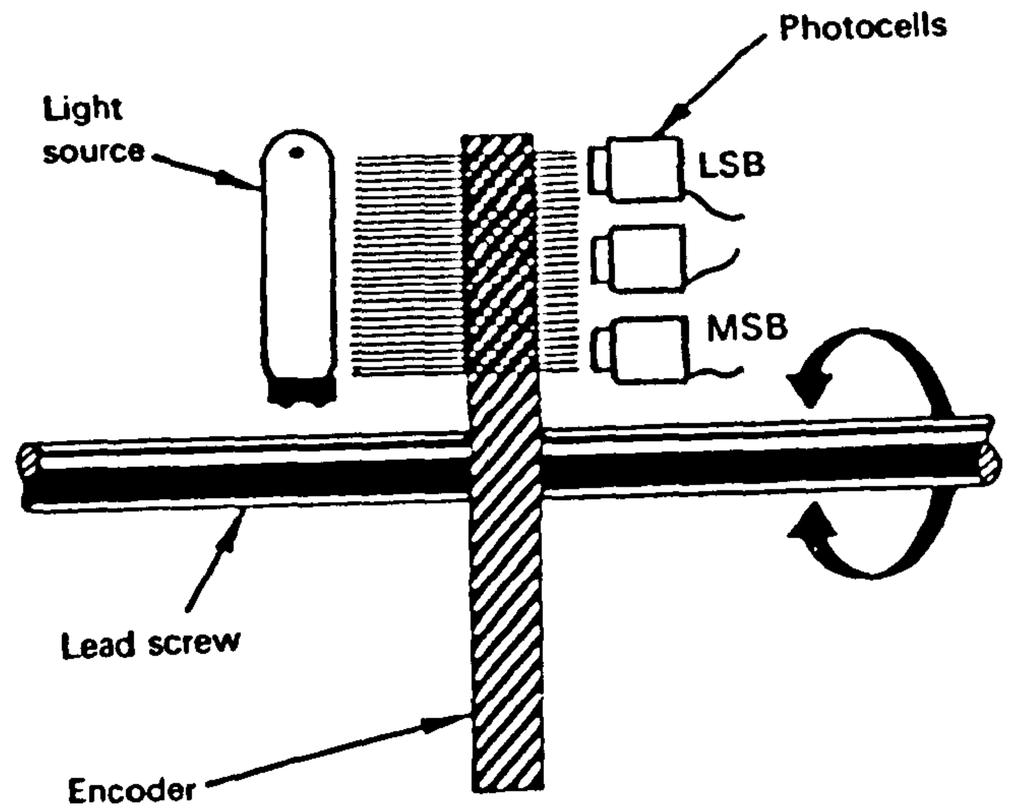

(b) Binary code (c) Grav code

Figure 1.16 Optical shaft encoder.

expand, the fast rate of such expansion makes it difficult to precisely predi
what the vehicle of the future will be without falling into the trap of qu
rightly predicting the future vehicle as a smart road vehicle with some fo
of intelligence able to self-diagnose, manage and take complex decisions
its performance and vehicle navigation. It is easier to categorize the use
sensory systems for road vehicles into their near-term technology and mo
adventurous and futuristic technology expected to mature into productic
at the end of the decade. Smart sensors and systems will play importa
roles in the near-term and future road vehicle.

The near-term sensory technology will include intelligent cruise contr
systems, automatic route guidance systems and enhanced vision systems
Intelligent cruise control systems will include the use of radar sensors linkec
to electronic devices which will maintain a set time interval of separation

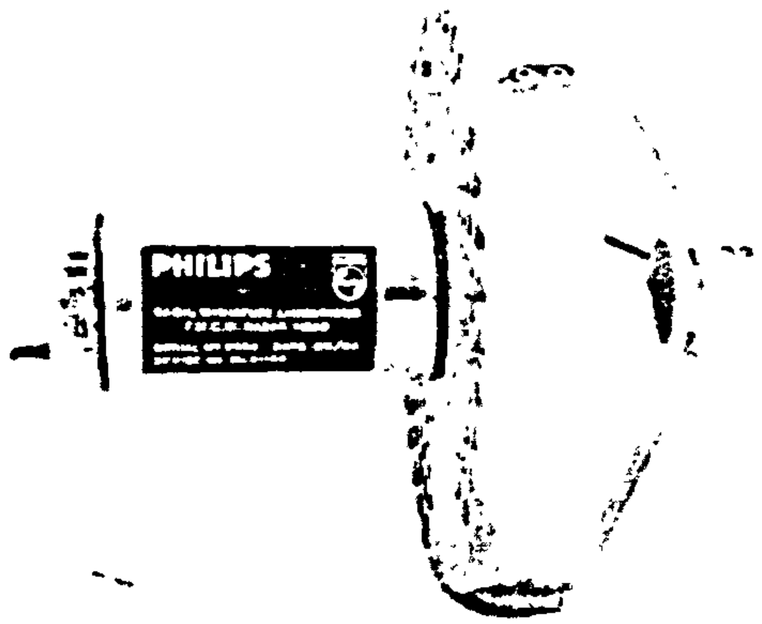

(a)

(b)

(c)

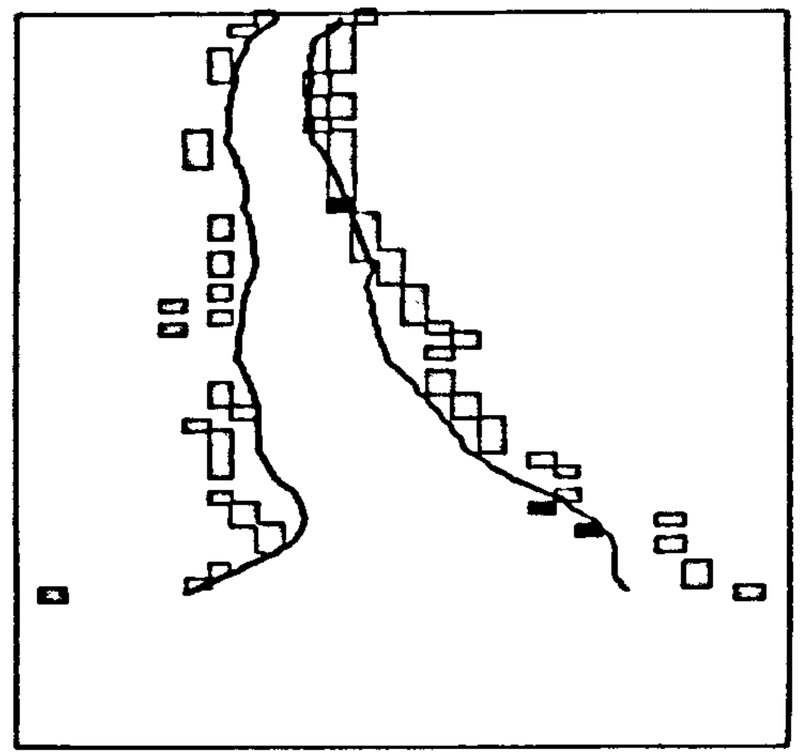

(d)

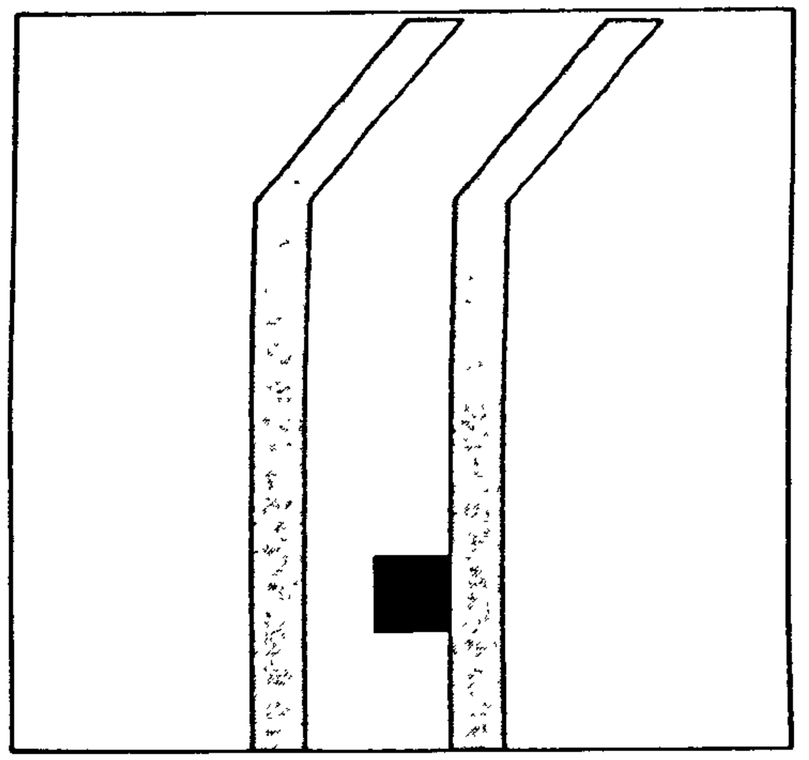

(e)

Figure 1.17 A vehicle obstacle avoidance radar system: (a) a radar antenna mounted on a vehicle; (b) country road being monitored by radar; (c) drawing of a raw radar map produced by the sensory system; (d) drawing of a processed radar map produced by the sensory system; (e) drawing of an enhanced map with blip to show target within roadway. (Courtesy Philips Research Laboratory, Redhill, UK.)

technology will obviously increase; some such safety systems will include the use of optical and visual sensory systems.

Systems which can be categorized as a long-term technology will involve the use of near infra-red illumination to increase the driver's depth of vision in conditions of low contrast, and at night. Some of the sensory technology will involve the use of thermal imaging sensors that utilize far infra-red

pedestrians at a far distance on the road will show up as white spots on the driver information display system.

The development of integrated collision avoidance systems with various sensory systems utilizing optical infra-red, radar and ultrasonic devices to detect where the road lies in poor visibility will continue. These systems will be capable of locating obstacles such as vehicles, people and objects that are likely to cross the driver's path. The system will have the intelligence to assess what threat is posed by the obstructing object and what help should be provided to the driver to select an appropriate course of action. Such a system may have the power of controlling the vehicle autonomously in the event of danger and accident. There are various basic systems being developed across the world at present. A typical example is the car collision avoidance system currently being developed at the Philips Research Laboratories. The sensory system uses a radar technique which draws the driver's attention to obstacles which are potentially hazardous. Shown in Figure 1.17a is the radar antenna which is mounted on the vehicle. This continuously transmits a signal which is acquired by an on-board computer system. In the event of any obstacle, the computer calculates the distance of the obstacle from the time taken for the radar signal to return from it. The obstacle's size is also calculated from the change in the signal frequency. Figure 1.17b shows a typical country road, and a drawing of a radar map of it is shown in Figure 1.17c. The map is processed in colour. Figure 1.17d shows a similar drawing in which the outlines of the road edges are depicted by black lines, with targets such as the road hedges (Figure 1.17a) illustrated by the shaded boxes (Figure 1.17d). The solid boxes at the right-hand road edges of Figure 1.17d are targets within the roadway. A concept for a driver information display format is shown in Figure 1.17e. The radar system may link with antilock braking or traction control to automatically trigger braking when a crash is imminent, thus minimizing or avoiding impact.

There will be a growth of sensory systems for co-operative driving which will allow for inter-vehicle communication. Such a system will provide the devices which will interact with cellular phone networks, satcom, satellite ground stations and satellite to track road vehicles. The integrated communication will form part of route planning and information exchange systems.

The vast number of sensory systems which will be made available for road vehicles will demand that expert systems are developed for multi-sensor fusion technology. The use of a neural network system which will monitor, through the multi-sensory systems, driver behaviour/reaction, vehicle performance, and control and navigation systems will be developed. This will require advanced data processing techniques to rationalize the sensory information and possibly *to take necessary system decisions. These will*

Other future systems could include those that use fuzzy logic and neural networks to monitor steering patterns, sounding an alarm when events such as no steering or unusually large movements indicate a driver may have dozed off or be intoxicated. There will be further developments in intoxication and sleep sensory systems; these can be linked to various interlock systems in the vehicle.

1.7 CONCLUSION

Undoubtedly, the automation of road vehicles has offered one of the greatest opportunities in the use of automotive sensors. This chapter has only presented introductory information on some of the sensory systems available. The description of some of the sensors has been cursory. These are the sensors which will be covered in more detail in subsequent chapters. Some of the sensory systems not covered in subsequent chapters have been discussed in more detail in this chapter. The future developments in automotive sensory systems have been discussed; there is no doubt that these sensors will be instrumental in revolutionizing and enhancing the performance and safety standards of road vehicles.

REFERENCES

1. Paulsen, J.J. (1989) The state of automotive electronics in the year 2000: perspective of the North America marketplace. *I. Mech. E.*, C39/KNI, 1–63.
2. Rivard, J.G. (1986) *Automotive Electronics in Year 2000.* SAE Technical Pap No. 861027.
3. Wolber, W.G. (1978) *A Worldwide Overview of Automotive Engine Control Senso Technology.* SAE Technical Paper No. 780207.
4. Fleming, W.J. (1982) *Engine Sensors: State of Art.* SAE Technical Paper N 820904.
5. Westbrooks, M.H. (1988) Automotive transducers: an overview. *IEE Proceedin* **135**, pt D5, 339–47.
6. Bertuol, B. (1991) Sensors as key component for automotive systems. *Sensors Actuators.*
7. Blauhaut, R.B., Horton, M.J. and Wilkinson, A.C.N. (1983) A knock detect system using spark plug ionization current, 4th International Conference Automotive Electronics (late paper not included in the proceedings), IEE, Lond
8. Nwagboso, C.O. and Pendlebury, M. (1992) Fibre optics for combustion pro monitoring of CNG engine. *Internal Communication VSRC*, 3.
9. Rhodes, D.M. and Weson, M.J. (1983) The petrol engine: a case of closed l control. *IEE Conference*, **229**, 62–6.
10. May, M.G. (1984) Flame Arrival Sensing Fast Response Double Closed L Engine Management. SAE Technical Paper No. 840441.
11. *Nwagboso, C.O. (1992) Integrated sensing technique for intelligent gear chang Systems in Advanced Vehicle Control, Proceedings of the Society o*

13. Mizuguchi, M. *et al.* (1984) *Chassis Electronic Control Systems for the Mitsubishi Galant*. SAE Technical Paper No. 840341.
14. Nwagboso, C.O. (1991) *Vehicle Dynamics*, Lecture Notes, BEng Automobile Engineering, Bolton Institute, UK.
15. Karnopp, D. (1983) Active damping in road vehicle suspension systems. *Vehicle System Dynamics*, 12, 291–311.
16. Dominy, J. and Bulman, D.N. (1985) An active suspension for a Formula 1 Grand Prix Car. *ASME Transactions, Journal of Dynamic Systems, Measurement and Control*, 107, 73–8.
17. Poyser, J. (1987) Development of a computer controlled suspension system. *International Journal of Vehicle Design*, 8, 74–86.
18. Cho, D. and Hedrick, J.K. (1985) Pneumatic actuators for vehicle active suspension applications. *ASME Transactions, Journal of Dynamic Systems, Measurement and Control*, 107, 67–72.
19. Yokoya, Y. (1974) *Toyota Electronics Modulated Suspension (TEMS) System for the 1983 Soarer*. SAE Technical Paper No. 840341.
20. Milliken, W.F. (1988) *Active Suspension*. SAE Technical Paper No. 880779.
21. Goto, T. *et al.* (1990) Toyota active control suspension system, in *22nd International Symposium on Automotive Technology (ISATA)*, Italy, pp. 857–64.
22. Prosser, S.J. and Moore, J.H. (1992) Advances in automotive sensors, in *Sensors and their Application V*, Institute of Physics, 1992.
23. Anon (1990) MTM – the intelligent monitor. *SAE Australian Journal*, May/June, 20–1.
24. Gay, P. and Bugnot, D. (1989) Real Time Tyre Pressure Electronic Monitoring System with Dashboard Possibility. SAE 221, Autotechnologies.
25. Goodyer, E.N. (1989) An overview of a range of novel automotive sensors. *I. Mech. E. Proc. Conf.* C391.

CHAPTER 2

Sensors in automobile applications

2.1 INTRODUCTION

The availability of more and more powerful and less expensive microelectronic devices for the vehicle, as in many other fields of application, represents the strongest innovative thrust able to satisfy and harmonize the demands of the individual with those of the community in terms of performance, safety, reliability, protection of the environment and resources.

Not only are technological developments in microelectronics and computer science fundamental elements in achieving these targets, but so also is the availability of sensors suited to control and perform system diagnostics. The development of new reliable and low-cost sensors planned for use in the automobile field has been made necessary. The progress which took place both in technologies and materials has allowed the acquisition of new sensing by means of new transducing principles or others which are already well known and used in other fields.

A thorough analysis of these components is quite complex, just as it is risky to actually classify the range of materials or technologies for future automotive sensors. However, it seems possible to foresee, with a certain degree of confidence, that there will be a greater appreciation of materials and technologies, allowing total or at least partial integration of sensors with conditioning electronics.

2.2 ENGINE CONTROL SENSORS

The necessity to check exhaust gas composition to limit urban traffic pollution and to reduce consumption forced the adoption of an engine electronic control system.

At the very beginning, the electronic control system included separate

increasing the slot width resolution. In addition the detectors are inherently matched which simplifies the electronic design and setting up procedure, and light losses are minimised, improving detector response.

The sensor package size has been further reduced by incorporating some of the signal processing electronics in the array package.

1.3 High Resolution Solution

Higher resolutions are usually obtained by either reducing the slot width or increasing the diameter of the chopper whee Ultimately however this approach is limi ed by the actual geometry of the steering column assembly. Smaller slot widths will also eventually stop the sensor functioning reliably, if at all, usually because there is insufficient light available to obtain a response from the detectors. As the geometries get smaller so too the manufacturing difficulties will increase.

Sira improved the resolution of the basic sensor concept by an optical techniq that has the added advantage that the coll ting area of the detector can actually be larger than the slot width. Figure 1.d shows the optical arrangement of the high resolution sensor. The concept is the same in that a chopper wheel is placed between a light source and a detector, but in addition a second identical chopper wheel is added and a lens is used to image the first wheel onto the second wheel. Because the lens inve ts the image of the first wheel as the wheels move in one direction the image moves in the opposite direction, effectively doubling the resolution of the slot pitch. The signals seen by the detectors are a pair of zero order Moire f inge patterns as used by many optical linear d splacement sensors as opposed to a series of ON & OFF pulses.

The detectors can now collect light from the h ole of the fringe pattern. This means that large sensor areas can be used, which has the dual advantages of low price and greater sensitivity.

2 FUEL LEVEL SENSOR

The fuel level sensor was originally developed for Drum Instrumentation Ltd for use in petrol delivery ro d tankers and is now in full scale production. The success of this development has resulted in the design of a number of spin-off products, most note ly a robust and accurate density probe for use with a range of fluids, and tank contents gauges for use with different fuels such as LPG.

The road tanker sensor is approved by the United Kingdom Weights and Meas es Department and is now in every day use. It is accurate to 0.15% and is available in a range of sizes capable of measuring tank volumes up to 1500 gallons.

Recently the Ford Motor Company sponsored Sira to investigate whether or not the design could also be used as the b is of a low cost level sensor for use in car uel tanks. This study was successful, and a new low cost sensor is now under development.

2.1 Operating Principle

The sensor's operating principle was derived from an existing concept developed by Marconi for measuring the level of electrolyte in aircraft batteries. The sensor is a tuned electromechanical resonator, which is achieved by attaching pairs of piezo electric crystals to the orthogonal axes of an aluminium rod. One crystal vibrates the rod whilst the other acts as a pickup. The loop is closed electronically by a phased lock loop circuit. When the rod is immersed in a fluid the resonant frequency changes. As the amplitude of the flexural vibrations created is extremely small (less than 1 micron), the change in resonance is primarily due to the mass of fluid that adheres to the rod, and not to sheer (or viscous) forces in the fluid. The sensor therefore measures true mass. Tank contents is calculated by an integral microcomputer using this data and information obtained from a number of oth r sensors that monitor fluid density and temperature. A calibration table of the tank shape is stored in a look up table, and is used to convert the level reading into a volume. Figure 2.a shows a schematic of the sensor, figure 2.b is a picture of a real sensor.

The basic design gives rise to an extremely accurate sensor; this is needed in order to meet the strict Weights & Measures requirements applying to road tanker operation. However variations of this design are available at a lower cost and can also boast excellent performance specifications. The density probe can be obtained as a separate item and has found a wide range of applications, most notably in oil exploration drilling operations.

3 DIM DIP SENSOR

First Inertia Ltd engaged Sira to develop a Dim Dip sensor that would be capable of automatically dipping a car's headlamps at night whenever an oncoming vehicle is seen on the opposite side of the road, or when the car comes close to a preceding car. In this respect the sensor is in advance of its competitors in that it is sensitive to both white headlamps and red tail lights.

3.1 Principle of Operation

Detecting an oncoming bright light source in itself is not a problem. The difficulty with this application is that the sensor has to 'look' at the correct place, and respond to both white headlamps and red tail lights in a different direction. The bulk of energy radiated from a tungsten lamp is in the infra red, and as the sensor is also required to respond to red tail lights a silicon detector (which has its sensitivity peak in the near infra red) is used. An infra red detector is also less sensitive to ambient visible light. The correct field of view is obtained by a low cost lens and a barrel shaped mask that takes account of the lens aberrations. Simple electronics threshold the detected signal and provide a switch output. Figure 3.a is a schematic of the sensor operation, and figure 3.b is a picture of an actual production sensor.

4 FUEL FLOW SENSOR

Sira developed the Fuel Flow sensor for the Ford Motor Company. The first prototype was constructed in 1986 , and was handed over to Sira's independent Instrument Evaluation Division for evaluation. The results of these tests showed that the sensor's optical principle is viable, but highlighted problems with the performance of the electronic signal processing unit, which is the subject of further research. The fundamental measuring principle is however sound, and can be used in other similar applications.

4.1 Operating Principle

Small particles of contamination are always present in fuel, and are carried along with it through the fuel lines. It is the presence of these particles that is the key to the sensor's operating principle. A transparent tube is placed in the fuel line and is illuminated by off axis light sources (see figure 4.a). such that no light will normally appear at the collecting lens. Particles carried along in the fuel will scatter the light so that some will fall onto the lens. The lens focuses the image of the illuminated particles onto a Fresnel beam splitter, which sends light alternately to the two collecting channels. The outputs from these channels are sinusoidal signals produced by particle images travelling along the length of the beam splitter. These signals are in antiphase.

The difference between the outputs of the two collecting channels is determined by the electronic signal processing unit. This will enhance the information obtained from the antiphase flow signals and remove common mode noise. The resulting sine wave output is squared up and used to generate a pulse train, the frequency of which is directly related to the fuel flow rate.

4.2 Sensor Assembly

Figure 4.b is a schematic drawing of the prototype sensor construction. This schematic shows fibre optic light guides as the means to bring the illumination into the sensor body and to take the collecting channel return signals away. This permits the electronics to be housed remotely from the sensor, away from the harsh engine environment. A lower cost solution was also developed which replaced the fibre assemblies with direct illumination and sensing using automotive light bulbs and low cost silicon detectors. Either approach is viable.

Figure 4.c shows the finished prototype sensor.

All optical components other than the tube are of plastic construction. The tube is glass, but could be substituted with plastic in a final model. The sensor does not use costly components or materials, and is a good example of how optical sensing can provide a low cost solution that is inherently immune to the electrical noise problems that are always present in the engine compartment.

4.3 Sensor Evaluation

A series of tests were carried out on the prototype sensor primarily to establish whether or not the optical sensing principle was viable in practice. Of particular interest in this application would be the repeatability and transfer function of the sensor.

Figure 4.d shows the results of the repeatability tests. It can be seen that the sensor is nonlinear, which is probably due to the fact that the flow profile front varies with velocity when under laminar flow conditions. The sensor is repeatable, but the margin of error is about 5%.

These results gave sufficient confidence in the optical technique to justify further development of the electronics unit, which was considered to be the main source of the 5% uncertainty on the measurement.

5 LINEAR POSITION SENSOR

Linear position detection has a wide range of applications in the automotive field, such as suspension arm position and wheel to road position. Sira has recently developed a prototype low cost optical sensor that could solve some of these difficult measurement problems. As yet no manufacturer has come forward to exploit this principle.

5.1 Operating Principle

Referring to figure 5, the sensor consists of a pair of detectors one of which is located at the focal point of a lens, the other is located in the same plane but shifted vertically. A light source is placed at the other end of the system, and is free to move with respect to the pair of detectors and lens. The detector at the focal point is chosen such that it is overfilled by the light that is focused onto it by the lens. The other detector is placed such that no light falls on it when the source is furthest away, as the light source moves closer the amount of out of focus light falling on this detector increases. It can be shown that the signal from the detector placed at the focal point is independent of light source distance from the lens (see appendix). This signal can be used as a normalising reference. The output from the other detector is related to the inverse square of the separation between light source and lens, and therefore is used as the basis of the output signal.

This principle is simple and low cost, but has the disadvantage that a light source and the detectors have to be fitted to different ends of the moving part. This can be overcome by using a mirror or a retroreflective system, but such an arrangement must be kept clean and free of contamination.

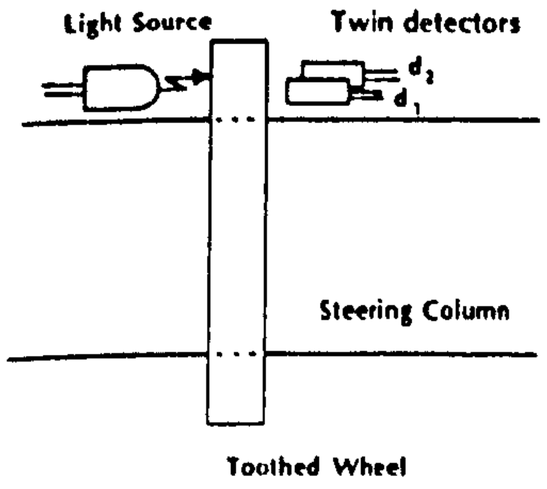

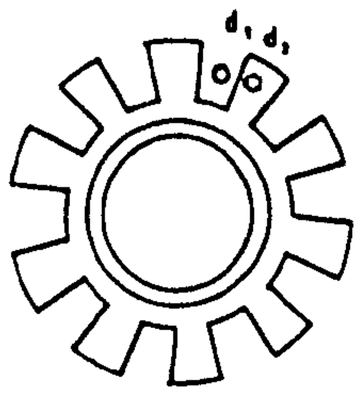

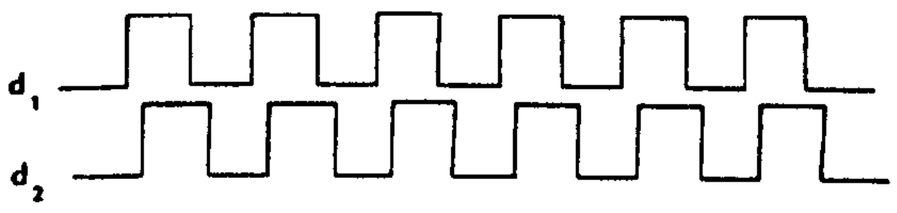

Usual Quadrature Type Angular Position Sensor

Fig 1a

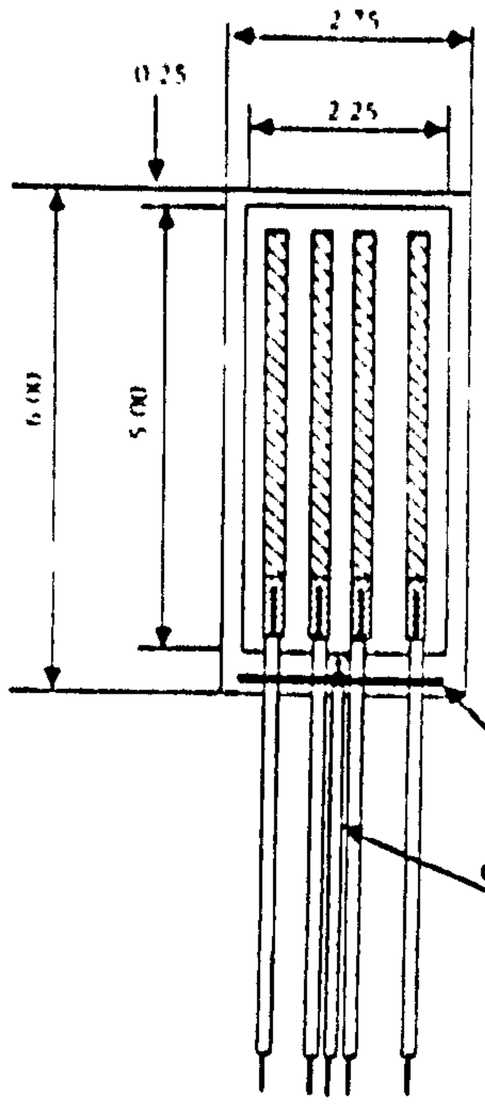

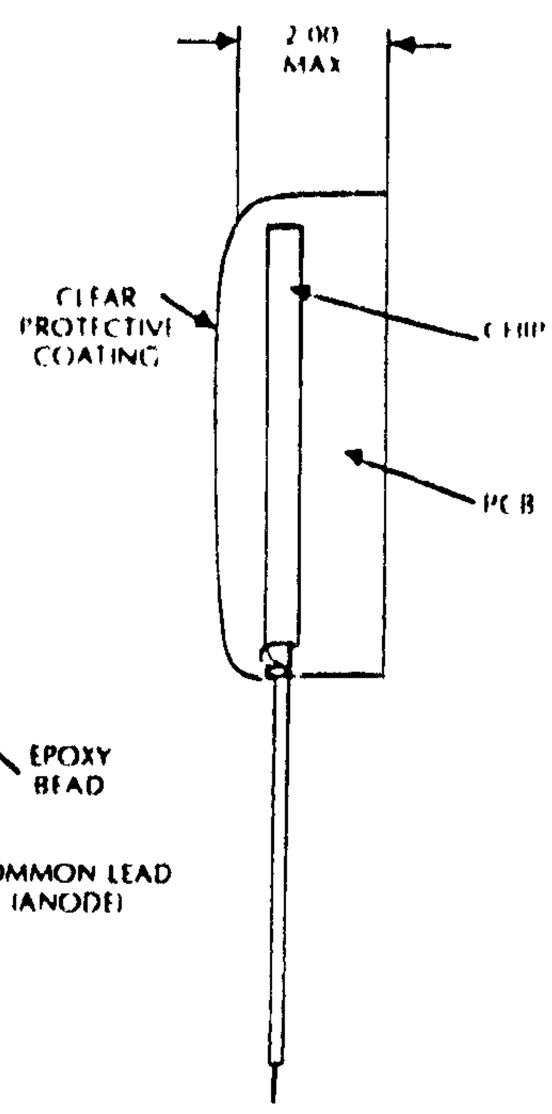

Fig 1c

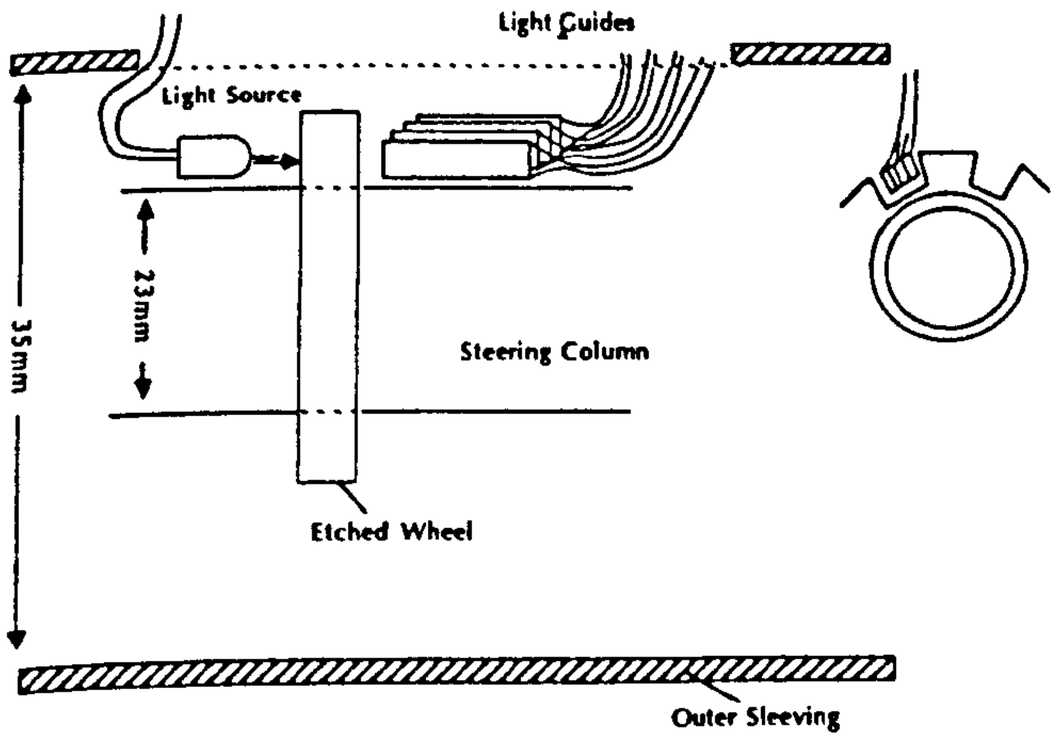

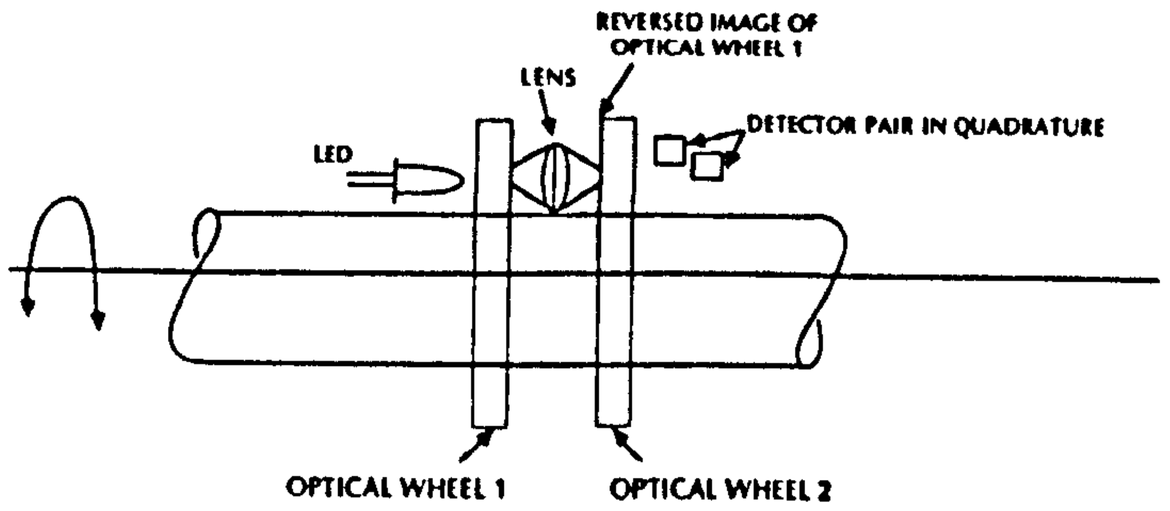

Fig 1d

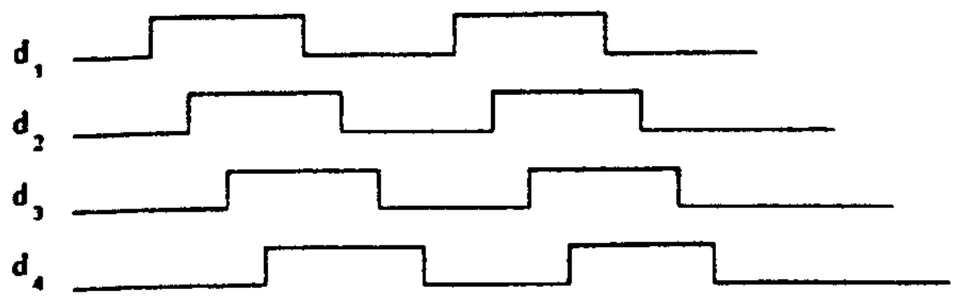

Light Guide Method

Fig 1b

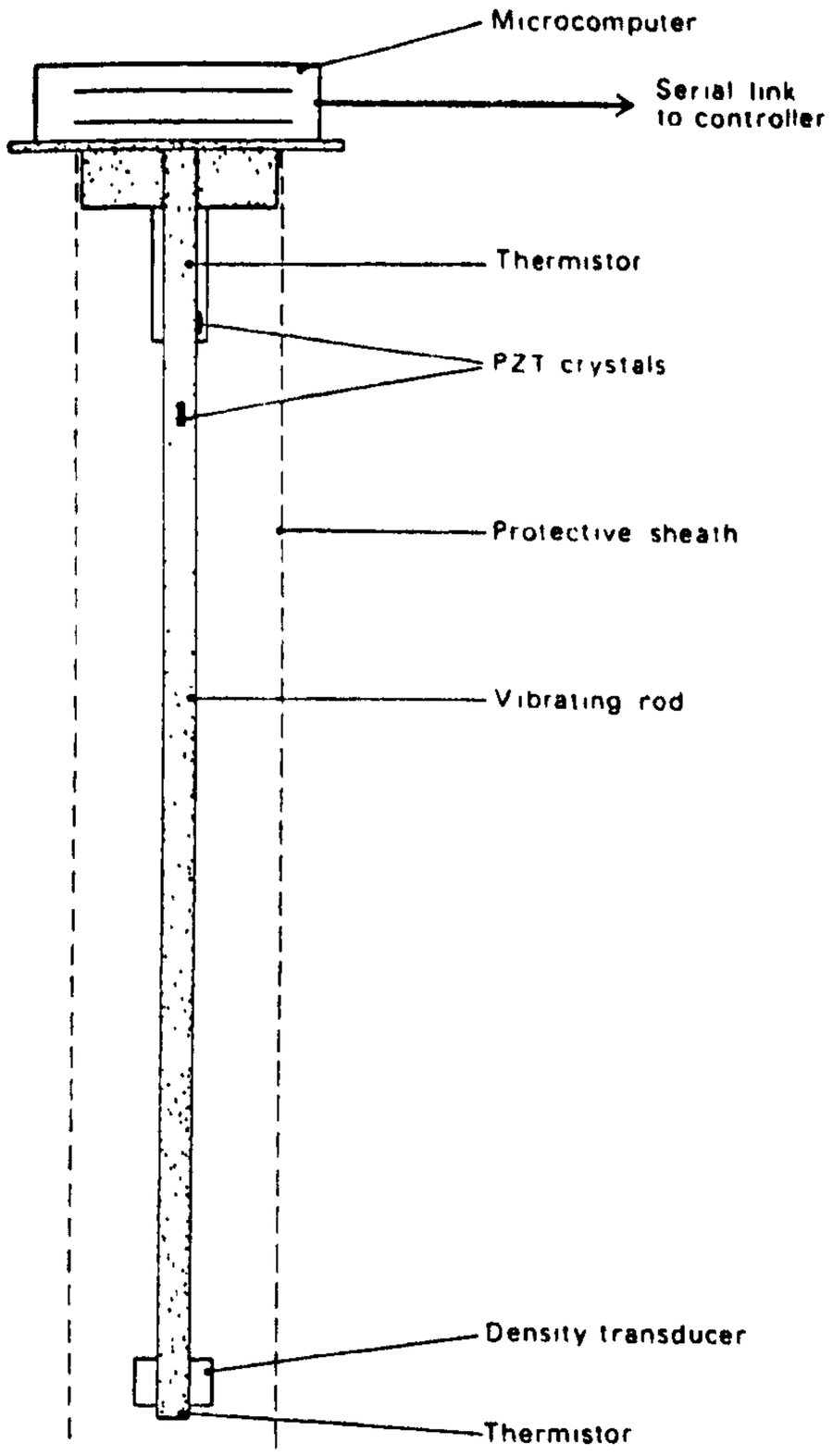

Fig 2a

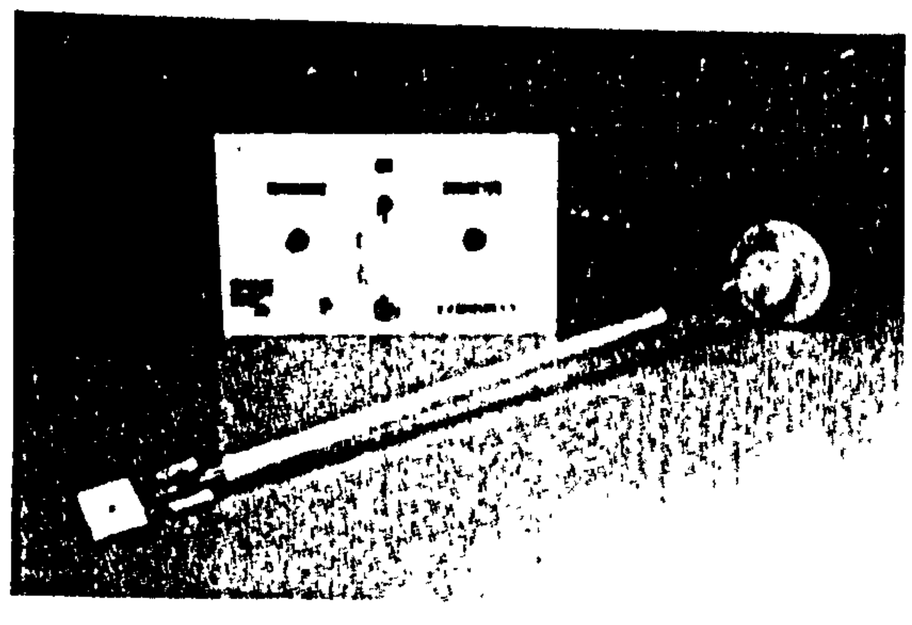

Fig 2b

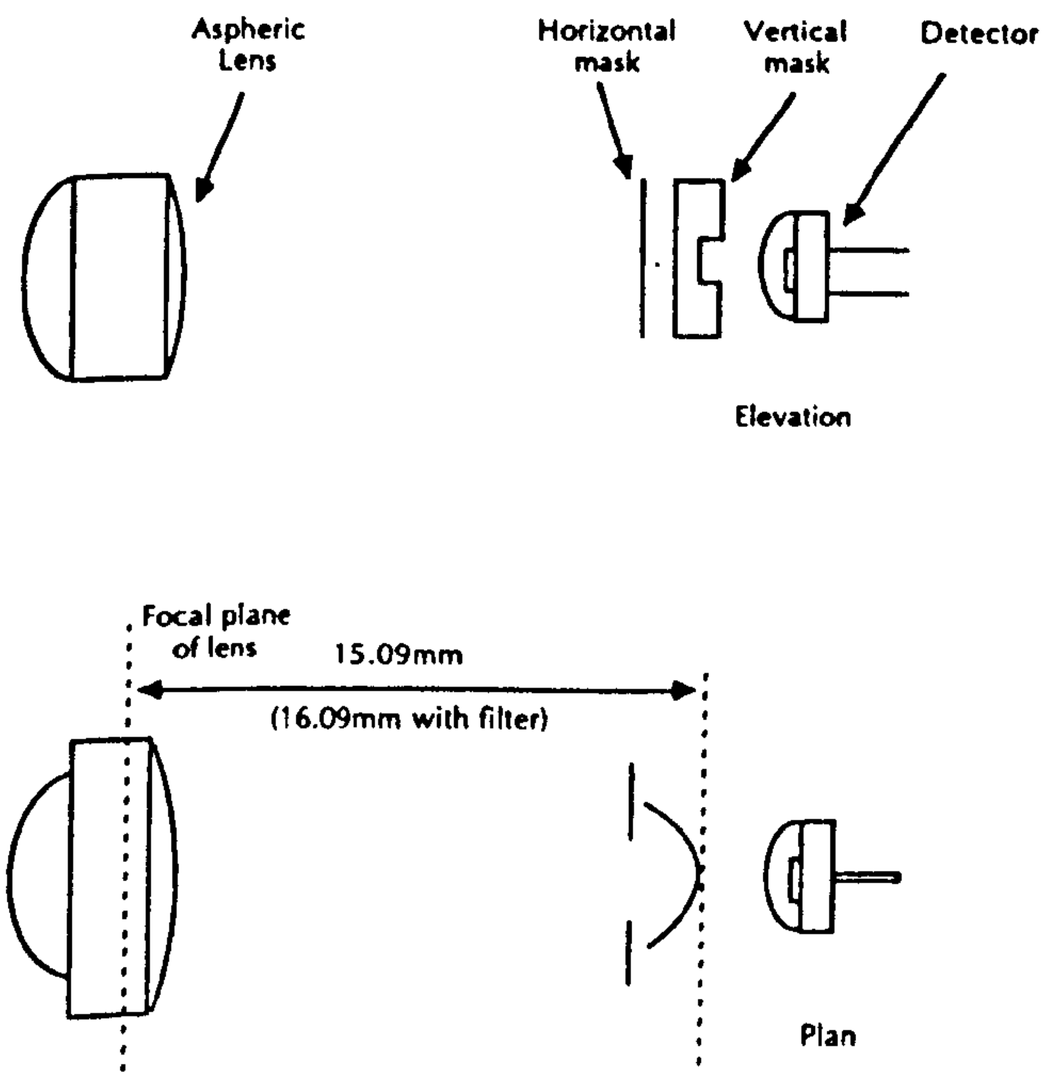

Optical layout of the Sira/FIS Autodipper

Fig 3a

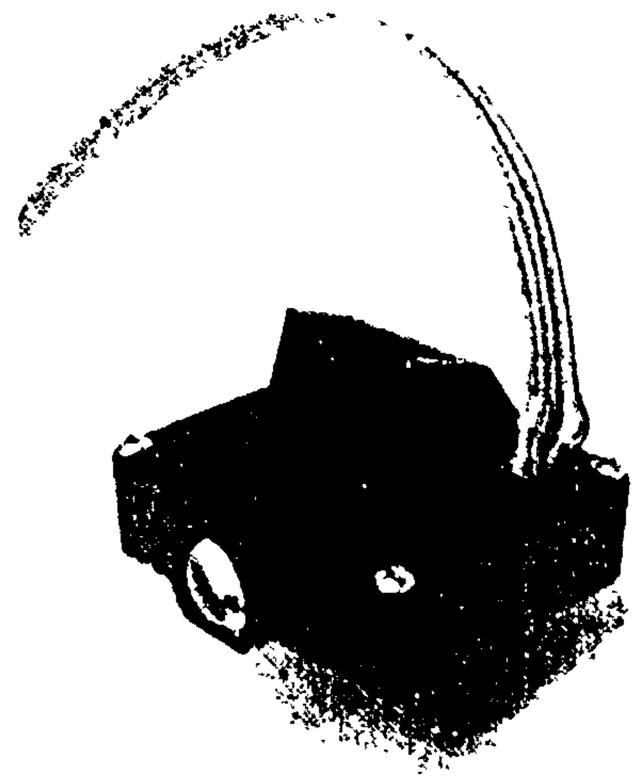

Fig 3b

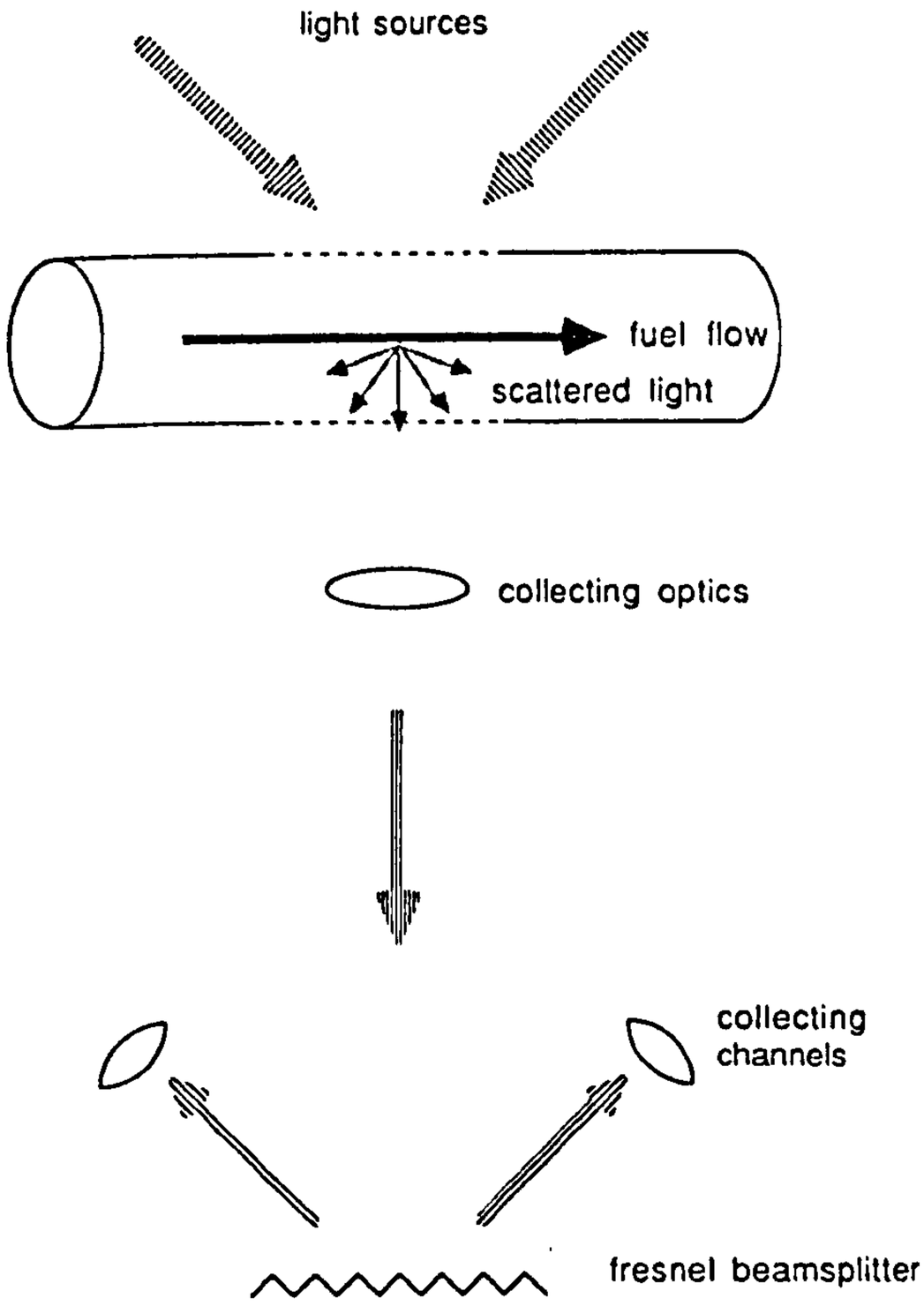

Fig 4a

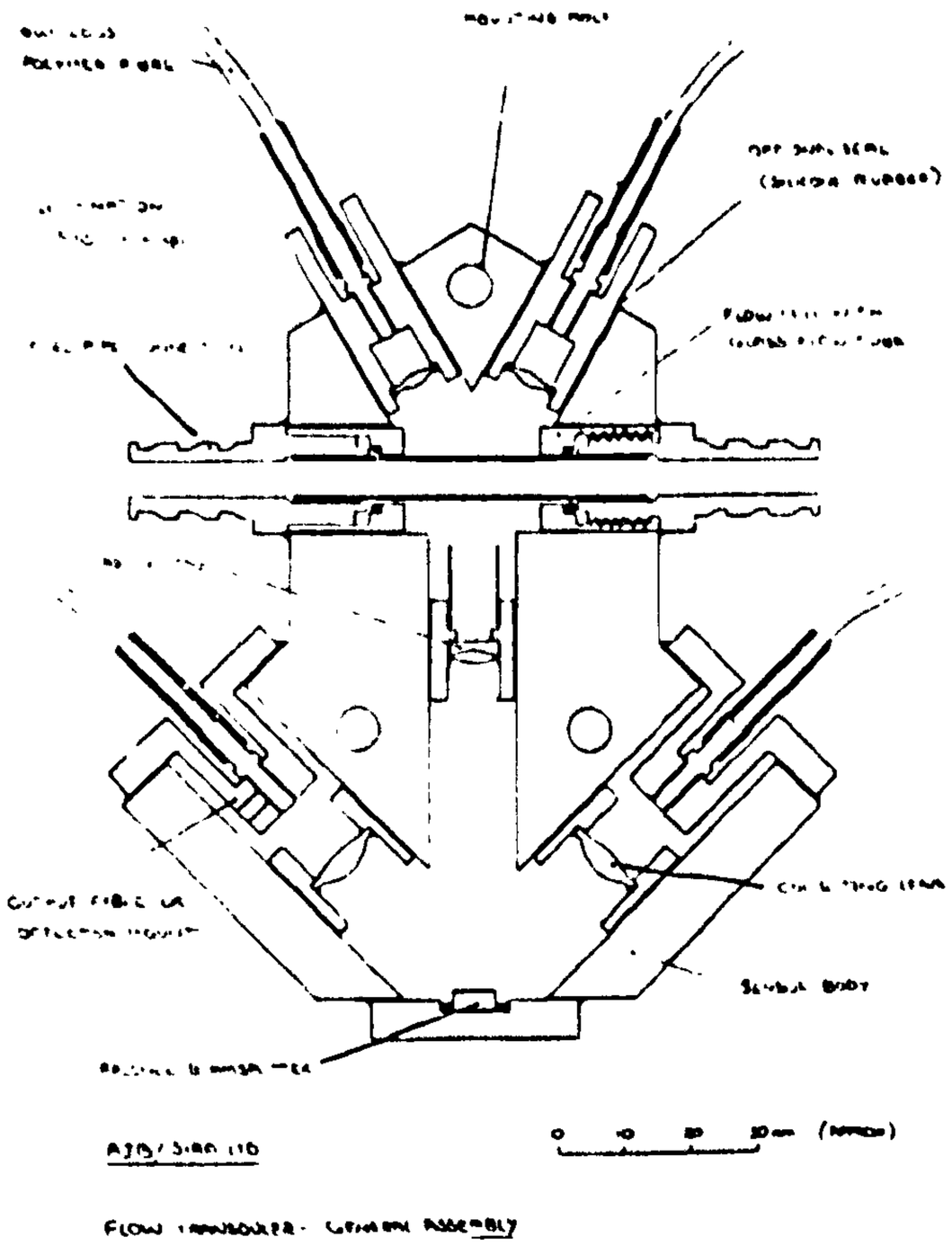

Fig 4b

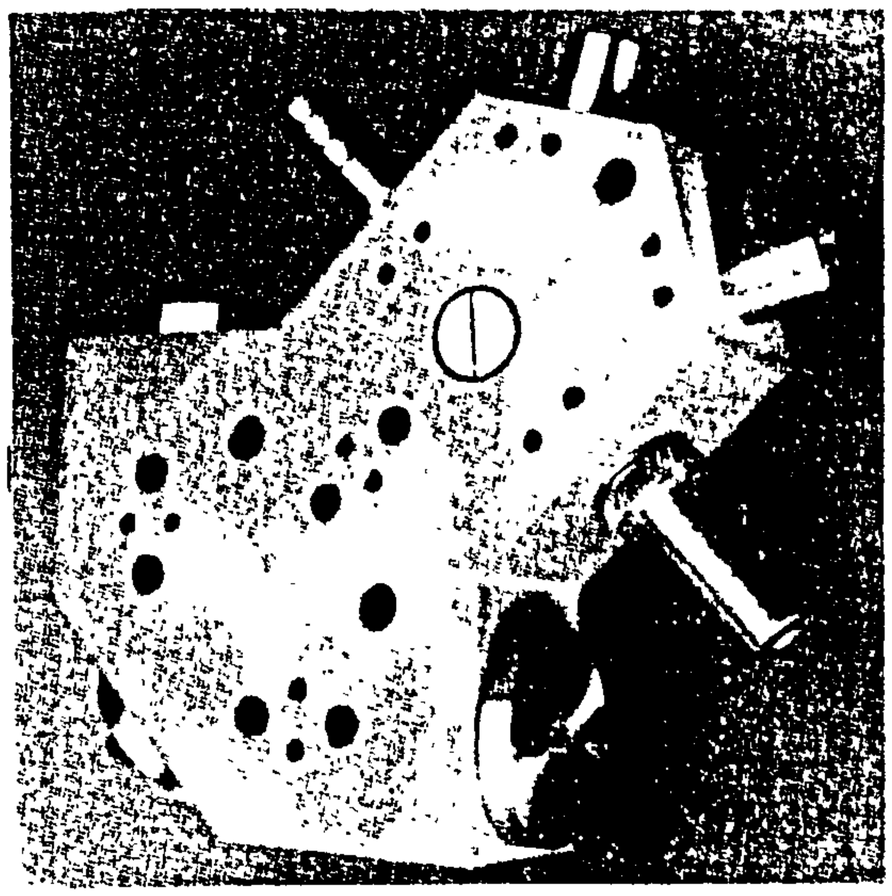

Fig 4c

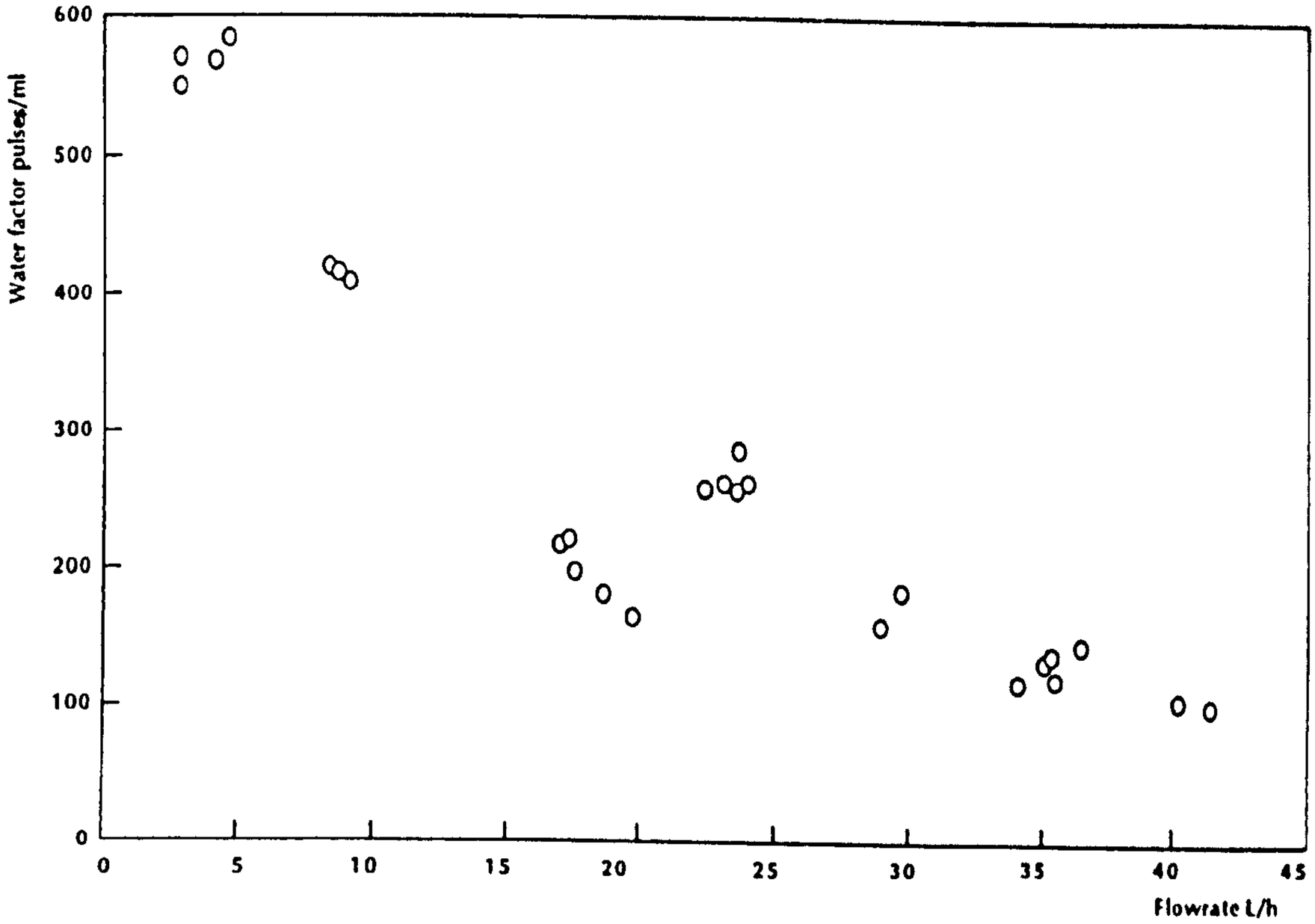

Linearity and repeatability

Fig 4d

d_1 on axis overfilled detector

d_2 off axis underfilled detector

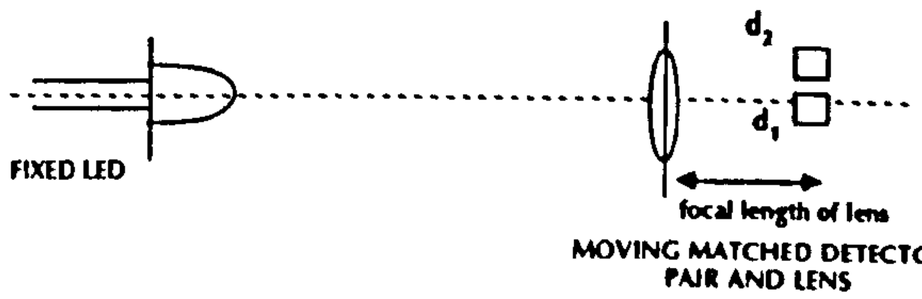

LOW COST OPTICAL POSITION SENSOR

Fig 5

APPENDIX

Requirement: detected power independent of source/detector distance

simple approximation

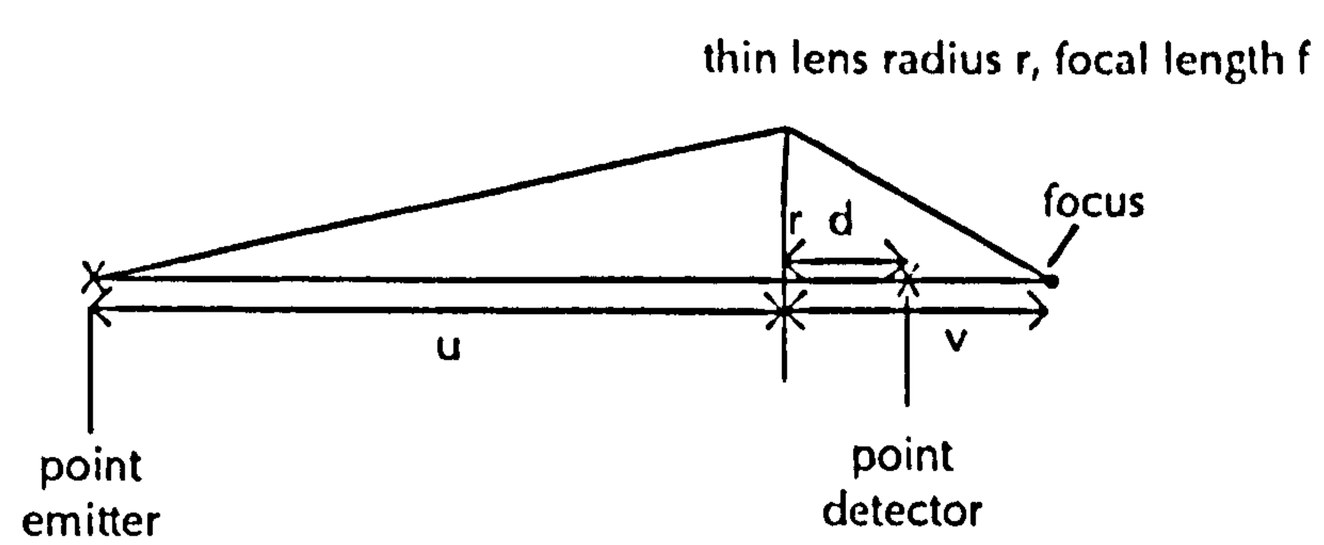

equivalent radiated power of emitter: P (ie power if radiated uniformly in all directions)

power intercepted by lens: $Q = \frac{P\pi r^2}{4\pi u^2}$ $(u >> r)$

radius of illuminated area in detector plane: $r_1 = \frac{(v-d)\,r}{v}$

power per unit area at detector: $i = Q / \pi\, r_1^2$

$$\Rightarrow i = \frac{P\pi r^2}{4\pi u^2}\left(\frac{v}{(v-d)r}\right)^2 \quad \frac{1}{\pi} = \frac{P}{4\pi u^2}\,\frac{1}{(1-\frac{d}{v})^2}$$

$$\frac{1}{f} = \frac{1}{u} + \frac{1}{v} \quad \Rightarrow \quad i = \frac{P}{4\pi u^2}\,\frac{1}{(1-d(\frac{1}{f}-\frac{1}{u}))^2}$$

$$\Rightarrow i = \frac{P}{4\pi}\,\frac{1}{(u(1-\frac{d}{f})+d)^2} \qquad \text{if set } d = f$$

$$\text{then } i = \frac{P}{4\pi f^2}$$

(independent of u)

Hence place detector at focal distance from lens

note: with real emitters and detectors, emitter must overfill lens which in turn must overfill detector. Also u >> r.

Novel sensors for measuring fuel flow and level

E.N. Goodyer

Sira Ltd, UK

ABSTRACT

This presentation will discuss a novel sensing method for measuring fuel flow which was developed for the Ford Motor Co by Sira Ltd. The fuel flow sensor uses an optical technique based on detecting light scattered from particles carried in the flowing fuel. Two off axis light sources illuminate the fuel flow region. As particles move with the fuel some light is scattered normal to the fuel flow direction. The scattered light is focused onto a course beam splitter which then directs the light onto two matched detectors. The course beam splitter has 5 linear reflecting grooves per mm each with an included angle of 135_1. As a particle that is smaller than the groove width moves across the field of view the effect is to focus scattered light from the particle alternately onto each of the two detectors. Each detector therefore receives optical modulation which is in antiphase to that received by the other detector. The difference of the two detector signals is then used. Also presented will be a new design for an optically based steering wheel position. The sensor is now in full scale production and is manufactured by First Inertia Switch Ltd. An assembly consisting of a number of parallel light guides, each 0.25mm wide, views the light reflected from a black and white striped tape that is stuck to the steering column. The signals from the detectors that are mounted remotely at the end of the light guides are interpreted by a PLA device to give rotational information. The sensor offers a higher resolution than traditional similar sensors while maintaining a low manufacturing cost.

1. INTRODUCTION

This paper discusses two novel sensors for use in automotive environments, one is a fuel flow sensor, the other is a steering wheel position sensor. The flow sensor uses an optical technique, based on viewing the light scattered by particles that are being carried along by the flowing fuel. The steering wheel sensor uses a traditional optical technique to measure angular movement, a coaxial chopper, but with the added refinement of dividing the light/dark transmissions into 8 different levels optically, thus increasing angular resolution.

2. FUEL FLOW SENSOR

The fuel flow sensor was developed by Sira Ltd for the Ford Motor Company. The first prototype was completed in 1986, and was then handed over to Sira's independent Instrument Evaluation Department for formal tests under reference and adverse conditions. These trials indicated that the sensor principle is viable, but that further long term research would be advisable in order to enhance the performance of the electronic signal processing. This work is now being carried out by Southampton University.

2.1 Principle of Operation

A transparent tube is placed into the fuel line which is lit by off axis light sources, in this way the only light that reaches the imaging lens is scattered from particles moving along with the fuel. The lens images the flow region onto a a Fresnel beamsplitter. Particles in the fuel appear as small spots of light moving across the beamsplitter. The beamsplitter deflects the scattered light alternately onto two light collecting channels, which produces a modulation frequency that is directly related to the flow rate. The two signals are inherently in antiphase with each other, whereas any unwanted signals due to large particles, air bubbles or off axis scattered light will generally be in phase. The output of the two channels are subtracted from each other which will in effect enhance the useful modulations which are in antiphase, and remove the common mode signals which are unwanted. Finally the difference is thresholded to produce a frequency output signal which is related to the fuel flow rate at the illuminated flow region.

This design approach is particularly advantagous for the automotive environment. It inherently overcomes the environmental problems of shock & vibration, electrical interference and temperature changes. As the sensor principle is fundamentally optical electrical interference is not as great a problem as for electronic and electromechanical sensors. There are no moving parts, making the sensor more resistant to shock and vibration. Temperature is still a problem as it will have an effect on the detectors and associated electronics. However judicial selection of components will minimise this problem.

2.2 Sensor Evaluation

The prototype sensor was examined by Sira's independent Instrument Evaluation Department. Our main concern at this stage was to determine what the sensors response characteristics were and whether or not the output signal was repeatable. The outcome of these tests would determine the future of the sensor.

Included in the figures is a reproduction of the repeatability test results. It can be seen that the sensor exhibits a non linear response, which may be due to the fact that the flow profile varies with flow rate. (A similar response is seen with ultrasonic type sensors). The sensor is repeatable, but is not adequate for a production sensor. Further examination indicated that the cause of the non linearity lay in the electronics rather than the optics.

As a result of these tests sufficient confidence was generated to justify further development of the electronics.

2.3 Future Development

The optical principles of the sensor have been established as viable. Further development work is now being undertaken by Southampton University who are concentrating on improving the signal conditioning electronics. When suitable electronics are developed then they will be redesigned such that it can be built at a low cost and be miniaturised.

3. STEERING WHEEL POSITION SENSOR

The steering wheel position sensor was designed by Sira Ltd for, and in close partnership with, First Inertia Switch Ltd, who are an established volume automotive components manufacturer. A joint development team was established that successfully combined Sira's expertise in optical systems design with First Inertia's experience of mass production techniques, and automotive requirements. This sensor is now in full scale production, and can be readily adapted for different mechanical arrangements.

3.1 Principle of Operation

Two sensors have been developed in order to take account of different styles of steering column. The optical sensing method is the same in both cases, the difference being the method of delivering light into the sensor. Illustrated in the figures is the transmissive method, the alternative, and preferable implementation uses a reflective method. For the transmissive method a perspex wheel is fitted around the steering column onto which are etched a series of darkened notches, such that the wheel acts as a chopper. This is a common technique already used in a number of commercially available rotational sensors, a pair of detectors being used to obtain quadrature pulses that have to be interpreted by a remote microcomputer.

The Sira design differs fundamentally in the method of detecting the light. Using the traditional method the angular resolution is given by the number of notches * 2. Sira has improved the resolution by replacing the twin detectors with a sandwich of flat light guides, each with an independent detector. Using this method the angular resolution is given by the number of notches * N, where N is the number of light guides in the sandwich that fit into a single notch gap. The resolution is solely limited by the width of the light guides used, as eventually insufficient light can be collected to be detected by a low cost sensor. The added advantage of the Sira optical collecting method is that the detectors and associated electronics no longer need to be situated near to the steering column. Small custom designed optical assemblies can be fitted into difficult positions, and the light brought out via the guides to the bulkier electronics package.

An alternative is to use a reflective method, where the perspex collar is replaced by a reflective tape, with black lines, stuck coaxially onto the steering column. The light guide sandwich now consists of alternate illuminating and detecting elements, which is directed normally to the surface of the steering column. As less light is obtained by this method it can only be used with large diameter steering columns at the present, with the tranmissive method used for small diameter columns.

The electronics incorporates a PLA device that decodes the 'grey code' pattern obtained from the detectors into a series of pulses, representing left and right rotations. Resolution is better than 2 degrees.

3.2 Future Development

A number of potential new developments are under consideration. The sensor itself is intended as a low cost device for use by car manufacturers. The principle however can be adapted for much higher resolutions if the cost constraint is removed.

For the automotive industry specific new developments include the addition of an angular rate of change signal output, the provision of analogue outputs, and the addition of a zero datum such that an absolute angular measurement is available.

4. OTHER OPTICALLY BASE AUTOMOTIVE SENSORS

Sira have developed a number of optically based automotive sensors for industrial clients. These have included a tilt sensor, an automatic headlight dimmer, and an accelerometer. These sensors are representative of the application of optical techniques to obtain low cost sensing solutions suitable for large scale manufacture. At the other end of the scale Sira also supply laser scanning Automatic Inspection systems , an example of which has been installed at an Austin Rover plant to inspect the paint finish on cars moving along the production line. Other inspection systems have been custom designed for a range of production lines and applications.

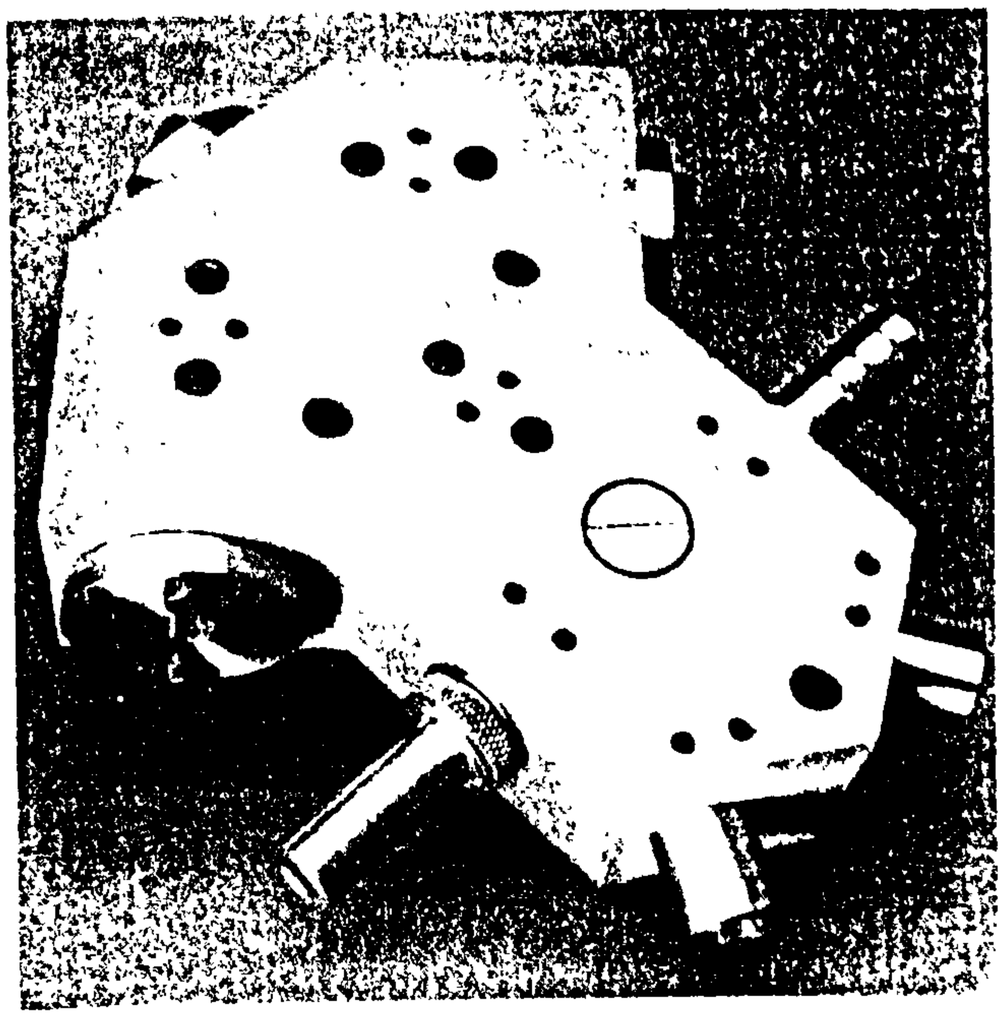

PHOTOTYPE FUEL FLOW SENSOR

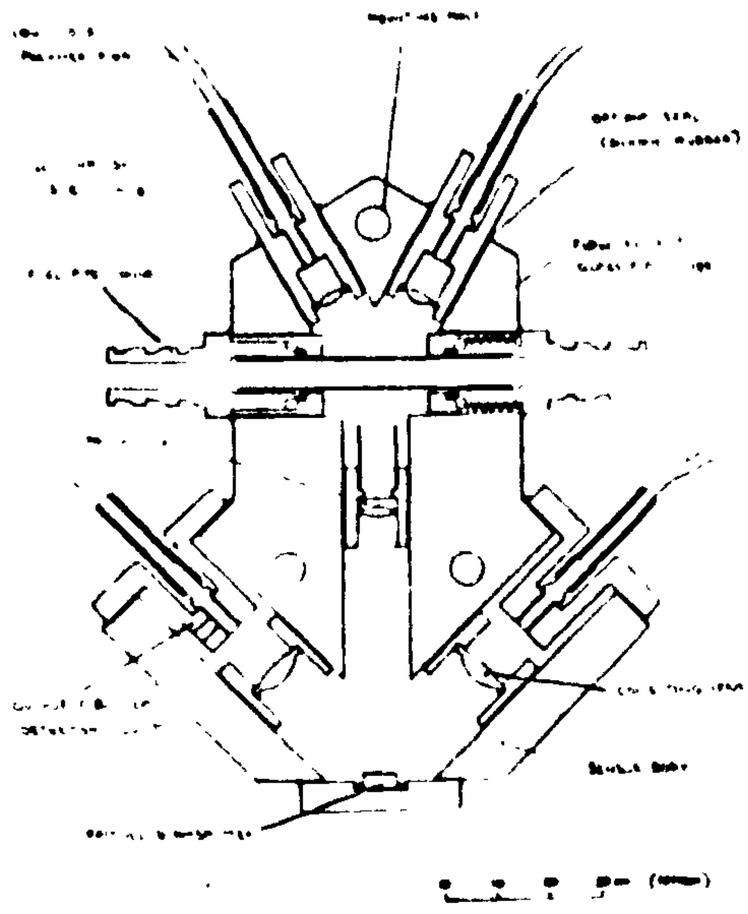

FUEL FLOW SENSOR GENERAL ASSEMBLY

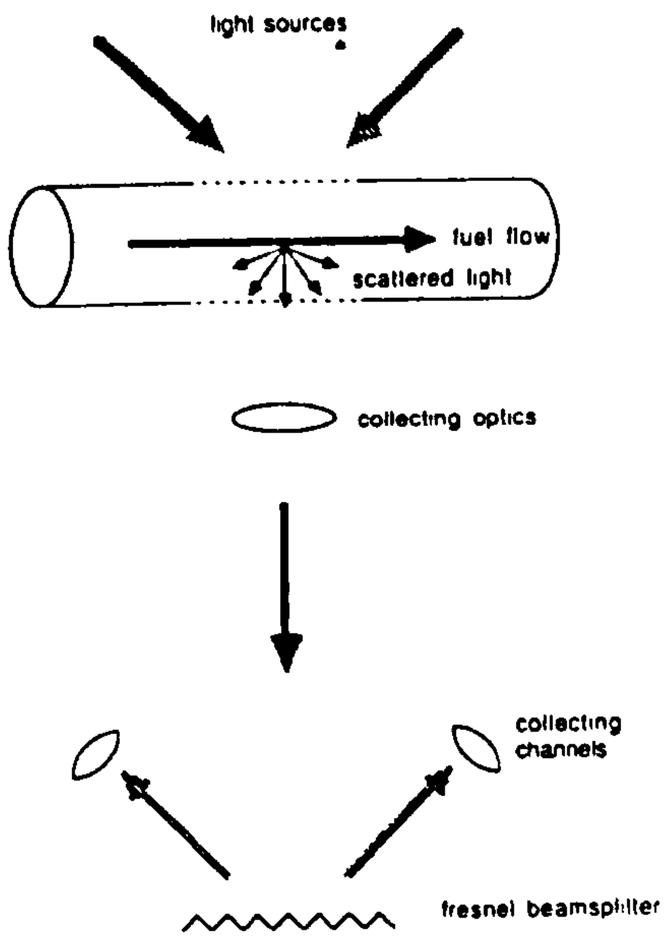

FUEL FLOW SENSOR
PRINCIPLE OF OPERATION

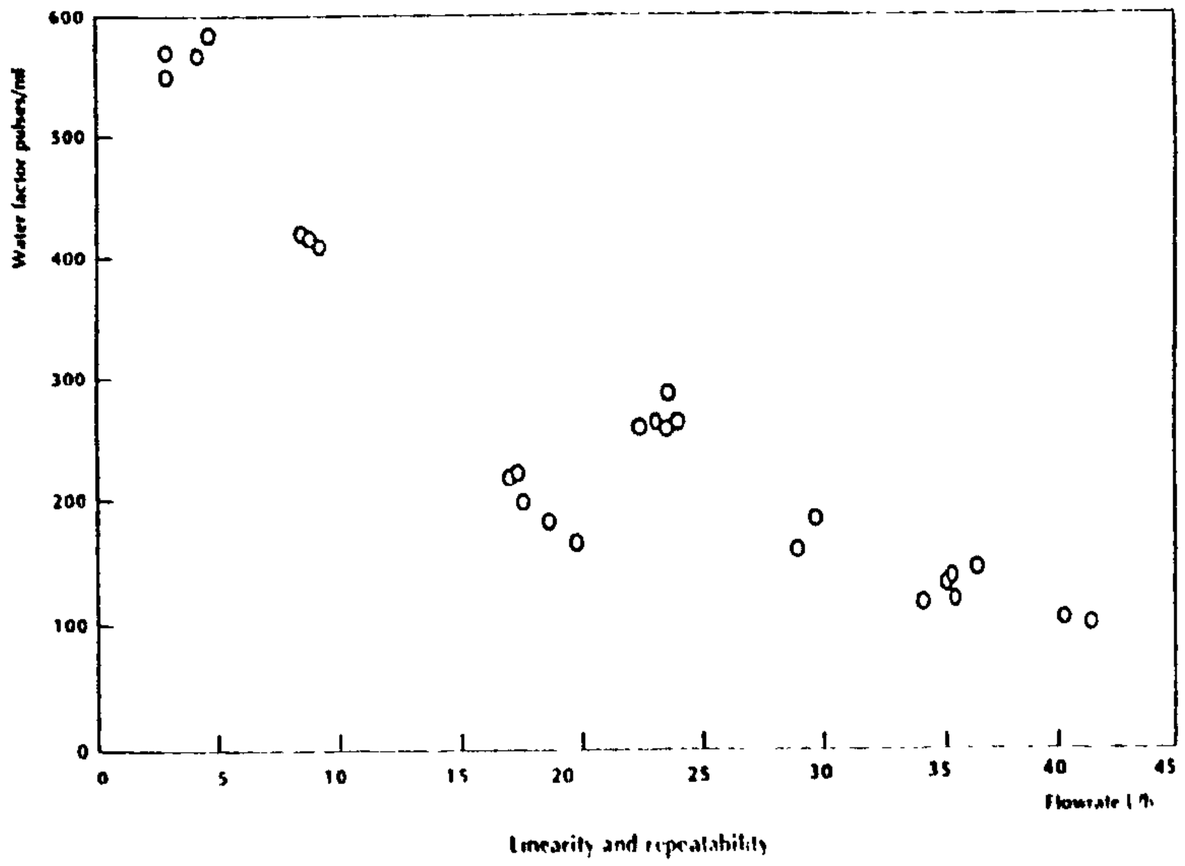

FUEL FLOW SENSOR
LINEARITY TEST

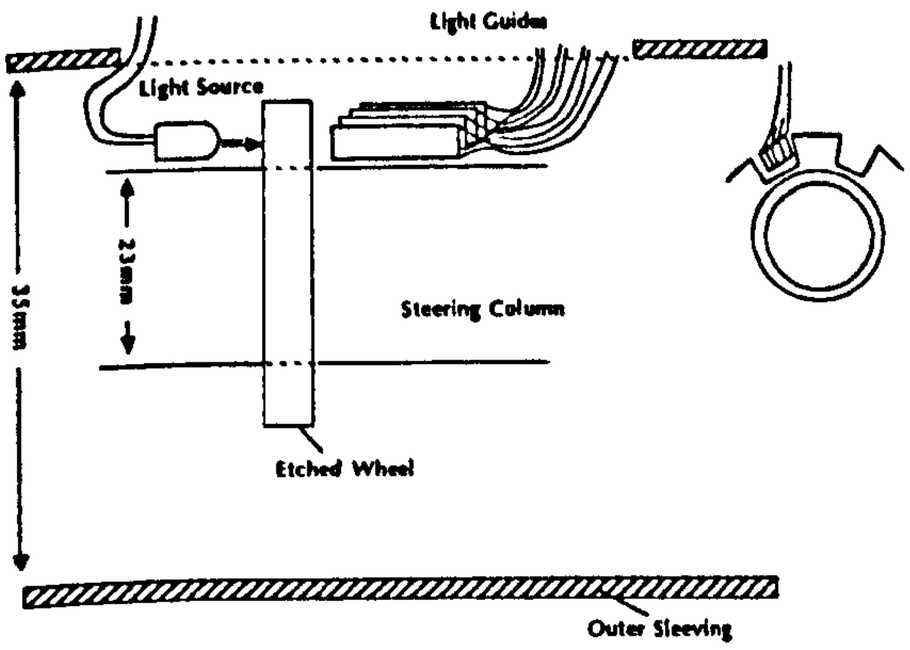

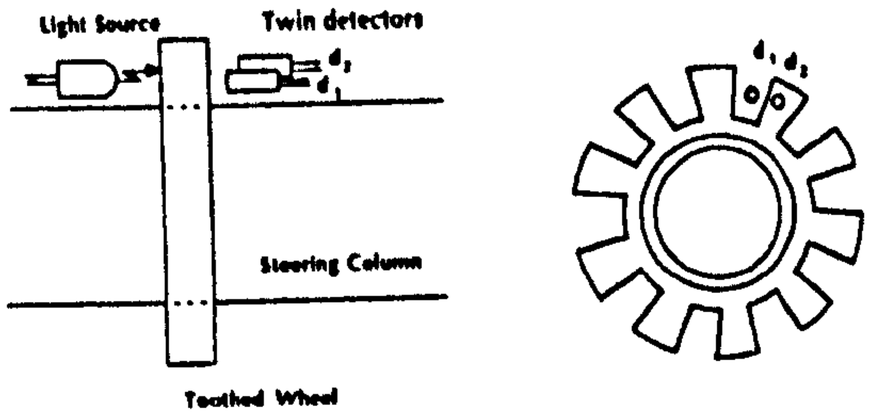

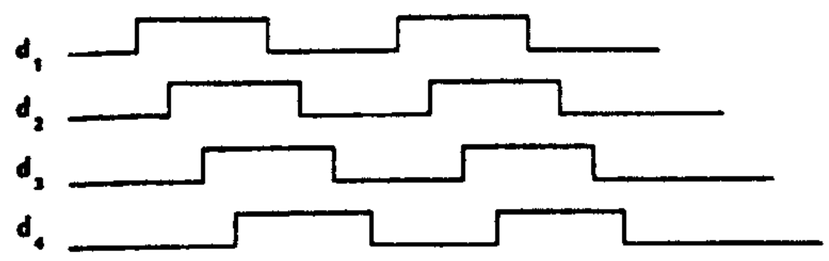

SIRA ANGULAR POSITION SENSOR
PRINCIPLE OF OPERATION

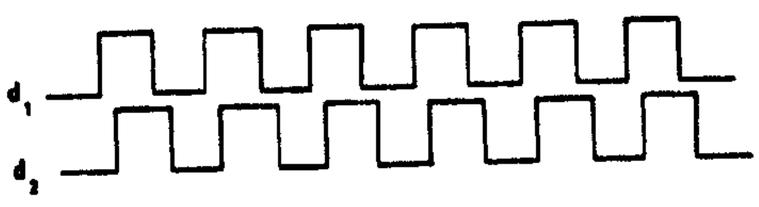

TRADITIONAL ANGULAR POSITION SENSOR

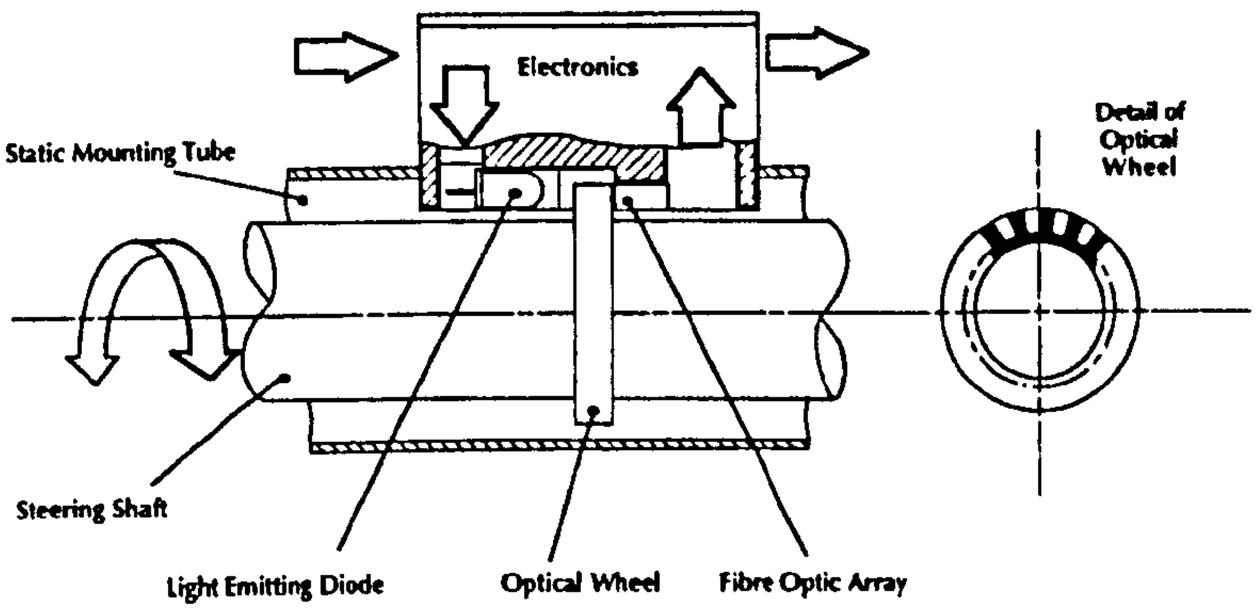

STEERING WHEEL POSITION GENERAL ASSEMBLY

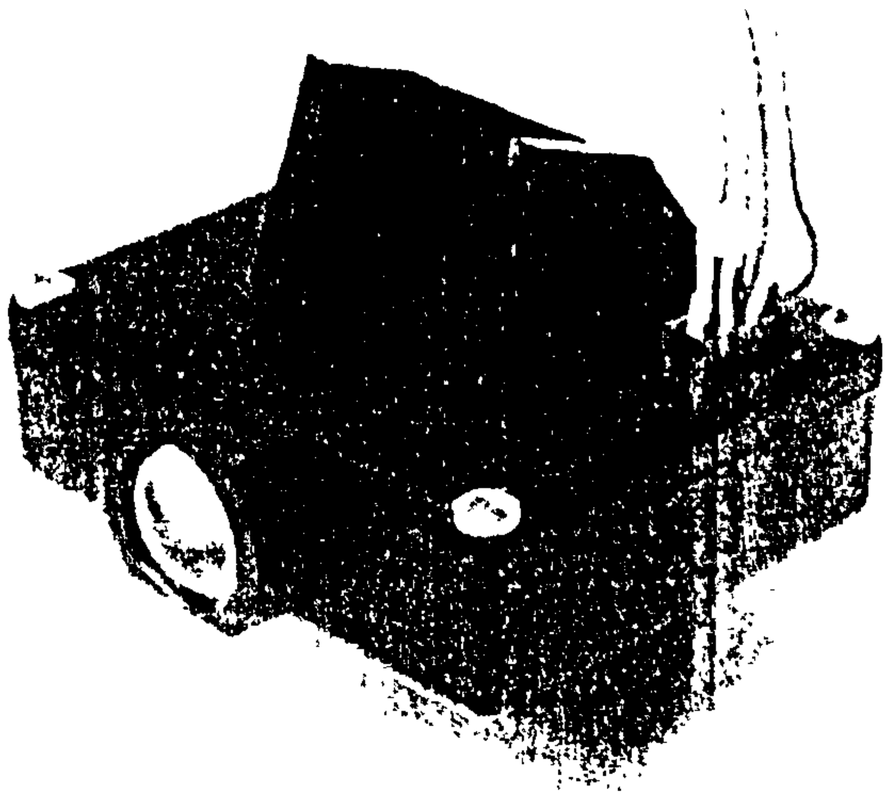

AUTOMATIC HEADLIGHT DIMMER

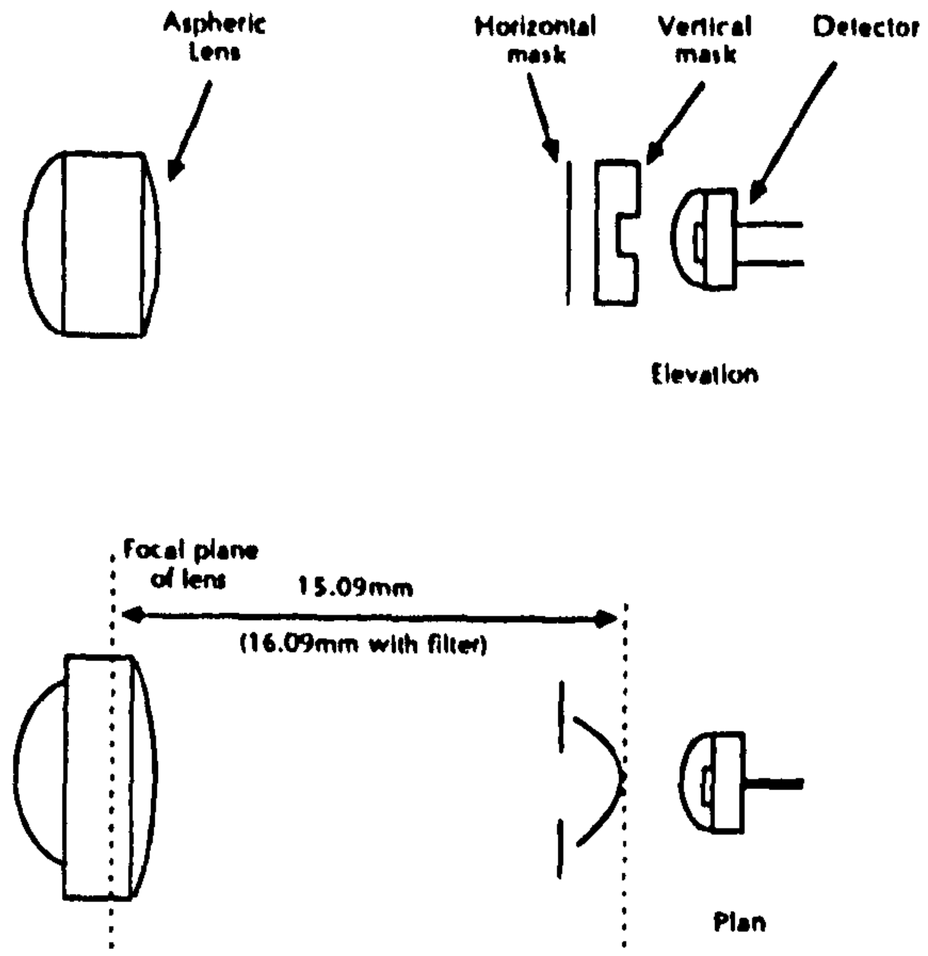

HEADLIGHT DIMMER
PRINCIPLE OF OPERATION

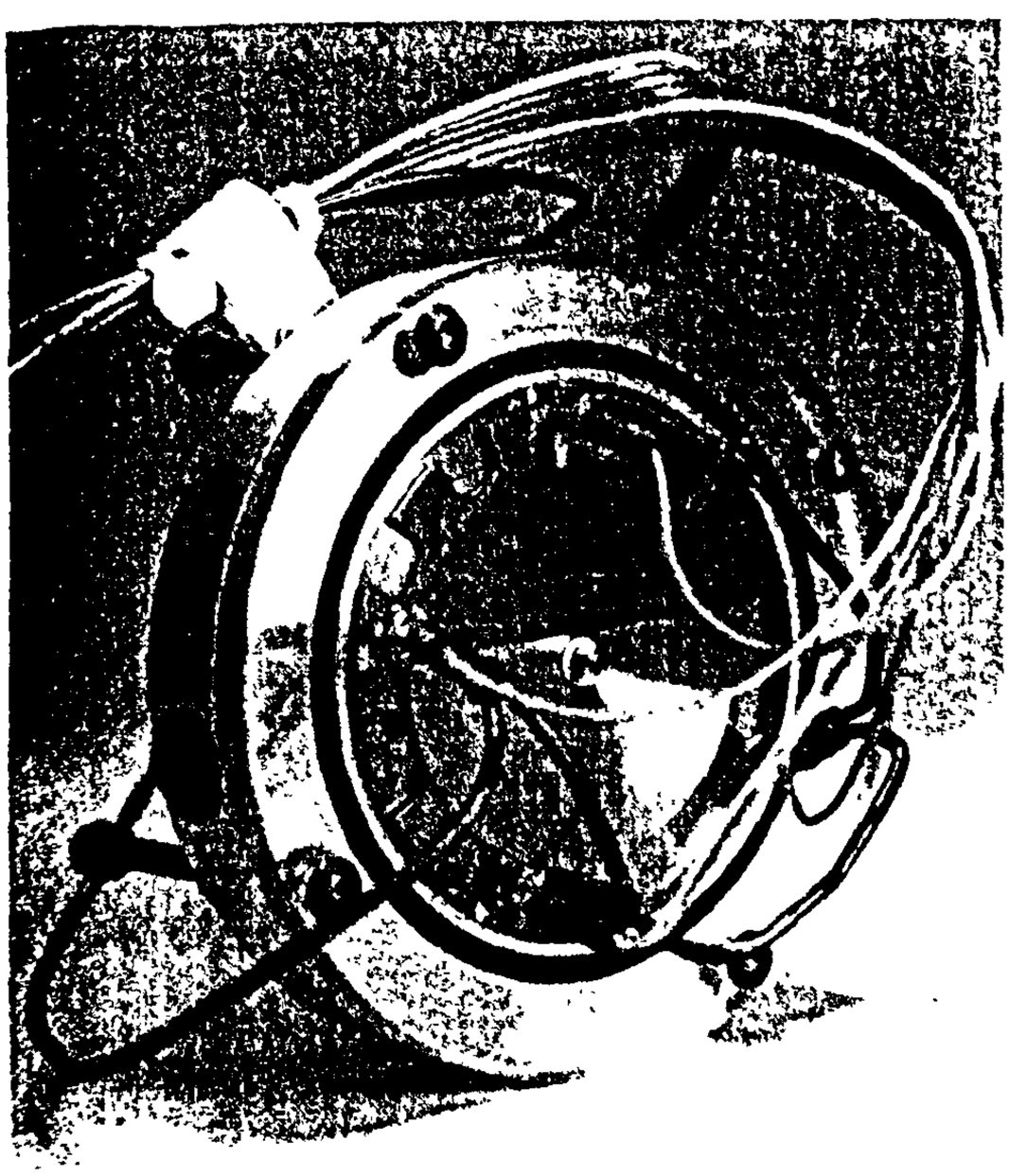

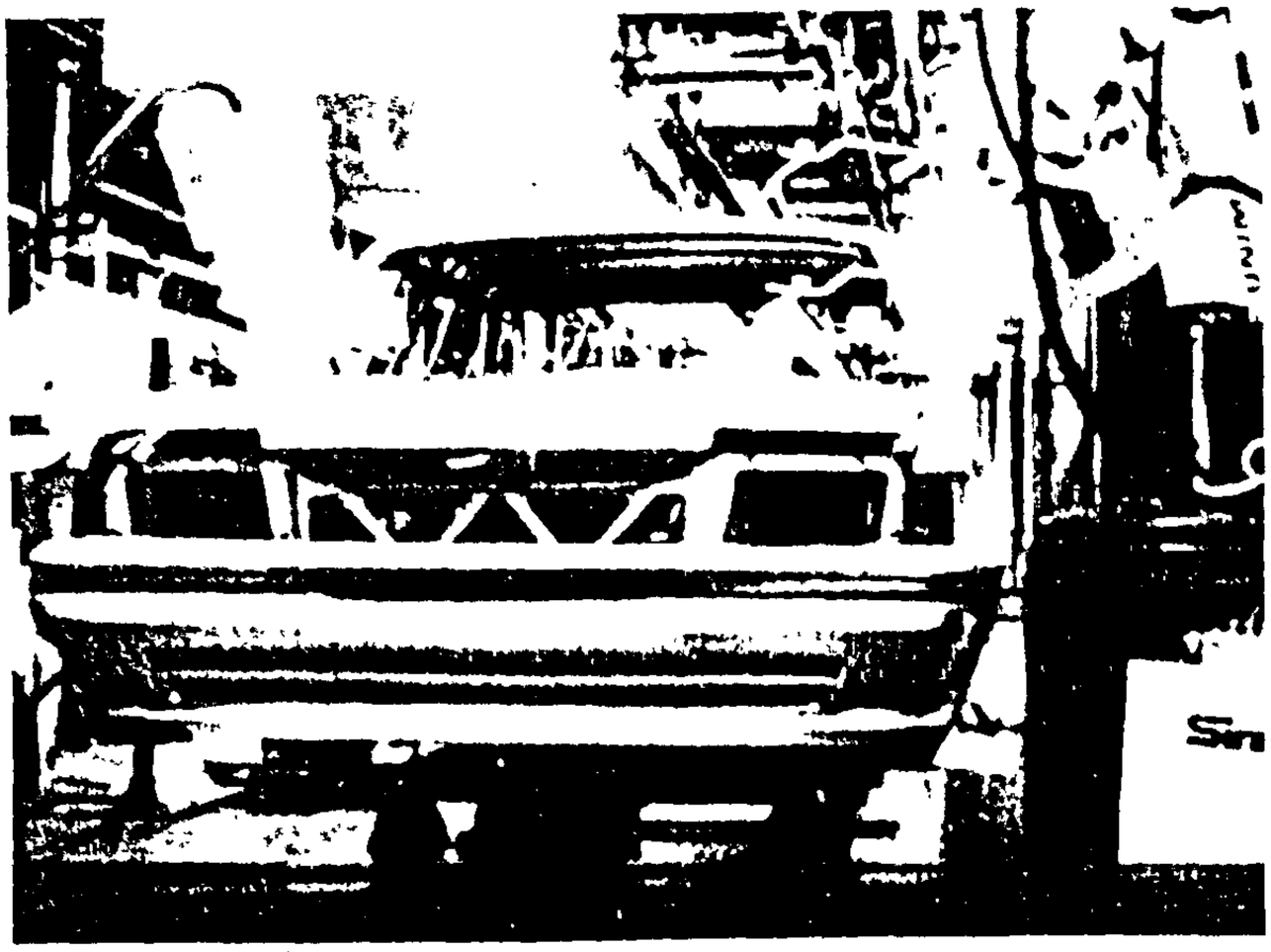

AUTOMATIC PAINT INSPECTION SYSTEM

PROTOTYPE TILT SENSOR

SENSORS FOR MEASURING FUEL FLOW AND LEVEL

Goodyer

Ltd, UK

ODUCTION

paper discusses two novel sensors for use in motive environments, one is a fuel flow r, the other is a fuel level sensor. The sensor uses an optical technique, based on ng the light scattered by particles that are carried along by the flowing fuel. The sensor uses an electromechanical technique, vibrates a rod that is immersed in the fuel easures the resonant frequency of the rod.

FLOW

uel flow sensor was developed by Sira for a car manufacturing company. A prototype or was constructed in 1986 and subjected to is under reference and adverse conditions by 's Instrument Evaluation Department. The usion from the results of these trials was the sensor principle was viable, and that it be useful to ask Southampton University to out some additional long term research of sensor.

ciple of Operation

ansparent tube inserted into the fuel line is y off axis light sources, such that only ered light can reach the imaging lens. This forms an image of the flow region onto the el beamsplitter. Small particles that are ed along by the fuel appear as small spots of moving across the beamsplitter. The mirror s on the beamsplitter deflect the scattered alternately onto two light collecting els, thus producing a modulation on the ting channels at a frequency that is related e flow rate. The beamsplitter ensures that are two signals available which are in hase with each other, whereas any unwanted s due to large particles, air bubbles or off scattered light will generally be in phase. ving the difference of the two channels modulation is enhanced, and unwanted s are removed. By thresholding the ence signal a frequency is obtained which is ed to the fuel flow at the illuminated flow

Advantange for Automotive Applications

el flow measuring technique is particularly le for use in an automotive environment as it ntly overcomes the main environmental prob- electrical interference, shock and on and temperature fluctuations. The main the sensor cannot be affected by electrical erence as it is based on an optical tech- Shock and vibration effects will be ed as these effects will move the fuel around flow tube, but the effect is small compared signal generated by the moving fuel. The oncern is temperature fluctuations, which ot affect the basic optical concept, but will the responsivity of the optical detectors. , detectors that are stable over wide tem- e ranges are available, so it is considered udicial selection of components will overcome foreseen temperature problems. The design also has no moving parts which should improve reliability over the traditional turbine flow meter.

Sensor Evaluation

A prototype fuel flow sensor was examined by Sira's instrument evaluation laboratory. At this stage of the development we were mainly interested in the repeatability of the sensor, in order to determine whether or not it was worth undertaking further development. Attached is a copy of the repeatability test results. The graph shows that the sensor exhibits a response which is non-linear. The repeatability is not yet good enough for a production sensor, but it is adequate to justify further development work.

Future Development

The general sensor principle has been established as viable. Current development work is concentrating on improving the signal conditioning electronics as this is thought to be the cause of the poor repeatability of the prototype sensor. When suitable electronics are developed then the next stage will be to redesign the sensor so that it can be built at a low cost and be miniaturised.

PETROL TANKER FUEL LEVEL SENSOR

The tanker fuel level sensor is the result of a collaborative development programme carried out by Sira, and two major engineering companies. Long term research is also being carried out by the City University. The requirement was to find a replacement for the traditional wooden dipsticks which are still widely used to measure the fuel level in road tankers. Sira were to assist in finding a suitable sensor and in developing a measuring system for road tankers that used the sensor. The sensor chosen for the application was based on another company's existing design for measuring the electrolyte level in batteries, among other applications. This design is now licensed to the original engineering company who have taken over responsibility for the design of sensors suitable for use in road tankers.

The petrol tanker fuel level sensor is now in full scale production by and is marketed under the name of Drumstic. It is also now fully approved by HM Weights and Measures Department and is therefore the first automatic dipstick commercially available for use in the UK.

Principle of Operation

The rod is manufactured from an aluminium extrusion, to which are attached two pairs of piezo electric crystals on orthogonal axes. One piezo of each pair is used to vibrate the rod, the other is used as a receiver. A phase locked loop circuit locks the electromechanical circuit onto the resonant frequency. The rod is vibrated flexurally, with a small amplitude. As well as the frequency information from the two pairs of piezo, the temperature of the fuel and the vapour above it, and the fuel density are also measured.

This data is fed into a microcomputer attached to each rod, where a mathematical model and calibration data are used to generate a volume reading that is accurate to better than 0.15% over a range of up to 1500 gallons. The probe head computer transmits all the available data from the probe down a serial interface. This data includes the fuel level, volume, density and temperature readings.

Drumstic is in principle a mass measuring instrument. When operating in mass rather than volume mode, the system error is reduced by one third.

Design Advantage for Automotive Applications

The basic sensor is a tuned electromechanical resonant device, with a well defined narrow operating frequency range. This makes the design of electronics that will reject unwanted noise far simpler. As the information is a frequency, the signal to noise and stability problems associated with linear signals do not arise. Also the integral processor within the sensor converts all the available information into a data stream that is transmitted via a serial link. This feature improves the integrity of the information that is gathered by the Central Display Unit (CDU).

Tanker Installation

A petrol tanker has a number of separate compartments, each fitted with its own Drumstic which is then connected via serial links to the CDU. The CDU is used for various functions including monitoring the level, density and temperature in the tank, recording the delivered quantity, and to give an alarm if the tank is about to overspill when being loaded. All transactions are data logged and tickets can be printed for each delivery. LPG tankers are normally single compartment and are fitted with only one Drumstic.

Mass being invariant with temperature makes stock reconciliation much more straightforward. Currently, however, mass display mode can only legally be used for LPG deliveries. In the future when mass is the accepted measuring unit (remember that Cornflakes used to be sold by volume!) Drumstic can still be used.

Future Developments

At the time of writing a number of enhancements to the system are being examined. Among these are tank valve control, stainless steel probes, and a petrol station forecourt interface for unattended (driver controlled) deliveries.

CAR FUEL TANK LEVEL GAUGE

Sira were requested to evaluate the road tanker level sensor just described to determine whether it was suitable for use in cars. To assist in this study a miniature probe was manufactured and installed into a car fuel tank. In order to reduce the cost of the sensor (an essential requirement if it is to be manufactured in large quantities for use in cars) the design was reduced to the bare minimum. The desired accuracy is far less than the stringent requirements of the Weights and Measures Department, therefore the design did not incorporate a densitometer. Instead the density of the fuel was determined by using the temperature reading and a look up table.

Sira then evaluated the operation of the mini sensor under reference conditions in the laboratory, and under adverse conditions when subjected to severe shock, vibration and temperature variations.

Test Results

There was initially a high degree of confidence in the measuring principle because it was already being used in road tankers. The main concern was whether the accuracy would be retained for the miniature probe. The other area that required investigation was whether the small probe would be as good as the larger road tanker sensor in withstanding severe shock and vibration.

Temperature effects were evaluated in two ways. The probe was placed in a tank containing a known mass of fluid. A series of mass readings were taken from the sensor at different temperatures. A second series of tests was then carried out using a constant volume of fuel.

The graphs show the effect of temperature variations on the readings. The constant volume tests show a near linear response (±1%) followed by a steadily rising response. The constant mass tests give a steadily rising response of ±3%.

These accuracies are an improvement on the existing float type level sensor used in cars. However, subsequent analysis of the results indicated that the mathematical model used for temperature variations in the larger tanker probe cannot be directly applied to the miniature probe. Changes to the model that take account of the different thermal characteristics of the mini probe should in future give a better performance.

The probe was subjected to shock tests of 15g for 12 ms duration. It was found that the level reading was hardly effected during the shock period, and returned to normal after the shock had subsided. The probe was then subjected to two vibration tests with a frequency sweep of 30 Hz to 1200 Hz at 0.6g and 1.5g accelerations. A resonance was found at about 150 Hz with the acceleration set to 0.6g which caused the electromechanical circuit to come out of lock, but the probe was able to recover. At 1.5g the probe was unable to operate at any frequency above about 150 Hz, possibly because it was unable to recover lock at this acceleration.

These tests demonstrate that the probe can be designed to operate under adverse conditions, and that it would be worthwhile to proceed to a full prototype development programme.

Design Advantage for Automotive Applications

In addition to the advantages already described, this level gauge has the added advantage that it contains no moving parts. The gauge should also be easier to manufacture, and can be auto calibrated in production. The absence of moving parts will improve reliability, and consequently maintenance costs and reduce failure rates.

Future Developments

The trials were sufficiently promising to justify further development of the car fuel tank level gauge. It is now necessary to redesign the sensor so that it can be manufactured at low cost and still take account of the harsh automotive environment. As the sensor does not have to meet the same stringent accuracy requirements of the road tanker sensor, there is a reasonable confidence that a successful sensor design will be produced.

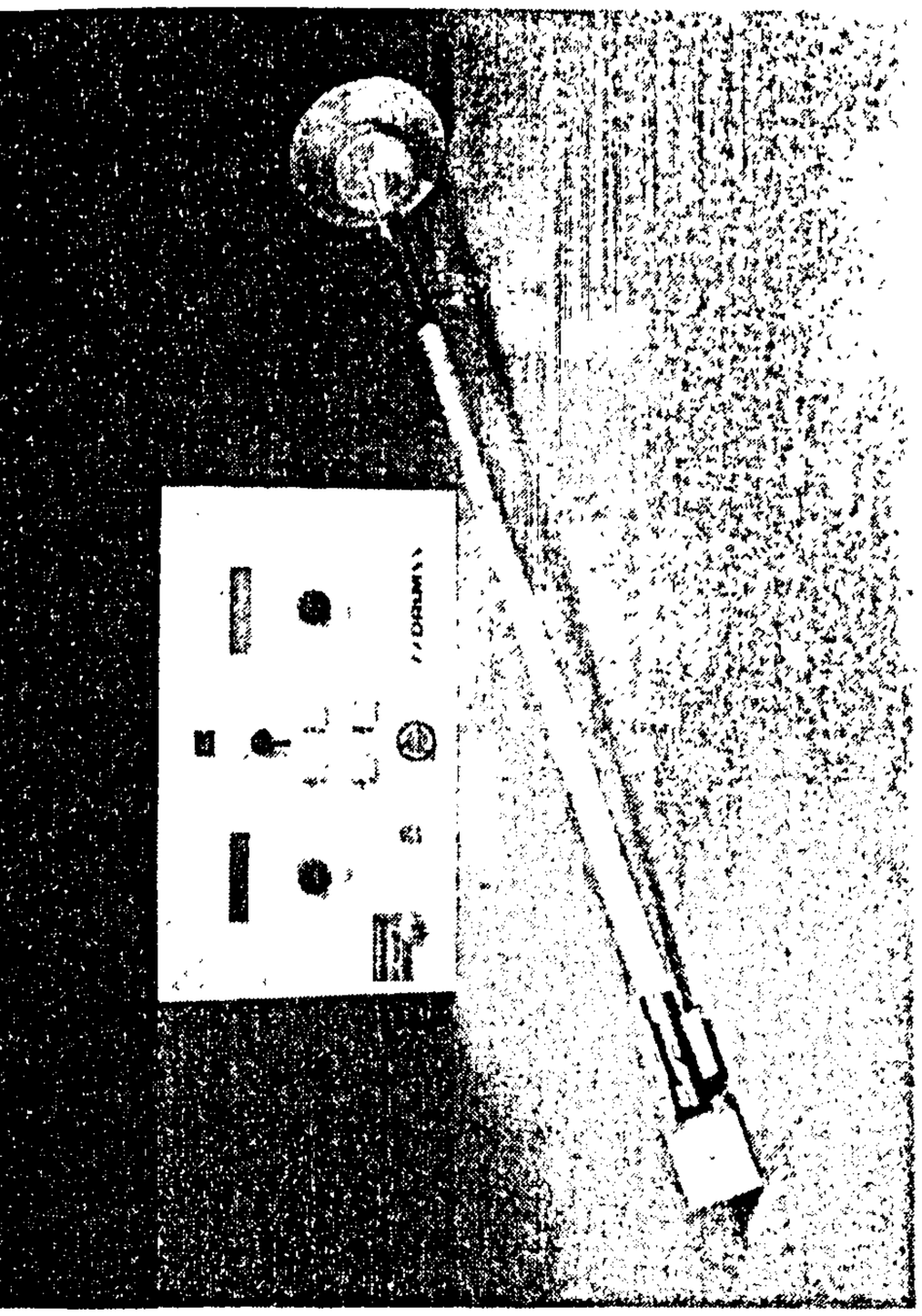

Petrol tanker level sensor

Traditional, now obsolete method of measurement.

Traditional dip stick

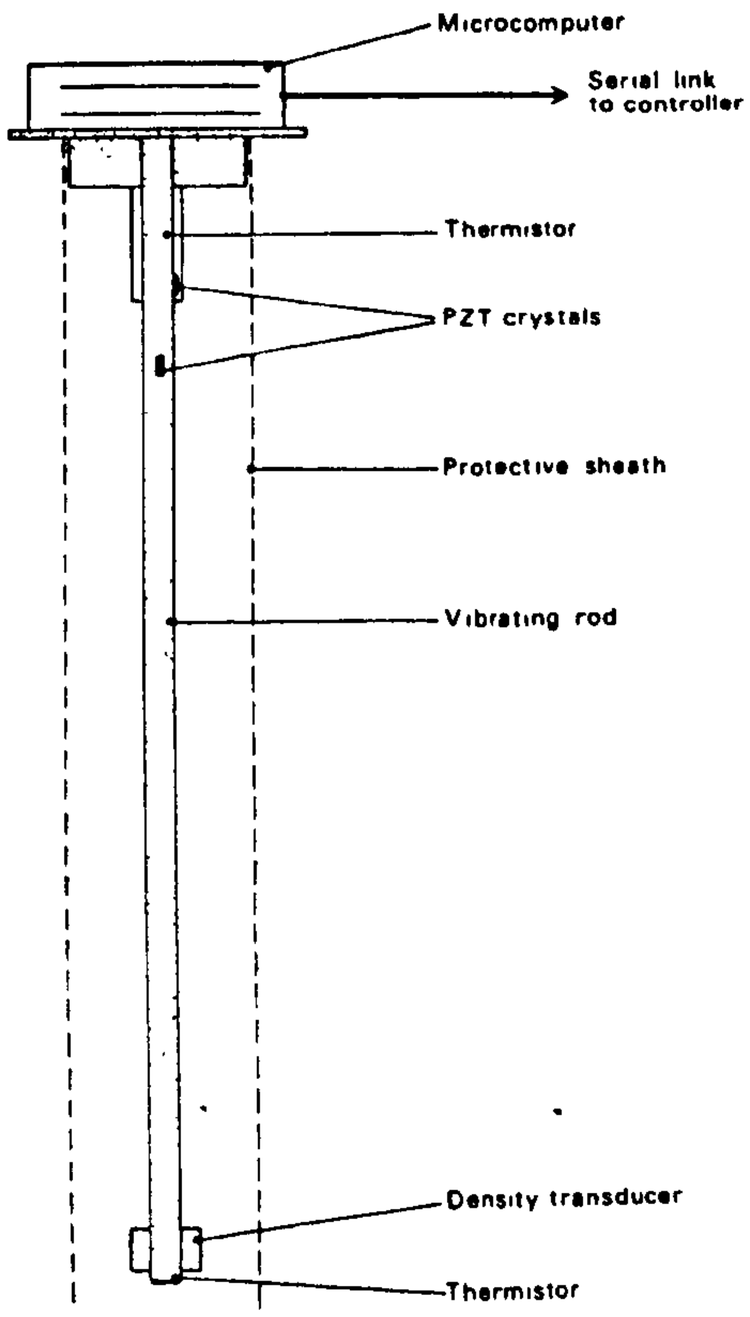

Principle of operation

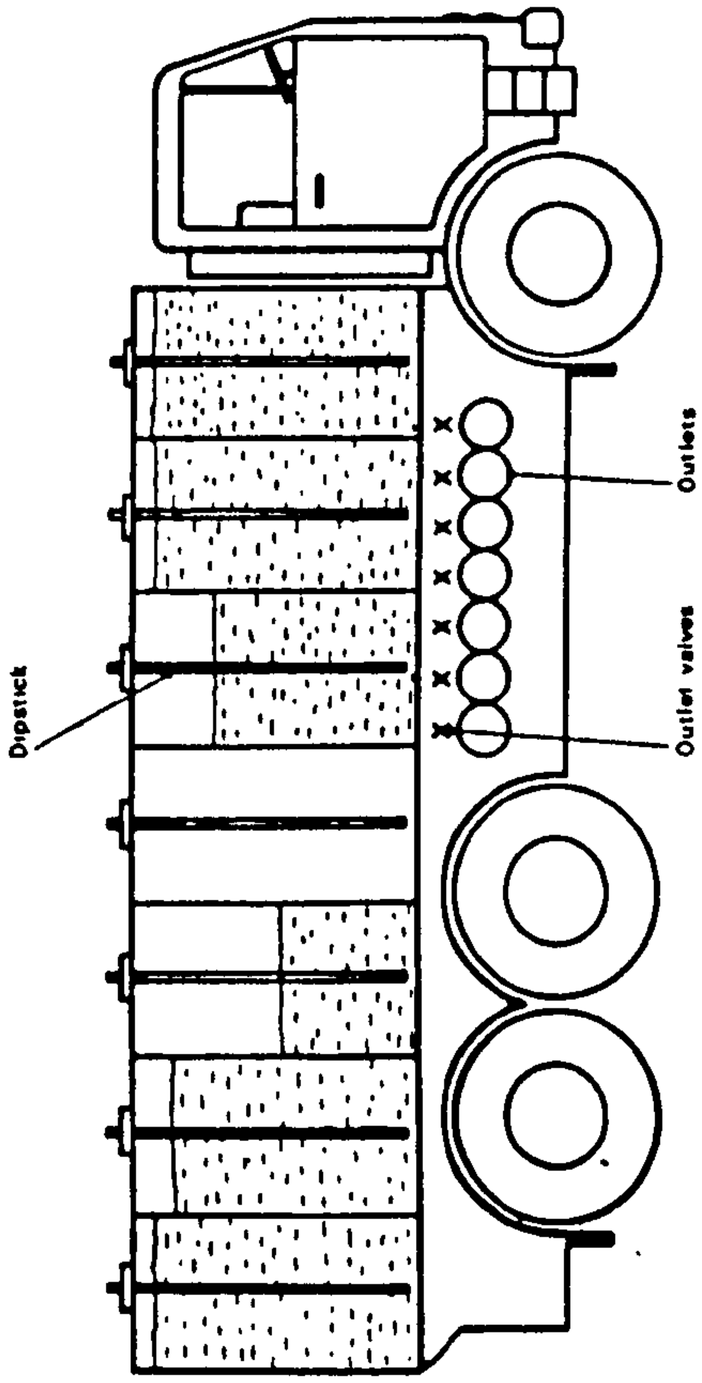

Complete tanker installation

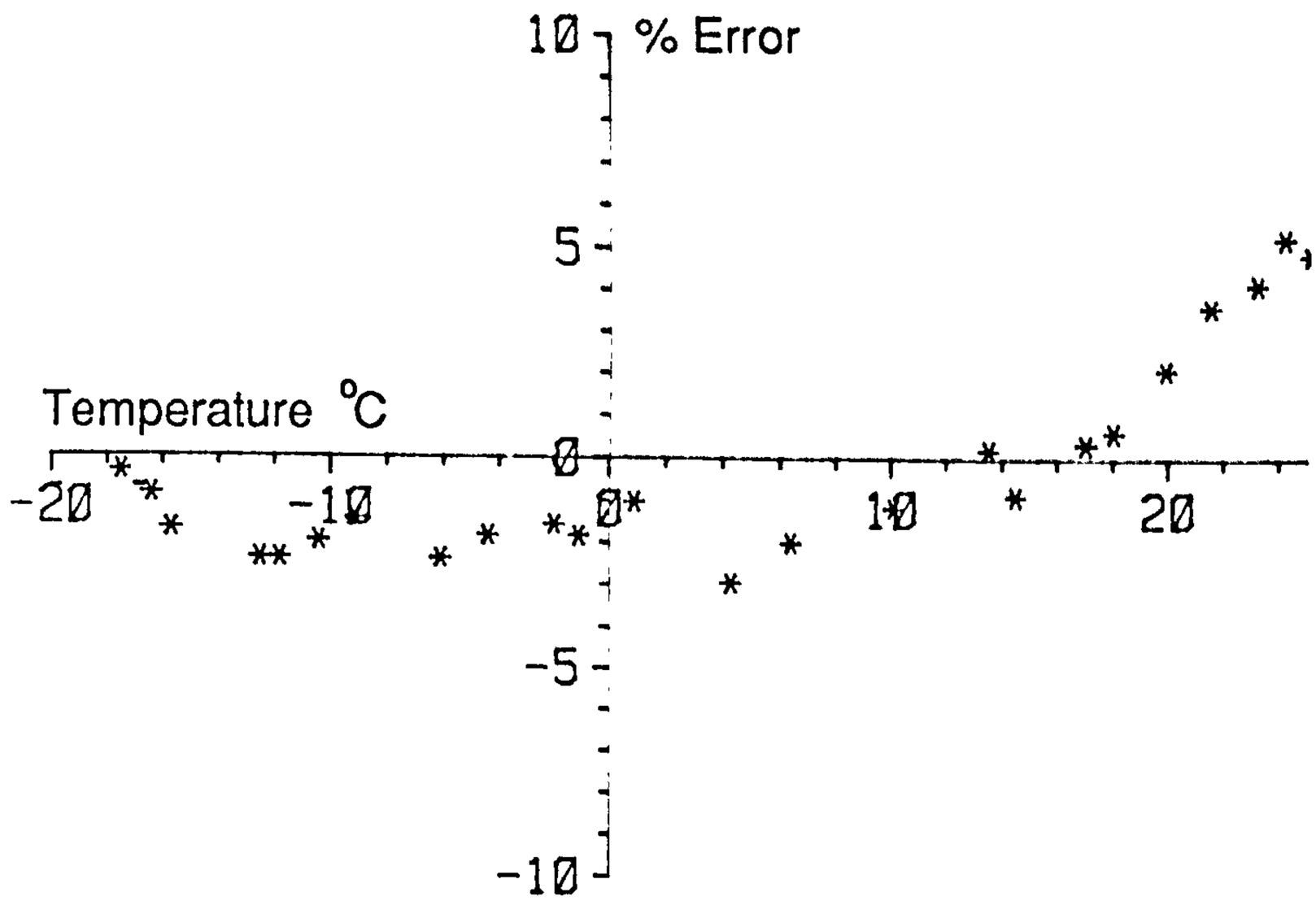

Constant mass test

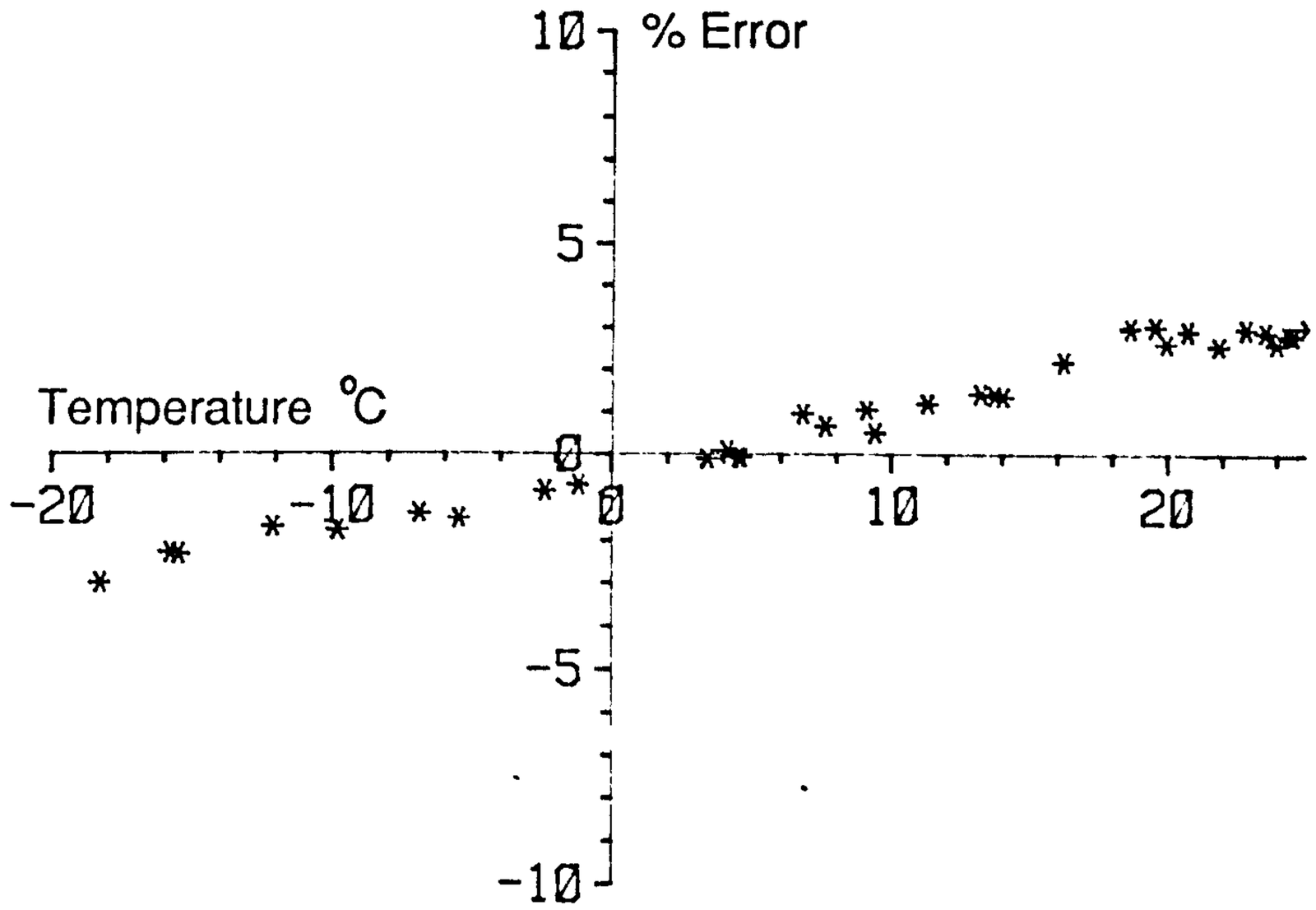

Constant volume test

Applications report

APPLICATION OF CMOS TECHNOLOGY TO PROCESS INSTRUMENTATION: SOME CASE STUDIES

Indexing term: Instrumentation

Abstract: The paper considers the application of CMOS technology to process instrumentation and gives examples of the use of CMOS in design.

Introduction

This paper discusses the reasons why CMOS is a desirable technology for some process instrumentation applications. Some examples are described which use CMOS exclusively in the design, giving the reasons why CMOS was used and the problems that were found while developing these instruments. All these examples are joint developments carried out by Sira Ltd. and a manufacturing company.

CMOS technology can be applied to advantage in process instrumentation, but the designer who is more familiar with NMOS and TTL devices must take into account the lower speed of CMOS components as compared with LS and NMOS equivalents, must avoid 'latch-up' conditions, and should apply all the normal design rules for LS and NMOS to the CMOS design.

Why choose CMOS for process instrumentation?

The growing use of CMOS components for process instruments is due primarily to the low-power requirement of the technology. The advantage of using low-power components is that it is far easier to design intrinsically safe and battery-operated instrumentation. Intrinsically safe instruments are essential for the energy industries (oil, gas, coal etc.) and for some process industries. The reliability of process control and measuring instruments is increased by being able to site the instrumentation in the hazardous environment, as opposed to relying on sensors connected by long lines to a remote instrument house. There are also ergonomic advantages in being able to install intelligent instruments close to the process under control. The main advantage of battery-operated instruments over traditional instruments which require a local supply is that they are portable. Portable test equipment can be carried onto site and used for on-site maintenance. Portable data logging and remote monitoring and control equipment can be installed in hostile environments for long periods of time, and collected only when necessary.

Some product examples

Sira has worked with a number of different companies on the collaborative development of various CMOS-based instruments over the last few years. The product examples discussed below are:

Gas flow volume corrector (Fig. 1)
BS Instruments Ltd.

System for tanker instrumentation and control (Fig. 2)
Drum Engineering Ltd.

Temperature readout for a hand-held thermal imager (Fig. 3)
Lasergage Ltd.

Gas flow volume corrector

The model 800 volume corrector jointly developed by BS Instruments and Sira is a battery-operated portable instrument that is now in large-scale production. The corrector is intended for use by industrial consumers of natural gas. Uncorrected flow rate is measured using a turbine meter. The static pressure and temperature are transduced and used to determine the gas compressibility factor, from which the true corrected volume flow can be calculated at a standard temperature and pressure. The corrector is intrinsically safe, and can be sited by the gas supply inlet.

The processor used is the Motorola 146805. This processor, as well as handling the analogue and pulsed turbine input, is also capable of performing the calculations required to determine corrected volume flow. A particular advantage of this device is the 'go to sleep until interrupt' command, which is used to prolong the battery life.

System for tanker instrumentation and control

Development of the DRUM-STIC was achieved through a four-way collaboration between Drum Engineering, Marconi, Sira and The City University. The product is a multiprocessor system consisting of satellite processors that measure the fluid volume in the separate compartments of a road tanker, and a central controller.

The level transducer is a vibrating rod developed by Marconi. The local intelligence that converts the frequency, density and temperature data into volume is a Motorola 146805-based single-board computer, developed by Sira and Drum Engineering, sited above each tank. The data from these satellite volume monitors are transmitted to a central controller based on a CMOS 8085. The central controller is responsible for interrogating the volume monitors, monitoring the front panel, driving the displays and controlling the tank valves.

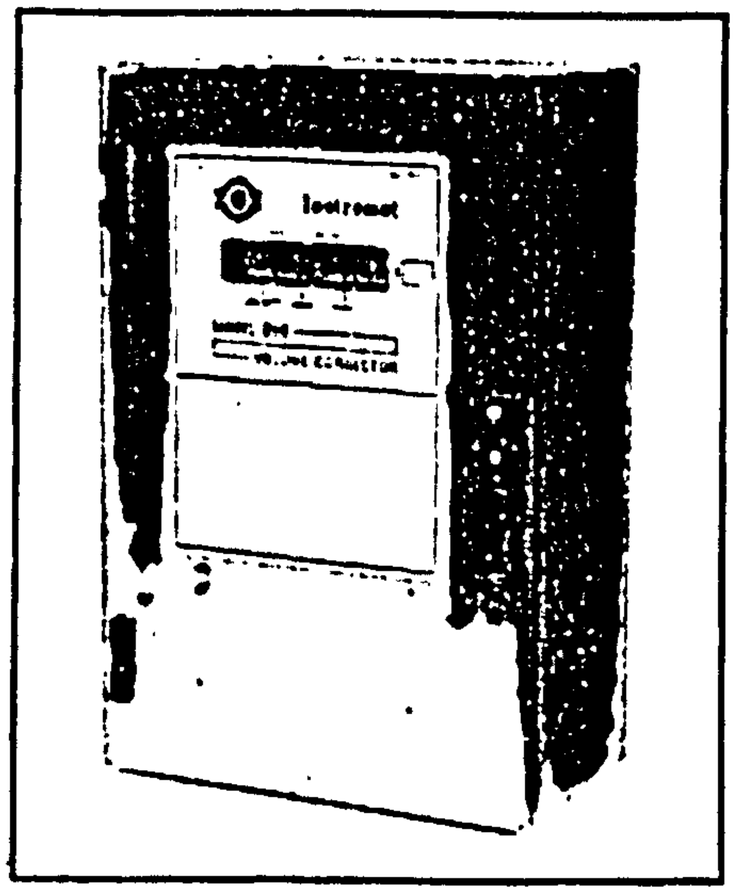

Fig. 1 Gas flow volume corrector
(BS Instruments Ltd.)

the CMOS processor invariably went into a latch-up mode. This was cured by adding extra decoupling to the supply lines.

Power on reset

A phenomenon that was discovered with a variety of processors was their failure to start their clocks oscillating on power up. As yet the cause has not been firmly established. The solution is to use an active reset device, such as the 4541, with a long time constant, and not rely on an RC network.

Conclusion

CMOS-technology components can be used in the engineering of process instruments. The design rules for CMOS-based instruments are more complex than those for NMOS and TTL instruments. This is because the engineer has not only to apply the same rules required for NMOS and TTL, but has also to take into account the additional rules that apply to CMOS.

E.N. GOODYER *3rd May 1984*

Electronics & Computing Systems Department, Sira Ltd., South Hill, Chislehurst, Kent, England

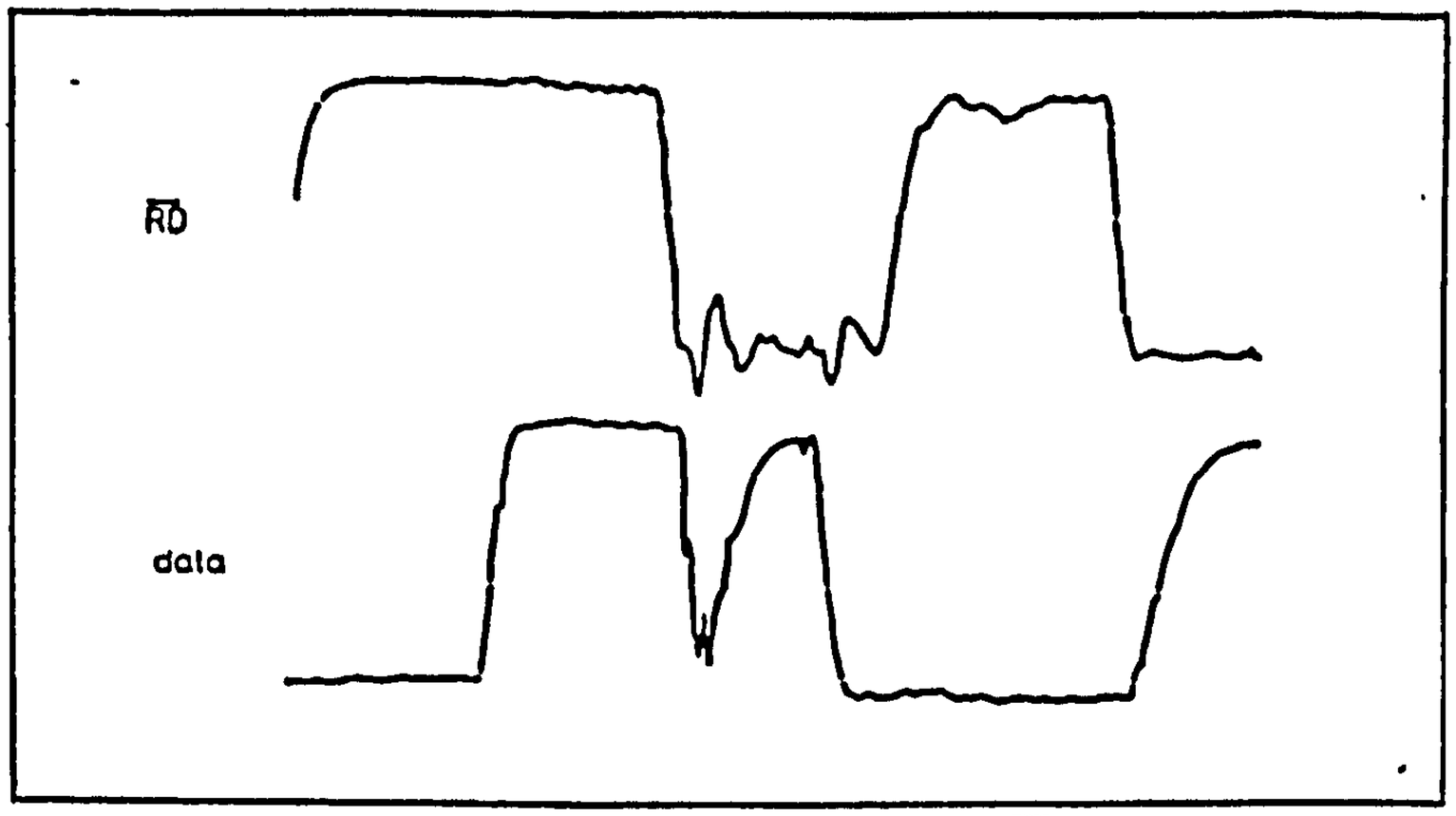

Fig. 5A Data output from 27C32 showing 1V switching spike on $\overline{RD}$ line

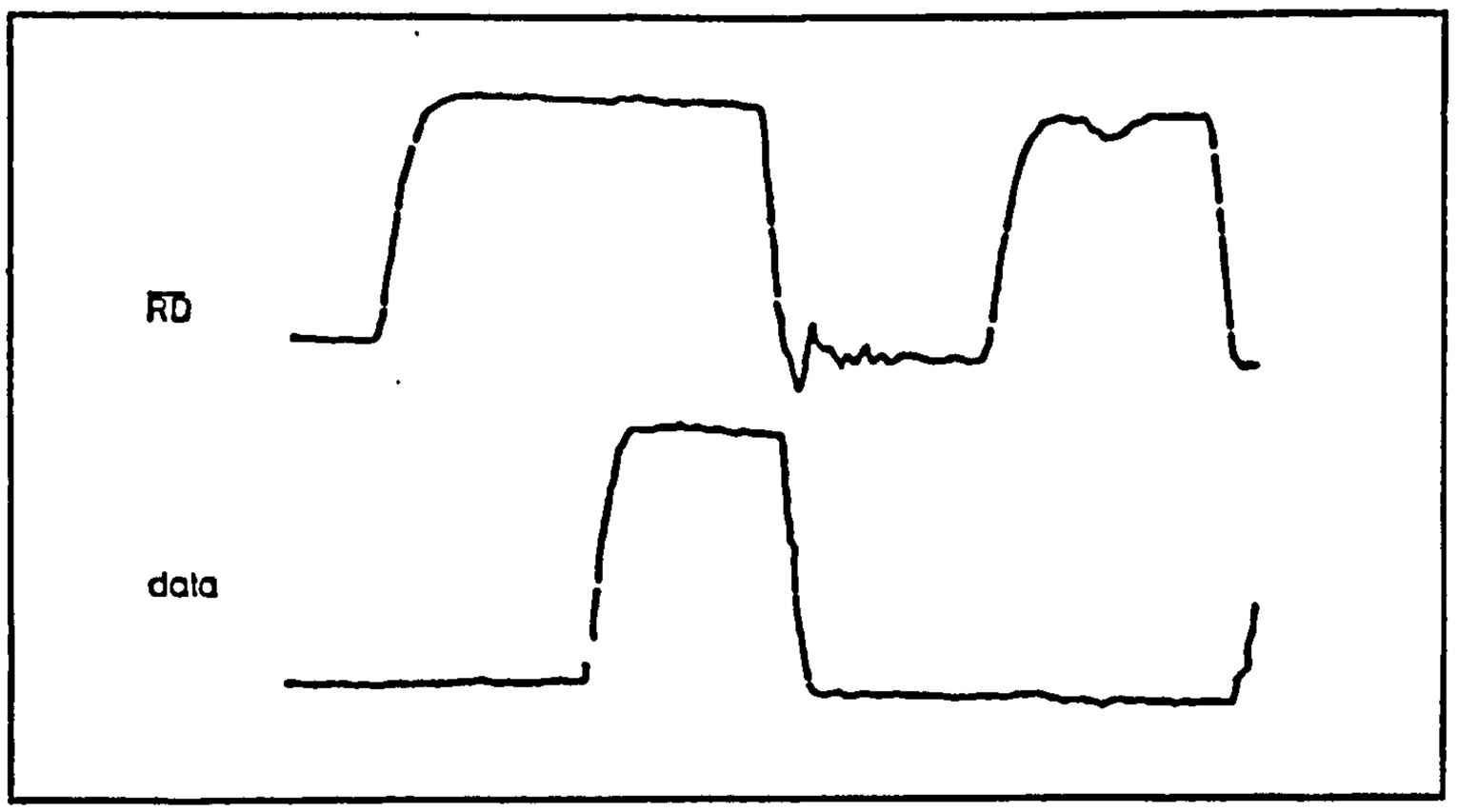

SM86 Fig. 5B Data output from 27C32 with correct PCB power gridding

Book review

Designing systems with microprocessors — a systematic approach
D. M. Freedman and L. B. Evans
Prentice-Hall 1983, 332pp., £28.75
ISBN: 0-13-201350-9

About a decade ago, in the early days of the microprocessor, it was the custom for logic designers to attend courses to introduce them to the new device. If the subject of top-down design was mentioned at all it was touched upon only briefly. Indeed, the object of the courses was to allow the participants to start producing code as quickly as possible, with a little perfunctory testing if time permitted. It is sobering to consider how much randomly designed code (with its attendant bugs) must exist to this day in assorted control systems around the world.

Fortunately, the past few years have seen an increased awareness of the need for a more structured approach to system design. Today, the terms 'top-down design' and 'software engineering' are commonplace. In keeping with this trend, the book by Freedman and Evans provides a welcome new variation upon the 'introduction to microprocessors' theme.

This attractively presented book is aimed at undergraduates and at practising engineers. The structure of the book reflects the 'top-down' nature of its subject. Anyone raised on more conventional microprocessor texts will be intrigued that the first five chapters of this book contain no mention of arithmetic logic unit. However, it is this lack of obsession with minute detail in the early chapters which makes this text so refreshing. Similarly, whereas most books dive directly into assembly language, the emphasis here is on the high-level language PL/M. Details of hardware and assembly language are covered later, only after the more abstract concepts have been established.

In keeping with its subject matter, the book itself is well structured: the authors present a diagram showing the relationship between the system design cycle and the chapters of the text. The reader is led from requirements definition, functional specification and system design, through hardware and software design and implementation, to system integration and evaluation. Continuity is provided by the use of a running example — a burglar alarm system.

Chapter 1 leads in gently with a discussion on the

APPLICATION OF LOW POWER MICROTECHNOLOGY TO PROCESS INSTRUMENTATION:

SOME CASE EXAMPLES

E N Goodyer

1 Introduction

This paper, using some product examples in the field of process instrumentation, seeks to examine some of the problems that can arise when applying CMOS technology, and offers some practical solutions to these problems.

Briefly mentioned are some of the reasons why CMOS is a desirable technology for process instrumentation applications.

The specific problems discussed are speed, power supply spikes and "latch up".

The overall conclusion is that CMOS technology can be successfully applied in process instrumentation, but the designer who is more familiar with NMOS and TTL devices should take into account the different characteristics of CMOS.

2 The case examples

Four successful products jointly developed by the named manufacturer and Sira were used as the source of the problems discussed below.

2.1 A low power flow corrector

This product is now in large scale production by BS Instruments Ltd. It is a battery operated product that is intended for use as a gas flow meter by industrial users. The processor used is a Motorola 146805.

2.2 A system for tanker instrumentation and control

This development, by Drum Engineering Ltd, will shortly be undergoing field trials by two major petrochemical companies.

It is a multiprocessor system that measures the fluid volume in the separate tanks of a road tanker. The data from these satellite fluid volume monitors are transmitted back to a central controller, that will eventually control the automatic loading and unloading of the individual tanks. The fluid volume monitors use a Motorola 146805, and the central computer uses a CMOS 8085.

2.3 Temperature readout unit for a thermal imager

This product is currently being developed for Lasergage Ltd. The unit is an optional addition to their range of existing thermal imagers. The temperature readout unit calculates the temperature of the target in the

E N Goodyer is with the Electronics and Computing Systems Department of Sira Ltd, Chislehurst, Kent.

centre of the field of view of the infra red image, and displays the measured temperature in the eyepiece display. The processor used is a National NSC 800.

2.4 Intelligent marine telemetry instrumentation

A series of battery powered telemetry equipments have been successfully developed and installed by Ocean Technical Systems Ltd. The applications vary depending upon the installation, but usually consist of a Remote Telemetry Unit situated in an undesirable environment, that is interrogated by a base station. The processor used is an RCA 1802.

2.5 Which processor?

Our experience of all the above-mentioned devices has led us to the conclusion that a processor is as good as the technical support and development equipment that is available for it.

Devices such as the NSC 800 and CMOS 8085 tend to be used when there is a requirement for complex mathematics. The 1802 and 146805 are preferable for I/O development systems. But these are not hard and fast rules. We have successfully implemented floating point maths on a 146805, trend analysis on an 1802, and I/O dependent control using an NSC 800 and a CMOS 8085.

3 The advantages of CMOS

The main advantages of CMOS technology arise from the fact that CMOS devices consume comparatively little power. The low power consumption means that it is now possible to develop lightweight, portable instrumentation, that can operate from batteries. The other large expanding field is that it is now possible to situate more intelligent instrumentation in hazardous environments.

Other advantages are battery backup capability when there is a power failure; and "power down" modes that allow CMOS instrumentation to idle when not in use, without switching off the power.

4 Some problems and their solutions

4.1 Speed

Standard 4000 series and 74C series devices have much longer switching times than their TTL equivalents.

Figure 1 gives a circuit example that demonstrates the problems that can arise. The decoder part of the circuit is used to select the I/O MAP of an NSC 800, CMOS 8085 or equivalent. The output latch is only selected during a write operation.

This circuit was found to be adequate on a processor system running at up to 4MHz, however any attempt to run it faster failed.

A quick examination of the worst case gate delays gives the reason. Each NAND gate has a typical delay of 125nS each, the OR gate takes 160nS, the decoder takes 550nS to settle and the setup time for the latch is 220nS, giving a total typical delay from address setup to chip select of 1180nS. The write cycle of an 8085/NSC800 is only 990nS when running at 6MHz.

The solution to this obvious problem, and other more subtle timing problems is to use high speed CMOS devices, such as the Signetics HEF series, or the 74PC (National) and 74HC (National, Motorola) devices which approach TTL speeds.

4.2 Power supply spikes

Just because CMOS technology takes less power than other equivalent technologies it is incorrect to assume that it does not generate current surges, and therefore voltage drops on supply lines.

Figure 2 shows two traces measured off a 27C23 CMOS EPROM when it is under maximum switching load. One trace is the Output Enable input signal, the other is a data output line. The bus is the multiplexed address/data bus of a CMOS 8085. The address is FF hex, the data is 00 hex, therefore the output buffers of the 27C32 are required to perform the maximum switching of pulling a bus all set high to their low states.

Despite the fact that the device is CMOS, the current surge generated when the output is enabled is sufficient to put a 1 volt spike on the supply lines. As a result the device was switched off and the data disappeared.

This problem was cured in the final prototype by the addition of a suitable power gridding network on the PCB. This is of course good engineering practice, however the lesson to be learnt is that despite CMOS's low power consumption, it is still capable of generating large switching spikes.

4.3 Latch up

CMOS, due to its construction, inherently has parasitic SCR junctions that in normal operation are reverse biased. If input signals exceed the power supply then these junctions become activated, causing SCR latchup and allowing high currents to pass which will easily destroy the device.

Sensible design can ensure that a latch up does not occur, the easiest method being to employ level shifting devices at input interfaces. A particular problem arose with a fast rising power supply that put some ringing on the supply lines. As a result, on power up the CMOS processor invariably went into a latchup mode. This was cured by adding extra decoupling to the supply lines.

4.4 Power on reset

A phenomenon that was discovered with a variety of processors was their failure to oscillate on power up. As yet the cause has not been firmly established.

The solution is to use an active reset device (and not rely on an RC network) such as the 4541 reset desive with a long time constant.

5 Conclusion

CMOS technology components can be used in the engineering of process instruments. As well as applying the design rules applicable to TTL, NMOS and equivalent technologies, the engineer must also take account of the operational differences of CMOS devices such as lower speed and latch up.

RD

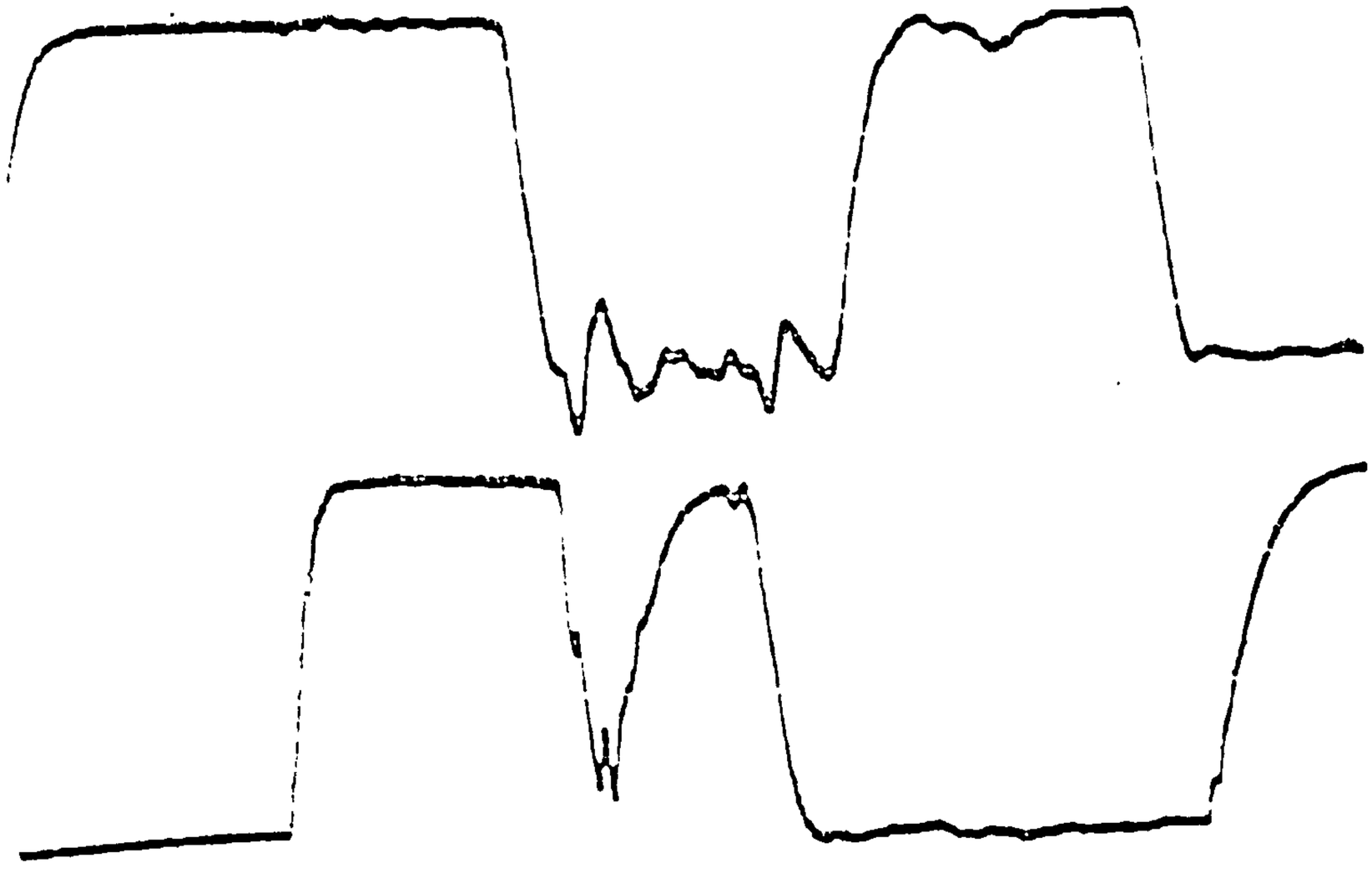

DATA

FIGURE 1

RD

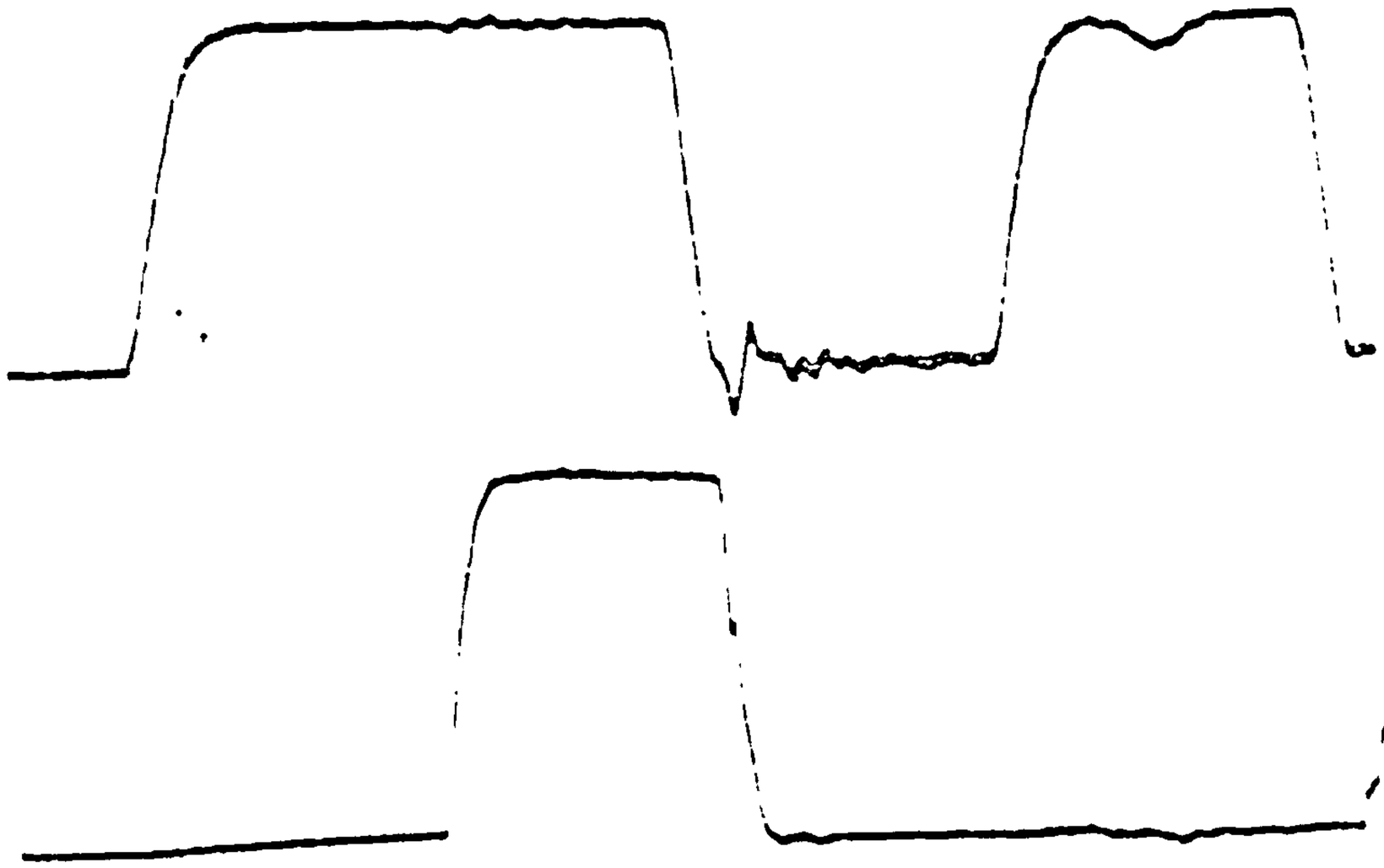

DATA

FIGURE 2

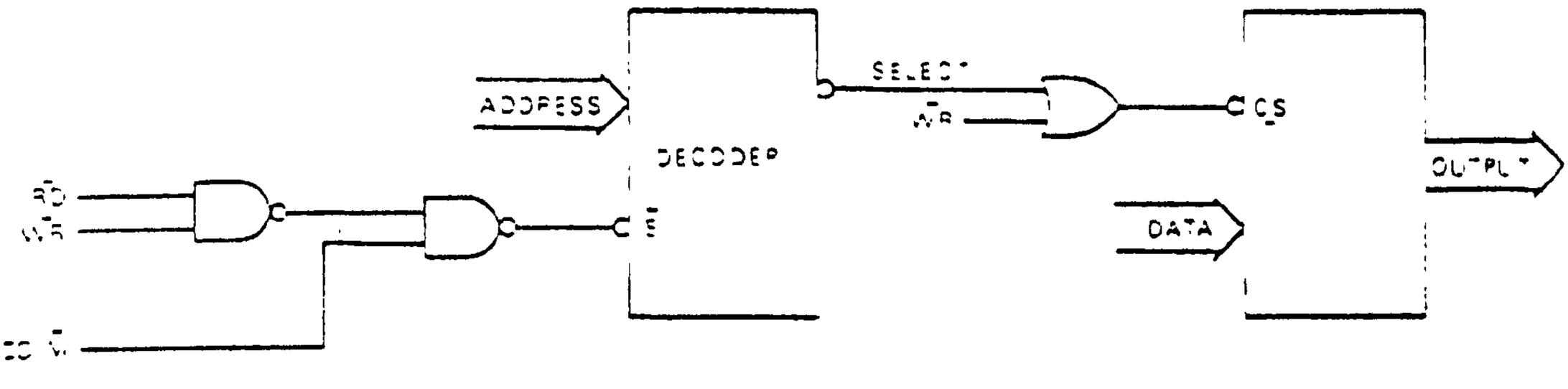

FIGURE 3

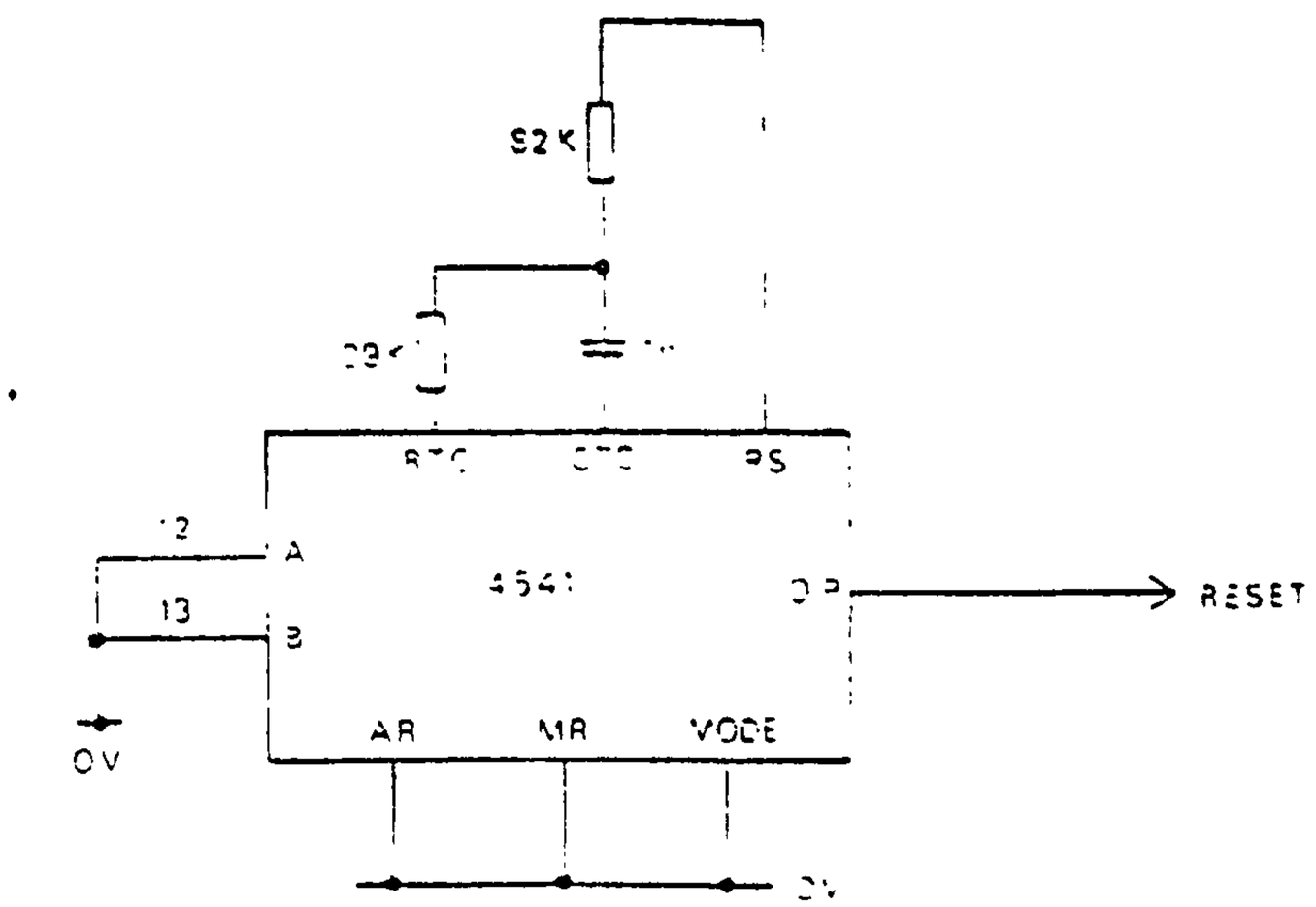

FIGURE 4

A MICROPROCESSOR-BASED GAS FLOW COMPUTER

E N Goodyer
Sira Institute Ltd, Chislehurst, Kent

This presentation discusses some of the problems in accurate measurement of the flow rate of hydrocarbon gas; briefly reviews the limitations of analogue solutions; and finally presents a viable solution that employs a microprocessor-based gas flow computer.

By adopting a microprocessor-based solution the engineer is able to use the programmability of the system to advantage. The gas flow computer can operate in 30 different modes, giving the choice between use of a turbine meter or orifice plate, output of mass flow or volume flow, with correction based upon compressibility calculation or densitometer input. Range limits and scaling factors are operator entered by means of a calculator type keypad. Self checking and error diagnosis procedures are incorporated and further illustrate enhancements provided by the microprocessor-based solution.

INTRODUCTION

Difficulties that arise when applying analogue techniques to calculating the flow rate of hydrocarbon gas are overcome with digital instrumentation. Such an instrument is the Instromet model 782 gas flow computer. The computer was conceived by KDG instruments Ltd, and the development carried out jointly by Sira Institute Ltd and KDG.

The intended application of this instrument is the custody transfer of natural gas. The computational accuracy is ± 0.05%.

DERIVATION OF FLOW RATE

Volumetric flow of hydrocarbon gas is in practice usually measured by means of a turbine meter, or an orifice plate, inserted into the stream of flowing gas. The measurand yielded is frequency of rotation or differential pressure respectively. This value is manipulated and scaled to give the volumetric flow rate of the gas, at the pressure and temperature of that gas.

Orifice Plate

Theoretically the differential pressure across an orifice plate is related to the flow rate of the fluid by a square root factor.

$$\frac{dV}{dt} \propto \sqrt{h} \qquad \text{.......} \quad (1)$$

where h = differential pressure

$\frac{dV}{dt}$ = flow rate

In reality account must be taken of the expansion factor of the orifice plate installation, which is dependent upon the ratio of the diameters of the orifice plate and the pipe, and the pressure of the fluid. The expansion factor (Y) is:

$$Y = 1 - (0.41 + 0.35B^4) \quad \frac{h}{P \times 1.3} \qquad \text{.......} \quad (2)$$

where B = ratio of orifice plate to pipe diameter
P = pressure of flowing gas

Turbine Meter

A turbine meter generates pulses that are equivalent to a volume of fluid. A simple method of obtaining the flow rate is to integrate the pulses over a known period of time, however, this approach inherently adds a quantisation error to the calculation.

A worst case example would be a rate of 1 pulse every 0.9 seconds, and an integration time of 1 second. For the first 9 integration periods the rate is measured as 1 pulse per second, and for the tenth period a rate of 2 pulses per second is measured. The solution is to integrate over a period of time that is far larger than the inter-pulse period, but even this approach will still contain a finite quantisation error.

To obtain a true measurement of turbine frequency it is necessary to know the actual time at which the first and last pulse arrived in a given period.

In Figure 1, t_o is the start of an integration period, t_p is the end of an integration period, t_f the time of the arrival of the first pulse, and t_l the time of arrival of the next pulse immediately after the end of the period. Using an integration approach the frequency would be given as:

$$\frac{7}{t_p - t_o} \qquad \ldots\ldots\ldots\ldots\ldots\ldots\ldots\ldots\ldots\ldots (3)$$

as 7 pulses would be seen during the integration period t_o to t_p.

The true frequency however is obtained by measuring the actual time of arrival of the first and eighth pulse, and using this time as the integration period. The true frequency is therefore given as

$$\frac{7}{t_l - t_f} \qquad \ldots\ldots\ldots\ldots\ldots\ldots\ldots\ldots\ldots\ldots (4)$$

To obtain this measurement the integrator must be capable of dynamically altering its integration period to relate to the true time of arrival of the pulses.

Once the frequency has been obtained it must be scaled by the maximum frequency output of the meter. The maximum frequency output of a turbine meter is a calibration factor that is usually different even for meters of the same type.

The flow rate is:

$$\frac{dV}{dt} = \frac{\text{frequency}}{\text{scaling factor}} \qquad \ldots\ldots\ldots\ldots\ldots\ldots\ldots\ldots\ldots\ldots\ldots\ldots (5)$$

where the scaling factor is dependent upon the maximum turbine frequency, and the required engineering units.

Compressibility Factor

As hydrocarbon gas is a compressible fluid, it is essential that the flow rate is expressed at a standard (or base) pressure and temperature. Various standards exist throughout the world, so for generality let us refer to these values as Pressure Base (P_b) and Temperature Base (T_b). The actual pressure and temperature of the gas shall be referred to as Pressure Flowing (P_f) and Temperature Flowing (T_f).

Given the gas equation

$$PV = RTZ \qquad \ldots\ldots\ldots\ldots\ldots\ldots\ldots\ldots\ldots\ldots\ldots\ldots\ldots\ldots\ldots\ldots (6)$$

where
- P = pressure
- V = volume
- R = gas constant
- T = temperature
- Z = the deviation of the gas from the ideal gas at P and T

then volumetric flow rate at base conditions dV_b/dt is related to the volumetric flow rate at flowing conditions dV_f/dt by:

$$\frac{dV_b}{dt} = \frac{dV_f}{dt} * \frac{P_f}{P_b} * \frac{T_b}{T_f} * \frac{Z_b}{Z_f} \qquad \ldots\ldots\ldots\ldots\ldots\ldots\ldots\ldots (7)$$

The calculation of the compressibility factor (Z) itself poses major problems. Specifically, for hydrocarbon gas it is necessary to take account of the non-hydrocarbon impurities present in the gas, thus a knowledge of the concentration of the primary impurities, CO_2 and N_2, and the specific gravity of the gas are required. From these values, measurands P_f and T_f are adjusted to eliminate the effect of the impurities on the calculations. Given the adjusted values the Z factor, which is a complex function of pressure and temperature, can be determined.

One widely accepted method of calculating Z is given by the American Gas Association Standard NX 19. This standard is laid down in a series of equations that cover 4 sides of A4 paper, and involves some 300 multiplications/divisions.

LIMITATIONS OF ANALOGUE TECHNIQUES

The overriding limitations of an analogue approach to the solution of the problems discussed above is the difficulty in implementing circuits that will perform the required calculations.

Commissioning of an analogue meter requires the presetting of a number of constants, including concentrations of CO_2 and N_2, orifice plate dimensions or maximum turbine frequency, pressure and temperature base conditions, and scaling constants. These presets are usually implemented with potentiometers, which are subject to drift and instability.

The implementation of a variable period integrator for turbine meters is possible but is complex.

Analogue square root circuits, for use with orifice plates are widely available. The calculation of the expansion factor is not as simple, and requires complex function generators.

Z factor circuits have been implemented in the past. These circuits do not calculate the equations laid down in the AGA standard, as it would require one operational amplifier to implement each stage of the calculation representing an extremely large analogue computer. The usual approach is to implement a transfer function that approximately matches the Z factor function.

A MICROPROCESSOR-BASED SOLUTION

An example of a digital solution to problems inherent in measuring gas flow is the Instromet model 782 gas flow computer.

Gas Flow Computer Inputs

The computer can use either a turbine meter or an orifice plate for the measurement of uncorrected flow rate (dV_f/dt). The transducer inputs required for each of the methods are:

Turbine:	pulse input (ranges from	1 - 100 hz to 1 - 5 KHz)
Orifice plate:	differential pressure	(4 - 20 mA)
	pressure	(4 - 20 mA)

To determine corrected flow the computer calculates Z factor as described above. The other transducer inputs required are:

Z factor:	pressure	(4 - 20 mA)
	temperature	(4 - 20 mA)
	specific gravity	(4 - 20 mA)

An alternative to calculating the Z factor is to measure the density of the gas, and to scale the flow rate by this measurand to obtain the mass flow rate. This method is preferred by some users, therefore a density input is also provided.

Flow may be required in terms of either mass or volume of gas. If the volume is required then there must be a specific gravity input.

In some applications the specific gravity, density or pressure is preset and not transduced. The computer has manual preset overrides for these three transducer inputs.

Gas Flow Computer Outputs

The outputs from the computer are a 4-20 mA current loop indicating flow rate (dV_b/dt), and two pulsed outputs indicating totalised flow, before and after correction by the Z factor.

There are two relay alarm outputs and a local LED display, which indicate the following conditions:

Low flow detected on turbine meter/orifice plate
Instrument failure
Transducer out of range
Preset data corrupted

Preset Constants

Various constants are required for the operation of the computer. Each of the transduced inputs requires some form of scaling factors:

Pressure range
Differential pressure range
Specific gravity maximum and minimum
Density maximum and minimum
Maximum turbine frequency

Depending upon the chosen method of obtaining corrected flow it is necessary to enter some of these values:

Temperature base
Pressure base
mol % CO_2
mol % N_2
B ratio
K factor

The engineer must also be provided with facilities for entering scaling factors for the gas flow computer outputs, and the low flow alarm level.

In total there are 16 possible preset constants, which are entered via a calculator-type keypad in decimal. If the engineer attempts to enter unrequired data the display indicates a selection error. The data entry routine also checks that the value is valid.

Operator Facilities

There is an LED display, upon which can be displayed any of the transduced values, the flow rate or the Z factor. Also provided are a counter which displays the totalised flow, and the LED indicators as described in 'Gas Flow Computer Outputs'.

Computation Cycle

The instrument's microprocessor (an Intel 8085) controls a computation cycle in which: five transducers are sampled to an accuracy of ±0.01%, the calculations (which involve some 300 multiplication and division routines) are executed to an accuracy better than ±0.05%, various self-checking routines are executed, the analogue and pulsed outputs are generated, and a transduced value is displayed. The cycle time is approximately 3 seconds.

Self Tests

Every cycle the computer executes various self-test programs. It checks that all the required preset data for the chosen mode of operation has been entered; and ensures that none of that data has been corrupted. If any transducer input is out of range or the turbine meter stops working, an error is indicated. If there is low flow; the analogue interface is acting suspiciously; the outputs go full scale, an error is indicated.

Other tests include examining the selection switch and key switch for open circuit or oscillation. Every 12 hours the whole of the read/write memory is tested for any failure, and the program is self-checked regularly to ensure that no bits are corrupted. In the event of a power failure, the memory has a battery backup facility to preserve all the data.

CONCLUSION

The digital computer overcomes the problems in measuring gas flow because it is capable of performing precise calculations, can take decisions under program control, and can store preset values in its memory.

The calculation of Z factor, the orifice plate expansion factor and other equations are performed digitally by the microprocessor, using floating point arithmetic which is far more precise than analogue computation and is far easier to implement.

The computer is capable of determining the true frequency of the turbine meter input. A 6 MHz crystal oscillator is used to update an internal real time clock. When pulses arrive from the turbine meter this clock is examined to obtain the actual time of arrival of that pulse.

The preset constants are free of the drift problems associated with analogue circuits, because they are entered via a keypad as opposed to a potentiometer, and are stored in the computer's memory.

The ability of the gas flow computer to perform self check programs gives the instrument a greater integrity than its analogue predecessors.

SYMBOLS USED

h = differential pressure

$\frac{dV}{dt}$ = flow rate

B = ratio of orifice plate to pipe diameter

P = pressure of flowing gas

t_o = start of an integration period

t_p = end of an integration period

t_f = time of the arrival of the first pulse

t_l = time of arrival of next pulse immediately after end of period

P_b = pressure base

T_b = temperature base

P_f = pressure flowing

T_f = temperature flowing

P = pressure

V = volume

R = gas constant

T = temperature

Z = the deviation of the gas from the ideal gas at P and T

Where:

Q_v = Volume flow rate

Q_m = Mass flow rate

t_f = Turbine meter output (pulse rate)

p_f = Static Pressure (bar, absolute pressure)

T_f = Gas Temperature (deg.C)

Z_f = Gas Compressibility factor (See Appendix 3)

d = Gas Density

G = Gas specific gravity

Z_b = Gas base compressibility factor (See Appendix 3)

P_b = Base pressure (bar, absolute pressure)

T_b = Base Temperature (deg.C)

t_{max} = Turbine meter output at maximum flow rate (pulse rate)

and K_1, K_2, K_3 and K_4 are scaling factors

APPENDIX C

Equations for Gas Flow using an Orifice Plate***

1 Volume Flow

(a) $Q_v = \frac{K_5 Y Z_b (T_b + 273.15)}{P_b} \cdot \frac{hP_f}{GZ_f (T_f + 273.15)}$

(b) $Q_v = K_6 \frac{Y}{G} hd$

2 Mass Flow

(a) $Q_m = \frac{K_7 Y Z_b (T_b + 273.15)}{P_b} \cdot \frac{hP_f G}{Z_f (T_f + 273.15)}$

(b) $Q_m = K_8 \frac{Y}{G} hd$

Where:

$Y = 1 - (0.41 + 0.35b^4) \frac{X}{K}$

Where:

$X = \frac{h}{P_f}$

K = 1.3 (Ratio of specific heats)

$b = \frac{\text{orifice diameter}}{\text{pipe diameter}}$

and Q_v = Volume flow rate

Q_m = Mass flow rate

h = Differential pressure (bar)

p_f = Static Pressure (bar, absolute pressure)

T_f = Gas Temperature (deg.C)

Z_f = Gas Compressibility factor (See Appendix 3)

d = Gas Density

G = Gas specific gravity

P_b = Base pressure (bar, absolute pressure)

T_b = Base Temperature (deg.C)

Z_b = Gas base compressibility factor (See Appendix 3)

and K_5, K_6, K_7 and K_8 are scaling factors

*** Instromet Series 782 Users Manual

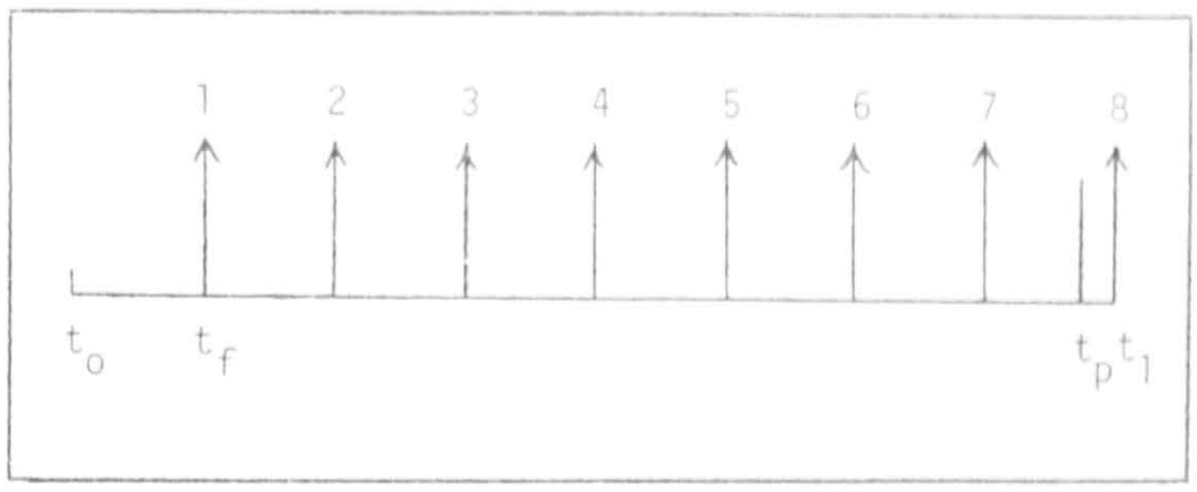

Figure 1 Turbine meter output

Figure 2 A gas flow computer